Biomechanical Modelling of the Whole Human Spine for Dynamic Analysis

by

Volkan Esat, BSc MSc

A Doctoral Thesis

Submitted in partial fulfilment of the requirements
for the award of
Doctor of Philosophy of Loughborough University
June 2006

ABSTRACT

Developing computational models of the human spine has been a hot topic in biomechanical research for a couple of decades in order to have an understanding of the behaviour of the whole spine and the individual spinal parts under various loading conditions. The objectives of this thesis are to develop a biofidelic multi-body model of the whole human spine especially for dynamic analysis of impact situations, such as frontal impact in a car crash, and to generate finite element (FE) models of the specific spinal parts to investigate causes of injury of the spinal components. As a proposed approach, the predictions of the multi-body model under dynamic impact loading conditions, such as reaction forces at lumbar motion segments, were utilised not only to have a better understanding of the gross kinetics and kinematics of the human spine, but also to constitute the boundary conditions for the finite element models of the selected spinal components. This novel approach provides a versatile, cost effective and powerful tool to analyse the behaviour of the spine under various loading conditions which in turn helps to develop a better understanding of injury mechanisms.

Keywords: Human Spine, Intervertebral Disc, Multi-Body Modelling, Finite Element Modelling, Biomechanics, Whiplash, Crash

Dedication

To My Family, and My Wife, Berna

ACKNOWLEDGEMENTS

I wish to express my full indebtedness to my supervisor *Dr. Memis Acar*, who chose me as his PhD student and introduced spinal biomechanics to me. Without his outstanding contributions, kind encouragement, stimulating discussions, everlasting support and patience, this thesis would not have been written.

I convey my most sincere thanks and deep appreciation to *Prof. Dr. Homer Rahnejat, Dr. B. Serpil Acar, Prof. Dr. Haluk Darendeliler, Prof. Dr. Mustafa Ilhan Gokler, Prof. Dr. Koshiro Ono, Dr. Leon Kazarian,* and *Dr. Serge Van Sint Jan* for their precious help and contributions.

I wish to thank my dear friend and housemate *Murat Ceran* gratefully for his never-ending support and fellowship. I would also like to extend my sincere thanks to my friends *Dr. Serhat Erpolat, Dr. Yasar Alper Ozkaya, Selcuk Himmetoglu, Sinan Eroglu, Dr. David van Lopik, Dr. Adnan Aziz, Senay Mihcin, Ebru Tascioglu, Dr. Yigit Tascioglu, Ozge Unverdi, Dr. Ozhan Unverdi, Selda Konukcu, Ozan Koseoglu, Behzat B. Kentel, Bilge Erdogan, and Alix Weekes,* who stood by me all the way.

The financial support from *Loughborough University* is gratefully acknowledged.

Last, but not least, I am utmost grateful to *my wife, Berna,* and *my family,* for their invaluable understanding, endless support, patience, and love.

TABLE OF CONTENTS

CHAPTER 1 1

Introduction 1

1.1 Research Issues and Computational Models 1

1.2 Aim of the Thesis 4

1.3 Objectives of the Thesis 4

1.4 Scope of the Thesis 6

1.5 Outline of the Thesis 6

CHAPTER 2 8

Biomechanics of the Human Spine 8

2.1 Introduction: The Human Spine 8

2.2 Spine Components 10

2.2.1 The Intervertebral Disc 11

2.2.2 The Spinal Ligaments 20

2.2.3 The Vertebra and the Facet Joints 26

2.2.4 The Spinal Muscles 33

2.2.5 Other Components 37

2.3 Biomechanics of the Regions of the Human Spine 37

2.3.1 The Cervical Spine 37

2.3.2 The Thoracic Spine 48

2.3.3 The Lumbar Spine 51

2.3.4 The Sacroiliac Region 57

2.4 Discussion 58

CHAPTER 3 61

Computational Models of the Human Spine 61

3.1 Introduction 61

3.2 Computational Human Spine Model Classifications 62

3.3 Analytical, Geometric, 2 Pivot, and Continuum Models 64

3.4 Multi-Body / Discrete Parameter Models 71

3.4.1 Multi-Body / Discrete Parameter Models of the Cervical Spine 71

3.4.2 Multi-Body / Discrete Parameter Models of the Lumbar Spine 79

3.4.3 Multi-Body / Discrete Parameter Models of the Whole Spine 82

3.5 Finite Element Models 87

3.5.1 FE Models of the Cervical Spine 88

3.5.2 FE Models of the Lumbar Spine 96

3.5.3 FE Models of the Whole Human Spine 100

3.5.4 FE Models of the Intervertebral Discs 102

3.6 Hybrid Multi-Body / Finite Element Models 106

3.7 Discussion 109

CHAPTER 4 *113*

Multi-Body Model Development *113*

4.1 Introduction 113

4.2 A Preliminary Multi-Body Model of the Lumbar Spine 113

4.2.1 Solid Model of the Lumbar Spine 113

4.2.2 Multi-Body Modelling of the Lumbar Spine 118

4.2.3 Analysis of the Multi-Body Model of the Lumbar Spine 125

4.3 Multi-Body Model of the Whole Human Spine 128

4.3.1 Solid Bodies: Vertebrae and Others 129

4.3.2 Intervertebral Discs 133

4.3.3 Ligaments 136

4.3.4 Muscles 137

4.3.4.1 External Software to Control Muscles: Virtual Muscle 138

4.3.4.2 Muscle Fibre Types. 141

4.3.4.3 Muscle Morphometry 143

4.3.4.4 Musculotendon Blocks 145

4.3.4.5 Muscle Descriptions and Attachment Locations 146

4.3.5 Final Multi-Body Model 165

4.4 Discussion 167

CHAPTER 5 *170*

Multi-Body Model Validation *170*

5.1 Motion Segment Responses in the Cervical Spine 171

5.1.1 Motion Segment Responses to Various Loads 171

5.1.2 Moment Generating Capacity of Neck Muscles 177

5.2 MB Model Responses in the Cervical Spine for Frontal and Lateral Impacts 179

5.2.1 Frontal Impact 180

5.2.2 Lateral Impact 185

5.3 Vertical Loading for the Cervical Spine 191

5.4 MB Model Responses of Thoracolumbar Region in Rear-End Impact 194

5.5 Discussion 199

CHAPTER 6 201

A MB Model Application: Simulating Whiplash 201

6.1 Experimental and Simulation Set-ups 203

6.2 MB Model Simulation Results 204

6.3 Ligament Forces 211

6.4 Intervertebral Disc Forces 213

6.5 Discussion 213

CHAPTER 7 215

Finite Element Models of the Intervertebral Discs 215

7.1 The Proposed Approach 215

7.2 First Model: A Disc Segment Investigation 216

7.3 Second Model: An FE Investigation on the Whole Disc Segment 218

7.4 Third Model: An Improved FE Model of the Whole Disc Segment 220

7.5 Fourth Model: FE Model of L2-L3 Level FSU 225

7.6 Fifth Model: Viscoelastic FE Model of Whole Cervical Spine Discs 227

7.7 Discussion 232

CHAPTER 8 233

Conclusions 233

8.1 Assessment of the Work 233

8.2 Final Conclusions 237

CHAPTER 9 _____ *239*

Suggestions for Further Work _____ *239*

REFERENCES _____ *241*

APPENDICES _____ *260*

Appendix A: Modelling/Material Property Data for Spinal Elements _____**261**

Appendix B: Mean and Standard Deviation Values for Force and Deflection at Failure for Human Spinal Ligaments _____**267**

Appendix C: Equations and Coefficients for 'Virtual Muscle' Muscle Model_**268**

Appendix D: A Survey of Human Musculotendon Actuator Parameters (Yamaguchi et al., 1990) _____**269**

VITA _____ *283*

LIST OF TABLES

Table 2.1 Stiffness coefficients and maximum load of the intervertebral disc (White and Panjabi, 1990) 17

Table 2.2 Representative anatomic properties for ligaments (Length in mm) (White and Panjabi, 1990) 22

Table 2.3 Representative values for ranges of rotation for the occipital-atlanto-axial complex (White and Panjabi, 1990) 38

Table 2.4 The distraction biomechanical data from isolated cervical intervertebral disc units as a function of spinal level (Yoganandan et al., 1996) 43

Table 2.5 Rotation ranges for the thoracic spine (White and Panjabi, 1990) 49

Table 2.6 Rotation ranges for the lumbar spine (White and Panjabi, 1990) 52

Table 3.1 Advantages and disadvantages in spine model classification of Reeves and Cholewicki (2003) 64

Table 4.1 Cross-sectional area and original length of lumbar ligaments (Pintar et al., 1992) 121

Table 4.2 Overall mean values of stiffness 121

Table 4.3 Stiffness of intact motion segments (Gardner-Morse and Stokes, 2004) 124

Table 4.4 Stiffness and damping data for cervical intervertebral discs. 135

Table 4.5 Muscle model fibre type parameters (Van Lopik, 2004). 142

Table 4.6 Histochemical composition of muscle fibre types in the muscles of the head-neck model (Van Lopik, 2004). 144

Table 5.1 Validation of the neck muscles in the MB model 178

Table 7.1 Material properties of the disc (Lee et al., 2000) 216

Table 7.2 The material properties of the parts of the FSU 222

Table 7.3 Material Constants of Annulus and Nucleus (Wang et al., 2000) 222

Table 7.4 Material constants of annulus and nucleus using Prony series (source: Lee et al.,2000, and Wang et al., 2000) 226

Table 7.5 Material properties of the discs 228

Table A.1 The failure strength of spinal ligaments (White and Panjabi, 1990) 261

Table A.2 Quantitative anatomy of vertebrae from T1 to T12 (White and Panjabi, 1990) 262

Table A.3 Rotation ranges for the middle and lower cervical spine (White and Panjabi, 1990) 262

Table A.4 Nomenclature for a typical lumbar vertebra (Panjabi et al., 1992) 263

Table A.5 Lumbar vertebral body dimensions (Panjabi et al., 1992) 263

Table A.6 Lumbar spinal canal dimensions (Panjabi et al., 1992) 263

Table A.7 Lumbar pedicle dimesions (Panjabi et al., 1992) 264

Table A.8 Geometric and morphologic features of the lumbar muscles (Bogduk et al., 1992) 264

Table A.9 Moment arms of lumbar muscles (Bogduk et al., 1992) 265

Table A.10 Maximum moments generated by lumbar muscles (Bogduk et al., 1992) 266

List of Tables

Table A.11 Biomechanical parameters of human lumbar ligaments (Pintar et al., 1992) ____ 266

LIST OF FIGURES

Figure 2.1 The three primary planes of a standing person (Tozeren, 2000) 9

Figure 2.2 Spinal column and the regions of the spine (Tozeren, 2000) 10

Figure 2.3 The intervertebral disc (A) A photo showing the annular fibers and their orientation (B) The nucleus pulposus and the annulus laminates (C) The orientation of annular fibers (White and Panjabi, 1990) 12

Figure 2.4 Tensile strength of the intervertebral disc (A) Disc specimens (B) The results of the tension tests in the form of contour maps (White and Panjabi, 1990) 14

Figure 2.5 Disc anisotropy (A) Tensile stiffness (B) Tensile strength (White and Panjabi, 1990) 15

Figure 2.6 Disc stresses in bending (A) During flexion, extension and lateral bending one side is in compression while the opposite side is in tension (B) The distribution of the tensile and compressive stresses (White and Panjabi, 1990) 16

Figure 2.7 Intradiscal loads on the disc (A) The needle pressure transducer in the nucleus pulposus (B) Load on the disc (White and Panjabi, 1990) 18

Figure 2.8 Ligaments of the spine (White and Panjabi, 1990) 22

Figure 2.9 A typical load-displacement curve of a ligament (White and Panjabi, 1990) 23

Figure 2.10 The load-displacement curve of the ligaments (A) Force-deformation curves of spinal ligaments of the lumbar region (B) Stabilizing function of a spinal ligament (White and Panjabi, 1990) 24

Figure 2.11 Functional biomechanics of ligamentum flavum (A) In flexion/extension (B) The stress-strain curve (White and Panjabi, 1990) 25

Figure 2.12 Quantitative anatomy of a vertebra (TP = transverse process; UE = upper end-plate; LE = lower end-plate; PD = pedicle; SP = spinous process; SC = spinal canal; PI = pars interarticularis; VB = vertebral body; W = width; A = area; D = depth; H = height; I = inclination. Suffixes are: t = transverse plane; p= posterior.) (White and Panjabi, 1990) 27

Figure 2.13 Orientation of the facet joints (A) Cervical spine (B) Thoracic spine (C) Lumbar spine (White and Panjabi, 1990) 28

Figure 2.14 Vertebral compression strength at slow loading rate (White and Panjabi, 1990) 30

Figure 2.15 Illustration of vertebral coordinate systems and JCS (Wu et al., 2002) 32

Figure 2.16 Location of the common origin of axes (A) The general case (B) The specific case of Y and y being parallel (Wu et al., 2002) 32

Figure 2.17 The x, y, and z directions shown locally on the upper plate of a vertebra as used throughout the thesis 32

Figure 2.18 A horizontal cross-section through the lumbar spine showing muscles (White and Panjabi, 1990) 34

Figure 2.19 Physical properties of a muscle (A) The force developed (B) Stiffness (White and Panjabi, 1990) 35

Figure 2.20 Functional model of muscle (White and Panjabi, 1990) 35
Figure 2.21 Muscle activity during the four physiological motions (A,B) In flexion and extension, gluteus and erector spinae muscles are active (C) Lateral bending is gathered by an imbalance of muscle forces on both sides of the back (D) During axial rotation, erector spinae muscles on the ipsilateral side, the rotators and multifidi on the contralateral side, and the gluteals on both the sides were found to be active (White and Panjabi, 1990) 36
Figure 2.22 (A) Sagittal plane motion of C1 on C2 with the approximate instantaneous axis of rotation (IAR) in combined flexion/extension of 20° (B) The anterior curvature of the dens can allow some degree of additional sagittal plane motion in both rotation and translation (White and Panjabi, 1990) 38
Figure 2.23 Rotation of C1 (White and Panjabi, 1990) 40
Figure 2.24 Translatory movements of the anterior aspect of C1 with respect to C2 (White and Panjabi, 1990) 40
Figure 2.25 A schematic approximation of the relative regional cephalocaudal variations in radii of curvature of the arches defined by the cervical vertebrae as they rotate and translate in the sagittal plane (White and Panjabi, 1990) 42
Figure 2.26 The overall rotational movements of the cervical spine vs. time (DeFrate et al., 1999) 44
Figure 2.27 Cross-sectional areas of the ligaments (Yoganandan et al., 1999) 44
Figure 2.28 Lengths of the ligaments (Yoganandan et al., 1999) 45
Figure 2.29 Stiffness of the ligaments (Yoganandan et al., 1999) 45
Figure 2.30 Failure energy of the ligaments (Yoganandan et al., 1999) 45
Figure 2.31 Failure stress of the ligaments (Yoganandan et al., 1999) 46
Figure 2.32 Force-deformation properties of the PLL (Yoganandan et al., 1999) 46
Figure 2.33 Failure strain of the ligaments (Yoganandan et al., 1999) 46
Figure 2.34 Force-deformation properties of the JC (Yoganandan et al., 1999) 47
Figure 2.35 Force-deformation properties of the ALL (Yoganandan et al., 1999) 47
Figure 2.36 Force-deformation properties of the LF (Yoganandan et al., 1999) 47
Figure 2.37 A schematic representation of the relative variations in the radii of curvature of the arches of the thoracic vertebrae (A) Flexion/extension (B) Lateral bending (White and Panjabi, 1990) 49
Figure 2.38 Coupling of lateral bending and axial rotation (White and Panjabi, 1990) 50
Figure 2.39 The approximate locations for IAR in the thoracic spine (White and Panjabi, 1990) 51
Figure 2.40 Values for rotational ranges of motion for different ranges of the spine (White and Panjabi, 1990) 52
Figure 2.41 Linear dimensions of vertebral body as functions of vertebral levels L1-L5. The linear dimensions are the upper (u) and lower (l) end-plates width (EPW) and depth (EPD), anterior (a) and posterior (p) vertebral body height (VBH) (Tan et al., 2001) 53

Figure 2.42 Linear dimensions of spinal canal, spinous process and transverse process as functions of vertebral levels L1-L5. The linear dimensions are the spinal canal width (SCW) and depth (SCD), spinous process length (SPL) and transverse process width (TPW) (Tan et al., 2001) 54

Figure 2.43 Linear dimensions of pedicles as functions of vertebral levels L1-L5. The linear dimensions are the left (l) and right (r) pedicle height (PDH) and width (PDW) (Tan et al., 2001) 54

Figure 2.44 Areas of end-plates, spinal canal and pedicles as functions of vertebral levels L1-L5. The areas are the upper (u) and lower (l) end-plates (EPA), spinal canal (SCA), left (l) and right (r) pedicle (PDA) (Tan et al., 2001) 55

Figure 2.45 Angular dimensions of end-plates and pedicles as functions of vertebral levels L1-L5. The angles are the upper (u) and lower (l) end-plates, transverse inclinations (EPI), and left (l) and right (r) pedicles, sagittal and transverse inclinations (PDI) (Tan et al., 2001) 55

Figure 2.46 Comparison of selected linear dimensions of present study with that of Panjabi (1982). The results from the latter are represented by C. The linear dimensions are the spinal canal width (SCW) and depth (SCD) and left (l) and right (r) pedicle width (PDW) (Tan et al., 2001) 56

Figure 2.47 Representative kinematics of the sacrum (A) 3mm anterior translation (B) Representative z-axis rotation of a total 3° (C) Representative y-axis rotation of 12°, totally (White and Panjabi, 1990) 58

Figure 3.1 Spine model of Borelli (1989) 62

Figure 3.2 Continuum beam model of the spine (Lindbeck, 1987) 66

Figure 3.3 Simple cantilever beam model of spine (Noone et al., 1991) 67

Figure 3.4 Schematic representation of the planar spinal model (Crisco III and Panjabi, 1992) 68

Figure 3.5 Loading system of the spine model (Case et al., 1999) 69

Figure 3.6 Lateral and anteroposterior views of a normal spine (Adler et al., 2002) 70

Figure 3.7 A flexed posture of the mathematical model (Acar and Grilli, 2002) 71

Figure 3.8 Cervical spine with rigid body representation (Williams and Belytschko, 1983) 72

Figure 3.9 Muscle and ligament elements in the model (Williams and Belytschko, 1983) 73

Figure 3.10 The simplified thoracolumbar model and its connection to the cervical model (Williams and Belytschko, 1983) 73

Figure 3.11 Responses of the head-neck model in frontal impact (-G_x impact acceleration) (a) with passive muscles, (b) with stretch reflex response (Williams and Belytschko, 1983) 74

Figure 3.12 Responses of the head-neck model in lateral impact (+G_y impact acceleration) (a) with passive muscles, (b) with stretch reflex response (Williams and Belytschko, 1983) 74

Figure 3.13 Multi-body model of Merrill, Goldsmith and Deng (1987) 75

Figure 3.14 Multi-body model of de Jager (1996) 76

Figure 3.15 Multi-body model of van der Horst (1997, 2002) 76

Figure 3.16 Isometric view of the cervical spine with all neck musculature (Van Lopik and Acar, 2002) 77

Figure 3.17 Multi-body model of the head and neck (van Lopik and Acar, 2004) 78

Figure 3.18 Model response to 15g frontal impact for 200 ms with 100% active musculature (van Lopik and Acar, 2004) 79

Figure 3.19 Model response to 7g lateral impact for 200 ms with 100% active musculature (van Lopik and Acar, 2004) 79

Figure 3.20 Human model with 19 body segments, 5 of which are lumbar vertebrae and discs (Jager and Luttmann, 1989) 81

Figure 3.21 Modeling components (Broman et al., 1996) 81

Figure 3.22 Anatomical diagram (A) of the lumbar spine and torso, and (B) the physical model (Cholewicki et al., 1999) 82

Figure 3.23 The spine model, where; X represents vertebral body, ▼ represents articular facet, ► represents transverse process, and ◄ represents spinous process locations (Schultz and Galante, 1970). 83

Figure 3.24 Geometric model of the human torso (Belytschko et al., 1973) 84

Figure 3.25 Several views from de Zee et al. (2003) model 85

Figure 3.26 Biomechanical multi-body model of Silva and Ambrosio (2004) 86

Figure 3.27 Biomechanical spine model of Ishikawa et al. (2005) 86

Figure 3.28 Discs and ligaments in the model (Ishikawa et al., 2005) 87

Figure 3.29 FE cervical spine model of Kleinberger (1993) 89

Figure 3.30 FE cervical spine model of Dauvilliers et al. (1994) 90

Figure 3.31 FE cervical spine model of Camacho et al. (1997) and Van Ee et al. (2000) 91

Figure 3.32 FE cervical spine model of Yang et al. (1998) 92

Figure 3.33 FE cervical spine model of Halidin et al. (2000) 92

Figure 3.34 C4-C6 cervical spine FE model of Kumaresan et al. (1997) 94

Figure 3.35 C4-C6 cervical spine FE model of Teo and Ng (2001) 95

Figure 3.36 Cut through the element mesh of the finite element model of the lumbar spine (Zander et al., 2002) 97

Figure 3.37 Four frames from an animation sequence of the lumbar spine (Cooper et al., 2001) 98

Figure 3.38 Yield contours of the lumbar vertebra under compressive load at two successive points on the load-deformation curve, where red colour shows the localized yield (Overaker et al., 1999) 99

Figure 3.39 Applied pressure to L5 (Nabhani and Wake, 2002) 99

Figure 3.40 Model of human spine (a) the orientation of the 22 vertebrae (b) modelled thoracic vertebra (c) modelled lumbar vertebra (Dietrich et al., 1991) 101

Figure 3.41 FE model of the human spine of Jost and Nurick (2001) within the whole FE human body model 102

Figure 3.42 The actual and simplified representation of the vertebral body and intervertebral disc (Spilker et al., 1984) 103
Figure 3.43 Vertebral disc FE model (Lee et al., 2000) 104
Figure 3.44 A flexible body connecting two rigid bodies (Ma and Lankarani, 1997) 106
Figure 3.45 Occupant with FE spine model (Ma and Lankarani, 1997) 107
Figure 3.46 FE model of the lumbar spine (Ma and Lankarani, 1997) 108
Figure 3.47 Computational model of head and cervical spine (Camacho et al., 2001) 108
Figure 4.1 Orthogonal views of a typical lumbar vertebra (Panjabi et al., 1992) 114
Figure 4.2 A typical lumbar vertebra 115
Figure 4.3 Front view of a typical lumbar vertebra 115
Figure 4.4 An oblique view of a typical lumbar vertebra 115
Figure 4.5 An isometric view of the lumbar spine 116
Figure 4.6 Frontal view of the lumbar spine 116
Figure 4.7 An isometric rear view of the lumbar spine 117
Figure 4.8 The orientation of the lumbar vertebrae in sagittal plane 117
Figure 4.9 The multibody model of the lumbar spine 118
Figure 4.10 Tracings of the posteroanterior and lateral radiographs showing the attachment sites of the lumbar muscles (Bogduk et al., 1992) 119
Figure 4.11 Muscles in the model 120
Figure 4.12 Ligaments and bushing constraint as intervertebral disc 121
Figure 4.13 Average biomechanical force-deformation curves for ALL, PLL and JC (Pintar et al., 1992) 122
Figure 4.14 Average biomechanical force-deformation curves for LF, ISL and SSL (Pintar et al., 1992) 123
Figure 4.15 Lumbar motion segment L4-L5 containing 2 vertebrae 125
Figure 4.16 The modified version of the lumbar spine multi-body model 126
Figure 4.17 The posture of the lumbar spine under 10 Nm flexion moment 127
Figure 4.18 The resultant global rotations at each vertebral level 127
Figure 4.19 The intersegmental rotations at each vertebra pair 128
Figure 4.20 Intradiscal pressures under 10 Nm flexion moment 128
Figure 4.21 Segments of the human skeleton, which were joined to form the solid model 129
Figure 4.22 Digitization of a full musculoskeletal system (from left to right and from top to bottom) (Van Sint Jan, 2005). 131
Figure 4.23 The solid model of the human spine used in the developed multi-body model: (a) the entire spinal column, (b) with the head, (c) with the head and the ribs, and (d) with the head, the ribs, the clavicles, the scapulas, and the iliacs. 132
Figure 4.24 The intervertebral disc in the multi-body model 133
Figure 4.25 Ligaments and the disc in the multi-body model 136

Figure 4.26 Average dimensionless force-strain curve used to determine the force-deflection curves for the missing ligament properties ____ 137
Figure 4.27 The order of muscle control (Cheng et al., 2001) ____ 139
Figure 4.28 Schematic of basic muscle model elements. The muscle fascicles are represented by the contractile element (CE) in parallel with the passive elastic element (PE). The series elastic element (SE) represents the combined tendon and aponeurosis. The inertial mass of the muscle is also applied in series to the fascicles. PE1 is a non-linear spring that resists stretch in the passive muscle, while PE2 is non-linear spring resisting compression during active contraction at short lengths. (Cheng et al., 2001) ____ 140
Figure 4.29 Schematic representation of Virtual Muscle's equations and terms. Complete descriptions of all elements shown can be found in Brown and Loeb (2000) and Brown et al. (1999). F_{Total} *- total force produced by muscle fascicles.* F_{PE} *- total passive force produced by parallel elastic element PE.* F_{CE} *- total active force produced by contractile element CE.* F_{PE1} *- passive visco-elastic properties of stretching a muscle.* F_{PE2} *- passive resistance to compression of the thick filaments at short muscle lengths. FL- tetanic Force-Length relationship. FV- tetanic Force-Velocity relationship. Af- isometric, activation-frequency relationship.* F_{eff} *- time lag between changes in firing frequency and internal activation (i.e. rise and fall times).* L_{eff} *- time lag between changes in length and the effect of length on the Af relationship. S represents the effects of 'sag' on the activation during a constant stimulas frequency. Y represents the effects of yielding (on activation) following movement during sub-maximal activation.* ____ 141
Figure 4.30 Virtual Muscle "BuildMuscles" interface (Cheng et al., 2001) ____ 145
Figure 4.31 Simulink model for scalenus medius muscle group. The switch is used to change the level of activation following a specified onset delay. ____ 146
Figure 4.32 The longus capitis (Warfel, 1985) ____ 147
Figure 4.33 The longus capitis, colli, and scalenus muscles in the MB model ____ 148
Figure 4.34 The longus colli (Warfel, 1985) ____ 149
Figure 4.35 The scalenus (a) anterior, (b) medius, and (c) posterior (Warfel, 1985) ____ 150
Figure 4.36 The sternocleidomastoid (Warfel, 1985) ____ 151
Figure 4.37 The sternocleidomastoid and other cervical muscles in the MB model ____ 151
Figure 4.38 Levator Scapulae along with some other neck muscles (Gray, 1980) ____ 152
Figure 4.39 Longissimus Capitis, Cervicis, Thoracis (Warfel, 1985) ____ 153
Figure 4.40 Multifidus (Warfel, 1985) ____ 155
Figure 4.41 Multifidus and semispinalis muscles in the MB model ____ 155
Figure 4.42 Semispinalis Capitis, Cervicis, Thoracis (Warfel, 1985) ____ 156
Figure 4.43 Splenius muscle (Warfel, 1985) ____ 158
Figure 4.44 Splenius and trapezius muscles in the MB model ____ 159
Figure 4.45 Rotatores (Warfel, 1985) ____ 161
Figure 4.46 Back muscles in the MB model ____ 162
Figure 4.47 Iliocostalis muscles (Warfel, 1985) ____ 163

Figure 4.48 Spinalis Thoracis (Warfel, 1985) _____ *164*

Figure 4.49 Abdominal muscles in the MB model _____ *165*

Figure 4.50 The developed MB model of the whole human spine _____ *166*

Figure 4.51 Three views of the MB model _____ *167*

Figure 5.1 Displacements of model motion segments C0-C1 in response to applied rotational loads of 1.5Nm against the experimental results (average ±1 SD) of Panjabi et al. (1988). Resulting displacements are shown along the vertical axis; translations on the left, rotations on the right. Anterior shear (+AS), posterior shear (-AS), left lateral shear (+LLS), right lateral shear (-LLS), tension (+TNS), compression (-TNS), right lateral bending (+RLB), left lateral bending (-RLB), flexion (+FLX), extension (-FLX), left axial rotation (+LAR) and right axial rotation (-LAR). _____ *173*

Figure 5.2 Displacements of model motion segments C1-C2 in response to applied rotational loads of 1.5Nm against the experimental results (average ±1 SD) of Panjabi et al. (1988). Resulting displacements are shown along the vertical axis; translations on the left, rotations on the right. Anterior shear (+AS), posterior shear (-AS), left lateral shear (+LLS), right lateral shear (-LLS), tension (+TNS), compression (-TNS), right lateral bending (+RLB), left lateral bending (-RLB), flexion (+FLX), extension (-FLX), left axial rotation (+LAR) and right axial rotation (-LAR). _____ *174*

Figure 5.3 Displacements of model motion segments C3-C4 in response to applied rotational load of 1.8 Nm shown against the experimental results of Moroney et al. (1988). Resulting displacements are shown along the vertical axis, translations on the left, rotations on the right. Anterior shear (+AS), posterior shear (-AS), left lateral shear (+LLS), right lateral shear (-LLS), tension (+TNS), compression (-TNS), right lateral bending (+RLB), left lateral bending (-RLB), flexion (+FLX), extension (-FLX), left axial rotation (+LAR) and right axial rotation (-LAR). *175*

Figure 5.4 Displacements of model motion segments C5-C6 in response to applied rotational load of 1.8 Nm shown against the experimental results of Moroney et al. (1988). Resulting displacements are shown along the vertical axis, translations on the left, rotations on the right. Anterior shear (+AS), posterior shear (-AS), left lateral shear (+LLS), right lateral shear (-LLS), tension (+TNS), compression (-TNS), right lateral bending (+RLB), left lateral bending (-RLB), flexion (+FLX), extension (-FLX), left axial rotation (+LAR) and right axial rotation (-LAR). *176*

Figure 5.5 Displacements of model motion segments C3-C4 (□) and C5-C6 (○) in response to applied translational loads of 20 N shown against the experimental results of Moroney et al. (1988). Anterior shear (+AS), posterior shear (-AS), left lateral shear (+LLS), right lateral shear (-LLS), tension (+TNS), compression (-TNS), right lateral bending (+RLB), left lateral bending (-RLB), flexion (+FLX), extension (-FLX), left axial rotation (+LAR) and right axial rotation (-LAR). _____ *177*

Figure 5.6 Average T1 acceleration and rotation used as input to the MB model to simulate frontal impact. (Acceleration in x-axis, rotation about y-axis) _____ *180*

Figure 5.7 Frontal impact simulation (all constraints, elements, and some parts of the model are hidden for better visualization) 181
Figure 5.8 Head and neck images for 0, 100, 170, and 200 ms, with all elements visible 181
Figure 5.9 Head centre of gravity resultant linear acceleration vs. time 182
Figure 5.10 Head centre of gravity angular acceleration vs. time 182
Figure 5.11 Head occiput and head centre of gravity trajectories in the horizontal (X) and vertical (Z) planes (OC lower, CG upper graph) 183
Figure 5.12 Head rotation vs. time 183
Figure 5.13 Neck rotation vs. time 184
Figure 5.14 Neck link length vs. time 184
Figure 5.15 Head Lag vs. time 185
Figure 5.16 Model inputs for lateral impact 186
Figure 5.17 Lateral impact simulation 187
Figure 5.18 x linear acceleration of head centre of gravity vs. time 187
Figure 5.19 y linear acceleration of head centre of gravity vs. time 188
Figure 5.20 z linear acceleration of head centre of gravity vs. time 188
Figure 5.21 x angular acceleration of head centre of gravity vs. time 189
Figure 5.22 z angular acceleration of head centre of gravity vs. time 189
Figure 5.23 Head rotation about x axis 190
Figure 5.24 Head rotation about z axis 190
Figure 5.25 Head occiput and head centre of gravity trajectories in the horizontal (Y) and vertical (Z) planes (OC lower, CG upper graph) 191
Figure 5.26 Two-pivot linkage model (Ziejewski et al., 1998) 192
Figure 5.27 Linear head acceleration at mouthpiece in z direction 193
Figure 5.28 Linear head acceleration at mouthpiece in x direction 193
Figure 5.29 Angular head acceleration about y axis 194
Figure 5.30 The JARI sled test (Ono et al., 1999) 195
Figure 5.31 Test and model instants for JARI sled test 195
Figure 5.32 Rotational angles of the MB model prediction (in red) compared with the experimental values for T1-T3. 196
Figure 5.33 Rotational angles of the MB model prediction (in red) compared with the experimental values for T4-T6. 196
Figure 5.34 Rotational angles of the MB model prediction (in red) compared with the experimental values for T7-T9. 197
Figure 5.35 Rotational angles of the MB model prediction (in red) compared with the experimental values for T10-T12. 197
Figure 5.36 Rotational angles of the MB model prediction (in red) compared with the experimental values for L1-L3. 198

Figure 5.37 Rotational angles of the MB model prediction (in red) compared with the experimental values for L4-S1. 198
Figure 6.1 Schematic views of S-shaped whiplash injury mechanism in a rear-end impact (S-shaped cervical spine in the middle figure) (Yoganandan et al., 2000) 201
Figure 6.2 Experimental set-up (Grauer et al., 1997) 203
Figure 6.3 T1 acceleration profiles used as input to the cervical spine model 204
Figure 6.4 Response of the model to 8.5g whiplash acceleration for 0, 60, 120 ms (respectively, from left to right). Muscles were deactivated completely. 204
Figure 6.5 Model head translations and rotations for 8.5 g case compared to experimental values (which are shaded with similar colour) 205
Figure 6.6 Intervertebral rotations at 8.5g impact 206
Figure 6.7 Model head translations and rotations for 6.5 g case 207
Figure 6.8 Model head translations and rotations for 4.5 g case 207
Figure 6.9 Model head translations and rotations for 2.5 g case 208
Figure 6.10 Maximum intervertebral angles achieved for C0-C1 208
Figure 6.11 Maximum intervertebral angles achieved for C1-C2 209
Figure 6.12 Maximum intervertebral angles achieved for C2-C3 209
Figure 6.13 Maximum intervertebral angles achieved for C3-C4 209
Figure 6.14 Maximum intervertebral angles achieved for C4-C5 210
Figure 6.15 Maximum intervertebral angles achieved for C5-C6 210
Figure 6.16 Maximum intervertebral angles achieved for C6-C7 210
Figure 6.17 Maximum intervertebral angles achieved for C7-T1 211
Figure 6.18 Alar ligament forces for 8.5 g impact 211
Figure 6.19 Apical ligament forces for 8.5 g impact 212
Figure 6.20 Transverse ligament forces for 8.5 g impact 212
Figure 6.21 Intervertebral disc forces for 8.5 g impact at C5-C6 level 213
Figure 7.1 The shape of the impulsive force (Lee et al., 2000) 217
Figure 7.2 The FE model 217
Figure 7.3 The boundary conditions 218
Figure 7.4 The whole FE model of the FSU 219
Figure 7.5 The equivalent von Mises stress distributions of the disc under a compressive impact load of 3000 N for a duration of t=5 ms 219
Figure 7.6 The improved model of L2-L3 disc segment 220
Figure 7.7 The disc, composed of nucleus and annulus 221
Figure 7.8 The ligaments as links 221
Figure 7.9 The force boundary conditions for the FE model 223
Figure 7.10 Maximum equivalent von Mises stresses 223
Figure 7.11 Maximum intradiscal pressure 224

Figure 7.12 (a) Disc before loading, (b) the maximum equivalent von Mises stress distribution at t=0.010 s under 10 Nm moment, and (c) the maximum equivalent von Mises stress distribution at t=0.010 s under 2000 N compressive force. 224

Figure 7.13 The FE model of L2-L3 motion segment 225

Figure 7.14 The equivalent von Mises stress distributions within the disc under (a) the compressive load of 2000 N, and (b) the the combined loading of 15 Nm flexion moment and 1000 N compressive force. 227

Figure 7.15 The FE model of the discs 228

Figure 7.16 Validation of the FE disc 229

Figure 7.17 Intervertebral disc loadings: (a) frontal impact, and (b) rear-end impact (van Lopik, 2004) 230

Figure 7.18 FE results: (a) Max. von Mises stresses in the annulus for frontal impact with multi-body head and neck response illustration, and (b) max. von Mises stresses in the annulus for rear-end impact with multi-body head and neck response illustration 231

Figure 7.19 Von Mises stress distribution of C56 disc at 200 ms for frontal impact 231

LIST OF SYMBOLS & ABBREVIATIONS

b_i : Damping coefficient
F_i : Force relative to the i-axis of the lower vertebrae
M_i : Moment relative to the i-axis of the lower vertebrae
θ_i : Relative rotation between the vertebrae
t_i : Relative translation between the vertebrae
v_i : Relative translational velocity of the disc centre
ω_i : Rotational velocity of the disc centre
k_i : Stiffness
A : Area
Af : Activation-Frequency Relationship
ALL : Anterior Longitudinal Ligament
CAD : Computer Aided Design
CE : Contractile Element
CL : Capsular Ligament
CT : Computerised Tomography
D : Depth
DoF : Degrees of Freedom
F_0 : Peak isometric active muscle force
$f_{0.5}$: Frequency at which half of maximal tetanic force is obtained
F_{CE} : Force created by CE
FE : Finite Element
FES : Functional Electrical Stimulation
FL : Titanic Force-Length Relationship
F_{PE} : Force created by PE
FSU : Functional Spine Unit
FV : Titanic Force-Velocity Relationship
H : Height
I : Inclination
IAR : Instantaneous Axis of Rotation
ISL : Interspinous Ligament
JC : Joint Capsules
L_0 : Muscle fibre length at peak isometric active muscle force (F_0)
L_0^T : Length of muscle tendon at maximal tetanic isometric force
LE : Lower End-Plate
LF : Ligamentum Flavum
L_{max} : Length of the fascicles at the maximal anatomical length of the muscle
LSM : Link-Segment Model
L_S^T : Tendon slack length
MB : Multi-Body
PCSA : Physiological Cross-Sectional Area

PD : Pedicle
PDH : Pedicle Cross-Section Height
PDIs : Pedicle Axis Inclination to the Sagittal Plane
PDIt : Pedicle Axis Inclination to the Transverse Plane
PDW : Pedicle Cross-Section Width
PE : Parallel Element
PI : Pars Interarticularis
PLL : Posterior Longitudinal Ligament
SC : Spinal Canal
SE : Series Element
SP : Spinous Process
SSI : Supraspinous Ligament
TP : Transverse Process
UE : Upper End-Plate
$V_{0.5}$: Shortening velocity required to produce half the maximum tetanic force
VB : Vertebral Body
W : Width
Δt : Impact Duration

CHAPTER 1

Introduction

The human spine is a mechanical structure, consisting of vertebrae, facets and discs, ligaments and muscles. As a mechanical system, the vertebrae can be regarded as levers while facets and discs behave like pivots. In this system, ligaments and muscles can be considered as passive restraints and actuators, respectively.

Biomechanics of the human spine and the problems related to it are a hot topic amongst researchers all over the world. Computational techniques are widely used to model, simulate and analyse the behaviour of the spinal segments in the human spine, which are by no means possible with *in vitro* and *in vivo* experimental studies. Computational models are highly important in reconstructing impact situations such as car crashes, where only a small range of experiments can be conducted with human volunteers. Clinical investigations also demand a higher level of support from computational modelling in order to aid in many applications such as fixture and fixation implementations, and corrections of scoliosis and kyphosis.

This thesis focuses on the development of a platform of computational models to investigate the kinetics and the kinematics of the whole human spine and its components and the response of selected soft tissues under complex dynamic loading histories, such as car crashes.

1.1 Research Issues and Computational Models

Testing on human volunteers is limited to non-traumatic situations and therefore only low acceleration impacts can be investigated. Cadaver and

dummy testing, where realistic impact conditions can be simulated, does not reflect the true human response due to the lack of live anatomical structure, whereas computational modelling offers a cost effective and practical alternative to experimental methods by having the potential to provide information on simulated situations that could not otherwise be obtained. Therefore, the estimate of injury risk in a wide variety of tasks is only possible through biomechanical modelling.

Various models were developed to investigate the aforementioned situations such as automobile impacts, recreational activity, industrial work, and clinical applications. The group of analytical, geometric, 2 pivot, and continuum models, which are often referred to as mathematical models, possess significant differences from biomechanical models such as multi-body (MB) or finite element (FE) models. When compared to biomechanical models, mathematical models seem to arouse less interest, mainly due to a belief that they cannot provide a relevant and satisfactory description of the spine because of their simplicity. These models are usually used for the evaluation of static loadings and ergonomics of work situations and are generally incapable of handling complex dynamic loading scenarios.

Multi-body/discrete parameter and FE models have the ability to simulate the global and local kinematics and kinetics of the human spine. A multi-body system is a collection of rigid bodies connected through kinematic joints as well as elements applying forces, whereas an FE system is capable of producing highly detailed models of bodies and systems by dividing the entities into a number of smaller elements, connecting those via nodes, and producing the realistic material behaviour by employing governing FE equations. The quality of FE models depends on many factors such as the number and type of elements, the structure of the mesh, geometric and contact properties, material property description, initial and boundary conditions, and various theoretical FE analysis options. Multi-body dynamics models have advantages such as less complexity, less demand on computational power, and relatively simpler validation requirements when compared to FE models. MB and FE models, and a combination of these two, hybrid MB-FE models are highly suitable for the simulation and analysis of dynamic situations such as automobile impacts.

Hybrid MB-FE models have the potential to offer an even better solution to dynamic problems, utilising the strengths of both techniques. Many MB, FE and hybrid MB+FE studies conducted regarding dynamic loading conditions are presented in *Computational Models of the Human Spine* Chapter in detail.

As an automobile impact injury, Whiplash or Whiplash Associated Disorders (WAD) is a very common problem of the cervical spine, occurring usually as a result of low speed, rear-end car crashes, in which the sudden differential movement between the head and torso results in abnormal motions in the neck causing damage to its soft tissue components. The injury mechanism of whiplash is insufficiently understood. Recent research has focused on the possibility of internal nerve damage to the spinal canal due to the rapid acceleration of the body with respect to the head, while intersegmental hyperextension, tearing of ligaments and muscles, lesions to discs, and facet joint injuries are also considered to be possible reasons for whiplash.

Whiplash not only leaves some patients with severe residual disability that may interfere with their ability to do their job and quality of life, but also burdens the economy with a huge cost. It has been estimated that 80% of personal injury claims made against British Insurers are related to whiplash, costing well over £1 billion every year and steadily rising (THATCHAM, 2001). In US, neck injuries cost at least $7 billion in U.S. insurance claims per year (IIHS, 2004). Similarly in Japan, neck injury accounted for an annual loss of 192.8 MYen in 2001 (Hasegawa and Shiomi, 2003). The costs in the early nineties have been estimated to be 700 MEuro in Germany, 210 MEuro in Sweden and 300 MEuro in Netherlands (van der Horst, 2002). These data do not include the lost working days due to injuries and their socioeconomic costs. In this thesis, whiplash injury is also investigated as a case study through the developed biomechanical models.

Biomechanical research is an ongoing process in the field of impact analysis in order to attempt and determine the mechanisms of injury and ultimately to improve vehicle safety. The main focus of this thesis is to provide a contribution to knowledge in this area by developing advanced MB and FE models, combining and utilising them in the form of a novel versatile platform and

investigating the effects of the dynamic impact loading conditions on the human spine as in whiplash injury. The developed MB model of the whole human spine offers a highly detailed anatomical structure combined with an advanced muscle model, possessing both passive and active behaviour, and highly realistic material properties such as non-linear viscoelasticity, whereas other existing models cannot.

1.2 Aim of the Thesis

The aim of this research is to develop a powerful, cost-effective and versatile platform to investigate the kinetics and the kinematics of the whole human spine and its components and the response of the intervertebral discs under complex dynamic loading histories occurring during impact situations. The platform combines a multi-body model of the whole human spine and FE models of the discs via a proposed novel approach. The rationale that motivated this research is that a fully validated detailed computational model of the whole human spine and the FE models of the spinal segments can help investigate and explain the injury mechanisms under impact conditions such as automobile crashes. A well-known example to be investigated is 'whiplash' injury in rear-end impacts. The combined platform is aimed to constitute a powerful tool in order to increase our understanding of the impact injuries by delving into the loads and deformations of the soft-tissue components as well as the critical loadings on the bony parts. The main novelty of the thesis and its contribution to knowledge are intended to be the multi-body model of the whole human spine itself.

1.3 Objectives of the Thesis

One of the main objectives of this thesis is to develop and validate a *biofidelic* multi-body model of the whole human spine. *Biofidelity* can be defined as the measure of how well a model simulates a human being. A biofidelic model is expected to respond like a human to a certain extent in terms of mechanical responses to ensure that the predictions obtained are truly representative of what would happen to a human being under similar conditions. The proposed

model is aimed to be one of the most sophisticated MB models in the literature, especially with its highly advanced material property definitions such as viscoelastic behaviour, active-passive muscles, and geometric nonlinearities. The multi-body model must be able to simulate the kinetics and the kinematics of the whole human spine as well as to predict the loads and deformations of the surrounding soft tissues.

Objectives also include the construction of several finite element models of the spinal segments, and the implementation of a proposed approach to establish a versatile platform in order to have a better understanding of injury mechanisms under impact loading conditions. This approach is thought to be another novelty for spinal biomechanics, where the predictions of the MB model as a result of these simulations such as intervertebral disc loadings will be used as loading boundary conditions for the FE models of the individual elements of the human cervical spine, such as the intervertebral discs. As it is practically almost impossible to determine what these loadings on the discs in a real life dynamic impact situation are, the validated MB model will act as a realistic source for determining these loadings on each and every one of the spinal elements, such as intervertebral discs, ligaments, or muscles.

This approach should help not only to visualise the global and local kinematics and kinetics of the human spine via the MB model, but also to avoid modelling, validation and computational power complications of a possible complicated FE model of the whole human spine.

Validation, which verifies the biofidelity of the developed models, is an important part of the objectives of this research, involving comparisons of the models' predictions against available experimental data. Multi-body model is aimed to be validated utilising motion segment responses in the cervical spine, model responses in the cervical spine for frontal and lateral impacts, vertical loading for cervical spine, and model responses of thoracic and lumbar regions in rear-end impact. Similarly, FE models are aimed to be checked against various experimental results.

1.4 Scope of the Thesis

The scope of the thesis is to construct and validate a *biofidelic* multi-body model of the whole human spine as well as finite element models of the spinal segments in order to investigate impact situations via a novel approach, which utilises the predictions of the MB model as loading boundary conditions for the FE models. The MB model development includes the preliminary MB model of the lumbar spine and the final whole human spine model. The FE modelling contains various models of the lumbar and cervical discs, disc segments, and functional spine units.

1.5 Outline of the Thesis

In Chapter 2, biomechanics of the human spine is explained in detail in order to reflect the background of all the modelling studies conducted. This chapter covers an introduction to the biomechanically essential parts of the human spine, namely; intervertebral disc, ligaments, muscles, and vertebrae. Following the subsections regarding the components, biomechanics of the segments of the human spine are presented in order to establish a background on the kinetics and kinematics of the human spine regions.

Chapter 3 discusses and attempts to comprehend the classifications of the computational human spine models and the reasoning behind the need for those. The assessment of all types of models constituted the initial steps of this study and not only leads to developing hybrid approaches for the previously addressed dynamic loading conditions the human spine is subjected to, but also forms the basis for the methodologies employed in developing the models. Hence, this chapter includes a comprehensive review of the classifications of human spine models as well as a broad literature survey on numerous prominent models developed. The final classification approach used in this thesis serves for understanding the mainstream of spinal modelling and helps to demonstrate the rapid developments and improvements within each methodology.

In Chapter 4, multi-body model development is described in detail. Two multi-body models are explained: first one is a preliminary multi-body model of the lumbar spine, which aimed to establish the principles to extend the model to a whole human spine MB model; second one is the final whole human spine MB model.

In Chapter 5, validation studies regarding the multi-body model of the whole human spine are presented. The validation is carried out against the results of several experimental studies; static, quasi-static or dynamic, and particularly for the cervical spine region. Validation attempts for the thoracic and lumbar regions are also included.

In Chapter 6, the MB model is used to simulate a ligamentous cervical spine undergoing whiplash trauma. Chapter 7 covers the use of finite element method in order to investigate intervertebral discs under various loading conditions. Several FE models are developed from simpler ones to more advanced models, incorporating different modelling parameters and techniques each time. Also, the proposed approach was explained and utilised in this chapter.

Conclusions are given in Chapter 8 and suggestions for further work are presented in Chapter 9.

CHAPTER 2

Biomechanics of the Human Spine

2.1 Introduction: The Human Spine

The human spine is a mechanical structure, consisting of vertebrae, facets and discs, ligaments and muscles. As a mechanical system, the vertebrae can be regarded as levers while facets and discs behave like pivots. In this system, ligaments and muscles can be considered as passive restraints and activators, respectively. The mechanical stability of the spine is mostly provided by the highly developed, dynamic neuromuscular system. The ligaments are the other elements to contribute the spinal stability. The spine structure protects the spinal cord, which resides at the centre of the system (White and Panjabi, 1990).

Spatial positions of several parts of the human body can be described referring to a Cartesian coordinate system that is located at the centre of gravity of the human body in the standing configuration (Fig. 2.1). The directions of the coordinate axes constitute the three primary planes of a standing person. These planes are also ascribed to spinal motions. Axes x_1 and x_3 form *the transverse plane*. It passes through the hip bone and lies at a right angle to the long axis of the body, separating it into superior and inferior parts. Any imaginary sectioning of the human body that is parallel to the (x_1, x_3) plane is called a transverse section or cross section. *The frontal plane* comprises the x_1 and x_2 axes of the coordinate system (Fig. 2.1). It is also called *the coronal plane*. *The frontal plane* divides the body into anterior and posterior sections. *The sagittal plane* is the plane made by the x_2 and x_3 axes (Fig. 2.1). *The sagittal plane* separates the body into left and right sections. It is the only plane of symmetry in the human body (Tozeren, 2000).

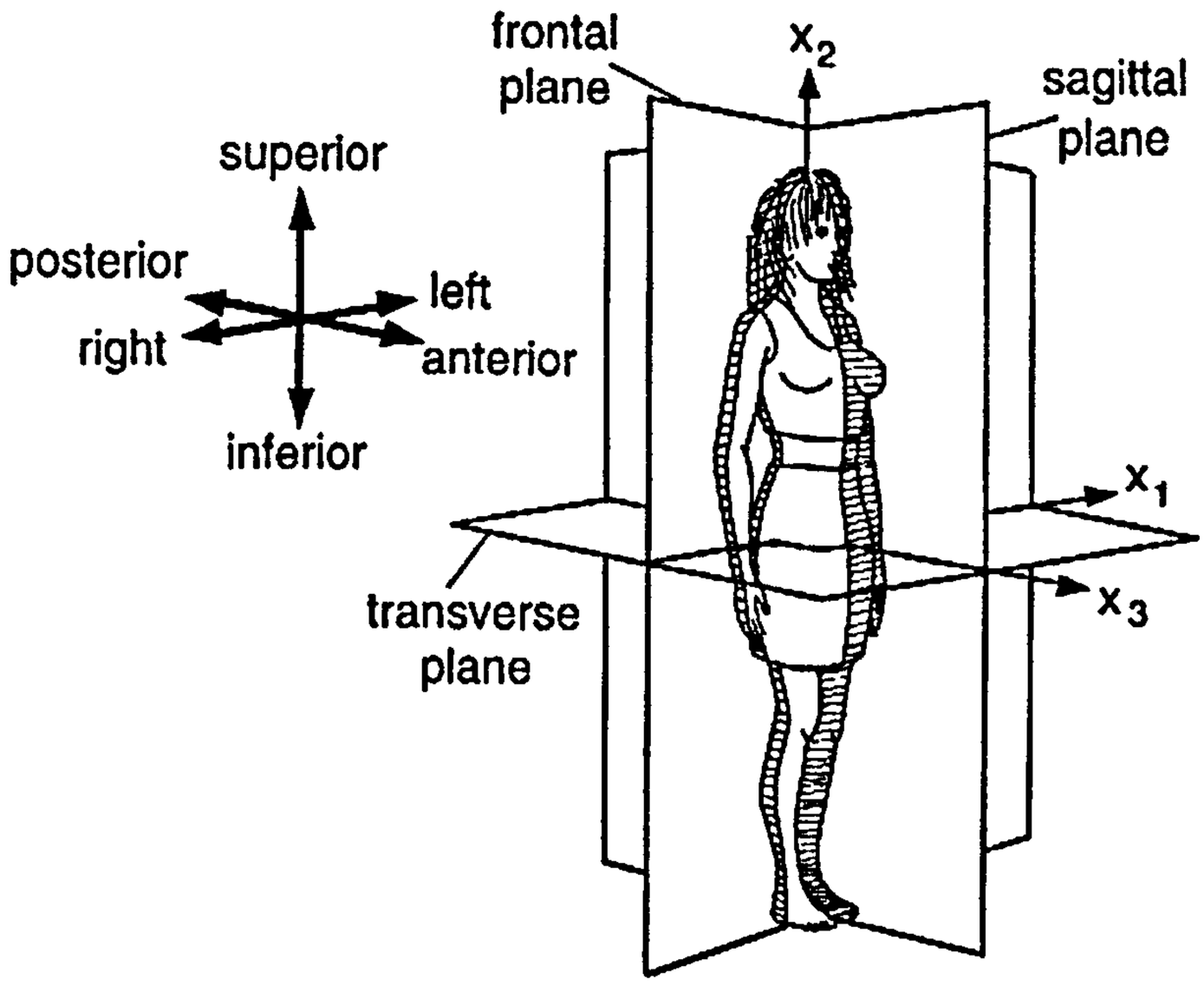

Figure 2.1 The three primary planes of a standing person (Tozeren, 2000)

The spine consists of four main segments; the cervical spine, the thoracic spine, the lumbar spine and the sacroiliac region, which embody seven cervical vertebrae, twelve thoracic vertebrae, five lumbar vertebrae, five fused sacral vertebrae, and three or four fused coccygeal segments (Fig. 2.2). As the spine is viewed in the frontal plane, it generally appears straight and symmetrical. In some individuals there may be a slight right thoracic curve, which may be due to either the position of the aorta or the increased use of the right hand. In the lateral or sagittal plane there are four normal curves, which are convex anteriorly in the cervical and lumbar regions and convex posteriorly in the thoracic and sacral regions. There is a mechanical basis for these normal anatomic curves; they provide the spinal column increased flexibility and augmented, shock-absorbing capacity, while at the same time, sustaining adequate stiffness and stability at the intervertebral joint level (White and Panjabi, 1990).

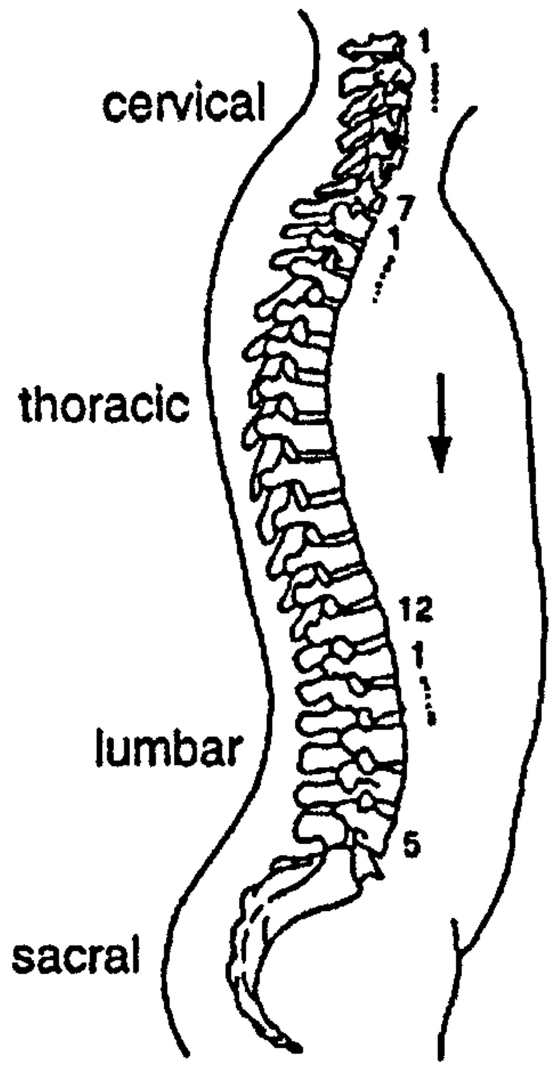

Figure 2.2 Spinal column and the regions of the spine (Tozeren, 2000)

The fundamental functions of the spine can be summarized as follows:

- The human spine transfers the weights and the resulting bending moments of the head, trunk and any weights being lifted to the pelvis.
- It allows sufficient physiologic motions between head, trunk, and pelvis.
- The most important of all, it preserves the fragile spinal cord from potentially damaging forces and motions, which are originating from both physiologic movements and trauma.

These functions are achieved through the highly specialized mechanical properties of the normal spinal anatomy (White and Panjabi, 1990).

2.2 Spine Components

In this section, the most essential parts of the human spinal column in terms of biomechanical modelling are introduced as intervertebral disc, ligaments, vertebrae, and the muscles, which all will constitute the fundamental elements considered in the developed multi-body model.

2.2.1 The Intervertebral Disc

Having many other functions, the intervertebral disc carries all of the compressive loading, to which the trunk is subjected. The intervertebral discs are mainly responsible for supporting various forces and moments acting on the spine. When a person is standing erect, the disc is subjected to much greater forces than the weight of the portion of the body above it.

The loads acting on the disc can be classified into two main categories according to the duration of application as short and long duration loads. Short duration loads are high amplitude loads such as jerk lifting while long duration loads are lower in magnitude due to more normal physical activities. This division is crucial as disc possesses time-dependent properties such as viscoelasticity.

Short-duration, high-level loads cause irreparable structural damage on the intervertebral disc when a stress value at a given point is higher than the ultimate failure stress. The mechanism of failure during long-duration, low-level, repetitive loading of relatively low magnitude is completely different and is due to fatigue failure. A tear develops at a point where the nominal stress is relatively high (but much less than the ultimate or even yield stress), and it eventually enlarges and results in complete disc failure (White and Panjabi, 1990).

The intervertebral disc is composed of three discrete parts: the *nucleus pulposus*, the *annulus fibrosus*, and the *cartilaginous end-plates*.

The nucleus pulposus is a centrally located area composed of a very loose and translucent network of fine fibrous strands that lie in a mucoprotein gel containing various mucopolysaccharides. The water content ranges from 70~90%. It is highest at birth and tends to decrease with age. The lumbar nucleus comprises 30-50% of the total disc area in cross-section. In the low back, the nucleus is usually more posterior than central and lies at about the juncture of the middle and posterior thirds of the sagittal diameter. The size of the nucleus and its capacity to swell are greater in the cervical and lumbar regions.

The annulus fibrosus is a portion of the intervertebral disc that gradually becomes differentiated from the periphery of the nucleus and constitutes the outer boundary of the disc. This structure is composed of fibrous tissue in concentric laminated bands (Fig. 2.3A, B). The fibers are arranged in a helicoid manner. They are located in about the same direction in a given band but in opposite directions in any two adjacent bands. They are oriented at 30° to the disc plane and therefore at 120° to each other in the adjacent bands (Fig. 2.3B, C). The annulus fibers are attached to the cartilaginous end-plates in the inner zone, while in the more peripheral zone they attach directly into the osseous tissue of the vertebral body and are called as *Sharpey's fibers*. This attachment to the vertebra is a much stronger than the other more central attachments, which is a useful characteristic in the clinical evaluation of spine trauma, clinical stability, and surgical constructs.

The cartilaginous end-plate is composed of hyaline cartilage that separates the other two components of the disc from the vertebral body (White and Panjabi, 1990).

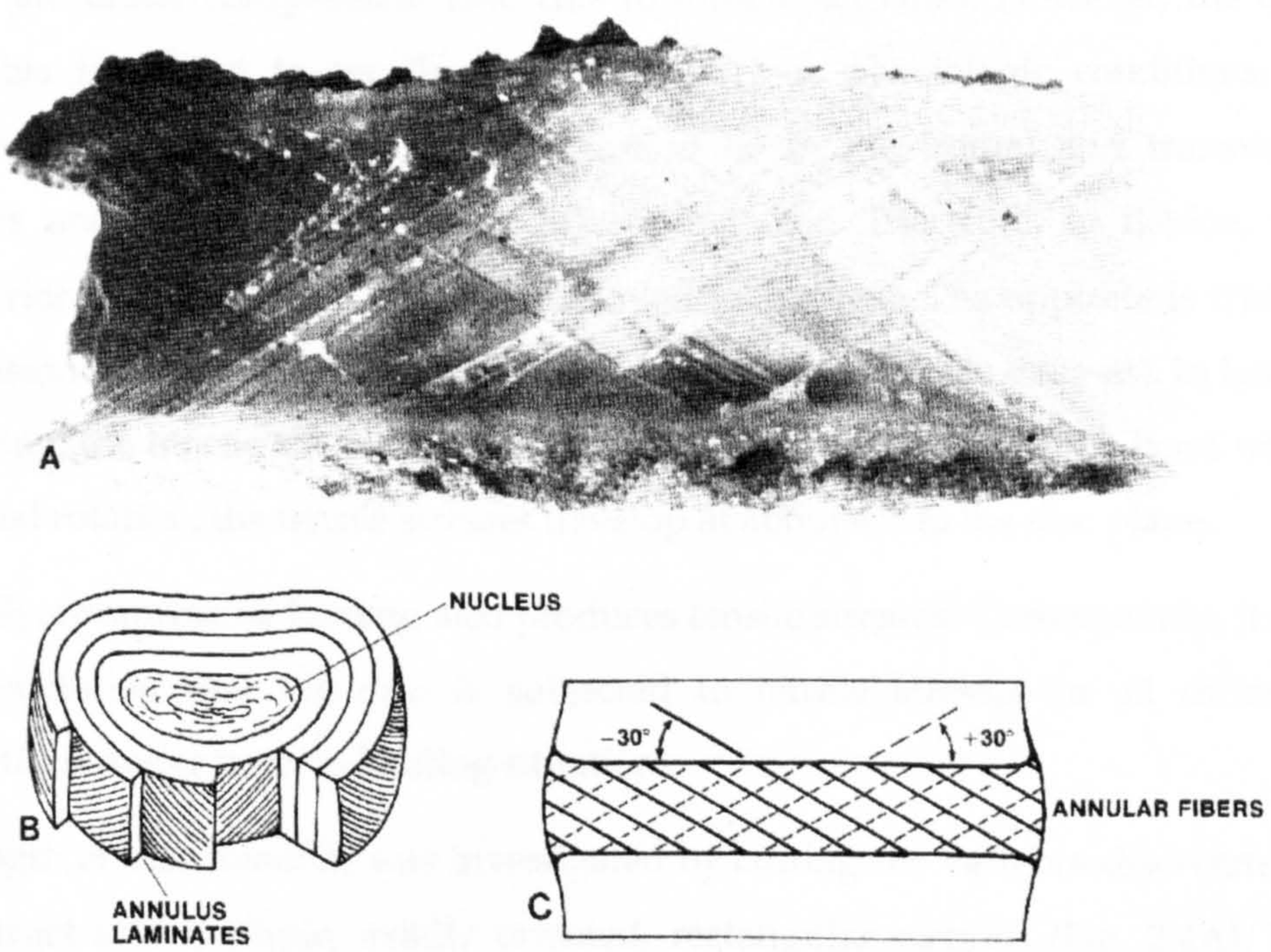

Figure 2.3 The intervertebral disc (A) A photo showing the annular fibers and their orientation (B) The nucleus pulposus and the annulus laminates (C) The orientation of annular fibers (White and Panjabi, 1990)

As the intervertebral disc is a viscoelastic structure, the mechanical tests should be carried out at relatively slow loading rates in order to minimize the viscoelastic effects. The compression test has been the most popular mechanical test for the study of the disc, probably as the disc is the major compression-carrying component of the spine. Many experiments have been done to determine the compressive properties of the disc. To compare the relative strength of the disc with that of the vertebral body in supporting compressive loads, static tests were conducted by Brown and colleagues on functional spinal units (FSUs), which are defined as pairs of adjacent vertebrae and the connecting disc and ligaments, but devoid of musculature, without posterior elements, of the lumbar region. It was found that the first component to fail in such a construct was the vertebra, because of fracture of the end-plates. No failure of the disc ever took place. The mode of failure was exclusively dependent on the condition of the vertebral body.

The intervertebral disc is hardly ever subjected to tensile loads under normal physiologic activities. Even under the application of traction to the spine, the discs are under compression load due to muscle activities. However, the disc annulus is subject to tensile stresses in various physiologic conditions. In flexion, the instantaneous axes of rotation lie in the frontal and transverse planes and pass through the middle of the disc. Therefore, in flexion, the posterior part of the disc is subjected to tensile stresses. The opposite is true in extension (i.e., the anterior part of the disc experiences tensile stresses). In lateral bending, the tensile stresses are produced on the convex side of the bend while in axial rotation; the tensile stresses develop at about 45° to the disc plane.

Finally, compressive loading also produces tensile stresses. Consequently, it can be concluded that the disc is subjected to tensile stresses in all different directions under various loading situations.

Strength of disc material was investigated by cutting the vertebra-disc-vertebra construct into multiple, axially oriented, rectangular sections (Fig. 2.4A). The specimens were stretched to failure in a tensile testing machine, and the load-displacement graphs were recorded. Failure load values were collected from various samples and combined as axial tensile strength maps of the disc. The

anterior and posterior regions of the disc are stronger than the lateral region, and the central region, consisting of the nucleus pulposus, is the weakest (Fig. 2.4B). This distribution may be "nature's attempt" to provide strength where most of the failures and herniations tend to occur (White and Panjabi, 1990).

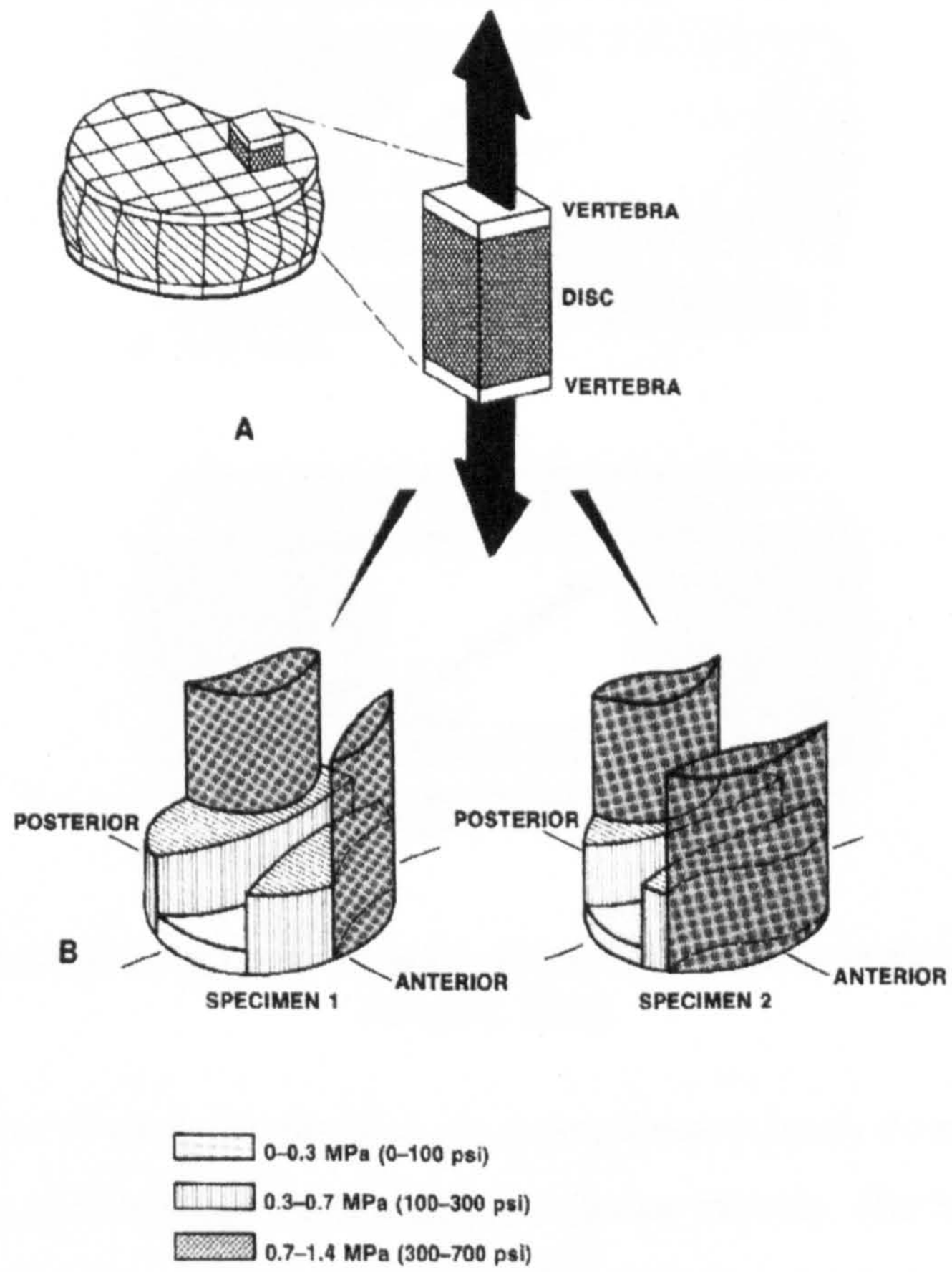

Figure 2.4 Tensile strength of the intervertebral disc (A) Disc specimens (B) The results of the tension tests in the form of contour maps (White and Panjabi, 1990)

Galante performed extensive biomechanical tests of the disc material. He cut the disc annulus into thin samples (1x2 mm) along different orientations and subjected these samples to tensile loads. His results for stiffnesses of the disc are summarized in Figure 2.5A. The stiffness was found to vary to a great extent with the orientation of the samples; the axial samples were the most flexible, while the samples taken at 15° to the horizontal plane were the stiffest. The strength results of the samples yield that the tensile strength in the fiber direction appears to be about three times stronger than the tensile strength along the horizontal direction (Figure 2.5B).

The stiffness and strength tests evidently show that the disc structure is anisotropic. It is able to support certain types of loads effectively while it can not resist the rest of the loadings in an equally efficient manner.

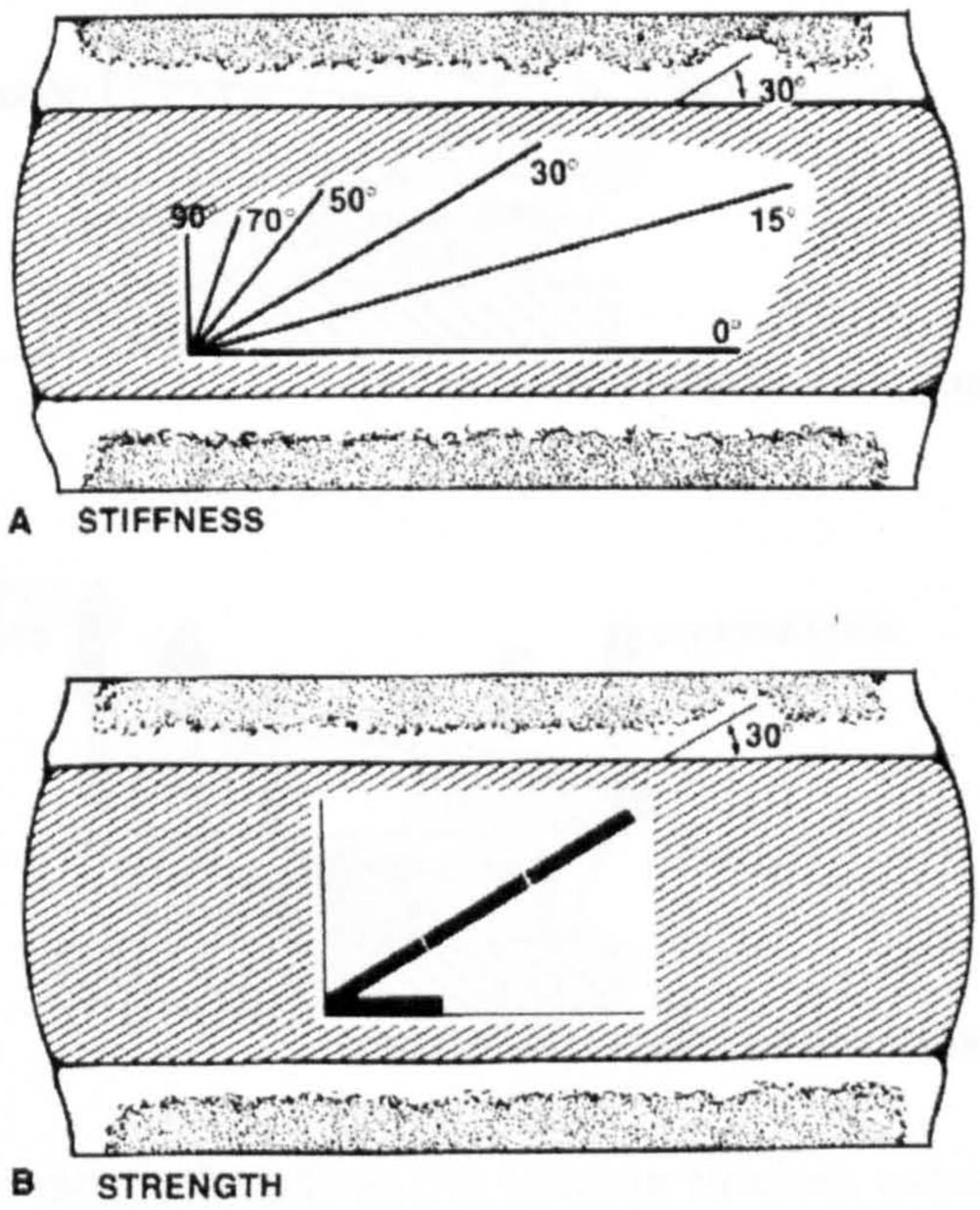

Figure 2.5 Disc anisotropy (A) Tensile stiffness (B) Tensile strength (White and Panjabi, 1990)

As experimental findings imply that pure compression loads do not damage the disc, bending and torsional loads attract particular interest. The lumbar disc did not seem to fail with a bending of 6-8° in the sagittal, frontal, and other vertical planes. However, after the posterior elements are removed, failure takes place with a bending of 15° (anterior flexion). Disc stresses in bending are illustrated in Figure 2.6. According to the studies of Farfan et al (In: White and Panjabi, 1990), the average angle at torsional failure for nondegenerated and degenerated discs was 16° and 14.5°, respectively. Generally, a large disc possessed large torsional strength. A round disc was found to be stronger than an oval disc.

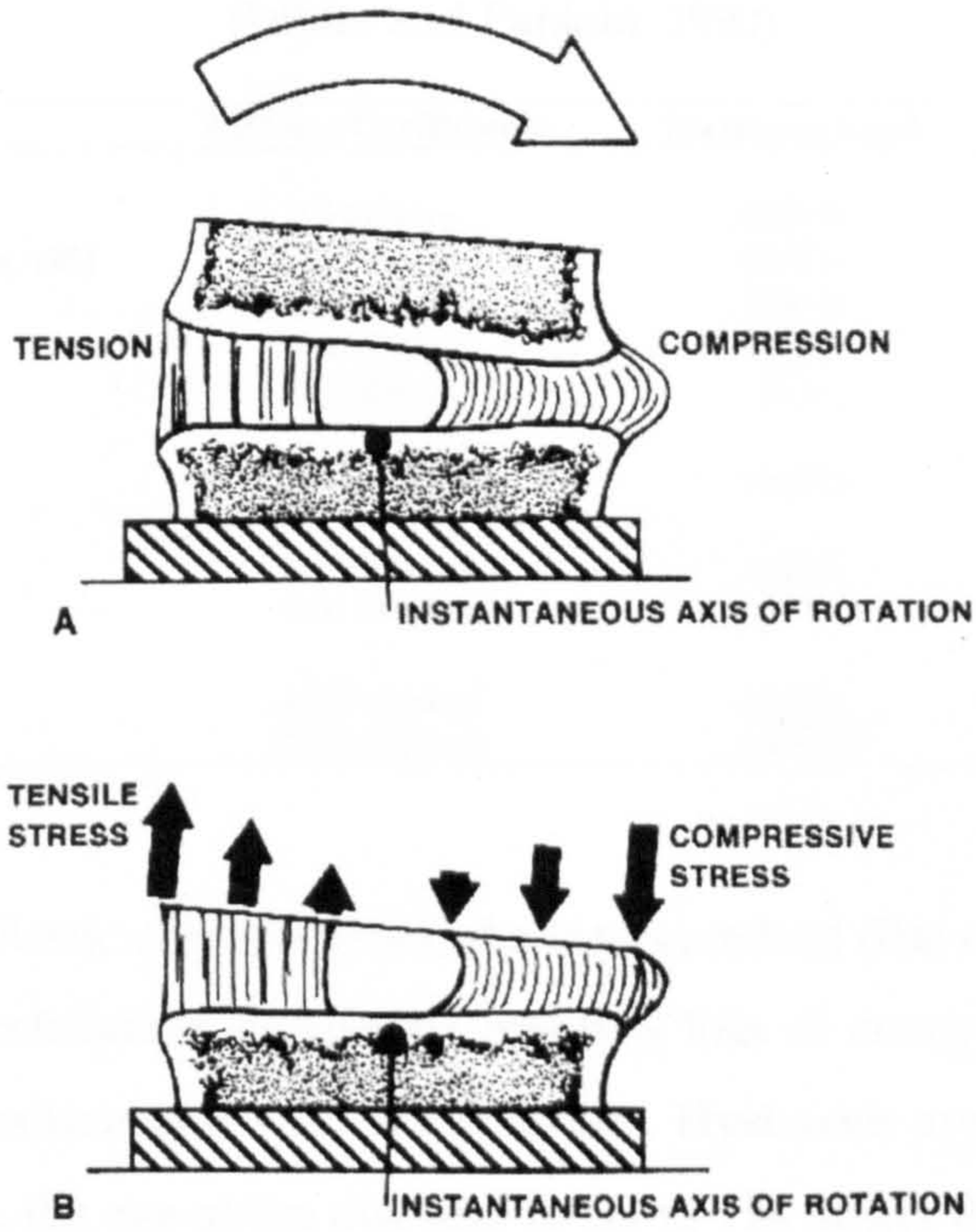

Figure 2.6 Disc stresses in bending (A) During flexion, extension and lateral bending one side is in compression while the opposite side is in tension (B) The distribution of the tensile and compressive stresses (White and Panjabi, 1990)

Although the disc is subjected to shear stresses during torsional loading, the stresses are not uniformly distributed. They are high along the periphery and low in the centre. Therefore, the torsional experiments do not provide precise information about the horizontal shear characteristics of the disc. Experiments had been conducted to investigate the lumbar disc in direct shear. The shear stiffness in the transverse plane (anteroposterior and lateral directions) was found to be around 260 N/mm. This is a high value and is clinically meaningful, showing that a large force is required to cause an abnormal horizontal displacement of a normal vertebral disc unit. This means that it is relatively rare for the annulus to fail clinically because of pure shear loading. Most likely, clinical evidence of annular disruption indicates that the disc has failed because of some combination of bending, torsion, and tension (White and Panjabi, 1990). Some numerical values for stiffness properties of the disc are given in Table 2.1.

Table 2.1 Stiffness coefficients and maximum load of the intervertebral disc (White and Panjabi, 1990)

Authors	Stiffness Coefficients	Maximum Load	Spine Region
Compression ($-F_y$)			
Virgin, 1951	2.5 MN/m	4500 N	Lumbar
Hirsch & Nachemson, 1954	0.7 MN/m	1000 N	Lumbar
Brown et al., 1957	2.3 MN/m	5300 N	Lumbar
Markolf, 1970	1.8 MN/m	1800 N	Thoracic & Lumbar
Moroney et al., 1988	0.5 MN/m	74 N	Cervical
Tension ($+F_y$)			
Markolf, 1970	1.0 MN/m	1800 N	Thoracic & Lumbar
Shear (F_x, F_z)			
Markolf, 1970	0.26 MN/m	150 N	Thoracic & Lumbar
Moroney et al., 1988	0.06 MN/m	20 N	Cervical
Axial Rotation (M_y)			
Fairfan et al., 1970	2.0 Nm/deg	31 Nm	Lumbar
Moroney et al., 1988	0.42 Nm/deg	1.8 Nm	Cervical

Due to its viscoelastic characteristics, the intervertebral disc exhibits hysteresis, and creep and relaxation. Hysteresis involves loss of energy when a body is subjected to repetitive load and unload cycles. Hysteresis appears to vary with the load applied, the age of the disc and its level. The larger the load the greater the hysteresis. The intervertebral disc also shows creep and relaxation. The higher loads produced result in greater deformation and faster rates of creep.

There are very few precise studies on the behavior of the spine components in vivo. Most of the work is done on cadaver materials. Although these studies have provided large amounts of precious information, the magnitude of the loads applied to the disc cannot be determined in vitro. Nachemson and Morris (In: White and Panjabi, 1990) determined for the first time the actual loads to which a disc is subjected in vivo. They employed the concept of nucleus pulposus as a load transducer. By means of in vitro experiments on vertebra-disc-vertebra preparations, they found that the fluid pressure within the nucleus is directly related to the axial compression applied to the disc (Fig. 2.7A). Nachemson et al (In: White and Panjabi, 1990) have measured the in vivo loads to which the lumbar discs are subjected when a person is resting in different body postures or performing a certain task. A sample of the results of their work is provided in Figure 2.7B.

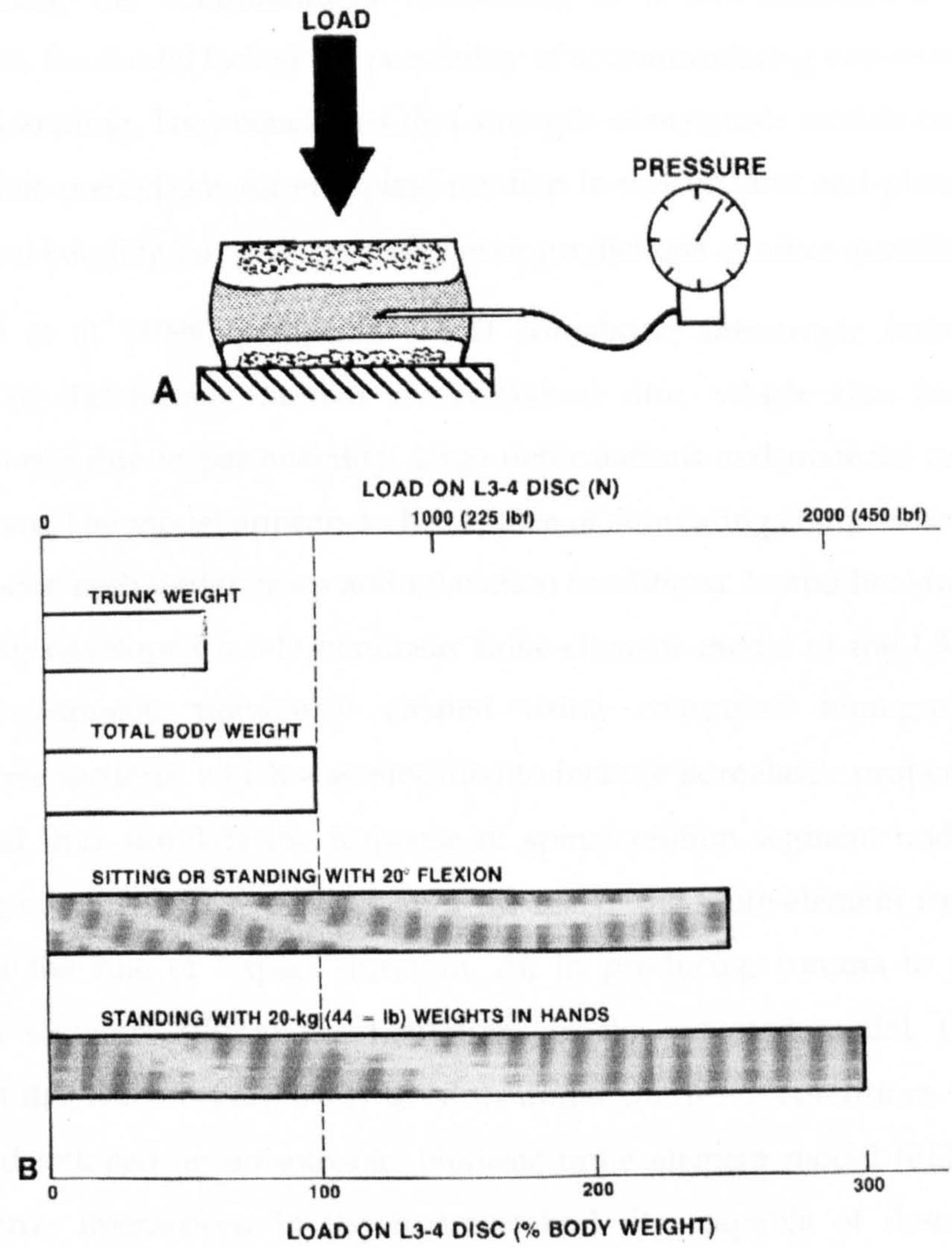

Figure 2.7 Intradiscal loads on the disc (A) The needle pressure transducer in the nucleus pulposus (B) Load on the disc (White and Panjabi, 1990)

The mechanical responses of intervertebral discs under different loading conditions have been investigated by several authors. Various models have been reported in order to analyze the disc behaviour and properties.

One of the most common techniques employed is finite element (FE) method. Spilker et al. (1984) proposed a simplified finite element model to explore the mechanical response of the disc under complex loading. Their model is axisymmetric about the longitudinal axis and the model motion segment is assumed to be symmetric with respect to its mid-transverse plane. The effects of gross disc geometry and soft tissue properties on mechanical behaviour had been studied for loading in compression, torsion, shear and moment, while

maintaining the computational efficiencies of a two-dimensional analysis. However, the model lacked the possibility of accommodating non-axisymmetric external loading. They concluded that strength-of-materials models can provide reasonable predictions for end-plate rotation in torsion, and end-plate tilting in shear and bending but give generally poor predictions of other quantities.

Dozzini et al. (1999) presented a 3-D poroelastic anisotropic finite element model of the human lumbar intervertebral disc, which also incorporates nonlinearity due to permeability, large deformations and material constitutive behaviour. The model appears to be capable of simulating compression, flexion, and torsion both under creep and relaxation conditions. In another study, Lee et al. (2000) developed a 3-D nonlinear finite-element model of the L3-L4 spinal motion segment, previously created using computed tomography (CT) transverse sections, which was modified to include poroelastic properties in the disc and thus simulate the response of spinal motion segment under impact loading conditions. The authors infer the use of the finite-element technique to address the role of impact duration, Δt, in producing trauma to the spinal motion segment. Within the limitations of the reported model, the results suggest that fractures are likely to occur under shorter Δt conditions. Baer et al. (2001) developed an anisotropic, biphasic finite element model (FEM) of disc cell-matrix interactions in the intervertebral disc capable of describing the anisotropy in the extra cellular matrix and the large strains which may occur in and around the cell. The outcomes of this study imply that zonal differences in cell micromechanical environment may play a role in known differences in the biosynthetic response of disc cells to mechanical loading.

Wagner et al. (1999) developed a constitutive formulation in order to specify a strain energy function which simultaneously predicts the mean response of the annulus to seven different experimental protocols - confined compression (two directions), uniaxial tension (two directions) and shear (three directions) and determined the material coefficients of the strain energy formulation which predicts within one standard deviation the mean response of the annulus fibrosus, both with and without invoking the traction free boundary conditions. Klisch and Lotz (2000) presented an intrinsically incompressible special mixture theory and have determined the material constants for healthy human annulus

fibrosus using new confined compression experimental data and in comparison to the aftermath of previous studies, they stated a higher initial water content, a lower aggregate modulus, and a higher initial permeability constant. Riches et al. (2002) investigated the mechanics of the intervertebral disc under cyclic loading by developing a one dimensional poroelastic model and conducting the experiment.

Some studies have been carried out on human and sheep intervertebral discs. Sheep lumbar discs have been used to investigate the effects of removing and replacing the nucleus. Reid et al. (2002) mainly investigated the water and collagen contents and fibre angles of sheep discs experimentally and concluded that a sheep disc can be used as a model of a human disc. Likewise, Costi et al. (2002) studied the hydration-over-time behaviour of ovine intervertebral discs and intact joints in a saline bath at body temperature and the effect on their stiffness compared to air at ambient temperature and demonstrated the similarities between human and sheep intervertebral discs.

2.2.2 The Spinal Ligaments

Ligaments are uniaxial structures mostly efficient in carrying loads along the fibres' direction. In this respect, they are much like rubber bands. They readily resist tensile forces but buckle when subjected to compression. Nature has designed the spine in such a way that when the functional spinal unit is subjected to different complex force and torque vectors, the individual ligaments resist tensile forces by developing tension.

The ligaments have many distinct functions. These can be summarized as follows:

- The ligaments must allow adequate physiologic motion and fixed postural attitudes between vertebrae, with a minimum expenditure of muscle energy.
- They must protect the spinal cord by restricting the motions within well-defined limits.

- They share with the muscles the role of providing stability to the spine within its physiologic ranges of motion.
- They must protect the spinal cord in traumatic situations in which high loads are applied at fast speeds. In these highly dynamic situations, not only is the displacement to be restricted within safe limits, but large amounts of energy that are suddenly applied to the spine must also be absorbed (White and Panjabi, 1990).

There are totally seven ligaments on the spine (Fig. 2.8), which are:

- *The anterior longitudinal ligament* (AAL) is a fibrous tissue structure that arises from the anterior aspect of the basioccipital and is attached to the atlas and the anterior surfaces of all vertebrae, down to and including a part of the sacrum. It fastens firmly to the edges of the vertebral bodies but is not so firmly attached to the annular fibers of the intervertebral disc.
- *The posterior longitudinal ligament* (PLL) starts from the posterior aspect of the basioccipital, covers the dens and the transverse ligament (where it is called the membrana tectoria), and overruns the posterior surfaces of all the vertebral bodies down to the coccyx. It has an interwoven connection with the intervertebral disc.
- *The intertransverse ligaments* pass between the transverse processes in the thoracic region and are identified as rounded cords intimately connected with the deep muscles of the back.
- *The capsular ligaments* (CL) are connected just beyond the margins of the adjacent articular processes. The fibers are generally oriented in a direction perpendicular to the plane of the facet joints.
- *The ligamenta flava* (LF) begin from the anteroinferior border of the laminae above to the posterosuperior border of the laminae below. They attach the borders of adjacent laminae from the second cervical vertebra to the first sacral vertebra. These ligaments are also referred to as yellow ligaments.

- *The interspinous ligaments* (ISL) combine adjacent spines, and their attachments start from the root to the apex of each process.
- *The supraspinous ligament* (SSL) arises in the ligamentum nuchae and goes along the tips of the spinous processes as a round, slender strand down to the sacrum.

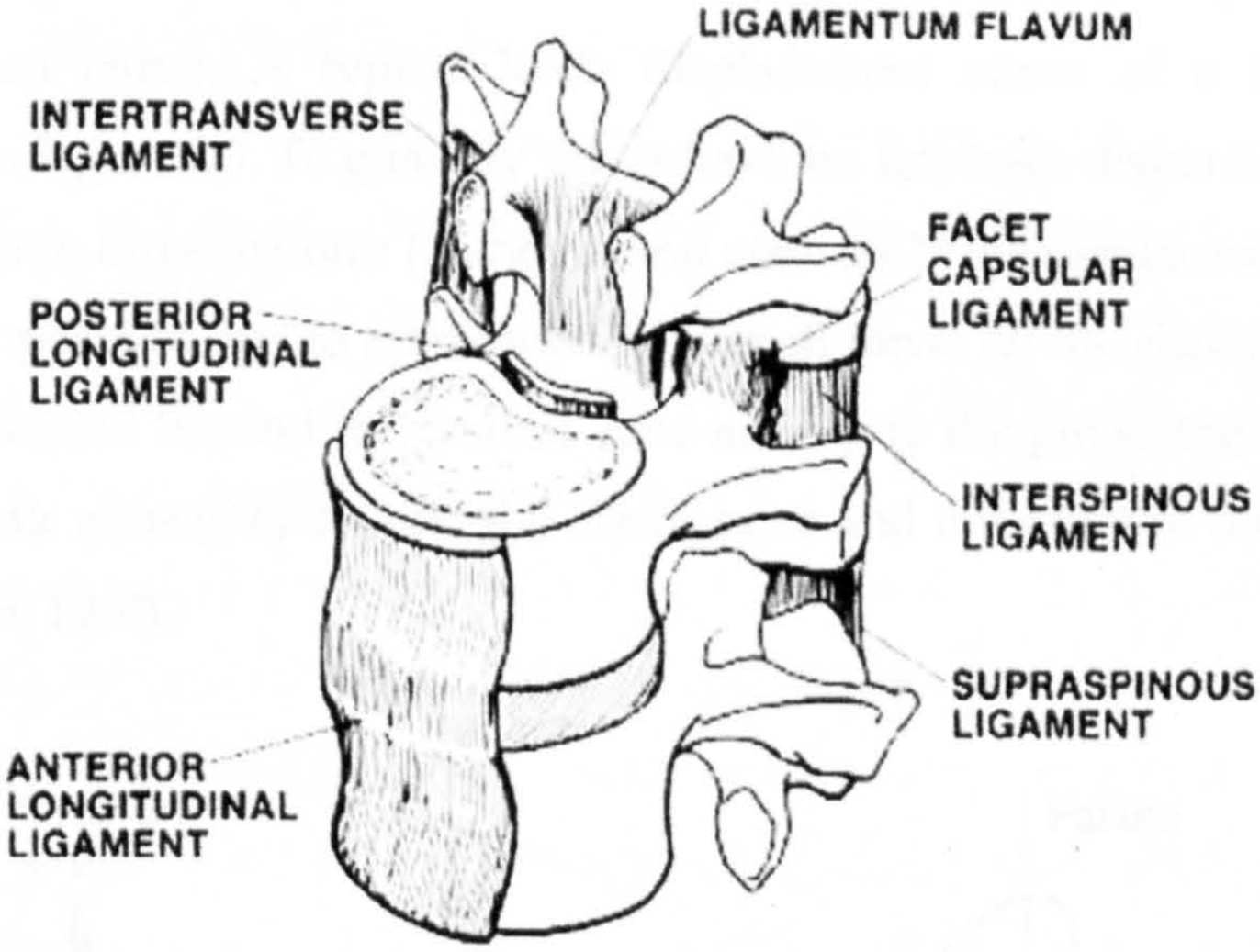

Figure 2.8 Ligaments of the spine (White and Panjabi, 1990)

Proper description of the quantitative anatomy of the ligaments, including ligament length, cross-sectional area and 3-D coordinates, is hardly ever available in the literature. A representative chart is provided in Table 2.2.

Table 2.2 Representative anatomic properties for ligaments (Length in mm) (White and Panjabi, 1990)

Region	Level	Ligament	Cross-sectional Area (mm^2)	Length
Cervical	C1-C2	Transverse	18	20
		Alar	22	11
Lumbar		ALL	53	13
		PLL	16	11
		LF	67	19
		CL	-	-
		ISL	26	-
		SSL	23	11

The biomechanical functions of the spine explained before are accomplished in part by the mechanical design of the individual ligaments and their locations and orientations with respect to the vertebrae to which they are connected.

Besides the strength of a ligament, which is important during spinal trauma (and only then), there are some other important characteristics that help obtain the physiologic functions. One such characteristic is the nonlinearity of the load-displacement curve. A typical load- displacement curve of a ligament is provided in Figure 2.9. To quantify this behaviour, the load- displacement curve is divided into three regions: (1) the neutral zone (NZ)-the displacement beyond the neutral position due to application of a small force; (2) the elastic zone (EZ)-the displacement beyond the neutral zone and up to the physiologic limit; and (3) the plastic zone (PZ)-beyond the elastic zone and until failure occurs (White and Panjabi, 1990).

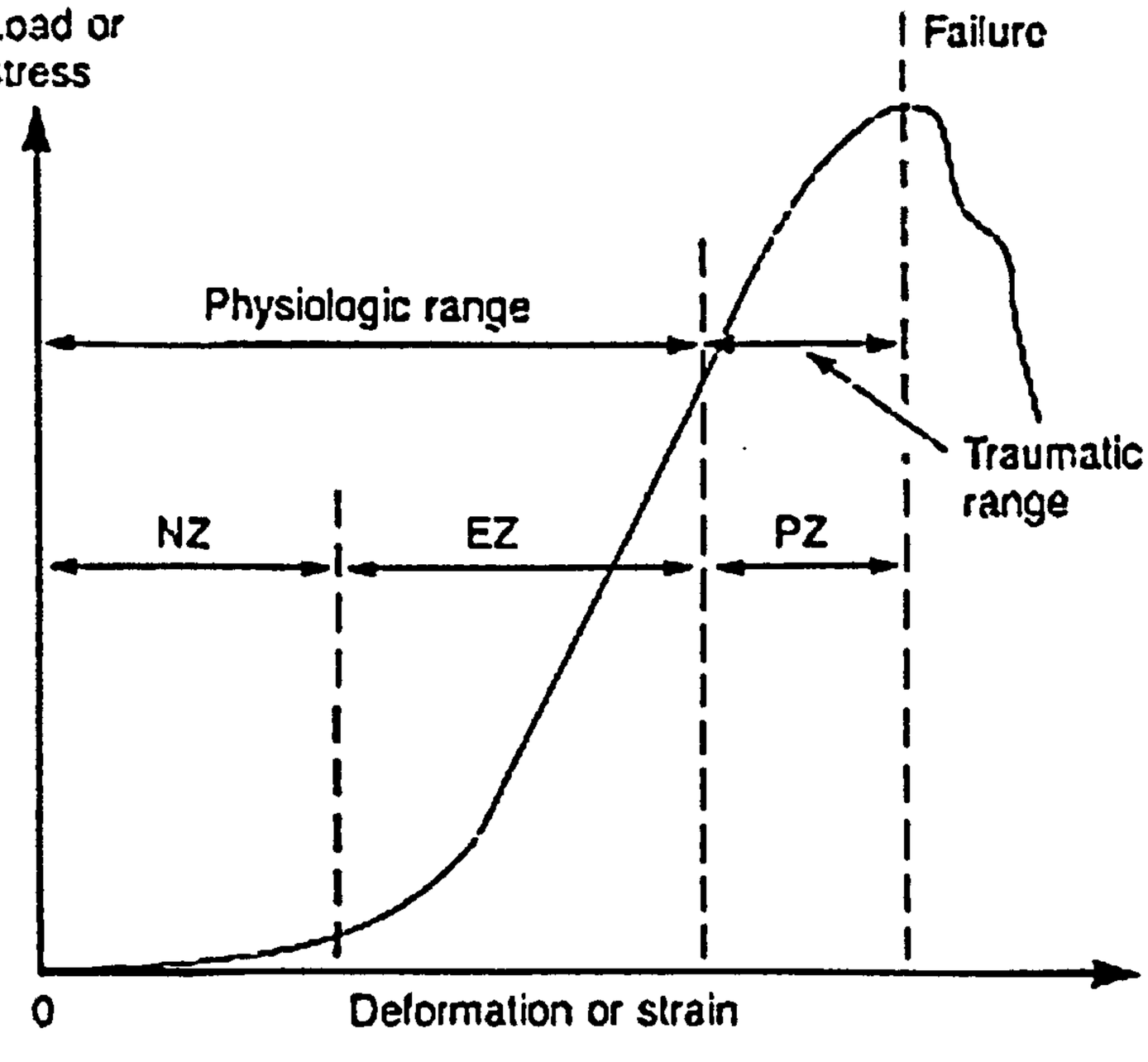

Figure 2.9 A typical load-displacement curve of a ligament (White and Panjabi, 1990)

The failure strengths of spinal ligaments are given in Table A.1 in Appendix A.

The appearance of the load-displacement curve of each of the ligaments is quite similar (Fig. 2.10). The nonlinearity of each of the curves in Figure 2.10A should

be noted (i.e., an initial phase in which a small force produces large deformation and a latter phase in which considerably larger force is required to produce the same deformation), where PLL = posterior longitudinal ligament; ALL = anterior longitudinal ligament; ISL = interspinous ligament; LF = ligamentum flavum; CL = capsular ligament; S SI, = supraspinous ligament. In Figure 2.10B, the two ligaments, A and B, are attached at point P to the moving vertebrae and having the same mechanical properties but oriented differently. As the spine flexes, the resistance provided by the two ligaments is proportional to the ligament force and the lever arm. Assuming that the moving vertebra is rotating around the instantaneous axis of rotation (IAR) as shown in the figure, then the resistance provided by ligament A will be (F_A x L_A). Similarly, the resistance offered by ligament B will be (F_B x L_B). If the ligaments applied equal forces, the resistance due to ligament A would be greater because $L_A > L_B$. In reality, the force F_A will be bigger than the force F_B because of the greater deformation of ligament A, again because $L_A > L_B$ (White and Panjabi, 1990). Each ligament is identified by its peerless combination of stiffness (the slope), maximum deformation, and failure load. These variations reflect the specific functional role of each of the ligaments.

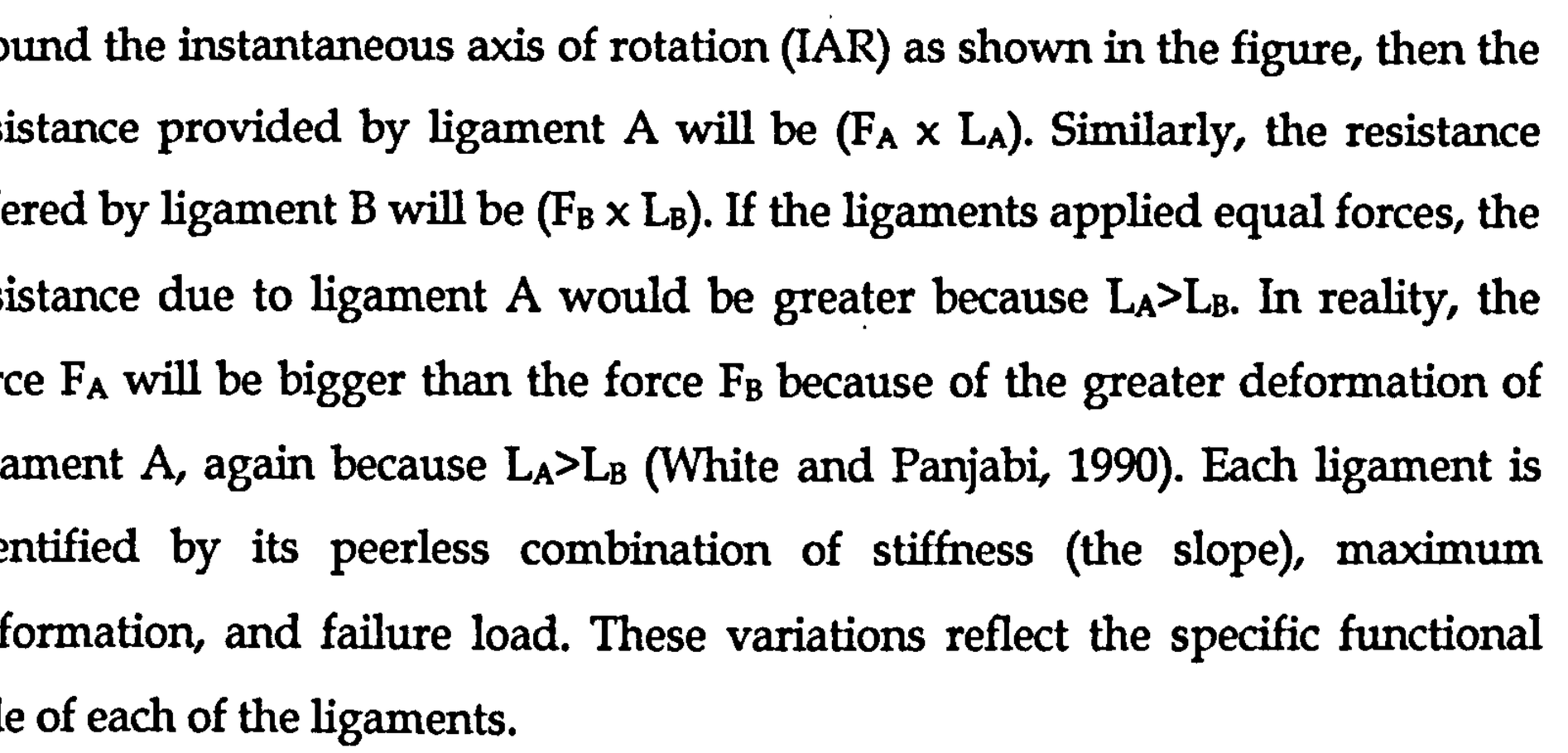

Figure 2.10 The load-displacement curve of the ligaments (A) Force-deformation curves of spinal ligaments of the lumbar region (B) Stabilizing function of a spinal ligament (White and Panjabi, 1990)

A typical stress-strain curve for the ligamentum flavum is provided in Figure 2.11.

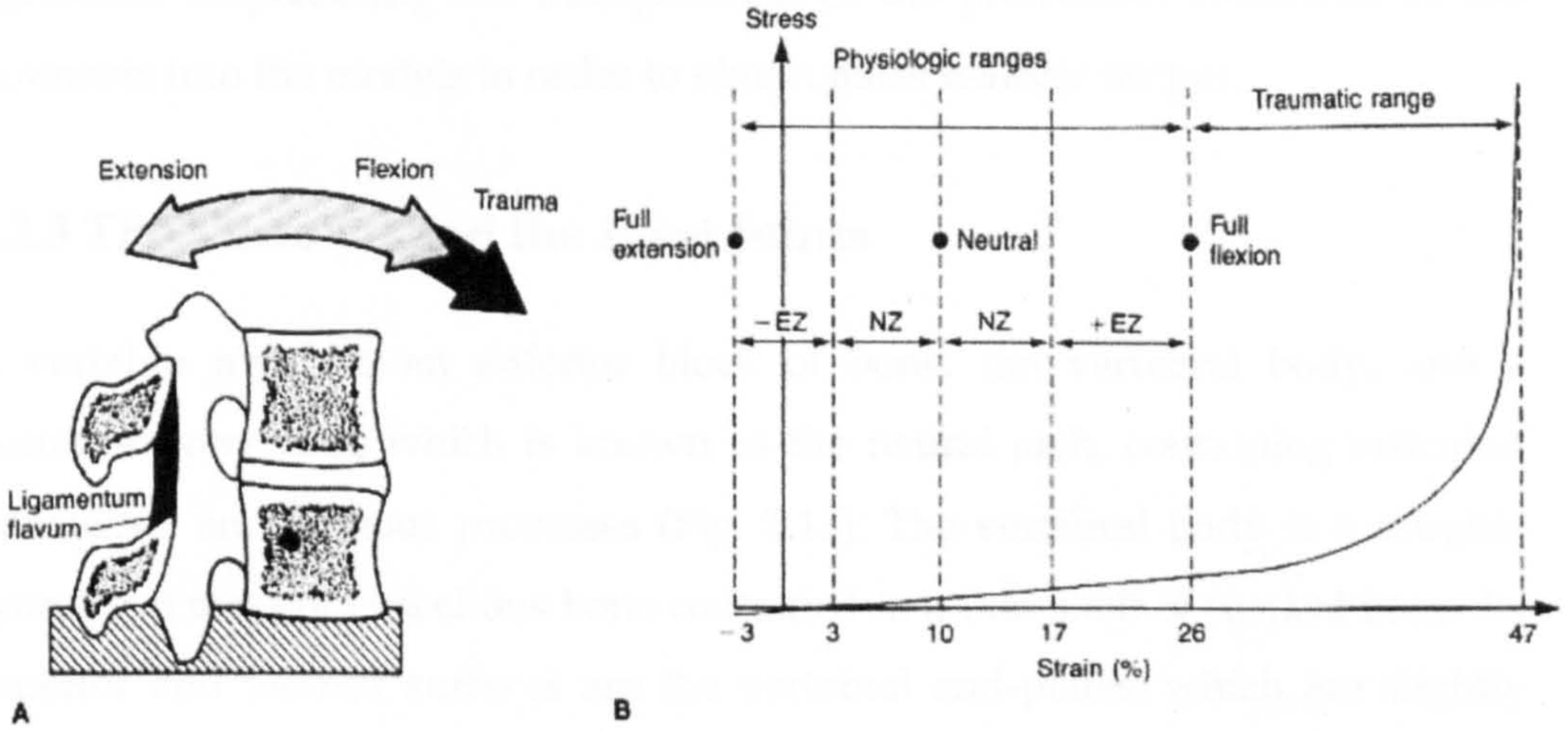

Figure 2.11 Functional biomechanics of ligamentum flavum (A) In flexion/extension (B) The stress-strain curve (White and Panjabi, 1990)

Dvorak et al. (1988) studied the biomechanics of the alar and transverse ligaments in the craniocervical region, using cadaveric spines and presented the in vitro strength of the alar ligaments as 200 N and the in vitro strength of the transverse ligaments as 350 N. The quantitative anatomy of the cervical spine ligaments had been reported by Panjabi et al. (1991) based on cadaveric specimens, including the orientations and origins of the ligaments. Similarly, Panjabi et al. (1998) carried out an in vitro study to determine the mechanical properties of human alar and transverse ligaments of the upper cervical spine at slow and fast extension rates, concluding that the strain and energy absorbed decreased to less than one tenth, while the stiffness increased to greater than ten times as the extension rate increased, for both the alar and transverse ligaments within the physiological limits and when failed at the faster rate, the alar ligament, although weaker of the two, absorbed greater energy to failure because of its higher failure strain. Also Yoganandan et al (2000) presented some geometric and mechanical properties of the human cervical spine ligaments of C2-T1 levels, including stiffness, stress, strain, energy, and Young's modulus.

Kumaresan et al (1999) developed a nonlinear finite element model of vertebral body-disc-vertebral body with the anterior and posterior longitudinal ligaments, emphasizing the incorporation of the pretension behaviour of the ligaments into the models in order to obtain more realistic output.

2.2.3 The Vertebra and the Facet Joints

A vertebra involves an anterior block of bone, the vertebral body, and a posterior bony ring, which is known as the neural arch, containing articular, transverse, and spinous processes (Fig. 2.13). The vertebral body is a roughly cylindrical mass of cancellous bone contained in a thin shell of cortical bone. Its superior and inferior surfaces are the vertebral end-plates, which are slightly concave. The neural arch consists of two pedicles and two laminae, from which seven processes originate.

Although the basic design of the vertebrae in the various regions of the spine from C3 to L5 is almost the same, the size and mass of the vertebrae increase from the first cervical to the last lumbar vertebra. This is a mechanical adaptation resulting from progressively increasing compression loads to which the vertebrae are subjected. There are also other differences. In the cervical region of the spine, there are foramina for the vertebral arteries. The thoracic vertebrae have articular facets for the ribs, and the lumbar spine has mammary processes. And lastly, the sacral spine is a unique structure among all. (White and Panjabi, 1990).

Although standard anatomic texts provide visual descriptions of vertebral anatomy, they rarely present any quantitative dimension. The latter type of information is necessary in the more widespread biomechanics research and the more precise clinical practice. The nomenclature is presented in Figure 2.12 while the data are provided in Table A.2 in Appendix A. It is crucial to remember that the shape, size, and physical properties of the vertebrae change with age.

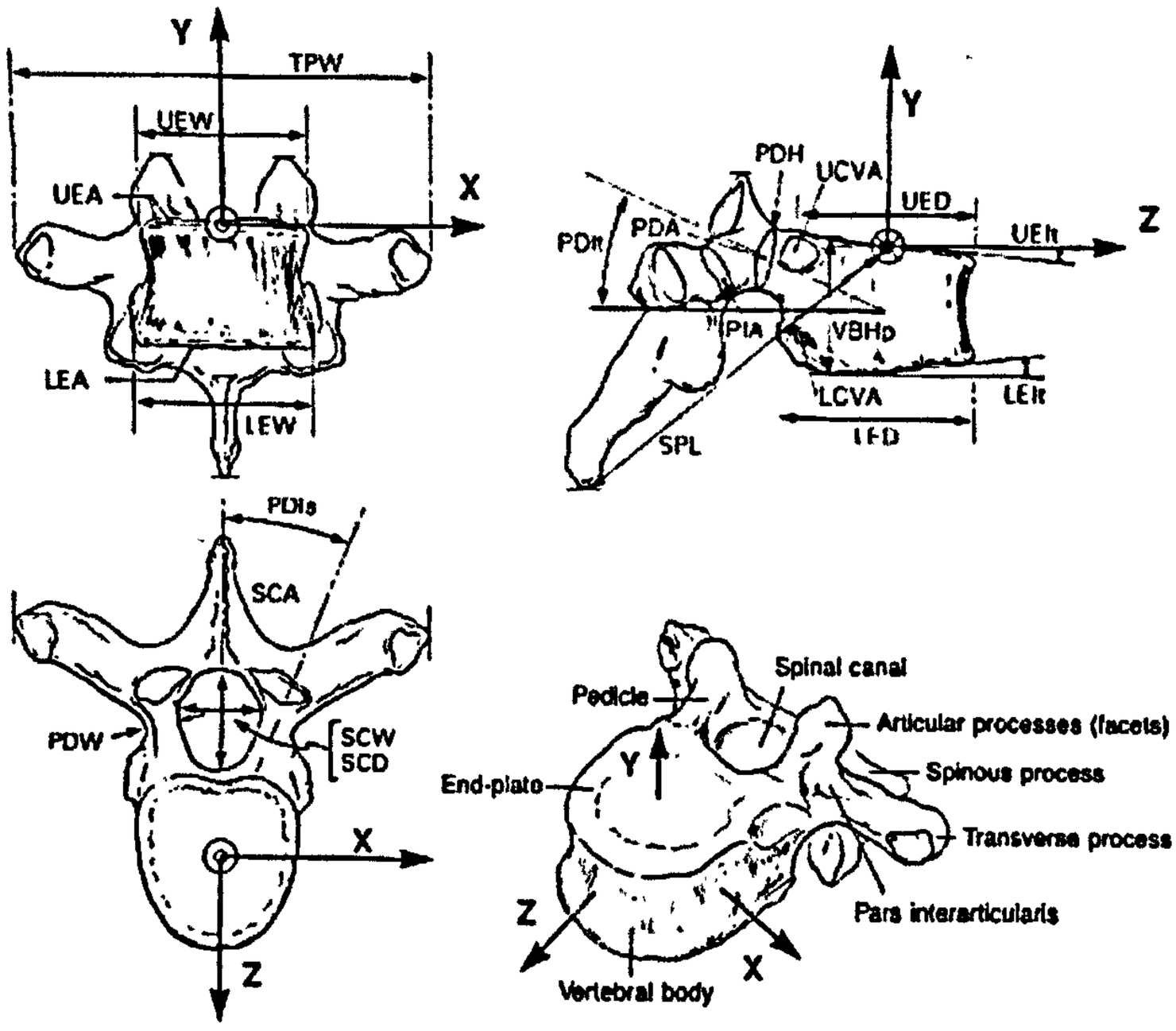

Figure 2.12 Quantitative anatomy of a vertebra (TP = transverse process; UE = upper end-plate; LE = lower end-plate; PD = pedicle; SP = spinous process; SC = spinal canal; PI = pars interarticularis; VB = vertebral body; W = width; A = area; D = depth; H = height; I = inclination. Suffixes are: t = transverse plane; p= posterior.) (White and Panjabi, 1990)

Among some other factors, the pattern of movements of the spine is dependent upon the shape and position of the articulating processes of the diarthrodial joints. It is the orientation of these joints in space that sets their mechanical importance. Figure 2.14 helps to demonstrate the changing pattern of the facet orientations, beginning from the inferior facets of C2 to L5. Two cards are initially located in the horizontal plane. A sequence of rotations of the cards about the various axes of the coordinate system shows the orientation of the facet joints they represent.

In the cervical spine, the inclination of the facet joint plane is demonstrated by first placing the two cards in the horizontal plane and subsequently rotating them through an angle of - 45° around the x-axis (Fig. 2.13A). In this position they show the inclination of the right as well as the left facet joints, C2-C3 to C7-T1.

Orientation of the thoracic facet joints, T1-T2 to T11-T12, is depicted in Figure 2.13B. Starting with the horizontal plane, a rotation of -60° about the x-axis is followed by a 20° rotation about the y-axis. The latter rotation should be positive for the right facet joint and negative for the left facet joint.

The facets of the lumbar region are not planar, but have considerably curved mating surfaces; the inferior facets are convex, while the superior facets are concave. Average planes of inclination of the facet joints, T12-L1 to L5-S1, are represented in Figure 2.13C. The horizontal cards are first given a negative rotation of about 90° around the x-axis, which is followed by a 45° rotation about the y-axis. This last rotation is positive for the left and negative for the right facet joint.

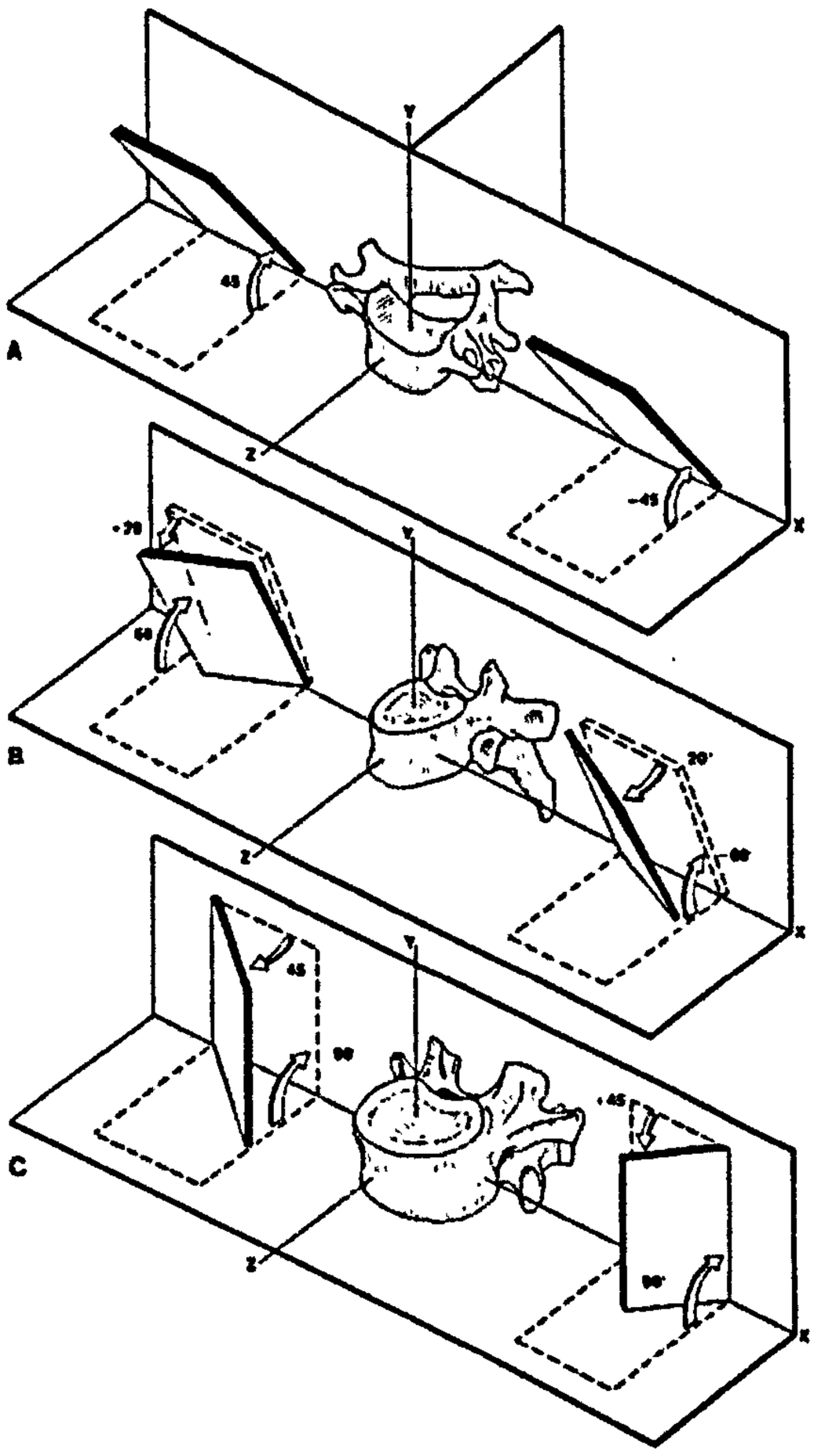

Figure 2.13 Orientation of the facet joints (A) Cervical spine (B) Thoracic spine (C) Lumbar spine (White and Panjabi, 1990)

Anatomy of the *pedicles* has gathered consequential clinical importance because of the accelerated use of pedicle fixation devices in the thoracic, lumbar, and lumbosacral regions. It is not enough to use the illustrations given in the standard anatomic text books. What is needed is a quantitative description of three-dimensional anatomy of the pedicles so that the pedicle screws may be securely and safely fixed into the vertebra. Four parameters appear to be necessary. They are pedicle cross-section height (PDH), pedicle cross-section width (PDW), pedicle axis inclination to the sagittal plane (PDIs), and pedicle axis inclination to the transverse plane (PDIt). The four parameters are graphically identified in Figure 2.12 (White and Panjabi, 1990).

Determination of compression strength of the human vertebrae has been the subject of research from the early days of biomechanics. One of motivations behind the research has been the problem of pilot ejection. Basically, it involves ejecting the pilot from the high-speed aircraft with the help of a rocket attached to the seat. To minimize the injury to the spine at the time of ejection, it is necessary to use a safe ejection acceleration. This requires a knowledge of the strength thresholds of the vertebrae. The results of some studies, in the form of strength vs. vertebral level, are summarized in Figure 2.14.

Lemosse et al. (1998) introduced a new method to determine the quantitative parameters which identify the mechanical behaviour of the costo-vertebral joint in order to help in developing numerical models of the thoracic spine, taking into account the thoracic cage. Although the whole joint mechanical behaviour, especially including the co-rotations and the non-negligible difference in behaviour from one level to another, can not be explained, yet, the authors provided quantitative information, non-existent so far, about the mechanical behaviour of the costo-vertebral joint such as ranges of motion, flexibilities in different loading directions and influence of the section of different ligaments on these parameters. Winkelstein et al. (1999) conducted a mechanical investigation to determine the role of the cervical facet capsule in whiplash injury and presented the complete strain field across the surface of the cervical facet capsule for both bending motions of flexion and extension and at failure.

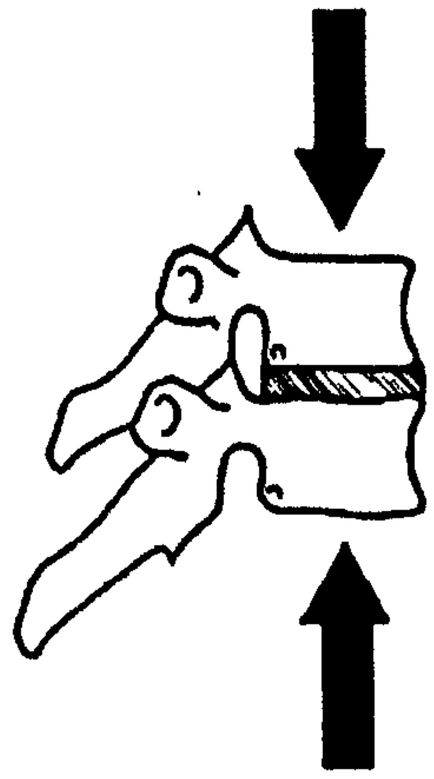

Figure 2.14 Vertebral compression strength at slow loading rate (White and Panjabi, 1990)

Kumaresan et al. (1998) modelled the facet joint capsule by employing four nonlinear finite element approaches; slideline, contact surface, hyperelastic, and fluid models. The authors presented force-displacement response, the load transmitted and maximum compressive stresses at the facet joint capsule.

Wu et al. (2002) introduced the International Society of Biomechanics (ISB) recommendations on definitions of the joint coordinate system (JCS) for the

spine. The authors explained the vertebral coordinate system and JCS as follows:

***Vertebral coordinate system* - *XYZ* (proximal) and *xyz* (distal)** (Fig. 2.15):

0(o): The origin is the intersection of the axes *Y* and *y* in the reference, neutral position (Fig. 2.16A). The neutral position must he specified, and must be in a position where the vertebral axes *Y* and *y* are coplanar. If *Y* and *y* are parallel (do not intersect at the common origin 0) the *Y*- and *y*-axis are constrained to be colinear, and the origin *0* is the mid-point between adjacent endplates (see Fig. 2.16B)

Y(y): The line passing through the centers of the vertebra's upper and lower endplates, and pointing cephalad.

Z(z): The line parallel to a line joining similar landmarks on the bases of the right and left pedicles, and pointing to the right.

X(x): The line perpendicular to the Y- and Z-axis, and pointing anteriorly.

JCS and motion for the spine (Fig. 2.15):

e_1: The axis fixed to the proximal vertebra and coincident with the Z-axis of the proximal vertebra coordinate system.

Rotation (α): flexion or extension.

Displacement (q_1): mediolateral translation.

e_2: The axis fixed to the distal vertebra and coincident with the y-axis of the distal vertebra coordinate system.

Rotation (γ): axial rotation.

Displacement (q_3): proximo-distal translation.

e_3: The floating axis, the common axis perpendicular to e_1 and e_3.

Rotation (β): lateral bending.

Displacement (q_2): antero-posterior translation.

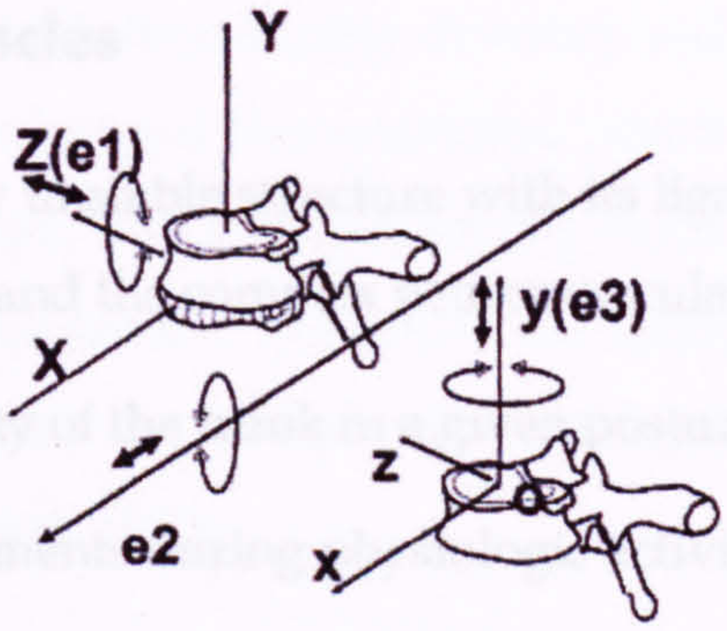

Figure 2.15 Illustration of vertebral coordinate systems and JCS (Wu et al., 2002)

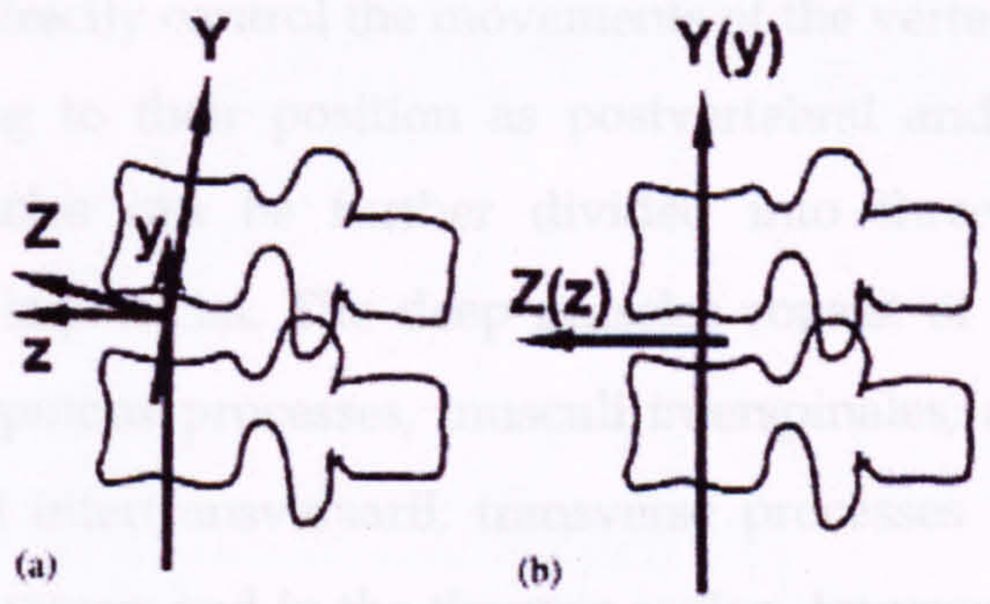

Figure 2.16 Location of the common origin of axes (A) The general case (B) The specific case of Y and y being parallel (Wu et al., 2002)

Throughout this thesis, a different coordinate axis system was used due to various conveniences within the computational multi-body and finite element software, as based on van Lopik (2004) studies (Fig. 2.17).

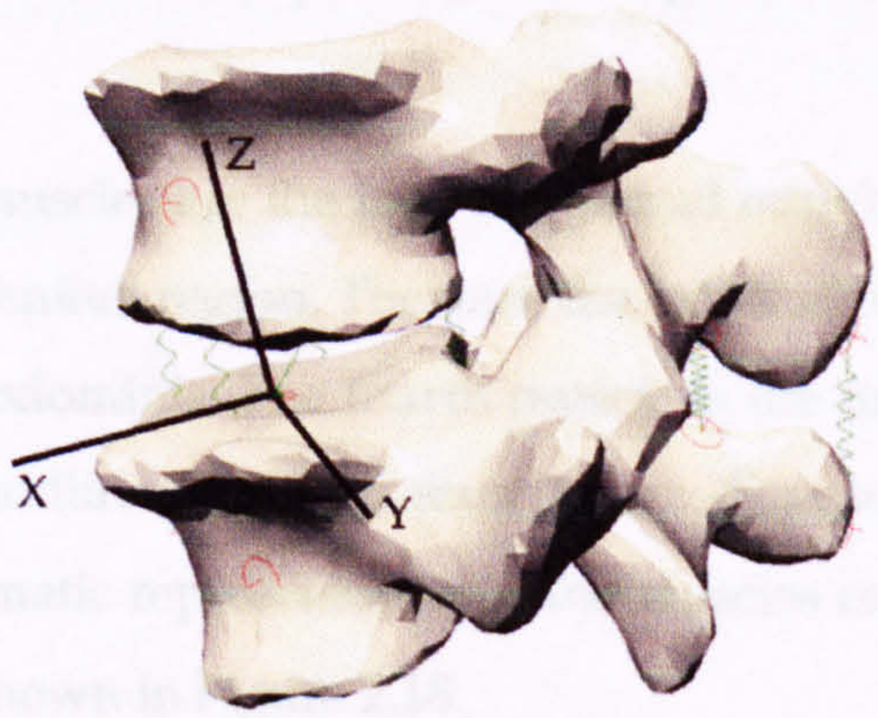

Figure 2.17 The x, y, and z directions shown locally on the upper plate of a vertebra as used throughout the thesis

2.2.4 The Spinal Muscles

The spine is a completely unstable structure with its ligaments intact but devoid of muscles. The muscles and the complex neuromuscular controls are needed:

- to provide stability of the trunk in a given posture, and
- to produce movements during physiologic activity.

The muscles may also play a role in protecting the spine during trauma in which there is time for voluntary control, and possibly in the postinjury phase.

The muscles that directly control the movements of the vertebral column can be classified according to their position as postvertebral and prevertebral. The postvertebral muscles can be further divided into three categories: deep, intermediate, and superficial. The deep muscles consist of short muscles that connect adjacent spinous processes, musculi interspinales; adjacent transverse processes, musculi intertransversarii; transverse processes below the laminae above, musculi rotatores; and in the thoracic region, transverse processes to the ribs, musculi levatores costarum. The intermediate muscles are more diffused, however certain components can be described. These muscles originate from the transverse processes of each vertebra and fasten to the spinous process of the vertebra above. According to the regions, they are the multifidus (lumbosacral), emispinalis thoracis, semispinalis cervicis, and semispinalis capitis. The superficial postvertebral muscles, collectively called as the erector spinae, are the iliocostalis (most laterally placed), the longissimus, and the spinalis (most medially placed).

The prevertebral muscles are the four abdominal muscles. Three of the muscles surround the abdominal region. They are the external oblique, internal oblique, and transversus abdominis. The fourth muscle is the rectus abdominis, located anteriorly at the midline. The four muscles are disposed in diversely different directions. A schematic representation of the muscles encircling the spine in the lumbar region is shown in Figure 2.18.

The spinal muscles have various biomechanical functions. Through their activity they generate body movements by inducing bending moments and torques. By the same mechanism, they also perform tasks and resist external

loads. Most important of all, they supply dynamic stability to the spine where very little exists. Two mechanical characteristics, which are essential to provide these physiologic functions, are; first, generating force isometrically as well as with changing length, and second, increasing the stiffness of the spinal system (ligamentous column and the surrounding musculature), thus increasing stability (White and Panjabi, 1990).

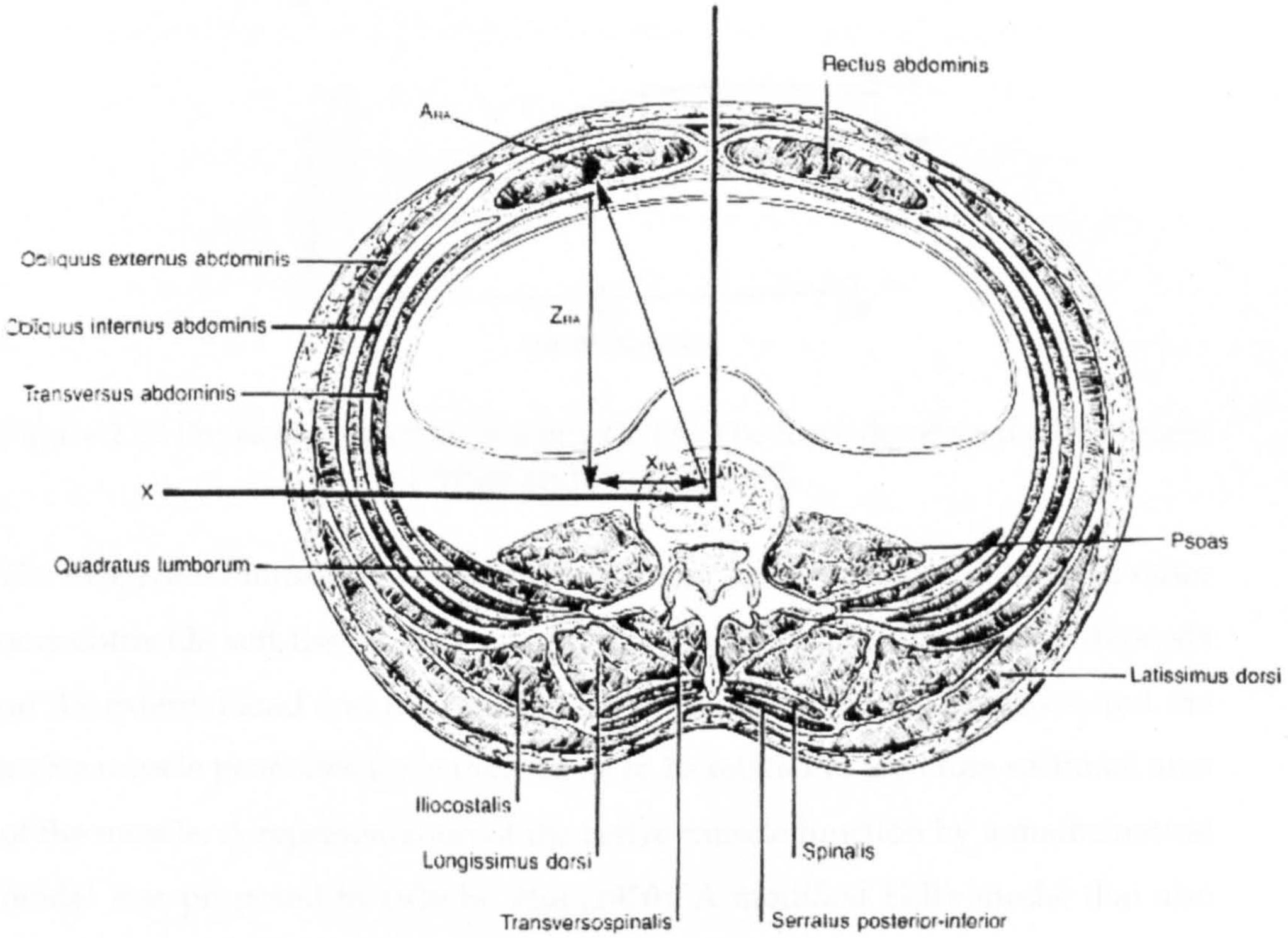

Figure 2.18 A horizontal cross-section through the lumbar spine showing muscles (White and Panjabi, 1990)

The passive/active force-length and stiffness-operating force curves are given in Figure 2.19.

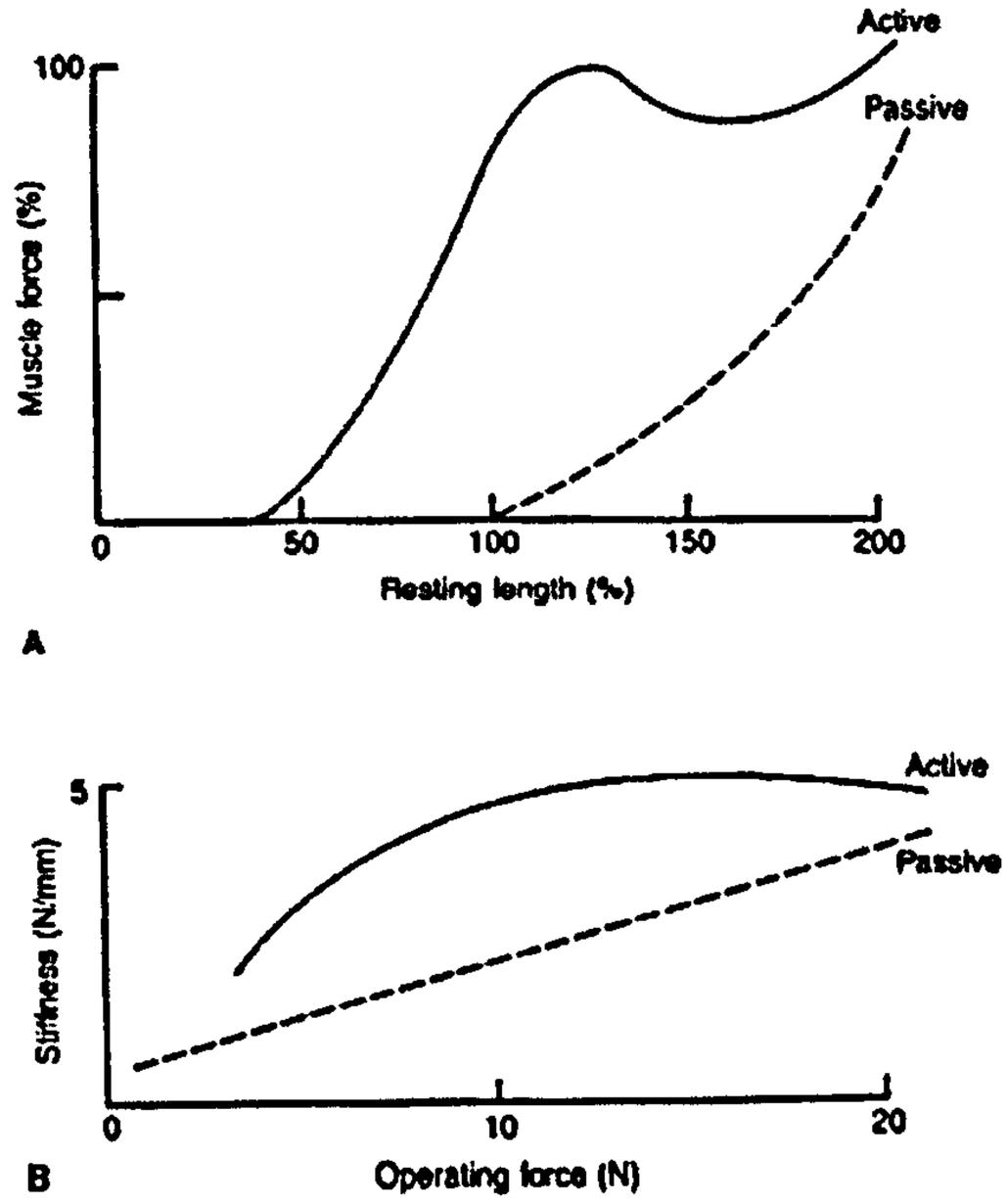

Figure 2.19 Physical properties of a muscle (A) The force developed (B) Stiffness (White and Panjabi, 1990)

The inactivated muscle has physical properties that are similar to those of other noncontractile soft tissues. The mechanical output of an active muscle depends on the external load and the muscle length. The passive muscle resists, and the active muscle generates force that seems to be related to the cross-sectional area of the muscle. A representation of the active muscle function by a mathematical model was proposed in 1939 by Hill (1970). A modified Hill's model that also includes the passive behaviour of the muscle is illustrated in Figure 2.20.

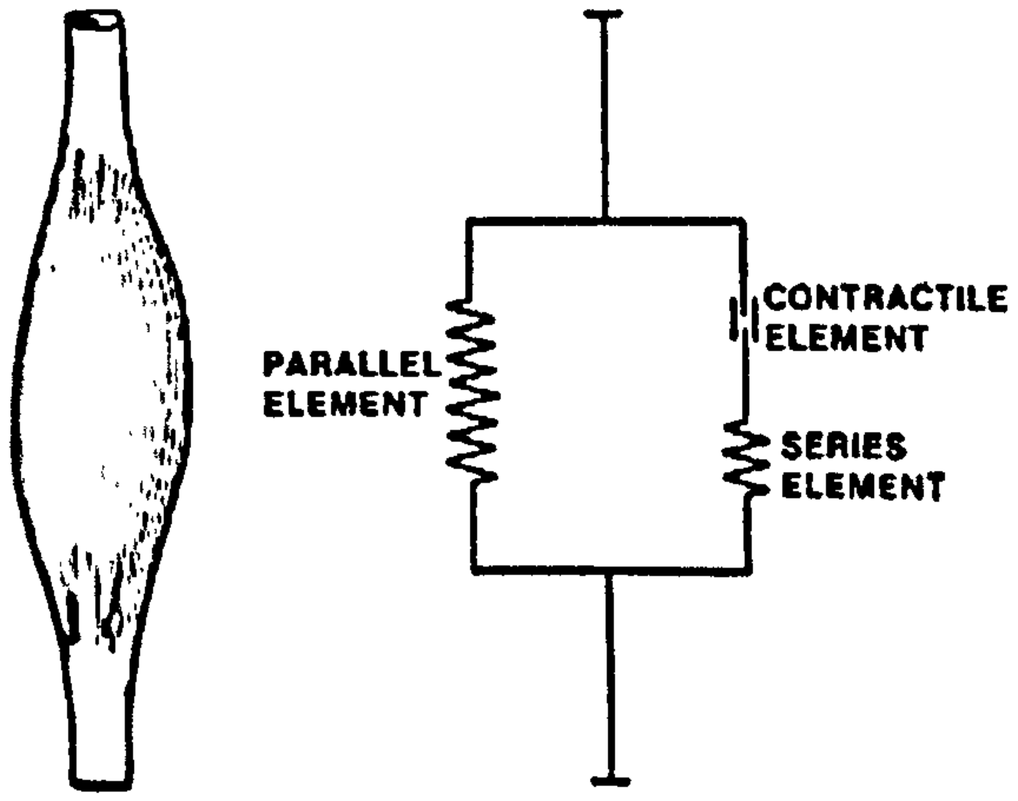

Figure 2.20 Functional model of muscle (White and Panjabi, 1990)

The model includes three elements - two springlike elastic elements (parallel and series) and one contractile element under the control of a neuromuscular signal. The passive behaviour of the muscle is entirely represented by the parallel element, because the contractile element remains inactive, and thus, no force is conducted by way of the series element. When a muscle is voluntarily contracted, it can remain in a fixed position with no change of muscle length (isometric contraction), or it may contract and shorten (isotonic contraction) to provide work against an external load. In both situations, the element shares the load together with the parallel element. This efficiently increases the muscle stiffness. It should be emphasized that the mathematical model presented in Figure 2.20 is not a physical representation of a muscle, but it is a simple and precise way to describe the actual mechanical behavior of the muscle. Such models have been used to investigate the protective role of the back muscles of the spine in front-end auto collisions (White and Panjabi, 1990).

Muscle activities during the four physiologic motions are illustrated in Figure 2.21.

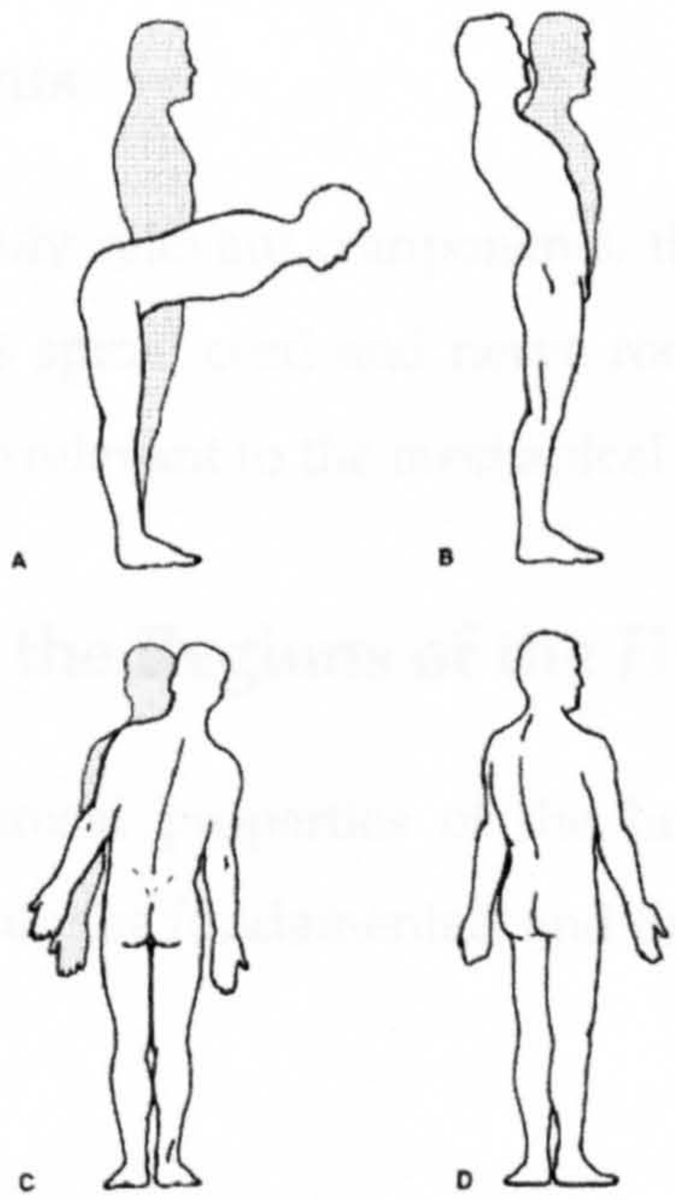

Figure 2.21 Muscle activity during the four physiological motions (A,B) In flexion and extension, gluteus and erector spinae muscles are active (C) Lateral bending is gathered by an imbalance of muscle forces on both sides of the back (D) During axial rotation, erector spinae muscles on the ipsilateral side, the rotators and multifidi on the contralateral side, and the gluteals on both the sides were found to be active (White and Panjabi, 1990)

Several studies have been carried out on spinal musculature. Seng (2001) developed an attachment device for measuring isometric neck muscle strength and submitted neck torque mean values in extension and lateral bending motions. In their study, Kettler et al. (2002) presented that mechanically simulated cervical spine muscles strongly stabilized intact and injured cervical spine specimens. The authors concluded that as a first step application of constant muscle forces and additional loading with pure moments appears to be a reasonable compromise for integration of muscles in *in vitro* experiments.

De Oliveira et al. (2001) investigated lumbar back muscle activity of helicopter pilots and the whole body vibration experimentally and concluded that the vibration produced by the helicopter does not seem to have an important influence on erector spine muscle activity and low back pain. Also Cholewicki and Van Vliet IV (2002) presented in their study that a single muscle can not be identified as the most important for the stability of the lumbar spine. They claimed that spine stability depends on the relative activation of all trunk muscles and other loading variables.

2.2.5 Other Components

Other than the mechanically relevant components, the human spine has some other components such as spinal cord and nerve roots. These components are not examined as they are irrelevant to the mechanical modelling concept.

2.3 Biomechanics of the Regions of the Human Spine

In this section, biomechanical properties of the human spine segments are introduced, which constitute the fundamentals and the limits for developing the computational models.

2.3.1 The Cervical Spine

Because of kinematic, kinetic, and clinical reasons, the cervical spine is classified into three subgroups; the upper cervical spine, namely, the occipital-atlanto-

axial complex (C0-C1-C2), the middle cervical spine (C2-C5), and the lower cervical spine (C5-T1).

The Occipital-Atlanto-Axial Complex (C0-C1-C2)

The occipital-atlanto-axial joints are anatomically and kinematically the most complex joints of the axial skeleton. Although there have been some thorough investigations of this region, there is significant controversy about some of the basic biomechanical characteristics. The representative values for the ranges of motion of the units of the occipital-atlanto-axial complex are given in Table 2.3.

Table 2.3 Representative values for ranges of rotation for the occipital-atlanto-axial complex (White and Panjabi, 1990)

Unit of Complex	Type of Motion	Representative Angles (deg)
Occipital-atlantal joint (CO-C1)	Combined flexion/extension (±θx)	25
	One side lateral bending (θz)	5
	One side axial rotation (θy)	5
Atlanto-axial joint (C1-C2)	Combined flexion/extension (±θx)	20
	One side lateral bending (θz)	5
	One side axial rotation (θy)	40

Both joints of the complex participate about equally during flexion/extension in total motion in the sagittal plane. Depending on radiographic study Werne (In: White and Panjabi, 1990) showed that sagittal plane movement is definitely present. An example from his studies is illustrated in Figure 2.22, with an angle of rotation indicated. It was found that the curvature of the dens in the sagittal plane may also allow some additional rotary displacement in that plane.

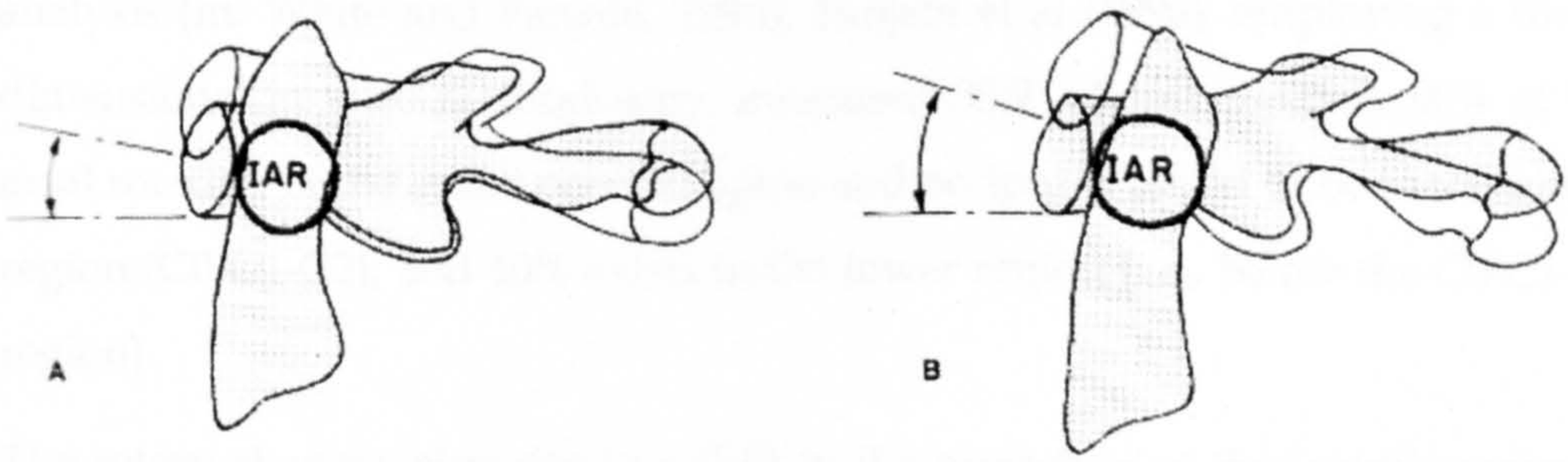

Figure 2.22 (A) Sagittal plane motion of C1 on C2 with the approximate instantaneous axis of rotation (IAR) in combined flexion/extension of 20° (B) The anterior curvature of the dens can allow some degree of additional sagittal plane motion in both rotation and translation (White and Panjabi, 1990)

Previously there was thought to be very little or no axial rotation between C0 and C1. However, various investigators have independently examined one side axial rotation in the range of 3-8°. Clark et al obtained an average of 4.8°; Worth, as well as Depreaux and Mestdagh, who presented an average of 3.2°; and Dvorak et al, employing computerized axial tomography in vivo, noted an average one side axial rotation of 4.3° (all in: White and Panjabi, 1990). Panjabi et al (1990) acquired 8° of one side axial rotation between C0 and C1 using a three-dimensional analysis.

However, it should be noted that the major axial rotation in the region is between C1 and C2. The anatomic structure of C0-C1 is somewhat cuplike in its design in both the frontal and the sagittal planes. Therefore, there is relatively little axial (y-axis) rotation. This is true even though there is little ligamentous restraint applied by the posterior atlantooccipital membrane.

On the contrary, however, both articular surfaces of the C1-C2 lateral masses possess a convex orientation in the sagittal plane. This geometric design allocates consequential mobility. The motion capacity is further intensified by the absence of any taut yellow ligament, which connects the posterior elements. Instead, and contrary to some anatomic diagrams, there is the loose, readily mobile atlanto-axial membrane connecting the posterior elements. The motion here was submitted by Werne as 47° to one side. Investigators have recently made similar observations on this issue. Dvorak and associates gathered unilateral C1-C2 axial rotation of 34° in an in vitro study and 41.5° in *in vivo* analysis (In: White and Panjabi, 1990). Panjabi et al (1990), employing a three-dimensional in vitro methodology, measured 38.9°. Approximately 60% of the axial rotation of the entire cervical spine and occiput is found to be in the upper region (C0-C1-C2), and 40% exists in the lower region (i.e., below the C0-C1-C2 region).

The rotary changes give rise to a shift in the projection of the lateral masses of C1 in relation to the dens. Werne has described this concept and demonstrated well by Shapiro et al (In: White and Panjabi, 1990). The rotary displacement pattern and the radiographic projection are shown diagrammatically in Figure 2.23. Although Hohl interpreted this aspect of C1-C2 kinematics differently, he

also made the point that apparent lateral displacement of up to 4 mm, between the dens and the lateral masses as an isolated radiographic finding is not indicative of subluxation or dislocation. This is nicely confirmed by the lateral (x-axis) translation of point A as provided in Figure 2.24, which is obtained experimentally (White and Panjabi, 1990).

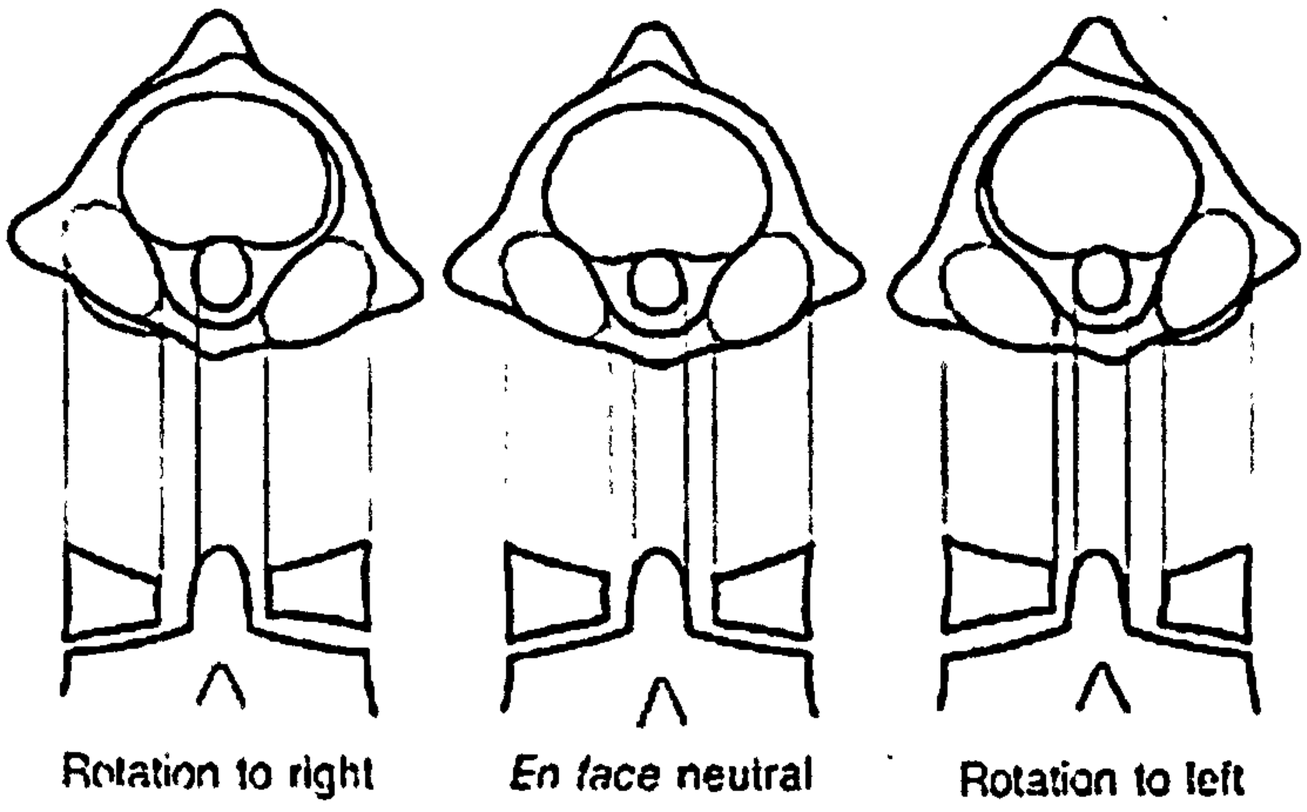

Figure 2.23 Rotation of C1 (White and Panjabi, 1990)

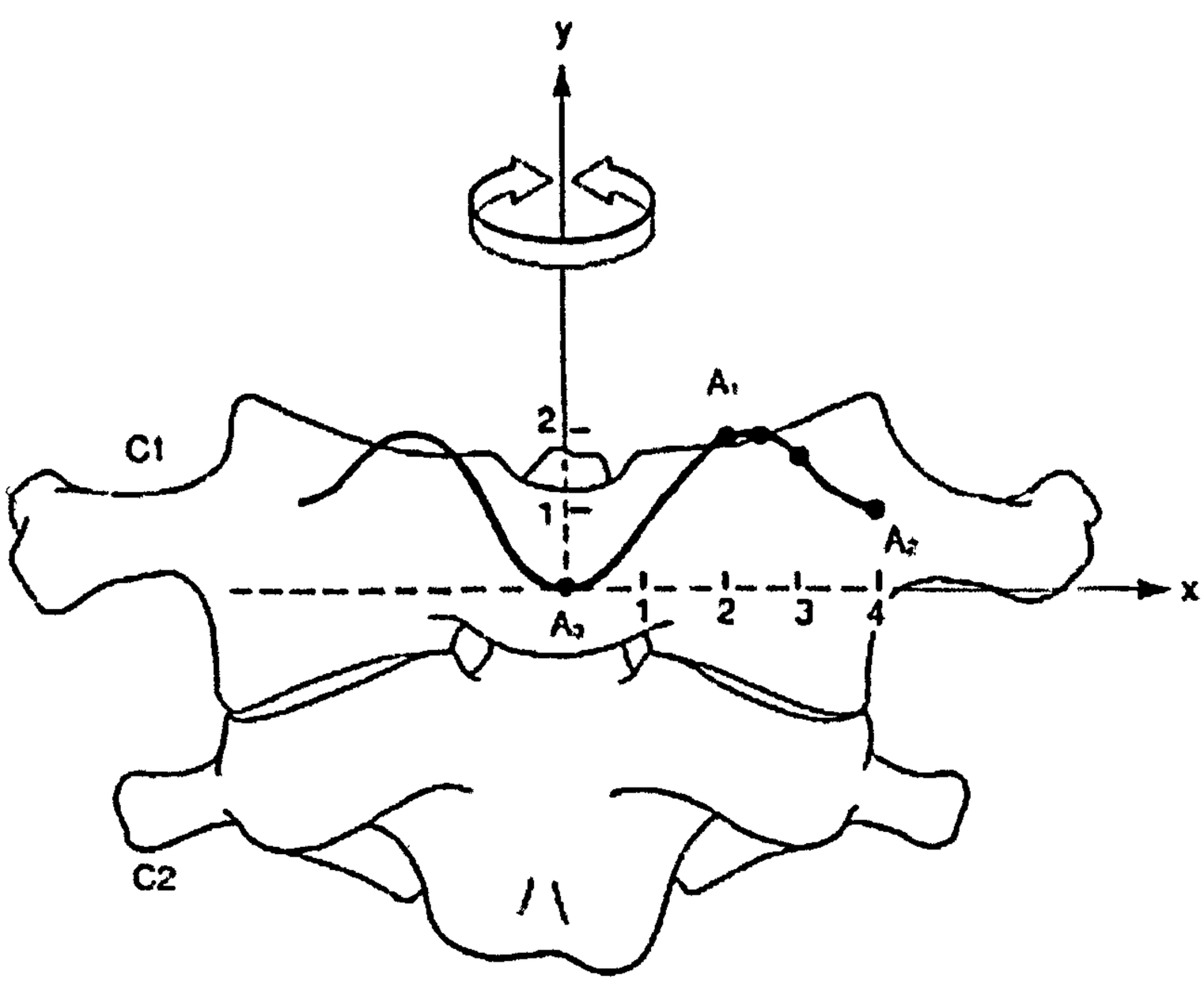

Figure 2.24 Translatory movements of the anterior aspect of C1 with respect to C2 (White and Panjabi, 1990)

The Middle and Lower Cervical Spine (C2-T1)

Most of the motion in flexion/extension occurs in the central region. The C5-C6 interspace is usually pondered to have the largest range. For lateral bending and axial rotation there exists a tendency for a smaller range of motion in the more caudal segments. The relationship between disc degeneration and motion had been investigated by Lysell (In: White and Panjabi, 1990). The intervertebral disc for each motion segment was cut and graded for degeneration. There seemed to be no change in range of motion as a function of disc degeneration. Other investigators have seen that a compensatory increase in motion occurs in cervical spine segments adjacent to interspaces with reduced motion due to either degeneration or post-traumatic changes (White and Panjabi, 1990). Rotation ranges for the middle and lower cervical spine are given in Table A.3 in Appendix A.

The pattern of motion of a vertebra within its ranges of motion is determined by a combination of the geometric anatomy of the structures and their physical properties. The positions of a vertebra from full extension to full flexion, for example, have certain similarities throughout the spine, and yet there are some characteristic local differences and even gradations of differences within regions. Lysell explained clearly that the routes were the same for any given vertebra whether it was moving from flexion to extension or vice versa. The movement is a combination of translation and rotation. He used what he called the "top angle" to indicate the steepness of the arch that was described by the vertebra while going from full extension to full flexion. The arches were flat at C2. The steepest was at C6, which is followed by C7. Those in between exhibit the same characteristics.

The route of motion in the sagittal plane is shown schematically in Figure 2.25. The acuity of the arc seemed to decrease in association with disc degeneration and this overall pattern was demonstrated to be a statistically significant variation. The route of motion in the sagittal plane consists of a strong coupling element.

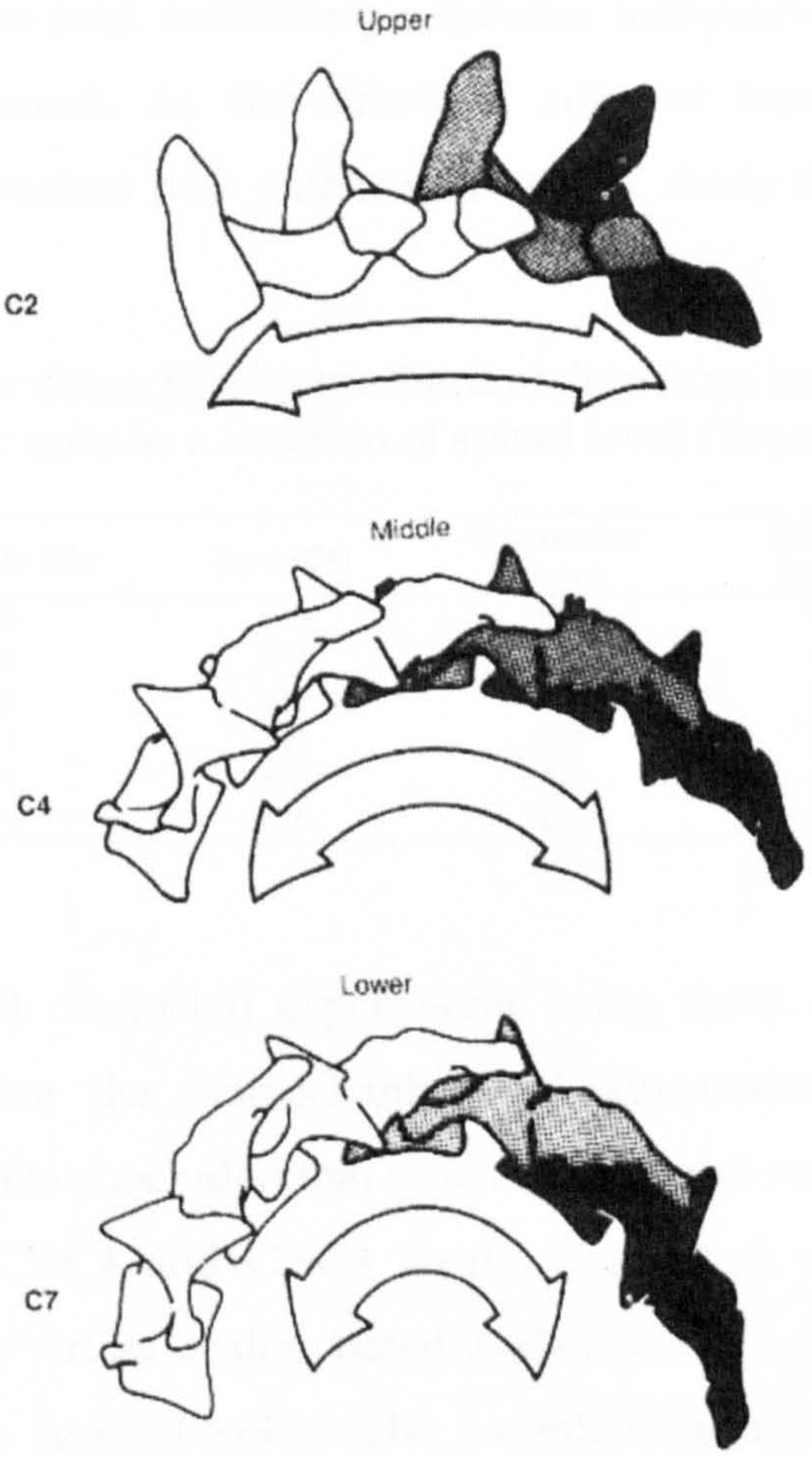

Figure 2.25 A schematic approximation of the relative regional cephalocaudal variations in radii of curvature of the arches defined by the cervical vertebrae as they rotate and translate in the sagittal plane (White and Panjabi, 1990)

Kinematics of the cervical spine has been studied by several authors. Goel et al. (1984) utilized a 3-D sonic digitizer to investigate the motion in flexion, extension, and right axial rotation as well as the effects of a number of injuries and stabilization. In another study, Goel et al. (1988) identified the effect of multiple-level laminectomies followed by stabilization on the load-deformation behaviour of the cervical spine. The authors found the facet wiring technique to be effective in stabilizing injured cervical spines. Moroney et al. (1988) conducted several compression, shear, flexion, extension, lateral bending and axial torsion tests and presented the principal and couple motions and stiffnesses. In a similar study, Yoganandan et al. (1996) performed axial tension tests to obtain the stiffness and energy absorbing characteristics of the cervical spine. The authors developed a "part-to-whole" approach, which assists in

obtaining the failure (and subfailure) responses independent of the otherwise connective environment, i.e. the effects of adjacent tissues and joints. The distraction biomechanical data gathered from this study is tabulated in Table 2.4.

Table 2.4 The distraction biomechanical data from isolated cervical intervertebral disc units as a function of spinal level (Yoganandan et al., 1996)

Spinal Level	Sample Size	Force (N)	Distraction (mm)	Stiffness (N/mm)	Energy (J)
C2-C3	5	636	11.4	63.5	3.7
C3-C4	5	590	12.1	69.8	4.4
C4-C5	3	571	9.3	66.8	5.5
C5-C6	1	391	12.7	22.0	2.6
C6-C7	2	505	9.9	69.0	3.3
C7-T1	4	510	11.3	82.2	3.3

Chang et al. (1999) conducted experiments using thirty canine specimens in order to investigate the biomechanics and kinematics of vertebrae with fixations. The authors concluded that when C4-C5 level was fixed, there was no compensation at C3-C4 and C5-C6 levels. DeFrate et al. (1999) reported a magnetic tracking/virtual reality based system for comprehensive kinematic assessment of the cervical spine. The overall rotational movements of the cervical spine vs. time during voluntary lateral bending by one subject with and without the aid of visual feedback are provided in Figure 2.26.

Yoganandan et al. (1999) presented geometrical and biomechanical properties of the human cervical spine ligaments, which are of value to develop computational models such as multi-body models and finite element models. Some essential data and curves are presented in Figures 2.27-36, where ALL: anterior longitudinal ligament, PLL: Posterior longitudinal ligament, JC: Joint capsules, LF: Ligamentum flavum, and ISL: Interspinous ligament.

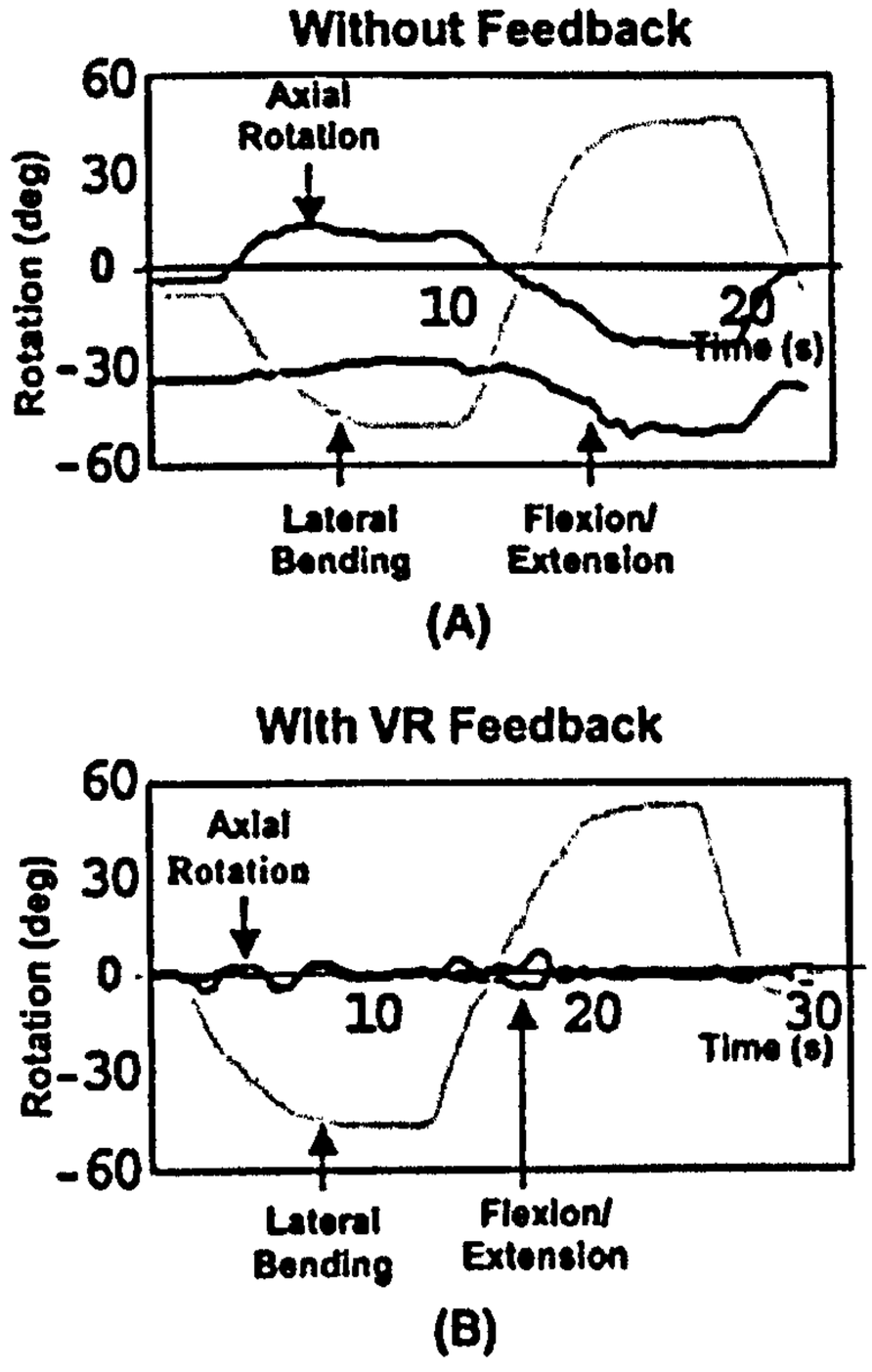

Figure 2.26 The overall rotational movements of the cervical spine vs. time (DeFrate et al., 1999)

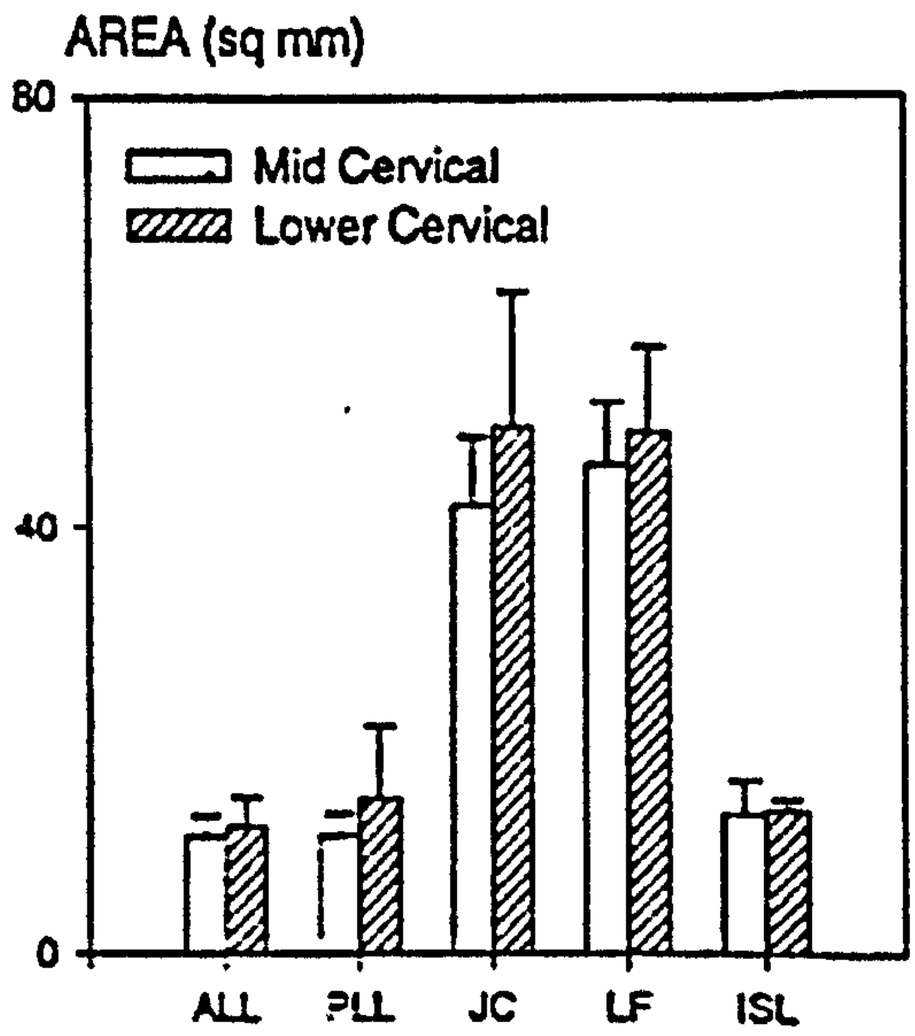

Figure 2.27 Cross-sectional areas of the ligaments (Yoganandan et al., 1999)

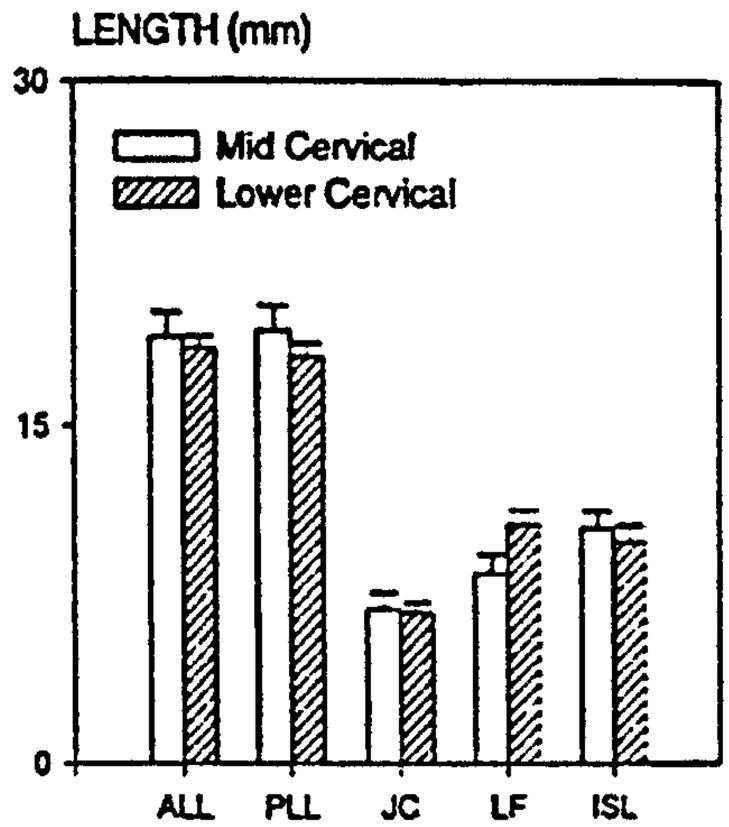

Figure 2.28 Lengths of the ligaments (Yoganandan et al., 1999)

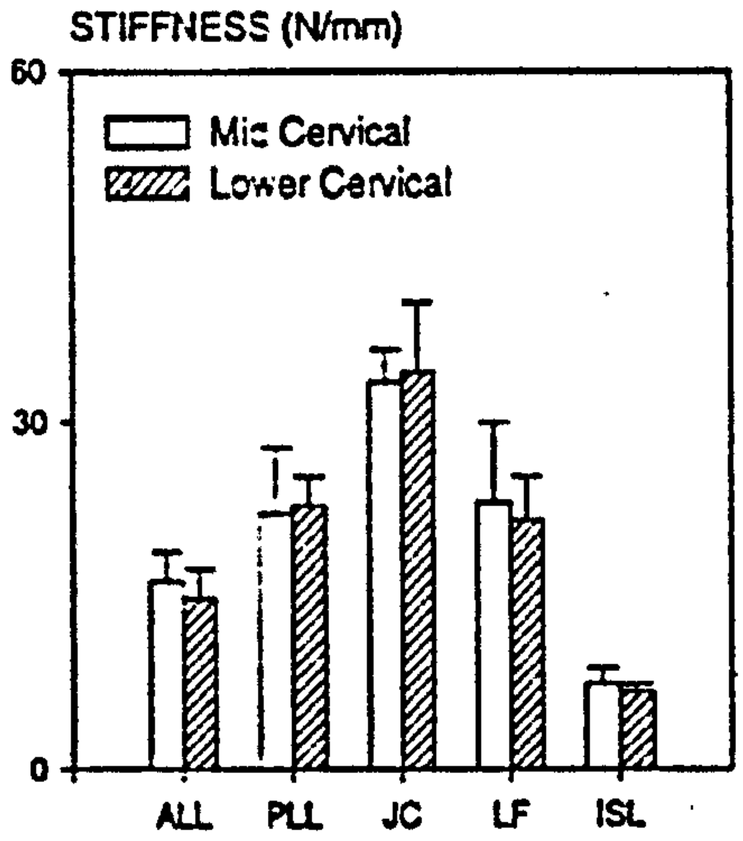

Figure 2.29 Stiffness of the ligaments (Yoganandan et al., 1999)

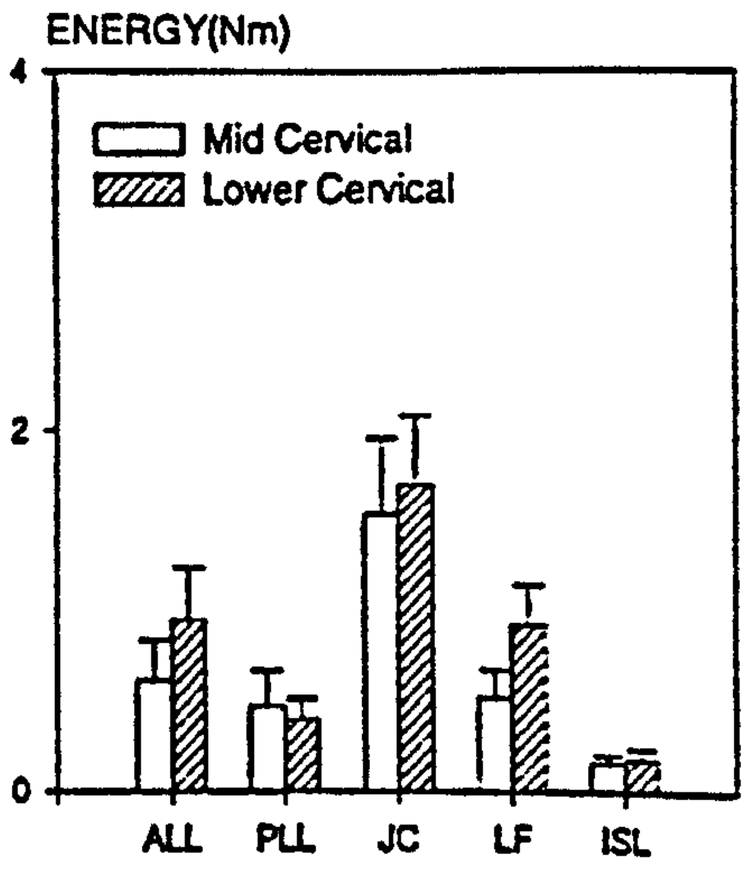

Figure 2.30 Failure energy of the ligaments (Yoganandan et al., 1999)

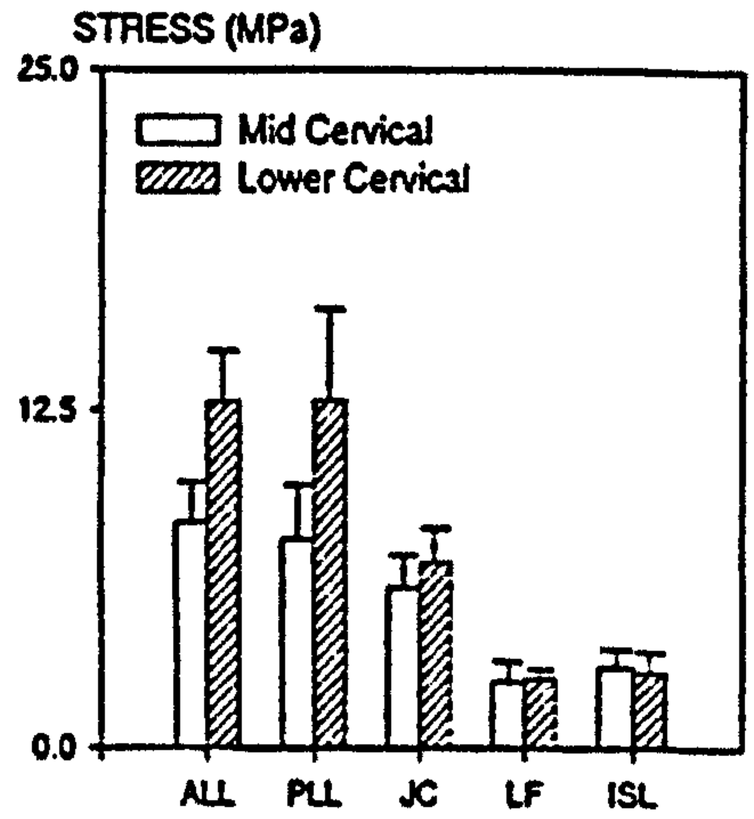

Figure 2.31 Failure stress of the ligaments (Yoganandan et al., 1999)

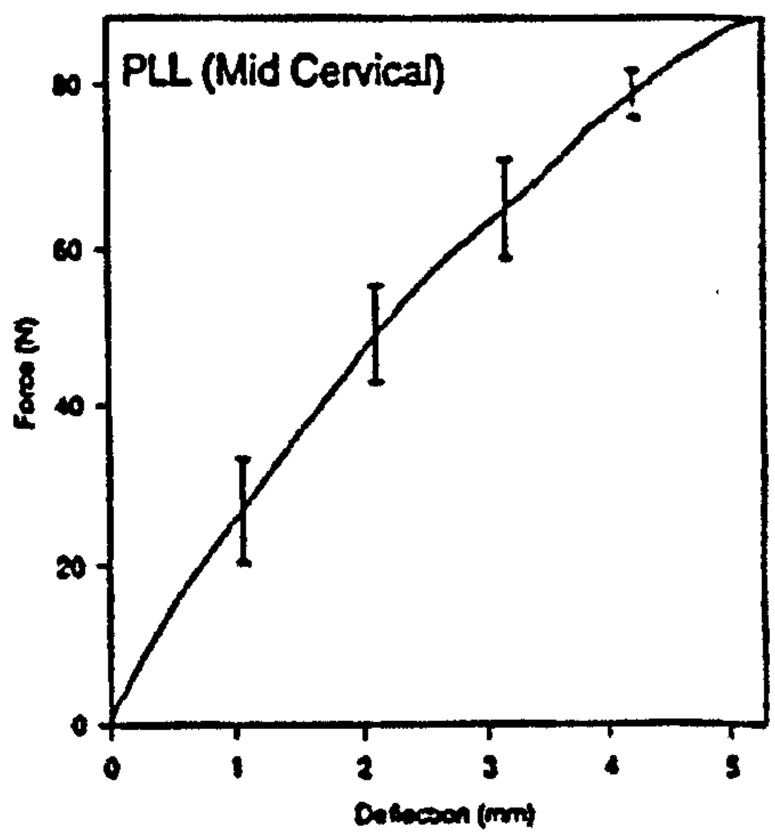

Figure 2.32 Force-deformation properties of the PLL (Yoganandan et al., 1999)

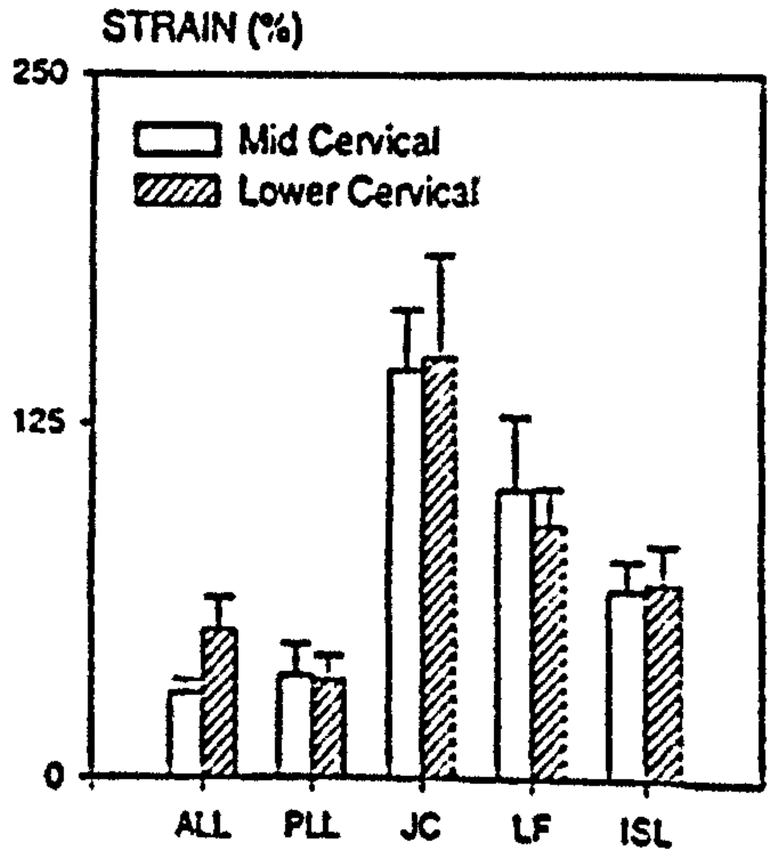

Figure 2.33 Failure strain of the ligaments (Yoganandan et al., 1999)

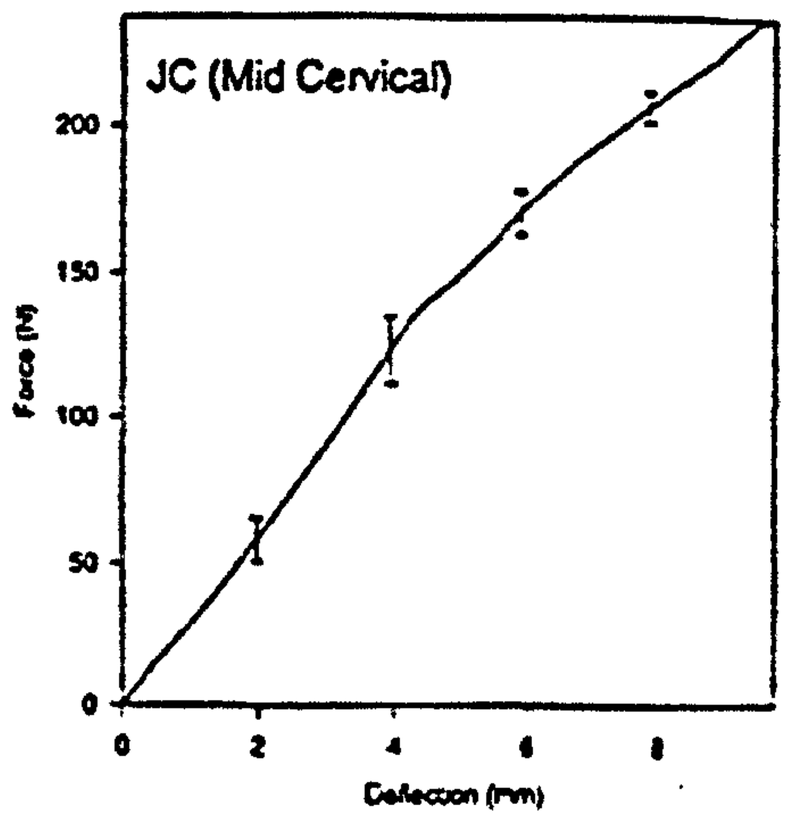

Figure 2.34 Force-deformation properties of the JC (Yoganandan et al., 1999)

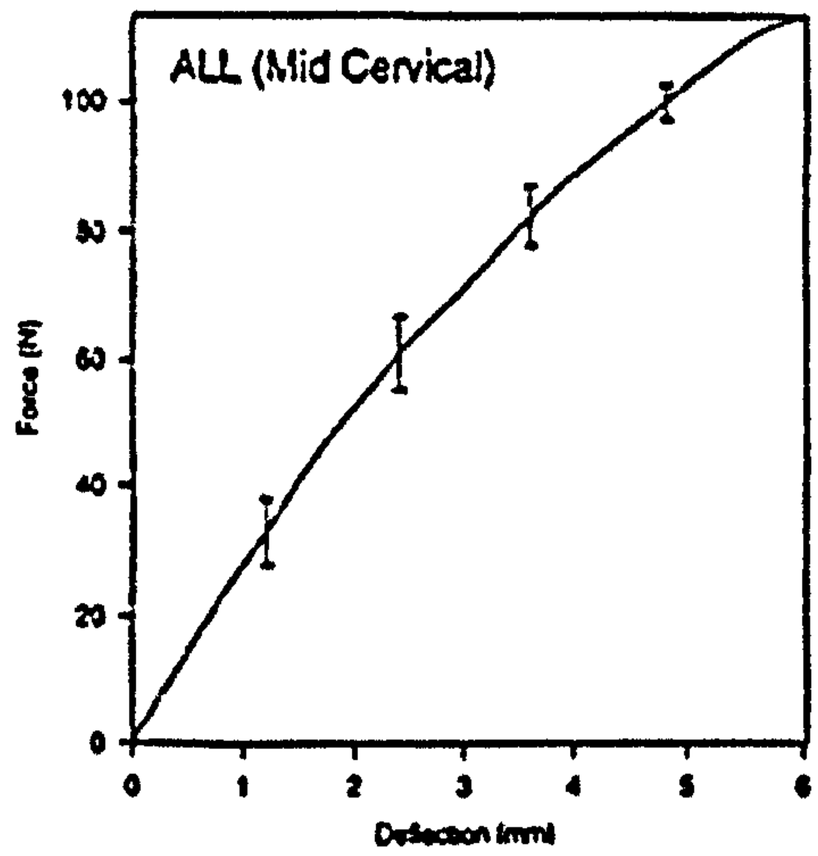

Figure 2.35 Force-deformation properties of the ALL (Yoganandan et al., 1999)

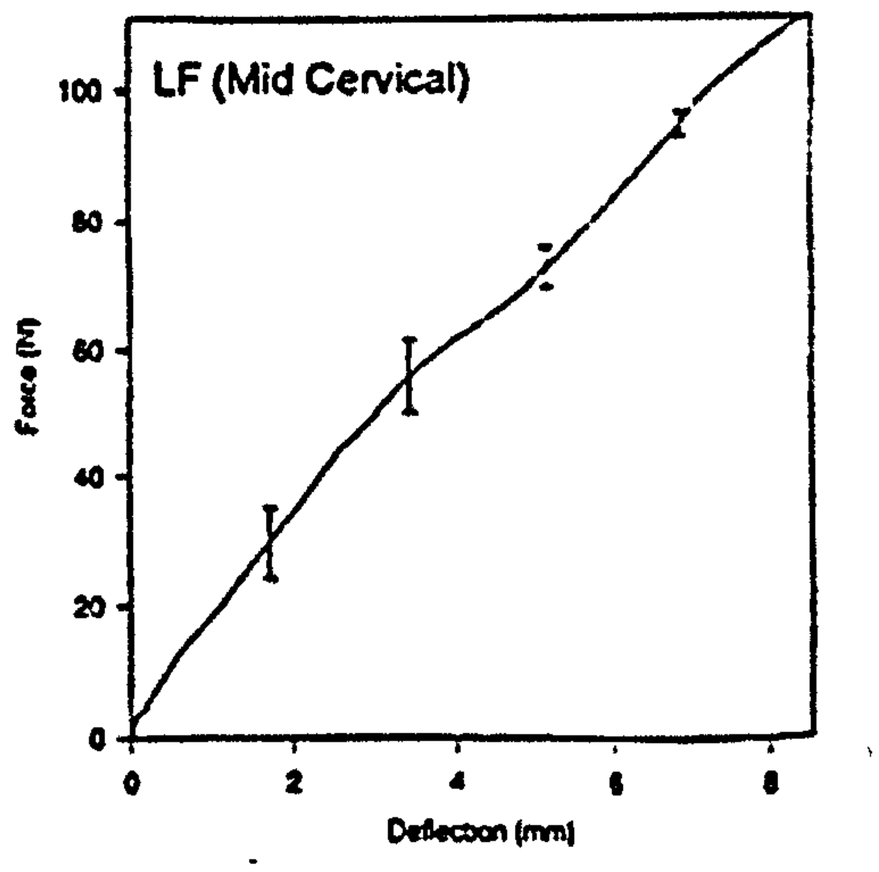

Figure 2.36 Force-deformation properties of the LF (Yoganandan et al., 1999)

Cusick and Yoganandan (2002) investigated biomechanics of the cervical spine by means of major injuries, where the authors discussed several external and human-related variables including force vectors responsible for injury causation, as well as potential influences of loading rate, gender, age and type of injury. Nightingale et al. (2002) concluded in their study that the upper cervical spine was significantly stronger than the lower cervical spine in extension. Frobin et al. (2002a, 2002b) investigated the kinematics of the cervical spine developing a new protocol which determines rotational and translational motion for all segments of the cervical spine imaged on the radiographic views.

2.3.2 The Thoracic Spine

The range of sagittal plane rotation (flexion/extension) for the thoracic spine is provided in Table 2.5. The median figure is 4° of motion in the upper portion of the thoracic spine and 6° of motion in the middle segments. In the lower portion (T11-12 and T12-L1), there are 12° of motion at each segment. In the frontal plane (lateral bending) there are 6° of motion in the upper thoracic spine, with 8° or 9° in the two lower segments. In the horizontal plane (axial rotation) there are 8-9° of motion in the upper half of the thoracic spine and 2° for each interspace of the three lower segments. Here, the values for axial rotation correspond somewhat with the in vivo findings of Gregersen and Lucas (In: White and Panjabi, 1990), who investigated axial rotation in some thoracic spines by inserting Steinmann pins into the spinous processes. They observed an average of 6° of rotation at each level, and when their subjects were walking the maximum amount of rotation was noticed at the middle portion of the thoracic spine. Figures for each interspace are given in Table 2.5.

The route of motion in the sagittal plane for the thoracic spine is somewhat analogous to that in the cervical spine. In identifying the patterns of cervical spine motion, the T angle, or "top angle," was employed to indicate the acuity of the arch formed by a given point as a vertebra moved in a plane. To calculate thoracic spine motion in the sagittal and frontal planes, the average curvature (the reciprocal of the radius of the arch) is utilized. In sagittal plane motion (flexion/extension), the average curvature is quite small, resulting in a rather

flat arch (Fig. 2.37A). There is no pattern of cephalocaudal variation. The average curvature in the frontal plane is also flat, but nevertheless greater, or steeper, than the arches of the sagittal plane (Fig. 2.37B).

Table 2.5 Rotation ranges for the thoracic spine (White and Panjabi, 1990)

Level	**Combined Flexion/Extension (±x-axis rotation)**		**One Side Lateral Bending (z-axis rotation)**		**One Side Axial Rotation (y-axis rotation)**	
	Limits of Ranges (deg)	Representative Angle (deg)	Limits of Ranges (deg)	Representative Angle (deg)	Limits of Ranges (deg)	Representative Angle (deg)
T1-T2	3-5	4	5	5	14	9
T2-T3	3-5	4	5-7	6	4-12	8
T3-T4	2-5	4	3-7	5	5-11	8
T4-T5	2-5	4	5-6	6	5-11	8
T5-T6	3-5	4	5-6	6	5-11	8
T6-T7	2-7	5	6	6	4-11	7
T7-T8	3-8	6	3-8	6	4-11	7
T8-T9	3-8	6	4-7	6	5-7	6
T9-T10	3-8	6	4-7	6	3-5	4
T10-T11	4-14	9	3-10	7	2-3	2
T11-T12	6-20	12	4-13	9	2-3	2
T12-L1	6-20	12	5-10	8	2-3	2

There are a number of different coupling methods. Of most interest at present in both the cervical and thoracic spines is coupling between lateral bending and axial rotation. Significant interest in the thoracic spine is due to the normal coupling and abnormal coupling in scoliotic deformities (White and Panjabi, 1990).

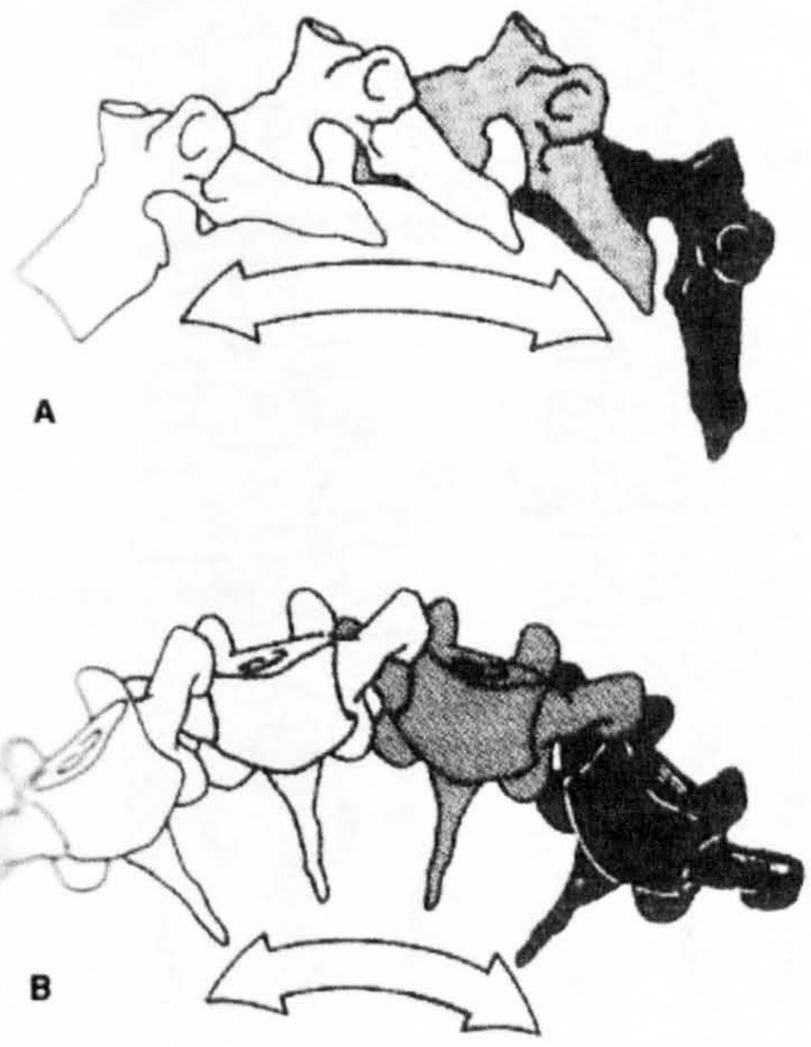

Figure 2.37 A schematic representation of the relative variations in the radii of curvature of the arches of the thoracic vertebrae (A) Flexion/extension (B) Lateral bending (White and Panjabi, 1990)

There has been relatively more interest in the coupling of axial rotation and lateral bending, which is mainly due to its relevance in the etiology, evaluation, and treatment of scoliosis. This coupling is also crucial in the mechanisms of injury in the cervical spine. Abnormal coupling patterns have been examined and analyzed to search for possible evidence of instability. Changes in coupling patterns have also been related to spinal fusions. Figure 2.38 demonstrates the coupling of lateral bending and axial rotation, describing the new biomechanical subdivisions of the spine.

The approximate locations of instantaneous axis of rotation centers for the thoracic spine are represented diagrammatically in Figure 2.39.

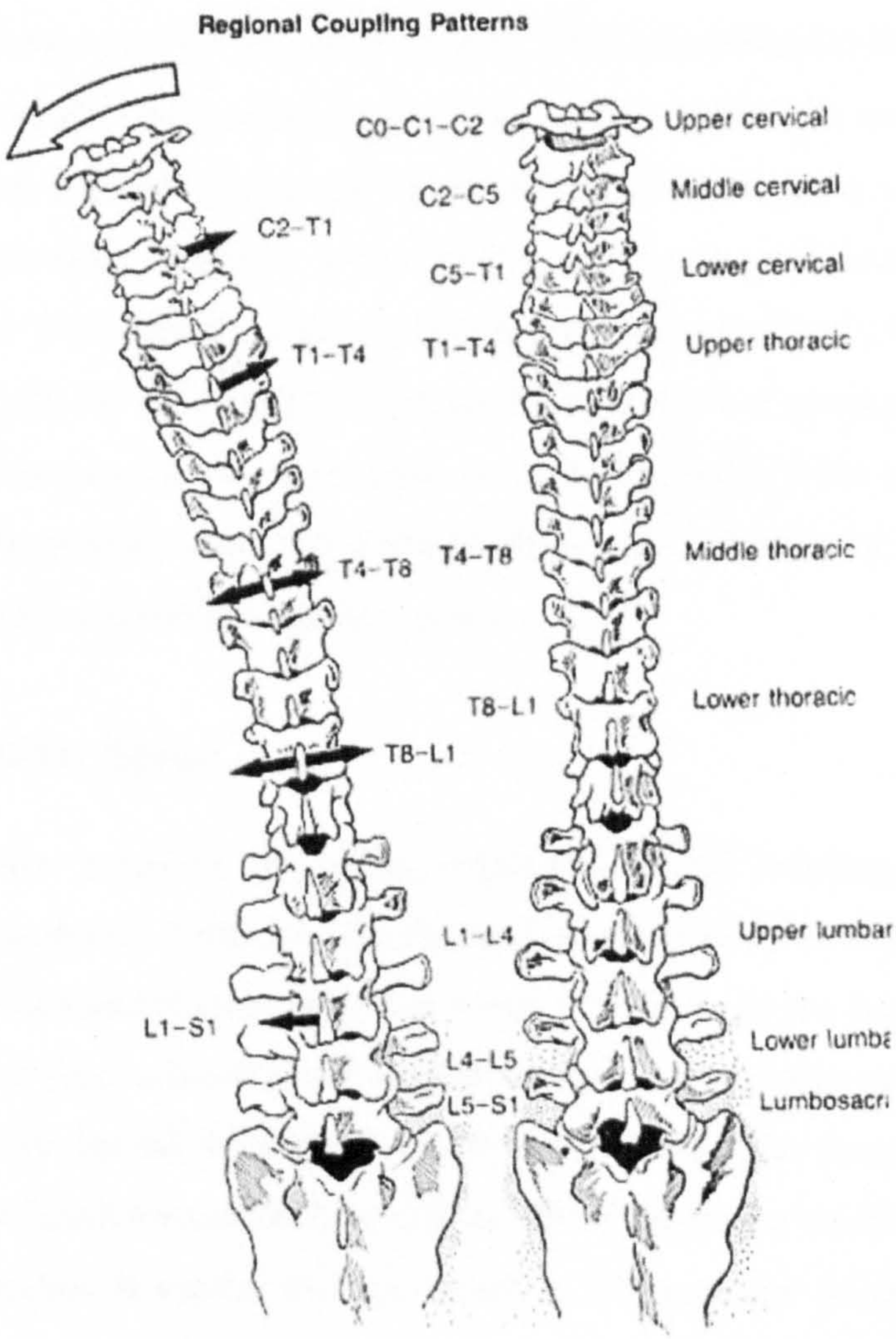

Figure 2.38 Coupling of lateral bending and axial rotation (White and Panjabi, 1990)

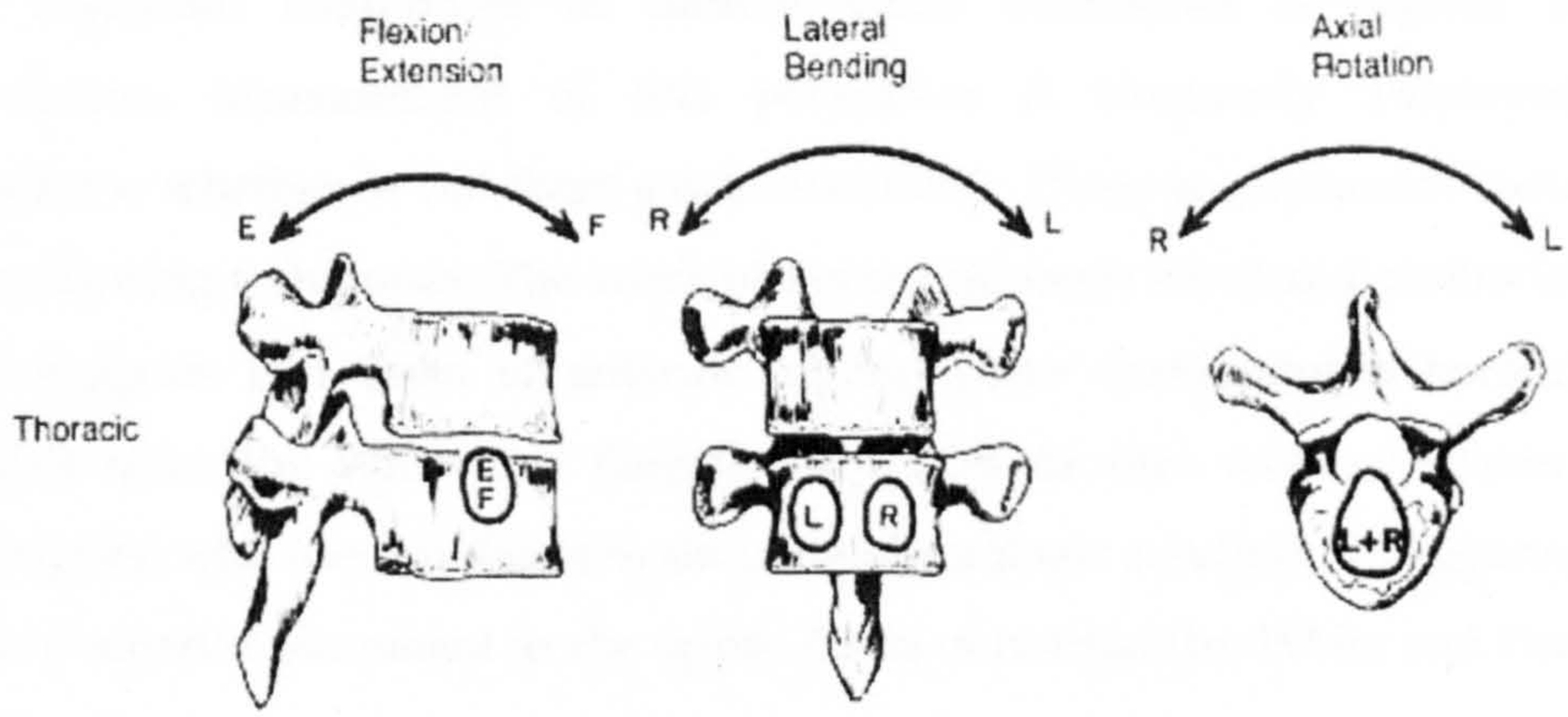

Figure 2.39 The approximate locations for IAR in the thoracic spine (White and Panjabi, 1990)

Kopperdahl and Keaveny (1999) and Yeni et al. (2001) investigated the vertebral bodies in the thoracic and lumbar regions by means of strength and stiffness. Gavin et al. (1999) developed a geometric model of a scoliotic spine to reveal the geometric relationship between post-correction thoracic and lumbar curve magnitudes and their effect on post-correction decompensation in idiopathic scoliosis. Bereznick et al. (2002) investigated the frictional properties at the thoracic skin-facia interface to determine the reaction forces from the thoracic vertebra to the overlying skin. The authors observed negligible friction, which results in relatively reasonable reaction forces.

2.3.3 The Lumbar Spine

The representative rotations in flexion/extension, lateral bending, and axial rotation are presented in Table 2.6 and Figure 2.40. In flexion/extension there is generally a cephalocaudal increase in the range of motion in the lumbar spine. The lumbosacral joint allows more sagittal plane motion than do the other lumbar joints. For lateral bending, each level is almost the same, with the exception of the lumbosacral joint, which exhibit a relatively small amount of motion. The situation is similar for axial rotation. It is sensible to claim that the high incidence of clinically evident disc disease at L4-L5 and L5-S1 may be related to mechanics. These two areas bear the highest loads and tend to sustain the most motion in the sagittal plane.

An important component of lumbar spine kinematics is sagittal plane translation. Measurement of this parameter is frequently employed to determine whether or not there exists instability. There is substantial variation in measuring techniques. The work of Pearcy depends on sound methodology and suggests that 2mm of anterior sagittal plane translation is normal for lumbar spine (In: White and Panjabi, 1990). The in vitro work of Posner and colleagues, who used preloads to simulate physiologic conditions, suggested 2.8 mm of anterior placement as the upper limits of normal (In: White and Panjabi, 1990).

Table 2.6 Rotation ranges for the lumbar spine (White and Panjabi, 1990)

	Combined Flexion/Extension (±x-axis rotation)		**One Side Lateral Bending (z-axis rotation)**		**One Side Axial Rotation (y-axis rotation)**	
Level	Limits of Ranges (deg)	Representative Angle (deg)	Limits of Ranges (deg)	Representative Angle (deg)	Limits of Ranges (deg)	Representative Angle (deg)
L1-L2	5-16	12	3-8	6	1-3	2
L2-L3	8-18	14	3-10	6	1-3	2
L3-L4	6-17	15	4-12	8	1-3	2
L4-L5	9-21	16	3-9	6	1-3	2
L5-S1	10-24	17	2-6	3	0-2	1

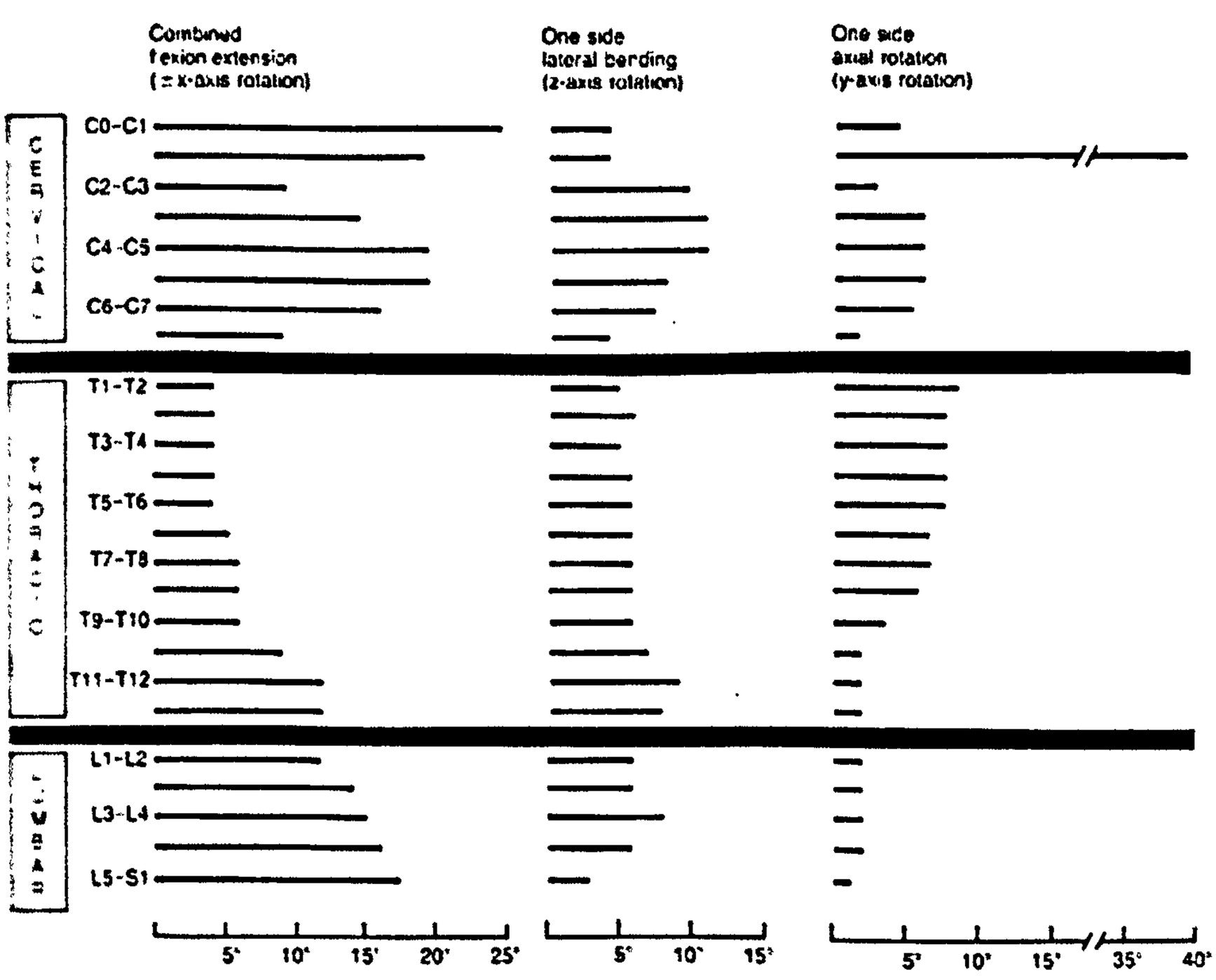

Figure 2.40 Values for rotational ranges of motion for different ranges of the spine (White and Panjabi, 1990)

Traditionally, coupling of axial rotation and lateral bending are regarded as reciprocal. In other words, if the spine is bent laterally and the associated axial rotation is measured, then the ratio between axial rotation and lateral bending would be the same as if the spine is rotated and the lateral bending is measured. Recent experiments have revealed that this assumption is not true, at least in the lumbar spine.

Tan et al. (2001) investigated the quantitative three-dimensional anatomy of lumbar vertebrae L1-L5 from Asian (Singaporean) subjects based on 60 lumbar vertebrae from 12 cadavers. The purpose of the study was to measure the dimensions of the various aspects of the lumbar vertebrae and then to compare the data with a study performed on Caucasian specimens, provided by Panjabi et al. (1982). Measurements had been carried out with the aid of a three-dimensional digitiser. Several parameters of the lumbar spine are provided in Figures 2.41-46.

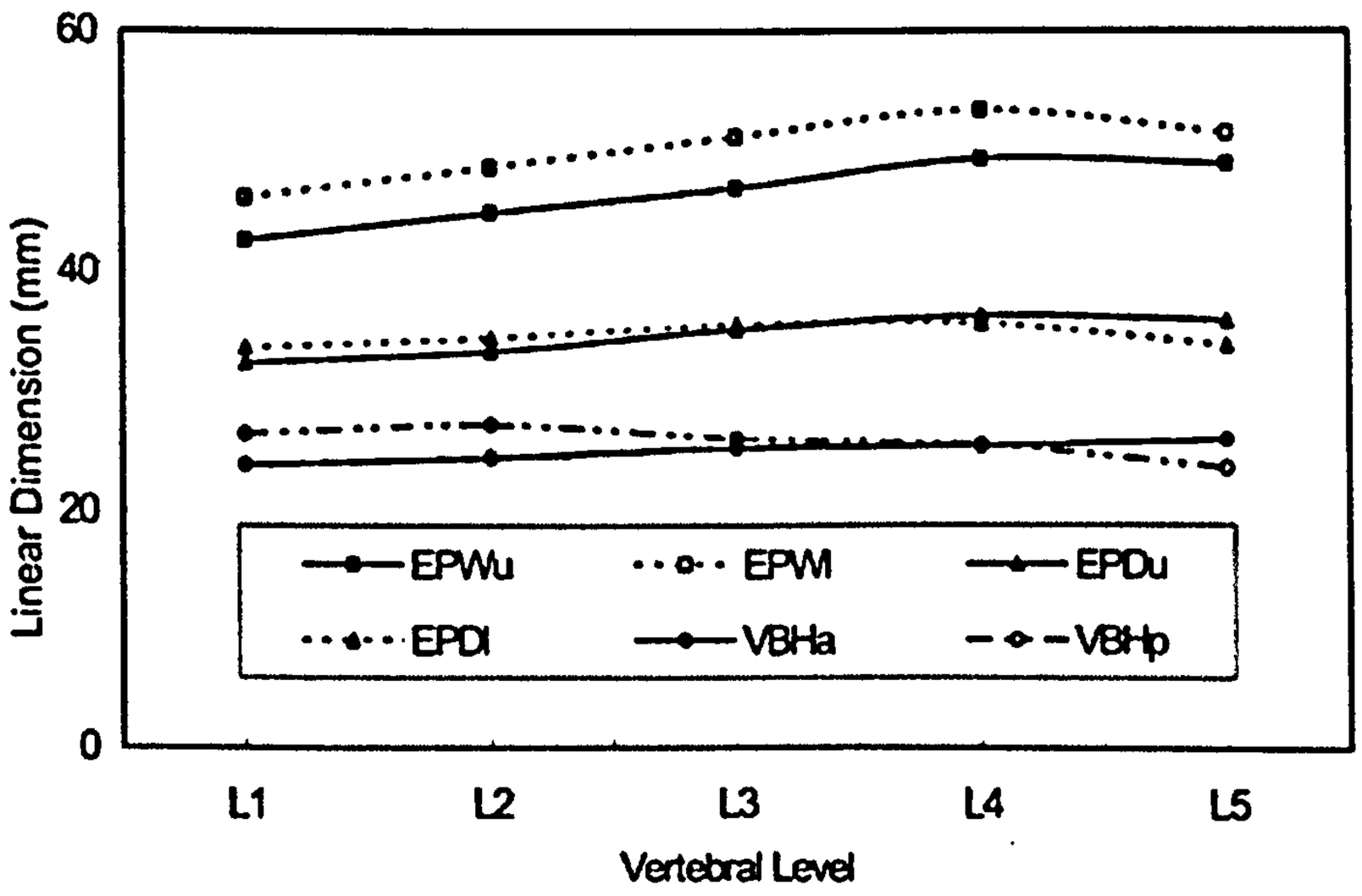

Figure 2.41 Linear dimensions of vertebral body as functions of vertebral levels L1-L5. The linear dimensions are the upper (*u*) and lower (*l*) end-plates width (*EPW*) and depth (*EPD*), anterior (*a*) and posterior (*p*) vertebral body height (*VBH*) (Tan et al., 2001)

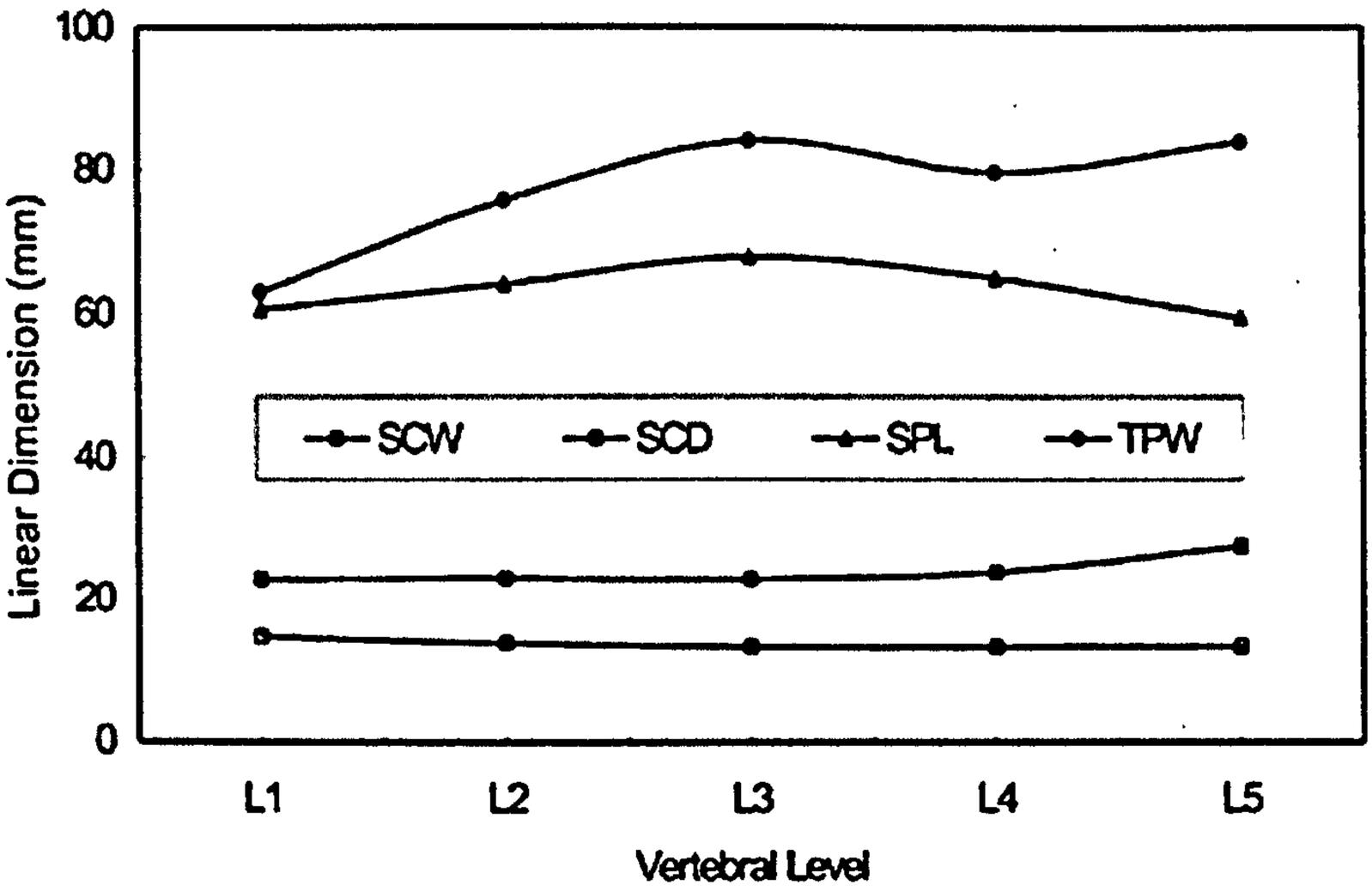

Figure 2.42 Linear dimensions of spinal canal, spinous process and transverse process as functions of vertebral levels L1-L5. The linear dimensions are the spinal canal width (*SCW*) and depth (*SCD*), spinous process length (*SPL*) and transverse process width (*TPW*) (Tan et al., 2001)

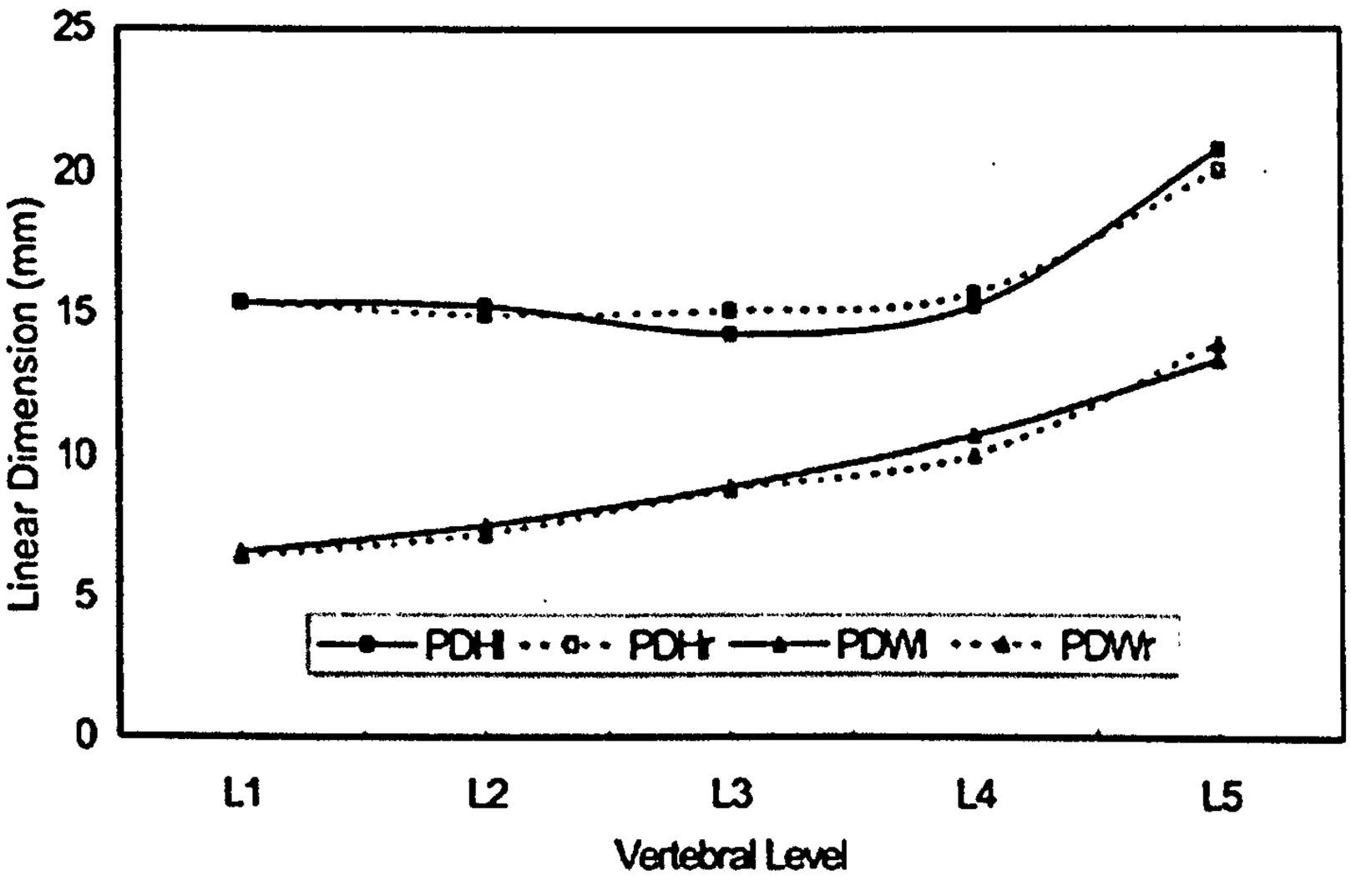

Figure 2.43 Linear dimensions of pedicles as functions of vertebral levels L1-L5. The linear dimensions are the left (*l*) and right (*r*) pedicle height (*PDH*) and width (*PDW*) (Tan et al., 2001)

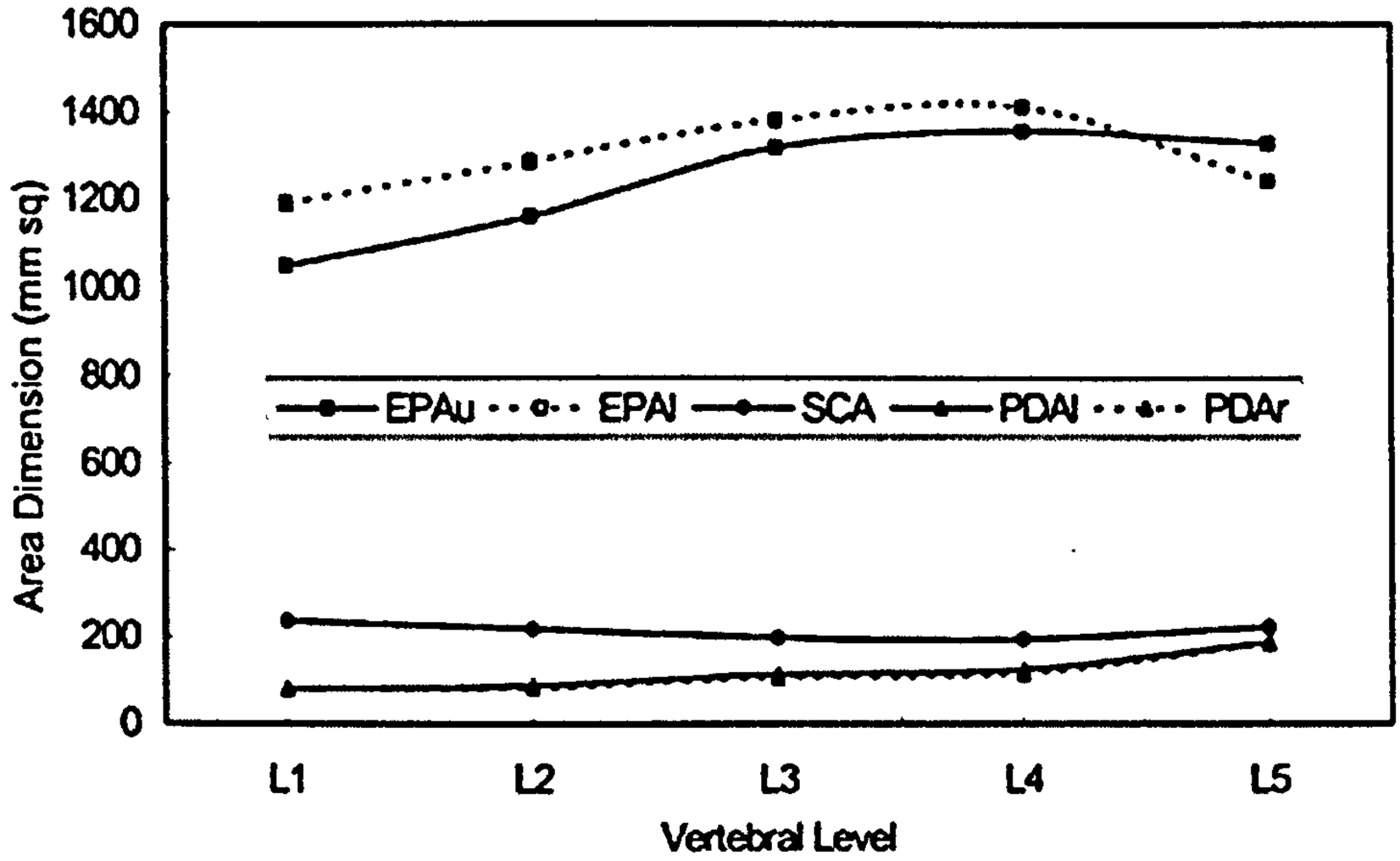

Figure 2.44 Areas of end-plates, spinal canal and pedicles as functions of vertebral levels L1-L5. The areas are the upper (*u*) and lower (*l*) end-plates (*EPA*), spinal canal (*SCA*), left (*l*) and right (*r*) pedicle (*PDA*) (Tan et al., 2001)

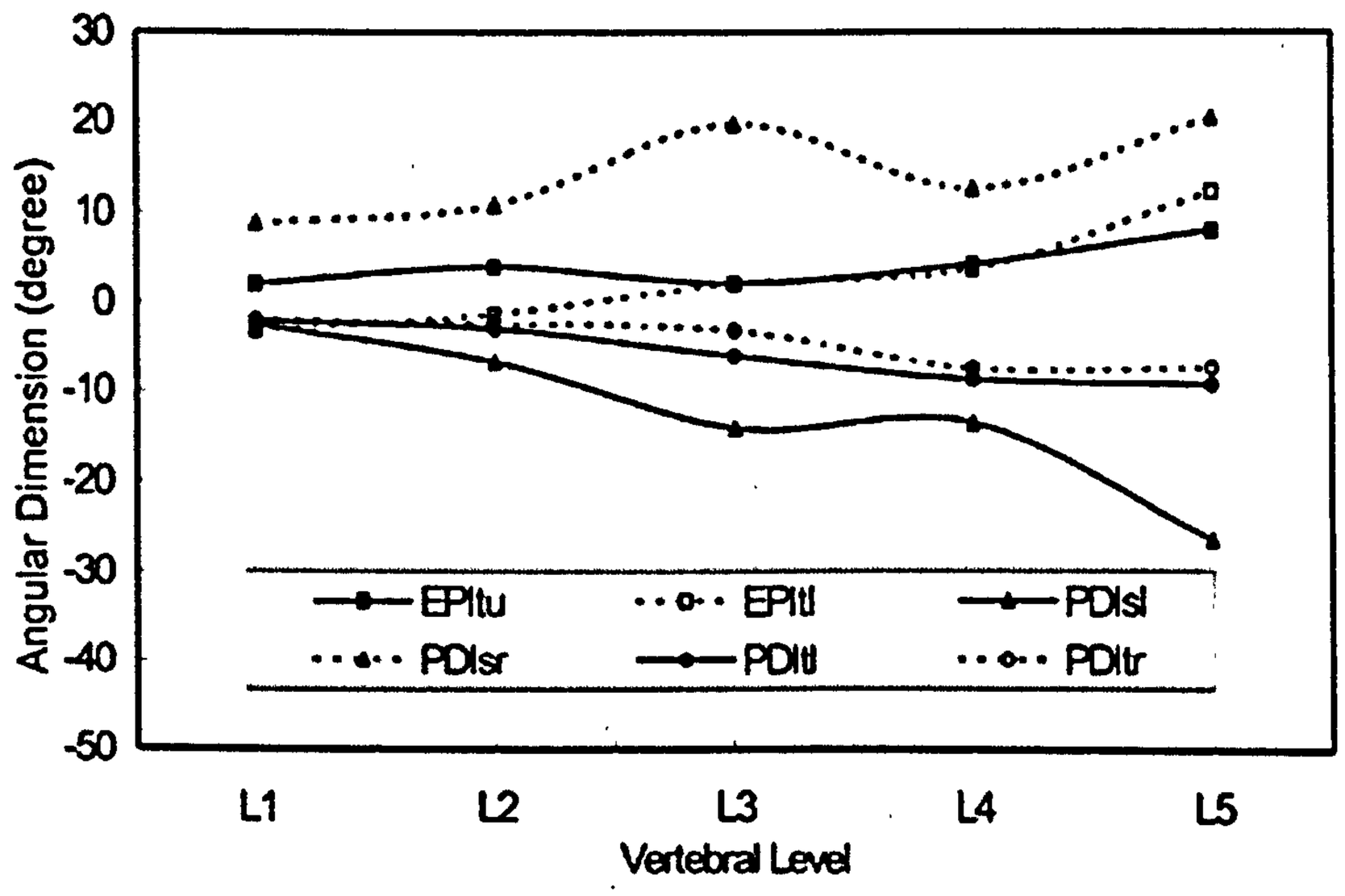

Figure 2.45 Angular dimensions of end-plates and pedicles as functions of vertebral levels L1-L5. The angles are the upper (*u*) and lower (l) end-plates, transverse inclinations (*EPI*), and left (*l*) and right (*r*) pedicles, sagittal and transverse inclinations (*PDI*) (Tan et al., 2001)

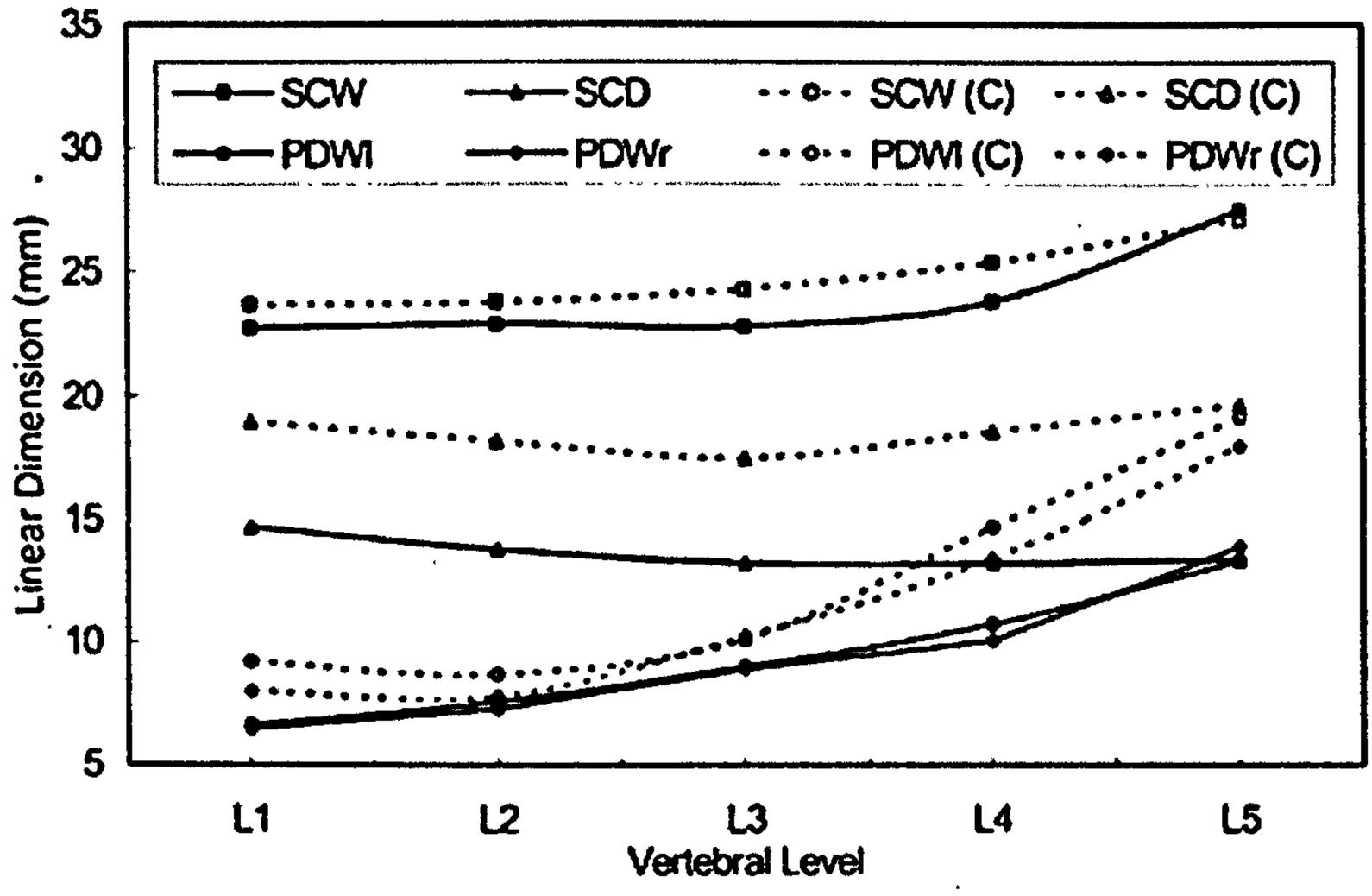

Figure 2.46 Comparison of selected linear dimensions of present study with that of Panjabi (1982). The results from the latter are represented by C. The linear dimensions are the spinal canal width (SCW) and depth (SCD) and left (l) and right (r) pedicle width (PDW) (Tan et al., 2001)

There are several studies on several aspects of the lumbar spine in the literature.

Patwardhan et al. (1999) investigated the possibility of a compressive follower load applied to the lumbar spine to minimize bending moments and shear forces and allow it to bear large compressive loads without damage or instability. The authors concluded that a 1200 N compressive preload increased the stiffness of the spine and caused the load-displacement behaviour to approach a more linear pattern in the flexion and extension segments.

Overaker et al. (1999) developed a 3-D physiologically realistic model of a lumbar vertebral body which includes a nonlinear foam model for the trabecular bone component. The authors demonstrated the effects of localized yield under compressive loads on the whole bone mechanical response. Similarly, Xinghua et al. (2002) proposed a high-order nonlinear equation of bone remodelling to incorporate with FEM by introducing two nonlinearities; remodeling coefficient, and the order of nonlinear remodeling equation.

Goh et al. (1999) investigated the extent to which cylindrical cages of progressively larger sizes can provide stability to the lumbar spine with its facets entirely removed for bilateral posterior lumbar interbody fusion. Doehring et al. (1999) presented a testing system that uses a hybrid control

algorithm for delineating the load-displacement characteristics osteoligamentous lumbar spine specimens.

Schibye et al. (2001) presented the mechanical load on the low back and shoulders during pushing and pulling a two wheeled container with the load during lifting and carrying the same amount of waste. The authors submitted the compression force at L4-L5 during pushing and pulling as 605-1445 N and claimed that no relation exists between the size of the external force and the torque at the low back and the shoulder. Similarly, some other studies had been carried out by Vogt et al. (2002), Essendrop et al. (2002), and Sakamoto et al. (1999) on kinematics and treatment of lumbar spine.

2.3.4 The Sacroiliac Region

Relatively little is known about the kinematics of this important set of articulations. This is the link through which the weight of the trunk is transmitted to the legs and a region in which the patient will often complain of localized back pain.

The sacroiliac joint is partly synovial and partly syndesmotic. It may be completely ankylosed in as much as 76% of subjects over 50 years of age. This fact makes the kinematic study of the joint a moot issue for a significant portion of the population. However, for many others these are rather stiff joints whose overall motion and stability depend largely upon the coarseness of the interdigitating articular surfaces (White and Panjabi, 1990).

Miller and colleagues investigated the kinematics of the sacroiliac region in eight fresh cadaver specimens aged 59-74. The joints were loaded, and displacements of the sacrum were measured in relation to one or both ilia. The key kinematics findings are illustrated in Figure 2.47. Lateral (x-axis) translation was measured at 0.76 mm (standard deviation [SD] 1.41), and anterior (+z-axis) translation was observed to average 2.74 mm (SD 1.07). Lateral rotation to one side (z-axis) averaged 1.40° (SD 0.71), and axial rotation (y-axis) in one direction was 6.21° (SD 3.29). These specimens may show relatively less motion as they were in older age group (White and Panjabi, 1990).

Swartz et al. (1991) investigated physical and mechanical properties of calf lumbosacral trabecular bone and concluded that calf spine is a good model of the young non-osteoporotic human spine.

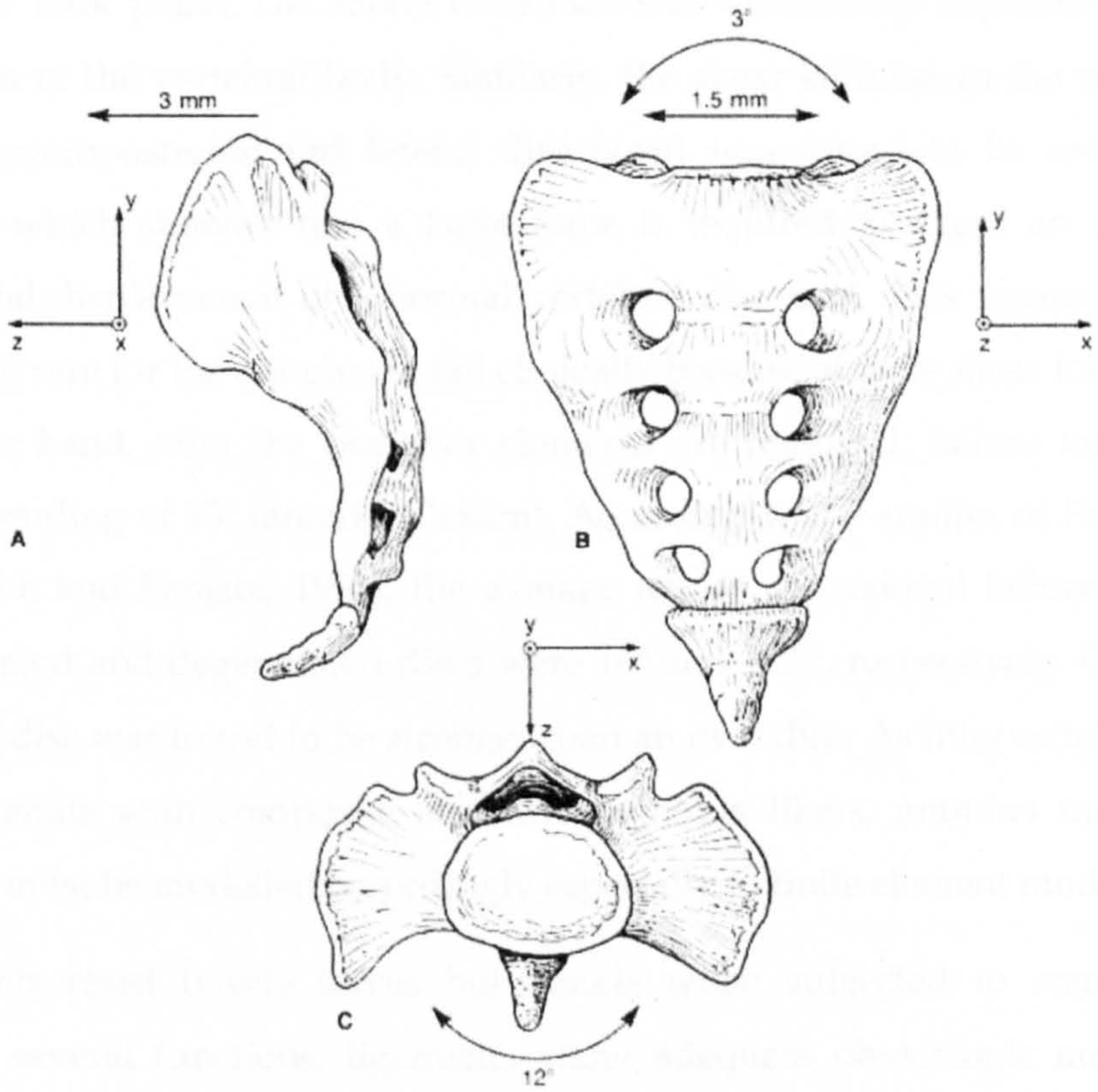

Figure 2.47 Representative kinematics of the sacrum (A) 3mm anterior translation (B) Representative z-axis rotation of a total 3° (C) Representative y-axis rotation of 12°, totally (White and Panjabi, 1990)

2.4 Discussion

This section covered an introduction to the biomechanically essential parts of the human spine, namely; intervertebral disc, ligaments, muscles, and vertebrae. Following the subsections regarding the components, biomechanics of the segments of the human spine were presented in order to establish a background on the kinetics and kinematics of the human spine regions.

The intervertebral disc carries all of the compressive loading the trunk is subjected to. Therefore, the intervertebral discs are the main responsible element for supporting the forces and moments acting on the spine. As they possess viscoelastic and anisotropic behaviour, the mechanical tests should be

carried out at relatively slow loading rates in order to minimize the viscoelastic effects. As a result of the compression test, it was found that the first component to fail was the vertebra, because of fracture of the end-plates. No failure of the disc ever took place. The mode of failure was exclusively dependent on the condition of the vertebral body. Similarly, the shear stiffness in the transverse plane (anteroposterior and lateral directions) was found to be around 260 N/mm, which showed that a large force is required to cause an abnormal horizontal displacement of a normal vertebral disc unit. This means that it is relatively rare for the annulus to fail clinically because of pure shear loading. On the other hand, after the posterior elements are removed, failure takes place with a bending of 15° (anterior flexion). According to the studies of Farfan et al (In: White and Panjabi, 1990), the average angles at torsional failure for non-degenerated and degenerated discs were 16° and 14.5°, respectively. Generally, a round disc was found to be stronger than an oval disc. As intervertebral discs are materials with composite structure; annulus fibers, annulus matrix and nucleus must be modelled accordingly especially in finite element modelling.

Ligaments resist tensile forces but buckle when subjected to compression. Having several functions, ligaments allow adequate physiologic motion and fixed postural attitudes between vertebrae, with a minimum expenditure of muscle energy, while protecting the spinal cord by restricting the motions within well-defined limits. They also contribute to the mechanical stability of the spine. In highly dynamic situations such as impacts, large amounts of energy suddenly applied to the spine are absorbed partially via ligaments. In vitro experiments showed that under slow and fast extension rates, the ligaments possessed rate dependent behaviour, and thus, viscoelasticity.

Although there are different joint coordinate system suggestions in the literature, a different coordinate axis system was used throughout this thesis due to various conveniences within the computational software, as based on van Lopik (2004) studies (Fig. 2.18).

Without muscles, spine is a completely unstable structure with its ligaments intact. The muscles not only provide stability to the trunk in a given posture, but also produce movements during physiologic activity, while protecting the

spine during trauma, in which there is time for voluntary control, and possibly in the postinjury phase. The modified Hill's model is the most common approach to model a muscle group, which includes the passive behaviour of the muscle as well as the active one via a contractile series element. Recent research revealed that spine stability depends on the relative activation of all trunk muscles and other loading variables. Therefore, incorporating muscles into computational models with passive and active properties is of fundamental importance.

This chapter also reviewed the types and ranges of motion of spinal segments. All spinal elements as discs, ligaments, muscles and vertebrae contribute to the spinal stability and determine the limits of motion. Cusick and Yoganandan (2002) investigated biomechanics of the cervical spine by means of major injuries, where several external and human-related variables such as force vectors responsible for injury causation, loading rate, gender, age and type of injury were found to be related.

There are various biomechanical aspects of the human spine as described in this chapter that are significant and essential for the computational modelling. One of them is the geometrical differences between vertebrae, which affect the overall kinematics of the cervical spine. Therefore, utmost attention was given to reflect the critical dimensions of the vertebrae, while developing the solid bodies of the models. Important coupling characteristics of the spine segments were discussed highlighting the importance of the facet joints. The facet joints can be assumed to be very stiff in compression and resistance to load of the facet capsule in other directions than compression is provided by the surrounding capsular ligaments. The in-vivo kinematic range of motion in all rotational directions for all motion segments of the spine are of fundamental importance, which can be utilised for validation purposes. Also, static properties of the spine ligaments and discs are provided with load-deformation characteristics defined. Generally, there is a lack of dynamic data for the response of the soft tissues and motion segments in the literature.

CHAPTER 3

Computational Models of the Human Spine

3.1 Introduction

This chapter reviews and attempts to comprehend the classifications of the computational human spine models and the reasoning behind the need for them. The assessment of all types of models constituted the initial steps of the present study and not only led to developing hybrid approaches for the previously addressed dynamic loading conditions the human spine is subjected to, but also formed the basis for the methodologies employed in developing the models. Hence, this chapter includes a comprehensive review of the classifications of human spine models as well as a broad literature survey on numerous prominent models developed. The final classification approach used in this thesis serves for understanding the mainstream of spinal modelling and helps to demonstrate the rapid developments and improvements within each methodology.

Maquet's review, Iatrophysics to Biomechanics (1992), reports that biomechanical modelling of the human spine and investigating the effects of spinal loadings date back to the 17th century. One of the first biomechanists, Borelli (1989), predicted the forces required by muscles to carry a load via an early model of the spine by employing a mechanical theory (Fig. 3.1). Various early investigators contributed to these efforts such as Weber and Weber (1992), who analysed kinematics of the movement, and Braune and Fisher (1985, 1988), who investigated the effects of centre of mass and radii of inertia via developing methods in order to observe the kinetics of movement. Early attempts as such

established the basis for contemporary biomechanical studies of the human body, and consequently, the human spine.

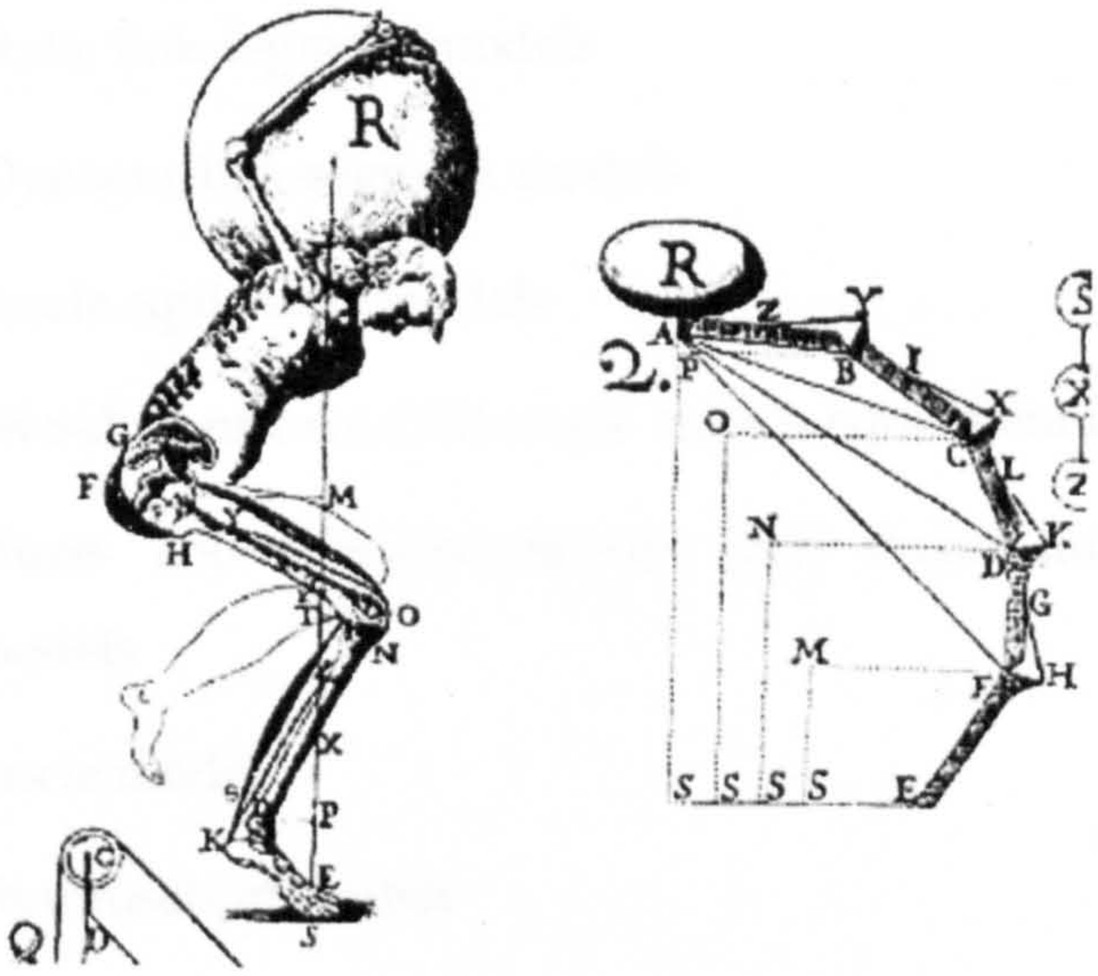

Figure 3.1 Spine model of Borelli (1989)

3.2 Computational Human Spine Model Classifications

Reeves and Cholewicki (2003) highlighted the fact that the single most important mechanical function of the spine is to support loads that arise from the interaction between external loads and muscular forces. Due to this function, trunk muscles with their relatively small moment arms in relation to external forces contribute significantly to loading across intervertebral joints, while challenging both tissue and structural tolerance of the spine. Therefore, they concluded that knowledge of loads sustained by the spine and its stability during physical activity is necessary for a more rational design of spine injury prevention strategies and rehabilitation programs, and consequently, the estimate of injury risk in a wide variety of tasks is only possible through biomechanical modelling. In their extensive review, they introduced a detailed classification of computational human spine modelling.

Reeves and Cholewicki (2003) classified spine models according to *levels of analysis* into two: *equilibrium-based models* and *stability-based models*. Consequently, the two main groups of *equilibrium-based models* and *stability-based models* were categorised into several subgroups.

Equilibrium-based models are:

- Link-segment models
    - Static link-segment models
    - Dynamic link-segment models
- Single muscle equivalent models
    - Two-dimensional (2D) single muscle equivalent models
    - Three- and four-dimensional (2D) single muscle equivalent models
- Multi muscle models
    - Optimisation models
    - EMG-assisted models
        - EMG-assisted optimisation (EMGAO)
        - EMG normalisation
    - Neural Network and Stochastic Models
- Finite Element (FE) Models

Stability-based models can basically be grouped as follows:

- Simple inverted pendulum models
- Multi-segment models
- Motor control and spinal stability based models

Equilibrium-based models employ the principles of mechanical equilibrium in order to estimate spinal loads, and therefore provide insight into the degree of loading sustained by various spinal tissues. Reeves and Cholewicki (2003) defined this process with a two-step approach; first one being the moment calculations using link-segment models (LSM), and secondly the estimation of joint reaction forces by using anatomical models of the spine. They defined mechanical equilibrium as a system in a state of balance between opposing forces and moments. The basic principles governing equilibrium-based models are based on Newtonian laws.

Stability-based models have been developed following the studies of several researchers such as Lucas and Bresler (1961), and Granata and Orishimo (2001), who have taken the buckling thresholds of the human spine into consideration, failure under which cannot be predicted with an equilibrium-based model under various circumstances.

A comparison to assess the advantages and disadvantages of Reeves and Cholewicki's (2003) classification of spine models is provided in Table 3.1.

Table 3.1 Advantages and disadvantages in spine model classification of Reeves and Cholewicki (2003)

	Equilibrium-based models	Stability-based models
Advantages	Estimation of spinal loading and risk of injury from overload can be evaluated	Injury from subfailure load, which compromises structural tolerance as opposed to tissue tolerance, can be predicted
Disadvantages	Injury from subfailure load cannot be predicted, which can compromise spinal stability	Current models are limited to static conditions and conservative systems

In this thesis, computational human spine models are categorised into four groups according to the modelling technique used. These groups are:

- Analytical, Geometric, 2 Pivot, and Continuum Models
- Multi-body (MB)/Discrete Parameter Models
- Finite Element (FE) Models
- Hybrid Multi-body/Finite Element Models

In the following sections, all of these groups were investigated thoroughly, reflecting the developments and advances in each category.

3.3 Analytical, Geometric, 2 Pivot, and Continuum Models

Although analytical, geometric, 2 pivot, and continuum models differ from each other with respect to their modelling principles, they are often referred to as

mathematical models and possess significant differences from biomechanical models such as multi-body or finite element models.

When compared to discrete parameter models, continuum models seem to arouse less interest. This is mainly due to a belief that they can not provide a relevant and satisfactory description of the spine because of their simplicity. However, several studies have revealed that a simple continuum model can give a reasonably correct description of the spine under various conditions.

Schultz and Galante (1970) constructed a mathematical model of the human vertebral column, which was idealised as a three-dimensional collection of rigid bodies interconnected by deformable or fixed length elements. The results revealed that this model demonstrated the geometry of three-dimensional motions of the spine in flexion, extension, lateral bending, and axial rotation as compared against *in vivo* studies in the literature.

Lindbeck (1987) employed a static continuum beam model of the human spine, proposed by Hjaimars (In: Lindbeck, 1987), and earlier used by him as a tool for the analysis of mild functional scoliosis, for the study of a spine, asymmetrically loaded in the frontal plane. In this study a mildly scoliotic spine, as observed from X-ray pictures, was investigated by means of a simple anisotropic beam model. In this model the lower part of the vertebral column, including the vertebrae L5-T8, is assumed to be an anisotropic elastic beam built-in at the pelvis. The part of the spine above T8 and segments connected to it are considered as a rigid body. The beam model was assumed an anisotropic constraint providing the beam, like the spine itself, a large resistance against longitudinal compression and a low flexural rigidity. This approach allowed a mathematical treatment without complications from changes in the beam length, when longitudinal forces are applied. A model of the vertebral column, supporting the upper part of the trunk and fixed at the pelvis, as an elastic beam AB supporting a rigid body in B and built-in in a fixed body at A is illustrated in Figure 3.2.

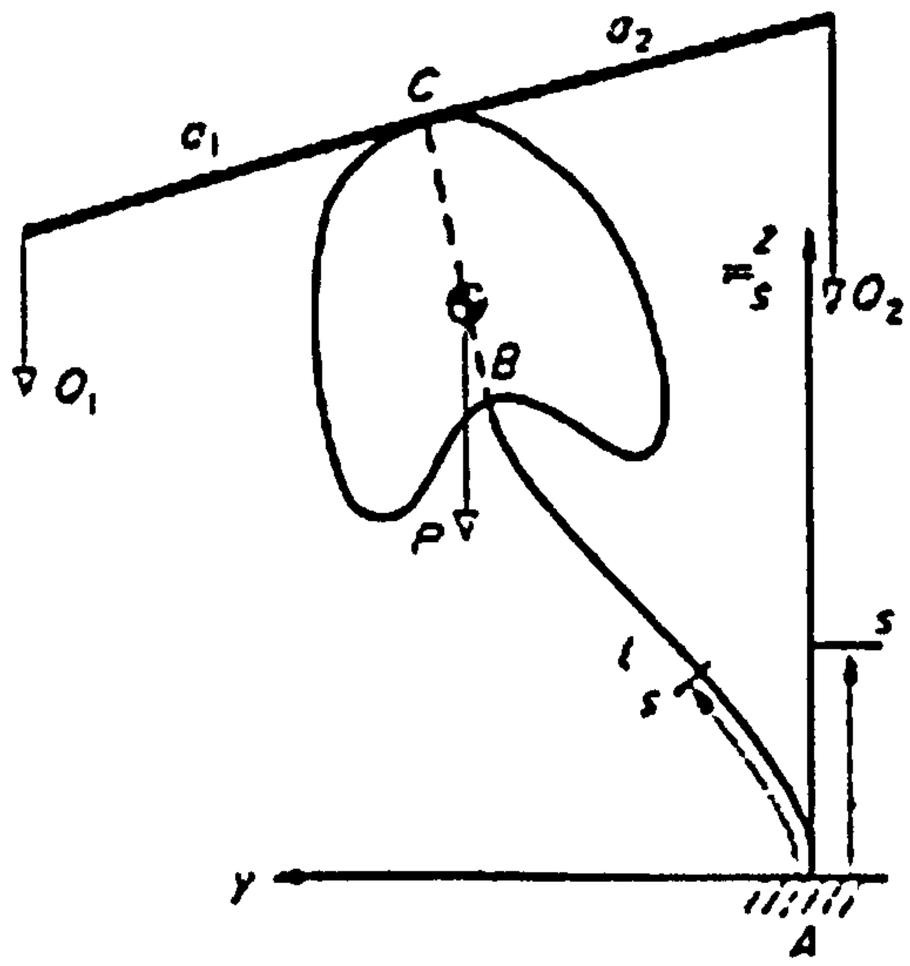

Figure 3.2 Continuum beam model of the spine (Lindbeck, 1987)

Lindbeck concluded that the suggested, very simple, beam model can fairly well predict and reproduce, at least qualitatively, the spinal lateral deflections and curvatures that occur in the frontal plane under muscle relaxation and various external loading conditions.

Aspden (1988) developed a new model, which regards that the spine functions in a similar way to an arch. This model had shown that spinal stresses are not as great as previously calculated using the traditional mathematical models such as cantilever ones and that, even without carrying any external loads; the stress is strongly dependent on posture of the spine. The arch model emphasized that the intra-abdominal pressure acts together with the lumbar lordosis to strengthen the spine.

In their study, Noone et al. (1991) modelled the human scoliotic spine mathematically by using the classical nonlinear curved beam-column theory. The authors incorporated a realistically representative muscle force system. Contraction of a muscle had been simulated by the application of equal and opposite forces to every node pair along the muscle line of action. The beam-column was assumed to be rigidly built in at its inferior end, but free to move without restraint at its superior end. The static model is illustrated in Figure 3.3. The authors concluded that the non-linear continuous beam-column model had its part to play in the study of gross spinal mechanics and with more work it

should be possible to construct a continuous spinal formulation incorporating a variable Young's modulus E and allowing curvature in the sagittal plane as well as axial rotations.

In another study by Monheit and Badler (1991), a kinematic model of the human spine and torso was developed from medical data and heuristics related to human kinesiology in order to establish realistic motions for a human motion model. This human spine model was a collection of vertebrae, connected by ligaments, small muscles, vertebral joints, and intervertebral discs. The model was designed as a black box with an initial state, input parameters, and an output state; using several input parameters such as initiator joint, resistor joint, and spine target position.

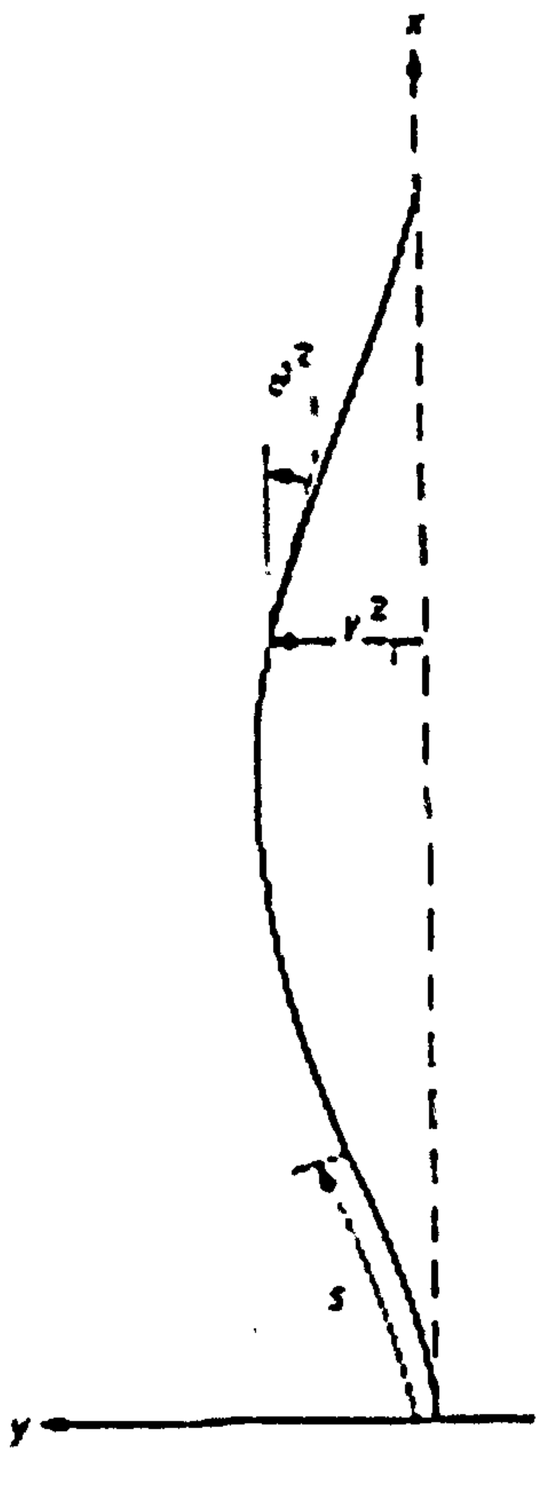

Figure 3.3 Simple cantilever beam model of spine (Noone et al., 1991)

Crisco III and Panjabi (1992) modeled the human ligamentous lumbar spine in the frontal plane as an Euler column for the purpose of rigorously studying its mechanical stability. Their objective was to study not only the buckling load, but also the postbuckling behaviour. Their model of the spine was assumed to

be static and restrained to the frontal plane (Figure 3.4). The vertebral bodies were assumed to be rigid and connected by simple pin joints. A single torsional spring simulated the behaviour of all intersegmental elastic elements in lateral bending. Two versions of the model were formulated. The linear model incorporated constant stiffness torsional springs, while the exponential model incorporated torsional springs with stiffnesses that were linearly proportional to load. After performing the necessary experiments, the authors concluded that, demonstrated to behave as an Euler column, the ligamentous lumbar spine is unstable in lateral bending under loads less than bodyweight.

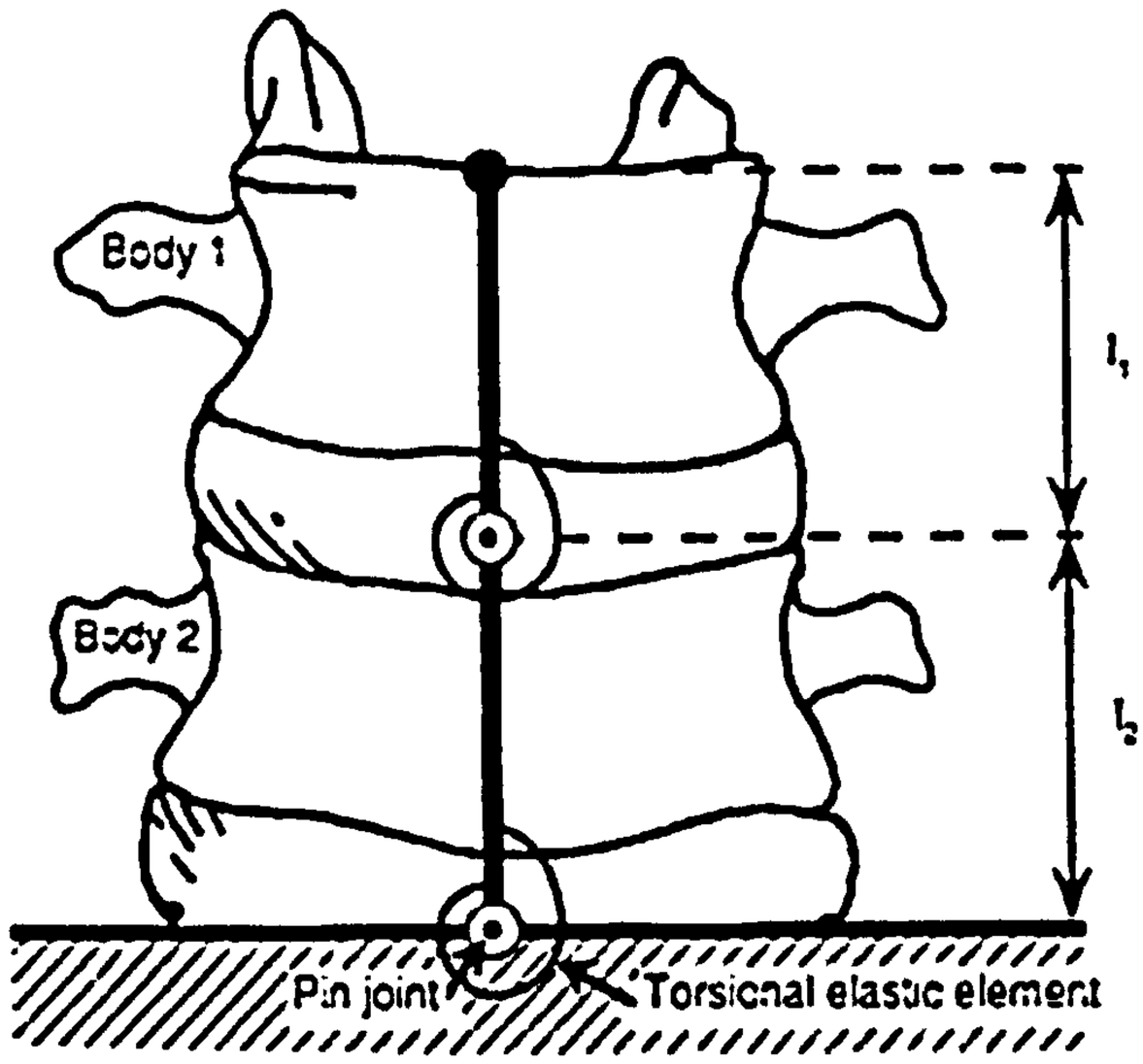

Figure 3.4 Schematic representation of the planar spinal model (Crisco III and Panjabi, 1992)

Case et al. (1999) developed an arch model, which allows for the establishment of a criterion for the failure of the spine with the assumptions that (a) loads are transmitted by compressive forces along the spine, (b) normal compressive forces are lower than the crushing strength of vertebrae and discs and (c) sliding failure cannot occur. The model included the optimization of the thrust line and was validated in comparison to the previous studies in the literature. The loading system of their model is illustrated in Figure 3.5.

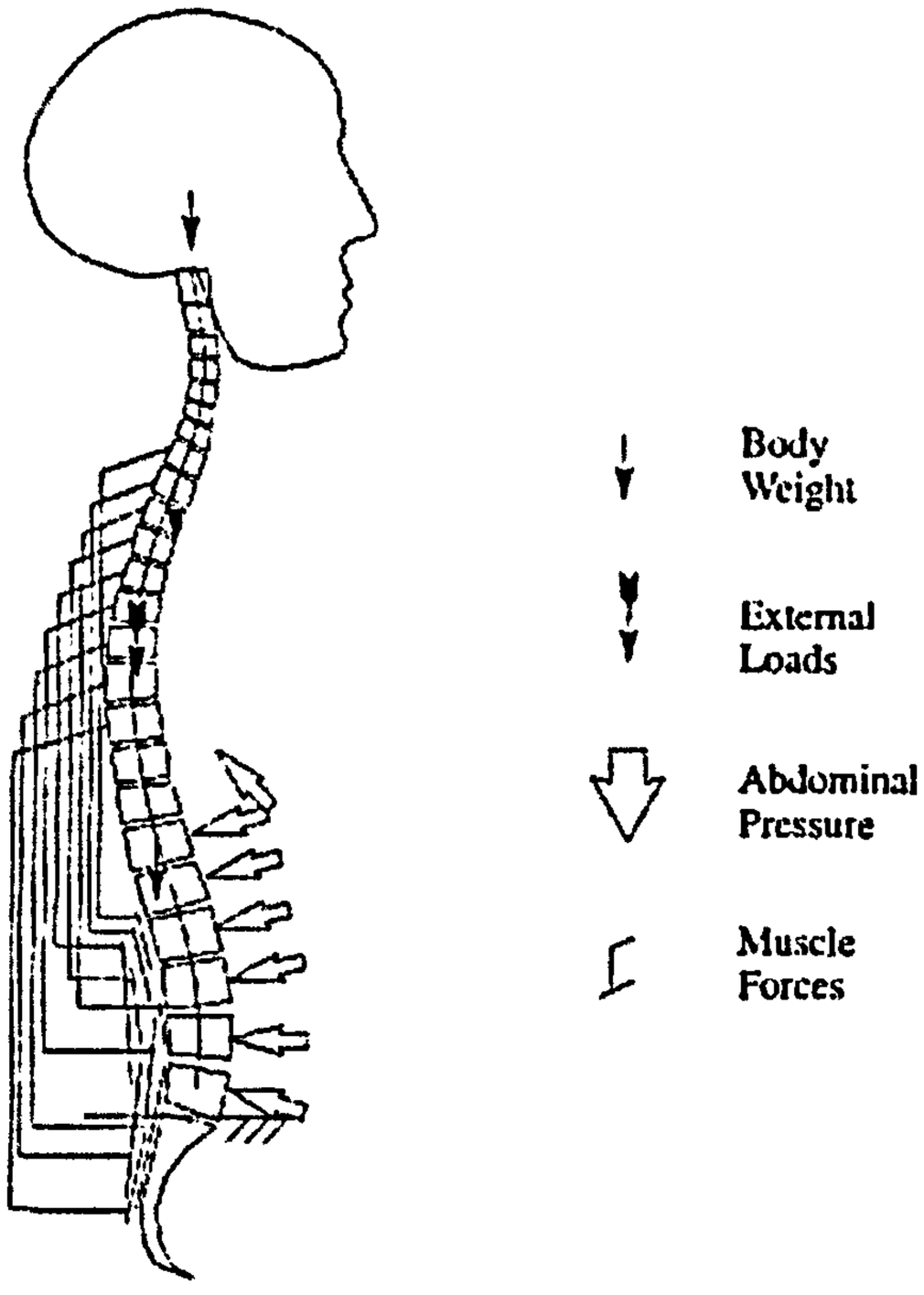

Figure 3.5 Loading system of the spine model (Case et al., 1999)

Patwardhan et al. (2001) used a two-dimensional, beam-column model to study the overall motion response of the whole lumbar spine in the frontal plane under the influence of gravitational and active muscle loads. The lumbar spine had been modelled as an isotropic flexible column. The authors verified that trunk muscles may coactivate to generate a follower load path to support physiologic compressive loads.

Li et al. (1991) developed a quasi-static analytical sagittal plane model of the cervical spine in extension and compression. Based upon the sensitivity of the test results, this model seems to be useful in determining the postural adjustment in reducing the axial loading on the cervical spine to more tolerable levels.

Granata and Wilson (2001) implemented an inverted double pendulum model of the spine, which is controlled by 12 muscle equivalents of the trunk to determine spinal load and stability. The authors concluded that spinal stability is influenced by posture and muscle recruitment patterns are more accurately explained by stability rather than by equilibrium alone.

Keller et al. (2002) constructed a mathematical model capable of describing the static and dynamic motion response of the lumbar spine to posteroanterior forces, which predicts lumbar segmental and inter-segmental motion responses to manipulative forces.

Similarly, Adler et al. (2002) developed a geometric model of the spine to resolve a certain optimization problem. Since the orientation of vertebrae can be specified by a frame of three orthogonal vectors in Euclidean three-space, the authors tried to find a constrained minimum, or at least a local minimum, of a real-valued function of special orthogonal groups. The function in question would turn out to be quadratic. Adler et al. claims that comparisons between the computed and measured spines had shown the pertinence of this approach. Lateral and anteroposterior views of a normal spine are provided in Figure 3.6.

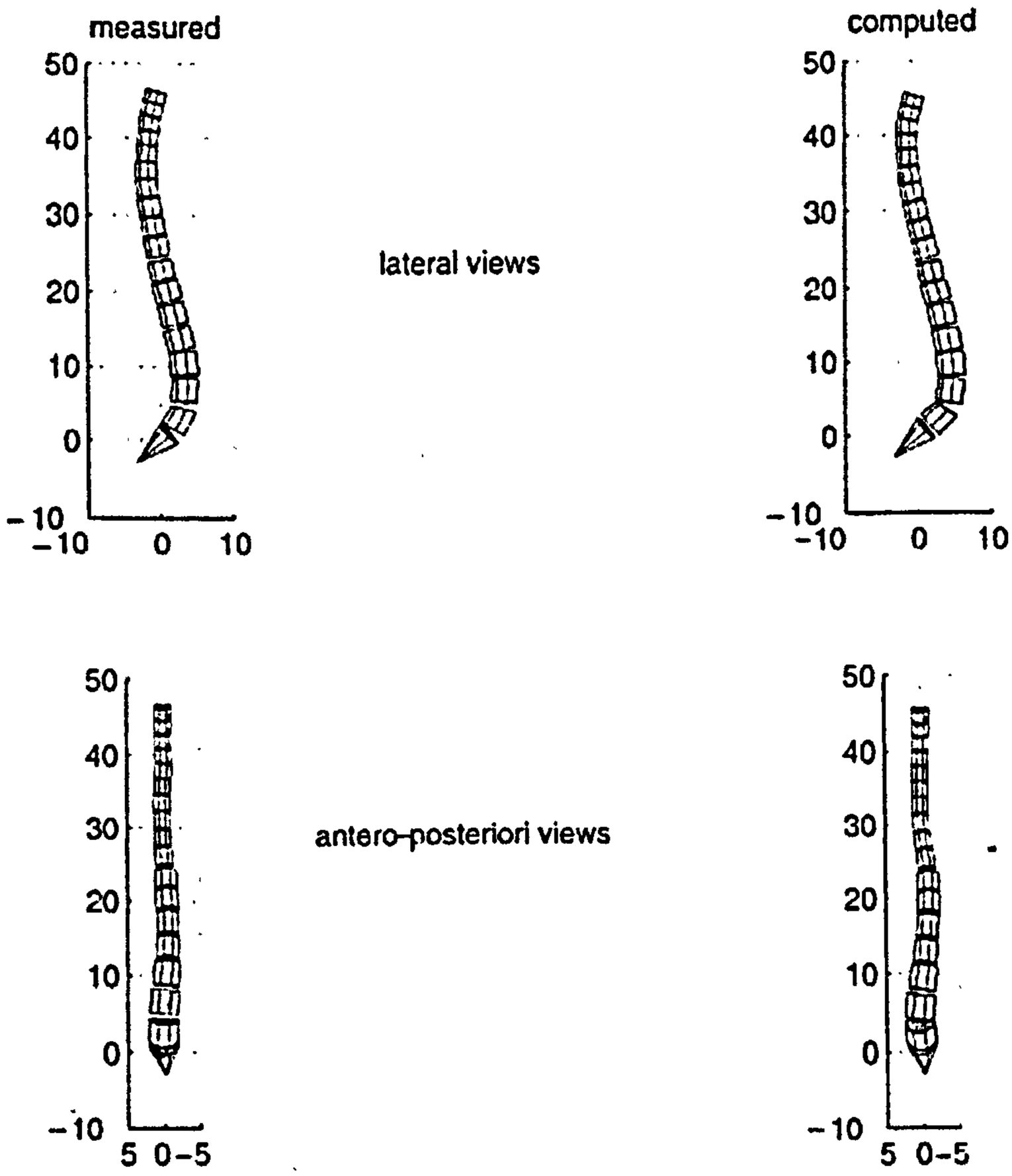

Figure 3.6 Lateral and anteroposterior views of a normal spine (Adler et al., 2002)

Acar and Grilli (2002) constructed a mathematical model of the human spine by using the modelling software, ADAMS (Fig. 3.7). Anatomic features regarding vertebral configuration and the applied body weights were incorporated into the model parametrically by using variables. They investigated a distributed loading pattern for the whole spine for different postures.

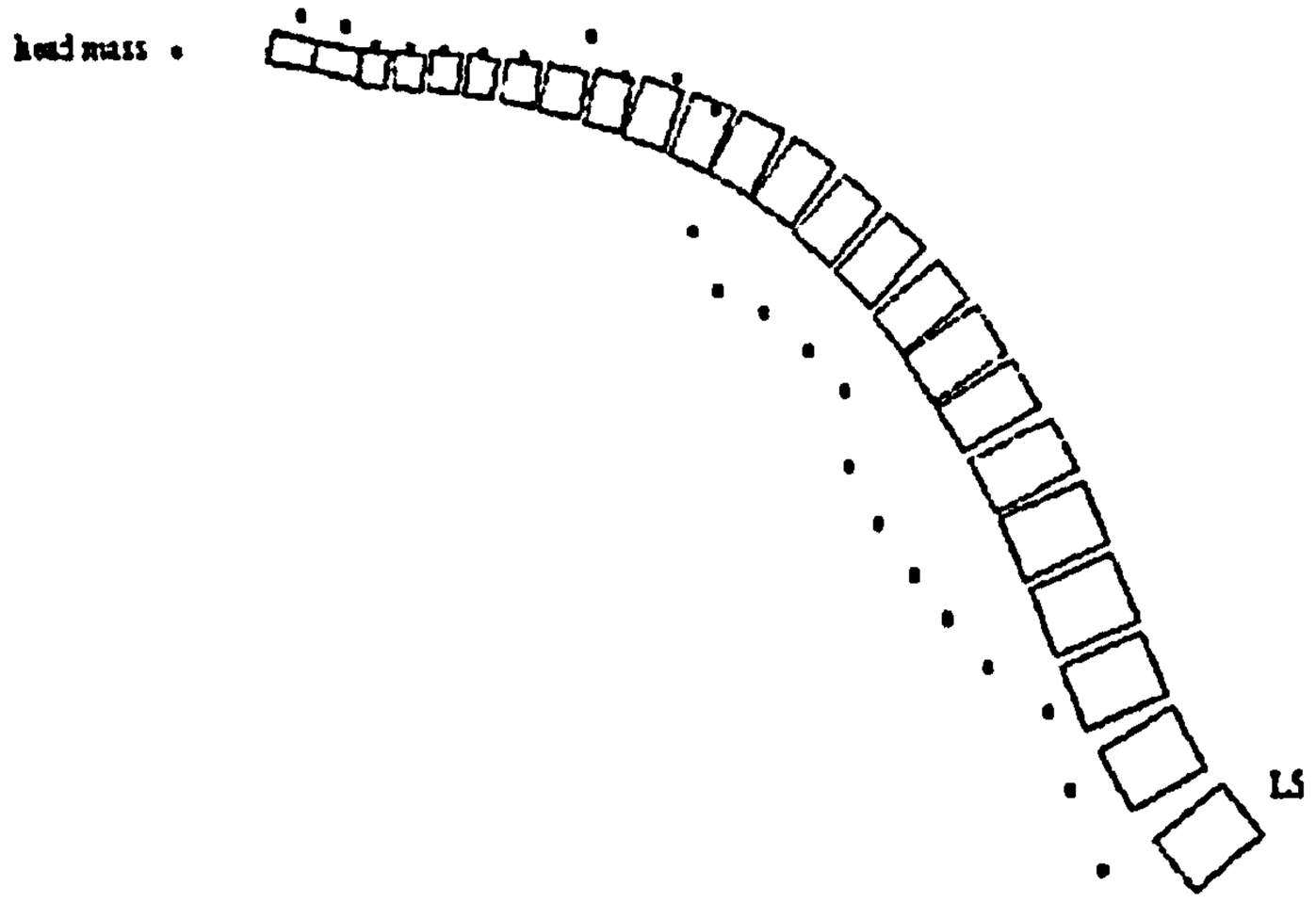

Figure 3.7 A flexed posture of the mathematical model (Acar and Grilli, 2002)

3.4 Multi-Body / Discrete Parameter Models

Multi-body/discrete parameter models have the ability to simulate the global and local kinematics and kinetics of the human spine. A multi-body system is a collection of rigid bodies connected through kinematic joints as well as elements applying forces. Multi-body dynamics models have advantages such as less complexity, less demand on computational power, and relatively simpler validation requirements when compared to FE models.

3.4.1 Multi-Body / Discrete Parameter Models of the Cervical Spine

Williams and Belytschko (1983) developed a three-dimensional human cervical spine model for impact simulation. A novel feature of this model had been the inclusion of a special facet element which allows the model to simulate both lateral and frontal plane motions, which appeared impossible with models of

the facet constraints composed of springs. In the cervical spine, the facets play a very important role in stabilizing the spine because of the very low stiffnesses of the intervertebral disks, and unless the facets are modelled adequately, unrealistically large shearing displacements occur between adjacent vertebrae. In addition a model for muscular contraction is included, which is shown to significantly affect the response of the neck. This study has been the first three-dimensional head and neck model to be validated for both frontal and lateral impact acceleration.

In modelling the head-neck region, vertebrae T1 through C1, and the head have been treated as rigid bodies interconnected by deformable elements. The geometry of the vertebrae had been compared with the rigid bodies in the model in Figure 3.8. Deformable elements (Figure 3.9) had been used to represent the soft tissue structures of the neck, including most of the major ligaments and -muscle groups, the intervertebral discs and the joints formed by the articular facets. The model consisted of the following deformable elements:

(a) spring elements, which have stiffness along the axis joining the two nodes which they connect;

(b) beam elements, which are elements with axial, bending and torsional stiffness;

(c) muscle elements, which are similar to spring elements except that the axial force may be activated independently of the elongation to mimic contraction of the muscle.

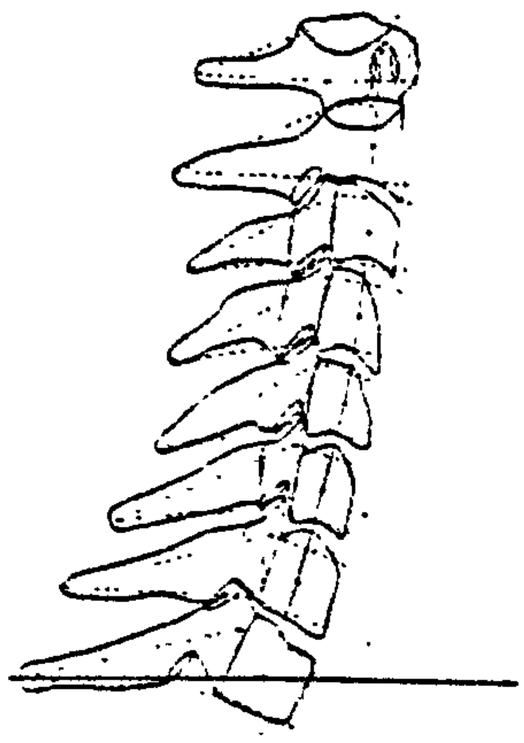

Figure 3.8 Cervical spine with rigid body representation (Williams and Belytschko, 1983)

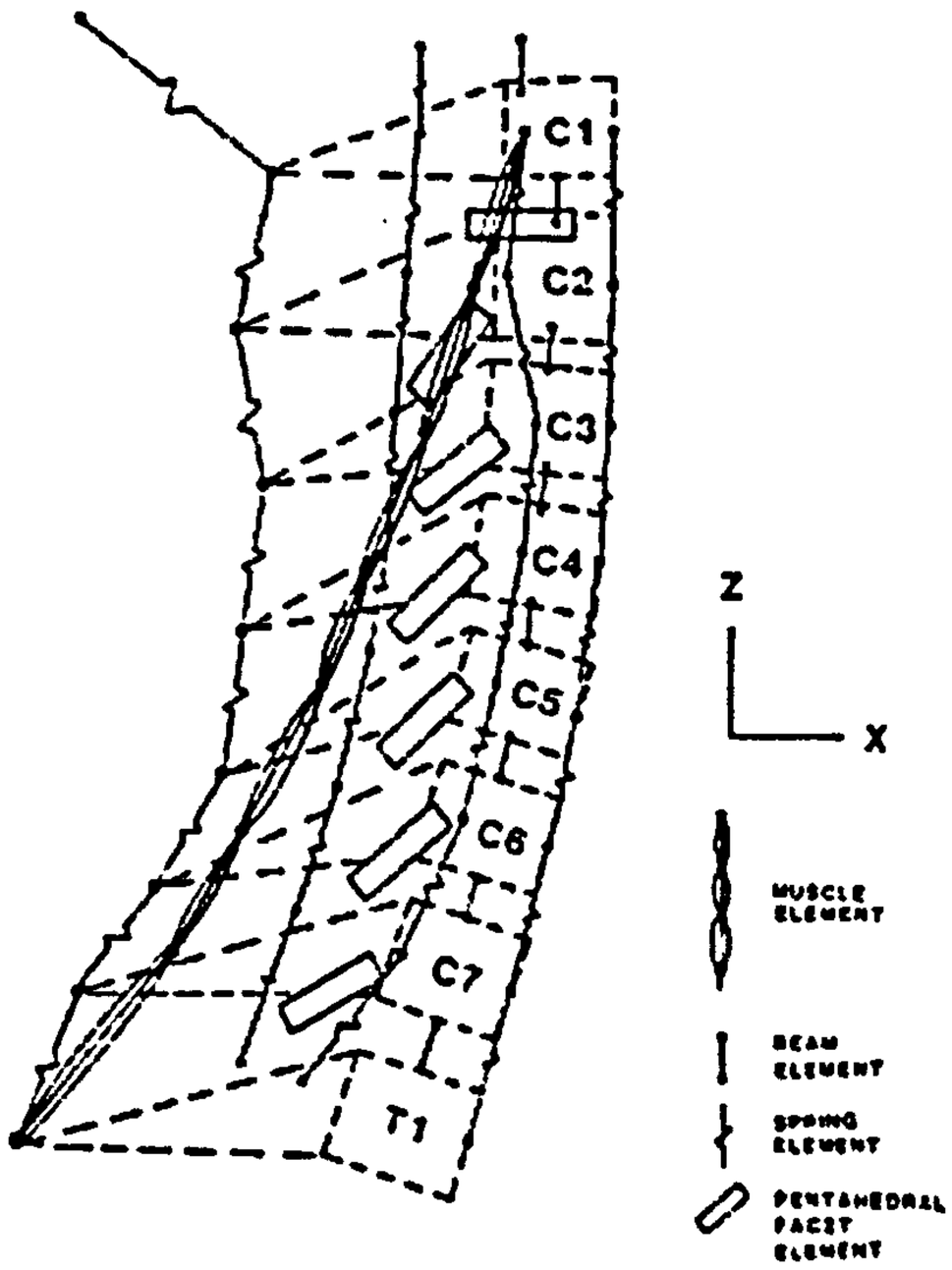

Figure 3.9 Muscle and ligament elements in the model (Williams and Belytschko, 1983)

The simplified thoracolumbar model and its connection to the cervical model is provided in Figure 3.10.

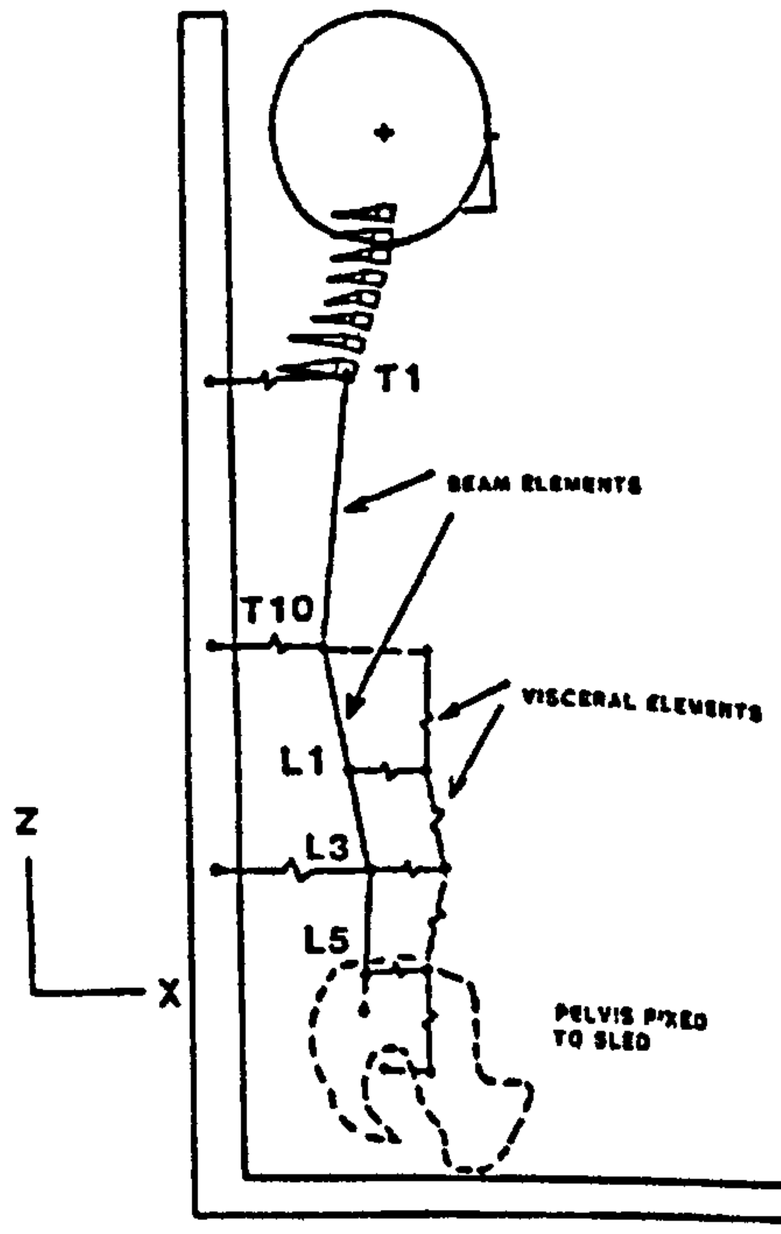

Figure 3.10 The simplified thoracolumbar model and its connection to the cervical model (Williams and Belytschko, 1983)

The results of this investigation had shown that the head-neck model was validated for both frontal and lateral impact situations by comparison with experimental results. Lateral impact appeared to be a severe validation test because of the three-dimensional motion involved. Williams and Belytschko claimed that they obtained good agreement with the tests.

Responses of the head-neck model in frontal and lateral impact conditions are illustrated in Figures 3.11 and 3.12, respectively.

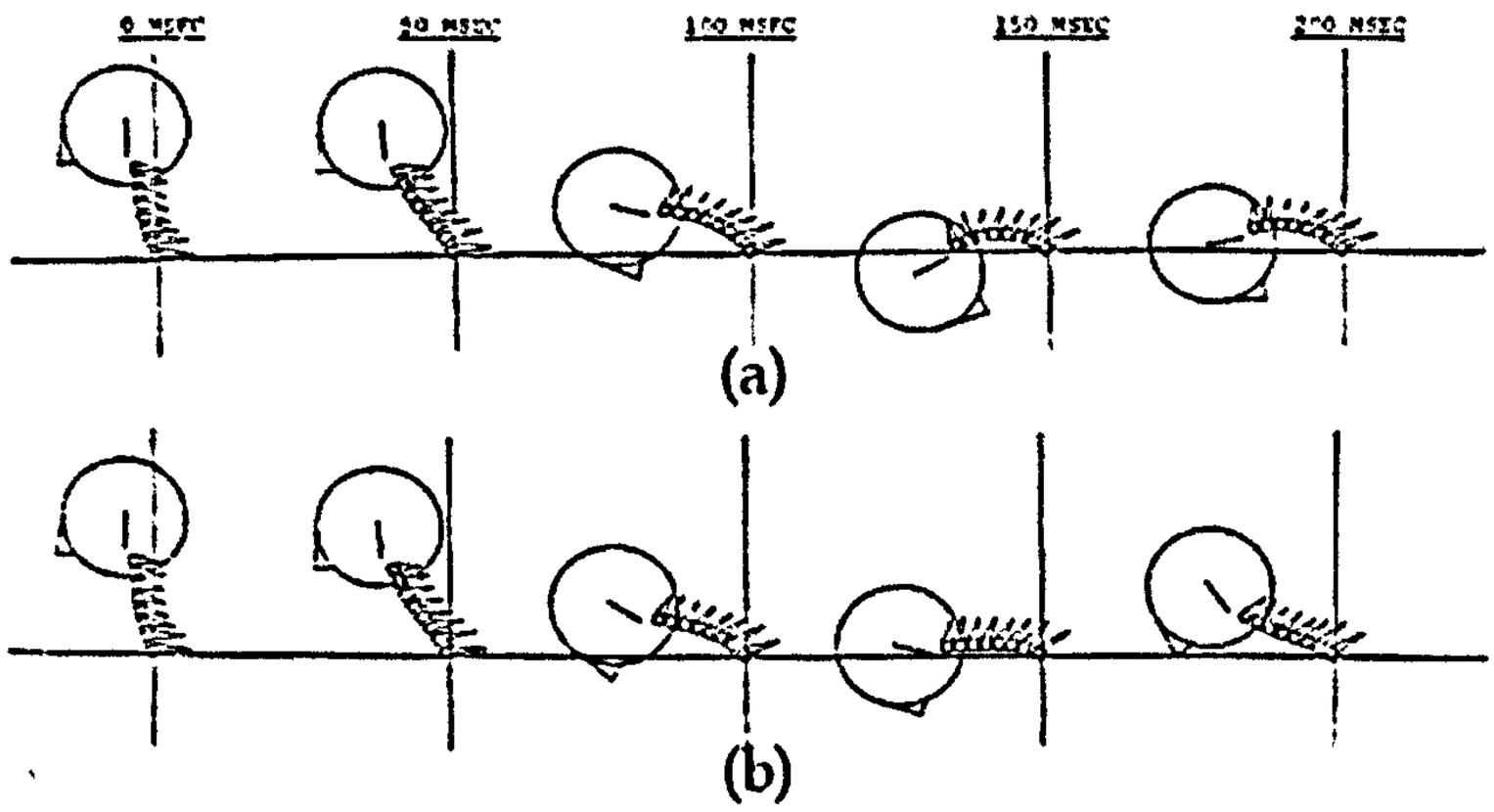

Figure 3.11 Responses of the head-neck model in frontal impact ($-G_x$ impact acceleration) (a) with passive muscles, (b) with stretch reflex response (Williams and Belytschko, 1983)

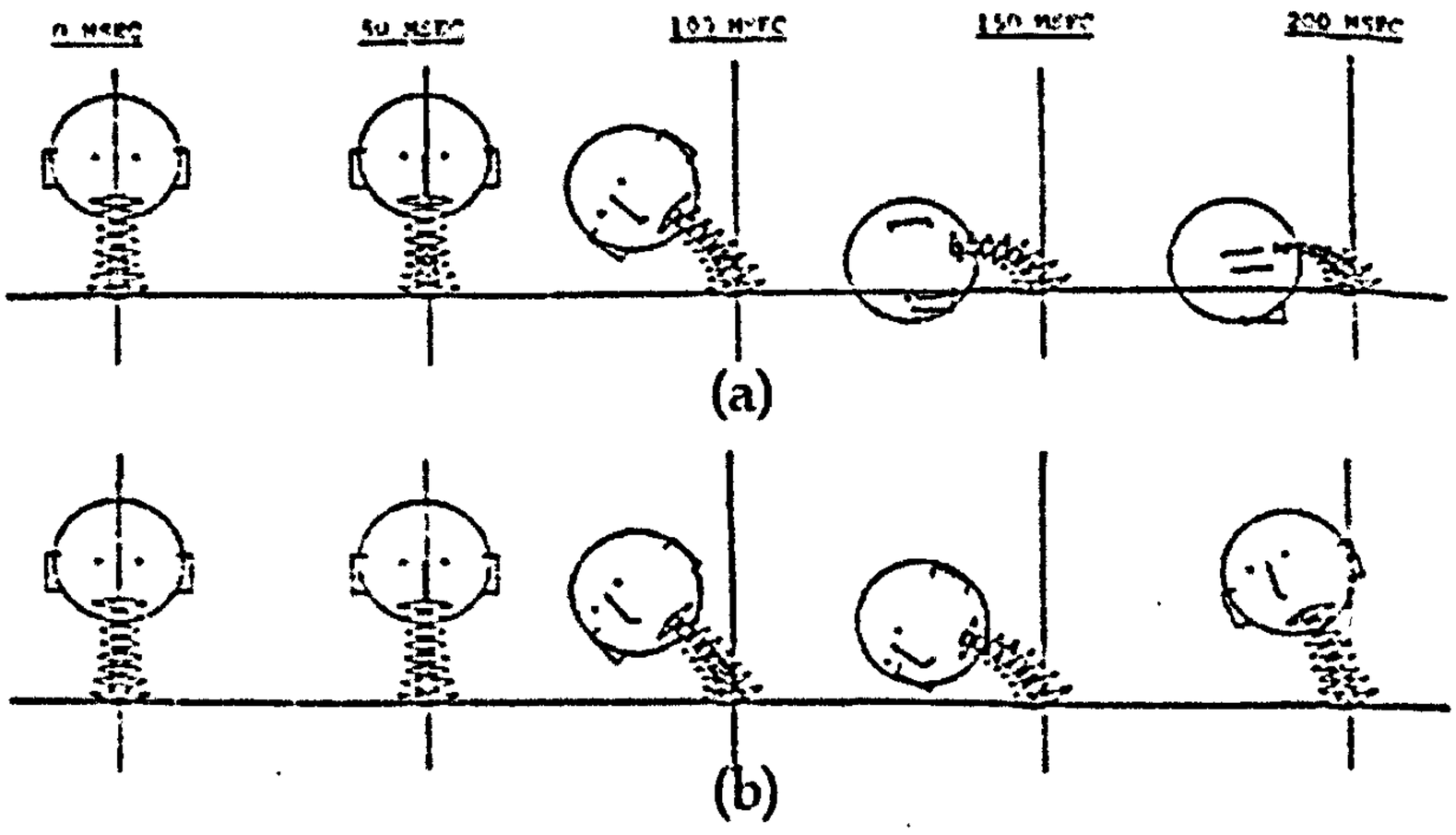

Figure 3.12 Responses of the head-neck model in lateral impact ($+G_y$ impact acceleration) (a) with passive muscles, (b) with stretch reflex response (Williams and Belytschko, 1983)

Merril et al. (1984) developed a three dimensional lumped parameter model improving the 2D model developed by Reber and Goldsmith (1979), which is illustrated in Figure 3.13. Deng and Goldsmith (1987) improved the model further, which was comprised of head, neck and upper torso with fifteen pairs of passive neck muscles. A single intervertebral joint defined the mechanical behaviour of each individual spinal unit possessing a linear stiffness matrix, which identified the segmental response.

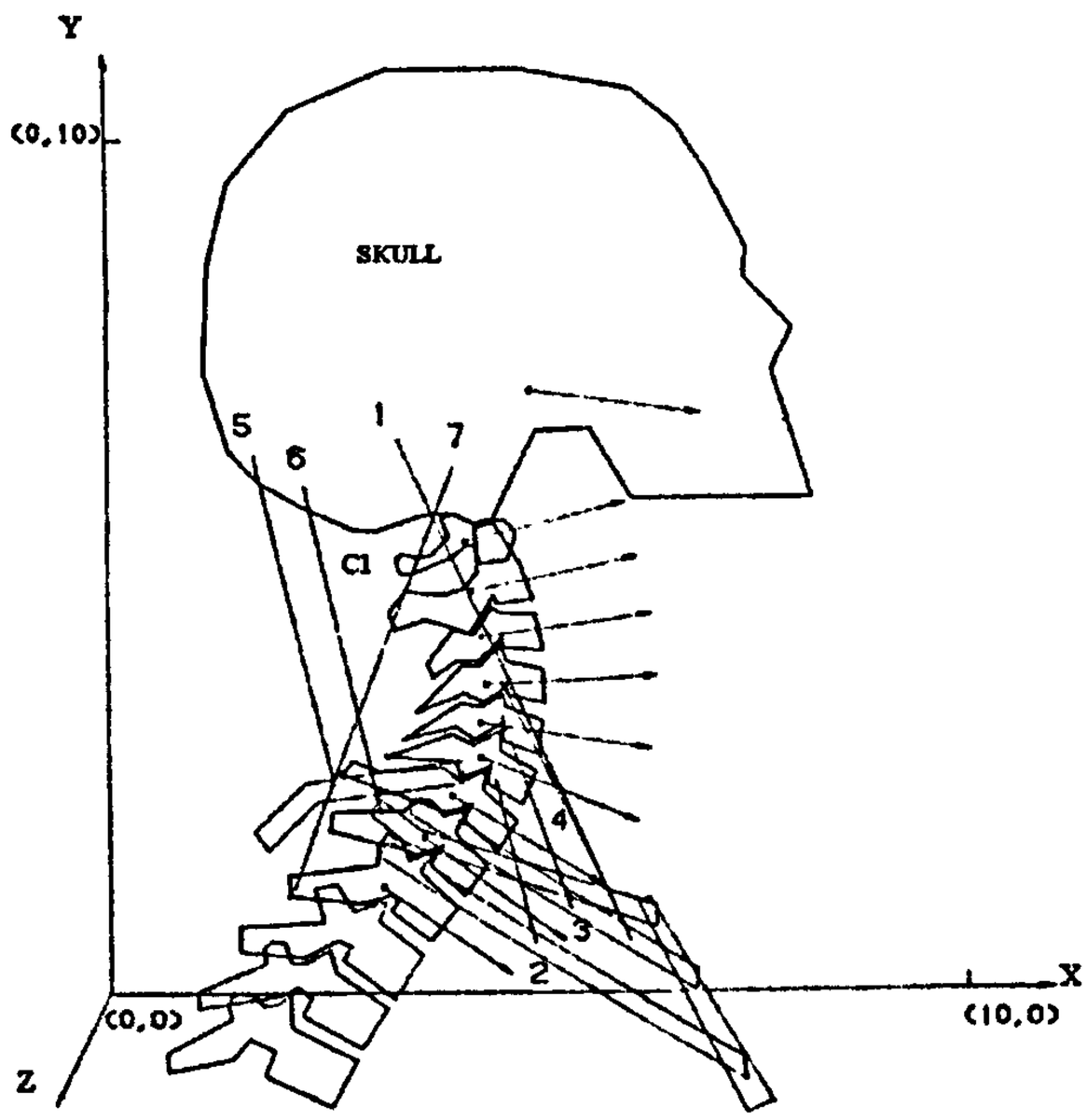

Figure 3.13 Multi-body model of Merrill, Goldsmith and Deng (1987)

De Jager (1996) developed a sophisticated model of the head and cervical spine by employing the multi-body software package Madymo. The model involved the head, the neck (cervical vertebrae, C1-C7) and the first thoracic vertebrae (T1). Intervertebral discs, facets joints, and various cervical ligaments were incorporated into the model as well as 14 pairs of the cervical spine's most significant muscle groups possessing both passive and active muscle behaviour. The model is illustrated in Figure 3.14.

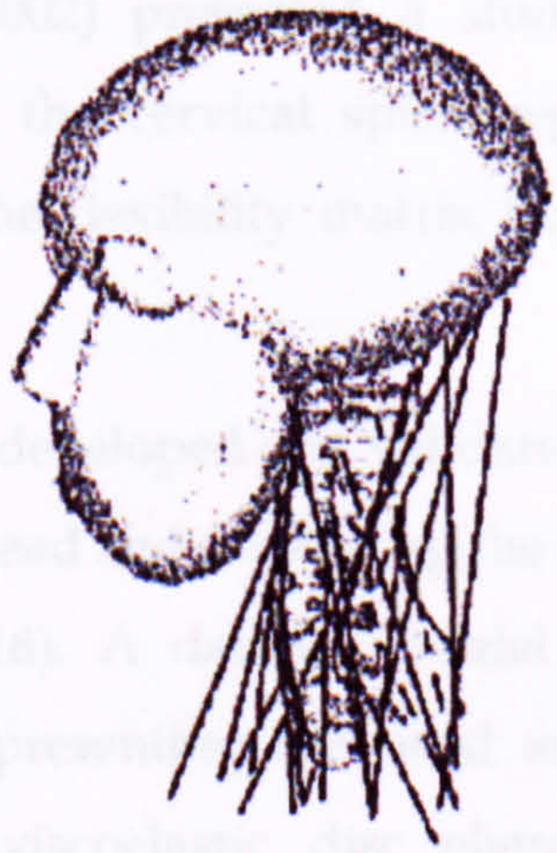

Figure 3.14 Multi-body model of de Jager (1996)

Van der Horst (1997, 2002) further improved the de Jager model by increasing the geometric details of the vertebrae, and updating the material properties of the soft tissues and the neck muscles in greater detail. She improved the material properties of the intervertebral discs for flexion, extension and compression, possessing nonlinear characteristics. Facet joints were modelled as three-dimensional non-linear compressive springs, and additionally, contact between spinous processes were included. Ligaments were represented by using 2D non-linear viscoelastic spring-damper elements and 68 muscle elements were implemented with improved geometry and allowing for curving around the cervical column. The Hill type muscle model in Madymo was employed to describe active and passive muscle behaviour. The model is provided in Figure 3.15.

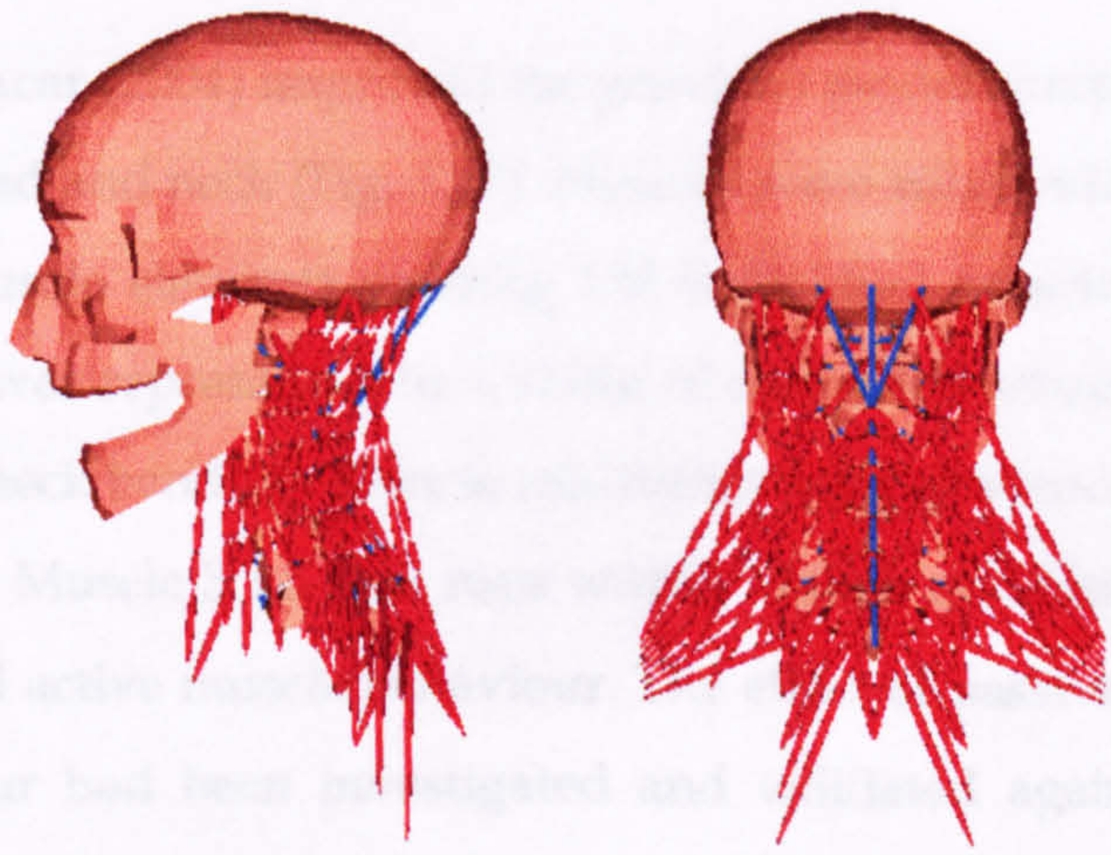

Figure 3.15 Multi-body model of van der Horst (1997, 2002)

Winkelstein and Myers (2002) presented a study, which tries to quantify flexibility relationships for the cervical spine segments and investigate the nonlinear components of the flexibility matrix that forms the basis of multi-body dynamics models.

Van Lopik and Acar (2002) developed and validated a three dimensional multi-body model of the human head and neck using the dynamic simulation package visuaINastran 4D (Fig. 3.16). A detailed model of the head-neck complex comprised rigid bodies representing the head and 7 vertebrae of the neck interconnected by linear viscoelastic disc elements, nonlinear viscoelastic ligaments, firictionless facet joints and contractile muscle elements describing both passive and active muscle behavior.

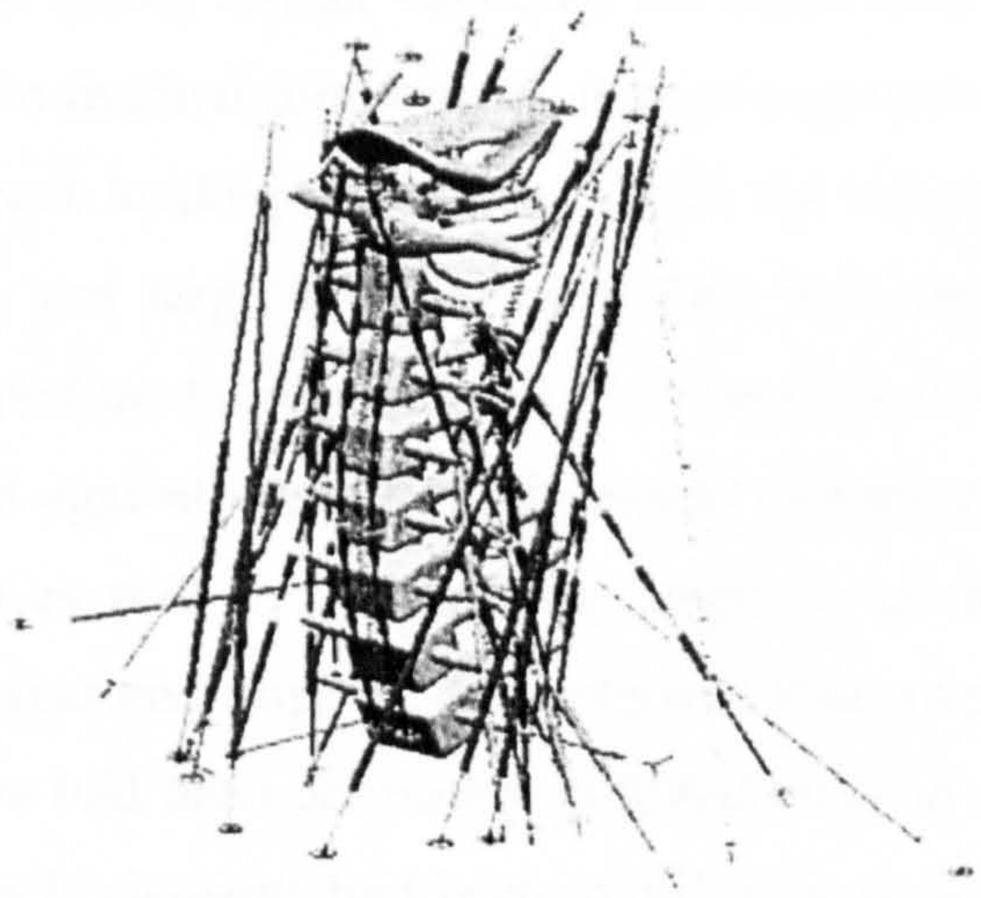

Figure 3.16 Isometric view of the cervical spine with all neck musculature (Van Lopik and Acar, 2002)

Van Lopik and Acar (2004) improved the previous model comprising 19 muscle groups of the head and neck (Fig. 3.17). Muscles were subdivided into a number of individual muscle elements yielding 138 individual muscle segments. Each muscle element was represented by a series of connected actuators allowing for curving during neck bending. Muscle mechanics were governed by the external software Virtual Muscle 3.1.5 that runs within Matlab and Simulink providing both passive and active muscle behaviour. The effect of passive and fully active muscle behaviour had been investigated and validated against experimental data, yielding good agreement for both impact directions.

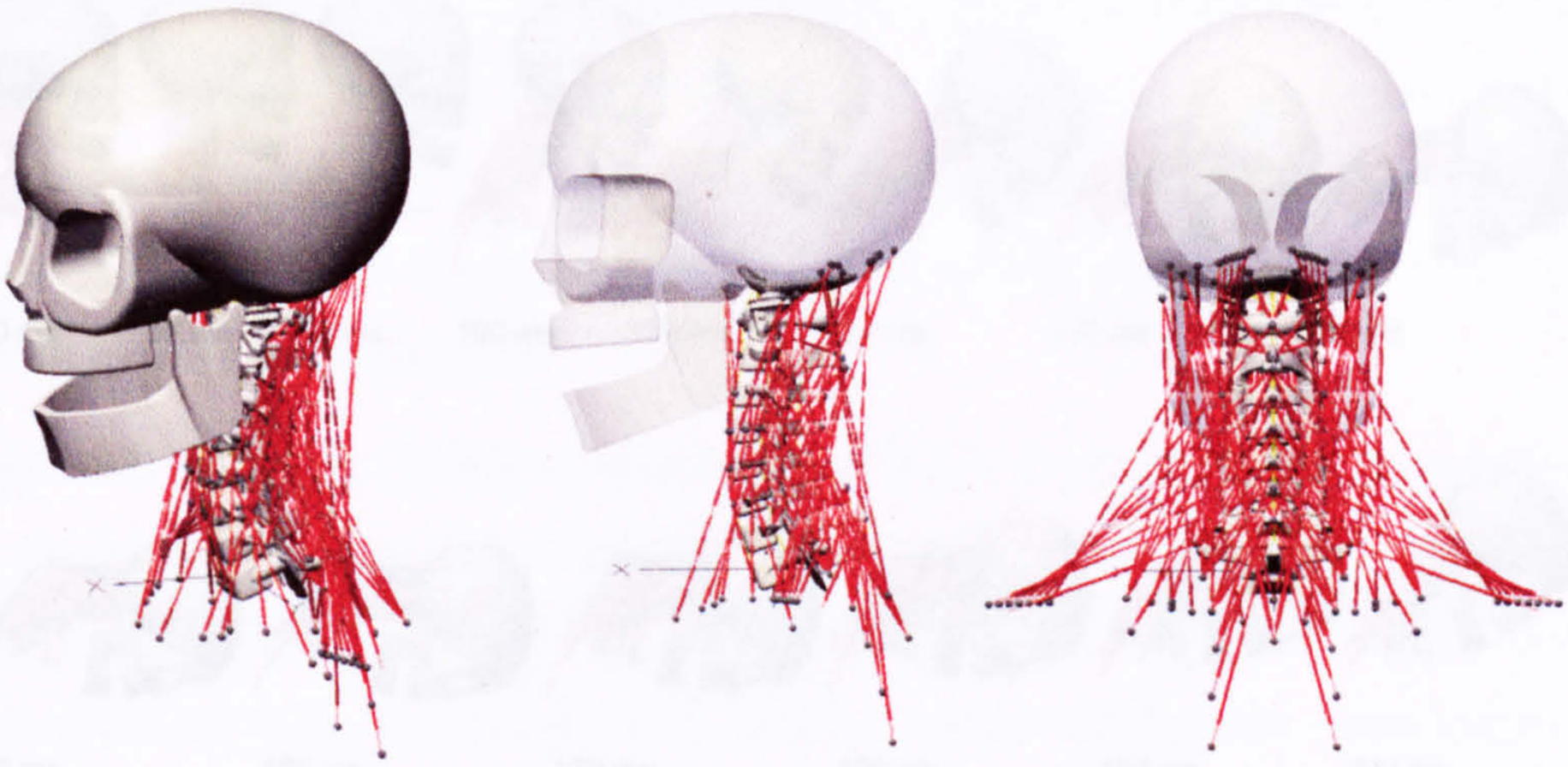

Figure 3.17 Multi-body model of the head and neck (van Lopik and Acar, 2004)

Van Lopik and Acar (2004) further validated the head-neck model by checking the accuracy of the individual components, motion segments and the model as a whole under different loading conditions. While the response of the motions segments to small and large static loading had been found to be in good agreement with experimental results in all directions, the completed model had also been validated against experimental results, including individual motion segment responses as well as the dynamic response of the whole model to frontal, lateral and rear end impacts. They showed that coupling characteristics of the cervical spine had been accurately imitated and the moment generating capacity of the muscle elements had been found to be realistic. The model had also been run to simulate bench-top trauma experiments using cadaveric isolated cervical spine specimens, which are devoid of musculature. They claimed that model had successfully reproduced the characteristic 'whiplash' motion and resulting head and vertebral rotations and displacements seen in the experimental results for rear impact accelerations. Model responses to 15g frontal impact and 7g lateral impact situations with 100% active musculature are illustrated in Figures 3.18 and 3.19, respectively.

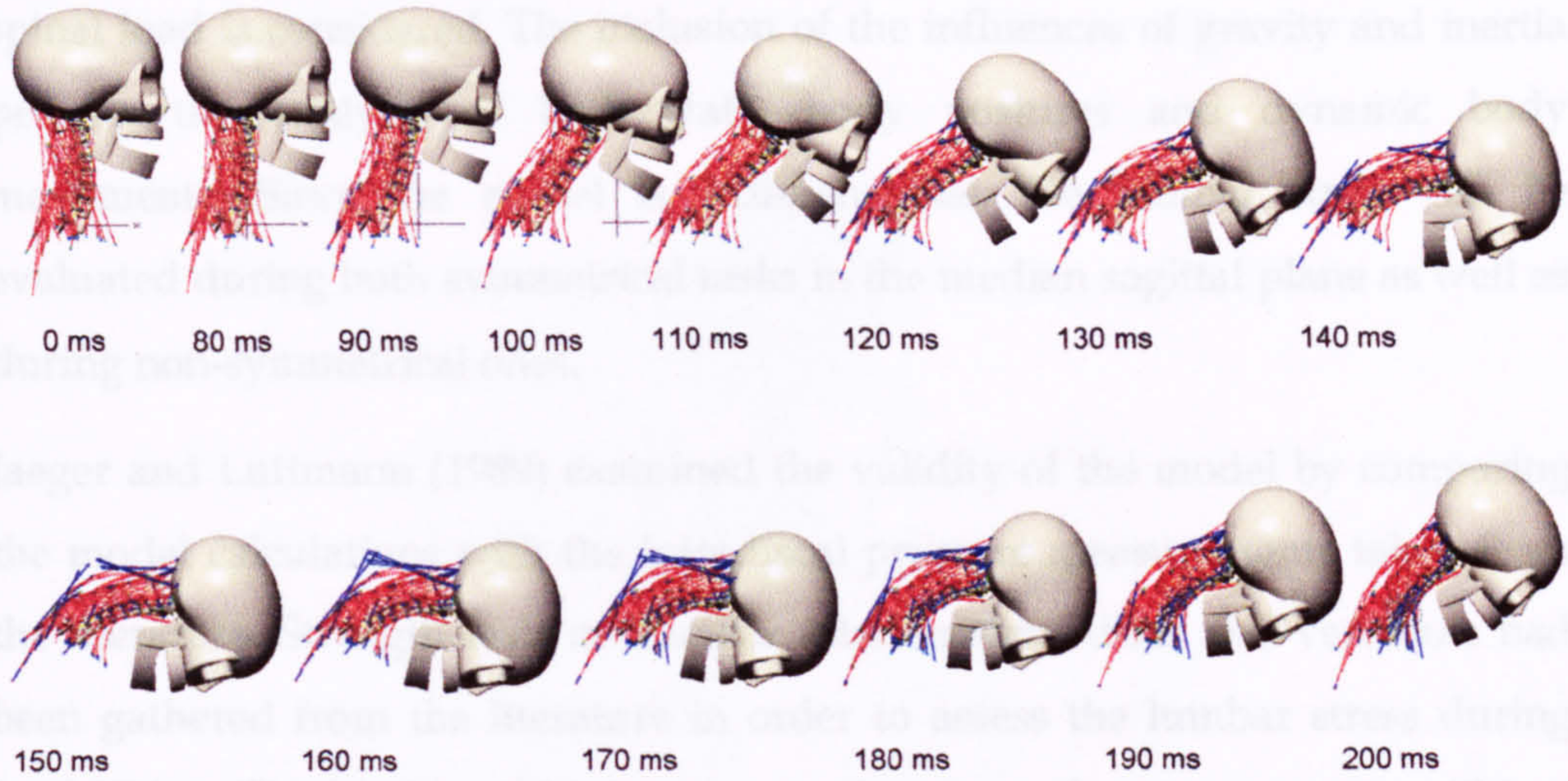

Figure 3.18 Model response to 15g frontal impact for 200 ms with 100% active musculature (van Lopik and Acar, 2004)

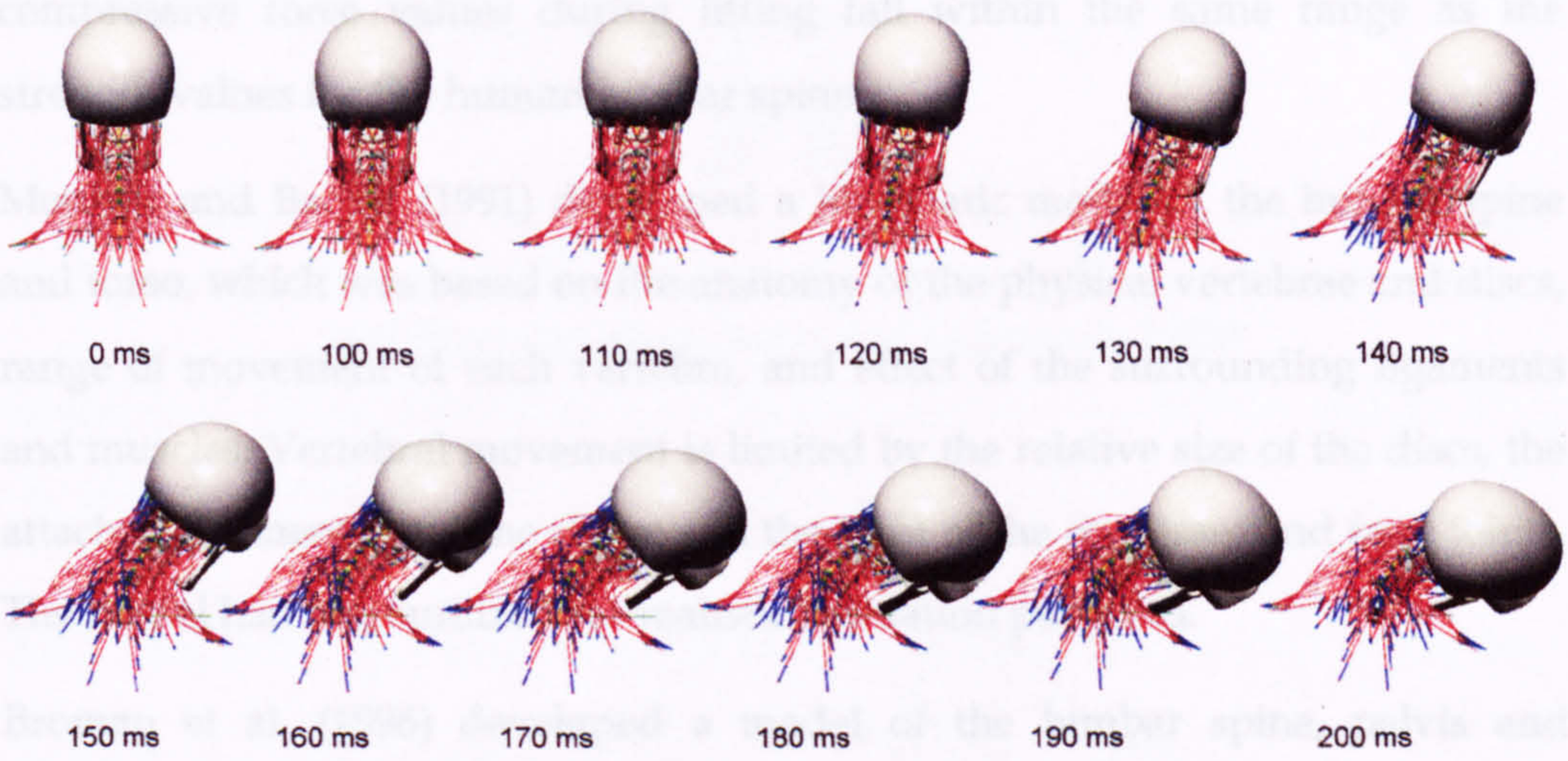

Figure 3.19 Model response to 7g lateral impact for 200 ms with 100% active musculature (van Lopik and Acar, 2004)

3.4.2 Multi-Body / Discrete Parameter Models of the Lumbar Spine

Jaeger and Luttmann (1989) presented a dynamic biomechanical human model which allows the quantification of mechanical parameters such as torque, compressive and shear forces, and pressure at the lumbar intervertebral discs. The human model includes a total of 19 body segments (Figure 3.20). Various trunk flexions can be analysed due to the provision of 5 joints at the level of the 5 lumbar intervertebral discs. The influence of intraabdominal pressure on

spinal load is considered. The inclusion of the influences of gravity and inertia permits the analysis of both static body postures and dynamic body movements. Since the model is 3-dimensional, the lumbar stress can be evaluated during both symmetrical tasks in the median sagittal plane as well as during non-symmetrical ones.

Jaeger and Luttmann (1989) examined the validity of the model by comparing the model calculations with the intradiscal pressure measurements taken from the literature. Strength tests on lumbar intervertebral discs and vertebrae had been gathered from the literature in order to assess the lumbar stress during load lifting. The lumbar ultimate compression strength seems to vary within a wide range. The mean value for a total of 307 lumbar segments amounts to 4.4kN, the standard deviation to 1.9kN. The authors concluded that lumbar compressive force values during lifting fall within the same range as the strength values for the human lumbar spine.

Monheit and Badler (1991) developed a kinematic model of the human spine and torso, which was based on the anatomy of the physical vertebrae and discs, range of movement of each vertebra, and effect of the surrounding ligaments and muscles. Vertebral movement is limited by the relative size of the discs, the attached ligaments, and the shape and the slant of the processes and facet joints. The model had been utilized for realistic animation purposes.

Broman et al. (1996) developed a model of the lumbar spine, pelvis and buttocks, based on linear horizontal and vertical systems along with a rotational subsystem. The model was aimed to simulate different experimental observations of transmission of vibrations from the seat to L3 in the sitting posture. The components of the model derived are illustrated in Figure 3.21. They concluded that the model had lacked detailed sophistication but on the other hand, had appeared to be qualitatively explanatory for the biomechanics of the seated vibrations.

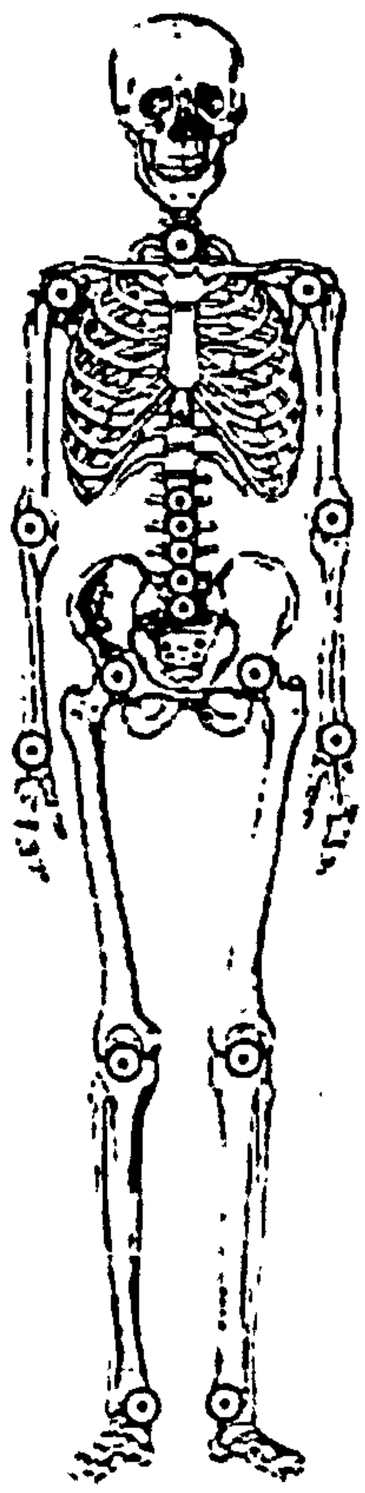

Figure 3.20 Human model with 19 body segments, 5 of which are lumbar vertebrae and discs (Jager and Luttmann, 1989)

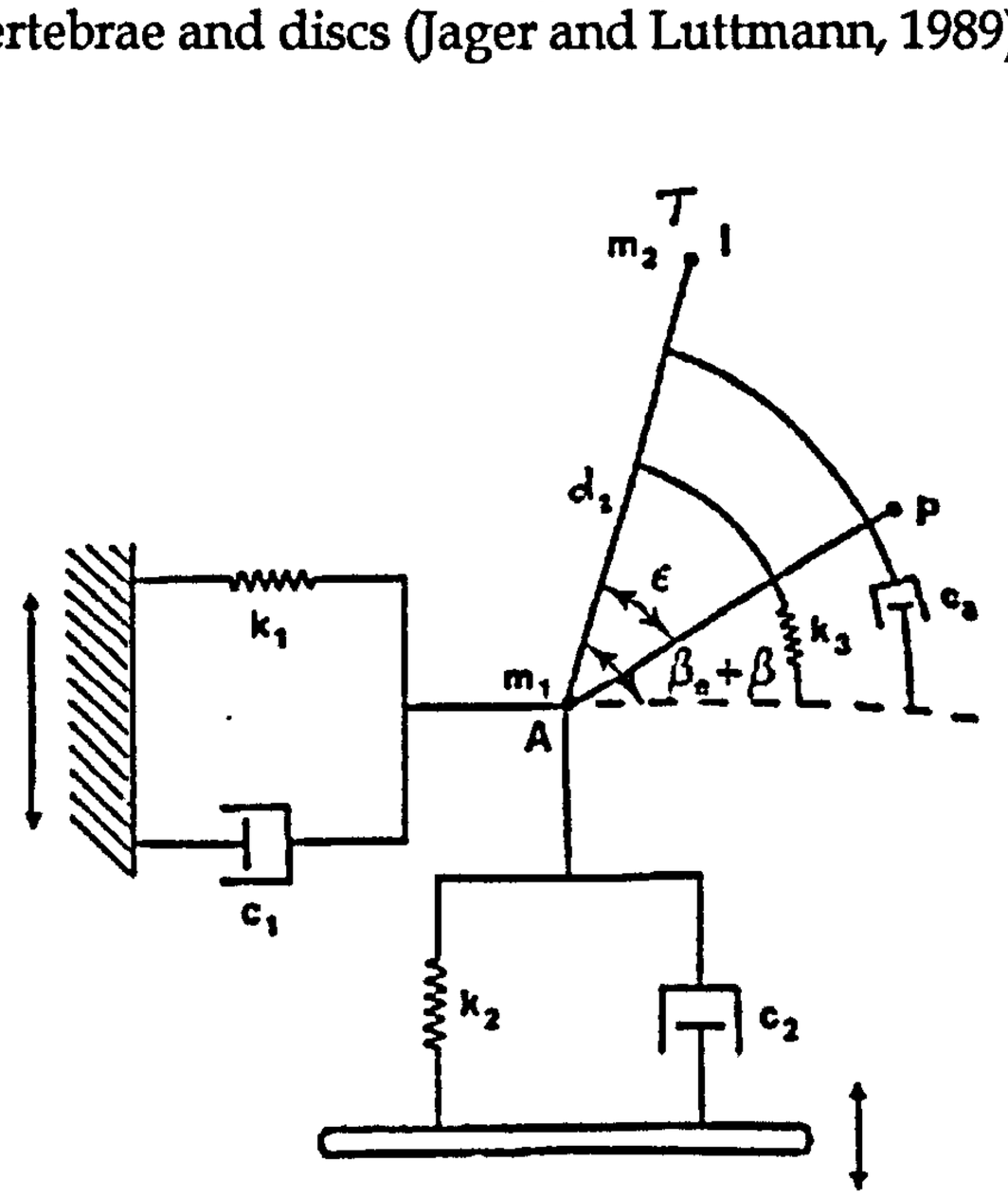

Figure 3.21 Modeling components (Broman et al., 1996)

Cholewicki et al. (1999) constructed a simplified physical model to illustrate a possible intra-abdominal pressure mechanism for stabilizing the spine (Figure

3.22). The model comprises an inverted pendulum with linear springs representing abdominal and erector spinae muscle groups.

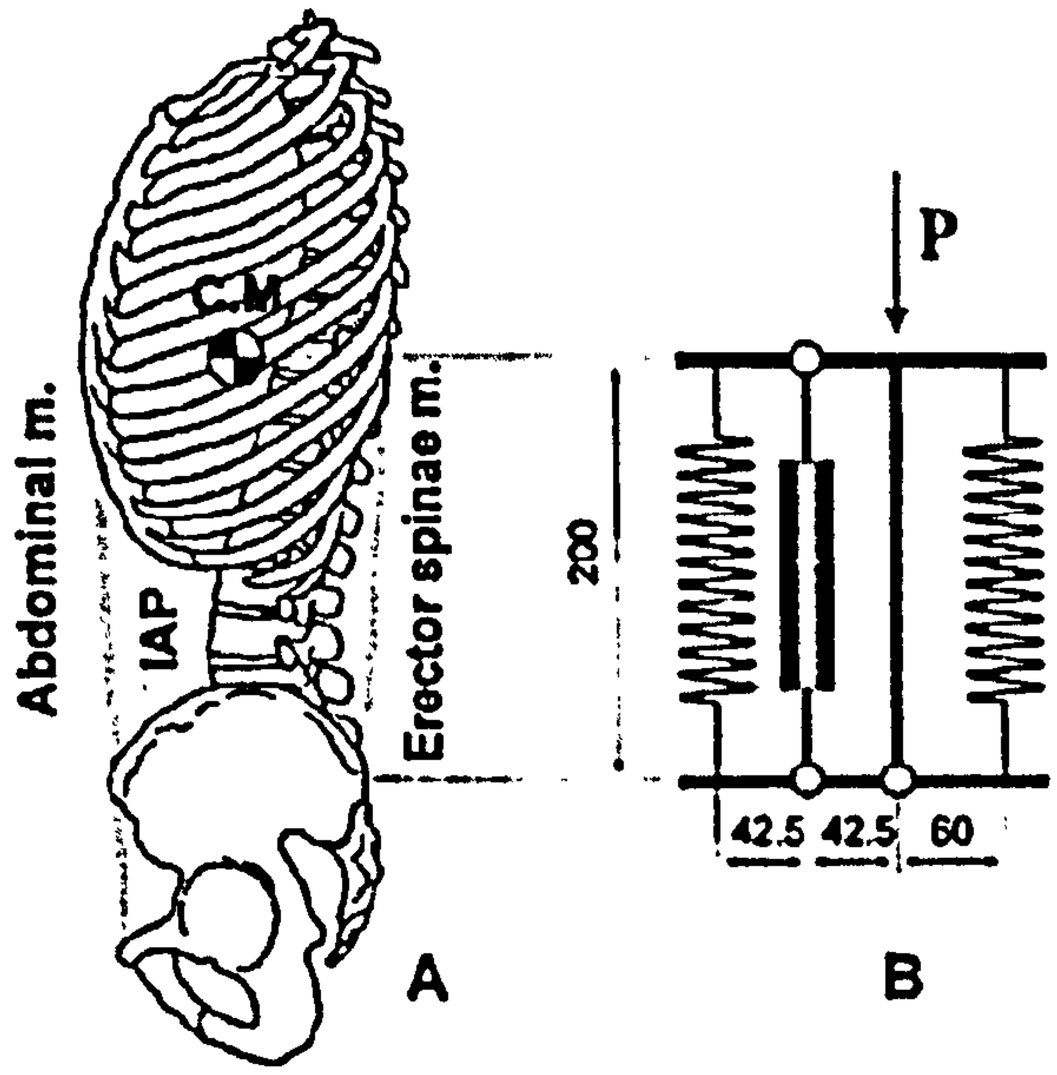

Figure 3.22 Anatomical diagram (A) of the lumbar spine and torso, and (B) the physical model (Cholewicki et al., 1999)

Stokes et al. (2002) introduced a method to measure the stiffness matrix of the six-degrees-of-freedom elastic behaviour of spinal motion.

3.4.3 Multi-Body / Discrete Parameter Models of the Whole Spine

Schultz and Galante (1970) constructed a multi-body model for studying the mechanical function of the human vertebral column (Figure 3.23). The column had been modelled as a collection of rigid bodies and equilibrium or geometrical configurations of the collection had been sought to satisfy constraints imposed in order to simulate the action of a real spine. In this model, adjacent vertebral bodies and spinous processes were connected each at one point, while articular facets and transverse processes were attached on both sides. They claimed that model had provided a reasonable understanding of the geometry of the vertebral column for lateral bending, extension, and flexion situations.

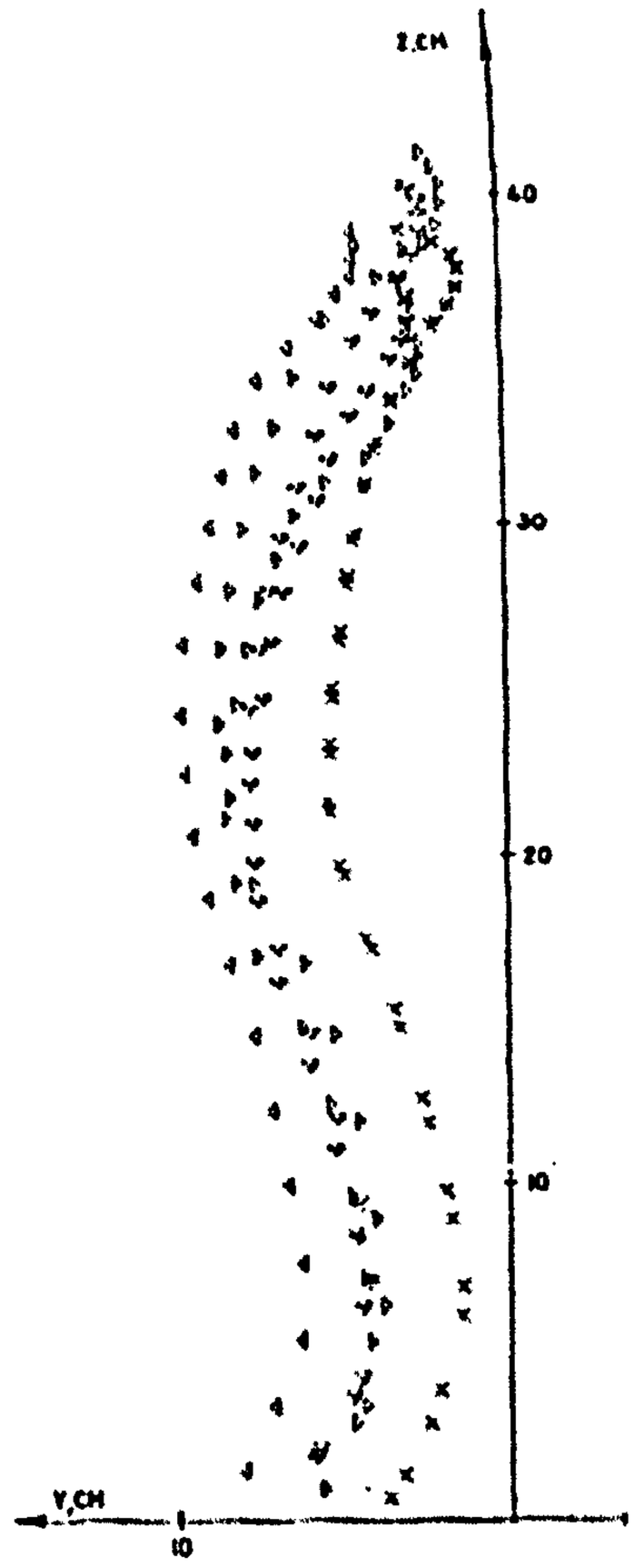

Figure 3.23 The spine model, where; X represents vertebral body, ▼ represents articular facet, ► represents transverse process, and ◄ represents spinous process locations (Schultz and Galante, 1970).

Belytschko et al. (1973) developed a computational model of the human spine and the rib cage, incorporating 39 rigid bodies interconnected by 236 spring and 59 beam deformable elements to represent the soft tissues of the motion segments, costal cartilages, and other ligamentous tissues of the trunk (Fig. 3.24). In this model, each spring element possessed one axial stiffness, while each beam element was characterised by six stiffnesses; one each for axial deformation, torsion, lateral bending, lateral shear, anteroposterior bending, and anteroposterior shear. The geometry and the material properties were reported to be found from literature. 78 muscle slips were incorporated into the model, applying significant forces to the trunk. Wynarsky and Schultz (1991) used the same model to develop a scheme for optimising configurations in models of skeletal structures in order to have an insight on scoliosis correction

biomechanics. They demonstrated the determination of the locations and magnitudes of the passive brace and active muscle forces for the correction of a right thoracic scoliosis. The results of this study suggested that, from a biomechanical viewpoint, both brace and muscle forces are capable of substantial correction of a model thoracic scoliosis. However, comparison of model results with long-term clinical results yields that even under optimal conditions it is unlikely that scoliosis can be fully corrected by passive brace forces or active muscle contractions. Nussbaum and Chaffin (1996) modified the same human spine model, including thoracic and lumbar motion segments, muscles, ribs, sternum, sacrum and pelvis. The modifications allowed for scaling to represent subject-specific anthropometry, deformation to mimic an arbitrary thoracolumbar posture, incorporation of new data regarding muscle geometry, estimation of passive reactive moments generated by muscles and lumbar motion segments, and generation of parameters required in subsequent muscle force algorithms. The predicted passive spinal moments were found to be comparable to those required to support body weight in different extreme postures.

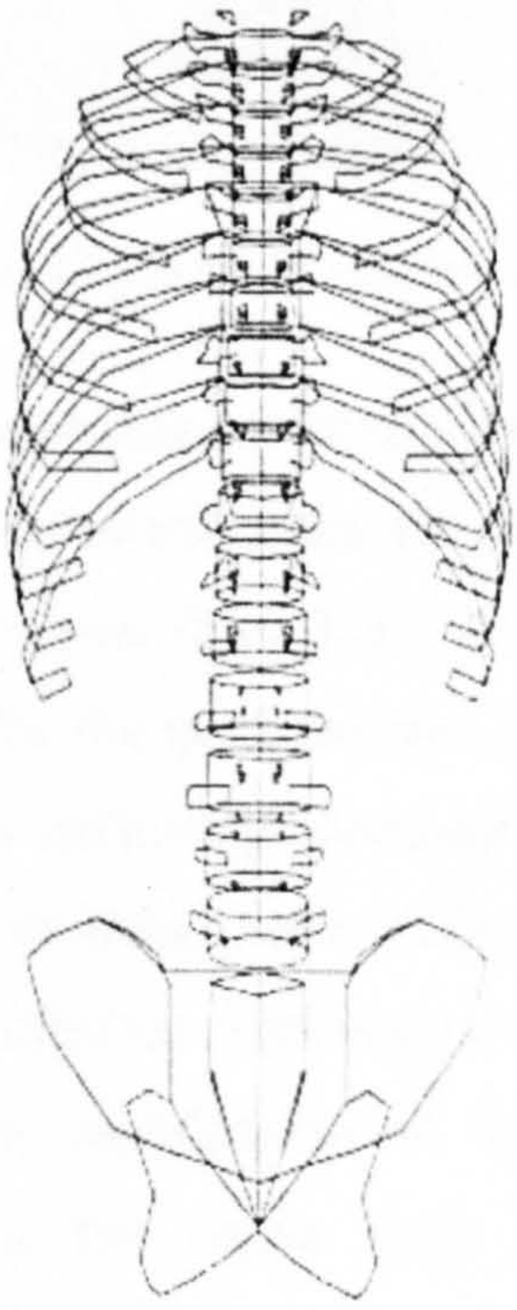

Figure 3.24 Geometric model of the human torso (Belytschko et al., 1973)

De Zee et al. (2003) developed a multi-body human spine model partially by using the AnyBody Modelling System, written in so-called AnyScript, which is a declarative, object-oriented language for development of multi-body dynamics models, and particularly for models of the musculoskeletal system (Fig. 3.25). Only the lumbar spine part was constructed, which consisted of seven rigid segments as pelvis, the five lumbar vertebrae and a thoracic part, where the joints between each vertebra set of two was modelled as a three degrees-of-freedom (dof) spherical joint. Four types of ligaments and several lumbar muscle groups including multifidi and psoas major were incorporated into the model. The model was incomplete in terms of including all lumbar muscle groups and it was solely constructed around the lumbar region.

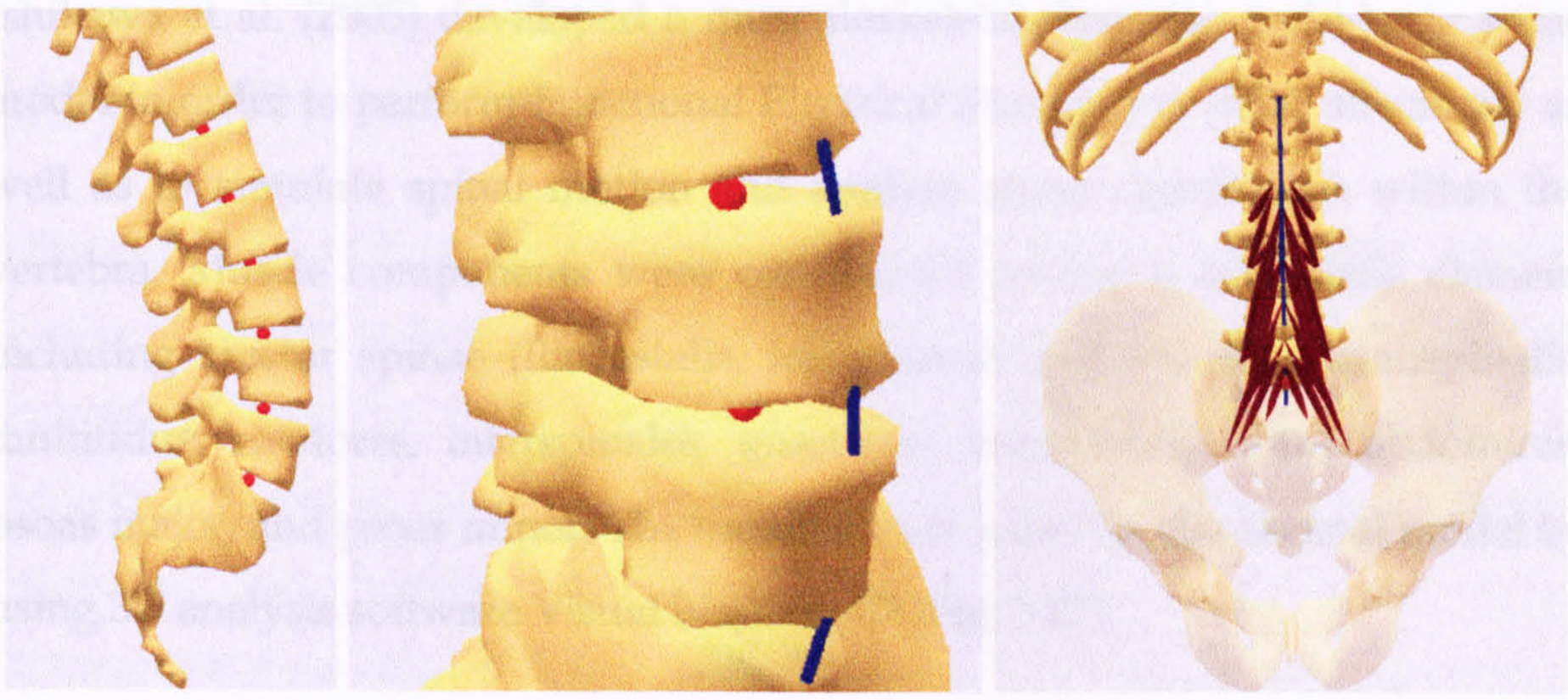

Figure 3.25 Several views from de Zee et al. (2003) model

Silva and Ambrosio (2004) constructed a biomechanical model, which describes the kinematic and dynamic characteristics of the human body, in order to perform inverse dynamic analysis (Fig. 3.26). The multi-body model utilised natural coordinates to describe the position and orientation of each rigid body in a three-dimensional space excluding kinematic constraints associated with revolute or spherical joints as these were defined by specifying points and vectors that were shared by different rigid bodies. The model was used in a gait analysis and the sensitivity calculations of the system response due to perturbations introduced in the input data during stride period were demonstrated.

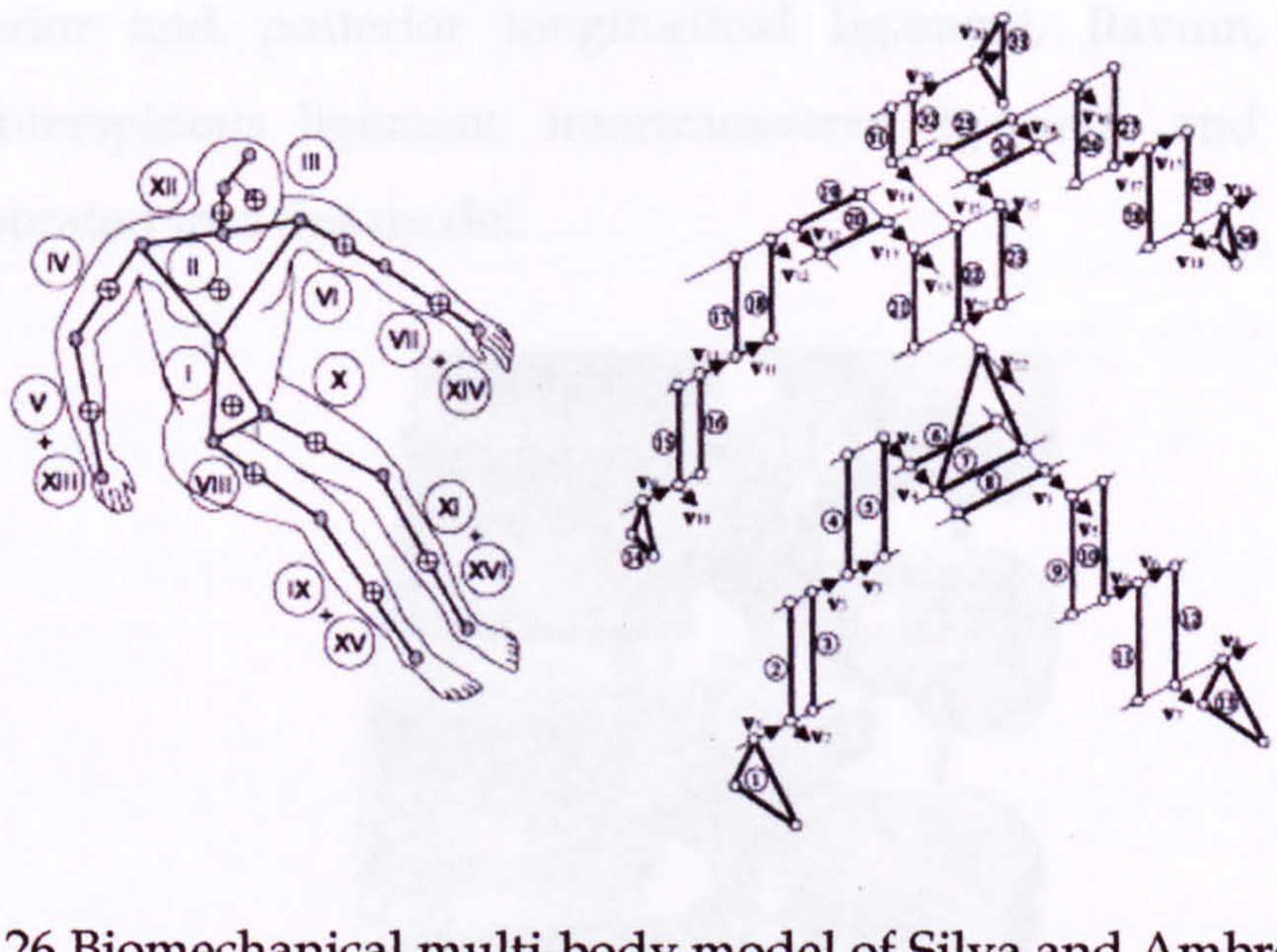

Figure 3.26 Biomechanical multi-body model of Silva and Ambrosio (2004)

Ishikawa et al. (2005) developed a musculoskeletal dynamic multi-body spine model in order to perform Functional Electrical Stimulation (FES) effectively as well as to simulate spinal motion and analyse stress distribution within the vertebra. Muscle components were constructed having a contractile element including erector spinae (iliocostalis, longissimus and spinalis), semispinalis, multifidus, rotatores, interspinales, quadratus lumborum, rectus abdominis, psoas major, and psoas minor. The muscles were joined to the skeletal model by using 3D analysis software Visual Nastran 4D (Fig. 3.27).

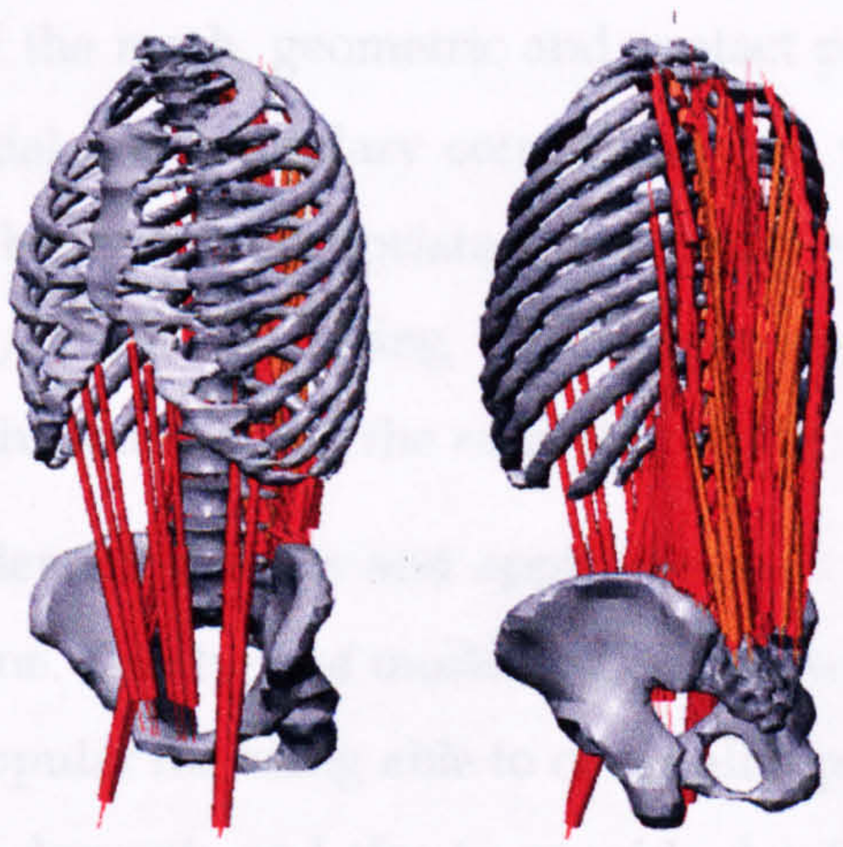

Figure 3.27 Biomechanical spine model of Ishikawa et al. (2005)

Intervertebral discs and ligaments were represented by spring-damper elements which were connected to two adjacent vertebral bodies to represent the disc so as to move the functional spinal unit multidirectionally (Fig. 3.28). The ligament

types; anterior and posterior longitudinal ligament, flavum, supraspinos ligament, interspinous ligament, intertransverse ligament, and also capsule were incorporated into this model.

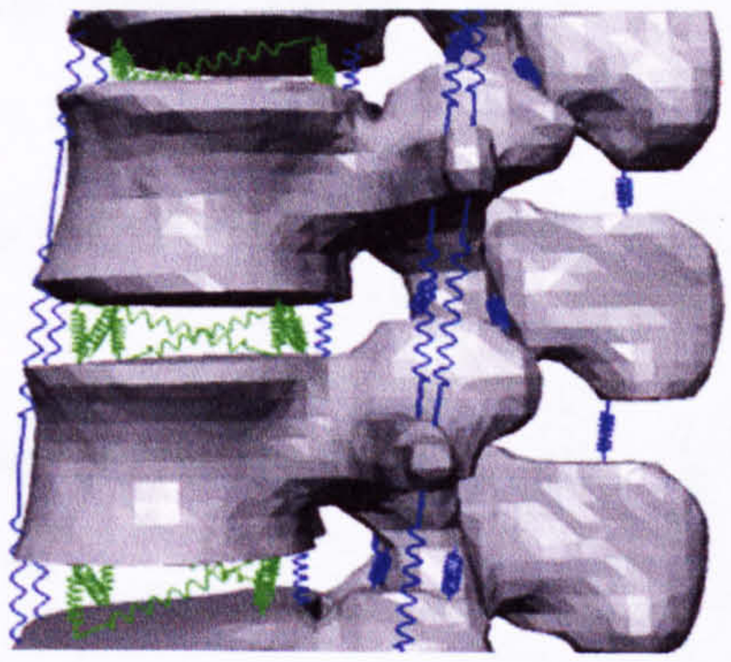

Figure 3.28 Discs and ligaments in the model (Ishikawa et al., 2005)

3.5 Finite Element Models

Generally, finite element (FE) modelling is capable of producing highly detailed models of bodies and systems by dividing the entities into a number of smaller elements, connecting those via nodes, and producing the realistic material behaviour by employing governing FE equations. As a result of being a hugely developed and detailed methodology, the quality and biofidelity of the biomechanical models depend on many factors such as the number and type of elements, the structure of the mesh, geometric and contact properties, material property description, initial and boundary conditions, and various theoretical FE analysis options. Wherever appropriate, sensitivity analysis based on material properties and/or FE modelling parameters such as number of elements needs to be conducted to check the reliability of the individual models.

There are several finite element models and applications on various aspects of modelling the human spine. This type of modelling is extensively used amongst researchers and highly popular for being able to cover all types of analysis such as static, quasi-static and dynamic and also to provide detailed results. On the other hand, FE techniques may require high computational power, detailed and realistic description of material properties, and complex validation requirements depending on the nature of the problem. Dietrich et al. (1991)

summarises the advantages of finite element technique so that FE modelling allows for:

- static analysis of forces occurring in the spinal system (muscles, vertebrae, ligaments, joints) and pressure in nuclei pulposi and in the abdominal cavity,
- investigation of the influence of the shape and dimensions of the spine as a whole,
- investigation of the influence of the system's initial tensions upon the distribution of forces,
- analysis of the influence of the control system expressed with various optimization criteria-upon the distribution of loads in the spine system,
- investigation of the spinal system stability (loss of stability causes a rise of primary curvatures and rotations of the spine),
- dynamic investigation of the spinal system at given kinematic or force excitations.

Some of the FE models of the human spine in the literature possess highly advanced modelling parameters and features such as detailed and realistic geometries, occasionally gathered from computerised tomography (CT) scans, and delineated material properties of the vertebral bodies, intervertebral discs, or ligaments. However, there are almost no FE models, which incorporate active muscle behaviour. Muscles are usually modelled as tissues with passive properties.

3.5.1 FE Models of the Cervical Spine

A vast amount of finite element studies have been conducted both on the segments and the whole cervical spine. Due to the type and purpose of the analysis, cervical spine FE models are carried out as whole head and neck models, partial cervical spine models, functional spine unit (two complete vertebra and a disc in between) models, disc segment (two vertebral bodies without processes and a disc in between) models or individual cervical vertebra/disc models.

Whole head and neck FE models include the head on top of the cervical spine to obtain a better representation of the head-neck complex. Liu (1986) developed a finite element model of the head and the cervical spine. The 3-D finite element model of a fluid filled skull had been used to simulate the spinal cord cavity.

Kleinberger (1993) constructed a 3-D *from head to T1* FE model of the cervical spine for linear static and dynamic analysis of automobile crashes in order to investigate whiplash injury (Fig. 3.29). The model had an assumed-simplified geometry of the complex, including vertebrae, discs and ligaments. The model possessed several simplifications such as facet angles, which were kept at 45° for all levels of the cervical spine, linear elastic material properties for the intervertebral discs, facet joints and ligaments and no muscular structure. Ligamentous attachments between the cervical spine and the skull were also neglected. The model had been validated against experimental data.

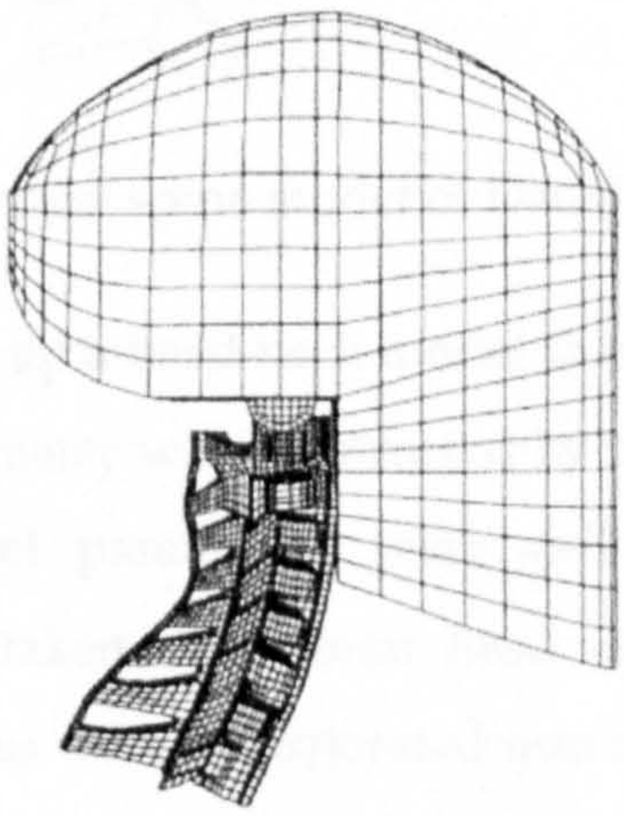

Figure 3.29 FE cervical spine model of Kleinberger (1993)

Dauvilliers et al. (1994) developed a head-T1 FE model for linear dynamic analysis. Vertebrae, discs, and ligaments were incorporated into the model. Cadaver x-rays were used where appropriate to determine the major geometric aspects of the components. All major ligaments of the lower neck were modelled as spring-damper elements, while intervertebral discs were represented by solid elements and disc fibres were incorporated as spring-dampers. Although, initially, material properties used were insufficient, they were calibrated to mimic a response similar to the volunteer test data for frontal

and lateral impact. Dauvilliers et al. claimed that the model yielded satisfactory results in most aspects of the lateral and frontal impact situations, while failing to produce satisfactory predictions at some points such as acceleration spikes, which didn't fall between response corridors of the validation data. They commented that the reason for this was likely to be due to insufficient damping of the model segments. This model is illustrated in Figure 3.30.

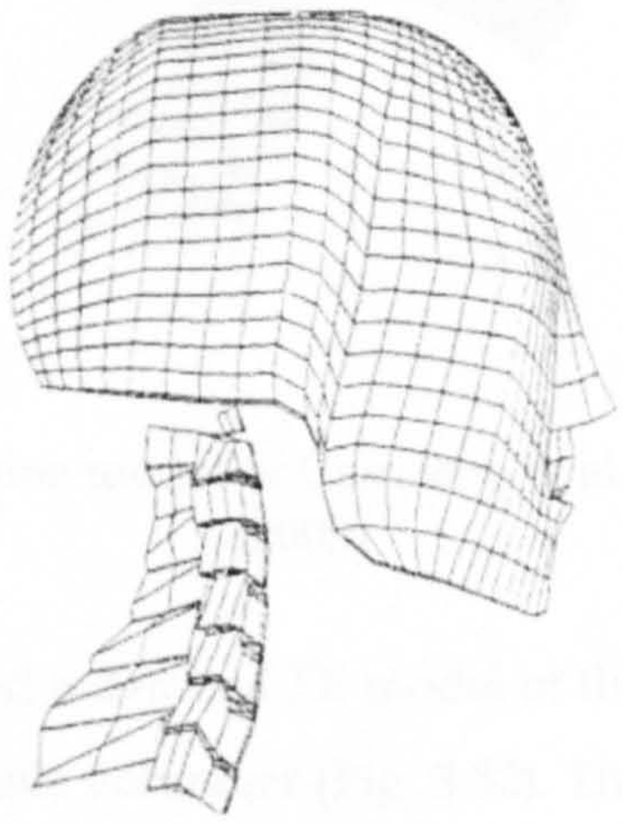

Figure 3.30 FE cervical spine model of Dauvilliers et al. (1994)

Camacho et al. (1997) built up a head-neck model to investigate a dynamic head impact situation. The geometry was constructed by using CT scans of the head and cervical spine. Model parameters were defined via flexion-extension flexibility measurements taken on human head and neck. The mechanical properties of the soft tissues were incorporated into a single intervertebral joint between each pair of adjacent vertebrae. It was presented that the FE spine model simulated the buckling behaviour of the spine specimens precisely in terms of resultant head and neck forces and resultant head acceleration. Van Ee et al. (2000) extended Camacho's model by including neck musculature and updated tensile properties of the intervertebral discs. Muscles were modelled as non-linear spring elements, some of which were divided into sub-segments each represented by a non-linear spring. Muscle force was calculated from the physiologic cross-sectional area of the muscle, initial muscle length and change in muscle length, where activation dynamics were not incorporated. This model is illustrated in Figure 3.31.

Figure 3.31 FE cervical spine model of Camacho et al. (1997) and Van Ee et al. (2000)

Yang et al. (1998) developed a detailed FE model of the cervical spine from MRI scans of a 50th percentile male volunteer (Fig. 3.32). The model was employed to study the mechanics of the head and neck when subjected to acceleration impacts. The vertebrae were modelled as 8-node brick elements with linear elastic-plastic material properties, while the intervertebral discs were modelled as linear viscoelastic materials by using solid elements. The ligaments were incorporated by using non-linear tension-only membrane and bar elements. Cervical muscles were included by integrating sixty tension-only spring elements, for which only the passive properties of the muscles were taken into consideration in the model simulations. Yang et al. claimed that the model was validated with reasonable success against the head and neck drop tests as well as cadaveric sled tests. The head and neck model was combined with a previously developed model of the upper torso and employed to simulate head and neck interaction with a pre-deployed air bag in order to predict head and neck kinematics, load histories and ligament forces.

Halidin et al. (2000) constructed a detailed finite element model of the head and neck in order to investigate the effect of axial impacts (Fig. 3.33). The model included facet joint contact and contact between spinous processes to conform to the nature of the specific loading, while muscles were not included in the model. Linear springs were employed to represent the ligaments of the neck. A

detailed FE model of the head was incorporated into the model to simulate load transfer accurately during near vertex head impact simulation. Validation was carried out for compression, shear and rotational loading on the C4-C5 segment against experimental data. The model was used in designing automobile roofs for injury prevention purposes.

Figure 3.32 FE cervical spine model of Yang et al. (1998)

Figure 3.33 FE cervical spine model of Halidin et al. (2000)

There are numerous *partial cervical spine FE modelling* studies conducted in the literature. Saito et al. (1991) developed a 2-D linear static FE model of the occiput-T2 complex. The model included discs, endplates, facets, ligaments, cortex and cancellous bone and the geometry of the model was simplified. The

effects of axial loading under 150 N force were investigated, however, no validation was carried out. Clausen et al. (1996) constructed a non-linear static model of the C5-C6 functional spine unit, where vertebrae, posterior elements, discs, endplates and all ligaments were incorporated. The geometries were obtained from axial CT scans and therefore modelled realistically. The model was run under 74 N compression, 1.8 Nm flexion, extension, lateral bending and axial torsion loadings and validated against experimental data. Nitsche et al. (1996) built an FE model of the human spine (C1-C7), comprising deformable vertebrae, intervertebral discs, facets, and ligaments, where geometric features were assumed and simplified from the literature. The model was linear elastic, while the intervertebral discs were isotropic, and the cartilages and ligaments were modeled as anisotropic. The model was validated against NBDL (Naval Biodynamics Laboratory) data for frontal and lateral impacts as utilised by De Jager (1996). No cervical muscles were included in the original model but later on Wittek et al. (2000) improved Nitsche's model by adding cervical muscles to study their effect in low speed rear-end impacts. The muscles were modelled as Hill Type muscle elements, and their geometry and attachment points were gathered from the literature. The model was further modified by modelling the intervertebral discs as visco-elastic elements by improving the anatomical representation of the articular facets and their orientation. Contact was sought between facet surfaces as well as spinous processes and the force-displacement properties of the longitudinal and flava ligaments were remodelled as non-linear. Kumaresan et al. (1997) developed a three-dimensional, anatomically accurate, geometrically and materially nonlinear FE model of the C4-C6 segment of the cervical spine (Figure 3.34). The geometrical features were obtained from 1.0 mm CT scan images (coronal and sagittal) and cryomicrotome anatomical sections of a human cadaver specimen. They used a subsequent imaging procedure so that natural lordosis of the cervical spine was incorporated. This model included all essential components of the cervical spine as vertebrae, intervertebral discs, synovial fluid in relevant joints, and ligaments. The model was vigorously validated by comparing computed force-displacement and moment-rotation responses and localised strain data against experimental results. Then, this model was utilised by Kumaresan et al. (1998,

1999a, 1999b, 2000, 2001) in various studies to have a better understanding of various problems associated with the cervical spine, such as modelling the ligaments and facet joint capsule in detail, biomechanical responses of pediatric cervical spine, and contribution of disc generation to osteophyte formation.

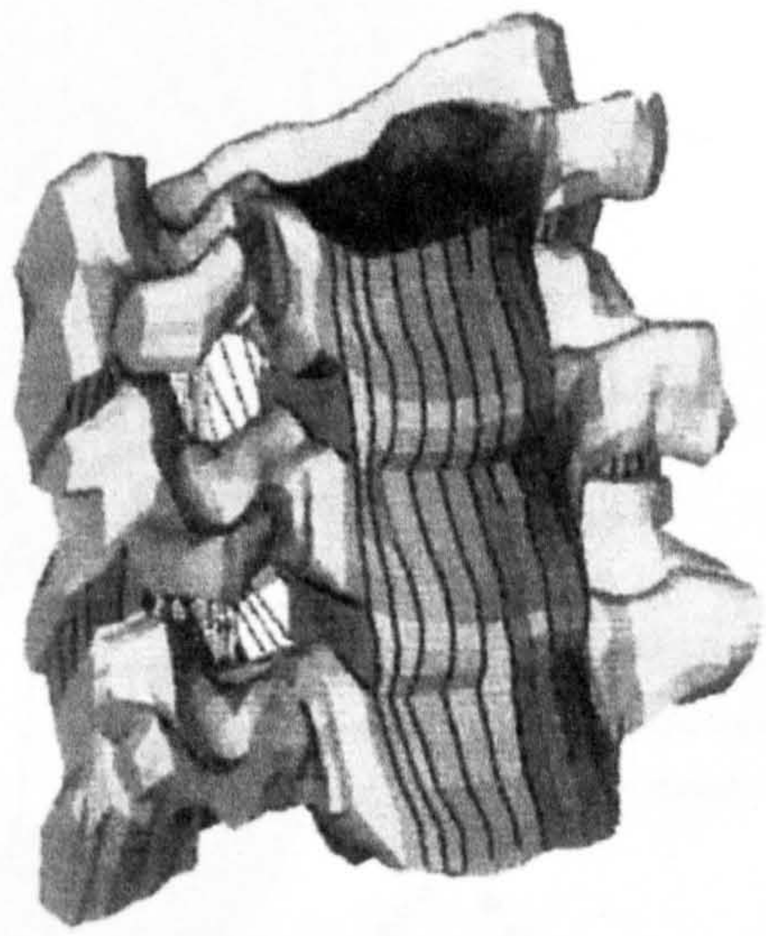

Figure 3.34 C4-C6 cervical spine FE model of Kumaresan et al. (1997)

Teo and Ng (2001) constructed another 3D FE model of the spinal motion segment C4-C6 (Fig. 3.35). The model was based on a 68-year-old cadaveric cervical spine, and assumed to be symmetrical about the mid-sagittal plane. Each vertebra was developed using 1632 eight-noded isoparametric solid elements for the cortical shell, the cancellous core, and the posterior arch. The material properties of the tissues between adjacent vertebrae were taken from literature. The model was validated against published experimental data and compared with existing analytical results under the same boundary conditions. Later on, Ng et al. (2004) used the same model to establish a systematic approach to analyse the influence of six spinal components (cortical shell, vertebral body, posterior elements, endplate, disc annulus, and disc nucleus) on the internal stresses and other biomechanical responses under compression, anterior, and posterior shear. They claimed that results indicated the influence of the material properties variation of the disc annulus significantly on the internal stresses in the disc. They also claimed that the study revealed for the first time the variation in the cortical shell modulus, which had a high influence on the mechanical responses under anterior and posterior shear.

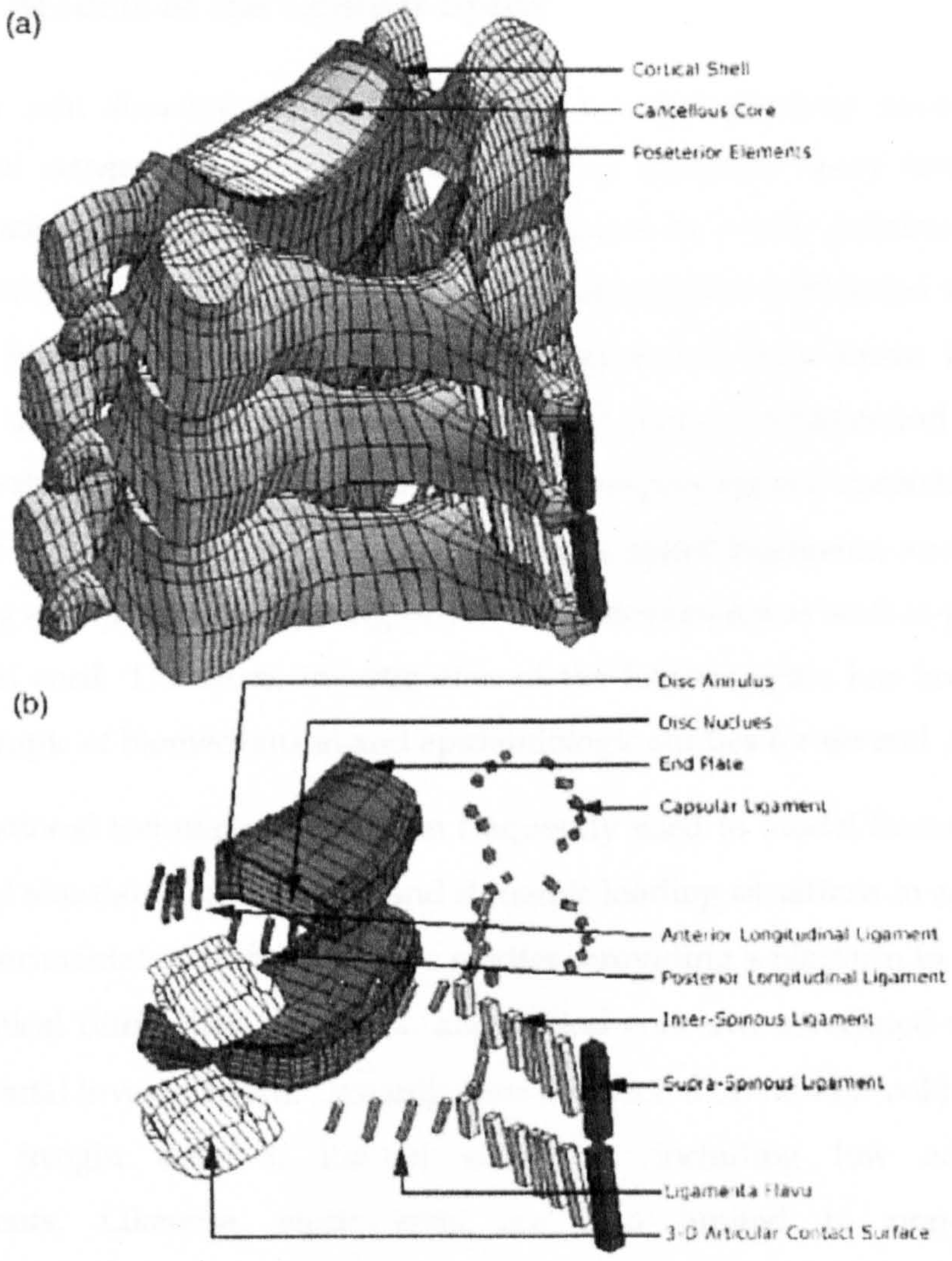

Figure 3.35 C4-C6 cervical spine FE model of Teo and Ng (2001)

FE models of the *cervical vertebrae* have also been investigated in various studies. Bozic et al. (1994) constructed a 3-D linear static FE model of the C4 vertebra. The model included the cortical shell and the cancellous bone, and the actual geometry was gathered via an automatic algorithm from CT scans. The model was run to simulate 4 mm axial compression, but no validation was carried out. In a similar study by Teo et al. (1994) C2 vertebra was modelled in 3-D. Actual geometry was implemented by using a coordinate measuring machine and a semi-automatic geometry generation. A load of 1000 N over 50 mm^2 was applied in different directions. The model was validated against experimental data.

3.5.2 FE Models of the Lumbar Spine

Low back pain disorders are one of the most prevalent problems associated with recreational activity and industrial work, involving physically heavy tasks, sudden lifting, bending, and twisting motions. These disorders are mainly associated with the *lumbar spine,* which is the lower part of the human spine positioned at the low back of human torso, below the thoracic spine and just above the sacral segment, supporting and transferring the largest portion of forces and moments acting on the human spine. Lumbar spine is a complex system, consisting of five vertebrae interconnected by intervertebral discs, spinal ligaments, and muscles, providing stability and producing physiologic movements as well as protecting the spinal cord. Therefore, investigation of the lumbar spine has been a very popular topic of biomechanical and epidemiologic studies for several years.

Computational techniques have been frequently used to model human lumbar spine and simulate various static and dynamic loading situations in accordance with experimental *in vitro* and *in vivo* studies, providing a platform to overcome the technical difficulties, high cost, and ethical concerns associated with such experimental investigations. Dynamic tests conducted on human volunteers can provide insight only to limited situations, including low acceleration experiments. Likewise, static tests are also limited to non-traumatic investigations. Under these circumstances, computational methods are frequently used to develop a better understanding of injury mechanisms regarding the lumbar spine, to aid the therapists in selecting the type of treatment for musculoskeletal disorders, and to develop guidelines for industrial safety.

Shirazi-Adl and Parnianpour (1996) performed a nonlinear finite element study of the ligamentous thoracolumbar spine to investigate the stabilizing role of two plausible mechanisms of combined moments and pelvic rotation on the human spine in axial compression. The passive system, by itself, was able to carry only a negligible fraction physiological compression loads without exhibiting large motions. Following this study, they (2000) developed a nonlinear finite element formulation of wrapping elements sliding over solid body edges in order to investigate biomechanics of the human spine under a novel compression

loading that follows the curvature of the spine. They concluded that the idealized wrapping loading stiffens the spine, allowing it to carry very large compression loads without hypermobility.

Zander et al. (2002) employed a three-dimensional nonlinear finite element model of the lumbar spine with internal spinal fixators and bone grafts in order to study mechanical behaviour after mono- and bisegmental fixation with and without stabilization of the bridged vertebra. Finite element analyses were performed to determine the influence of four different graft positions, five loading conditions, and six different pretensions in the longitudinal fixator rod. The following parameters were considered: the maximum contact pressure at the interface between the bone graft and vertebral body, the force transmitted by the bone graft, and the size of the contact area between the graft and the vertebral body. The finite element model of the lumbar spine is provided in Figure 3.36.

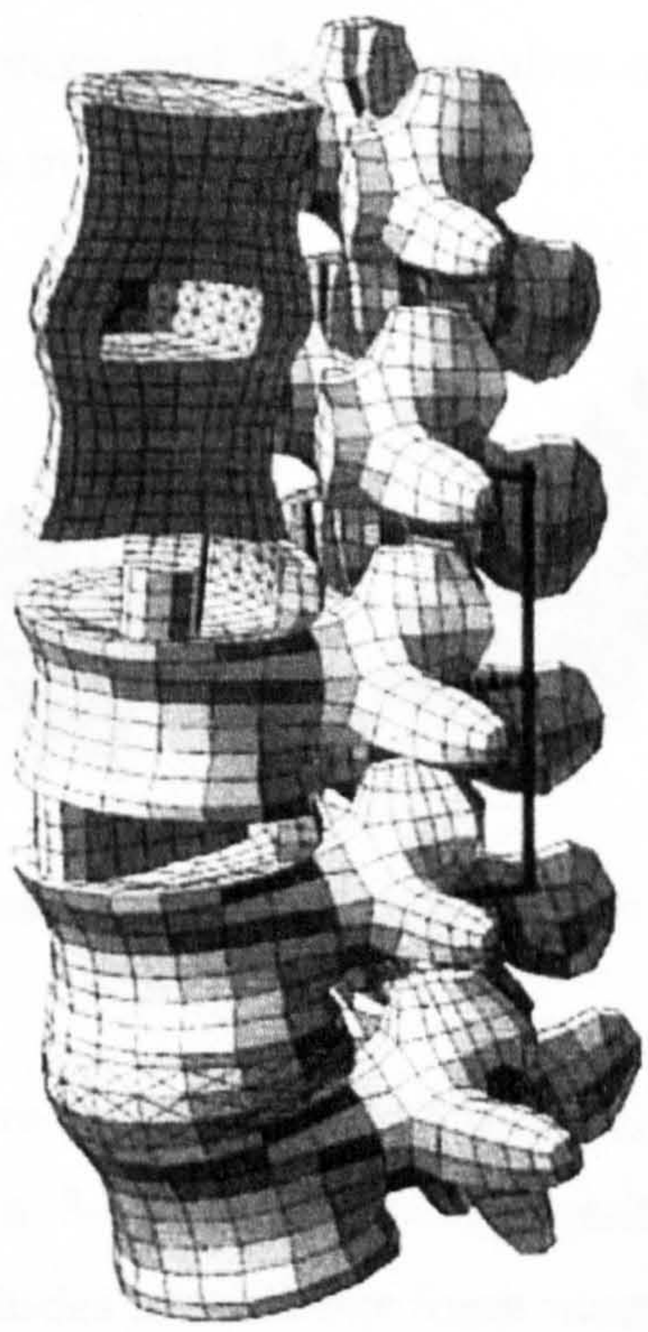

Figure 3.36 Cut through the element mesh of the finite element model of the lumbar spine (Zander et al., 2002)

They created a three-dimensional, nonlinear finite element model of the human osteoligamentous lumbar spine. The model consists of about 8000 volume elements and has more than 30,000 degrees of freedom. The nucleus pulposus had been simulated by an incompressible fluid-filled cavity and the anulus fibrosus by volume elements with superimposed spring elements representing the fibres. The spatial orientation of the facet joints had been modelled according to measurements taken by Panjabi. The facet joints could only transmit compressive forces. The capsule of the facet joints and the six ligaments of the lumbar spine were included. The authors concluded that their model showed no clear differences between mono- and bisegmental fixation. Additional stabilization of the bridged vertebra exerted a partly adverse influence on the parameters studied. Pretension in the bridged region had a strong effect on the mechanical behaviour (Zander et al., 2002).

In their study, Cooper et al. (2001) developed a three-dimensional visualisation tool of the human lumbar spine (Fig. 3.37). Motion data are acquired from fluoroscopic image sequences and the kinematics of the lumbar spine was visualised via the software interface.

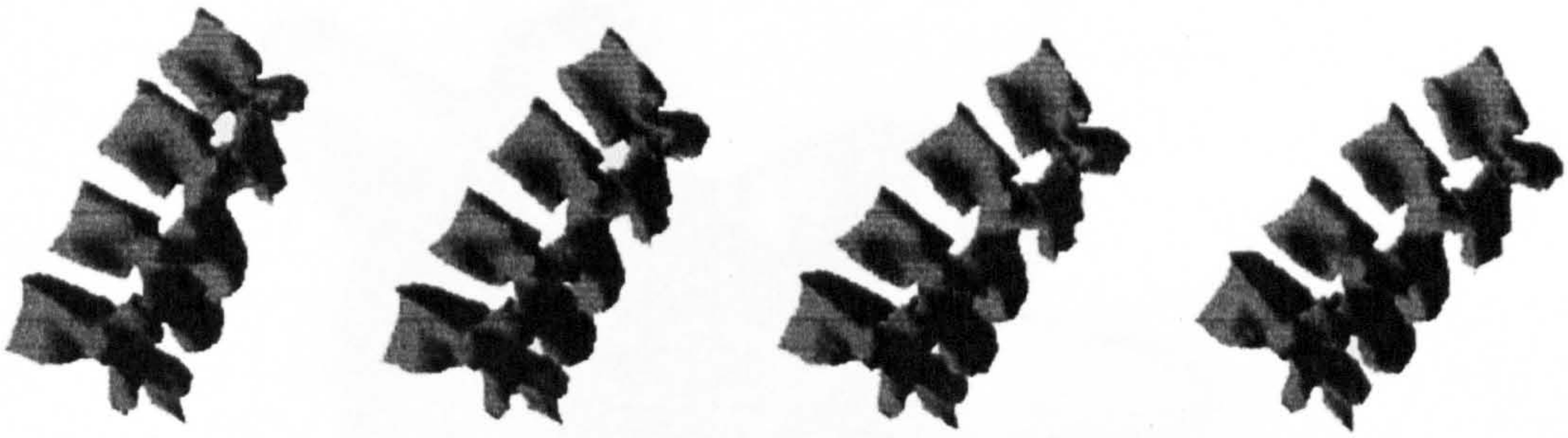

Figure 3.37 Four frames from an animation sequence of the lumbar spine (Cooper et al., 2001)

Lumbar vertebral bodies were also modelled by utilising FE techniques. Overaker et al. (1999) developed a 3-D physiologically realistic model of a lumbar vertebral body which includes a nonlinear foam model for the trabecular bone component. The authors demonstrated the effects of localized yield under compressive loads on the whole bone mechanical response (Figure 3.38). Nabhani and Wake (2002) used I-DEAS software to reconstruct the lumbar vertebrae by transferring data points, which yielded a very realistic model of the

vertebra (Figure 3.39). And then, finite element analysis had been carried out to simulate several loading conditions.

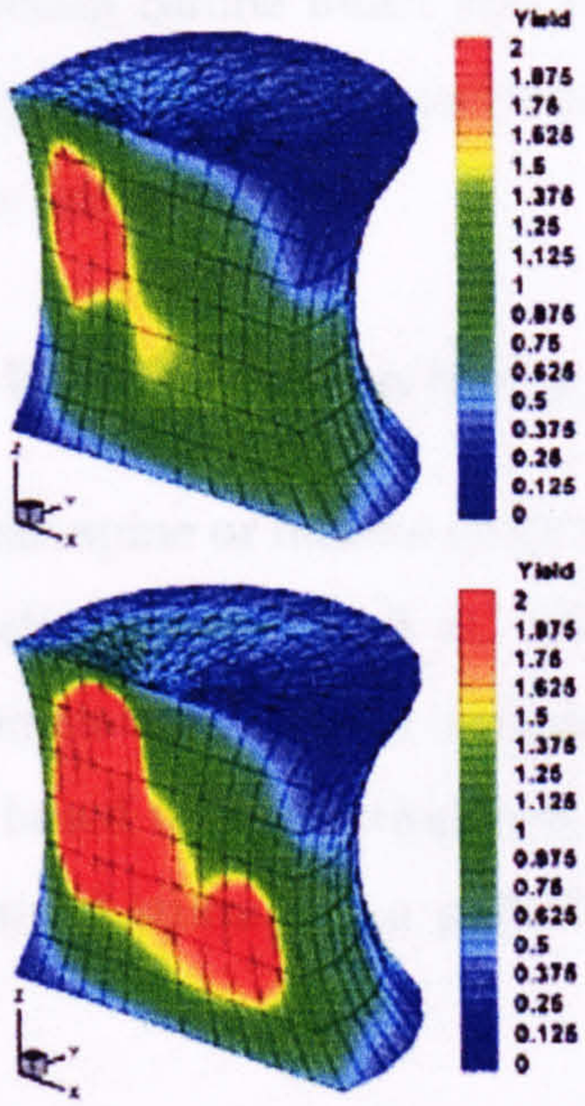

Figure 3.38 Yield contours of the lumbar vertebra under compressive load at two successive points on the load-deformation curve, where red colour shows the localized yield (Overaker et al., 1999)

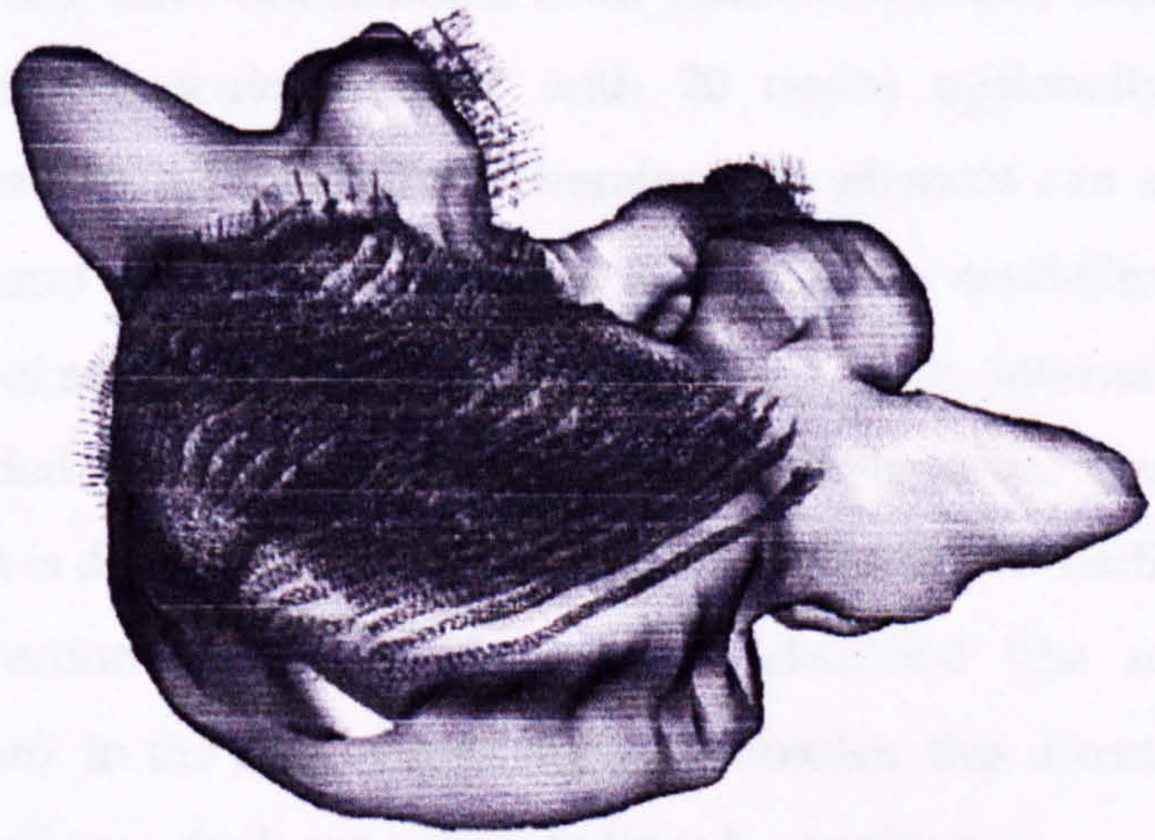

Figure 3.39 Applied pressure to L5 (Nabhani and Wake, 2002)

Xinghua et al. [2002] proposed a high-order nonlinear equation of bone remodelling to incorporate with FEM by introducing two nonlinearities; remodeling coefficient, and the order of nonlinear remodeling equation.

There are some other studies, which attempt to investigate the similarities between human and animal lumbar spinal segments. Lim et al. (1994) employed finite element method to obtain canine intact and stabilized motion segments. The outcomes of the study yields that a canine is a suitable model for the biomechanical studies of the lumbar spine.

3.5.3 FE Models of the Whole Human Spine

There are a few whole human spine or human body FE models conducted in the literature. In an early model, Vanderby et al. (1986) proposed a numerical algorithm in order to estimate the in vivo segmental stiffness properties of individual spine segments based upon existing load-displacement data. A static nonlinear finite element model stimulates a pathological spine and corrective instrumentation system.

Dietrich et al. (1991) presented a finite element model of the whole human spinal system (Fig. 3.40). The most important original concepts for this study are:

- Design of a three-dimensional finite element specially adjusted to model the skeletomuscular system with 20 nodes optionally located and connected by a broken line. Therefore the element can adopt different shapes and dimensions, and thus is suitable for modelling the complex shapes of anatomic elements of the spinal system. Internally the element is divided into 48 simple tetrahedral subelements. Geometry of the element is described in a local curvilinear system of coordinates in which the direction of one of the axes is identified (the so-called active direction). In the case of modelling of muscles, this direction runs along muscle fibres which can generate force by contraction.
- Description within one FEM model, of both rigid and deformable bodies as well as fluids.
- Description of muscle force as a function of its elongation and stimulation by nerves.

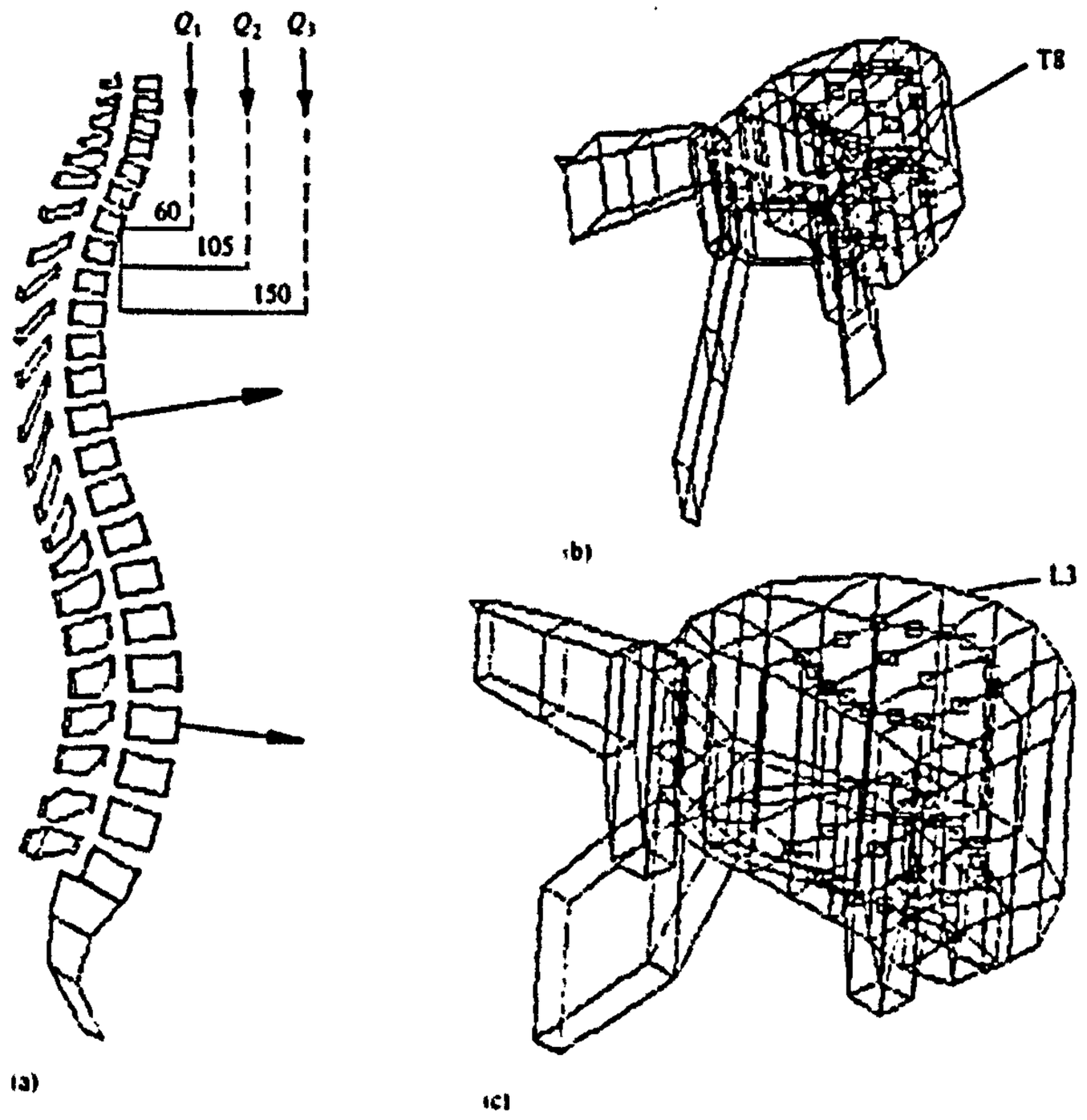

Figure 3.40 Model of human spine (a) the orientation of the 22 vertebrae (b) modelled thoracic vertebra (c) modelled lumbar vertebra (Dietrich et al., 1991)

Huang et al. (1994) developed an FE model of the human body in order to simulate the gross motion of cadavers in sled tests. To simplify the model and therefore to reduce the computational time, the FE mesh of the whole human spine was relatively coarse. The model was used to predict and interpret the injury responses for the chest in lateral impact sled tests.

Lee et al. (1995) generated a linear three dimensional finite element model in order to predict the vertebral displacements resulting from a posteroanterior force applied by a therapist. Consequently, intervertebral translations were predicted to be 1 mm or more at up to four intervertebral joints away from the point of load application.

Lizee et al. (1998) constructed a relatively advanced FE model of the human body, which was validated through various impactor and sled tests. The model included a limited number of 10000 elements for the sake of simplicity. They claimed that the validation results showed the feasibility of a biofidelic FE model of the human body.

Jost and Nurick (2001) developed an FE model of the human body for simulating damage during vehicle side impacts (Fig. 3.41). The model consisted of skeleton modelled with shell elements and the surrounding soft tissue of muscles, ligaments, and internal organs modelled with solid, membrane, and spring-damper elements. The muscles possess passive behaviour as modelled with solid elements. They claimed that the model operated numerically stable and did not exceed processing times of 48 hours for a 100 ms impact simulation. The model predictions were claimed to show good agreement with the results of pendulum impactor tests.

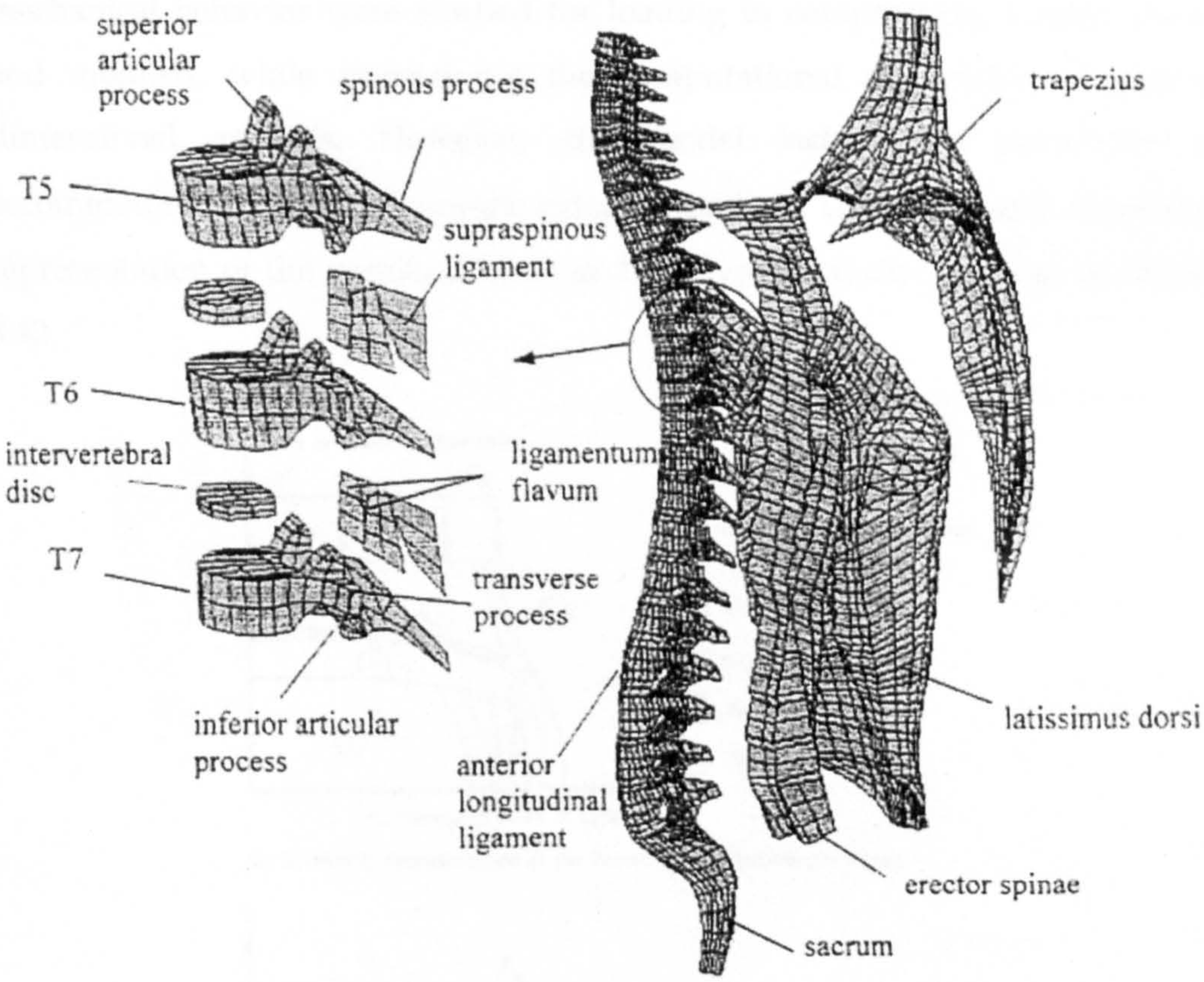

Figure 3.41 FE model of the human spine of Jost and Nurick (2001) within the whole FE human body model

3.5.4 FE Models of the Intervertebral Discs

The mechanical responses of intervertebral discs under different loading conditions have been investigated by several authors. Various models have been reported in order to analyze the disc behaviour and properties. For these

purposes, one of the most common techniques employed is the finite element method.

Spilker et al. (1984) proposed a simplified finite element model to explore the mechanical response of the disc under complex loading. Their model was axisymmetric about the longitudinal axis and the model motion segment is assumed to be symmetric with respect to its mid-transverse plane. The nucleus was assumed to be a hydrostatic incompressible fluid, while the annulus and the vertebral body/end-plates are assumed to be isotropic linear elastic materials. The effects of gross disc geometry and soft tissue properties on mechanical behavior were studied for loading in compression, torsion, shear and moment, while maintaining the computational efficiencies of a two-dimensional analysis. However, the model lacked the possibility of accommodating non-axisymmetric external loading. The actual and simplified representation of the vertebral body and intervertebral disc is given in Figure 3.42.

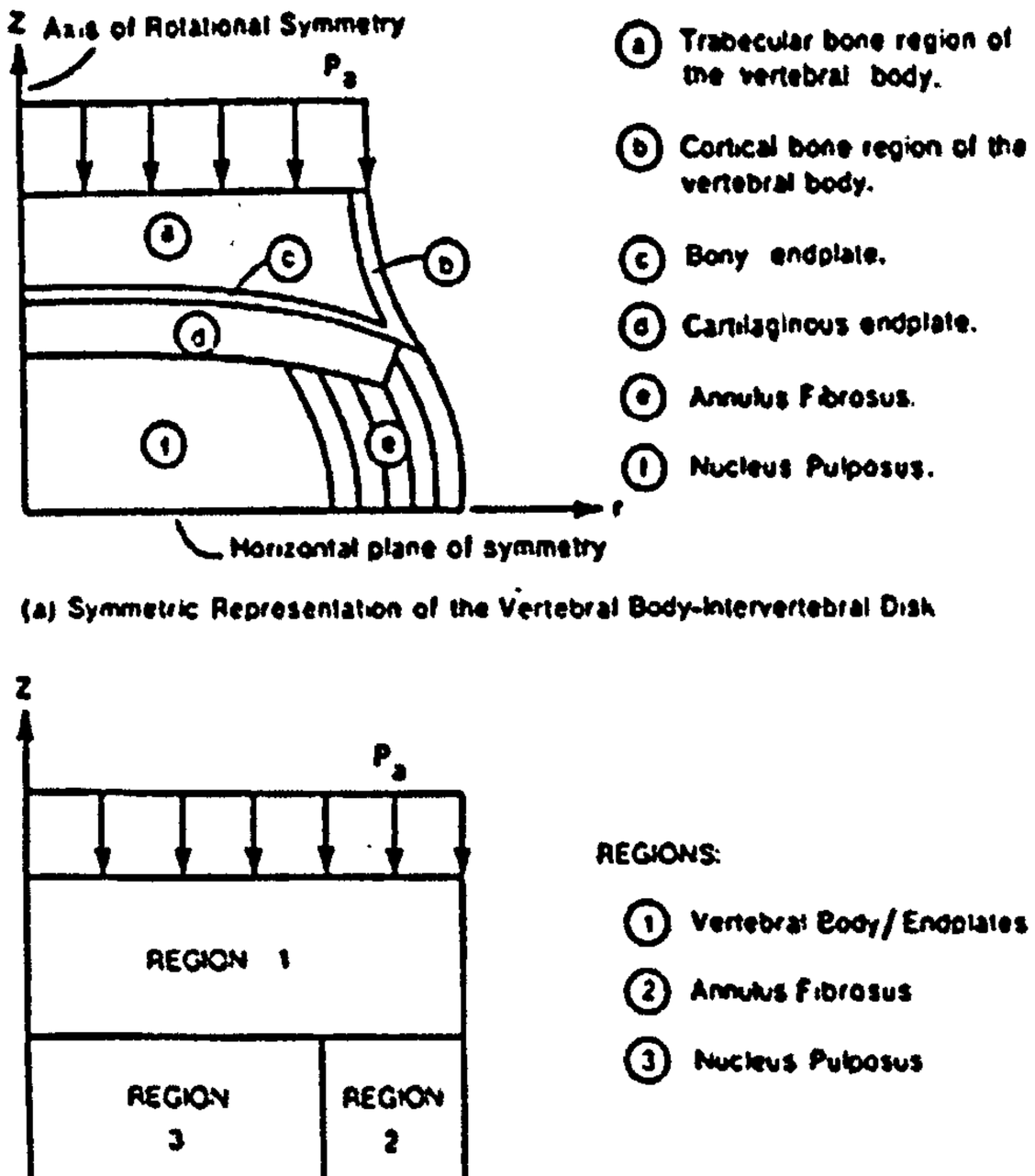

Figure 3.42 The actual and simplified representation of the vertebral body and intervertebral disc (Spilker et al., 1984)

Spilker et al. concluded that strength-of-materials models can provide reasonable predictions for end-plate rotation in torsion, and end-plate tilting in shear and bending but give generally poor predictions of other quantities.

Dozzini et al. (1999) presented a 3-D poroelastic anisotropic finite element model of the human lumbar intervertebral disc, which also incorporates nonlinearity due to permeability, large deformations and material constitutive behaviour. The model appears to be capable of simulating compression, flexion, and torsion both under creep and relaxation conditions. In another study, Lee et al. (2000) developed a 3-D nonlinear finite-element model of the L3-L4 spinal motion segment, previously created using computed tomography (CT) transverse sections, which was modified to include poroelastic properties in the disc and thus simulate the response of spinal motion segment under impact loading conditions. They used half of the vertebral body and disc model in order to reduce the overall mesh size and emphasize the behaviour of the disc and vertebral body (Figure 3.43).

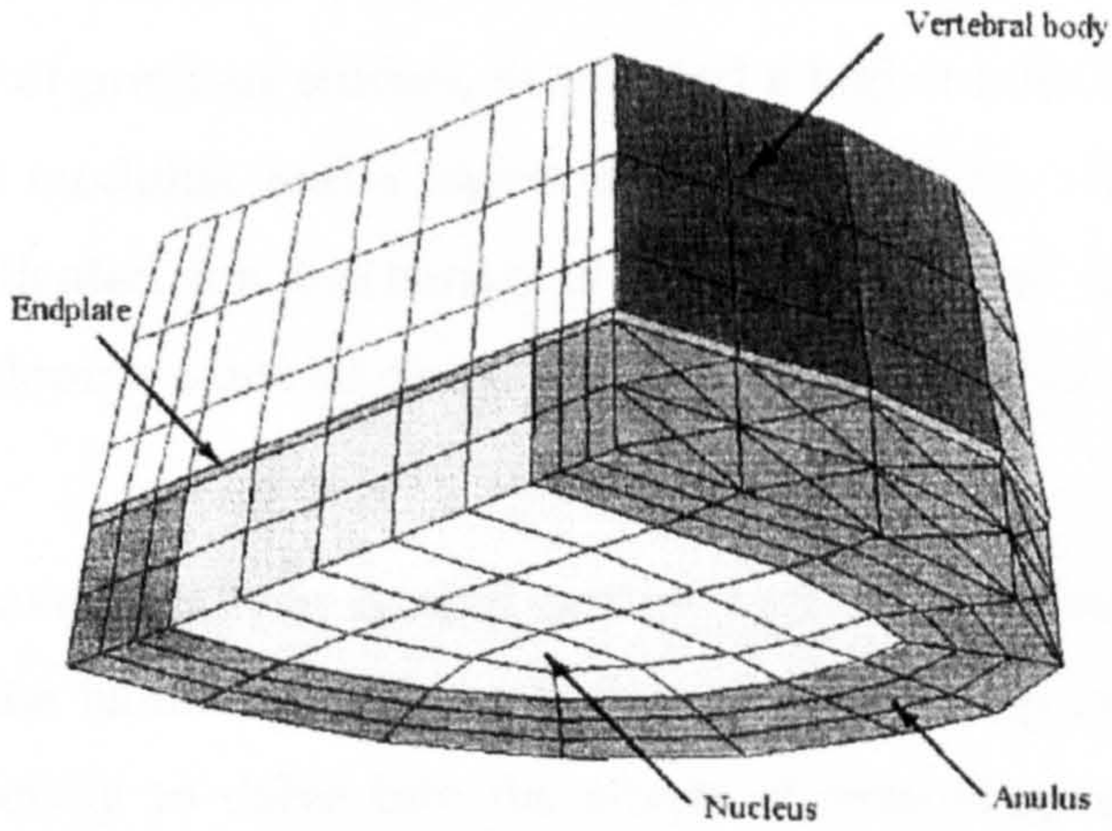

Figure 3.43 Vertebral disc FE model (Lee et al., 2000)

They infer the use of the finite-element technique to address the role of impact duration, Δt, in producing trauma to the spinal motion segment. Within the limitations of the reported model, the results suggest that fractures are likely to occur under shorter Δt conditions. They concluded that fractures can be initiated in the end-plate region or the posterior wall of the cortical shell depending on the strength of the region. Baer et al. (2001) developed an

anisotropic, biphasic finite element model (FEM) of disc cell-matrix interactions in the intervertebral disc capable of describing the anisotropy in the extra cellular matrix and the large strains which may occur in and around the cell. The outcomes of this study imply that zonal differences in cell micromechanical environment may play a role in known differences in the biosynthetic response of disc cells to mechanical loading.

Wagner et al. (1999) developed a constitutive formulation in order to specify a strain energy function which simultaneously predicts the mean response of the annulus to seven different experimental protocols - confined compression (two directions), uniaxial tension (two directions) and shear (three directions) and determined the material coefficients of the strain energy formulation which predicts within one standard deviation the mean response of the annulus fibrosus, both with and without invoking the traction free boundary conditions. Klisch and Lotz (2000) presented an intrinsically incompressible special mixture theory and have determined the material constants for healthy human annulus fibrosus using new confined compression experimental data and in comparison to the aftermath of previous studies, they stated a higher initial water content, a lower aggregate modulus, and a higher initial permeability constant. Riches et al. (2002) investigated the mechanics of the intervertebral disc under cyclic loading by developing a one dimensional poroelastic model and conducting the experiment.

Some studies have also been carried out on human and sheep intervertebral discs to reveal the biomechanical similarities of both. Sheep lumbar discs have been used especially to delve into the effects of removing and replacing the nucleus. Reid et al. (2002) mainly investigated the water and collagen contents and fibre angles of sheep discs experimentally and concluded that a sheep disc can be used as a model of a human disc. Likewise, Costi et al. (2002) determined the hydration-over-time behaviour of ovine intervertebral discs and intact joints in a saline bath at body temperature and the effect on their stiffness compared to air at ambient temperature and demonstrated the similarities between human and sheep intervertebral discs.

3.6 Hybrid Multi-Body / Finite Element Models

Multi-body dynamics constitute a powerful tool for investigating the gross motion of multi-body mechanical systems. Multi-body dynamics approach provides a platform for gathering kinematic and kinetic data for the motion analysis of systems such as vehicle occupant segments. Via this method, calculation of joint reaction forces is also possible as a kinetic output. On the other hand, determining internal loads and deformations of the structures is only possible through structural analysis as in FE method. In order to utilise these two methods to make the most of their advantages, hybrid multi-body/finite element models are used, where a multi-body system is constructed to have a set of interconnected rigid and deformable bodies (Fig. 3.44). Successful applications for this technique depend on individual codes or capabilities of relevant commercial software, which are not very common.

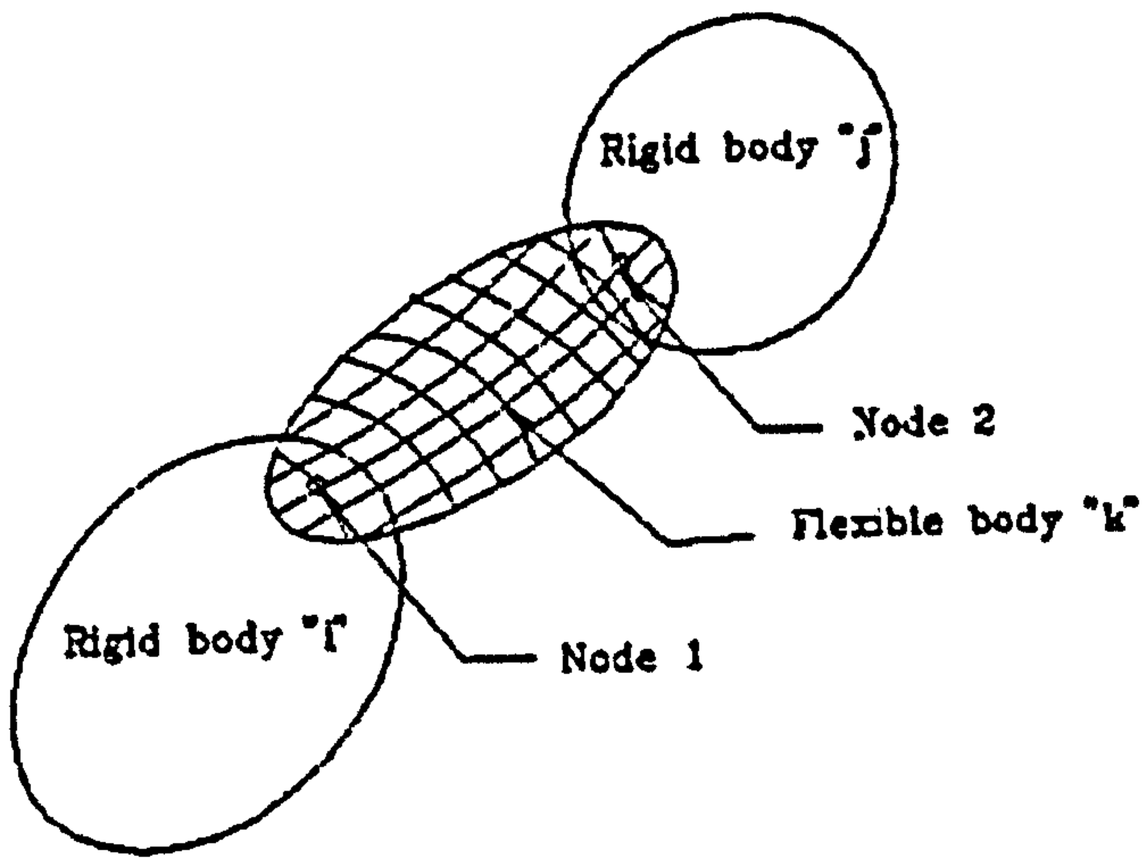

Figure 3.44 A flexible body connecting two rigid bodies (Ma and Lankarani, 1997)

Ma and Lankarani (1997) employed a hybrid multi-body/finite element analysis approach for modelling of crash dynamic responses of ground vehicle or aircraft occupants. The formulation was solved at every time step to determine the corresponding reaction forces and moments at the boundaries and also the structural deformations. Based on this technique, a multi-body model of the occupant with a nonlinear finite element model of the lumbar spine was developed for a Hybrid II anthropomorphic crash test dummy. The two-

dimensional occupant model was represented by eleven rigid segments including head, upper and lower torso, pelvis, upper arms, forearms, thighs, and lower legs as shown in Figure 3.45. The rotor cup, elbow, pelvic, knee, and head-neck joints were hinge-type connections. Deformable elements with simple force-deflection data were used for the lumbar and cervical spine. Rotations at the joints are resisted by torsional spring-dampers.

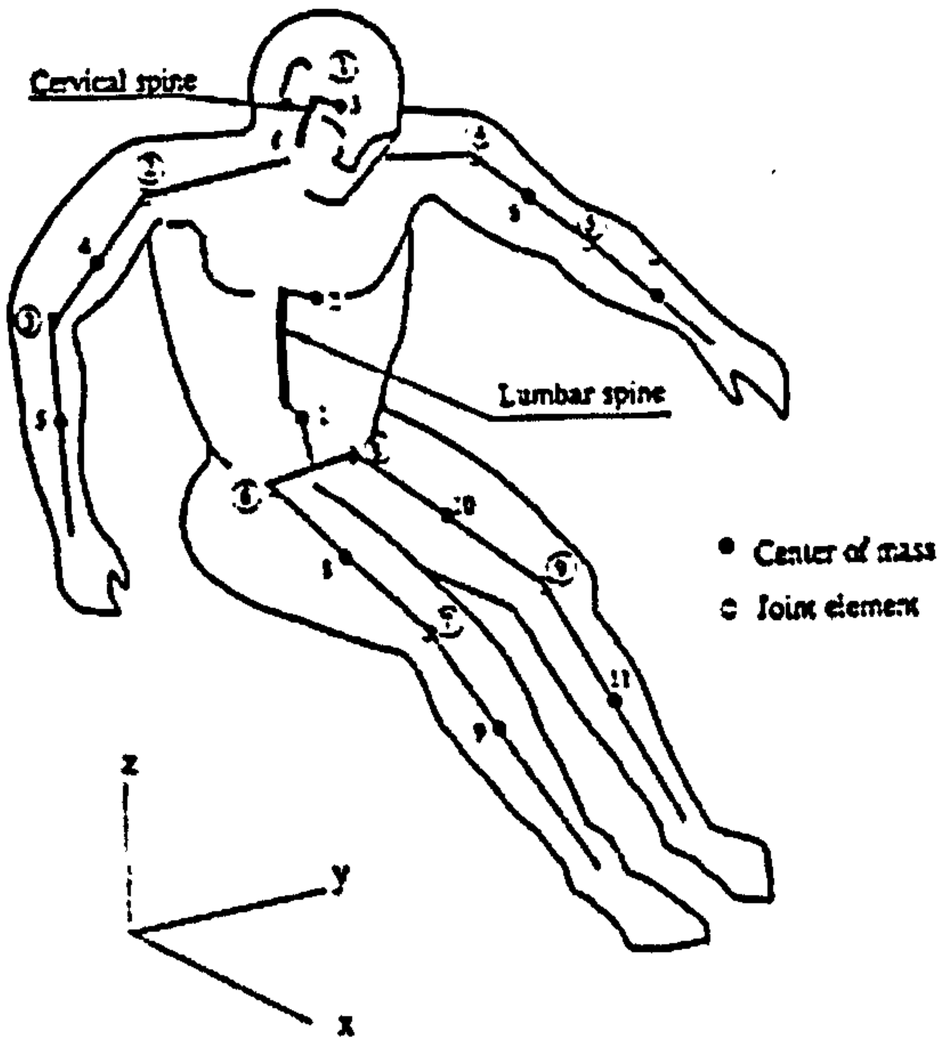

Figure 3.45 Occupant with FE spine model (Ma and Lankarani, 1997)

For the purpose of assessing the possibility of spine injury, the lumbar spine FE model for a Hybrid II test dummy was created. This model consisted of ten straight beam elements with rigid bodies at the top and bottom, which represent the pelvis and thorax. The beam elements included both axial and bending stiffness, which represented five vertebrae and discs, respectively. There were eleven nodes with thirty three degrees-of-freedom. The initially curved configuration of the finite element model was shown in Figure 3.46. The displacements (deformations) and corresponding forces were evaluated and transformed to global coordinates using the transformation matrices.

Consequently, the comparison of the results was reported to show better correlation between the analyses and the experiments compared to earlier studies.

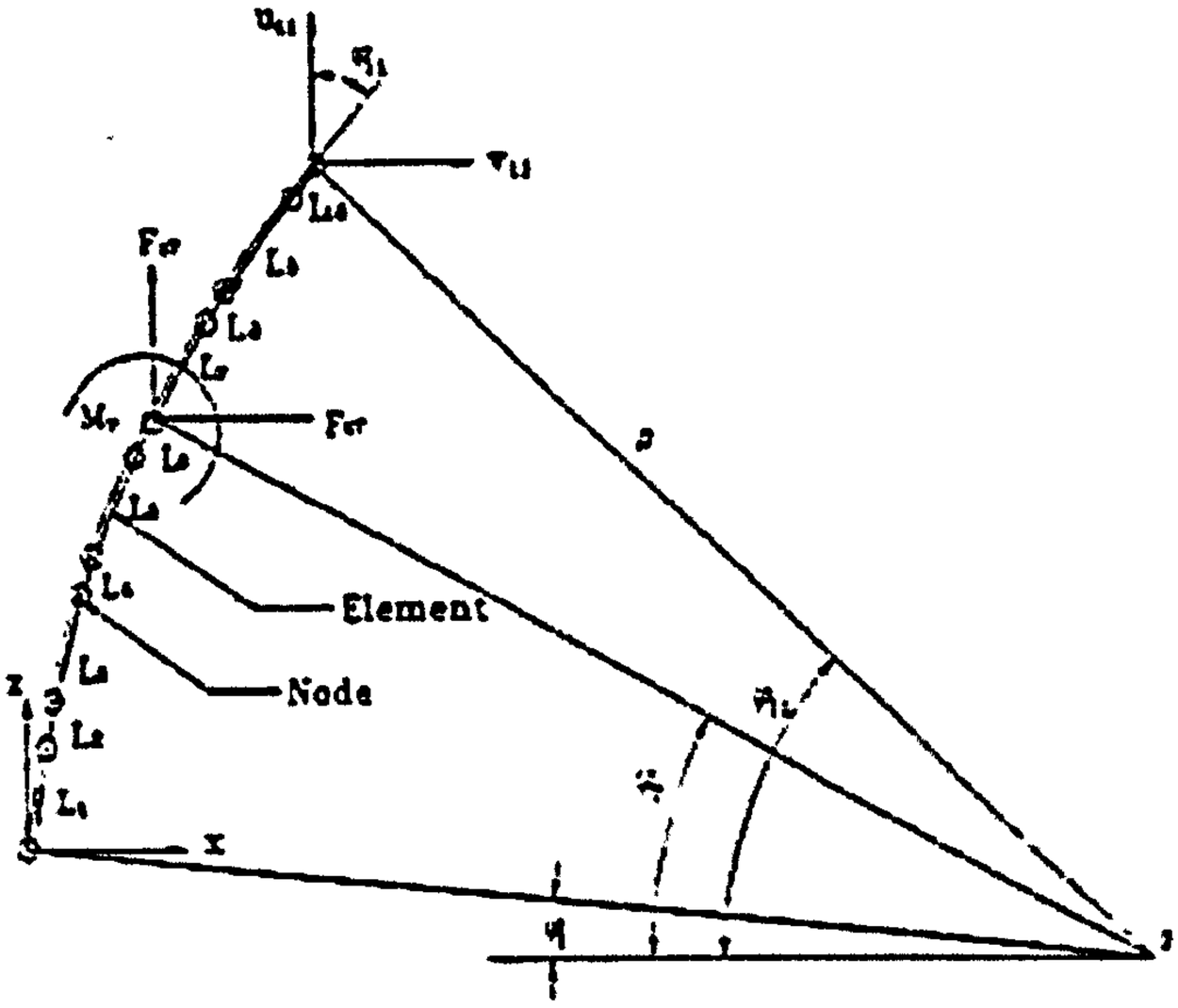

Figure 3.46 FE model of the lumbar spine (Ma and Lankarani, 1997)

In another study, Camacho et al. (2001) utilized an experimentally validated computational head-neck model, consisting of a lumped parameter neck model and a finite element head model, in order to investigate the influence of surface padding properties on head and neck injury. The model can be seen in Figure 3.47.

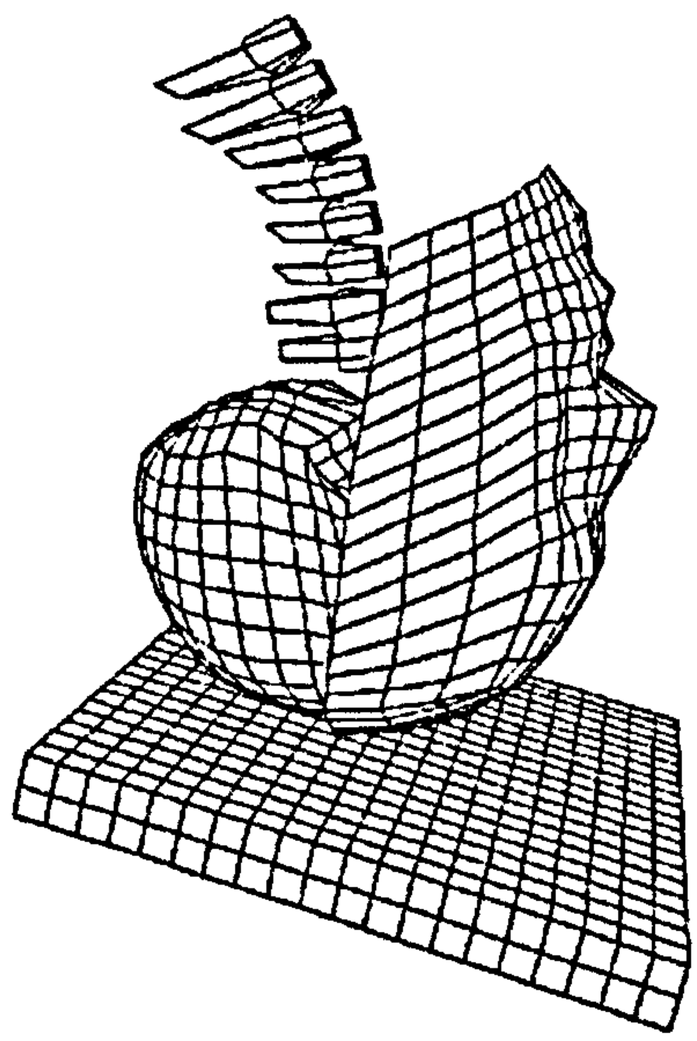

Figure 3.47 Computational model of head and cervical spine (Camacho et al., 2001)

3.7 Discussion

This chapter discussed the classifications of the computational human spine models as well as the reasoning behind the need for those. A comprehensive review of the classifications of human spine models and a broad literature survey on numerous prominent models developed were presented. A final classification approach was proposed for understanding the mainstream of spinal modelling, which helped to demonstrate the rapid developments and improvements within each methodology. Therefore, the assessment of all types of models constituted the initial steps of this study, which not only led to developing hybrid approaches for the previously addressed dynamic loading conditions such as car crashes and impacts, but also formed the basis for the methodologies employed in developing the models.

The first group of computational spine models introduced was *analytical, geometric, 2 pivot, and continuum models,* which are often referred to as *mathematical models* and possess significant differences from biomechanical models such as multi-body or finite element models. When compared to discrete parameter models, continuum models seem to arouse less interest due to a belief that they cannot provide a relevant and satisfactory description of the spine because of their simplicity. However, several studies have revealed that a simple continuum model can give a reasonably correct description of the spine under various specific conditions. These models were usually employed for static or quasi-static analyses such as lifting activities or spinal postures under static loading. One advantage of these models is required computational power and time, which is quite low when compared to more complex models such as multi-body and FE ones.

Multi-body models constituted the second group of computational human spine models discussed. As mentioned before, multi-body/discrete parameter models have the ability to simulate the global and local kinematics and kinetics of the human spine. A multi-body system is a collection of rigid bodies connected through kinematic joints as well as elements applying forces. These models provide a suitable platform to introduce active muscle properties as well as passive behaviour as in Van der Horst (1997, 2002) and Van Lopik and Acar

(2004) models. As in active muscle modelling, the capability of combining multi-body software such as visualNastran with advanced mathematical packages such as Matlab and Simulink provides a sophisticated medium to create more biofidelic and realistic biomechanical models. Multi-body dynamics models have advantages such as less complexity, less demand on computational power, and relatively simpler validation requirements when compared to FE models. Due to the nature of multi-body modelling, it is not possible to conduct structural analysis directly in order to gain information on internal forces and deformations such as stresses and strains within the segments of the human spine.

Author's multi-body model of the whole human spine as described in this thesis was started to be constructed in 2002. The two similar models of De Zee et al. (2003) and Ishikawa et al. (2005) were built in a manner close to the techniques employed in this study. However, De Zee model was an incomplete spine model in terms of only including all lumbar muscle groups and it was solely constructed around the lumbar region. Ishikawa et al. musculoskeletal dynamic multi-body spine model was developed in order to perform Functional Electrical Stimulation (FES) but only a few details were disclosed about how the components of the spine were modelled, and in particular, how muscles were developed and governed to possess active behaviour.

The other widely used group was the *finite element* models. Finite element (FE) modelling is capable of producing highly detailed models of bodies and systems by dividing the entities into a number of smaller elements, connecting those via nodes, and producing the realistic material behaviour by employing governing FE equations. As a result of being a hugely developed and detailed methodology, the quality and biofidelity of the biomechanical models depend on many factors such as the number and type of elements, the structure of the mesh, geometric and contact properties, material property description, initial and boundary conditions, and various theoretical FE analysis options. Wherever appropriate, sensitivity analysis based on material properties and/or FE modelling parameters such as number of elements needs to be conducted to check the reliability of the individual models.

FE modelling is highly popular for being able to cover all types of analysis such as static, quasi-static and dynamic and also to provide detailed structural results such as stress and strain distributions. Dietrich et al. (1991) summarised the advantages of finite element technique, which allows for; static analysis of forces occurring in the spinal system (muscles, vertebrae, ligaments, joints) and pressure in nuclei pulposi and in the abdominal cavity, investigation of the influence of the shape and dimensions of the spine as a whole, investigation of the influence of the system's initial tensions upon the distribution of forces, analysis of the influence of the control system expressed with various optimization criteria-upon the distribution of loads in the spine system, investigation of the spinal system stability (loss of stability causes a rise of primary curvatures and rotations of the spine), and finally dynamic investigation of the spinal system at given kinematic or force excitations. On the other hand, FE technique may require high computational power, detailed and realistic description of material properties, and complex validation requirements depending on the nature of the problem. Some of the FE models of the human spine in the literature possess highly advanced modelling parameters and features such as detailed and realistic geometries, occasionally gathered from computerised tomography (CT) scans, and delineated material properties of the vertebral bodies, intervertebral discs, or ligaments. However, there are almost no FE models, which incorporate active muscle behaviour. Muscles are usually modelled as tissues with passive properties.

The last group introduced was *hybrid multi-body/finite element models*. While multi-body dynamics models play an important role in investigating the gross motion of multi-body mechanical systems, it provides a platform for gathering kinematic and kinetic data for the motion analysis of systems such as vehicle occupant segments. On the other hand, determining internal loads and deformations of the structures is only possible through structural analysis as in FE method. Hybrid multi-body/finite element models were formulated to utilise these two methods to make the most of their advantages. Successful applications for this technique depend on individual codes or capabilities of relevant commercial software, which are not very common.

Having discussed all the relevant modelling approaches, this thesis includes a proposed hybrid approach (not a hybrid model), combining independent multi-body and FE models, which is explained in the forthcoming chapters in detail. Roughly, the loading conditions as predicted from the analyses of the multi-body model were used as dynamic loading boundary conditions for the FE models. This proposed approach not only provides a detailed loading history of the impact on the spinal parts via the validated MB model but also provides information via the validated FE models on how the relevant spinal part is affected during the loading.

CHAPTER 4

Multi-Body Model Development

4.1 Introduction

In this chapter, multi-body model development is described in detail. Two multi-body models are explained: the first one is a preliminary multi-body model of the lumbar spine, which aimed to establish the principles to extend the model to a whole human spine MB model; the second one is the final whole human spine MB model.

4.2 A Preliminary Multi-Body Model of the Lumbar Spine

A 3-D CAD (Computer Aided Design) model of the segments of the lumbar spine was established in order to employ in the multi-body analysis. In order to develop the solid models of the vertebrae, commercially available software Solid Edge v11 and I-DEAS have been utilized.

4.2.1 Solid Model of the Lumbar Spine

The lumbar vertebrae (L1-L5) are the largest and strongest vertebrae. They are situated between thorax and the pelvis. The arrangement of the facets on the articular processes of each vertebra maximizes forward and backward bending, however, lateral bending is limited while rotation is practically eliminated (Carola et al., 1992).

In order to develop the lumbar human spine, quantitative anatomy of the lumbar vertebrae in the literature (Panjabi et al. (1992), Dolan and Adams (2001), and Shirazi-Adl (1994)) was employed (Figure 4.1 and Tables A.4-A.7 in Appendix A).

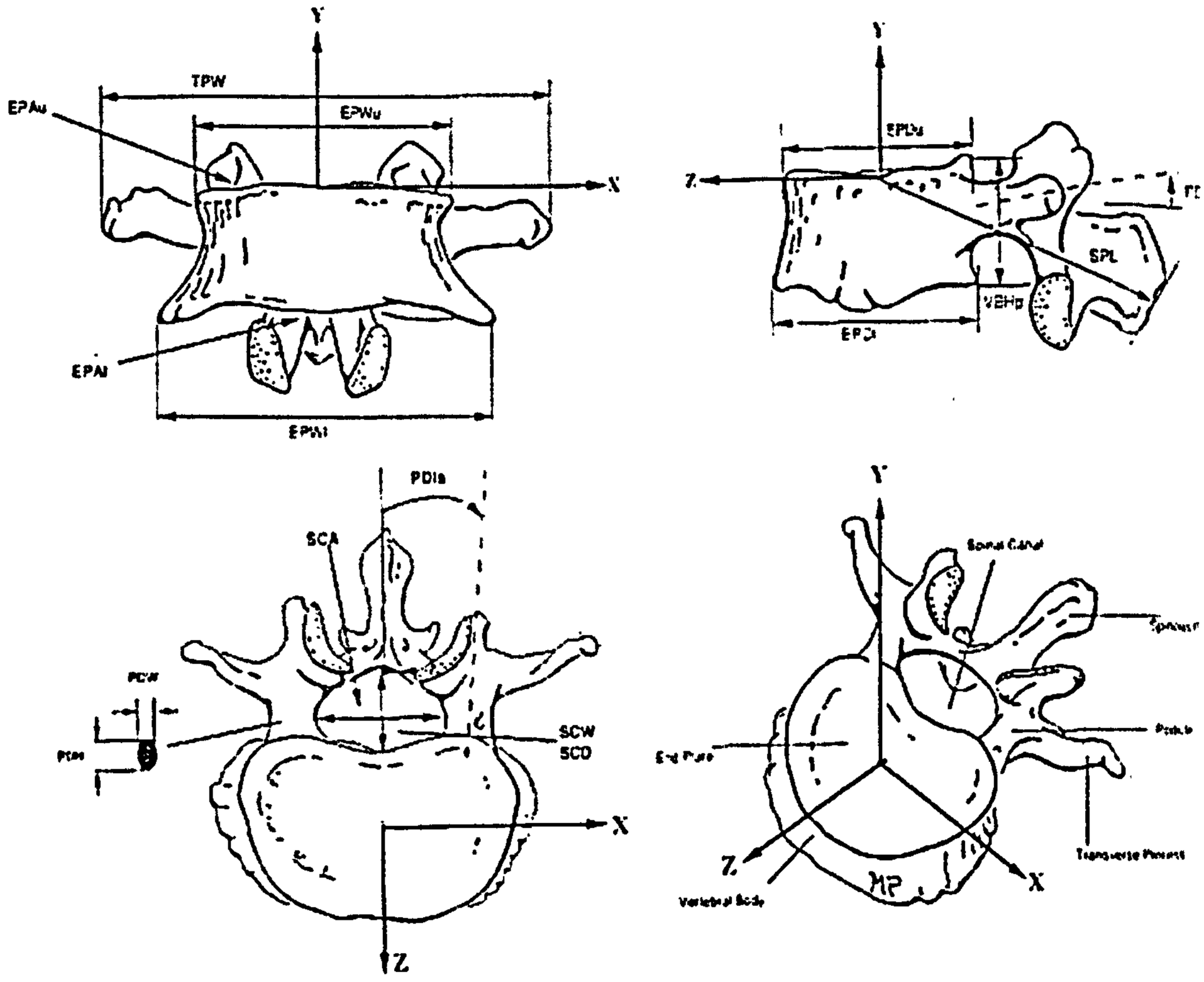

Figure 4.1 Orthogonal views of a typical lumbar vertebra (Panjabi et al., 1992)

The developed solid models of an individual typical vertebra and the whole lumbar spine are provided in Figures 4.2-4.7. The orientation of the lumbar vertebrae was established based on the studies of Shirazi-Adl and Parnianpour (1996) and (2000), and Adler et al. (2002) (Figure 4.8).

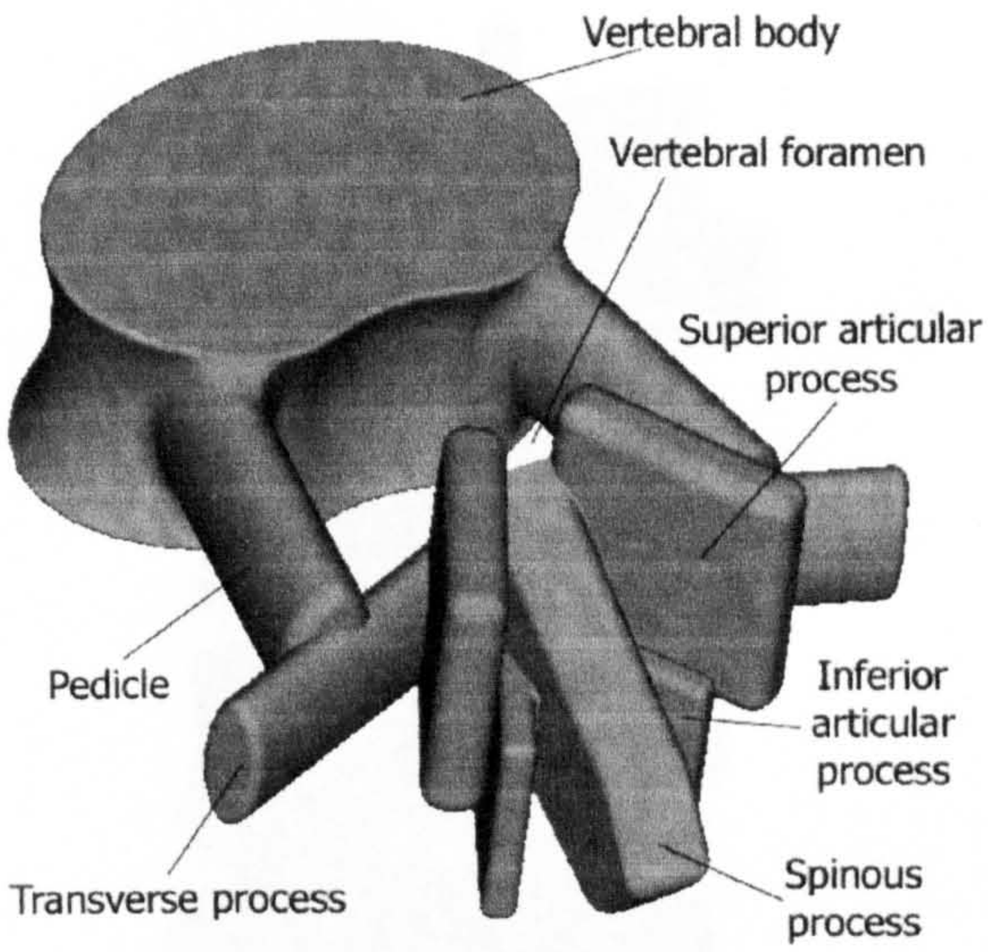

Figure 4.2 A typical lumbar vertebra

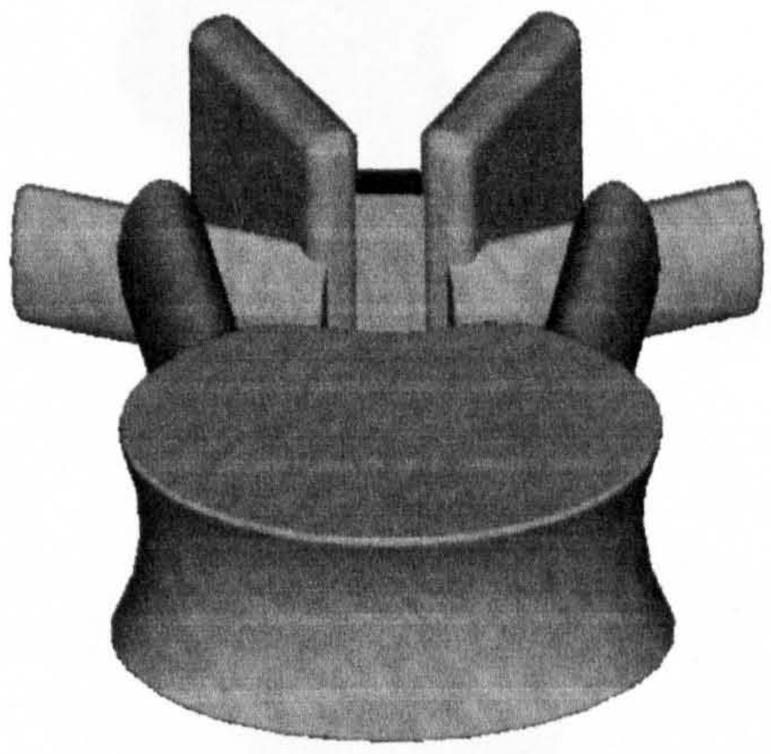

Figure 4.3 Front view of a typical lumbar vertebra

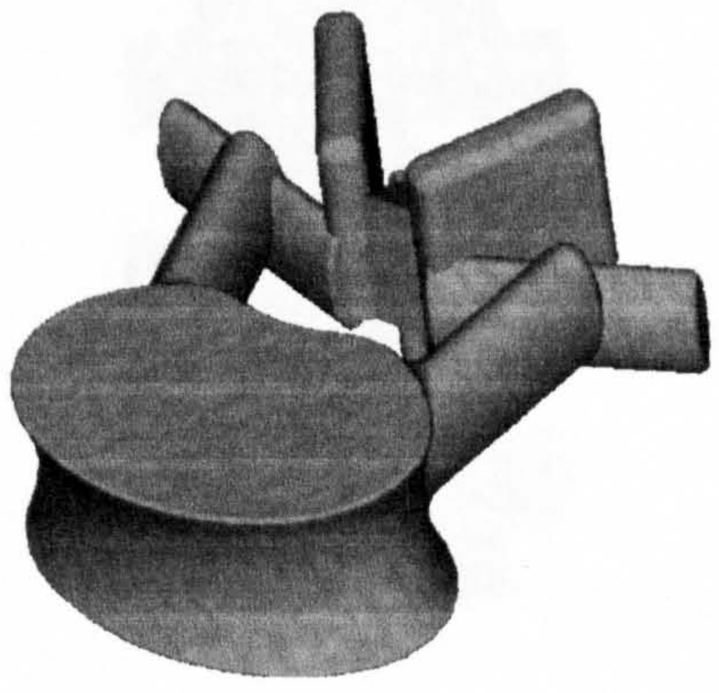

Figure 4.4 An oblique view of a typical lumbar vertebra

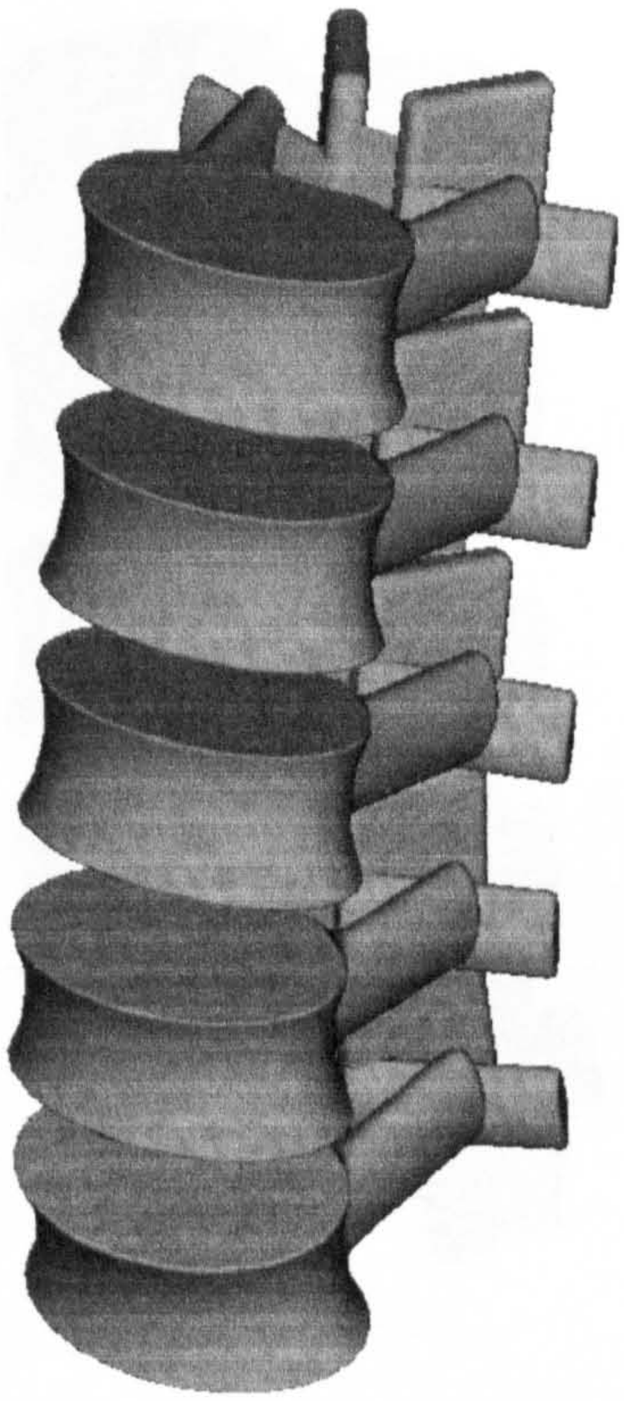

Figure 4.5 An isometric view of the lumbar spine

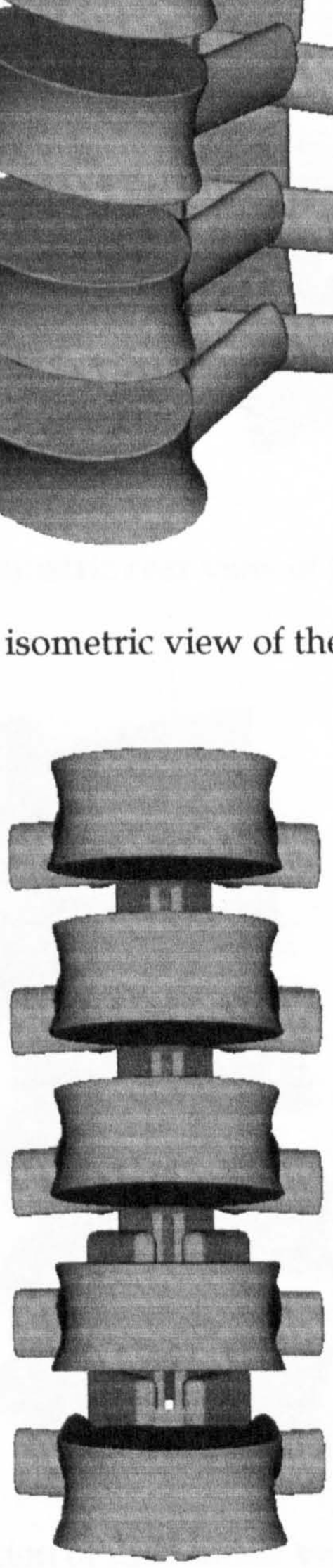

Figure 4.6 Frontal view of the lumbar spine

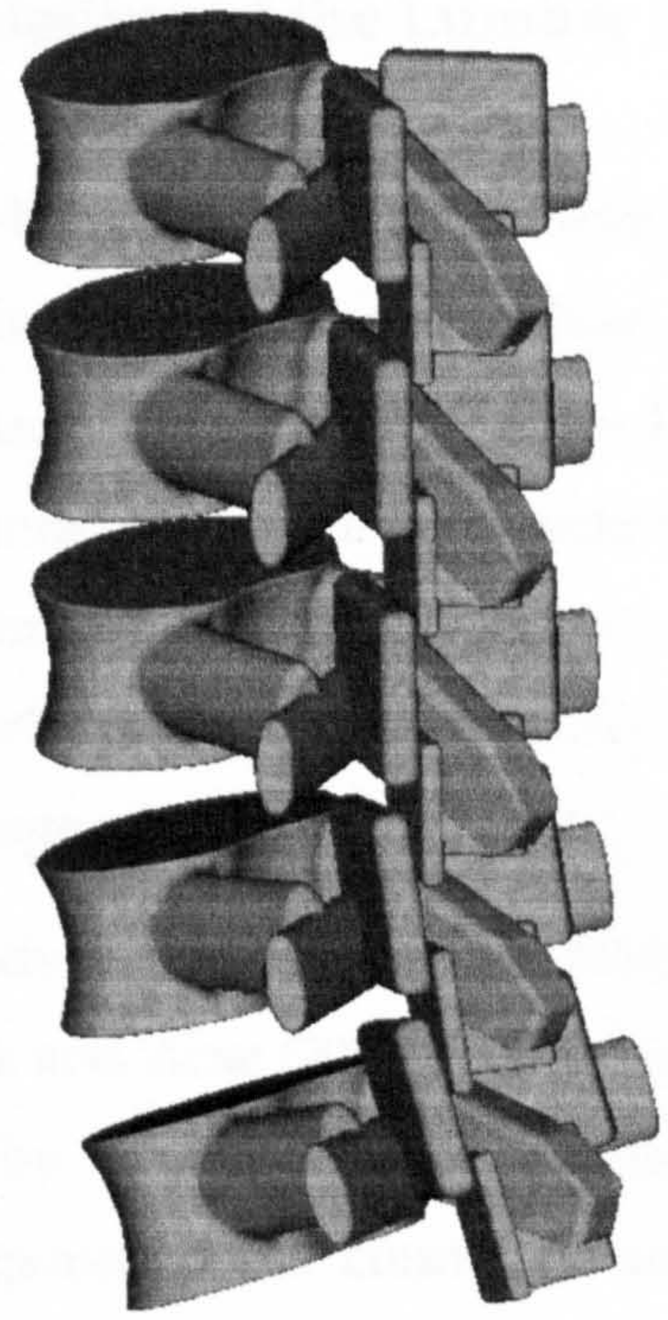

Figure 4.7 An isometric rear view of the lumbar spine

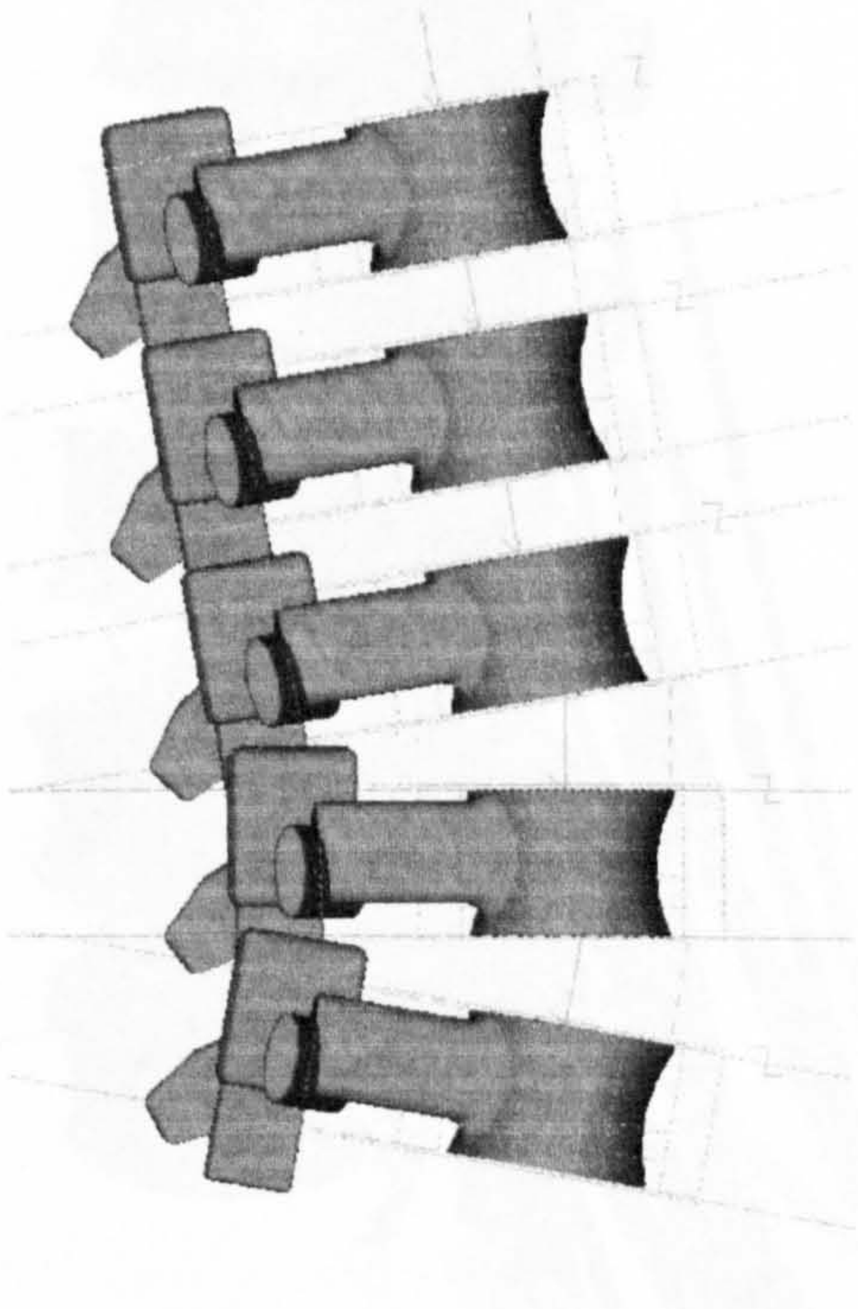

Figure 4.8 The orientation of the lumbar vertebrae in sagittal plane

4.2.2 Multi-Body Modelling of the Lumbar Spine

In constructing the multi-body model of the lumbar spine, four elements of the human spine were considered; the lumbar vertebrae, the muscles, the ligaments and the intervertebral discs. The vertebrae of the lumbar spine have already been modelled and presented in the previous section. The anatomical data and some essential specifications of the other elements are discussed and submitted in this chapter. The model has been built by using the commercially available dynamic simulation package *visualNastran 4D 2001*.

The constructed multi-body model has been handled as the cervical spine multi-body model of van Lopik and Acar (2002). The vertebrae are modelled as rigid bodies, interconnected by linear viscoelastic intervertebral disc elements, nonlinear viscoelastic ligaments and contractile muscle elements possessing both passive and active behaviour (Figure 4.9).

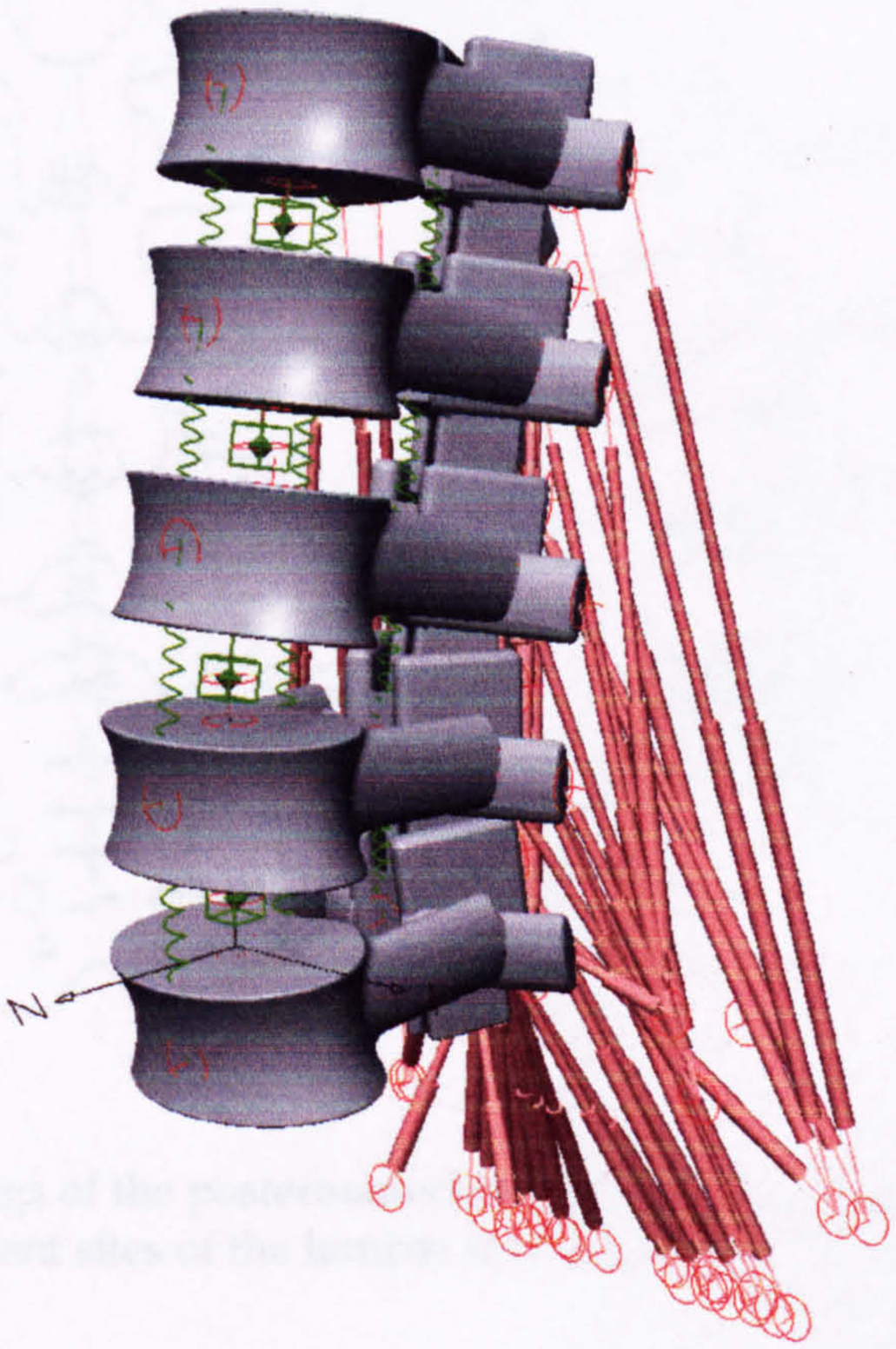

Figure 4.9 The multibody model of the lumbar spine

The Muscles

In the model the lumbar back muscles were constructed incorporating fascicles of the lumbar erector spinae and multifidus. The attachment sites and sizes of fascicles were illustrated in Figure 4.10. Calculations revealed that the thoracic fibres of the lumbar erector spinae contribute 50% of the total extensor moment exerted on L4 and L5; multifidus contributes some 20%; and the remainder is exerted by the lumbar fibres of erector spinae (Bogduk et al., 1992). At upper lumbar levels, the thoracic fibres of the lumbar erector spinae contribute between 70% and 86% of the total extensor moment. In the upright posture, the lumbar back muscles exert a net posterior shear force on segments L1 to L4, but exert an anterior shear force on L5. Collectively, all the back muscles exert large compression forces on all segments. A force coefficient of $K = 46\ Ncm^{-2}$ had been determined to apply for the back muscles (Bogduk et al., 1992).

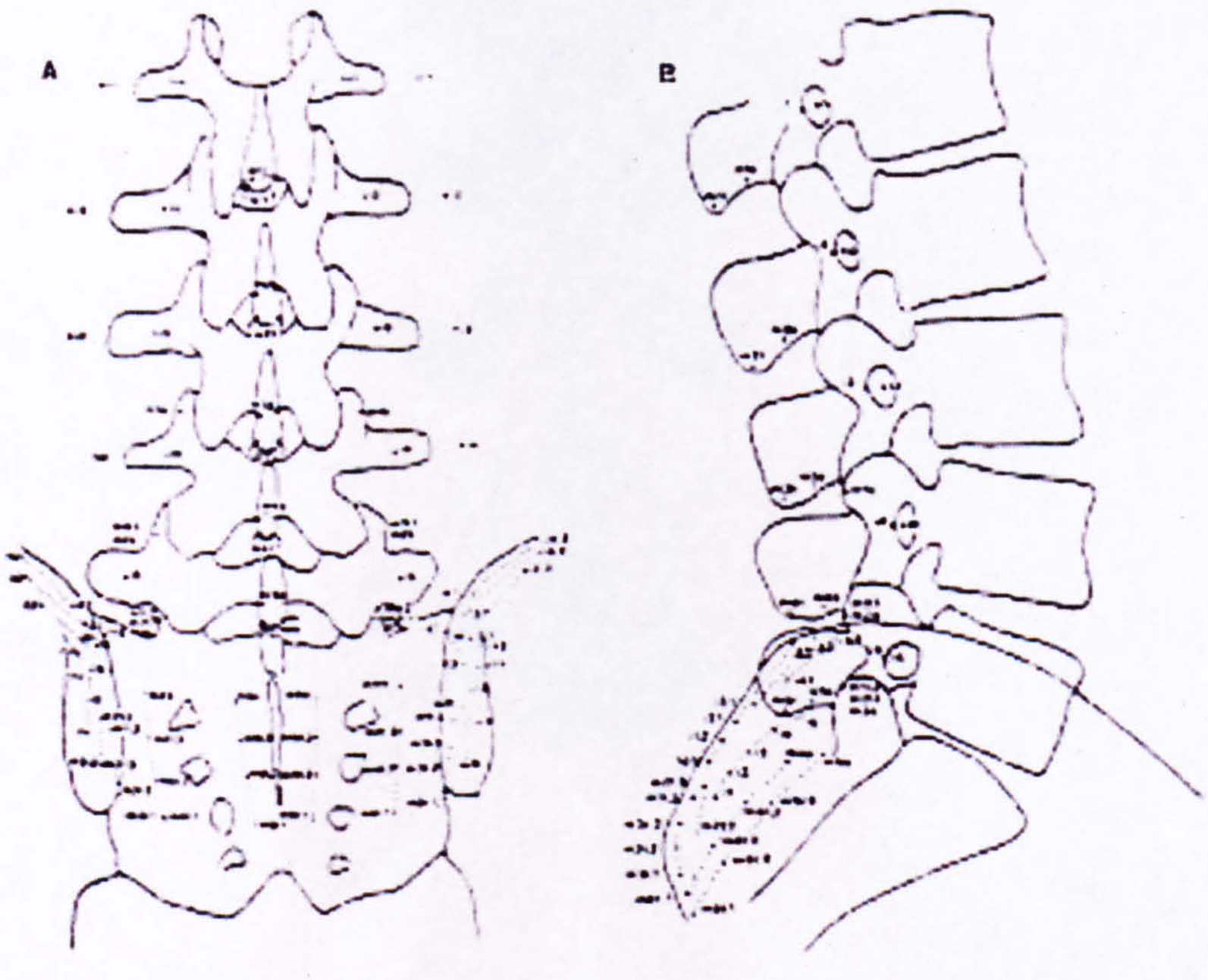

Figure 4.10 Tracings of the posteroanterior and lateral radiographs showing the attachment sites of the lumbar muscles (Bogduk et al., 1992)

Some geometric and morphologic features, and maximum moments generated and the moment arms are presented in Tables A.8 – A.10.

In the model, muscles were modelled as contractile muscle elements possessing both passive and active behaviour. In visualNastran, linear actuator constraint was employed, which have been governed by an external software, Virtual Muscle v.3.1.5 of Alfred E. Mann Institute at the University of Southern California, that runs within Matlab/Simulink and communicates with visualNastran where appropriate (Figure 4.11). The principles of Virtual Muscle are explained in detail in multi-body modelling of the whole human spine section of this chapter. The linear actuator constraint applies a controlled force between two bodies, or between the background and a body. The actuator can be specified to (1) apply a specified force, (2) maintain a specified acceleration, (3) maintain a specified velocity, or (4) maintain a specified length (MSC visualNastran Theory Manual, 2001).

Figure 4.11 Muscles in the model

The Ligaments

The ligaments in the present model are chosen as nonlinear viscoelastic ligaments. All six types of lumbar ligaments were introduced to the model as ALL (anterior longitudinal ligament), PLL (posterior longitudinal ligament), LF (ligament flavum), JC (joint capsules), ISL (interspinous ligament) and SSL (supraspinous ligament) (Figure 4.12). Some essential biomechanical properties of lumbar spine ligaments are presented in Tables 4.1 – 4.2, Table A.11, and Figures 4.12 – 4.14.

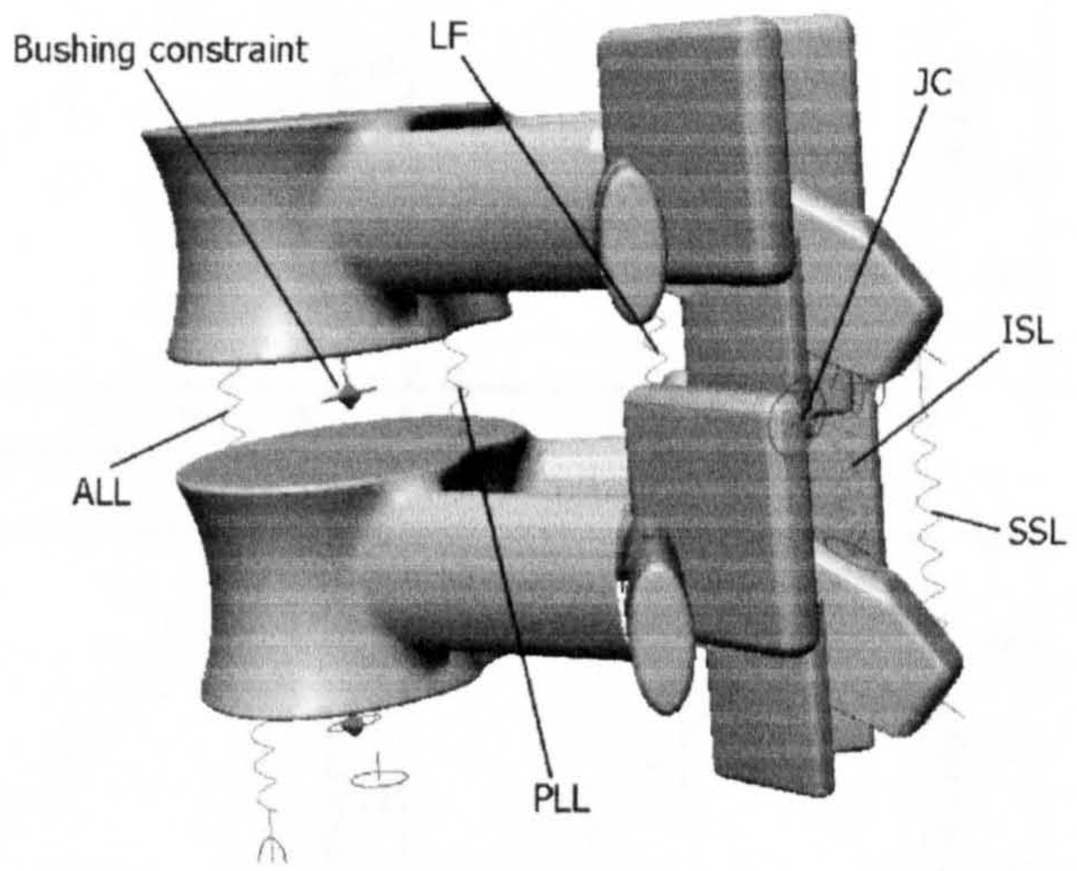

Figure 4.12 Ligaments and bushing constraint as intervertebral disc

Table 4.1 Cross-sectional area and original length of lumbar ligaments (Pintar et al., 1992)

		Cross-sectional area (mm^2)		Original length (mm)	
Ligament	n	Range	Mean±S.D.	Range	Mean±S.D.
ALL	25	10.6-52.5	32.4±10.9	30.0-48.5	37.1±5.0
PLL	21	1.6-8.0	5.2±2.4	27.8-36.7	33.3±2.3
JC	24	19.0-93.6	43.8±28.3	12.8-21.5	16.4±2.9
LF	22	57.2-114.0	84.2±17.9	13.0-18.0	15.2±1.3
ISL	18	13.8-60.0	35.1±15.0	6.7-20.0	16.0±3.2
SSL	22	6.0-59.8	25.2±14.0	17.0-33.5	25.2±5.6

Table 4.2 Overall mean values of stiffness

Ligament	Mean±S.D.
ALL	33.0±15.7
PLL	20.4±11.9
JC	33.9±10.7
LF	27.2±9.2
ISL	11.5±6.6
SSL	23.7±10.9

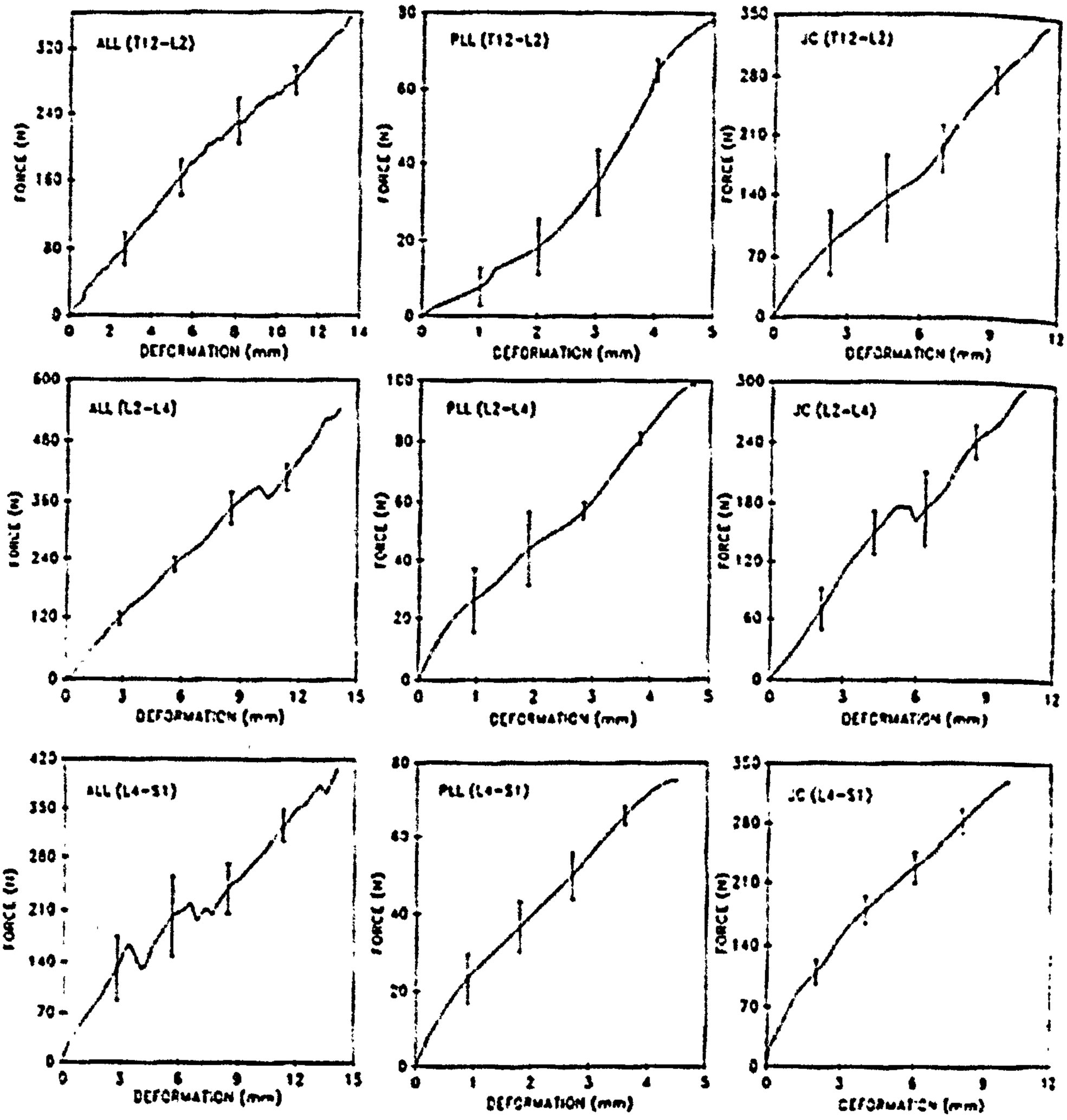

Figure 4.13 Average biomechanical force-deformation curves for ALL, PLL and JC (Pintar et al., 1992)

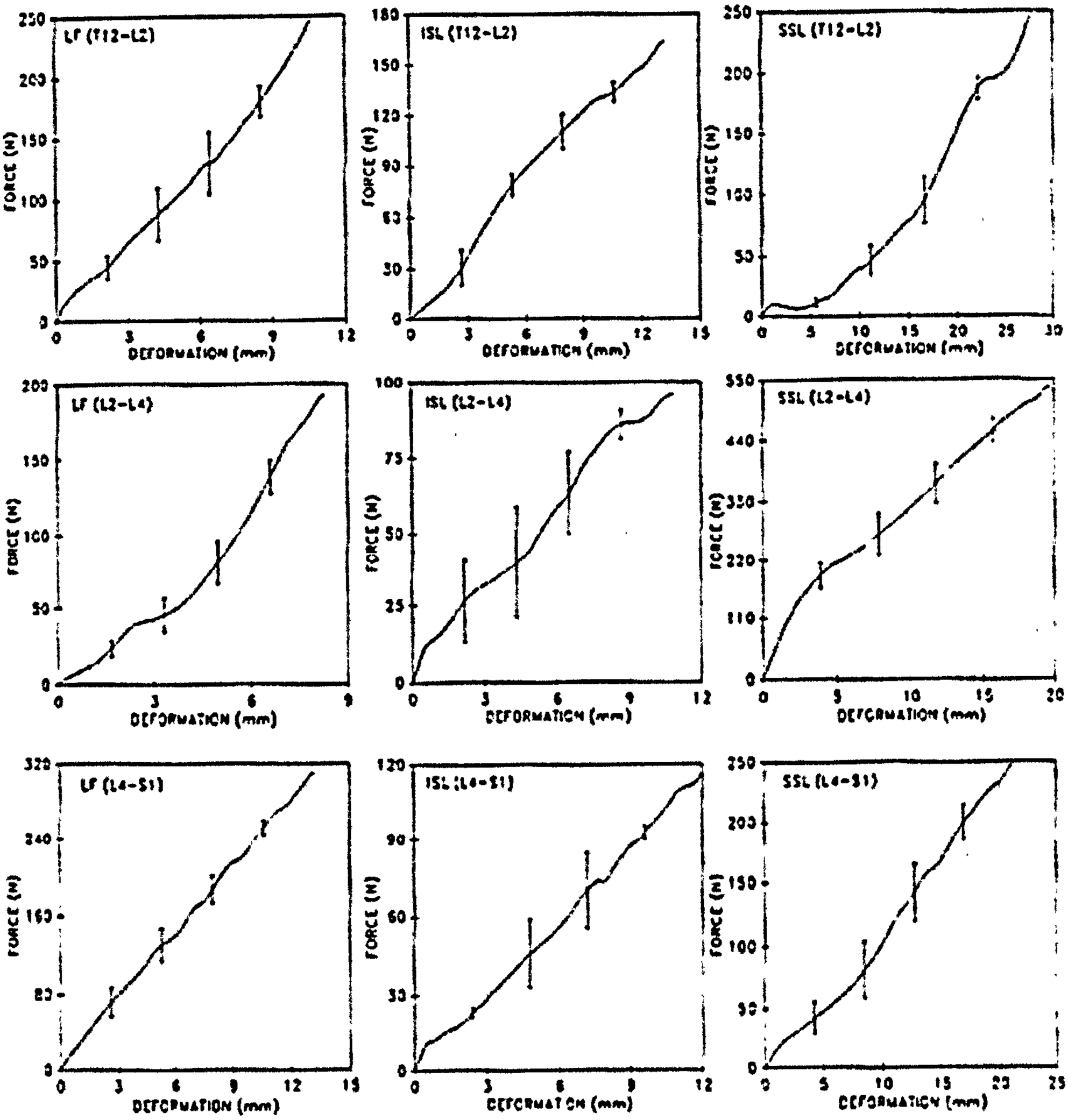

Figure 4.14 Average biomechanical force-deformation curves for LF, ISL and SSL (Pintar et al., 1992)

The Intervertebral Disc

In the present model, intervertebral discs are modelled as bushing elements. The bushing constraint models "slop" in rigid, revolute, and spherical joints. A revolute type bushing restricts the motion of the attached body to rotation about its revolute axis, similar in spirit to a revolute joint. Unlike a revolute joint, however, a revolute bushing's axis can deviate from its initial configuration during the simulation according to the applied loads and the bushing parameters.

All translational and rotational degrees of freedom are allowed in a bushing element, but they are restricted through spring-damper relationships. These relationships govern the deviation of the bushing configuration from its primary constraint goals: the deviation of a single goal is inversely proportional to the spring constant (of stiffness) prescribed for that goal; the settling time to the deviated configuration is governed by the damping constant (MSC visualNastran Theory Manual, 2001).

The translational damping coefficients of the discs were chosen as 1000 kg/s and rotational coefficients as 1.5 Nm/s as a preliminary estimation based on those used by de Jager as no actual disc damping coefficients have been reported in the literature. Also, the motion segment stiffness matrix results of the study of Gardner-Morse and Stokes (2004) have been utilized in the modelling (Table 4.3).

Table 4.3 Stiffness of intact motion segments (Gardner-Morse and Stokes, 2004)

Level		Δ_1	Δ_2	Δ_3	Δ_4	Δ_5	Δ_6
Axial compressive preload at 0 N (Mean of L2-L3 and L4-L5)							
F_1		438±92					-1370±519
F_2			251±42				6510±969
F_3				332±64	11000±2000	-6960±1100	
F_4					564000±89000	-235000±38200	
F_5			(symmetric)			174000±20500	
F_6							241000±33100
Axial compressive preload at 250 N							
F_1	L2-L3	1700±67					-4280±1130
	L4-L5						
F_2	L2-L3		346±63				8340±1240
	L4-L5		389±76				10200±1790
F_3	L2-L3			447±68	12100±1740	-9360±971	
	L4-L5						
F_4	L2-L3				668000±144000	-25000±34200	
	L4-L5				744000±137000		
F_5	L2-L3		(symmetric)			211000±17900	
	L4-L5					301000±29900	
F_6	L2-L3						266000±33000
	L4-L5						467000±80500
Axial compressive preload at 500 N							
F_1	L2-L3	2420±158					-5180±1940
	L4-L5						
F_2	L2-L3		397±68				9000±1330
	L4-L5		473±78				11100±2160
F_3	L2-L3			523±73	13400±1890	-10400±1760	
	L4-L5					-11600±1250	
F_4	L2-L3				734000±170000	-272000±33500	
	L4-L5				832000±129000		
F_5	L2-L3		(symmetric)			236000±12900	
	L4-L5					377000±44800	
F_6	L2-L3						287000±27000
	L4-L5						575000±137000

4.2.3 Analysis of the Multi-Body Model of the Lumbar Spine

First, a motion segment containing 2 vertebrae was run in visualNastran (Figure 4.15). Following the successful results of the motion segment in flexion and compression, the rest of the model has been constructed (Figure 4.16). The details of the multi-body model were discussed in the previous section. Throughout the analysis process, some minor modifications have been made on the geometry of the solid model in order to tune and validate the multi-body model.

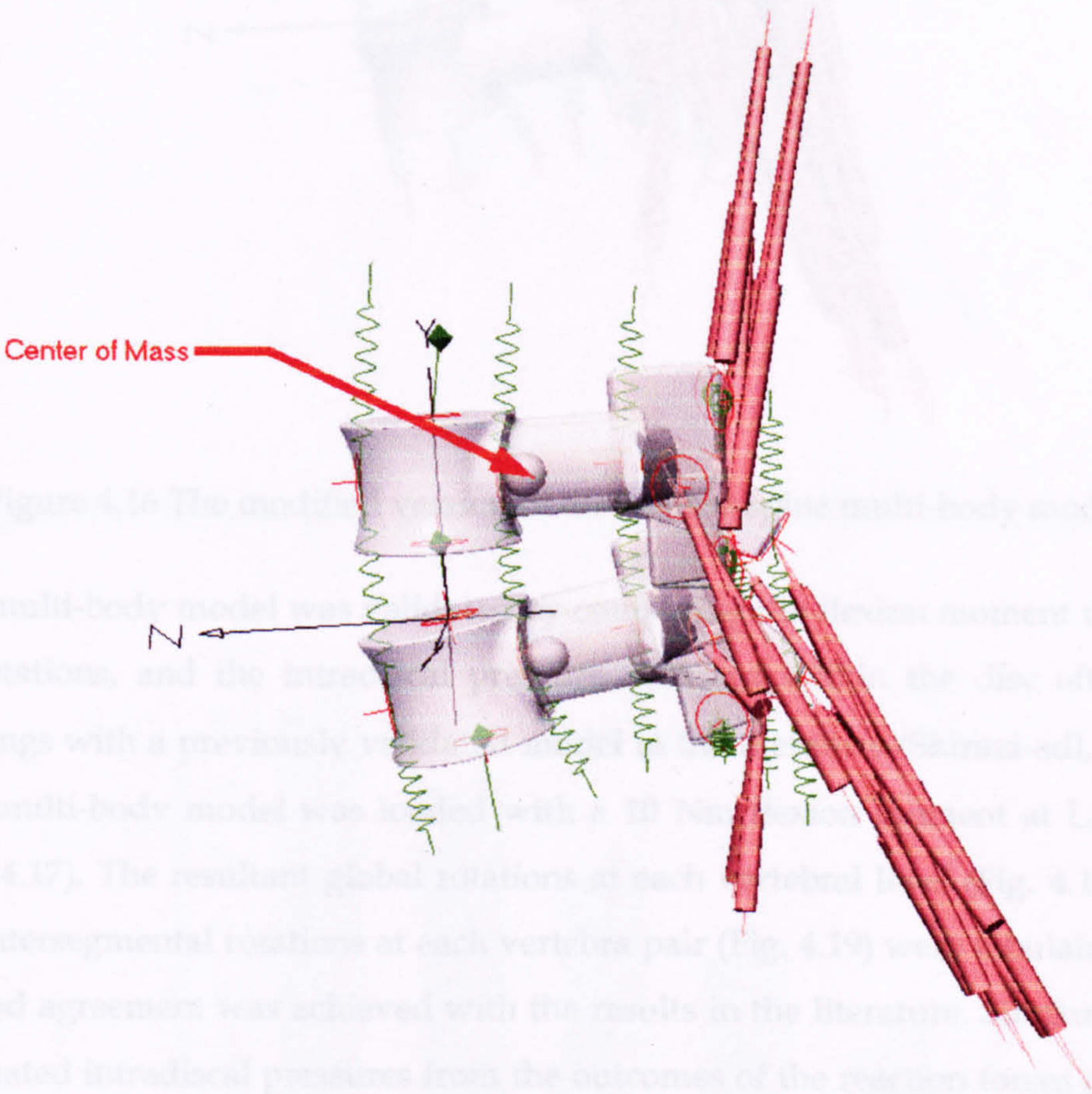

Figure 4.15 Lumbar motion segment L4-L5 containing 2 vertebrae

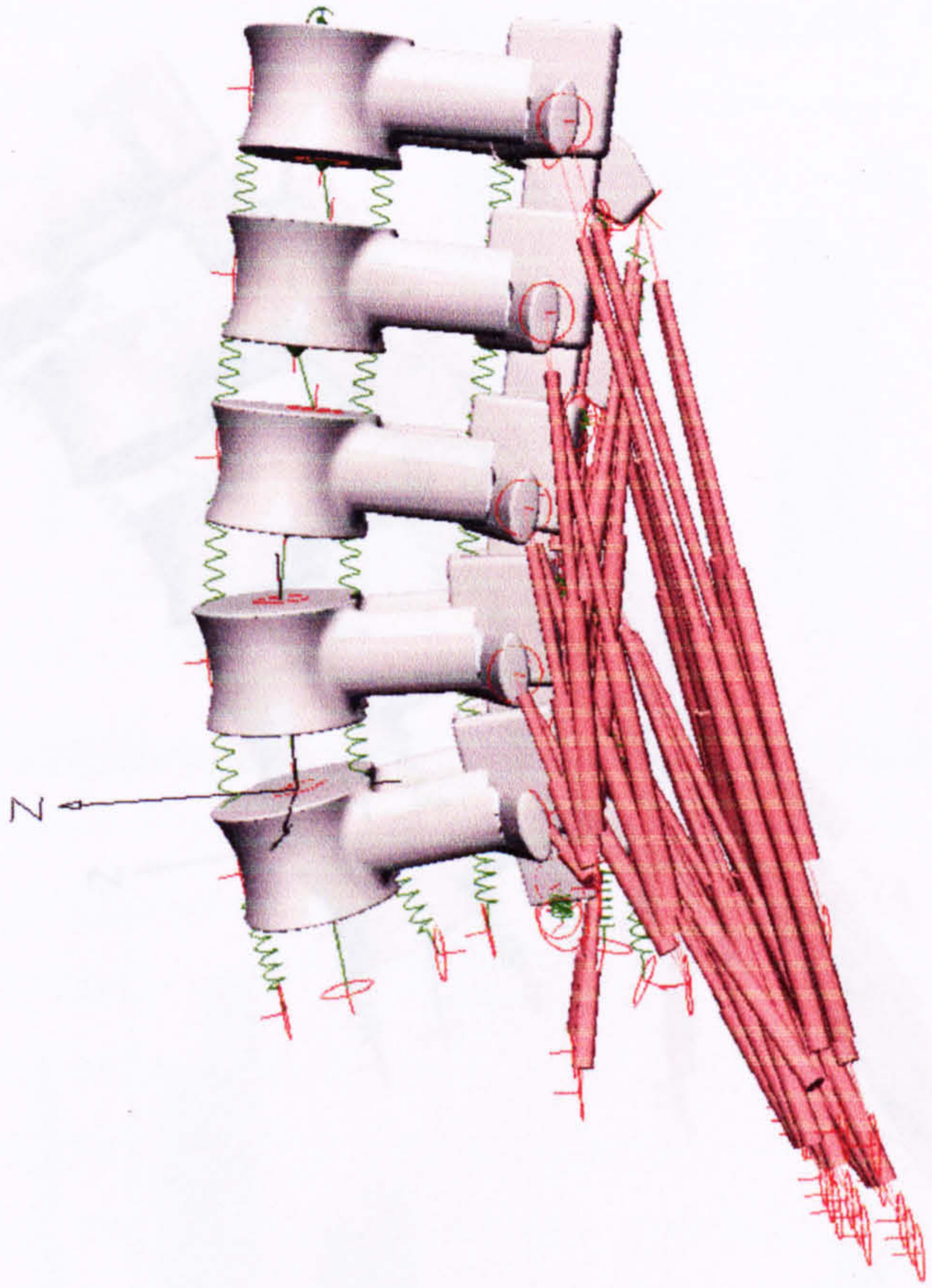

Figure 4.16 The modified version of the lumbar spine multi-body model

The multi-body model was validated by comparing the flexion moment results, as rotations, and the intradiscal pressure occurred within the disc after the loadings with a previously validated model in the literature (Shirazi-adl, 1994). The multi-body model was loaded with a 10 Nm flexion moment at L1 level (Fig. 4.17). The resultant global rotations at each vertebral level (Fig. 4.18) and the intersegmental rotations at each vertebra pair (Fig. 4.19) were tabulated and a good agreement was achieved with the results in the literature. Similarly, the evaluated intradiscal pressures from the outcomes of the reaction forces at each intervertebral disc were compared with the results in the literature and another good agreement was achieved (Fig. 4.20).

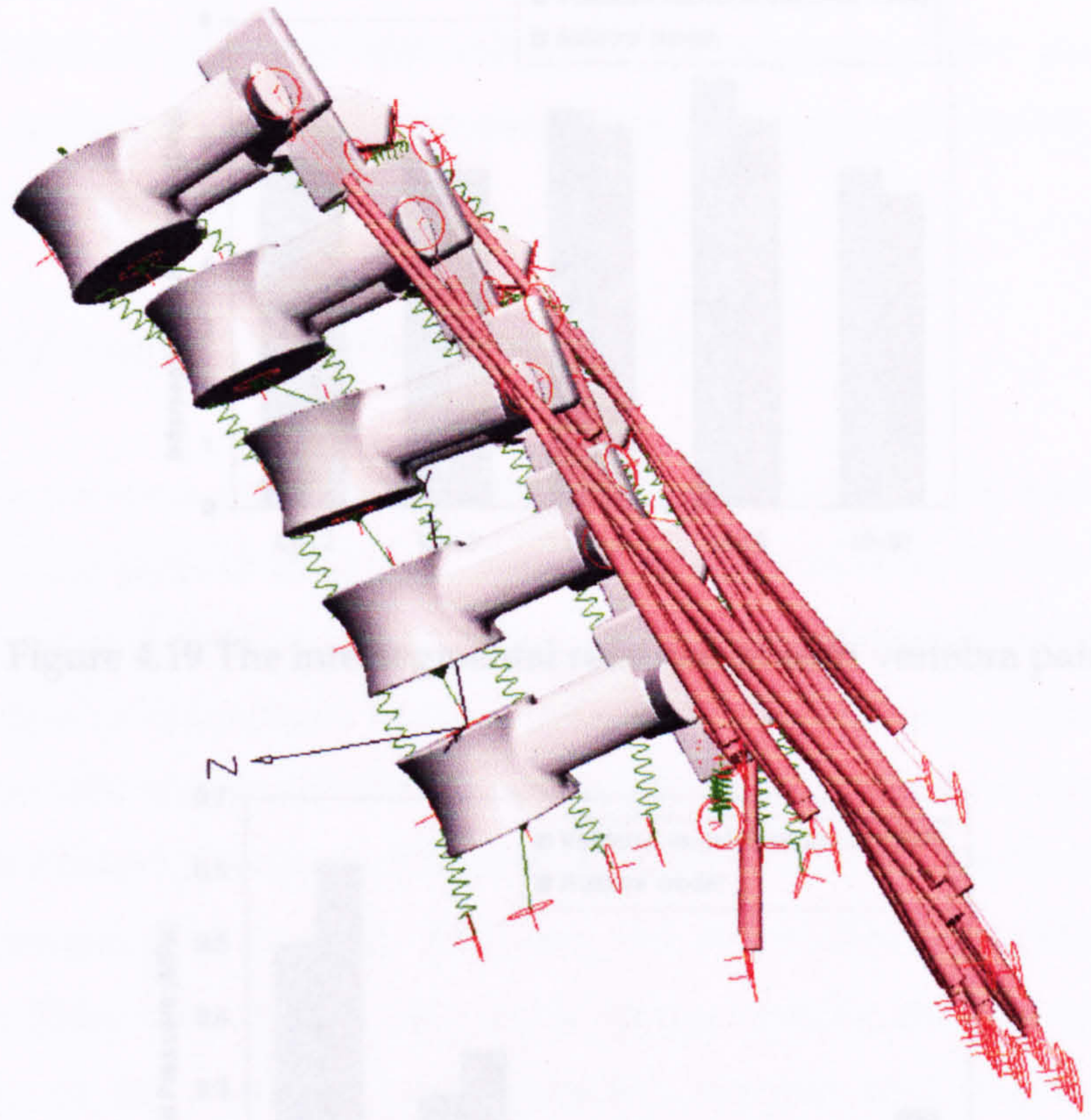

Figure 4.17 The posture of the lumbar spine under 10 Nm flexion moment

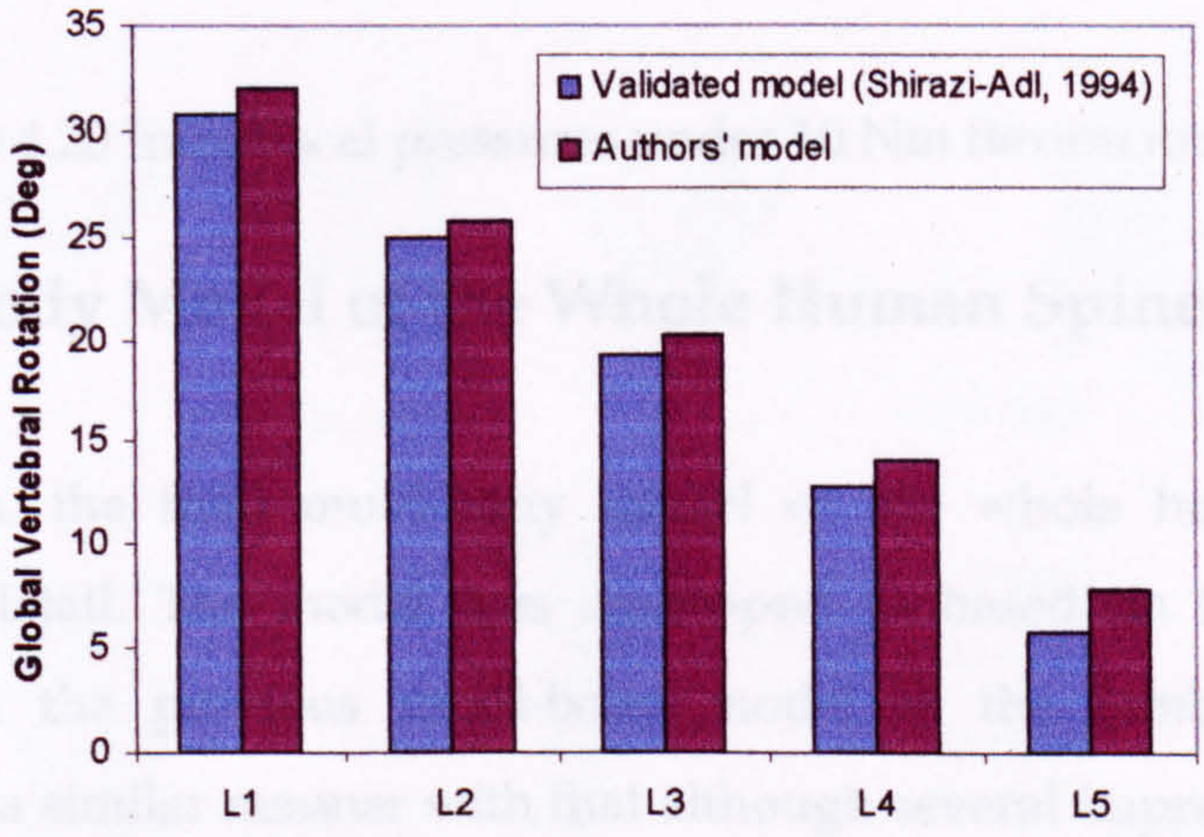

Figure 4.18 The resultant global rotations at each vertebral level

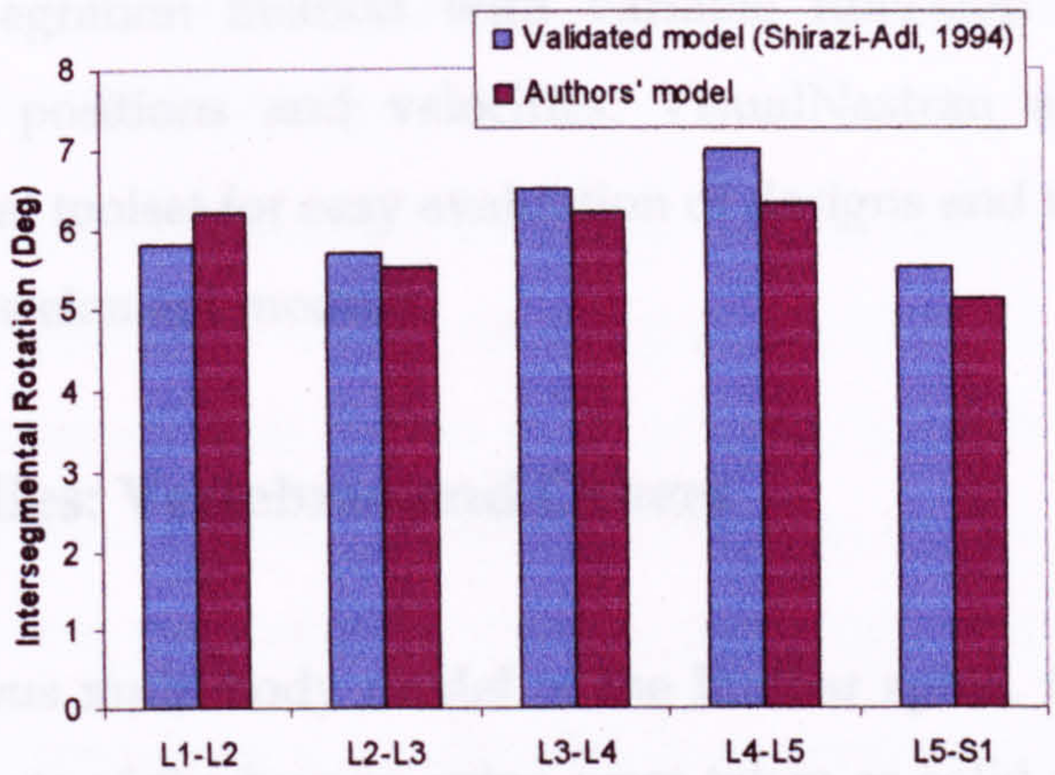

Figure 4.19 The intersegmental rotations at each vertebra pair

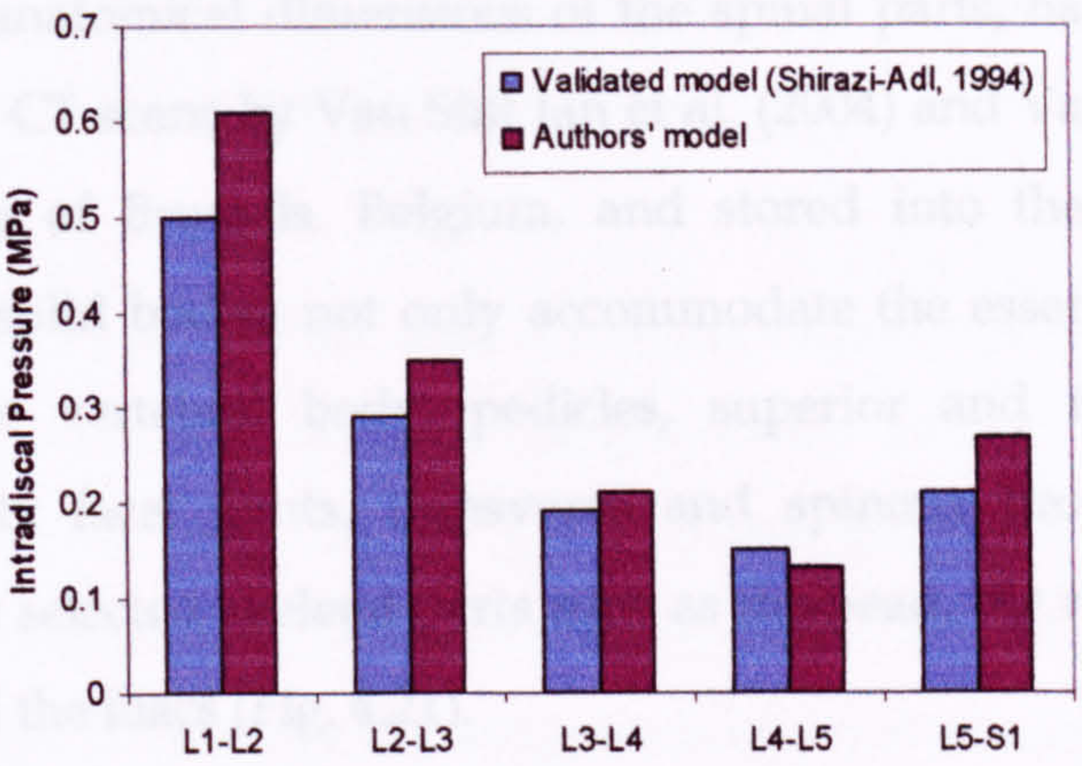

Figure 4.20 Intradiscal pressures under 10 Nm flexion moment

4.3 Multi-Body Model of the Whole Human Spine

In this section, the final multi-body model of the whole human spine is explained in detail. The model was developed as based on the experience acquired from the previous multi-body model of the lumbar spine and constructed in a similar manner with that although several improvements were made in different aspects of the model.

The model was developed in the commercially available dynamic simulation package *visualNastran 4D 2001* from MSC Software Company. VisualNastran uses numerical methods to solve the motion of mechanical systems, which are governed by differential equations arising from mechanics principles. The

Kutta-Merson integration method with variable time-step is employed to calculate bodies' positions and velocities. VisualNastran also provides an extensive analytical toolset for easy evaluation of designs and models as well as an integrated finite element module.

4.3.1 Solid Bodies: Vertebrae and Others

Unlike the previous multi-body model of the lumbar spine, the vertebrae and the other bony parts of the human spine were taken as solid models of the CT scans of human skeletal segments from a study called Multimod, carried out by a consortium of institutions around Europe. The geometrical surfaces, which possess realistic anatomical dimensions of the spinal parts, have been entirely constructed from CT scans by Van Sint Jan et al. (2004) and Van Sint Jan (2005) at the University of Brussels, Belgium, and stored into the software, Data Manager. These solid bodies not only accommodate the essential parts of the vertebrae; as the vertebral body, pedicles, superior and inferior articular processes, namely facet joints, transverse and spinous processes, but also involve the other selected skeletal parts such as the head, the ribs, the clavicles, the scapulas, and the iliacs (Fig. 4.21).

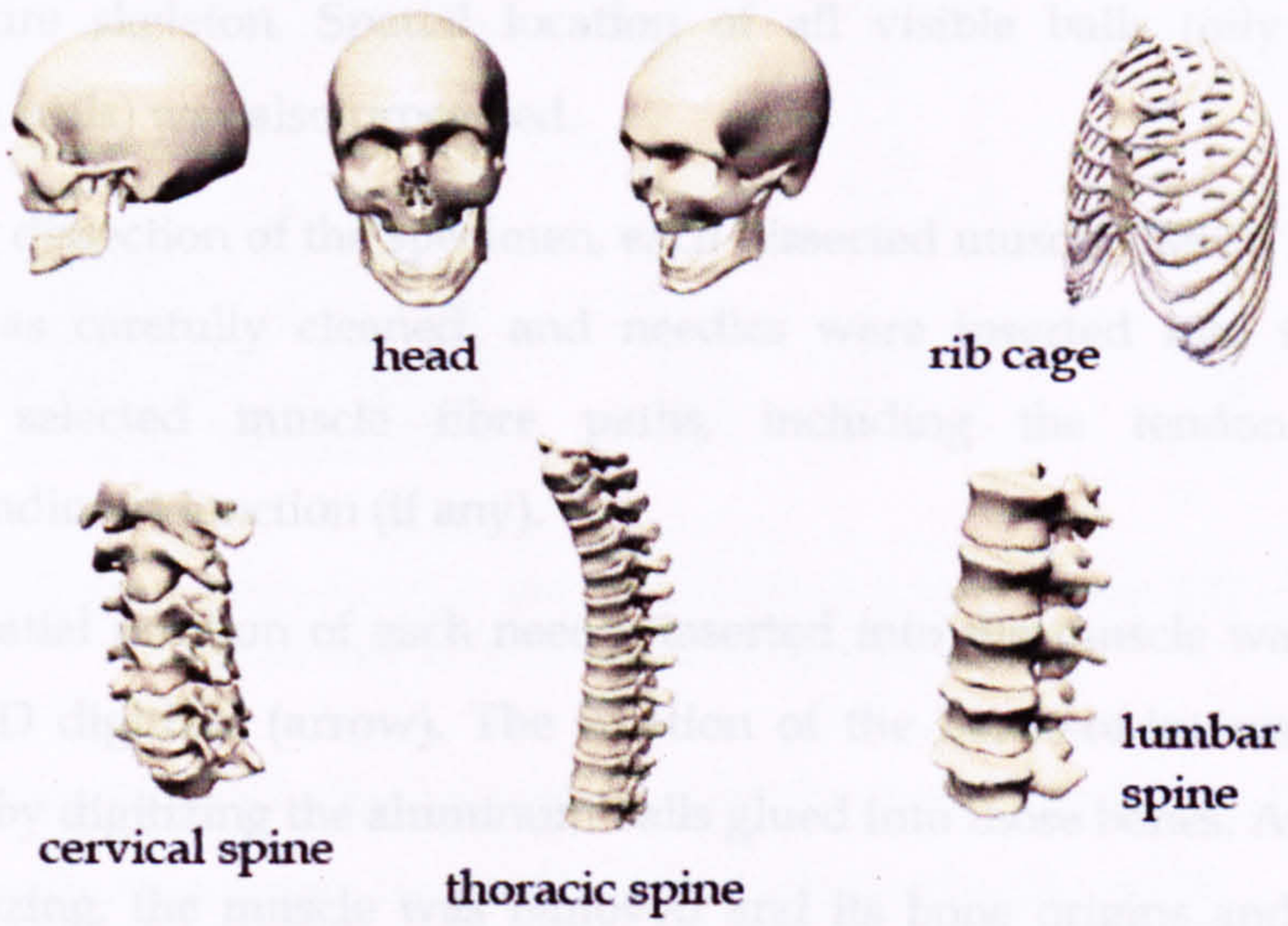

Figure 4.21 Segments of the human skeleton, which were joined to form the solid model

The details of the CT scanning and digitising process are illustrated and explained in Figure 4.22. In the figure:

(A) A specimen (male, 59 years old) of average size (172 cm) and weight (69 kg) was selected from the Body Donation program of ULB. No visible problem related to the musculoskeletal system was apparent. Large balls filled with an oily solution were set at different locations on the skin surface. These balls were visible in both CT scan and magnetic resonance imaging (MRI).

(B) In each major bone (here a left clavicle), four aluminium balls (diameter: 4 mm) were inserted and glued. These balls were visible in the CT scan and remained in place during further dissection.

(C) Both full-body MRI and CT scan imaging were performed the same day. A special jig ensured that the body position was similar in both medical imaging datasets.

(D) Slices obtained from MRI allowed extracting information related to muscle volume and location of the oily balls using so-called segmentation operations. On this image, segmentation of the gluteusmajor muscle is highlighted (see arrow). Each segmented structure was then reconstructed three dimensionally. Segmentation of the CT data (not shown) enabled the attainment of 3-D models of the entire skeleton. Spatial location of all visible balls (oily balls and aluminium balls) was also processed.

(E) During dissection of the specimen, each dissected muscle (here a left deltoid muscle) was carefully cleaned, and needles were inserted into the muscle following selected muscle fibre paths, including the tendon and the musculotendinous junction (if any).

(F) The spatial position of each needle inserted into the muscle was digitized using a 3-D digitizer (arrow). The location of the bones-of-interest was also processed by digitizing the aluminum balls glued into those bones. After muscle fibre digitizing, the muscle was removed and its bone origins and insertions were digitized, as well. Weight and volume of each muscle were also obtained.

(G) Registration of the digitized muscle fibre coordinates with the CT skeleton looks anatomically correct [here the left deltoid muscle shown in (E)].

(H) Registration of the digitized muscle origins and insertions toward the 3-D skeleton lead to anatomical cartography (view of the posterior aspect of the femoral bone).

(I) MRI volume models registered with the CT skeleton were also performed (displayed muscles: sartorius, rectus femoris, and gracilis).

(J) Further processing allows combining MRI volume data with the digitized fibre path and CT skeleton (displayed muscle: vastus lateralis and vastus medialis) (Van Sint Jan, 2005).

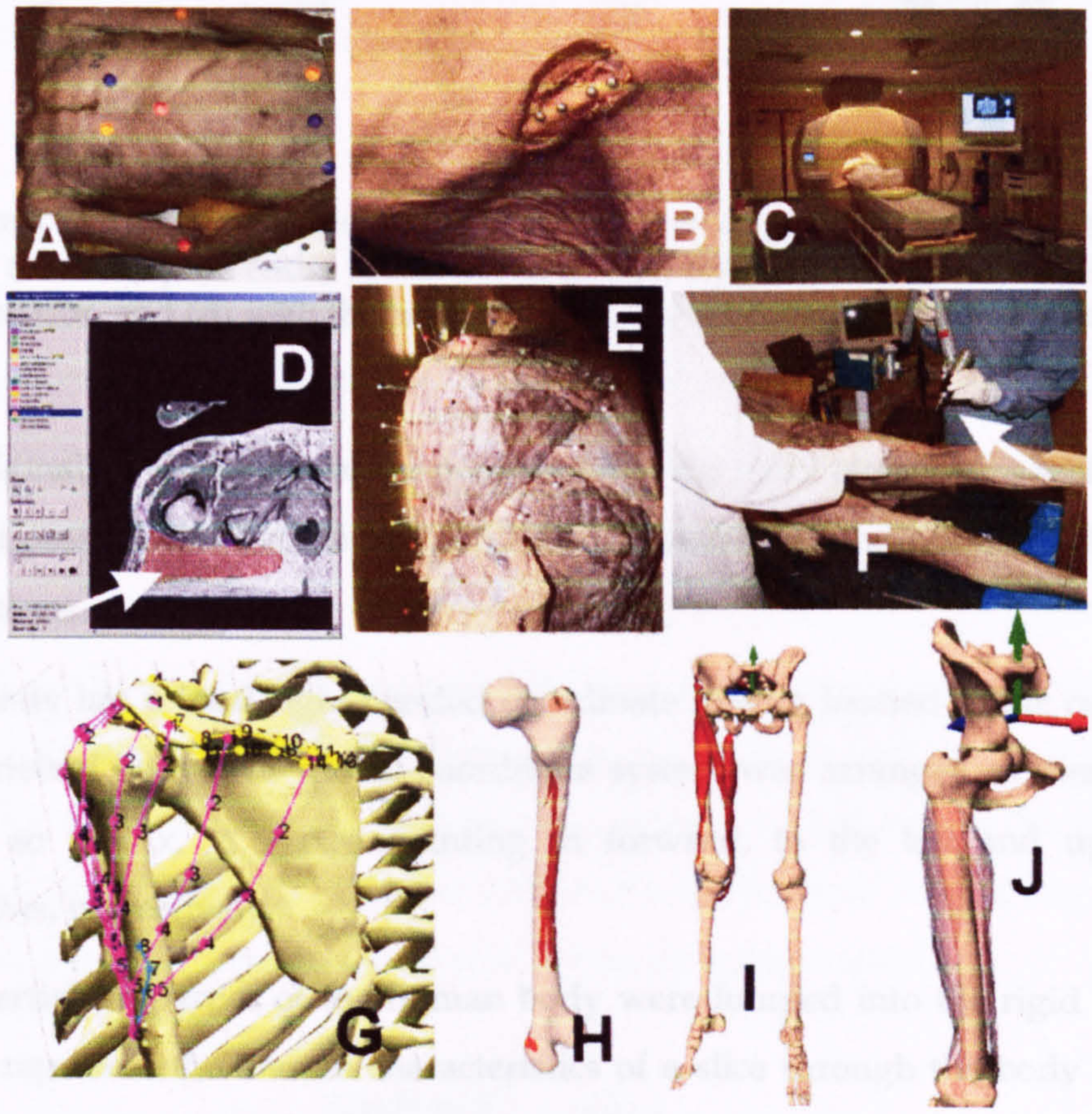

Figure 4.22 Digitization of a full musculoskeletal system (from left to right and from top to bottom) (Van Sint Jan, 2005).

All the bodies were included into the multi-body model in addition to the spinal parts to be able to simulate the model more realistically (Fig. 4.23).

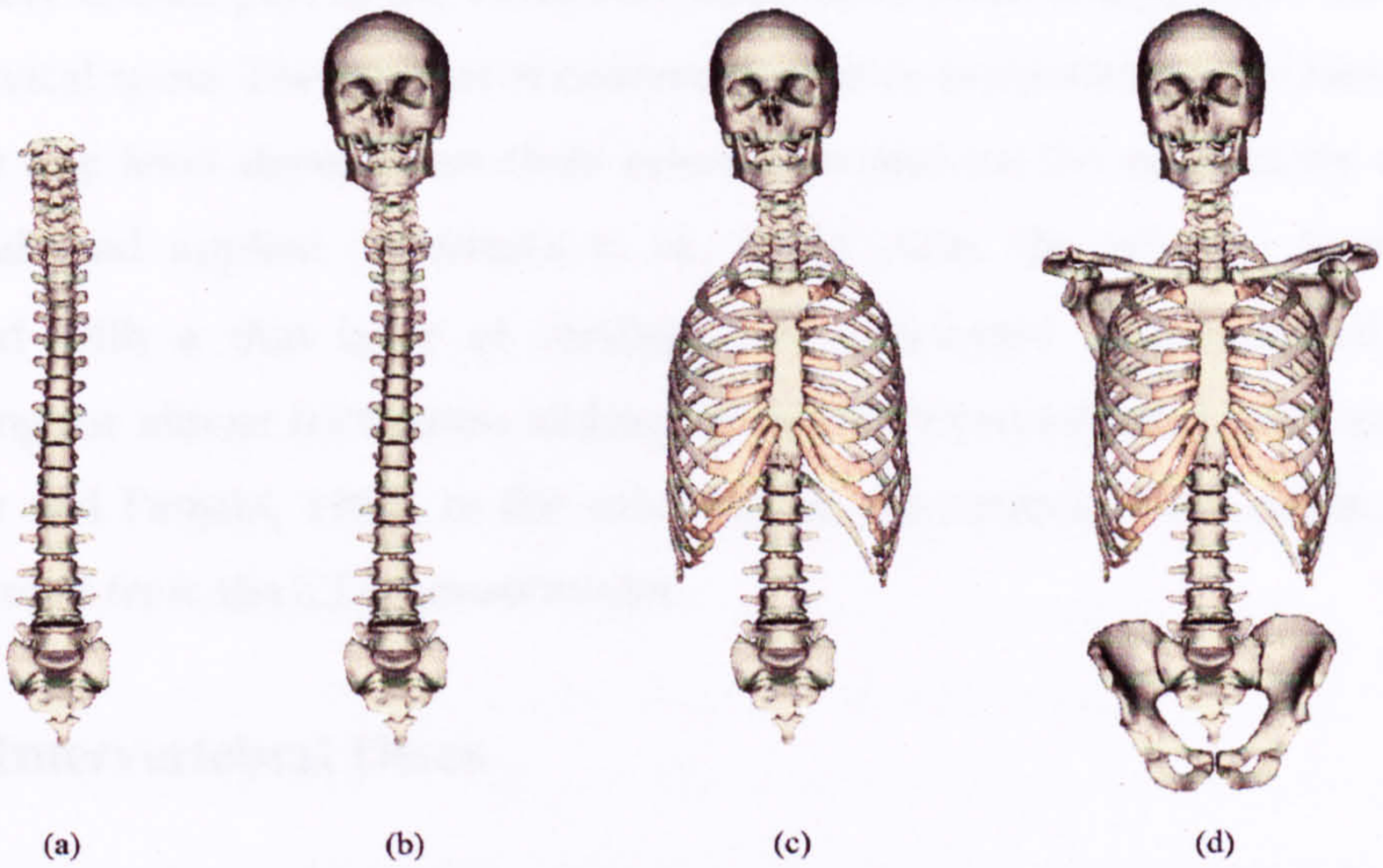

Figure 4.23 The solid model of the human spine used in the developed multi-body model: (a) the entire spinal column, (b) with the head, (c) with the head and the ribs, and (d) with the head, the ribs, the clavicles, the scapulas, and the iliacs.

The original configuration of the vertebrae and the other elements as well as the upright posture of the spine was preserved as an initial condition in multi-body simulations.

Each body has a local right-handed coordinate system located at the centre of the vertebral body. The global coordinate system was arranged as mentioned before so that x, y, z-axes pointing in forward, to the left and upwards directions, respectively.

The inertial properties of the human body were lumped into the rigid bodies, which represent the inertial characteristics of a slice through the body at each vertebral level containing all surrounding soft tissues. The properties used are those derived by de Jager (1996), who calculated the moment of inertia at each cervical level by assuming the straightened neck as a cylinder made up of 7 segments, each with a height equal to the distance between adjacent vertebral body origins. An average density of 1170kg/m^3 was used for all levels as reported by Walker et al. (1973) and used to determine the moments of inertia at each vertebral level.

As a very crucial part of the vertebrae, facet joints resist compressive forces in the cervical spine. The amount of compressive force supported by the facet joint pair at any level depends on their orientation and on the eccentricity of the external load applied (Nowitzke et al., 1994). Also, the articular facets are covered with a thin layer of cartilage and lubricated with synovial fluid allowing for almost frictionless sliding motion between adjacent facet surfaces (White and Panjabi, 1990). In the solid model, the articular facet surfaces are actual ones from the CT scanned model.

4.3.2 Intervertebral Discs

The constructed multi-body model was handled in the same manner as the cervical spine multi-body model of van Lopik and Acar (2002). The vertebrae were modelled as rigid bodies, interconnected by linear viscoelastic intervertebral disc elements, nonlinear viscoelastic ligaments and contractile muscle elements possessing both passive and active behaviour.

In the present model, intervertebral discs were modelled as bushing elements (Fig. 4.24). All translational and rotational degrees of freedom are allowed in a bushing constraint, but they are restricted through spring-damper relationships. These relationships govern the deviation of the bushing configuration from its primary constraint goals: the deviation of a single goal is inversely proportional to the spring constant (of stiffness) prescribed for that goal; the settling time to the deviated configuration is governed by the damping constant.

Figure 4.24 The intervertebral disc in the multi-body model

The intervertebral discs were located at the centre of the space between the upper and lower end plates of adjacent vertebrae at a fixed distance relative to the centre of the upper vertebrae. There were no discs between the axis, atlas and occiput.

In visualNastran, the direction and magnitude of a spring force is determined by the distance between its two end points for a translational spring or by the relative angle between its two end points for a rotational spring. Similarly, the direction and magnitude of a damper force is determined by the relative velocity between its two end points for a translational damper or by the relative angular velocity between its two end points for a rotational damper. Hence, the loads exerted by the bushing constraint on the vertebrae can be formulated as:

$$F_i = k_{ti} \cdot t_i + b_{ti} \cdot v_i \qquad [1]$$

$$M_i = k_{\theta i} \cdot \theta_i + b_{\theta i} \cdot \omega_i \qquad (i = x, y, z) \qquad [2]$$

where F_i and M_i are the components of the forces and moment relative to the i-axis of the lower vertebrae, t_i and θ_i are the relative translations and rotations between the vertebrae measured from the geometric centre of the disc and v_i and ω_i are the relative translational and rotational velocities of the disc centre. The stiffnesses k_i and the damping coefficients b_i govern the intervertebral disc behaviour.

In visualNastran collisions are detected geometrically by finding intersections between bodies. All body-to-body collisions are reduced to one or more point-to-point contacts, where a vertex of a body collides with a face of another body, the contact point can be identified on the face with a simple geometric calculation. When bodies collide, visualNastran computes the forces and/or impulses necessary in order to prevent interpenetration and applies these responses at the contact points.

Material properties of the intervertebral discs are required for all directions of loading as flexion, extension, tension, compression, anterior and posterior shear, lateral shear, axial rotation and lateral bending. Due to the mid-sagittal symmetry of the cervical spine, disc response can be regarded the same for left and right lateral bending, lateral shear and axial rotation. Vertebral disc responses are obtained by subjecting a motion segment (vertebra-disc-vertebra) or a disc segment (body-disc-body) to external loading. Disc stiffnesses reported by Moroney et al. (1988) and Yoganandan et al. (2001) were used for the cervical spine. As no other data on cervical disc stiffnesses can be found Moroney's values have been used for axial rotation, lateral bending and all shear stiffness coefficients. Camacho et al. (1997) presented non-linear load-displacement curves at various levels. The translational damping coefficients of the discs are set to 1000kg/s and rotational coefficients to 1.5Nm/s as based on those used by de Jager as no actual disc damping coefficients have been reported in the literature. These damping coefficients were shown not to account for the dynamic stiffening of the disc but instead were employed to attenuate vibration accelerations of the head (de Jager, 1996). In the model, the dynamic stiffness of the disc is assumed to be twice the static stiffness. For lumbar spine, the motion segment stiffness matrix results of the study of Gardner-Morse and Stokes (2004) was utilized in the modelling (Table 4.3). For thoracic spine, the stiffness values in Table 2.1 were employed in the modelling. Material properties for cervical spine discs are tabulated in Table 4.4.

Table 4.4 Stiffness and damping data for cervical intervertebral discs.

Loading Direction	Stiffness k [N/mm]						Damping b
	C2-C3	C3-C4	C4-C5	C5-C6	C6-C7	C7-T1	C2-T1 [Ns/m]
Anterior Shear	62	62	62	62	62	62	1000
Posterior Shear	50	50	50	50	50	50	1000
Lateral Shear	73	73	73	73	73	73	1000
Tension	63.5	69.8	66.8	68.0	69.0	82.2	1000
Compression	637.5	765.3	784.6	800.2	829.7	973.6	1000
	[Nm/rad]						[Nms/rad]
Flexion	Load Curve from Camacho et al., (1997) /2						1.5
Extension	Load Curve from Camacho et al., (1997) /2						1.5
Lateral Bending	0.33	0.33	0.33	0.33	0.33	0.33	1.5
Axial Rotation	0.42	0.42	0.42	0.42	0.42	0.42	1.5

4.3.3 Ligaments

Ligaments of the neck not only provide stability to the motion segments allowing motion within physiological limits but also dissipate energy during trauma. Ligaments are uniaxial structures that resist only tensile forces as they become slack in compression.

The ligaments in the present model were chosen as nonlinear viscoelastic ligaments. All six common types of ligaments were introduced to the model, which are ALL (anterior longitudinal ligament), PLL (posterior longitudinal ligament), LF (ligament flavum), JC (joint capsules), ISL (interspinous ligament) and SSL (supraspinous ligament) (Fig. 4.25).

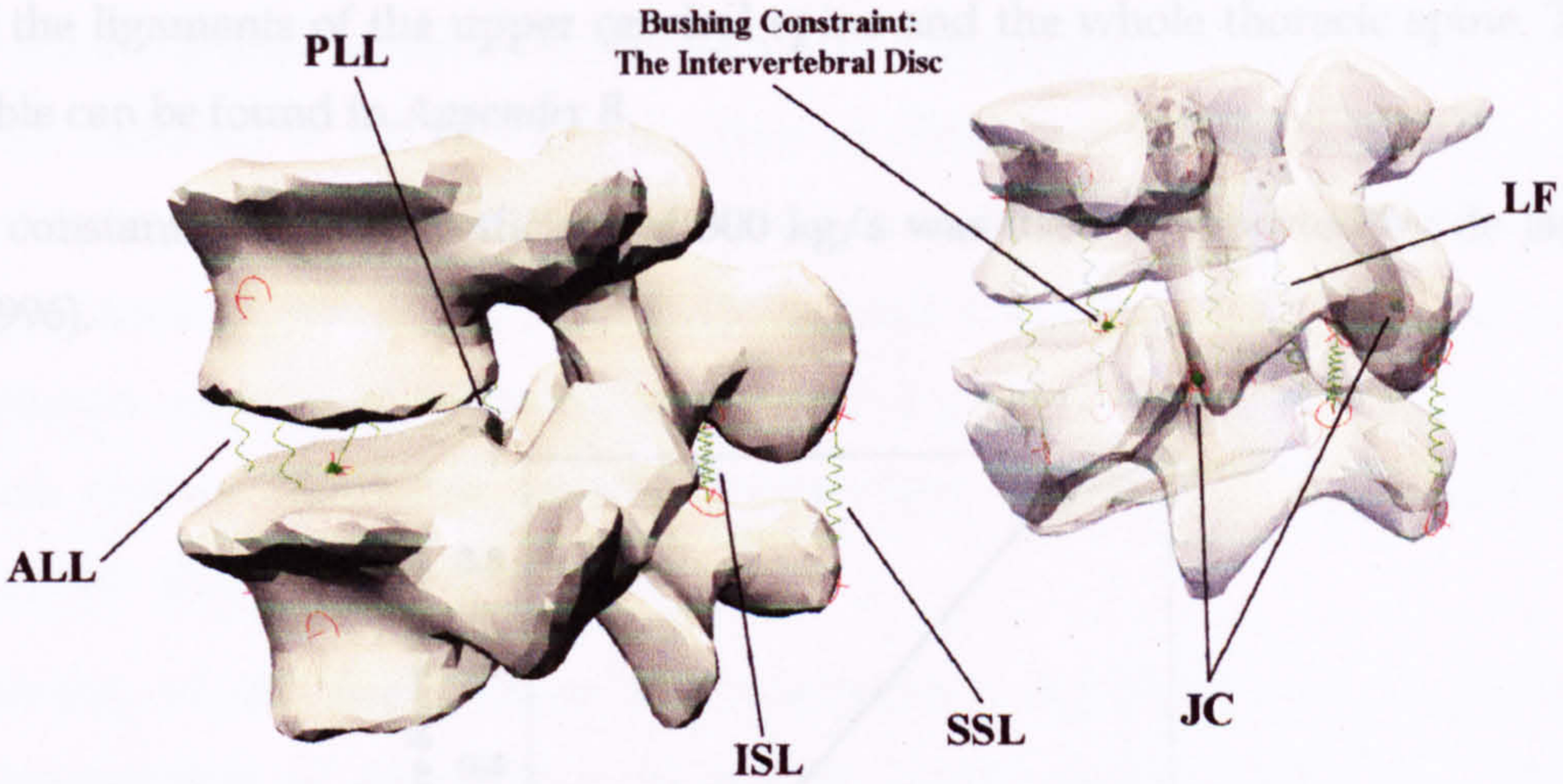

Figure 4.25 Ligaments and the disc in the multi-body model

The necessary non-linear biomechanical properties of human spine ligaments were taken from the literature (Pintar et al., 1992, Teo and Ng, 2001, Yoganandan et al., 1999) (Figures 2.28-2.37 for cervical ligaments, and Figures 4.13-4.14 for lumbar ligaments).

The curves were implemented as look-up tables in visualNastran with the elements defined as being active for positive values of deflection only i.e. the ligament elements produce force in tension only. The ligaments' rest lengths were input as the element lengths in the initial body position.

No force-deflection curves were characterized for the ligaments of the upper cervical spine as well as thoracic spine although Yoganandan et al. (2001) have presented failure force and deformation for each. Chazal et al (1985) identified the non-linear force-strain behaviour of ligaments from the thoracic and lumbar spine. The average dimensionless force-strain curve, normalized relative to the failure force F_{max} and failure strain E_{max}, for all ligaments reported by Chazal et al. is shown in Figure 4.26. This curve shows that spinal ligaments exhibit almost identical behaviour in dimensionless form, and so the curve can be used together with measured failure force and deformation to characterise the non-linear response of any specific spinal ligament. The curve was employed together with the force and deformation at failure, presented as a table in Myklebust et al. (2001), to define the non-linear force-deflection curves for each of the ligaments of the upper cervical spine and the whole thoracic spine. The table can be found in *Appendix B*.

A constant damping coefficient of 300 kg/s was used as reported by de Jager (1996).

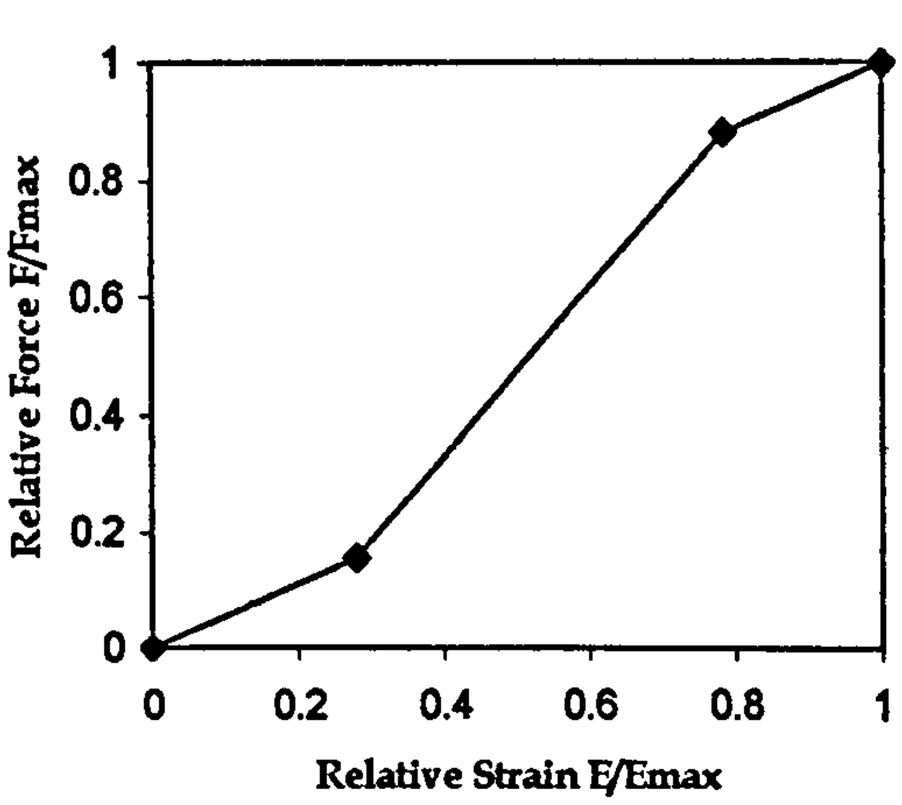

Figure 4.26 Average dimensionless force-strain curve used to determine the force-deflection curves for the missing ligament properties

4.3.4 Muscles

In the model the muscles were constructed incorporating all the muscle groups, including fascicles of the erector spinae and multifidus. Necessary geometric and morphologic features such as the origins, insertions and dimensions are

taken from various studies in the literature (Bogduk et al., 1992, Winters and Woo, 1990, Johnson et al., 1994, Cheng et. al., 2000). Muscles were modelled as contractile muscle elements possessing both passive and active behaviour. In visualNastran, linear actuator constraint was employed to model the muscles, which have been governed by an external software, Virtual Muscle v.3.1.5 of Alfred E. Mann Institute at the University of Southern California, that runs within Matlab/Simulink and communicates with visualNastran where appropriate. The linear actuator constraint applies a controlled force between two bodies, or between the background and a body. The actuator can be specified to (1) apply a specified force, (2) maintain a specified acceleration, (3) maintain a specified velocity, or (4) maintain a specified length. In the model, these selections are all handled by the external software.

19 muscle groups of the head and neck and 9 main muscle groups of the trunk were included in the model. As many of these muscles cross two or more vertebral pairs distributed between multiple sites of attachment, muscles with broad areas of attachment are subdivided into a number of individual muscle elements resulting in 280 individual muscle segments. Muscle attachment sites were chosen depending on other researchers' decisions and on published anatomic descriptions in the literature.

Curving of the musculature is an important aspect for a more realistic representation of the change in muscle length during head-neck motion. However, due to the complexity of the model and simplification purposes, muscle curving was compromised as almost all muscles segments were modelled as one piece of actuator. The following section describes the muscle model used, and the muscle groups included in the model.

4.3.4.1 External Software to Control Muscles: Virtual Muscle

Muscle mechanics is governed by external application called Virtual Muscle v. 3.1.5, developed at the Alfred E. Mann Institute at the University of Southern California that runs within Matlab and Simulink. Virtual Muscle has been created to be used in the context of a hierarchical model of motor control with itself being the intermediate layer (Figure 4.27). Realistic muscle properties

provided by Virtual Muscle manage the skeletal dynamics that are in turn governed by visualNastran being the lowest level of the system. At the top-level, muscle activation is controlled.

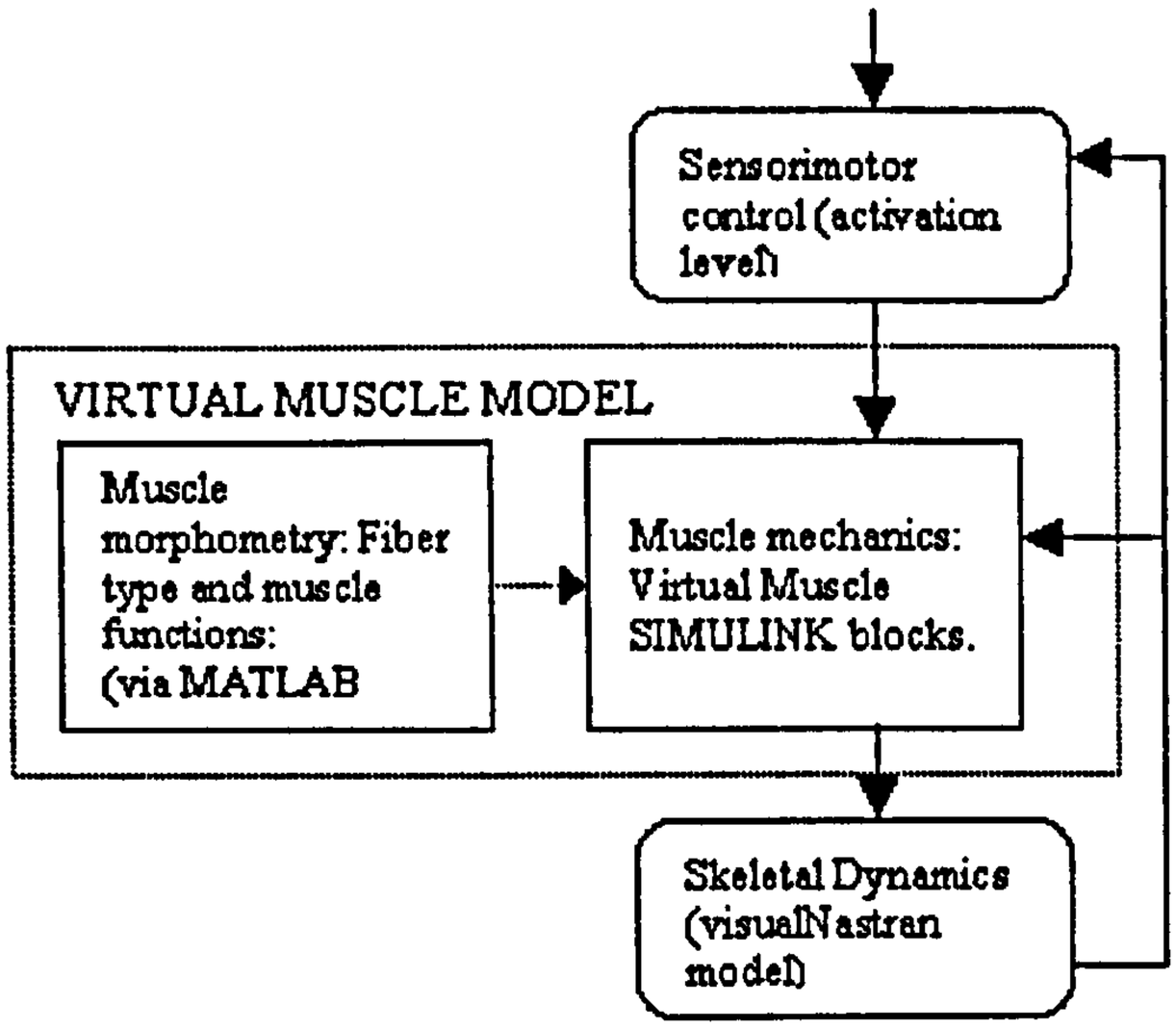

Figure 4.27 The order of muscle control (Cheng et al., 2001)

The basic form of the muscle model is generally similar to those of Hill (1970) and Zajac (1990), which is illustrated schematically in Figure 4.28. The model consists of an active contractile element (CE) describing active force F_{CE} with activation, length and velocity dependencies in parallel with a viscoelastic element (PE) describing the passive properties of fascicles F_{PE}. The total fascicular force is applied in series to the inertial mass of the muscle and a series elastic element (SE) for tendon and aponeurosis. The mass and a small amount of viscosity in the passive muscle establish realistic damping that prevents computational instability (Brown and Loeb, 2000).

Formulations for the models' fascicular force are stated in Equations 3-5.

$$F = F_{CE} + F_{PE} \quad [3]$$

$$F_{CE} = Af \cdot FL \cdot FV \quad [4]$$

$$F_{PE} = F_{PE1} + Af \cdot F_{PE2} \quad [5]$$

A schematic description of these main elements of the model along with their associated sub-elements is illustrated in Figure 4.29 with a description of the contribution of each constituent physiological component (see *Appendix C* for model equations). In Equation 3, *F* is the total force produced by the muscle fascicles while F_{CE} and F_{PE} are the forces produced by the *CE* and *PE*, respectively. In Equation 4, *Af* is defined as the activation-frequency relationship and is a unitless quantity ($0 \leq Af \leq 1$, Af=1 for tetanic stimulation). *FL* is defined as the tetanic force-length relationship and has units of F_0 (maximal potentiated isometric force), and *FL* is primarily dependent upon fascicle length. *FV* is defined as the tetanic force-velocity relationship and is unitless (*FV*=1 for isometric condition); *FV* is based primarily upon fascicle velocity, which is identified as positive for lengthening velocities. In Equation 5, F_{PE1} and F_{PE2} are spring-like components with units of F_0 and are non-linear functions of length (Brown et al., 1999).

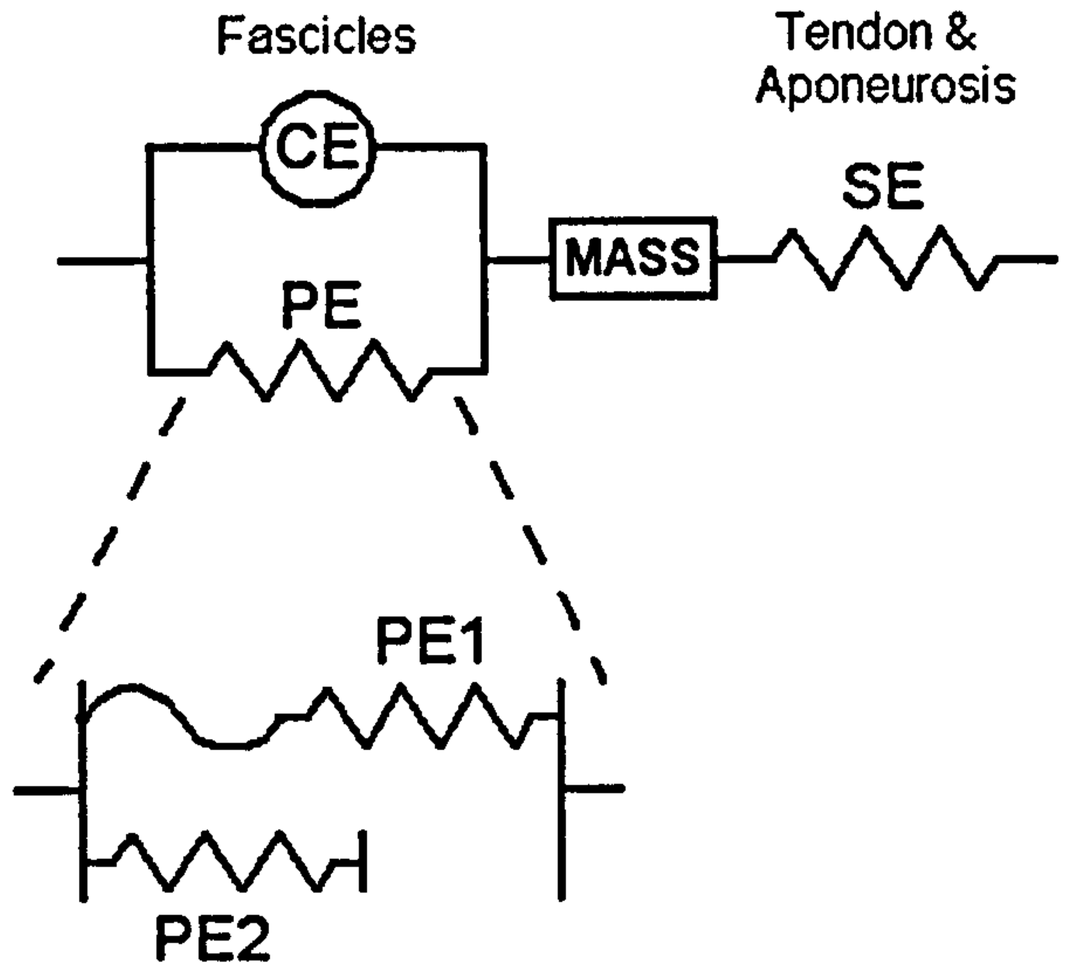

Figure 4.28 Schematic of basic muscle model elements. The muscle fascicles are represented by the contractile element (CE) in parallel with the passive elastic element (PE). The series elastic element (SE) represents the combined tendon and aponeurosis. The inertial mass of the muscle is also applied in series to the fascicles. PE1 is a non-linear spring that resists stretch in the passive muscle, while PE2 is non-linear spring resisting compression during active contraction at short lengths. (Cheng et al., 2001)

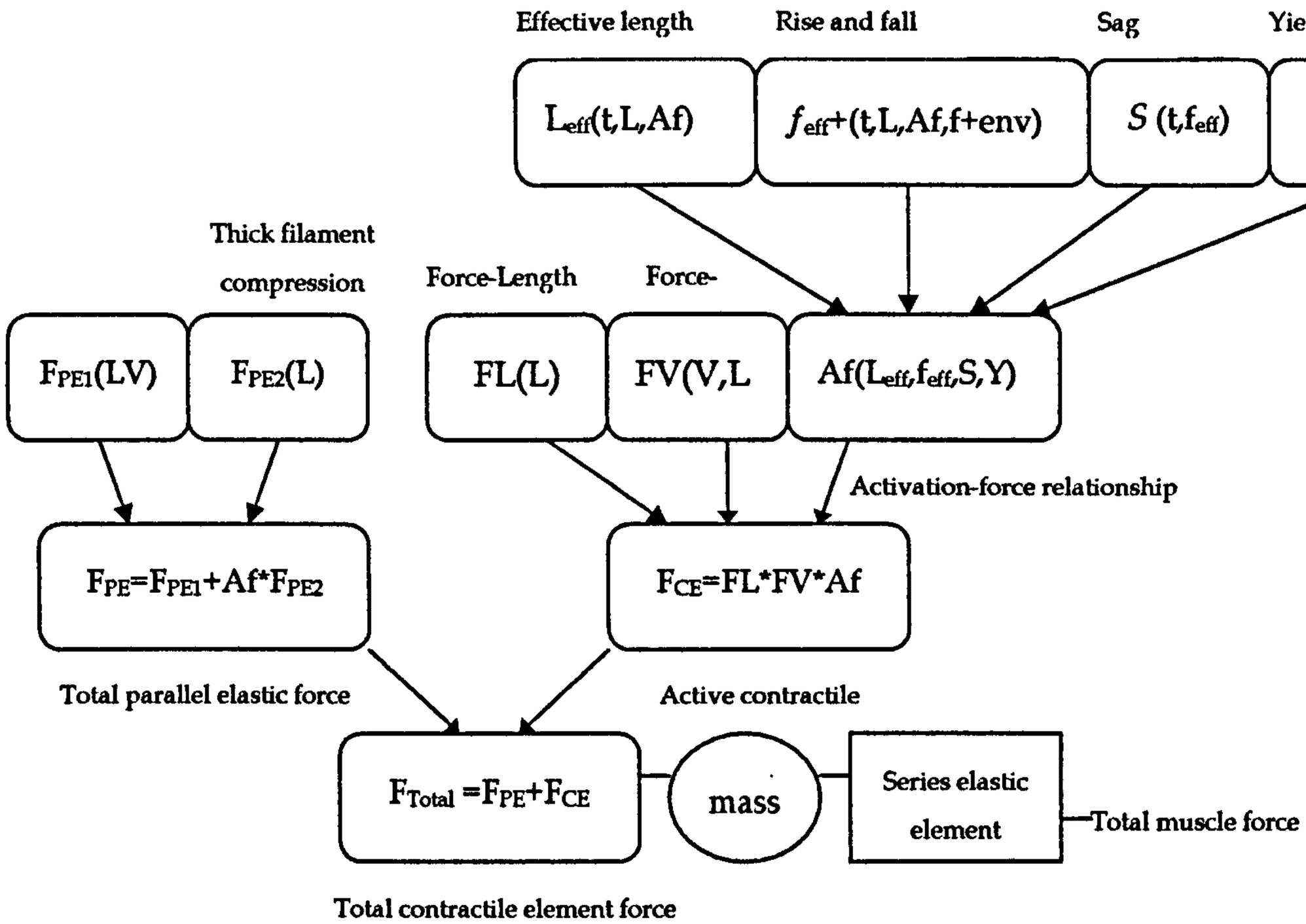

Figure 4.29 Schematic representation of Virtual Muscle's equations and terms. Complete descriptions of all elements shown can be found in Brown and Loeb (2000) and Brown et al. (1999). F_{Total}- total force produced by muscle fascicles. F_{PE}- total passive force produced by parallel elastic element PE. F_{CE}- total active force produced by contractile element CE. F_{PE1}- passive visco-elastic properties of stretching a muscle. F_{PE2}- passive resistance to compression of the thick filaments at short muscle lengths. FL- tetanic Force-Length relationship. FV- tetanic Force-Velocity relationship. Af- isometric, activation-frequency relationship. F_{eff}- time lag between changes in firing frequency and internal activation (i.e. rise and fall times). L_{eff}- time lag between changes in length and the effect of length on the Af relationship. S represents the effects of 'sag' on the activation during a constant stimulas frequency. Y represents the effects of yielding (on activation) following movement during sub-maximal activation.

4.3.4.2 Muscle Fibre Types.

Zajac (1989) showed that the behaviour of the contractile element of muscle varies from the sarcomere level up to the whole muscle fibre and again up to the level of an entire recruitment group of motor units. By introducing the properties of each fibre type that will be used throughout the muscle model in a single database, permits the muscle model to use these properties when fibre types are joined in varying percentages to form a typical mixed-fibre-type

muscle. In this study, the *generic fast twitch* and *typical slow twitch* fibre types derived for human muscles as presented in Cheng et al. (2000) are utilised (see Appendix C for fibre type best-fit constants and associated equations). The parameters used to identify these fibre types are tabulated in Table 4.5. The optimal sarcomere length of 2.7 μm was gathered from Herzog et al. (1992), which shows close agreement with the value 2.8 μm reported in another study by Rack and Westbury (1969). This value is employed to scale the active and passive force-length properties. The recruitment rank identifies which fibre type is recruited first in a muscle composed of more than one fibre type. $V_{0.5}$ is the shortening velocity required to produce half the maximum tetanic force (0.5 F_0) at 1.0 L_0 (fascicle length at which F_0 is elicited). $f_{0.5}$, the frequency at which half of maximal tetanic force is obtained (isometric at 1.0 L_0), scales the rise and fall times. Details of how $V_{0.5}$ and $f_{0.5}$ were obtained are explained by Cheng et al. (2000).

The specific tension is defined as the maximal isometric force produced at the optimal length per unit cross-sectional area. The default value of 31.8N/cm² has been used based on Scott et al. (1996) and Brown el al. (1998). On the other hand, the value was estimated to be anywhere between 20 and 100 N/cm² by Winters and Stark (1988) and it is claimed that a higher value than 31.8 may be required to truly represent the maximum muscular forces that can be exerted by a human subject and that the value of specific tension is likely to vary between subjects due to gender differences and different levels of muscular development.

Table 4.5 Muscle model fibre type parameters (Van Lopik, 2004).

Fibre Type Parameter	'typical' slow-twitch fibre type	generic fast-twitch fibre type
Optimal Sarcomere Length (μm)	2.7	2.7
Recruitment Rank	1	2
$V_{0.5}$ (L_0/s)	-1	-1.67
$f_{0.5}$ (pps)	12	20
Specific Tension (N/cm²)	31.8	31.8

4.3.4.3 Muscle Morphometry

The parameters needed for the muscle model that are independent of fibre type and are specific to individual muscles are F_0, L_0, L_0^T and $L_{max.}$ L_0 is the muscle fibre length at peak isometric active muscle force (F_0), where L_0 and F_0 are specific to the muscle fascicles). L_0^T is the length of muscle tendon at maximal tetanic isometric force, which is different from the more commonly used tendon slack length (L_S^T) Zajac (1989). L_S^T is less well defined than L_0^T. Also, L_S^T tends to be around 5% shorter (Cheng et al., 2000). L_{max} is the length of the muscle fascicles at the maximal anatomical length of the muscle.

The morphometric values required for the model are *muscle mass, optimal fascicle length, optimal tendon length* and the *maximal anatomical musculotendon path length.* These measures are then utilised either directly or to calculate the required parameters of the models equations. Optimal fascicle length and optimal tendon length correspond to L_0 and L_0^T. By using muscle mass and fascicle length, the physiological cross-sectional area (PCSA) of the muscle is obtained, which is proportional to F_0. L_{max} is calculated from the difference of the maximum whole-muscle length and the tendon L_0^T, scaled by muscle fascicle length L_0 (Van Lopik, 2004).

Mass and optimal fascicle length of most cervical spine muscles have been provided by Kamibayashi and Richmond (1998). Optimal tendon length was approximated by using 105% of tendon slack length (Cheng, 2001). Tendon slack length was calculated as the difference between the musculotendon length at the neutral head position of the model and the muscle fascicle length. Kamibayashi and Richmond claim that the measured muscle fascicle length in the neutral posture are within 15% of their optimal length. Values of maximal musculotendon path length were selected based on the path length of the muscle elements in the head-neck model at extreme positions of the head so as to give values of L_{max} between 1.1 and 1.42 (Cheng, 2001). In the virtual muscle model, the muscle fascicle lengths reported were employed for each of the sub-elements of a given muscle. Muscle mass was either divided equally between the sub-volumes or proportionally in order to give the required PCSA of the individual elements and the overall muscle.

Once the specific morphometry of an individual muscle is established, the muscle must be assigned to the relevant muscle fibre types. Table 4.6 tabulates the fibre type distribution for the neck muscles included in the model along with the source of reference. Some of the required muscle morphometry data to be used in the model can be found in Appendix D.

Finally, the number of motor units to be used to simulate each fibre type in the muscle is specified. Normally a muscle comprises about 100 or more motor units. In order to simplify the model to gain from computation time, a small number of motor units were chosen, where each unit represents a group of 'real' motor units. For example the Splenius Capitis consists of 37% slow- and 63% fast-twitch muscle fibres, with three motor units allocated to the slow-twitch portion and 5 motor units to the fast-twitch portion of the muscle.

Table 4.6 Histochemical composition of muscle fibre types in the muscles of the head-neck model (Van Lopik, 2004).

Muscle Name	Fibre Type Distribution/ Number of Motor Units		Reference
	Slow-twitch	Fast-twitch	
Suboccipital			
Rectus capitis post. Major	60% / 4	40% / 3	a
Rectus capitis post. Minor	60% / 4	40% / 3	a
Obliquus capitis superior	50% / 3	50% / 3	a
Obliquus capitis inferior	30% / 2	70% / 4	a
Longissimus capitis	33% / 2	67% / 4	b
Longissimus cervicis	45% / 3	55% / 3	b
Splenius capitis	37% / 2	63% / 4	b
Splenius cervicis	50% / 3	50% / 3	a
Semispinalis capitis	35% / 2	35% / 4	b
Semispinalis cervicis	35% / 2	35% / 4	b
Scalenus			
Scalenus anterior	29% / 2	71% / 4	b
Scalenus medius	29% / 2	71% / 4	b
Scalenus posterior	29% / 2	71% / 4	b
Sternocleidomastoid			
Sternomastoid	23% / 2	77% / 4	b
Cleidomastoid	23% / 2	77% / 4	b
Cleido-occipital	28% / 2	72% / 4	b
Trapezius	26% / 2	74% / 4	b
Longus colli	54% / 3	46% / 3	c
Longus capitis	40% 3	60% / 4	d
Levator scapulae	26% / 2	74% / 4	d
Multifidus	77% / 4	23% / 2	c

a. Winters and Woo (1990)

b. Richmond et al. (2001)

c. Boyd-Clark et al. (2001)

d. Estimated. Not present in the literature.

4.3.4.4 Musculotendon Blocks

Once fibre types were determined and the morphometry of the individual muscle volumes and sub-volumes were defined, the stand-alone Simulink muscle blocks were created (Fig. 4.30). Each musculotendon block requires inputs for activation and for musculotendon path length. The output from the musculotendon element is force in Newtons. A schematic general view of the Simulink model is depicted in Figure 4.31.

It is assumed here that the activation input of a muscle is determined by a single neural input where the level of activation lies between 0 and 1, 0 for passive muscle and 1 for maximally activated muscle. For muscle activation it is assumed that the level of activation changes instantaneously from 0 to 1 after a certain onset/reflex delay. Reflex time is defined as the activation time of a muscle in reaction to an external disturbance, which in the case of a motor vehicle collision may be a visual signal, a loud noise, or impact induced motion (Van Lopik, 2004). Reported reflex times for neck muscles range from 25 to 90 ms (Snyder et al., 1975, Reid et al., 1981, Ono et al., 1997, Brault et al., 2000).

The length of the actuators representing the individual muscle elements is read from visualNastran at each time step of simulation and passed to Simulink as the input for musculotendon path length. This along with level of activation is used to calculate the muscle force which in turn is passed back to the MB model in visualNastran.

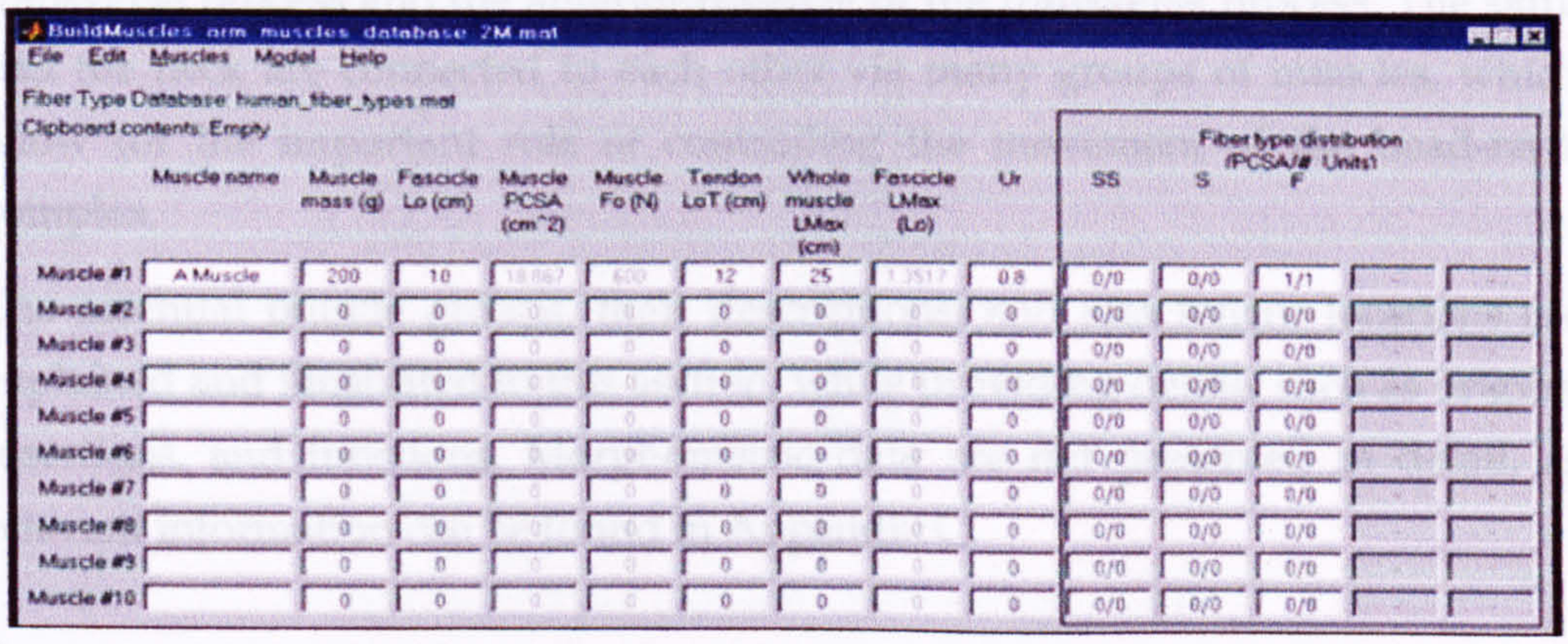

Figure 4.30 Virtual Muscle "BuildMuscles" interface (Cheng et al., 2001)

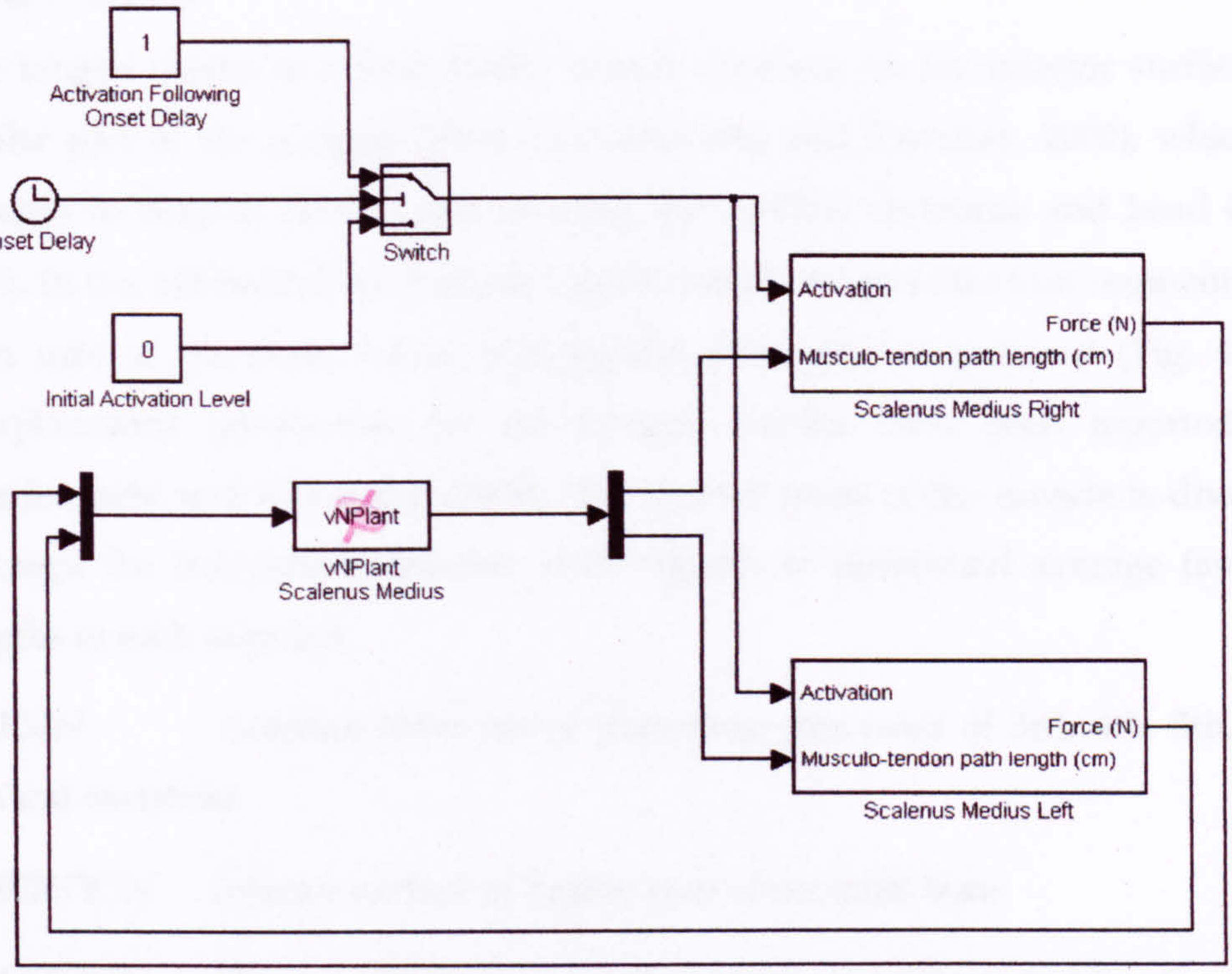

Figure 4.31 Simulink model for *scalenus medius* muscle group. The switch is used to change the level of activation following a specified onset delay.

4.3.4.5 Muscle Descriptions and Attachment Locations

This section covers the most important and essential muscle groups implemented into the model, which preserves the spinal stability. Although muscles are attached all around the vertebrae, three main areas of muscle attachment can be grouped as the tip of the spinous process, the tip of the transverse process and the anterior tubercle of the transverse process. The skull and the neck are connected to each other via many groups of muscles, which allow for the important role of controlling the movement of the head-neck complex.

The essential muscle groups, their descriptions, and attachment locations are explained and illustrated in this section, while providing details such as origins, insertions, and functions. Morphometric data are not presented in detail, as relevant information can be found in Appendix C.

Longus Capitis

The longus capitis is a long fleshy muscle inserted on the inferior surface of basilar part of the occipital bone (Gurumoorthy and Twomey, 2000), which is thought to help in flexing and rotating the cervical vertebrae and head (Fig. 4.32). In the MB model, the Longus Capitis muscle is split into four segments on each side of the neck, where mid-sagittal symmetry is assumed (Fig. 4.33). Morphometric parameters for the Longus Capitis have been reported by Kamibayashi and Richmond (1998). The overall mass of the muscle is divided amongst the individual elements with regards to individual average fascicle lengths of each segment.

ORIGIN : Anterior tubercles of transverse processes of 3rd, 4th, 5th, 6th cervical vertebrae

INSERTION : Inferior surface of basilar part of occipital bone

FUNCTION : Flexes and assists in rotating cervical vertebrae and head

NERVE : Muscular branches of 1st, 2nd, 3rd, 4th cervical

ARTERY : Ascending cervical of inferior thyroid; prevertebral of ascending pharyngeal; muscular of vertebral (Warfel, 1985)

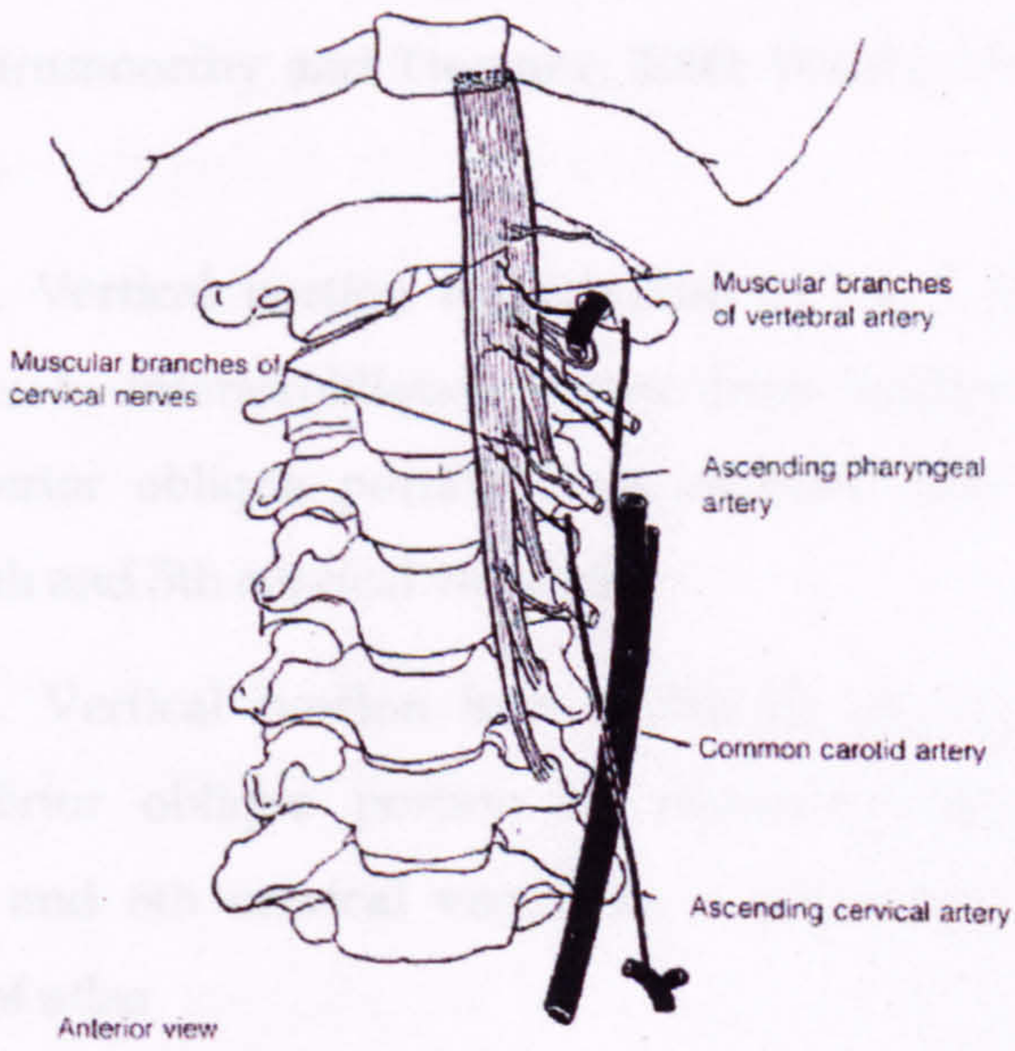

Figure 4.32 The longus capitis (Warfel, 1985)

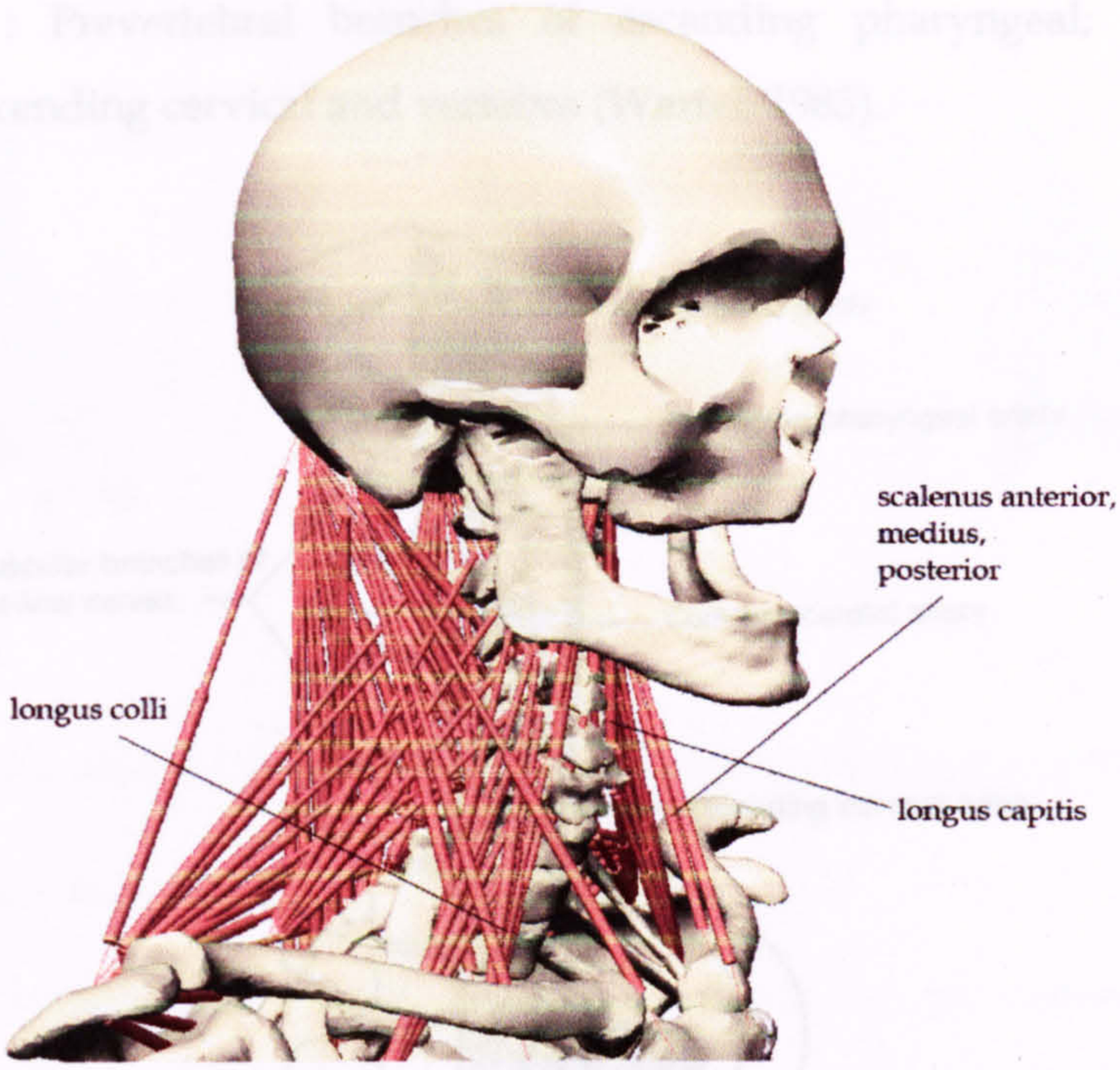

Figure 4.33 The longus capitis, colli, and scalenus muscles in the MB model

Longus Colli

The longus colli is a long, flat muscle being the deepest muscle found in the pre-vertebral region of the cervical spine, situated on the anterior surface between the atlas and T3 vertebrae. The longus colli is thought to be a flexor of the cervical spine (Gurumoorthy and Twomey, 2000; Warfel, 1985) and illustrated in Figures 4.33-34.

ORIGIN : a. Vertical portion from bodies of 1st 3 thoracic and last 3 cervical vertebrae; b. inferioroblique portion from bodies of 1st 3 thoracic vertebrae; c. superior oblique portion from anterior tubercles of transverse processes of 3d, 4th and 5th cervical vertebrae

INSERTION : a. Vertical portion into bodies of 2d, 3d and 4th cervical vertebrae; b. inferior oblique portion on anterior tubercles of transverse processes of 5th and 6th cervical vertebrae; c. superior oblique portion on anterior tubercle of atlas

FUNCTION : Flexes and assists in rotating cervical vertebrae and head; acting singly flexes column laterally

NERVE : Branches of anterior primary rami of 2d to 8th cervical

ARTERY : Prevertebral branches of ascending pharyngeal; muscular branches of ascending cervical and vertebra (Warfel, 1985).

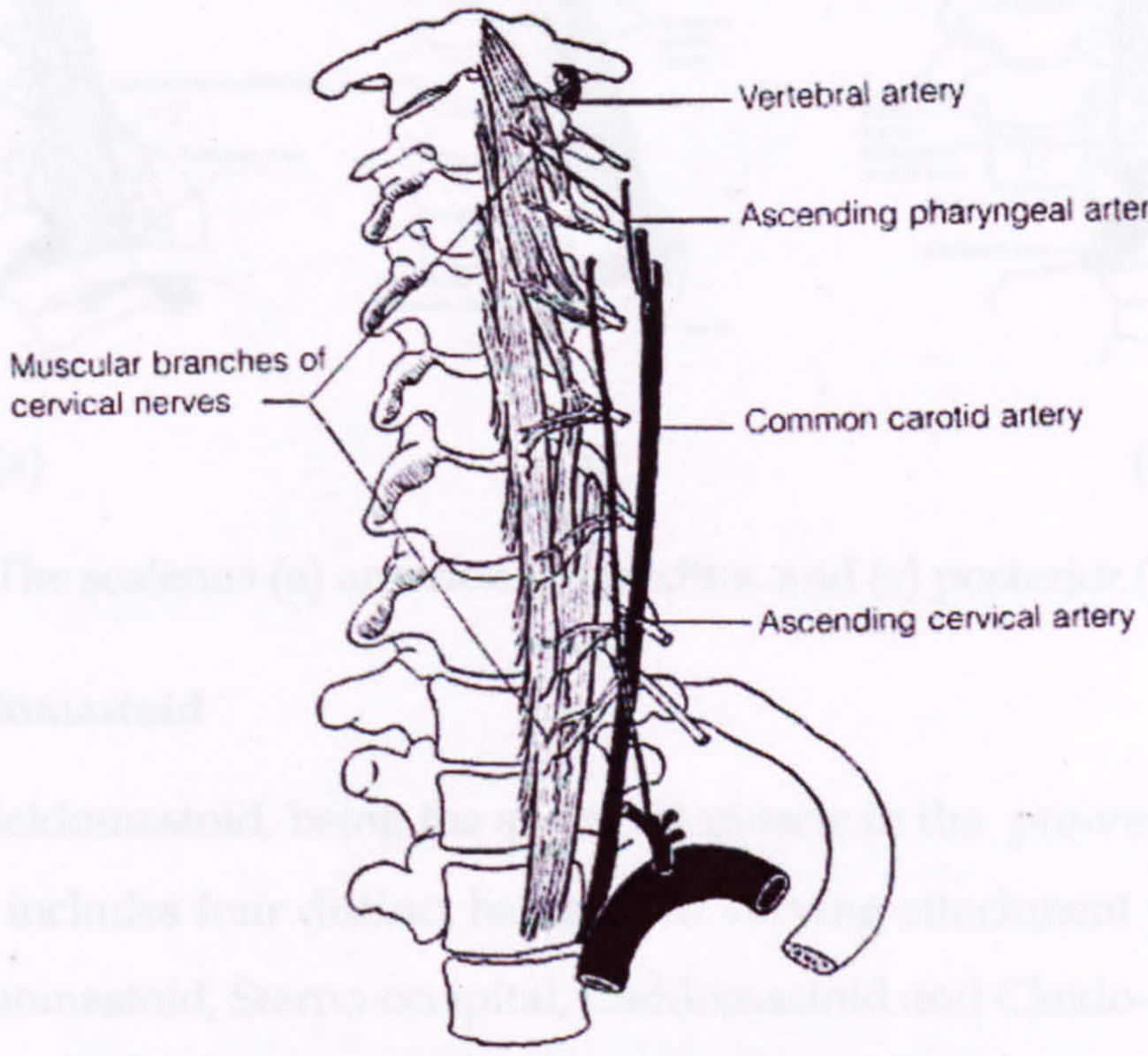

Figure 4.34 The longus colli (Warfel, 1985)

Scalenus: Anterior, Medius, and Posterior

The three Scalenus muscles are attached on either side of the anterior aspect of the cervical spine connecting the transverse processes of the middle and lower vertebrae to the first and second ribs (Fig. 4.35).

The *Scalenus Anterior* has its origin on the scalene tubercle of the first rib and inserts onto the transverse processes of C3 through C6. The *Scalenus Medius* starts from the posterior aspect of the first rib behind the subclavian artery inserting onto the transverse processes of C2 through C7. The *Scalenus Posterior* takes its origin from the superior border and lateral aspect of the second rib, while inserting via three tendinous slips onto the transverse processes of C4-C6. In the MB model, each Scalenus muscle is represented by a single muscle element on each side of the neck (Fig. 4.33), having the origins on the ribs as based on the above descriptions from the anatomical drawings (Warfel, 1985; Gray, 1980) and decisions made by other researchers (de Jager, 1996).

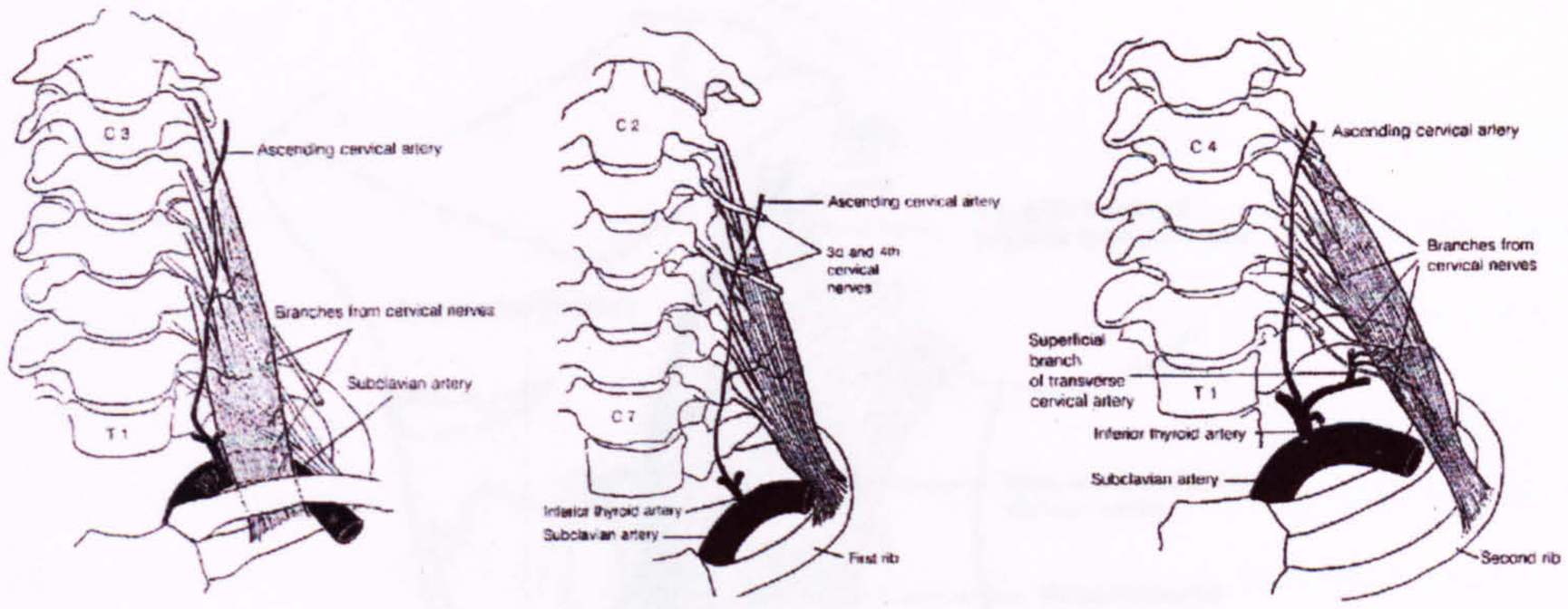

(a) (b) (c)

Figure 4.35 The scalenus (a) anterior, (b) medius, and (c) posterior (Warfel, 1985)

Sternocleidomastoid

The sternocleidomastoid, being the strongest muscle in the pre-vertebral region of the neck, includes four distinct bands with varying attachment points; which are the Sternomastoid, Sterno-occipital, Cleidomastoid and Cleido-occipital (Fig. 4.36). Sternocleidomastoid produces flexion in the cervical spine via contraction on both sides of the neck, and also they can be used to flex the atlanto-occipital joints without flexion of the neck.

ORIGIN : Sternal head, anterior surface of manubrium; clavicular head., upper surface of medial 3d of clavicle.

INSERTION : Lateral surface of mastoid process; lateral half of superior nuchal line of occipital bone

FUNCTION : Draws head toward shoulder and rotates it pointing chin cranially and to opposite side; together, flex head; raise thorax when head is fixed

NERVE : 2d cervical and spinal portion of accessory

ARTERY : Sternocleidomastoid branch of superior thyroid and occipital muscular of suprascapular, occipital of posterior auricular (Warfel, 1985).

In the MB model, the Sternocleidomastoid is represented by three muscle elements on each side of the neck as illustrated in Figure 4.37.

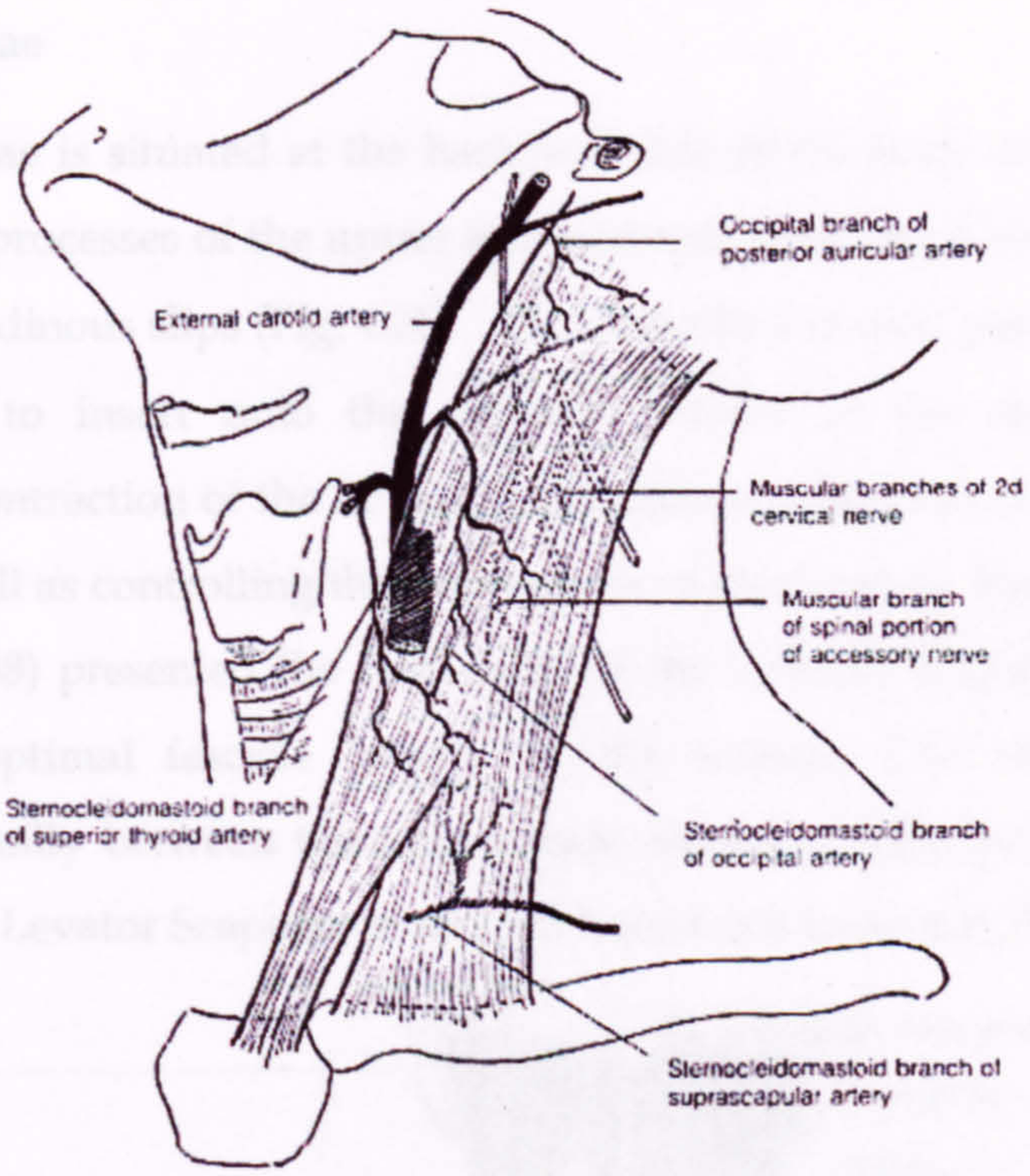

Figure 4.36 The sternocleidomastoid (Warfel, 1985)

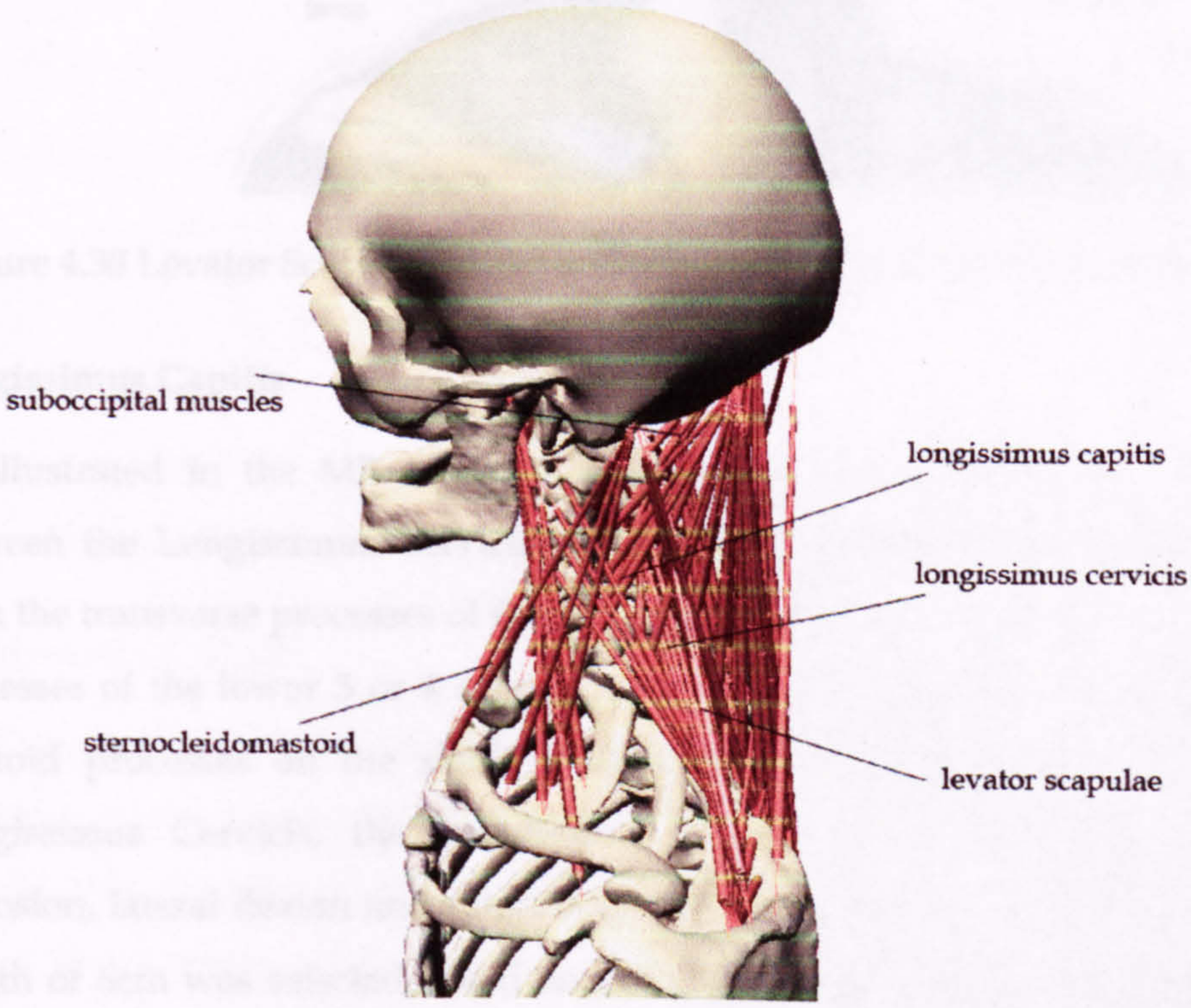

Figure 4.37 The sternocleidomastoid and other cervical muscles in the MB model

Levator Scapulae

Levator Scapulae is situated at the back and side of the neck originating from the transverse processes of the upper four cervical vertebrae, C1-C4 in the form of four thin tendinous slips (Fig. 4.38). This strap-like muscle passes downward and outward to insert onto the superior border of the medial scapula. Symmetrical contraction of the Levator Scapulae can assist the cervical spine in extensionas well as controlling the movements of the scapula. Kamibayashi and Richmond (1998) presented the total mass of the Levator Scapulae along with the average optimal fascicle length for the muscle. The total mass was distributed equally between the four muscle elements with the same average fascicle length. Levator Scapulae in the MB model can be seen in Figure 4.37.

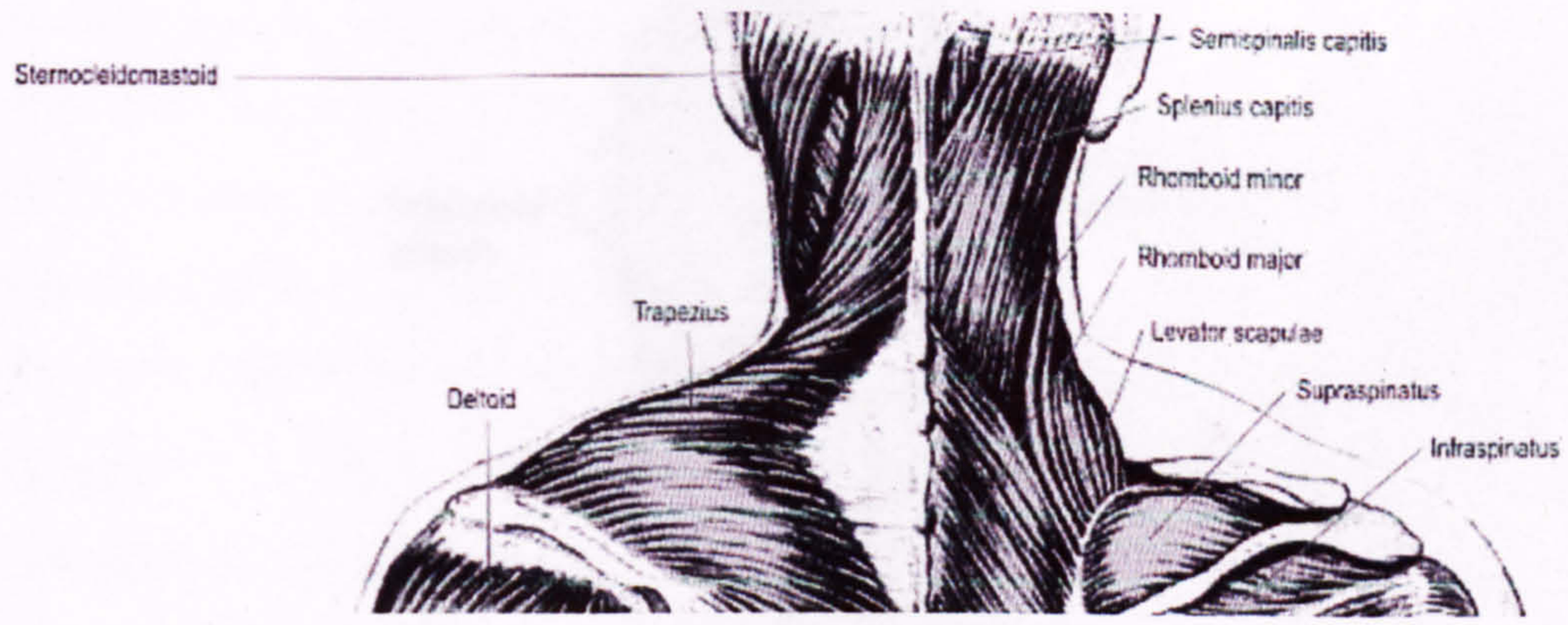

Figure 4.38 Levator Scapulae along with some other neck muscles (Gray, 1980)

Longissimus Capitis

As illustrated in the MB model in Figure 4.37, the Longissimus Capitis is between the Longissimus Cervicis and the Semispinalis Capitis. It originates from the transverse processes of the upper 4 or 5 thoracic and from the articular processes of the lower 3 or 4 cervical vertebrae to the posterior margin of the mastoid processes on the skull (Warfel, 1985) (Fig. 4.39). Along with the Longissimus Cervicis, the Longissimus Capitis has a role in producing extension, lateral flexion and rotation of the cervical spine. An optimal fascicle length of 6cm was selected based on the initial length of the muscle elements and on the fascicle length reported by Vasavada et al. (1998).

ORIGIN : L. capitis, transverse processes upper 4 or 5 thoracic, articular processes lower 3 or 4 cervical vertebrae

INSERTION : L. capitis, posterior margin mastoid process

FUNCTION : Extension, lateral flexion and rotation of column

NERVE : Posterior primary rami of spinal nerves

ARTERY : Muscular branches of occipital, deep cervical branch of costocervical trunk (Warfel, 1985)

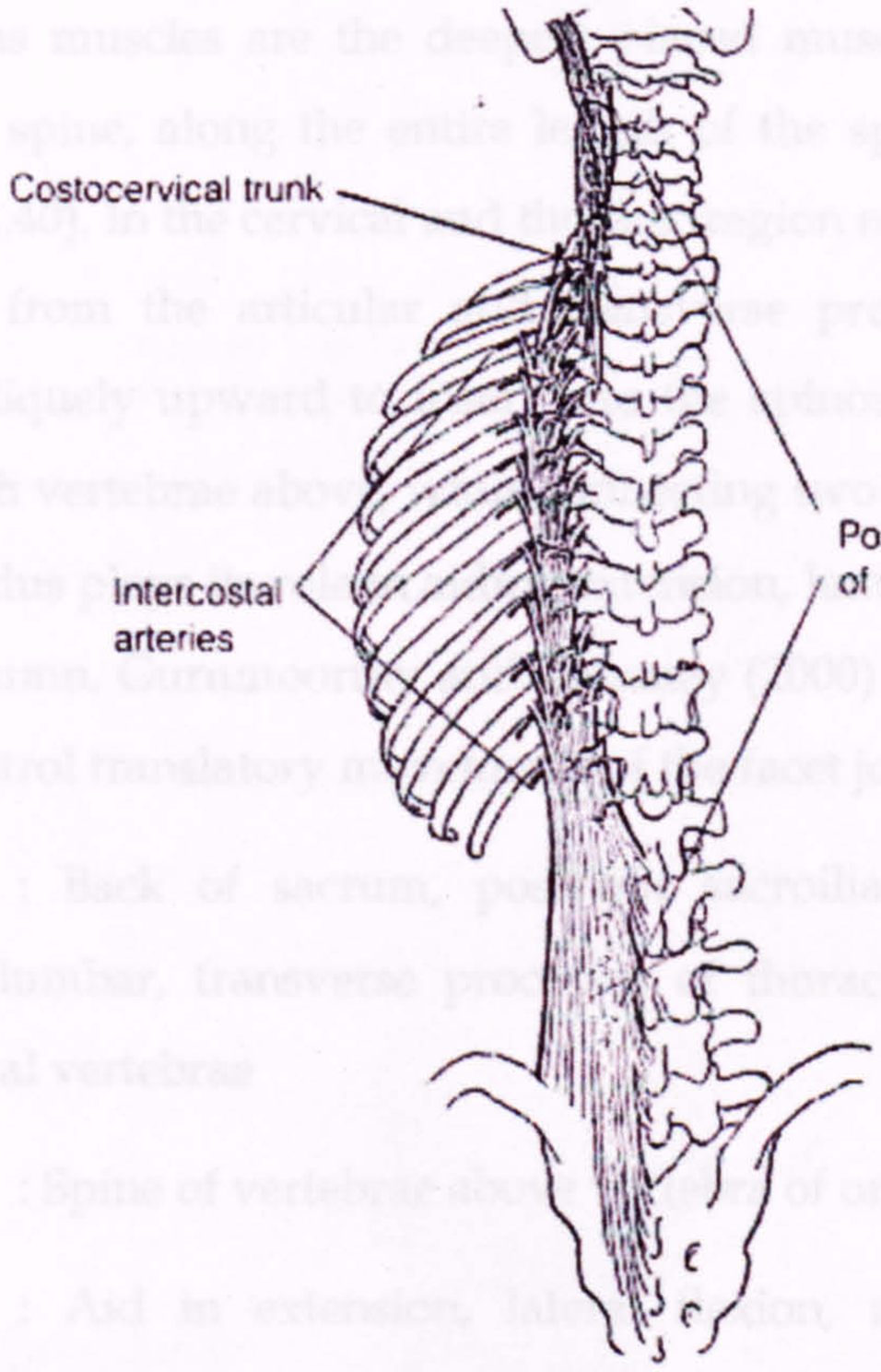

Figure 4.39 Longissimus Capitis, Cervicis, Thoracis (Warfel, 1985)

Longissimus Cervicis

The Longissimus Cervicis arises from the upper 4 or 5 thoracic vertebrae with insertions on the transverse processes of C2 to C6 (Warfel, 1985). Along with the Longissimus Capitis, the Longissimus Cervicis produces extension, lateral flexion and rotation of the cervical column (Fig. 4.39). In the MB model, the Longissimus Cervicis is integrated by five muscle elements on each side of the neck originating from a point connected to T1 at the approximate position of the

transverse process of T2 (Fig. 4.37). An optimal fascicle length of 4.4cm was used based on the initial length of the muscle elements.

ORIGIN : L. cervicis; transverse processes upper 4 or 5 thoracic vertebrae

INSERTION : L. cervicis; transverse processes 2d to 6th cervical vertebrae

FUNCTION : Extension, lateral flexion and rotation of column (Warfel, 1985)

Multifidus

The Multifidus muscles are the deepest placed muscles in the post-vertebral region of the spine, along the entire length of the spine from the axis to the sacrum (Fig. 4.40). In the cervical and thoracic region muscle fasciculi of varying length starts from the articular and transverse processes of the vertebrae, ascending obliquely upward to insert into the spinous process of the second, third and forth vertebrae above, while connecting two adjacent vertebrae (Gray, 1970). Multifidus plays its role in aiding extension, lateral flexion and rotation of the spinal column. Gurumoorthy and Twomey (2000) claim that the Multifidus also helps control translatory movements of the facet joints.

ORIGIN : Back of sacrum, posterior sacroiliac ligament, mammillary processes of lumbar, transverse processes of thoracic, articular processes of lower 4 cervical vertebrae

INSERTION : Spine of vertebrae above vertebra of origin

FUNCTION : Aid in extension, lateral flexion, and rotation of column, extension and lateral movement of pelvis

NERVE : Posterior primary rami of all spinal nerves

ARTERY : Medial muscular branches of posterior intercostals and lumbars; deep cervical branch of costocervical trunk (Warfel, 1985)

In the MB model, all Multifidus muscles were included (Fig. 4.41).

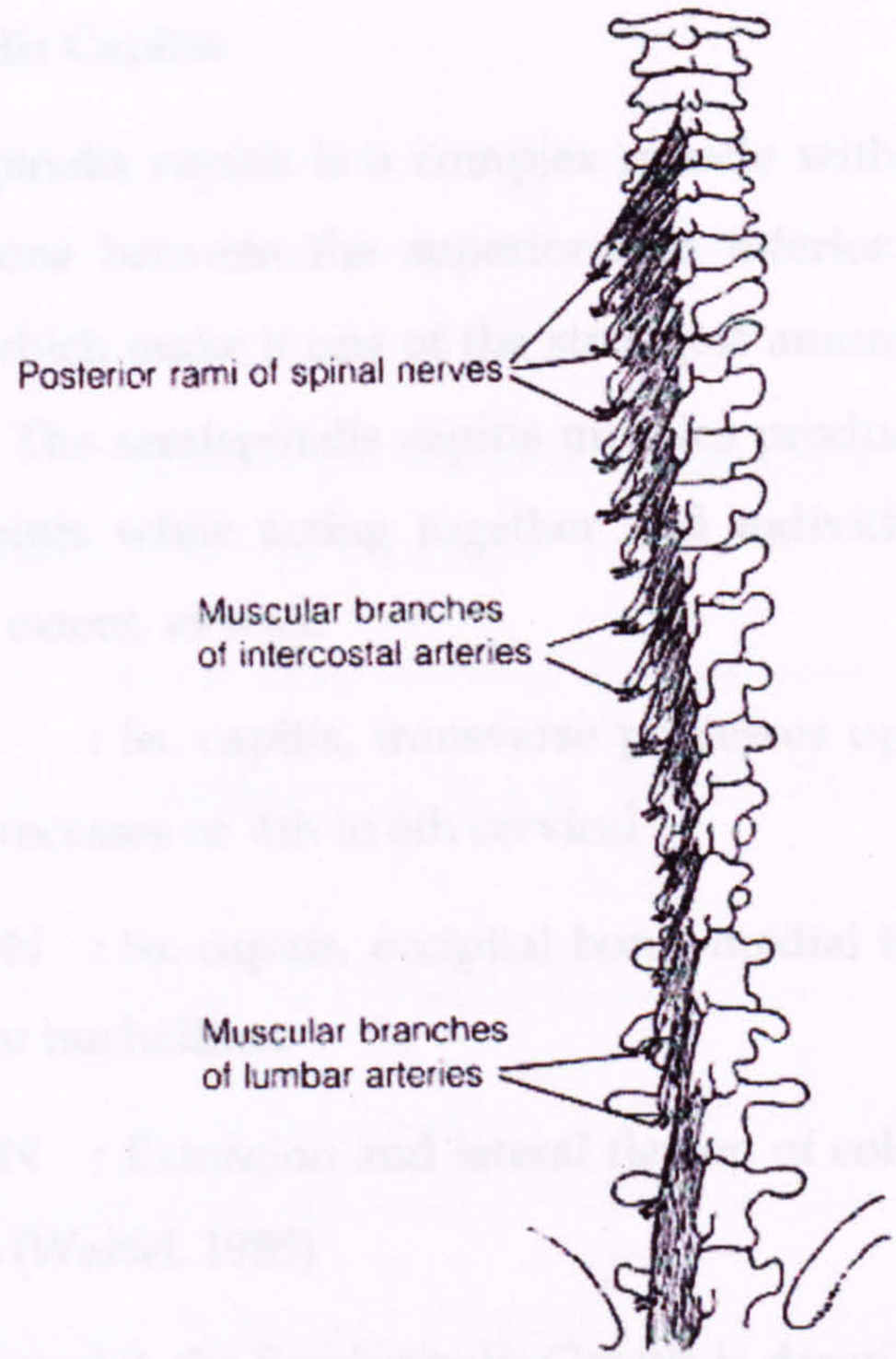

Figure 4.40 Multifidus (Warfel, 1985)

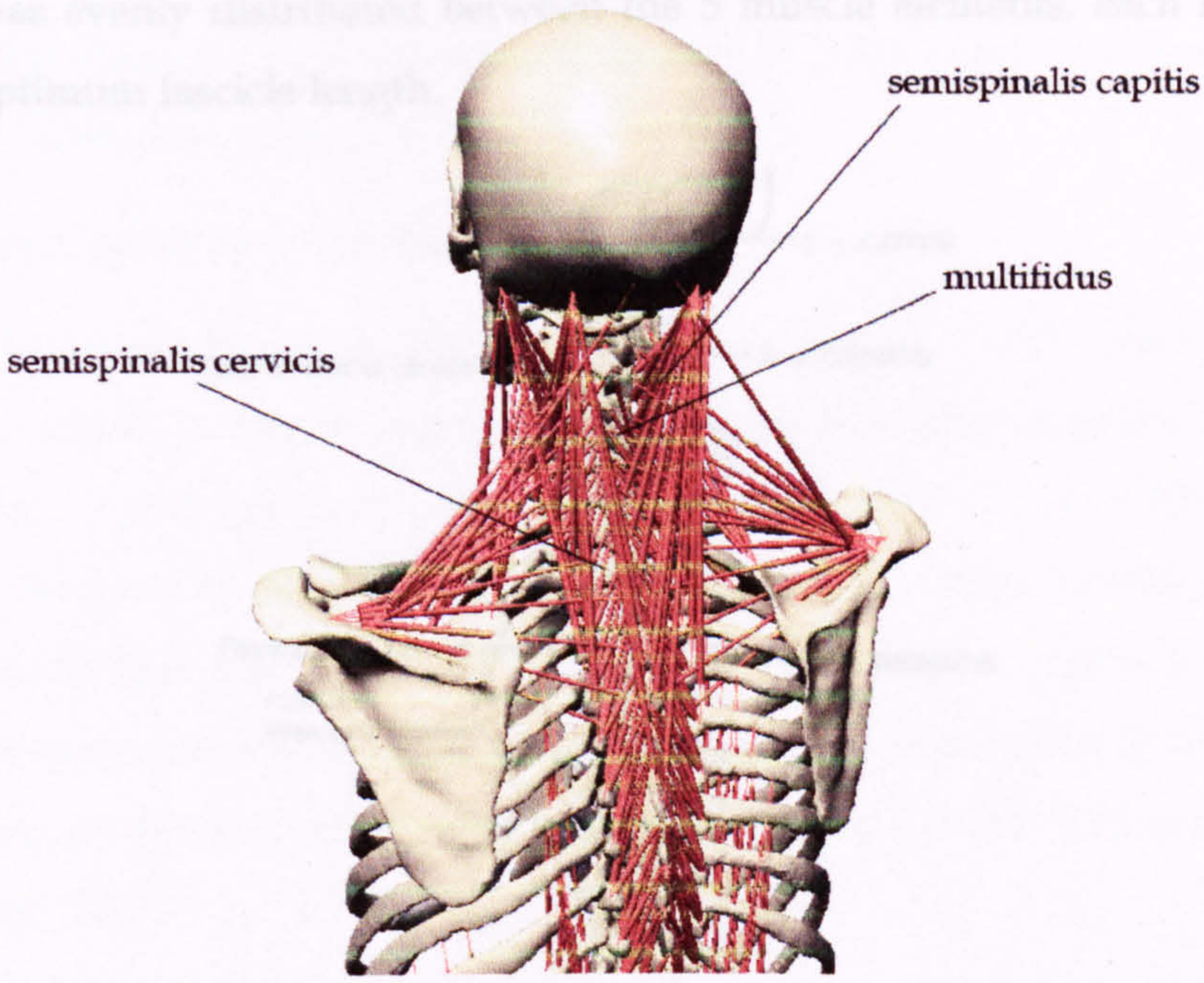

Figure 4.41 Multifidus and semispinalis muscles in the MB model

Semispinalis Capitis

The semispinalis capitis is a complex muscle with a broad insertion onto the occipital bone between the superior and inferior nuchal lines, the size and length of which make it one of the strongest among the post-vertebral muscles (Fig. 4.42). The semispinalis capitis muscles produces extension in the atlanto-occipital joints while acting together and individual contraction extends the head to an extent, as well.

ORIGIN : Ss. capitis, transverse processes upper 6 thoracic, 7th cervical, articular processes of 4th to 6th cervical

INSERTION : Ss. capitis, occipital bone, medial impression between superior and inferior nuchallines

FUNCTION : Extension and lateral flexion of column; extension of head, ribs and pelvis (Warfel, 1985)

In the MB model, the Semispinalis Capitis is described by 5 muscle elements on each side of the neck (Fig. 4.41). Kamibayashi and Richmond (1998) report the total mass of the muscle as 38.5g with the average fascicle length as 6.8cm. The mass was evenly distributed between the 5 muscle elements, each having the same optimum fascicle length.

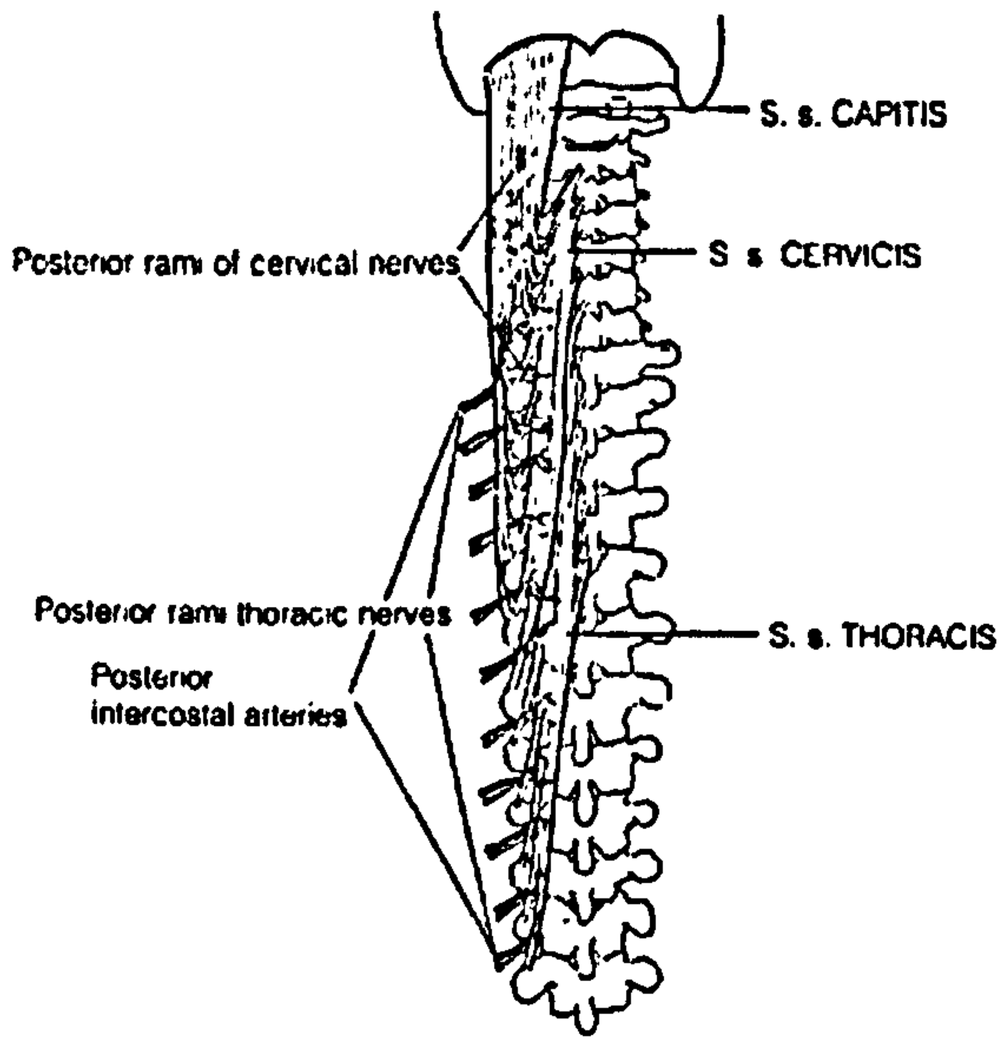

Figure 4.42 Semispinalis Capitis, Cervicis, Thoracis (Warfel, 1985)

Semispinalis Cervicis

The semispinalis cervicis originates from the transverse processes of the upper 5 thoracic vertebrae and ends on the spinous processes of C2 through C6 (Fig. 4.42).

ORIGIN : Ss. cervicis, transverse processes upper 6 thoracic, articular processes lower 4 cervical vertebrae

INSERTION : Ss. cervicis, spines of 2d to 5th cervical vertebrae

FUNCTION : Extension and lateral flexion of column; extension of head, ribs and pelvis

NERVE : Ss. cervicis, posterior rami of lower 3 cervical

ARTERY : Muscular branches of posterior intercostals; descending branch of occipital; deep cervical branch of costocervical trunk (Warfel, 1985)

Kamibayashi and Richmond (1998) failed to include the semispinalis cervicis in their study of neck muscle morphometry so the values used in the model were based on other researchers decisions (van der Horst, 1997). The same optimal fascicle length as that of the semispinalis capitis was used and the mass of the individual elements was determined to give PCSA's similar to those used by van der Horst (2002) (Fig. 4.41).

Splenius: Capitis and Cervicis

The Splenius muscle is situated at the back of the neck and upper part of the thoracic region, having its origin as a single muscle arising from the last cervical vertebrae C7 and the upper six thoracic vertebrae (T1-T6) (Fig. 4.43). From this origin, the muscle runs obliquely upward and outwards dividing into two sections, the Splenius capitis and the Splenius cervicis. The muscle is believed to work in conjunction with the semispinalis capitis as an extensor of the head and with part of the sternocleidomastoid for rotating the head (Gurumoorthy and Twomey, 2000).

ORIGIN : Sp. capitis from lower half of ligamentum nuchae and spine of 7th cervical and upper 3 or 4 thoracic vertebrae; Sp. cervicis from spines of 3rd to 6th thoracic vertebrae

INSERTION : Sp. capitis into mastoid process of temporal bone and lateral part of superior nuchal line; Sp. cervicis into posterior tubercles of transverse processes of upper 3 or 4 cervical vertebrae

FUNCTION : Together they extend, laterally flex head and neck and rotate head slightly

NERVE : Lateral branches of posterior primary rami of middle and lower cervical

ARTERY : Muscular and descending branches of occipital, superficial branch of transverse cervical (Warfel, 1985)

Kamibayashi and Richmond (1998) provide a single weight of 42.9g for the entire Splenius muscle but give the optimal fascicle lengths for the Splenius and Cervicis separately. Based on the study by Vasavada et al. (1998), the mass of the muscle was distributed as two-thirds to the Splenius capitis and one-third to the Splenius cervicis. The muscle is provided in Figure 4.44.

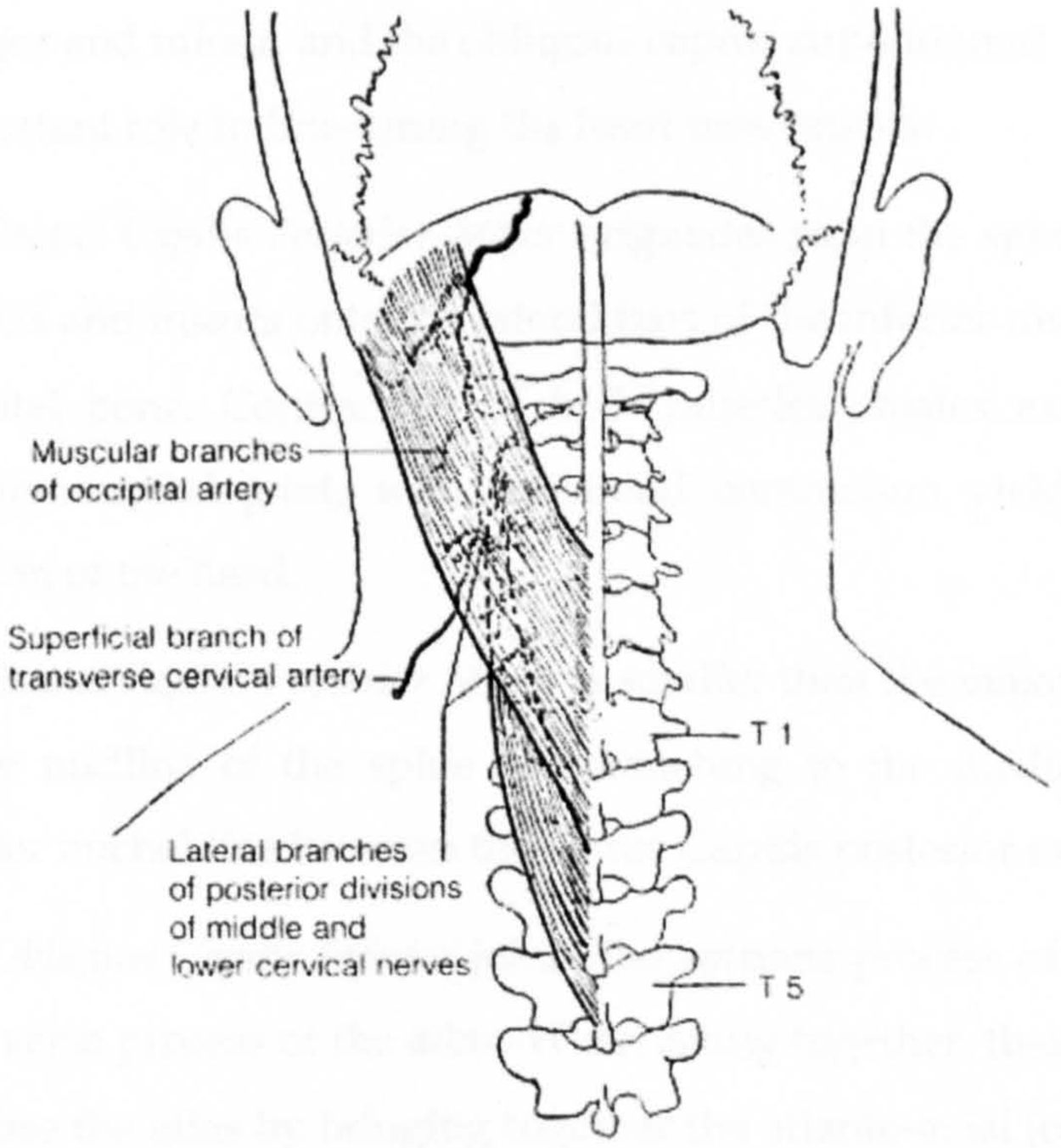

Figure 4.43 Splenius muscle (Warfel, 1985)

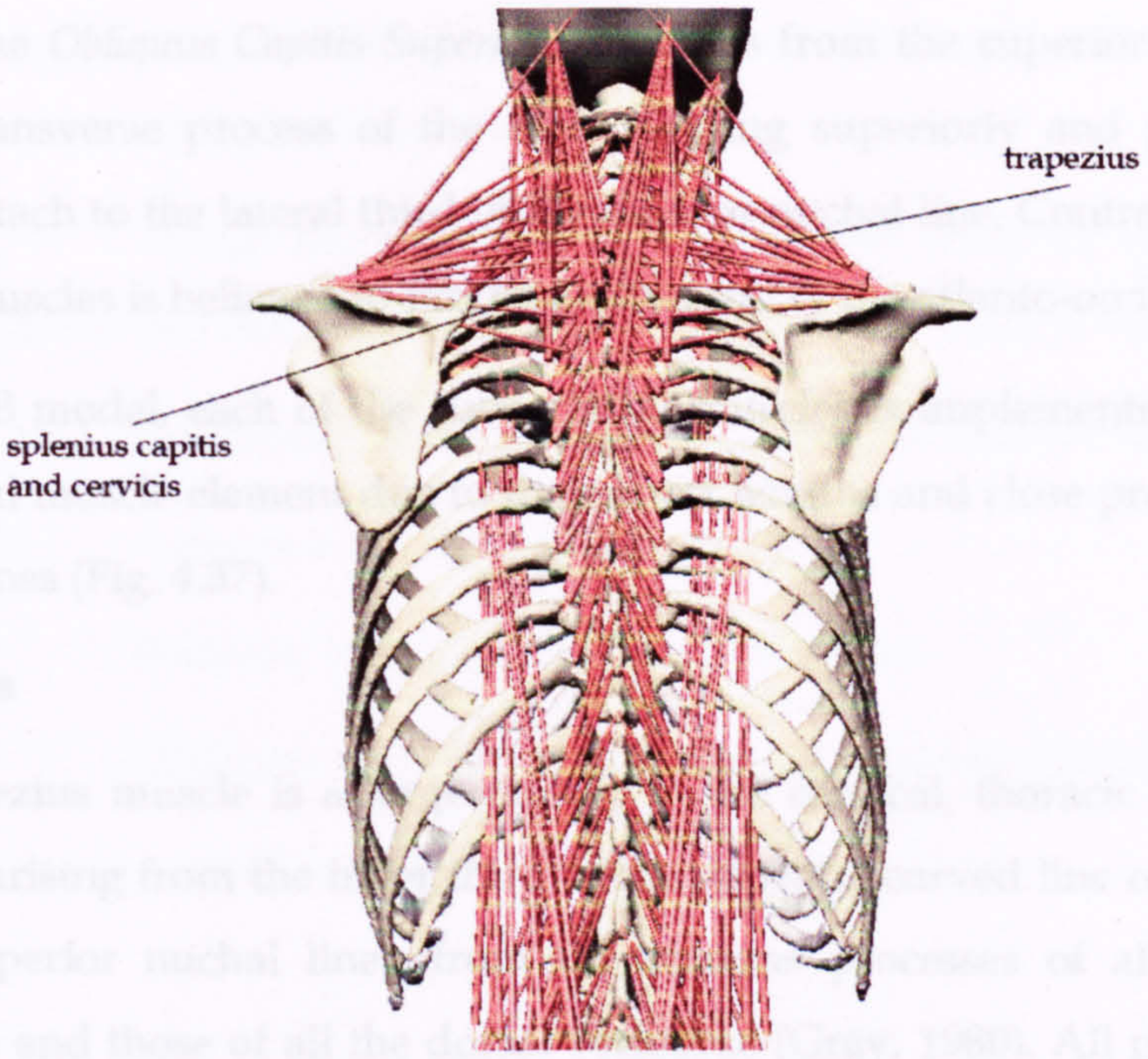

Figure 4.44 Splenius and trapezius muscles in the MB model

Suboccipital Muscles

The suboccipital muscles of the cervical spine are composed of the rectus capitis posterior major and minor, and the obliquus capitis superior and inferior, which have an important role in fine-tuning the head movements.

- The *Rectus Capitis Posterior Major* originates from the spinous process of the axis and inserts onto the lateral part of the inferior nuchal line of the occipital bone. Contraction of both muscles creates extension of the atlanto-occipital joint, with unilateral contraction yielding ipsilateral rotation of the head.
- The *Rectus Capitis Posterior Minor* is smaller than the major located closer to the midline of the spine and attaching to the medial third of the inferior nuchal line between the rectus Capitis posterior major muscles.
- The *Obliquus Capitis Inferior* joinss the spinous process of the axis to the transverse process of the atlas. When acting together, these muscles help stabilise the atlas by bringing together the atlanto-axial joints in order to allow movements in the atlanto-occipital joints (Gurumoorthy and Twomey, 2000).

- The *Obliquus Capitis Superior* originates from the superior aspect of the transverse process of the atlas running superiorly and posteriorly to attach to the lateral third of the inferior nuchal line. Contraction of these muscles is believed to produce extension of the atlanto-occipital joints.

In the MB model, each of the suboccipital muscles is implemented by a single individual muscle element due to their short lengths and close proximity to the spinal bones (Fig. 4.37).

Trapezius

The trapezius muscle is a large muscle in the cervical, thoracic and shoulder regions, arising from the inner third of the superior curved line of the occipital bone (superior nuchal line), from the spinous processes of all the cervical vertebrae and those of all the dorsal vertebrae (Gray, 1980). All portions of the muscle were included in the model. The upper section of the trapezius also known as the clavotrapezius, with origins above the level of C7, extends onto the clavicle (Fig. 4.38). The individual muscle fascicles attach systematically along the posterior border of the distal third of the clavicle bone, such that the fascicle from the superior nuchal line assumes the most anterior and medial attachment, followed in sequence by the fascicle from the spinous processes of the descending vertebrae, with the fibres from C6 inserting into the distal corner of the clavicle as far as the acromioclavicular joint (Johnson et al., 1994).

In the MB model, the trapezius muscle was divided into 8 separate muscle elements (Fig. 4.44). Positions of insertions onto the clavicle and scapula are based on anatomical drawings and descriptions in the literature. Johnson et al. (1994) reported fascicle length, PCSA and maximum force of each section of the muscle.

Rotatores

Rotatores thoracis involves eleven pairs of small roughly quadrilateral muscles, each of which joins the upper and posterior part of the transverse process of one vertebra to the lower border and the lateral surface of the lamina of the vertebra immediately above (Fig. 4.45). Rotatores cervicis and lumborum are represented

only by irregular and variable muscle bundles, whose attachments are similar to those of rotators thoracis (Gray, 1980).

ORIGIN : Lying deep to the muffifidus they form 11 pairs of small muscles; each arises from the transverse process of one thoracic vertebra

INSERTION : Into lamina of vertebra directly above vertebra of origin

FUNCTION : Assist in rotating vertebral column

NERVE : Posterior primary rami of spinal nerves

ARTERY : Muscular branches of posterior intercostals (Warfel, 1985)

The rotatores in the MB model are illustrated in Figure 4.46.

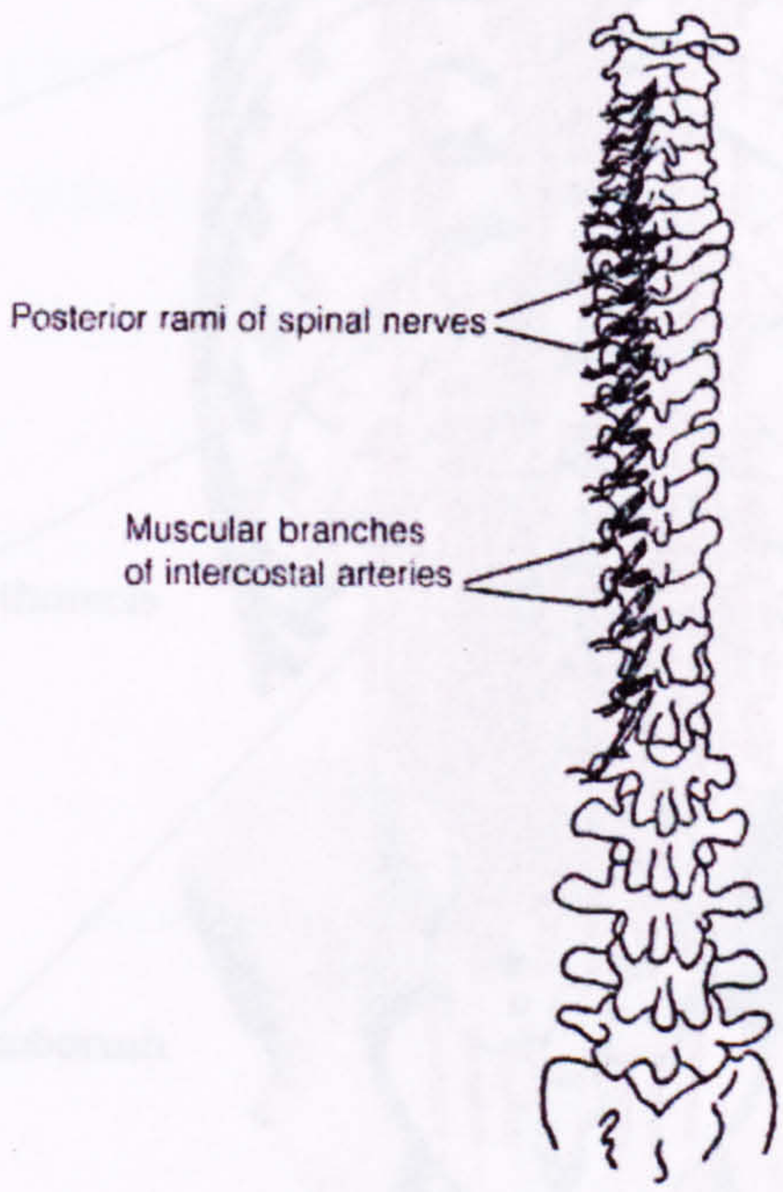

Figure 4.45 Rotatores (Warfel, 1985)

Longissimus Thoracis

As another part of the longissimus muscles, longissimus thoracis aids for extension, lateral flexion and rotation of the spinal column (Fig. 4.39).

ORIGIN : L. thoracis, transverse processes lumbar vertebrae, lumbodorsal fascia

INSERTION : L. thoracis, transverse processes thoracic vertebrae, lower 9 or 10 ribs proximal to angles

FUNCTION : Extension, lateral flexion and rotation of column; lateral movement of pelvis

NERVE : Posterior primary rami of spinal nerves

ARTERY : Posterior rami of intercostals and lumbars; muscular branches of occipital: deep cervical branch of costocervical trunk (Warfel, 1985).

The longissimus thoracis in the MB model are illustrated in Figure 4.46.

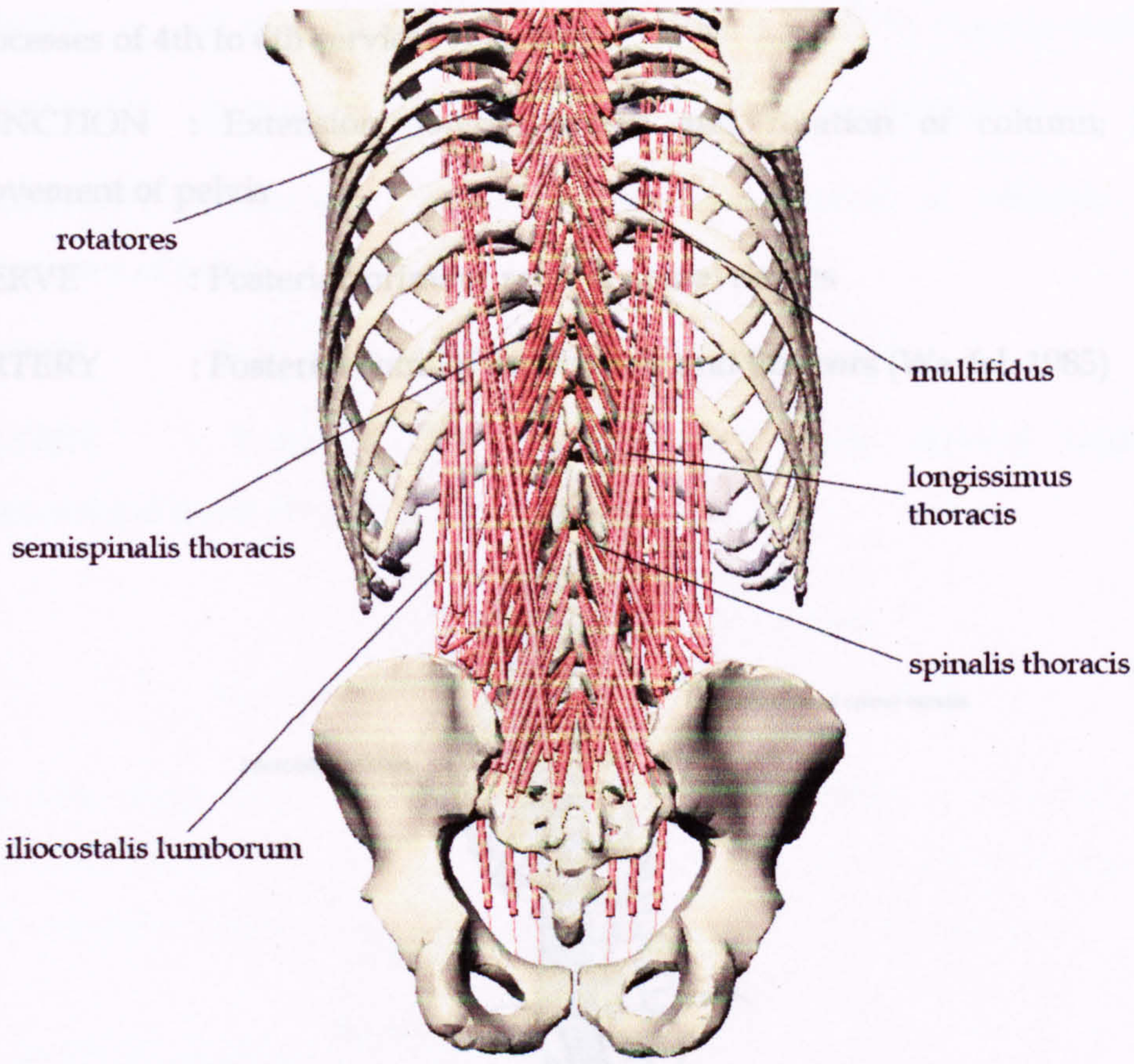

Figure 4.46 Back muscles in the MB model

Iliocostalis Lumborum, Thoracis, Cervicis

The erector spinae muscle complex lies on either side of the vertebral column. Varying in size and composition at different levels, it forms a large musculotendinous mass. In the upper lumbar region, it expands to form a thick fleshy mass. Being a part of erector spinae, iliocostalis lumborum is attached to

the inferior borders of the angles of the lower six or seven ribs (Fig. 4.47). I. thoracis attaches below to the upper borders of the angles of the lower six ribs, while I. cervicis attaches to the angles of the third to the sixth ribs (Gray, 1980). Iliocostalis muscles in the MB model are illustrated in Figure 4.46.

ORIGIN : a. I. lumborum, body of sacrospinalis in lumbar region; b. I. thoracis, angles of lower 6 ribs medial to insertion of I. lumborum; c. I. cervicis, angles of 3rd to 6th ribs

INSERTION : a. I. lumborum, lower borders of angles of lower 6 or 7 ribs; b. I. thoracis, upper borders of angles of upper 6 ribs; c. I. cervicis, transverse processes of 4th to 6th cervical vertebrae

FUNCTION : Extension, lateral flexion and rotation of column; lateral movement of pelvis

NERVE : Posterior primary rami of spinal nerves

ARTERY : Posterior rami of intercostals and lumbars (Warfel, 1985)

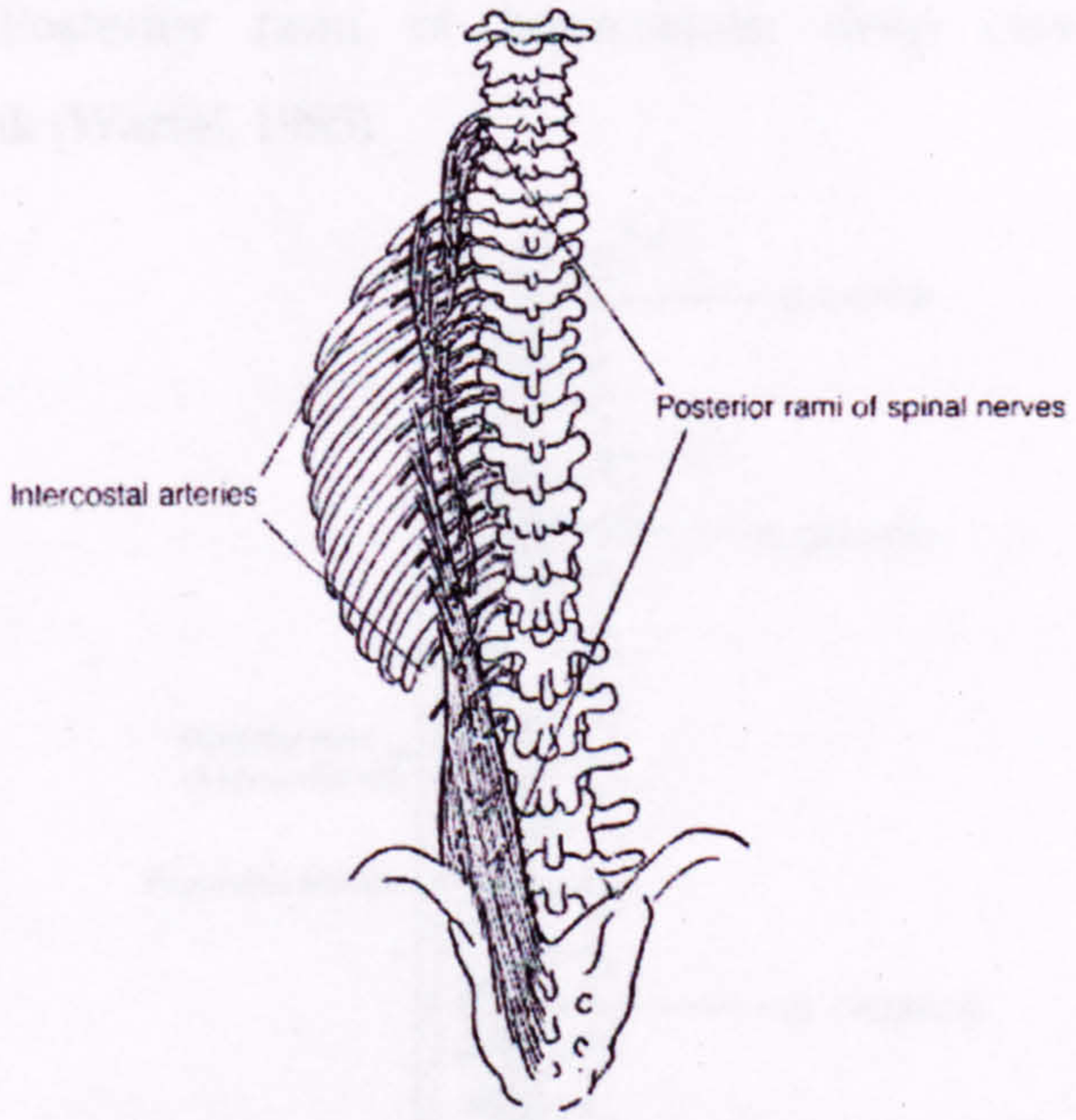

Figure 4.47 Iliocostalis muscles (Warfel, 1985)

Semispinalis Thoracis

Being similar in function to semispinalis cervicis, semispinalis thoracis aid the spine in extension and lateral bending as well as in extension of head, ribs and pelvis (Fig. 4.42).

ORIGIN : Ss. thoracis, transverse processes lower 6 thoracic vertebrae;

INSERTION : Ss. thoracis, spines of first 4 thoracic, last 2 cervical (Warfel, 1985)

Semispinalis thoracis muscles in the MB model are provided in Figure 4.46.

Spinalis Thoracis

Spinalis thoracis originates from the upper points of the lumbar spine and lowest points of thoracic spine, and inserts in the upper portions of the thoracic region (Fig.4.48).

ORIGIN : S. thoracis, spines 1 st, 2d lumbar, 11 th, 12th thoracic vertebrae

INSERTION : S. thoracis, spines upper 4 to 8 thoracic vertebrae

FUNCTION : Extension, lateral flexion and rotation of column; lateral movement of pelvis

NERVE : Posterior primary rami of spinal nerves

ARTERY : Posterior rami of intercostals; deep cervical branch of costocervical trunk (Warfel, 1985)

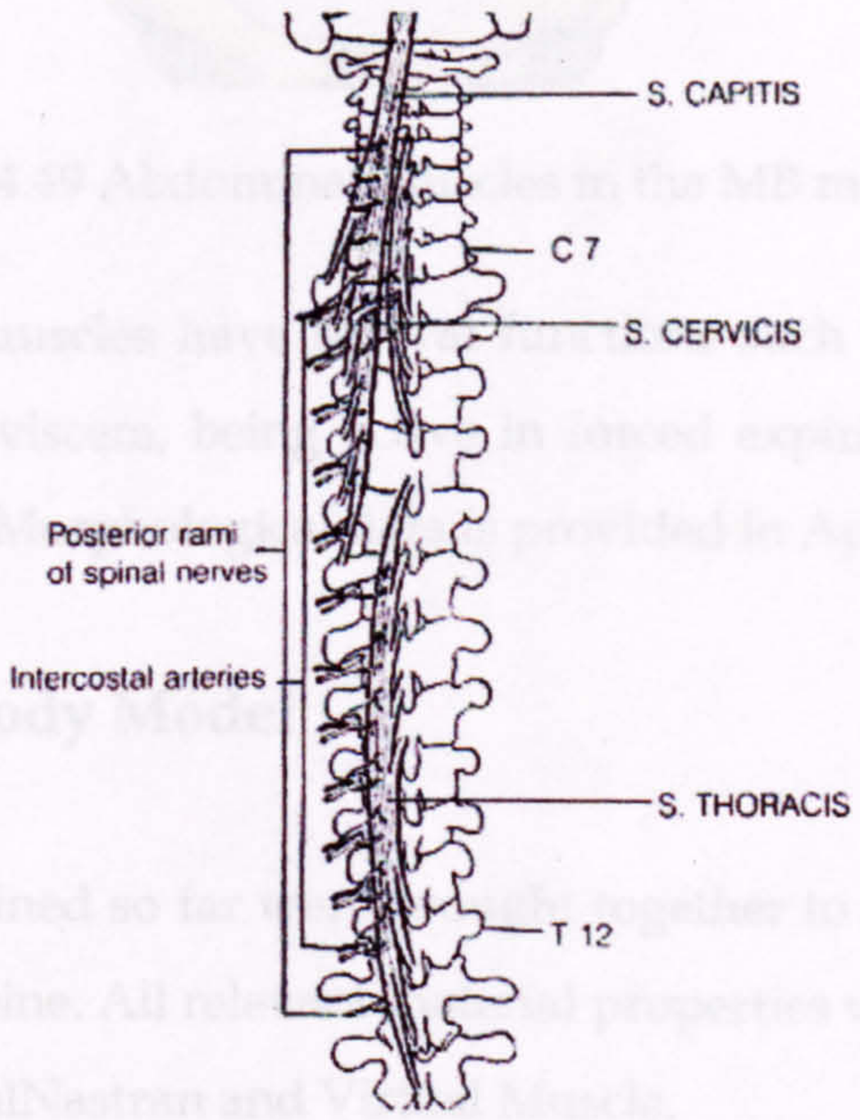

Figure 4.48 Spinalis Thoracis (Warfel, 1985)

The spinalis thoracis muscles in the MB model are illustrated in Figure 4.46.

Abdominal Muscles

In order to implement a simplified, yet effective group of abdominal muscles into the MB model; obliquus externus abdominis, obliquus internus abdominis, and rectus abdominis muscles were incorporated (Fig. 4.49). A total of 6 linear actuators were modelled to act as abdominal muscles to preserve the spinal stability.

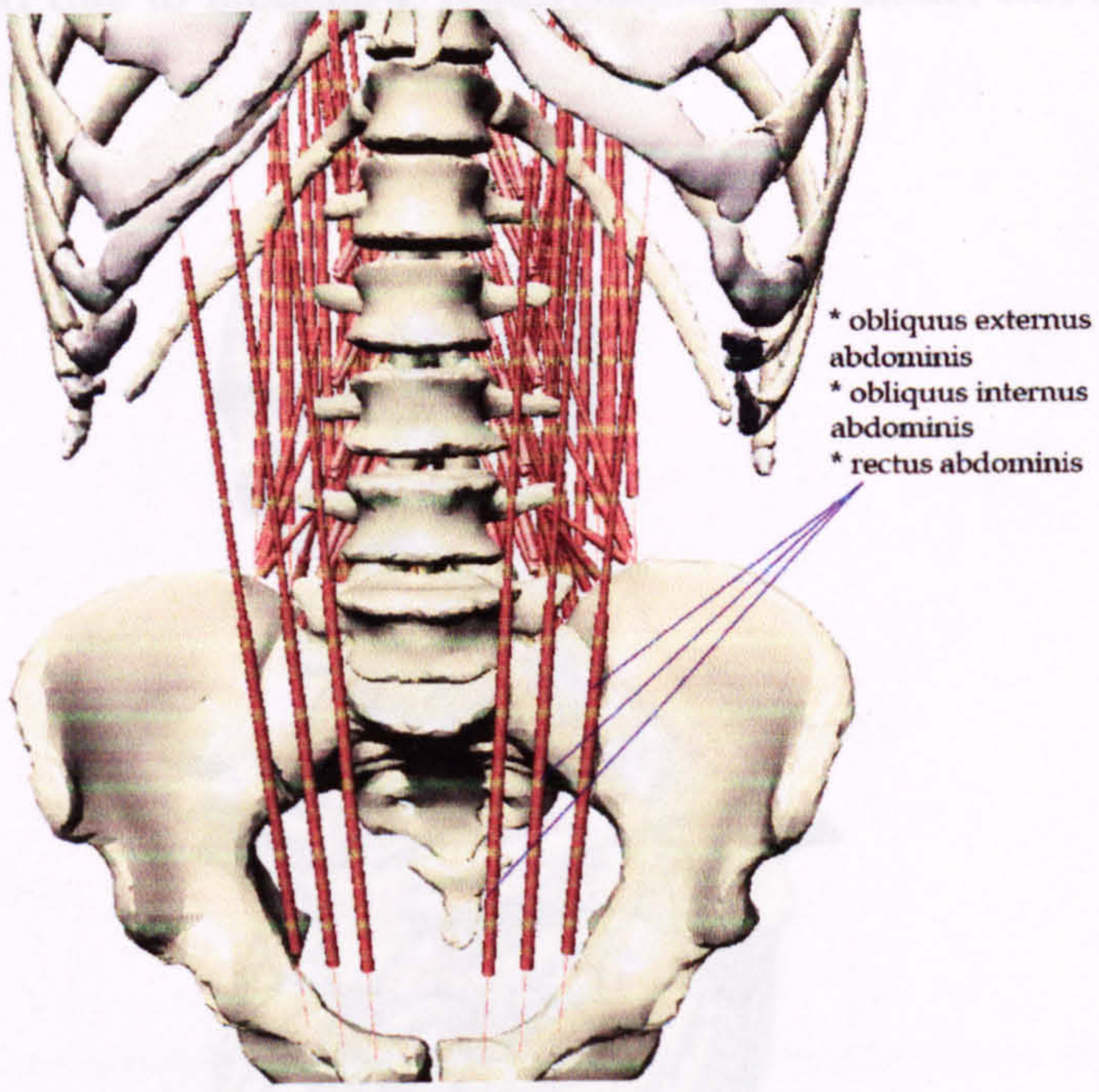

Figure 4.49 Abdominal muscles in the MB model

All these abdominal muscles have several functions such as compressing the abdomen, supporting viscera, being active in forced expiration, flexing pelvis and vertebral column. Morphological data is provided in Appendix C.

4.3.5 Final Multi-Body Model

All the elements explained so far were brought together to form the MB model of the whole human spine. All relevant material properties were introduced into the model within visualNastran and Virtual Muscle.

As the human spine is a very complex and detailed biomechanical structure, various simplifications and assumptions were made in order to keep the model within reasonable computational limits and requirements. Some other relatively

insignificant spinal muscles were neglected, and some muscle attachments and insertions especially to and from clavicles, iliacs, and scapulae were compromised. To maintain the integrity and biofidelity of the model, necessary structural elements such as clavicles or sternum were kept in position via spring-damper elements with very high stiffnesses and damping coefficients, which help to counteract for all the muscles and ligaments they normally should have, but neglected due to modelling requirements. The model can be seen in Figures 4.50-4.51.

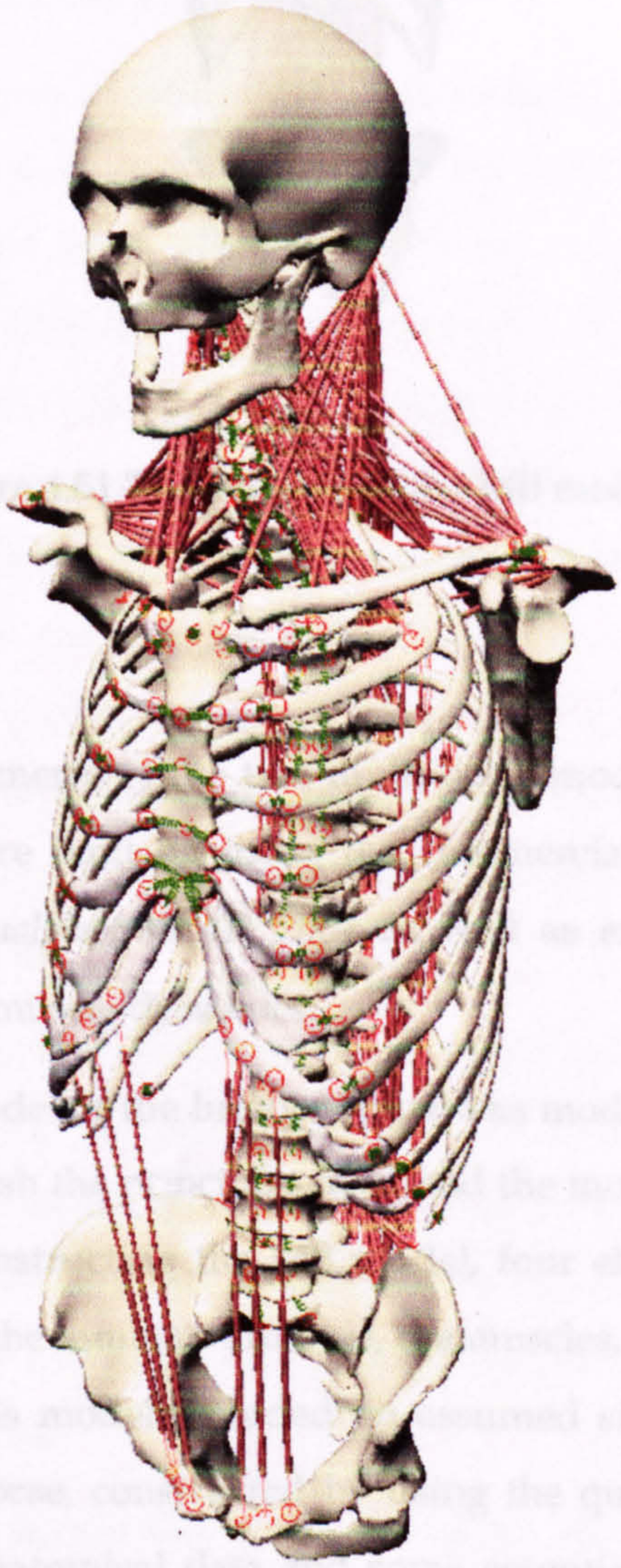

Figure 4.50 The developed MB model of the whole human spine

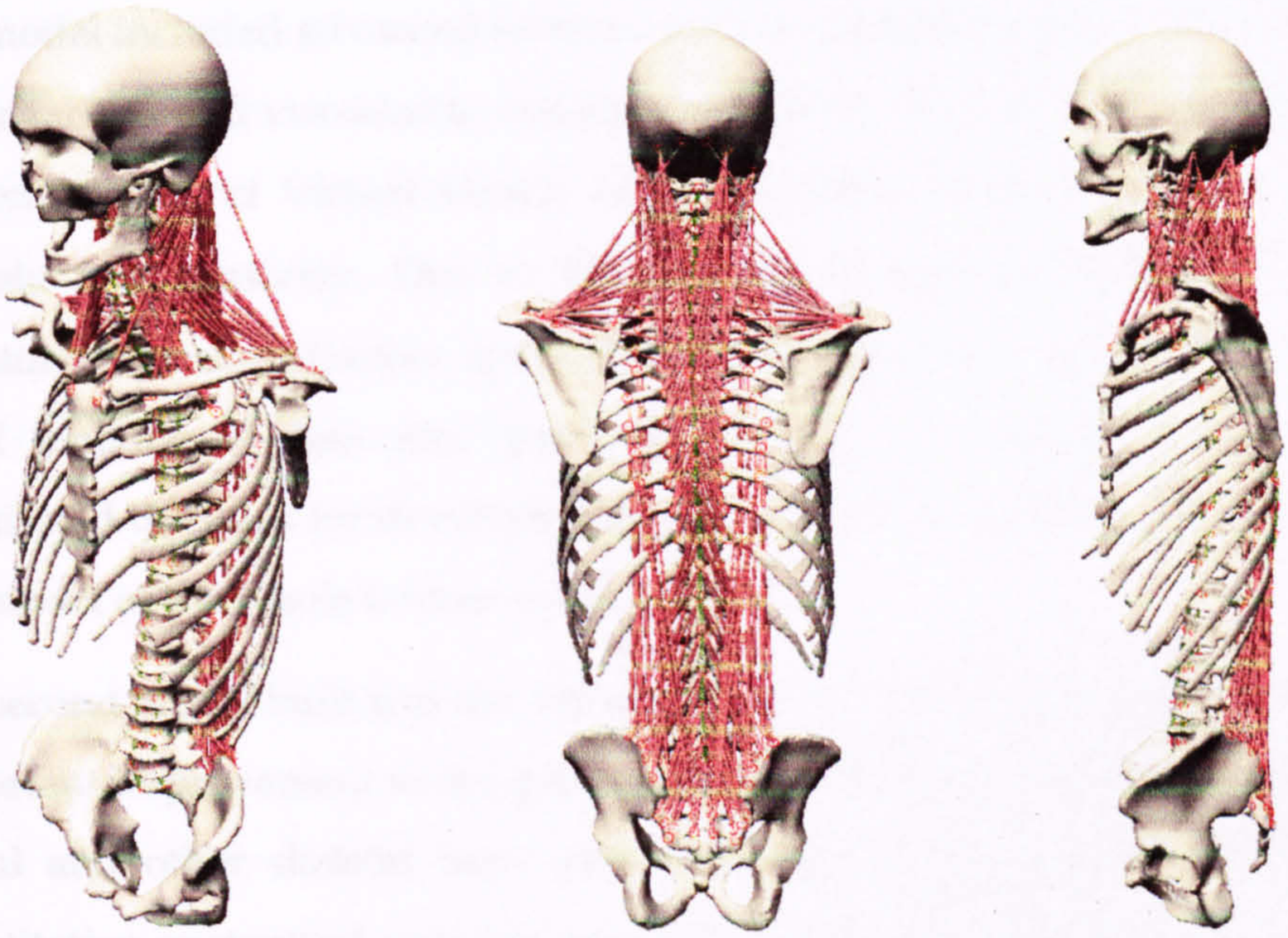

Figure 4.51 Three views of the MB model

4.4 Discussion

In this chapter, developments of the two multi-body models were explained in detail. Both models were built by using the commercially available dynamic simulation package *visualNastran 4D 2001* as well as employing an external package for controlling muscle dynamics.

The first multi-body model of the lumbar spine was modelled as a preliminary model, aiming to establish the principles to extend the model to a whole human spine MB model. In constructing the MB model, four elements of the human spine were considered; the lumbar vertebrae, the muscles, the ligaments and the intervertebral discs. This model included an assumed simplified geometry of the lumbar spine vertebrae, constructed by using the quantitative anatomy of the spinal parts. The anatomical data and some essential specifications of the other elements were discussed and submitted. The constructed multi-body model was handled as the cervical spine multi-body model of van Lopik and Acar (2002). The vertebrae were modelled as rigid bodies, interconnected by linear viscoelastic intervertebral disc elements, nonlinear viscoelastic ligaments

and contractile muscle elements possessing both passive and active behaviour. The model included advanced features such as material property and geometric nonlinearities and viscoelastic material properties. One of its strengths was the implementation of Virtual Muscle as an external software to control muscles actively and passively. Due to the paucity of experimental results in the literature regarding lumbar spine dynamics, validation was carried out with small amount of data and good agreements were achieved. This model constituted the basis for developing the more advanced, detailed, and biofidelic MB model of the whole human spine.

The second model built was the MB model of the whole human spine. As a very important improvement to the previous model, the solid bodies comprising the spinal and other skeletal bony elements were no more modelled by using quantitative anatomical data but imported from a CT scanned cadaver human spine study. Due to the technique used, it was highly realistic, and helped define more realistic contact surfaces within the MB model. These solid bodies not only accommodated the essential parts of the vertebrae; as the vertebral body, pedicles, superior and inferior articular processes, namely facet joints, transverse and spinous processes, but also included the other selected skeletal parts such as the head, the ribs, the clavicles, the scapulae, and the iliacs, which is of essential importance in order to build a biofidelic model with realistic element and joint locations.

The intervertebral discs and ligaments were modelled with highly realistic material properties, incorporating nonlinearities and viscoelasticity. All spinal intervertebral discs and all ligaments associated with the spinal column were introduced. The other skeletal parts such as the ribs, clavicles, and scapulae played a very important role especially in attaching the ligaments and muscles into their realistic locations.

Another strength of the model lies in the modelling and defining the muscles. The external software Virtual Muscle was employed to develop very detailed and realistic muscle behaviour, both active and passive. The morphological and mechanical properties of all muscle groups were incorporated by using the data available in the literature.

The developed MB model of the whole human spine reflects one of the novelties of this thesis, being one of the highly detailed, biofidelic models developed so far. Considering the size and the detail of the model, there had to be several assumptions and simplifications as in most of the engineering and computational models, especially due to lack of material property data such as damping characteristics of the intervertebral discs. The validation and sample simulations are presented in the following chapters.

CHAPTER 5

Multi-Body Model Validation

In this chapter, validation studies regarding the multi-body model of the whole human spine are presented. The validation was carried out against the results of several experimental studies; static, quasi-static or dynamic, and particularly for the cervical spine region. There is a paucity of tests in the literature regarding the kinetic and kinematic behaviour of the thoracic and lumbar regions, when compared to cervical spine investigations. Nevertheless, validation attempts for the thoracic and lumbar regions were also included in this thesis.

The validation process is the domain of the researcher who ensures that the real system is properly idealised, the proper algorithms are selected for various sub-mechanisms, and the database of parameters are appropriate (Kaleps, 1998). In the light of this information, validation preparations in this thesis started right from the beginning of the modelling attempts by choosing powerful computational media, which have the capacity to model the human spine in great detail. The human spine was modelled by employing the most recent data such as advanced material properties and model parameters, incorporating nonlinearities, wherever possible.

The validation process requires comparison of the predicted and real system variables and judgement of validity is based on differences between the model predictions and the real system responses (Kaleps, 1998). The main principle followed in validation in this thesis is that the reference (biofidelity) tests for validation **should not be** the same tests as used for determination of model input data (Wismans et al., 2005). Therefore, any data used in constructing the model was not used for validation.

This chapter covers validation sections as motion segment responses in the cervical spine, MB model responses in the cervical spine for frontal and lateral impacts, vertical loading for cervical spine, MB model responses of thoracic and lumbar regions in rear-end impact, and a discussion on thoracic response to lateral impact.

5.1 Motion Segment Responses in the Cervical Spine

In this section, model responses to various loads and moment generating capacity of the neck muscles are presented.

5.1.1 Motion Segment Responses to Various Loads

The model of the upper cervical spine (atlas, axis and occiput) was validated against the experimental studies by Panjabi et al. (1988), who applied static moments of 1.5Nm on the upper cervical spine specimens and evaluated the main and coupled rotations. In their experiments, C2 was fixed while moments were applied to the occiput and the corresponding rotations were measured at the centres of C1 and C0. Validation could not be conducted on the translational loading response of the upper cervical spine motion segments as experimental data is not available in the literature. For all simulations an acceleration field of 9.81m/s^2 in the z-axis was assumed to incorporate the effect of gravity.

Motion segment responses of the lower cervical spine were compared against the experimental results reported by Moroney et al. (1988). In their experiment, Moroney et al. tested *intact segments*, which are anatomically complete segments comprising the two adjacent vertebrae, disc, facet joints and ligaments, and *disc segments*, where only the vertebral bodies and intervertebral disc were considered.

For load-displacement testing, the superior vertebra was free to move in response to the applied loads, while the inferior vertebra was rigidly fixed. The motion segments were applied small static loads of 20N and 1.8 Nm in all loading directions; the resulting three-dimensional displacements were measured at the geometric centre of the upper vertebra.

For simulating the segment tests, the model motion segments were set up similarly, where the lower of the two vertebrae being fixed while leaving the upper vertebra free to move in all directions. Loads are exerted on the model as an external torque or force applied at the centre of the vertebra. In the experimental tests, the load was applied again at the centre of the intervertebral disc. The resulting displacements were measured at the centre of the local body coordinate system of the upper vertebra and compared against the reported displacements. The dynamic stiffening factor for the disc and ligaments was set to 1 for all static tests (van Lopik, 2004).

Figure 5.1 and 5.2 illustrate the main and coupled displacements of C0-C1 and C1-C2, respectively, in response to rotational loading. The model results were plotted against the experimental results of Panjabi et al (1988) including average standard deviations. In both figures, the response to each rotational loading direction, flexion, extension, lateral bending and axial rotation, are shown separately. The responses in all directions are shown along the horizontal axis, the labels representing the positive direction of the response, left lateral shear (LLS), anterior shear (AS), tension (TNS), right lateral bending (RLB), flexion (FLX) and left axial rotation (LAR), while negative values represent the opposite direction of loading, i.e. RLS, PS, CMP, EXT and RAR. The magnitudes of the translation (left side) or rotation (right side) were plotted on the vertical axis.

As can be seen from Figure 5.1, almost all displacements of C0-C1 are all within one SD of the reported experimental values. In extension loading case, the model shows almost no lateral bending, while in axial rotation case, the model produces a very small lateral bending, which is within the SD limits. This is thought to be because of the construction of the atlanto-occipital joints and their orientation within the model. C1-C2 segment displacements are also in good agreement with experimental data for all kinds of loading, except flexion and extension cases, where displacements in tension/compression and flexion directions are a bit away from the average, but still within the limits.

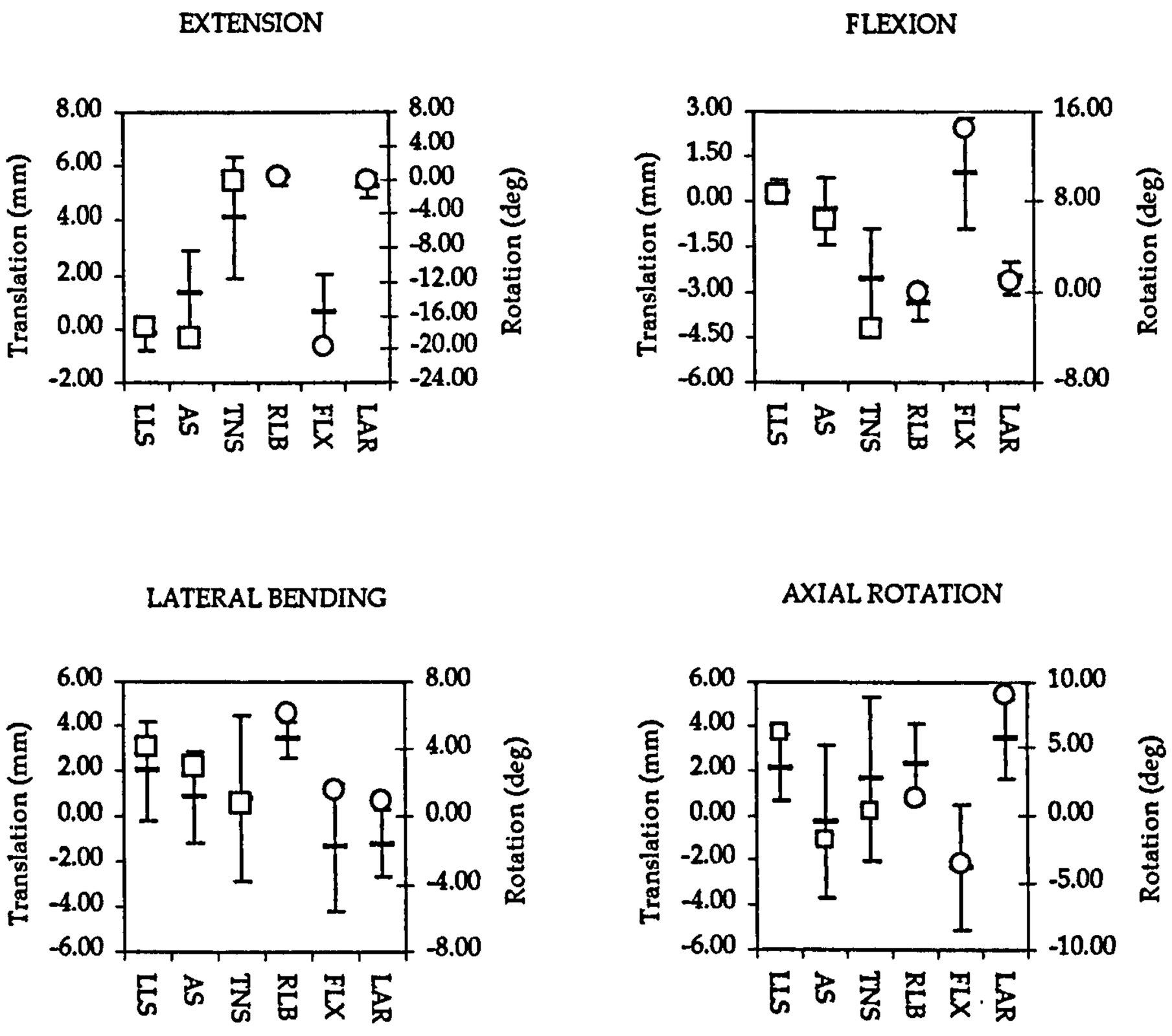

Figure 5.1 Displacements of model motion segments C0-C1 in response to applied rotational loads of 1.5Nm against the experimental results (average ± 1 SD) of Panjabi et al. (1988). Resulting displacements are shown along the vertical axis; translations on the left, rotations on the right. Anterior shear (+AS), posterior shear (-AS), left lateral shear (+LLS), right lateral shear (-LLS), tension (+TNS), compression (-TNS), right lateral bending (+RLB), left lateral bending (-RLB), flexion (+FLX), extension (-FLX), left axial rotation (+LAR) and right axial rotation (-LAR).

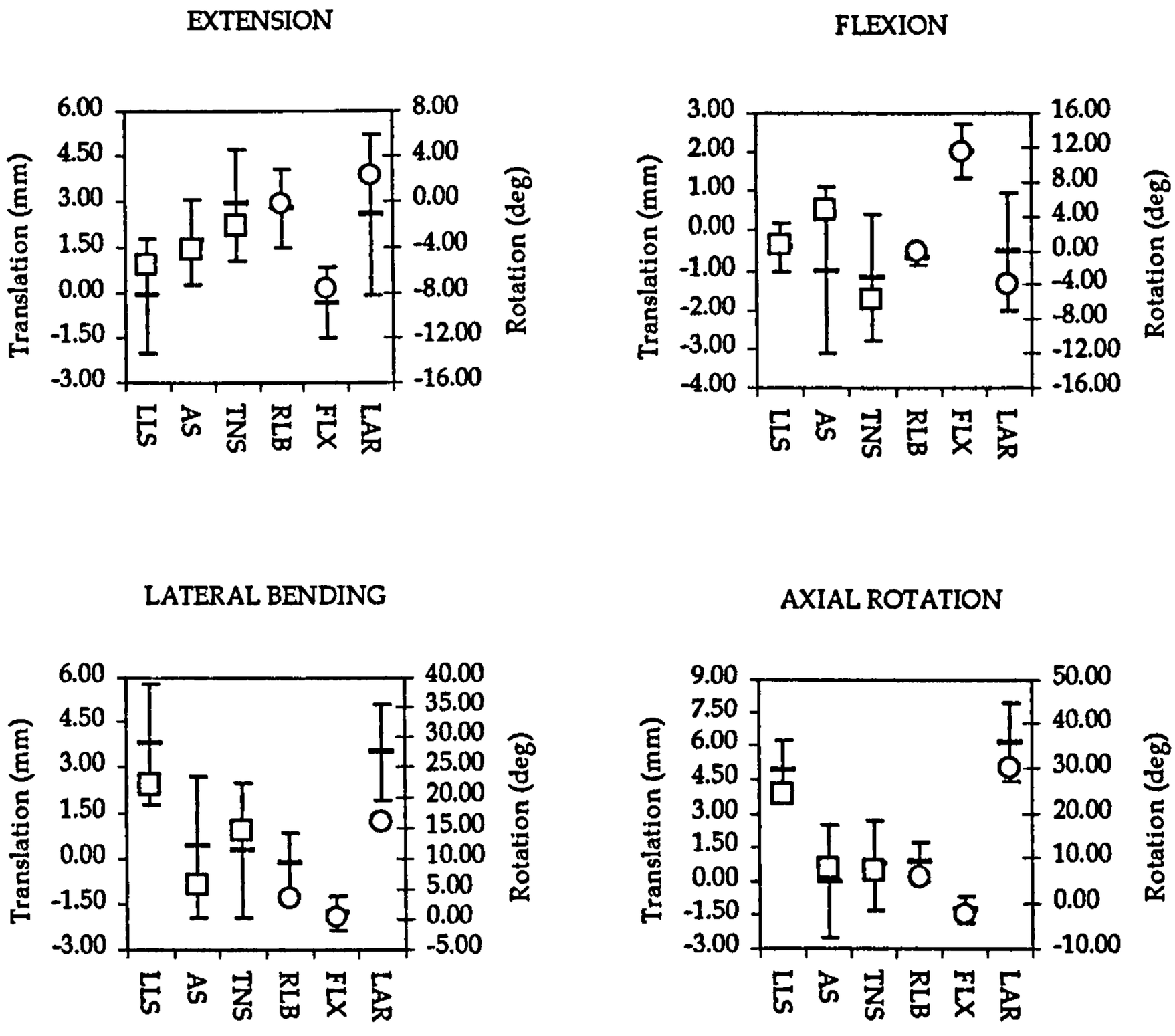

Figure 5.2 Displacements of model motion segments C1-C2 in response to applied rotational loads of 1.5Nm against the experimental results (average ± 1 SD) of Panjabi et al. (1988). Resulting displacements are shown along the vertical axis; translations on the left, rotations on the right. Anterior shear (+AS), posterior shear (-AS), left lateral shear (+LLS), right lateral shear (-LLS), tension (+TNS), compression (-TNS), right lateral bending (+RLB), left lateral bending (-RLB), flexion (+FLX), extension (-FLX), left axial rotation (+LAR) and right axial rotation (-LAR).

For lower cervical spine motion segment model investigations, motion segment models C3-C4 and C5-C6 were selected The facet orientations of these two spinal units possess different configurations; the facets of C3-C4 point backwards and inwards, while the facets of C5-C6 are located backwards and outwards. It is expected that responses of these two motion segments should slightly vary due to different ligament stiffness' and different disc properties.

The displacements of C3-C4 and C5-C6 in response to 1.8 Nm for flexion, extension, right lateral bending and CCW axial rotation loadings are depicted in Figures 5.3 and 5.4, respectively. Figure 5.5 shows the segments response to

translational loading of 20N for anterior shear, posterior shear, right lateral shear and compression for both segments.

In Figures 5.3-5.5, almost all main displacements and rotations are within 1 SD of the mean reported value except for axial rotation and flexion cases, where the model segments appear to be slightly too flexible. Generally the results are in good agreement with Moroney's data. In flexion loading, little anterior shear is present for both cases in comparison to the reported mean, which is thought to be because of the facet positioning and orientation.

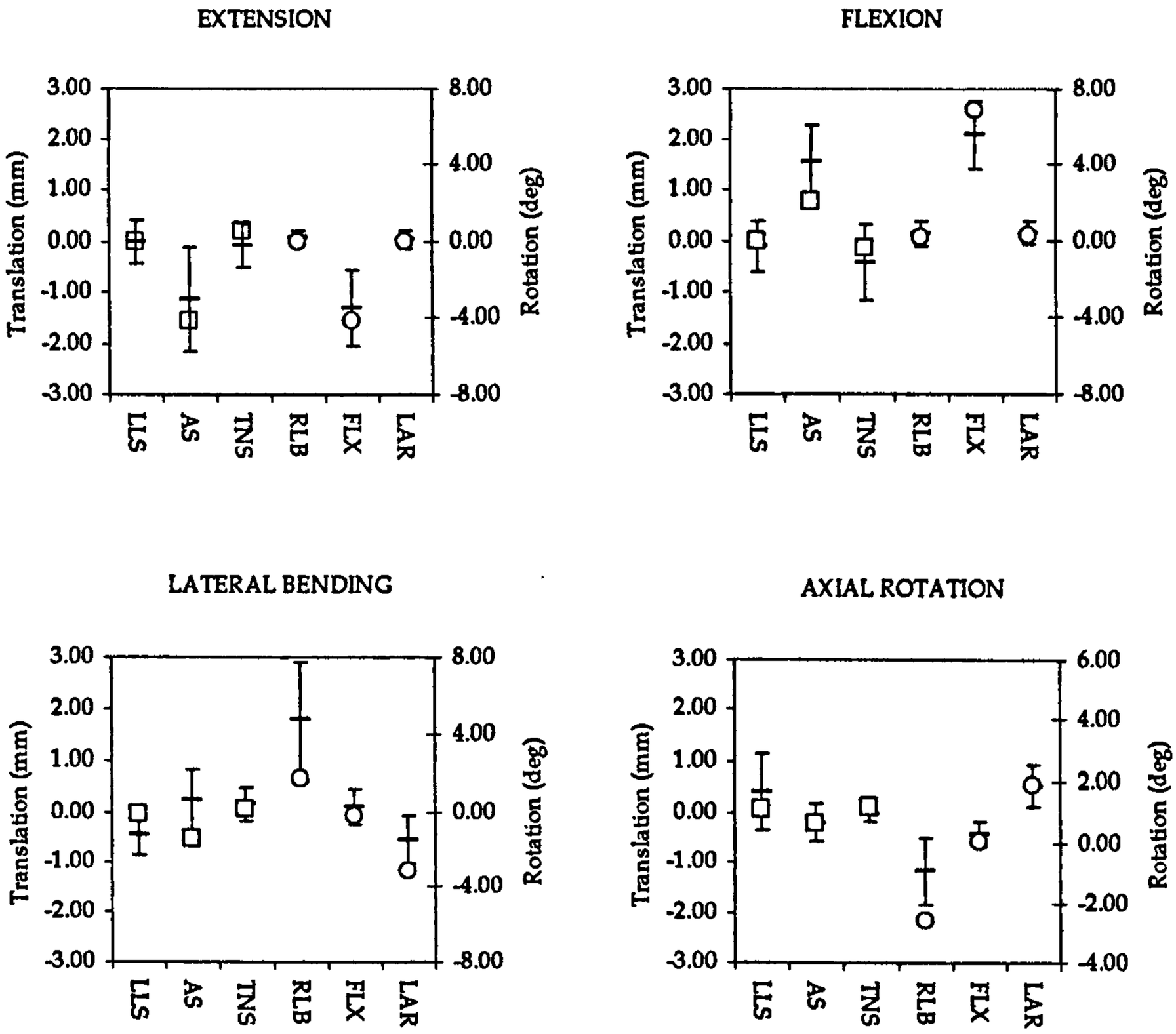

Figure 5.3 Displacements of model motion segments C3-C4 in response to applied rotational load of 1.8 Nm shown against the experimental results of Moroney et al. (1988). Resulting displacements are shown along the vertical axis, translations on the left, rotations on the right. Anterior shear (+AS), posterior shear (-AS), left lateral shear (+LLS), right lateral shear (-LLS), tension (+TNS), compression (-TNS), right lateral bending (+RLB), left lateral bending (-RLB), flexion (+FLX), extension (-FLX), left axial rotation (+LAR) and right axial rotation (-LAR).

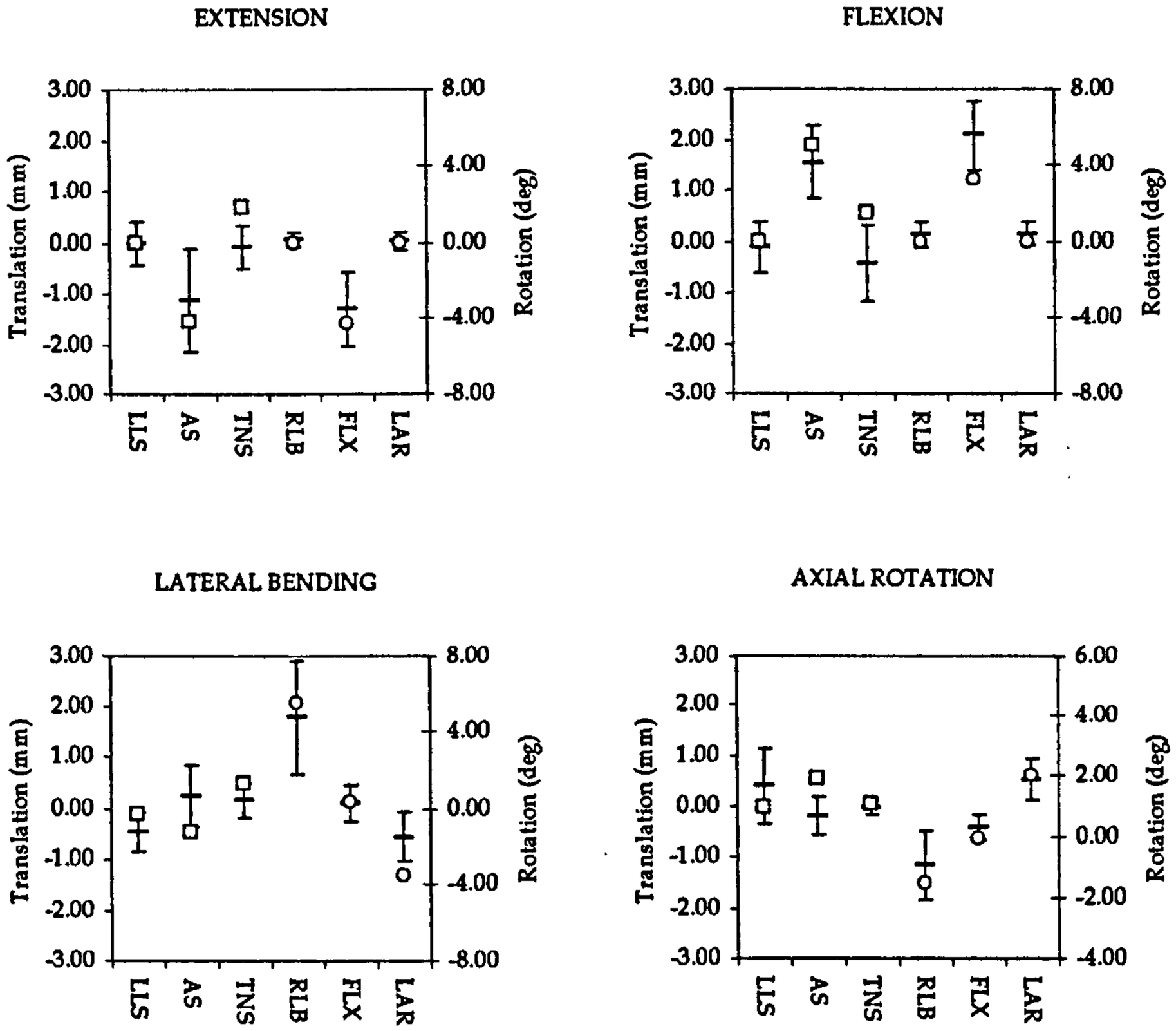

Figure 5.4 Displacements of model motion segments C5-C6 in response to applied rotational load of 1.8 Nm shown against the experimental results of Moroney et al. (1988). Resulting displacements are shown along the vertical axis, translations on the left, rotations on the right. Anterior shear (+AS), posterior shear (-AS), left lateral shear (+LLS), right lateral shear (-LLS), tension (+TNS), compression (-TNS), right lateral bending (+RLB), left lateral bending (-RLB), flexion (+FLX), extension (-FLX), left axial rotation (+LAR) and right axial rotation (-LAR).

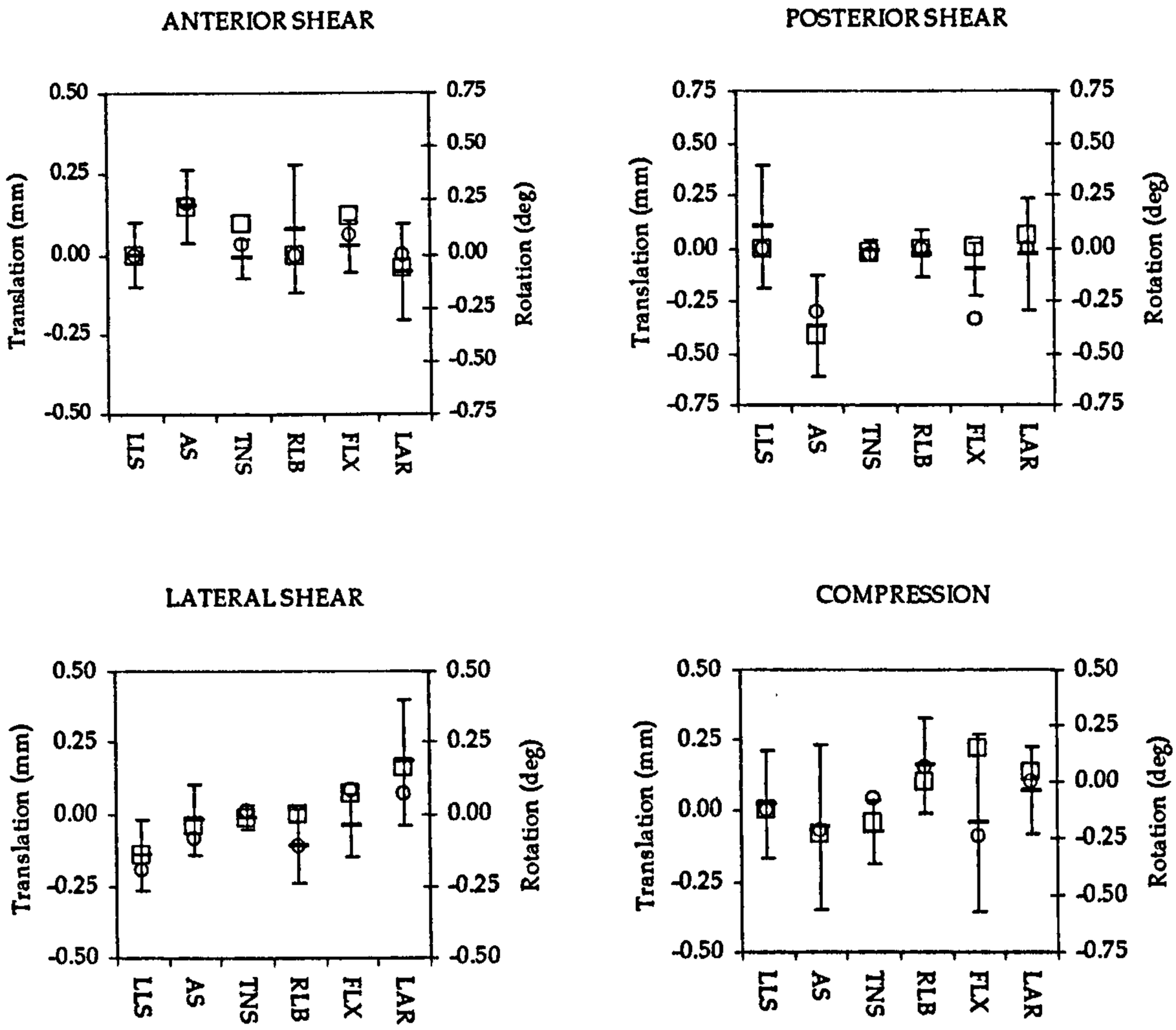

Figure 5.5 Displacements of model motion segments C3-C4 (□) and C5-C6 (○) in response to applied translational loads of 20 N shown against the experimental results of Moroney et al. (1988). Anterior shear (+AS), posterior shear (-AS), left lateral shear (+LLS), right lateral shear (-LLS), tension (+TNS), compression (-TNS), right lateral bending (+RLB), left lateral bending (-RLB), flexion (+FLX), extension (-FLX), left axial rotation (+LAR) and right axial rotation (-LAR).

5.1.2 Moment Generating Capacity of Neck Muscles

The total moment generating capacity of the neck muscle elements were validated via comparing them against experimental human volunteer data. In Vasavada et al. (2001) study, 11 men and 5 women volunteers with mean age of 31 years were asked to produce maximum head force in extension, flexion, lateral bending and axial rotation in an upright sitting position with shoulders and torso restrained. The measured forces in each direction were used to calculate the moments about the base of the neck for each of the loading directions. The isometric strength of the neck muscles was simulated by activating each muscle group maximally while fixing the rigid bodies of the

model in their initial position. Moments were calculated about the T1 anatomical coordinate system to calculate the moment generating capacity of each muscle element about the three axes of revolution. The moments generated were in flexion and extension (force generated by muscles on both sides of the neck), axial rotation and lateral bending (force generated on one side only). The results of this study were used to validate the muscles in the MB model as compared to some other prominent studies. The results were tabulated in Table 5.1.

Table 5.1 Validation of the neck muscles in the MB model

Study	No. & Gender of Subjects	Extension Moment (Nm)	Flexion Moment (Nm)	Axial Rotation Moment (Nm)	Lateral Bending Moment (Nm)
Harms-Ringdahl & Schuldt (1988)	10F	29			
Jordan et al. (1999)	50M	55 (14)	21 (8)		
	50F	48 (15)	19 (4)		
Mayoux-Benhamou et al. (1993)	5M, 10F	53 (12)			
Queisser et al. (1994)	12M	60 (9)			
Vasavada et al. (2001)	11M	52 (11)	30 (5)	15 (4)	36 (8)
	5F	21 (12)	15 (4)	6 (3)	16 (8)
Van Lopik Model (2004)	-	47	17	19	39
Current MB Model	-	37	25	17	29

Note. Mean (and standard deviation (SD) where available). M-males, F-females.

The results seemed to be in good agreement with Vasavada et al. (2001) study. When compared to van Lopik head-neck model, all moments generated except flexion case appeared to be lower. With all muscles maximally activated, the model yielded a total extension moment of 37 Nm with the Semispinalis Capitis and Cervicis (35%), Multifidus (21%) and Levator Scapulae (17%), having the most significant contribution. The remaining 27% of the total extension moment was generated by the remaining muscles. The Sternocleidomastoid produced most of the flexion moment about T1 (62%). The total axial rotation moment was predicted to be 17 Nm with the Trapezius muscle having the most significant contribution (47%). In lateral bending, the total moment-generating capacity appeared to be 29 Nm with the Trapezius (25%) and Scalenus (29%) muscles

providing over half the moment. The value of specific tension used in the model simulations was 50 N/cm², which is considered to represent an average male with reasonably developed musculature. Obviously, the choice of specific tension value affects the total-moment generating capacity predicted by the model but on the other hand does not affect the relative contributions of the muscles.

5.2 MB Model Responses in the Cervical Spine for Frontal and Lateral Impacts

In this section, the MB model responses to frontal and lateral impacts were validated against human volunteer response data. Response corridors based on sled acceleration tests with human volunteers were used to evaluate the model and investigate the effect of muscle activation on the head-neck motion. The response corridors used in this study were also used by other researchers for validation purposes (De Jager, 1996; van der Horst, 1997, 2002; and Thunnissen et al., 1995). The response corridors define the response boundaries that a valid human spine model should meet. The impacts were run with active muscle behaviour. The local loads in the soft-tissue elements were analysed. The effects of muscle specific tension, reflex time and level of activation on the kinematic response of the model were discussed.

The dynamic experimental data used is gathered from sled acceleration tests with human volunteers performed at the Naval Biodynamics Laboratory (NBDL). NBDL data contain male human volunteers as seated in an upright position on a sled driven HYGE accelerator and exposed to short duration accelerations simulating 15g frontal and 7g lateral impacts. The resulting three-dimensional motions of the cervical spine were monitored by anatomically mounted accelerometers and photographic targets. In the frontal impact tests the test subjects were constrained with shoulder straps, a lap belt and a pelvic strap to prevent movement of the torso during testing. Arm and wrist restraints were also utilised to prevent flailing. An additional chest strap was used in the lateral impacts to minimise loading of the right shoulder and a lightly padded

wooden board was placed against the right shoulder to limit torso motion further (Wismans et al., 1986).

Wismans et al. (1986) presented results of the NBDL tests for frontal and lateral impacts while a new analysis of the most severe frontal impacts was conducted later by Thunnissen et al. (1995). The original data were used to validate the models response to lateral impact while the response corridors presented by Thunnissen et al. (1995) were used to validate the models response to frontal impact. Also, van Lopik (2004) used the same data to validate his head-neck model. Thunnissen et al. (1995) analysed frontal tests that had a peak sled acceleration of 14.5g or higher; which yielded in 9 tests with 5 volunteers (all but one were tested twice). The average volunteer height was 169.1 cm and the average weight was 67.9kg. The neck link was flexible in the axial direction. It was found that the peak acceleration of T1 was twice as high as the applied sled acceleration due to deformation of the thorax/restraint system.

5.2.1 Frontal Impact

In simulating the frontal impact, the acceleration time history of T1 has been used as input to the head and neck model to have a highly similar computational environment with the original tests. Vertical acceleration during the sled tests was small enough to be ignored. The average acceleration and rotation time histories of T1 for the 15g frontal impacts are provided in Figure 5.6.

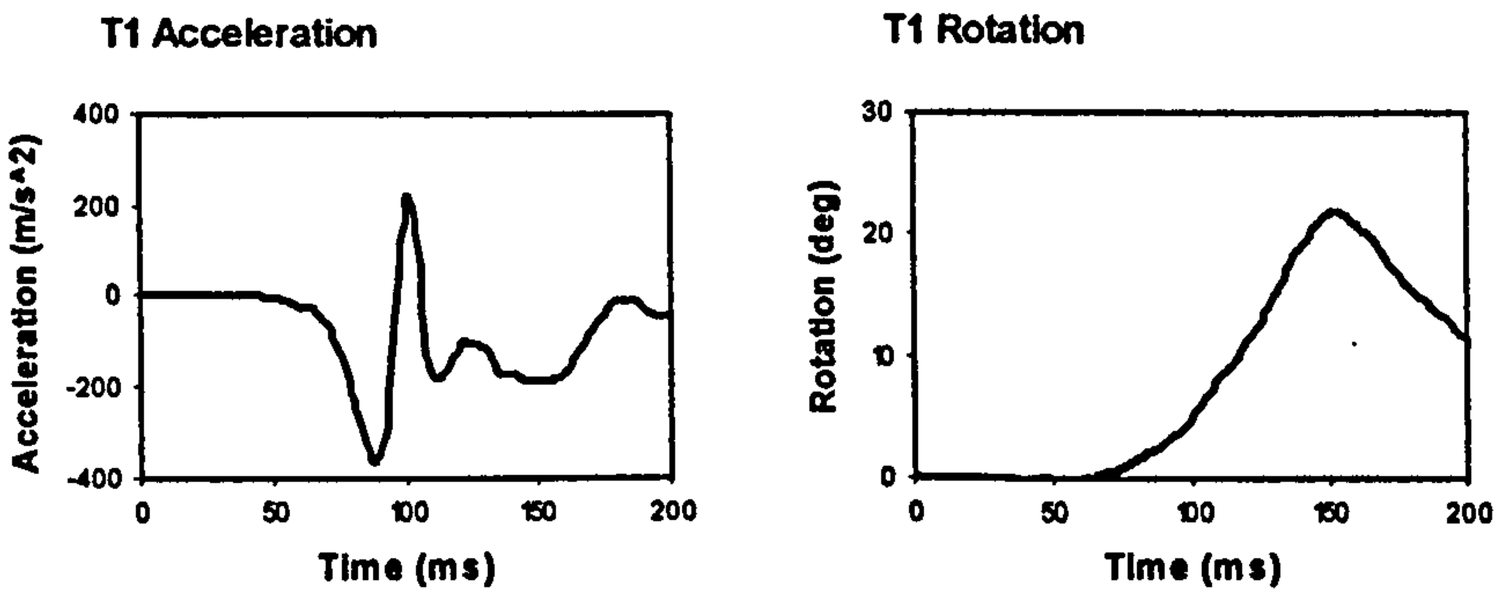

Figure 5.6 Average T1 acceleration and rotation used as input to the MB model to simulate frontal impact. (Acceleration in x-axis, rotation about y-axis)

In both impact simulations, motion of the T1 vertebrae was limited to the direction of impact while the rest of the model was left free to move in all directions. In frontal impact simulation, T1 was accelerated in the x-axis and rotated about the y-axis. For all other directions motion was found to be negligible in the analysis of the volunteer results (Wismans et al., 1986 and Thunnissen et al., 1995). An initial reflex response time of 75 ms has been used in the frontal and lateral impact simulations. All muscles are activated together 100% after the 75ms reflex time.

All simulations were conducted on a standard desktop PC with Pentium® 4 CPU XP 2.00 GHz, and 1GB PC2700 DDR RAM, 200 ms of simulation taking around 12,300 cpu seconds. Snapshot images from the simulation are illustrated in Figures 5.7-5.8.

Figure 5.7 Frontal impact simulation (all constraints, elements, and some parts of the model are hidden for better visualization)

Figure 5.8 Head and neck images for 0, 100, 170, and 200 ms, with all elements visible

The results of the simulations are provided in Figures 5.9-5.15 below, where the black curves represent the response corridors of the NBDL tests, and red ones the simulation results.

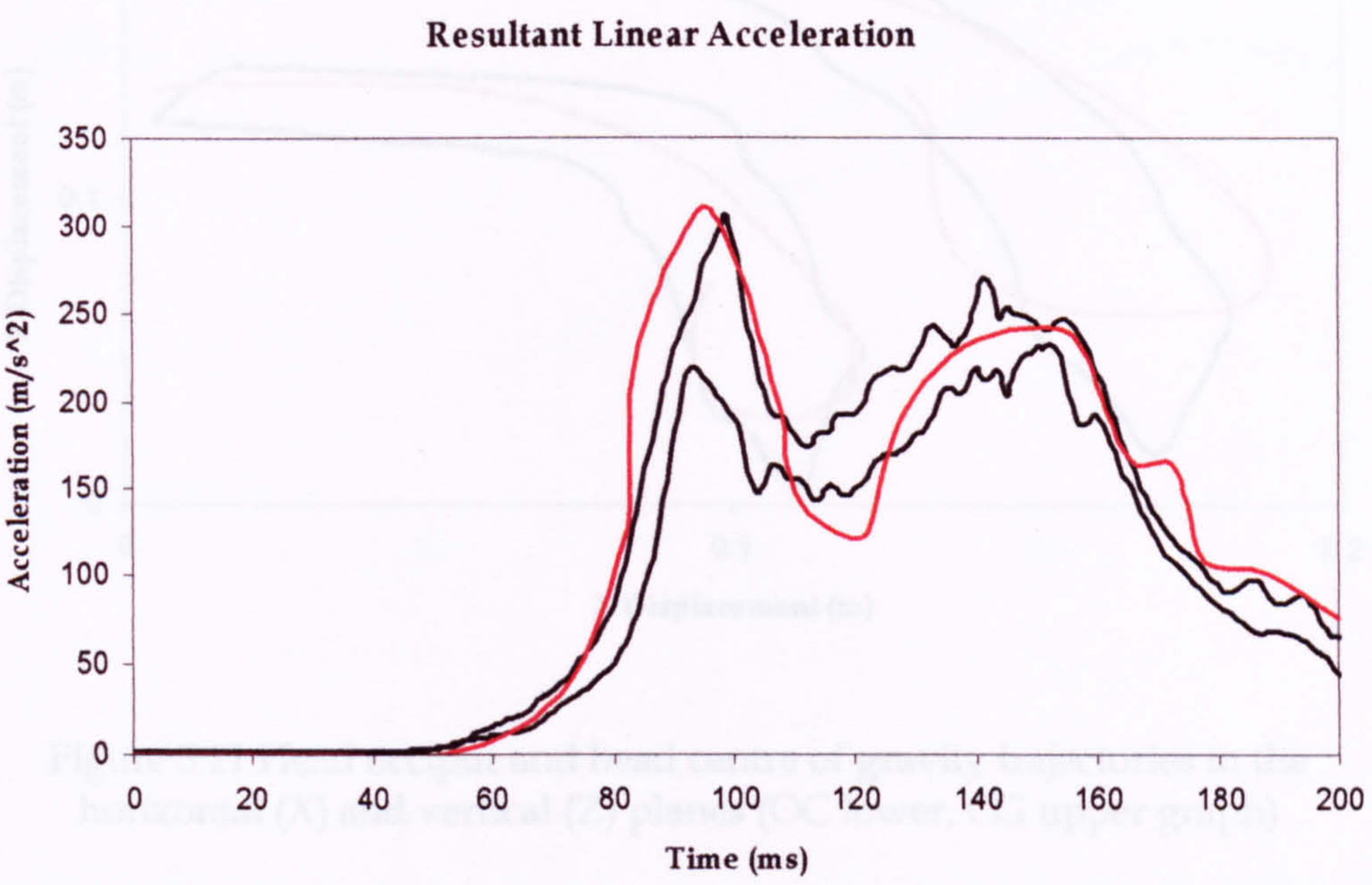

Figure 5.9 Head centre of gravity resultant linear acceleration vs. time

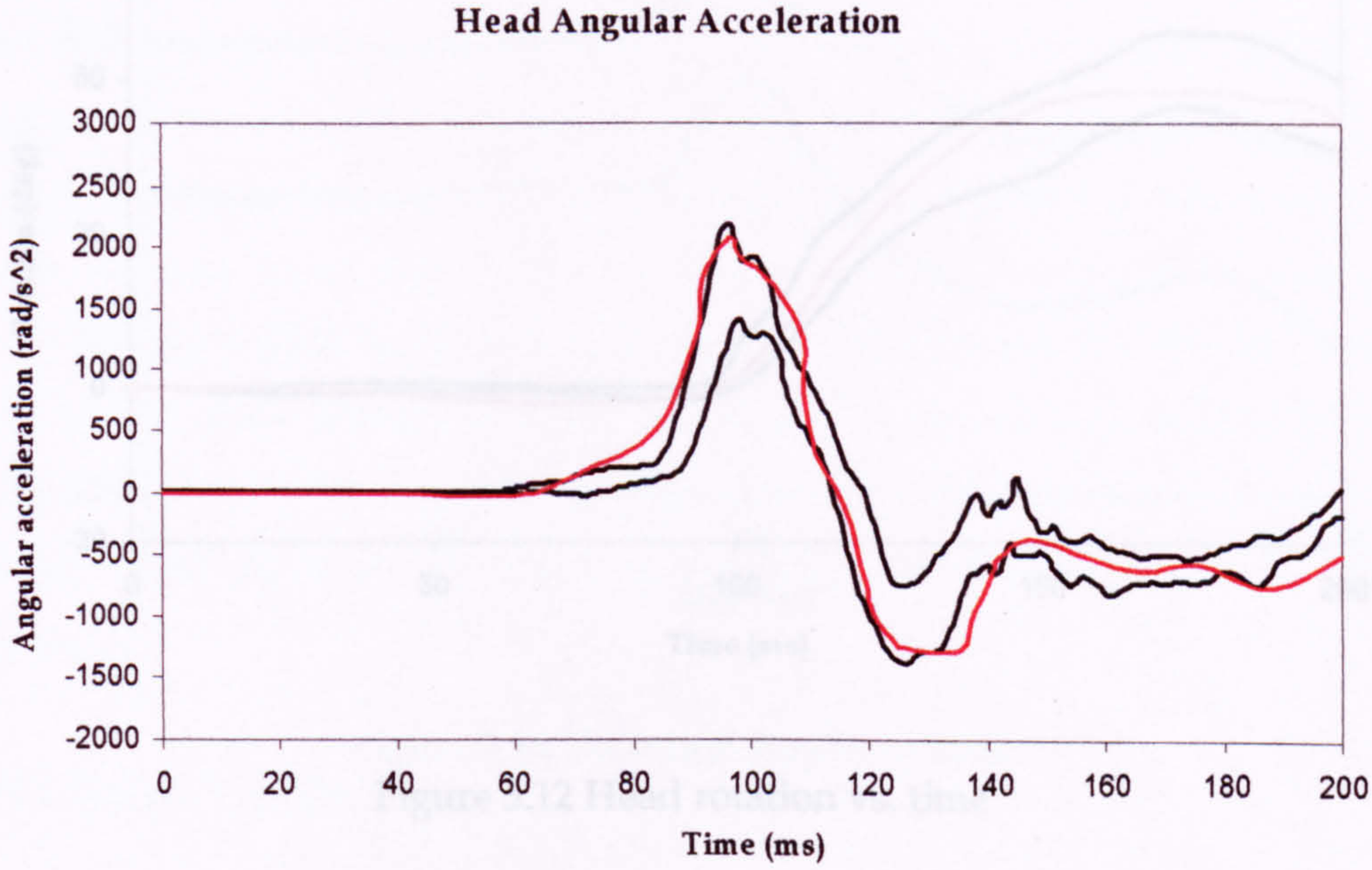

Figure 5.10 Head centre of gravity angular acceleration vs. time

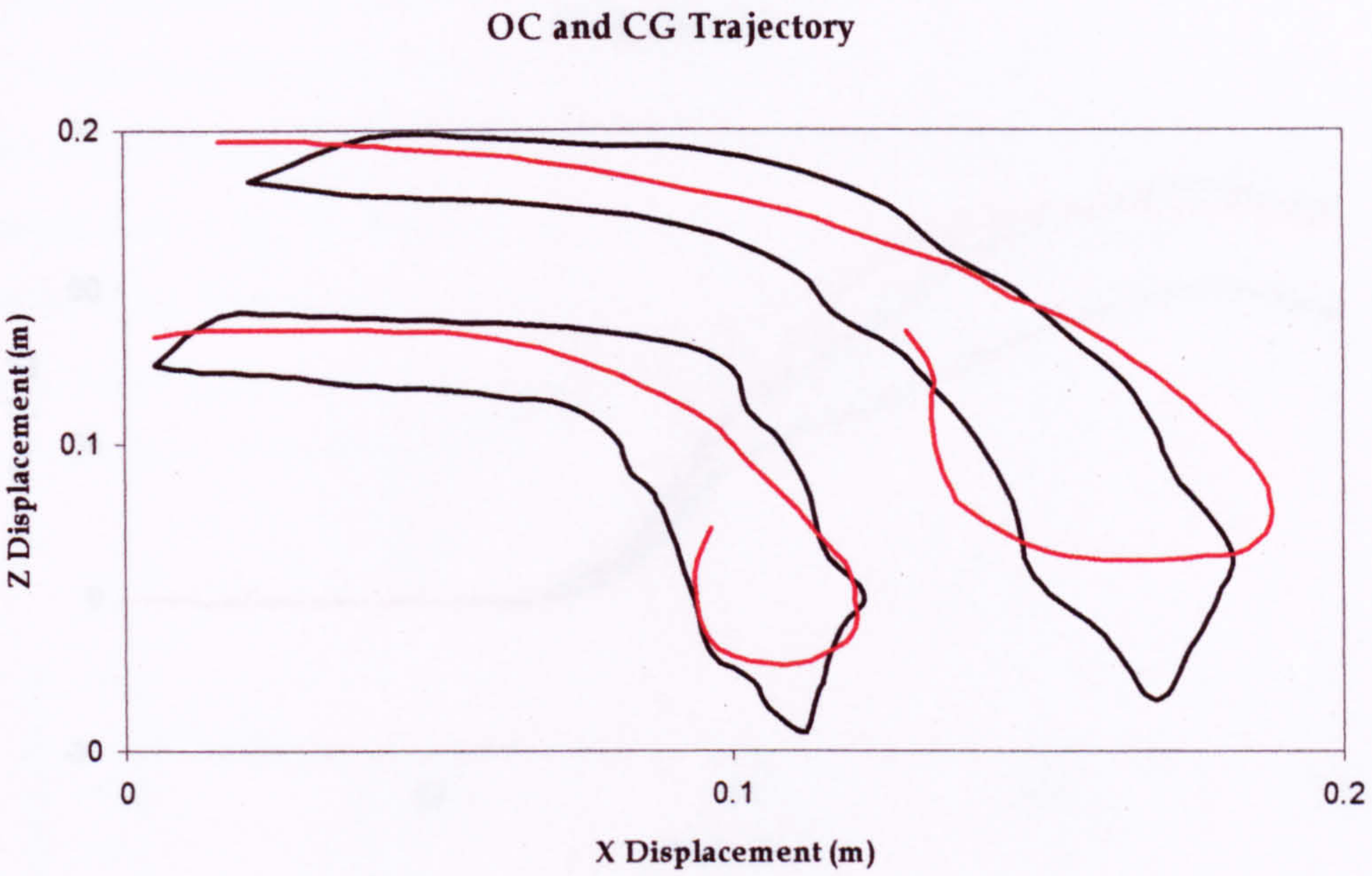

Figure 5.11 Head occiput and head centre of gravity trajectories in the horizontal (X) and vertical (Z) planes (OC lower, CG upper graph)

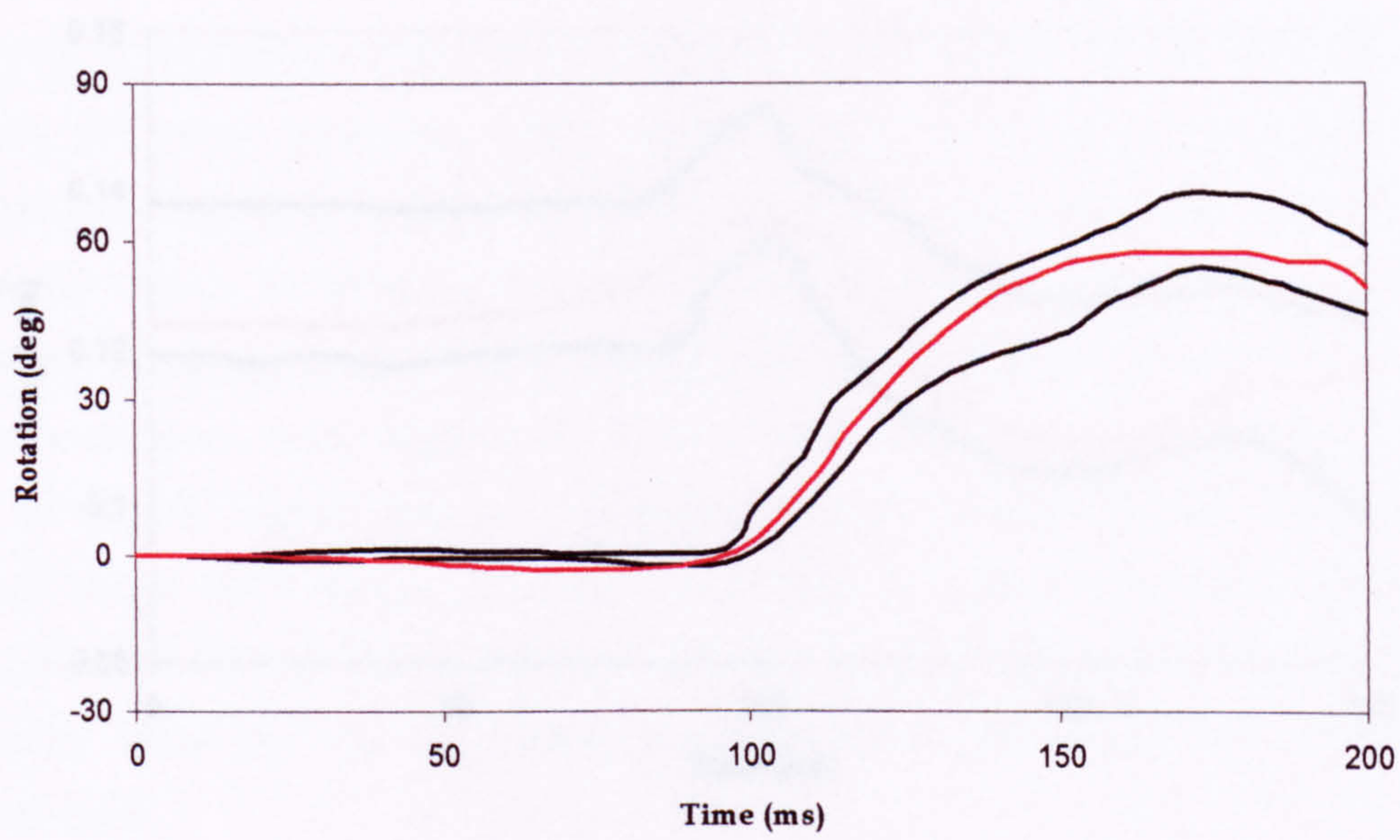

Figure 5.12 Head rotation vs. time

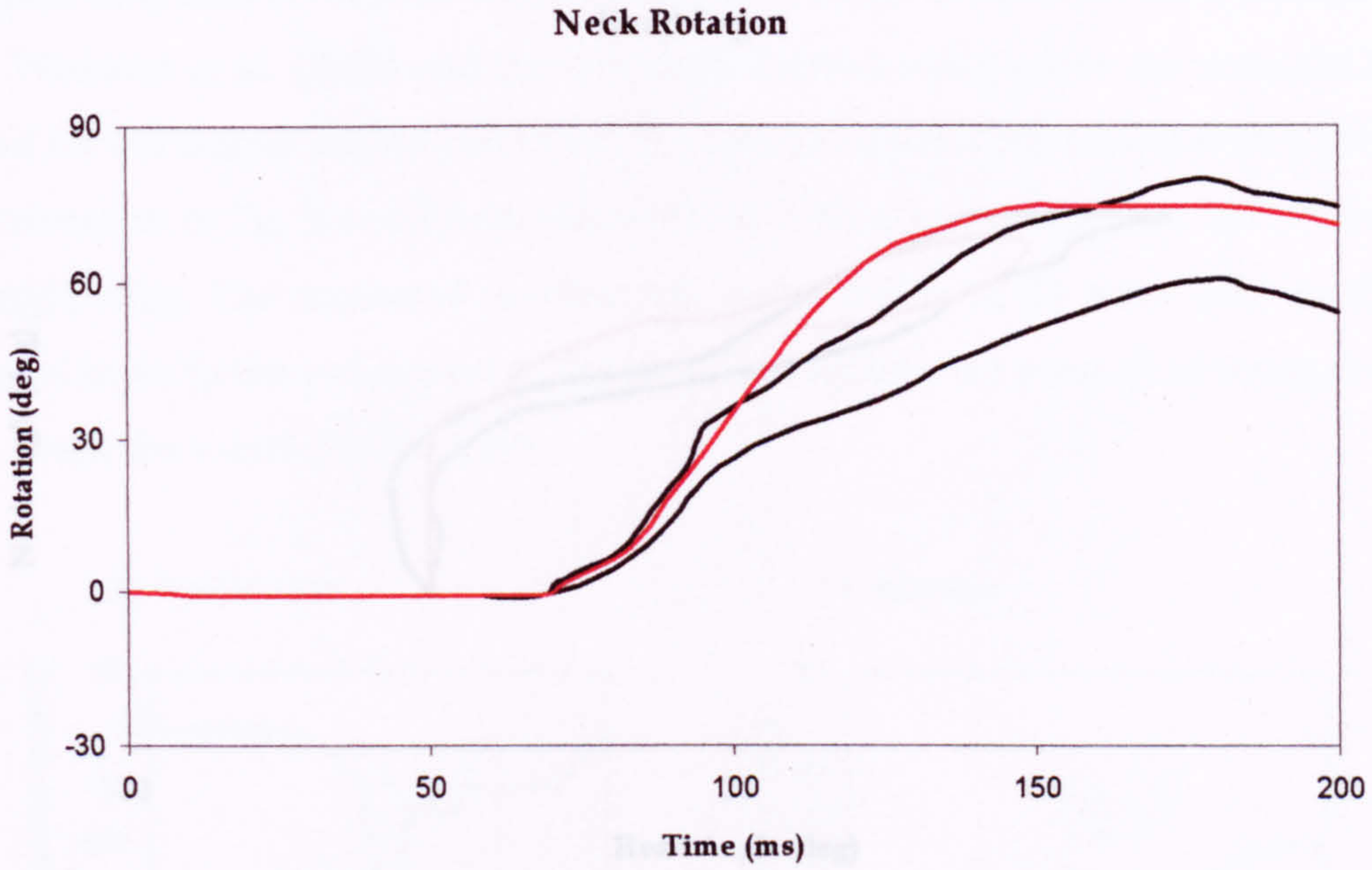

Figure 5.13 Neck rotation vs. time

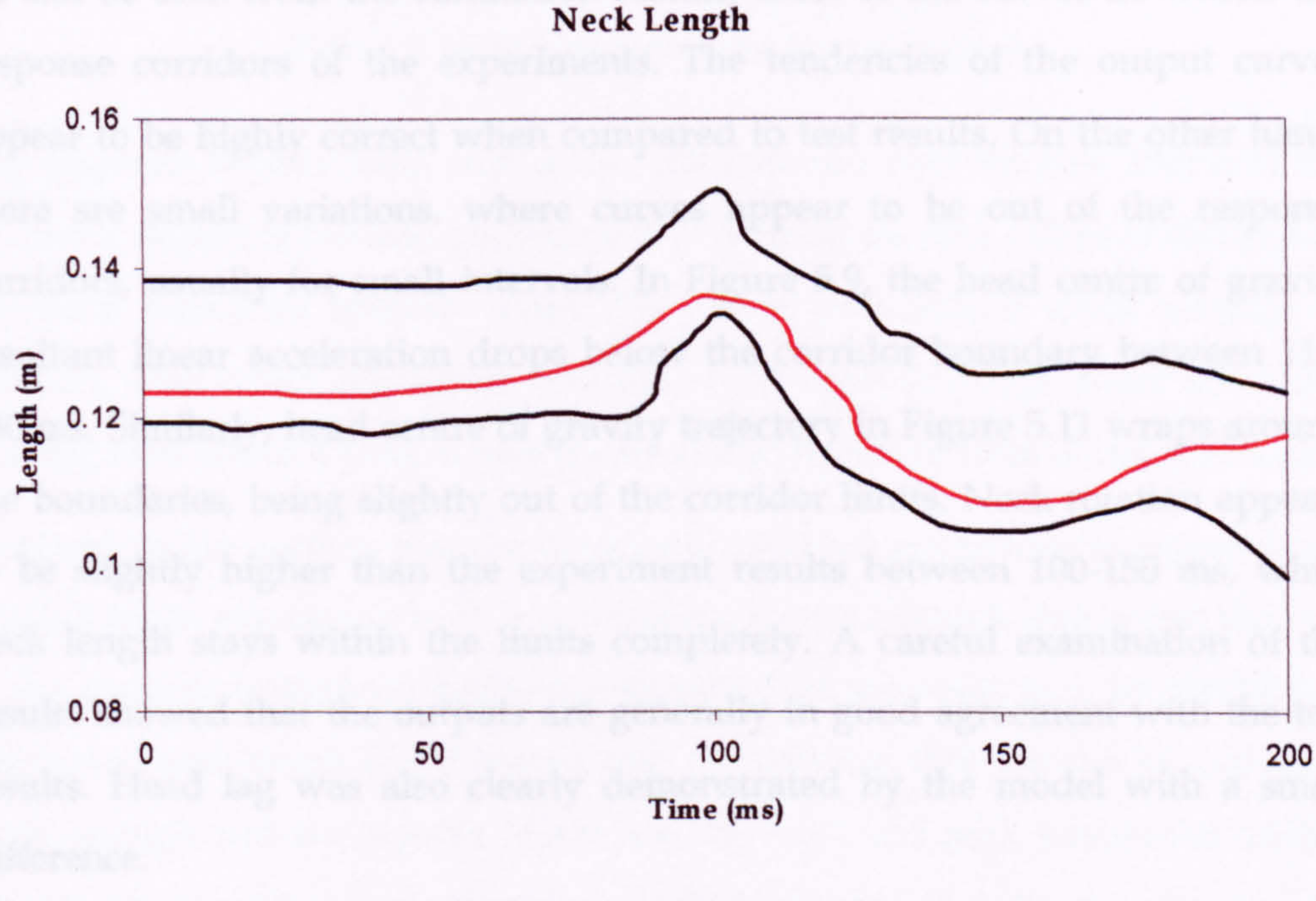

Figure 5.14 Neck link length vs. time

Figure 5.15 Head Lag vs. time

As can be seen from the simulation results, most of the curves lie within the response corridors of the experiments. The tendencies of the output curves appear to be highly correct when compared to test results. On the other hand, there are small variations, where curves appear to be out of the response corridors, usually for small intervals. In Figure 5.9, the head centre of gravity resultant linear acceleration drops below the corridor boundary between 110-130 ms. Similarly, head centre of gravity trajectory in Figure 5.11 wraps around the boundaries, being slightly out of the corridor limits. Neck rotation appears to be slightly higher than the experiment results between 100-150 ms, while neck length stays within the limits completely. A careful examination of the results showed that the outputs are generally in good agreement with the test results. Head lag was also clearly demonstrated by the model with a small difference.

5.2.2 Lateral Impact

In lateral impact simulation, T1 was accelerated along the y-axis and rotated about the x-axis. A similar set of response corridors were produced from lateral

impact sled tests on human volunteers at the NBDL. These tests were analysed by Wismans et al. (1986) and the corridors derived using a two-pivot model as used for the frontal impact corridors. The lateral impacts performed with a peak acceleration of 7g. 9 volunteers were tested with a mean height of 177cm and weight 76kg. The measured acceleration and rotation at T1 were used as the model input in the y-direction to simulate the impact with prescribed rotation of T1 about the x-axis (Figure 5.16).

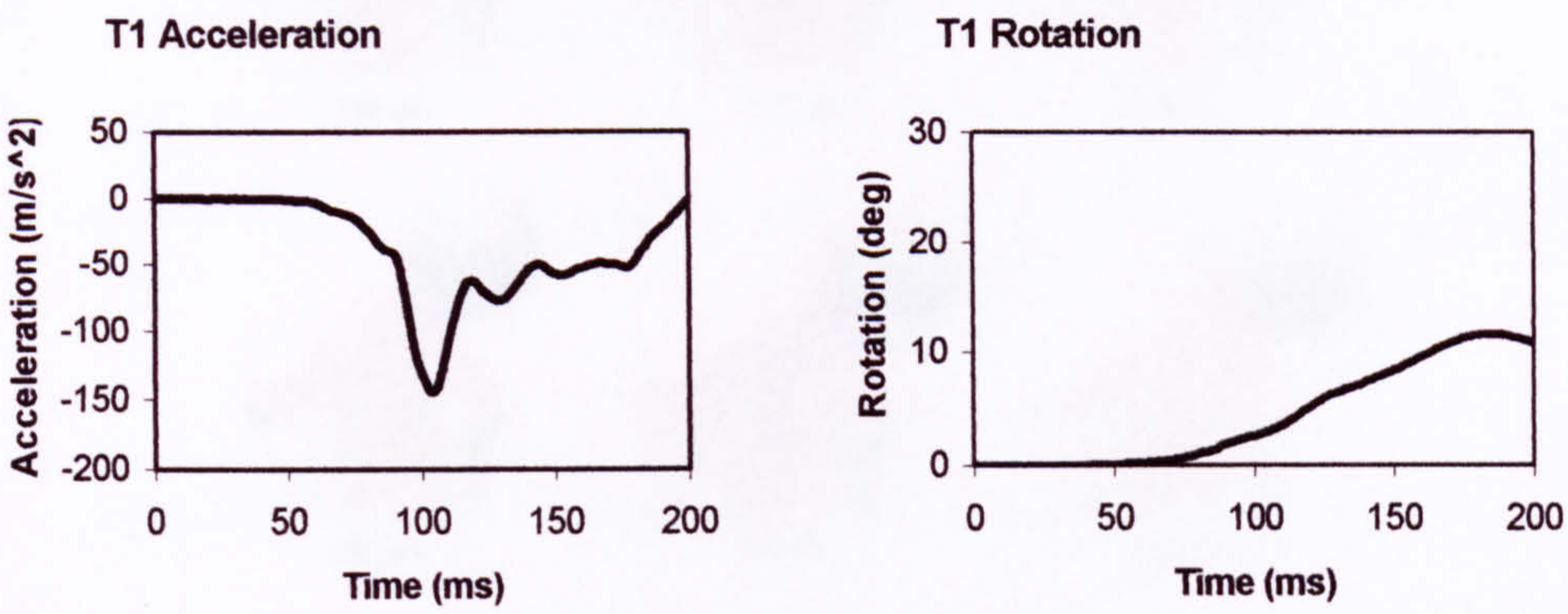

Figure 5.16 Model inputs for lateral impact

The response of the model with active musculature over the first 200ms of the 7g lateral impact is provided in Figure 5.17. During the first 110ms of the impact the head translates laterally along the y-axis with only a small amount of rotation, after which significant rotation of the head develops about the x-axis starting from about 130ms, where the head also begins to twist about the z-axis.

Contrary to the opinion that the muscles of the neck are unable to respond fast enough when exposed to high speed trauma recent research shows that the role of the muscles in limiting head-neck motion during impact may be significant. Siegmund and Brault (2000) stated that the cervical muscles can be activated early enough and are capable of altering the head and neck kinematics during impact trauma. There are a number of possible ways that the muscles may be triggered; during an impact there is a rapid sequence of events that may lead to the muscle reflex such as a loud noise on impact, vehicle motion and vibration and induced whole-body motion (Van Lopik, 2004). As in frontal impact, an initial reflex response time of 75 ms was used in the lateral impact simulations.

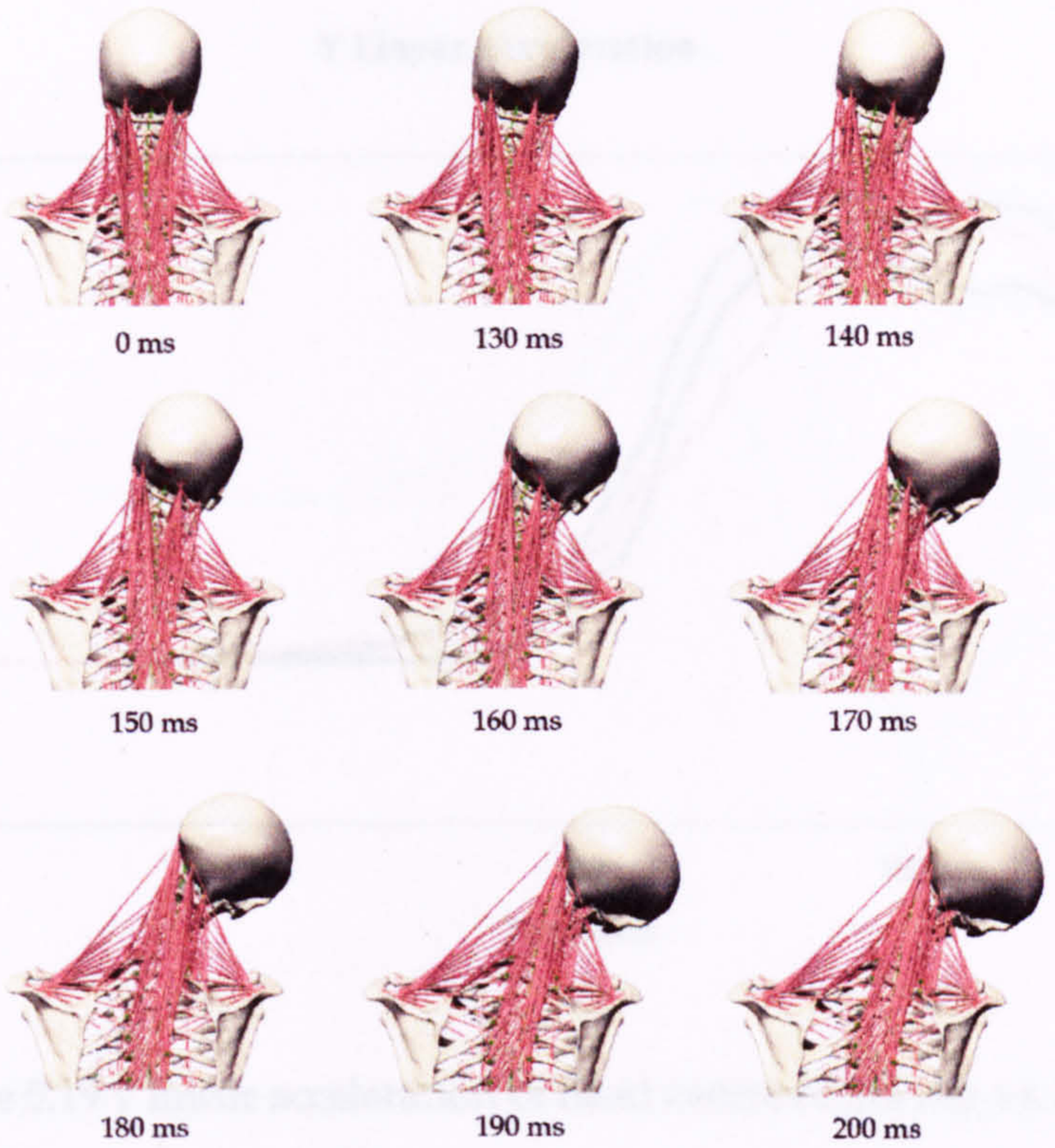

Figure 5.17 Lateral impact simulation

The predictions of the MB model in lateral impact case are illustrated in Figures 5.18-5.25.

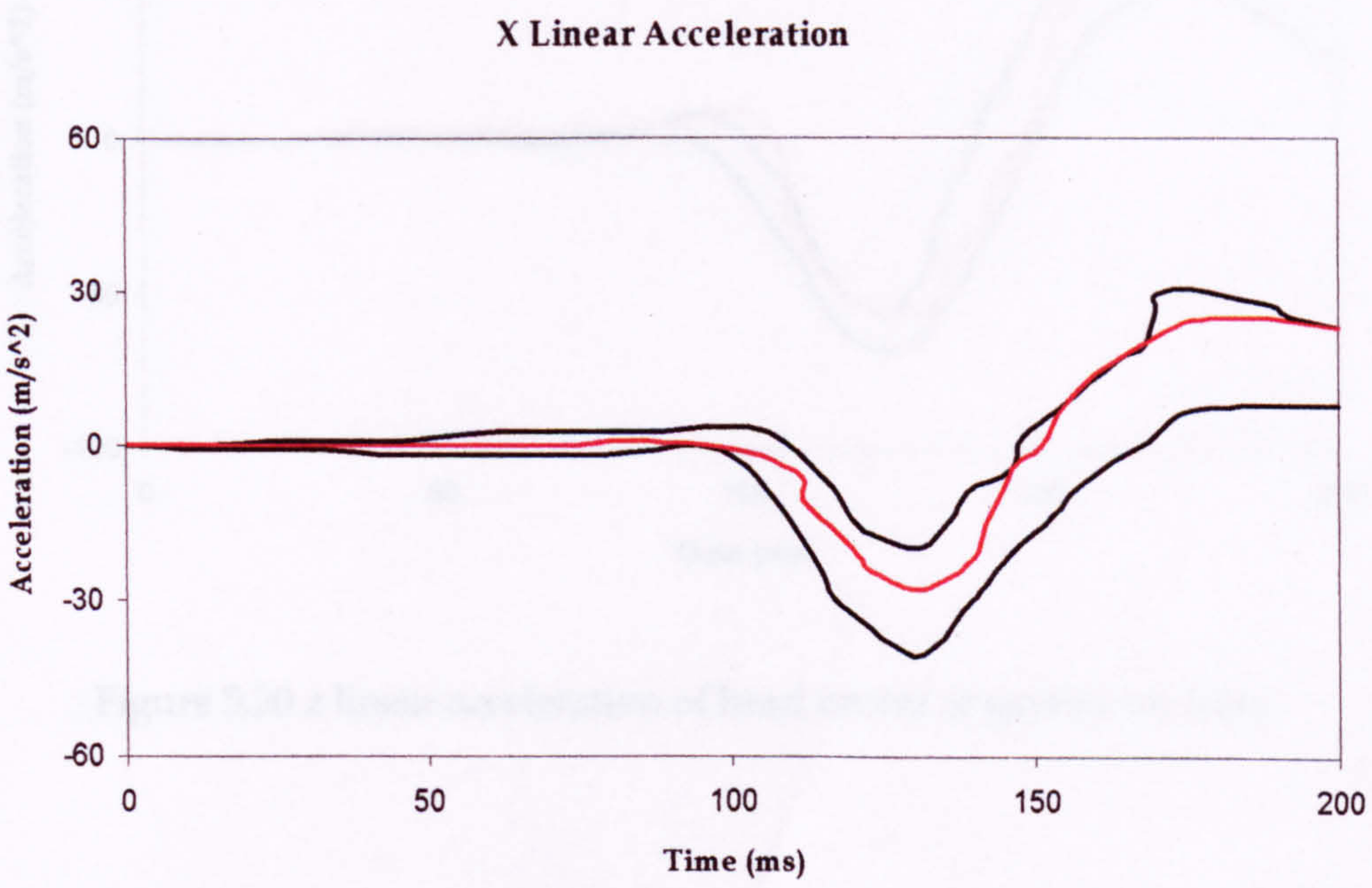

Figure 5.18 x linear acceleration of head centre of gravity vs. time

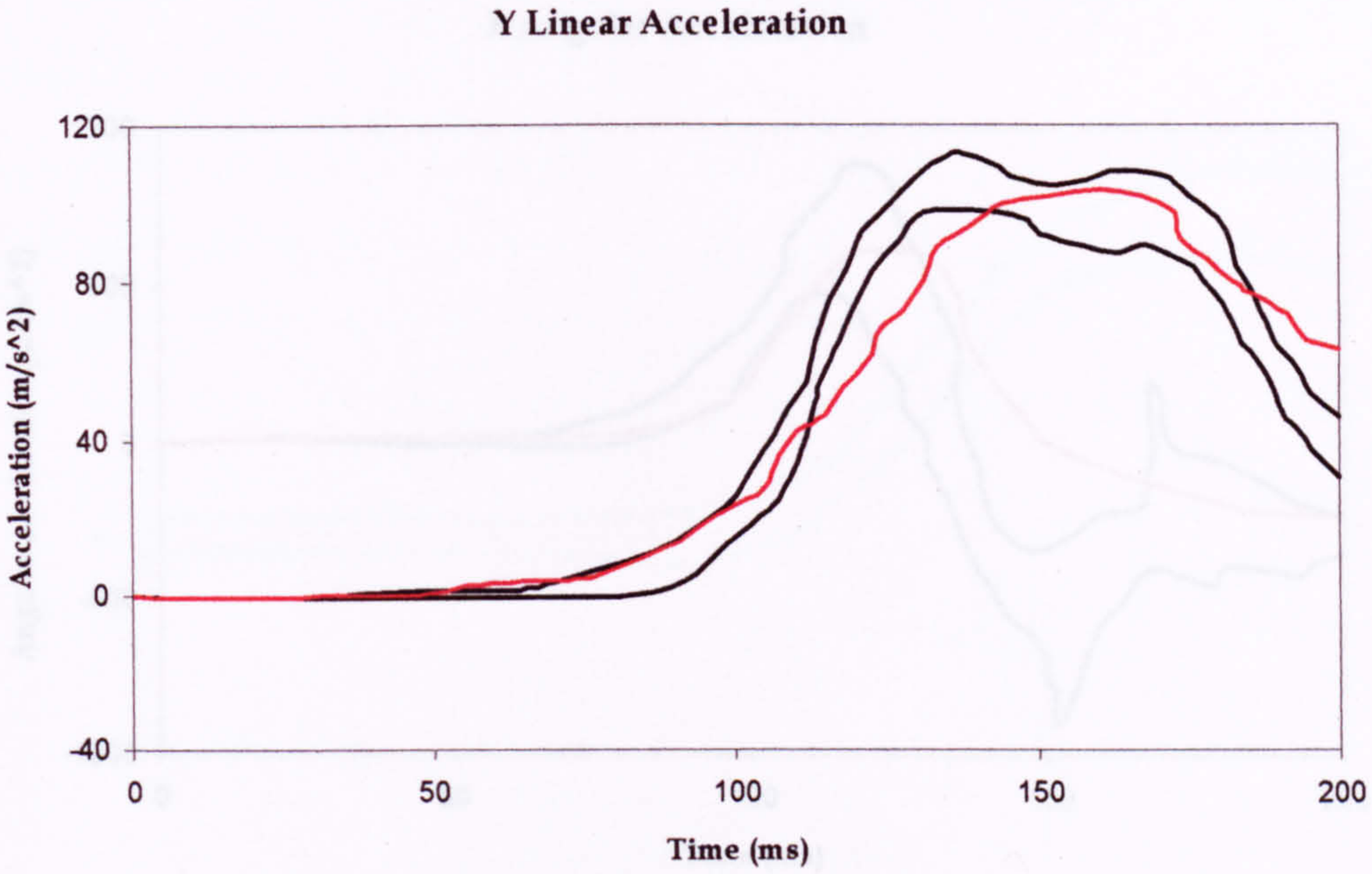

Figure 5.19 y linear acceleration of head centre of gravity vs. time

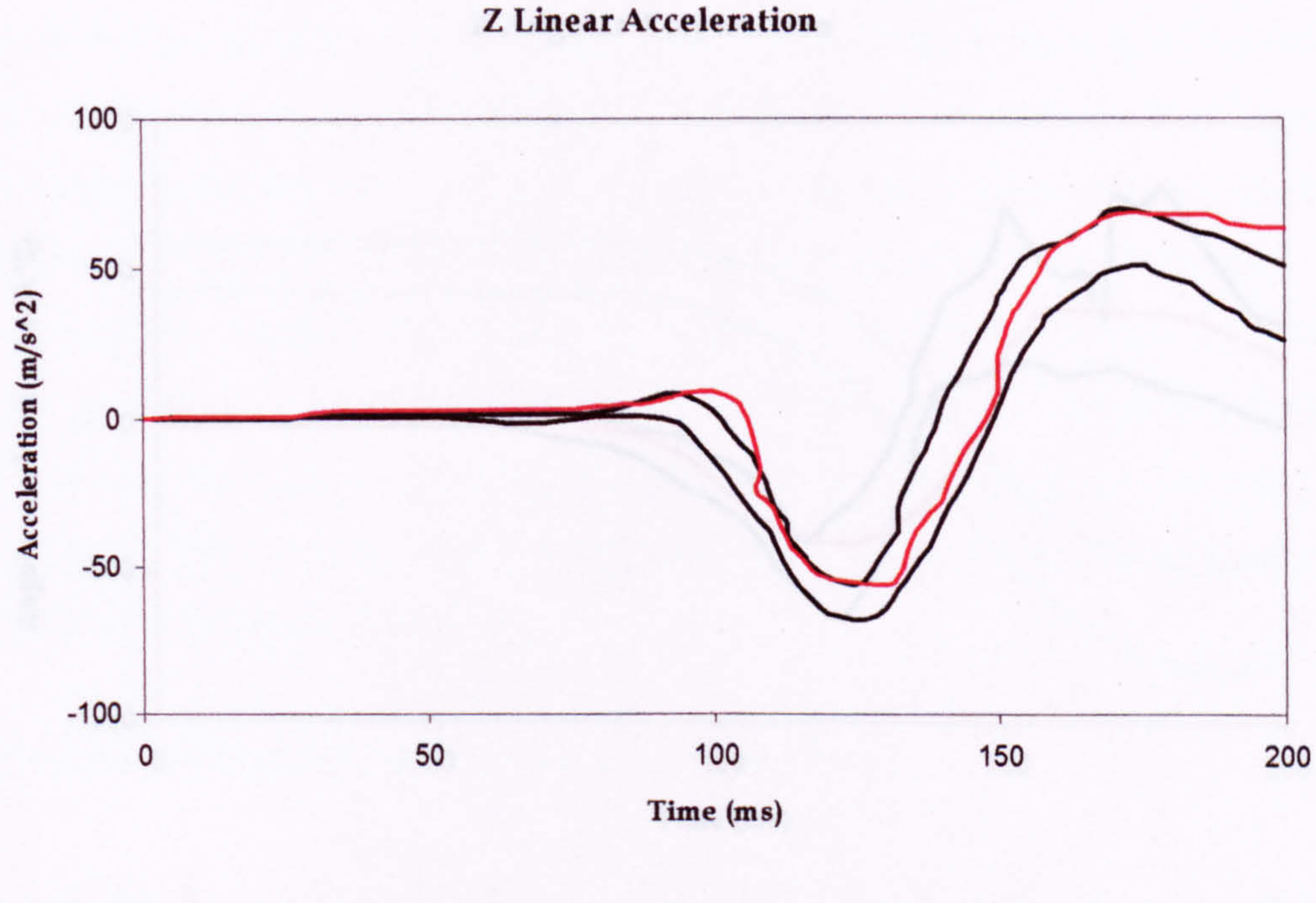

Figure 5.20 z linear acceleration of head centre of gravity vs. time

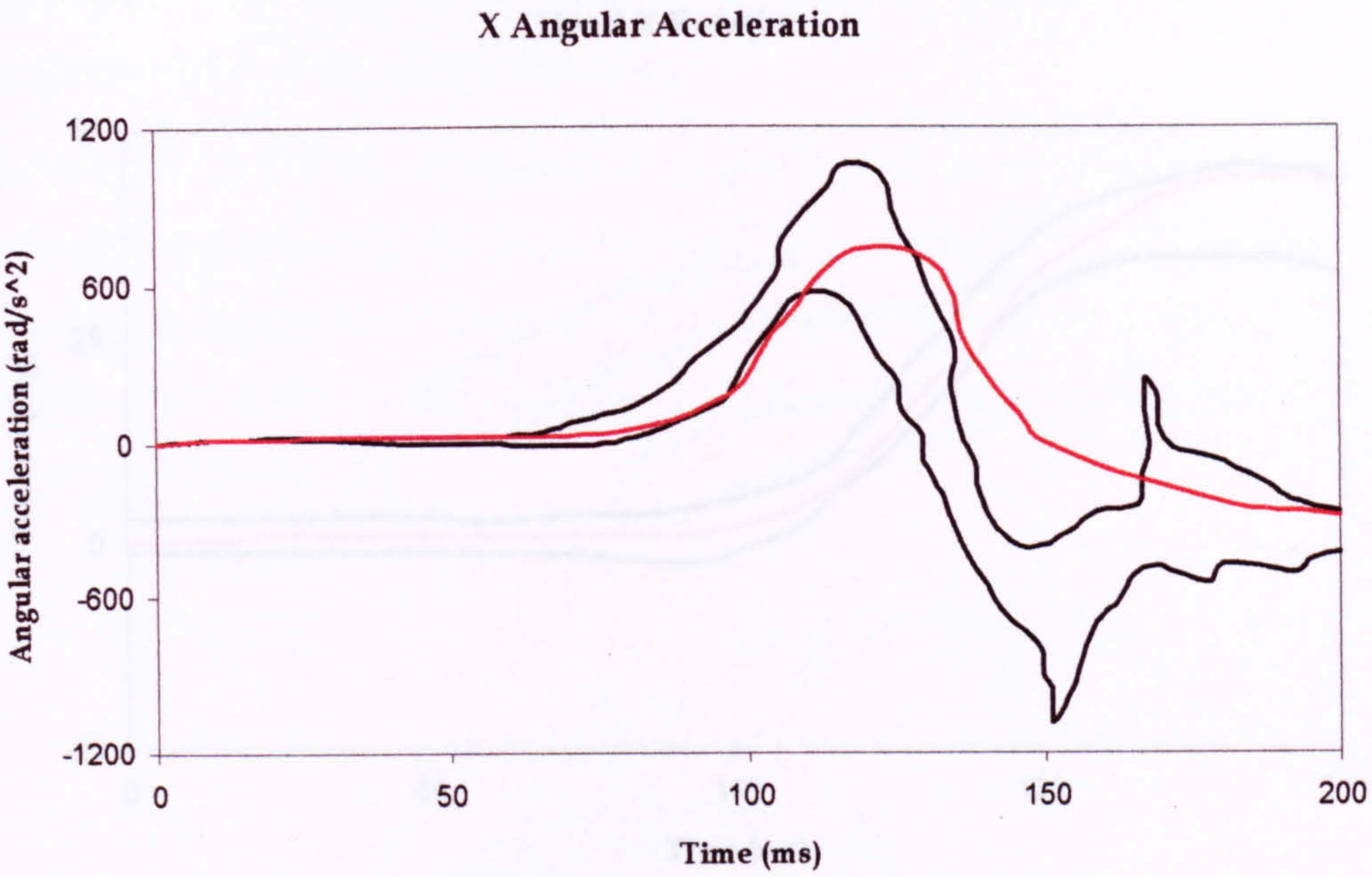

Figure 5.21 x angular acceleration of head centre of gravity vs. time

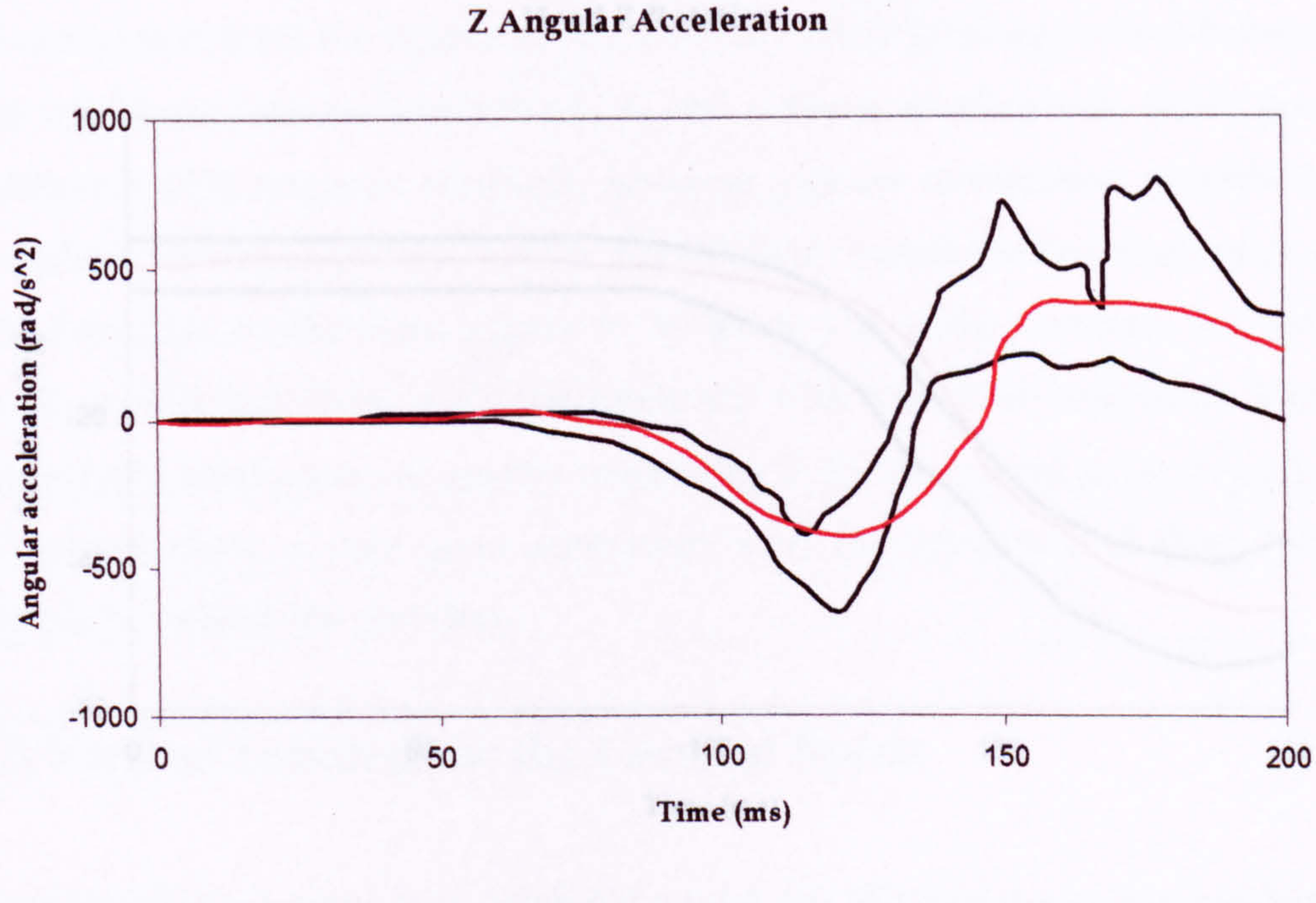

Figure 5.22 z angular acceleration of head centre of gravity vs. time

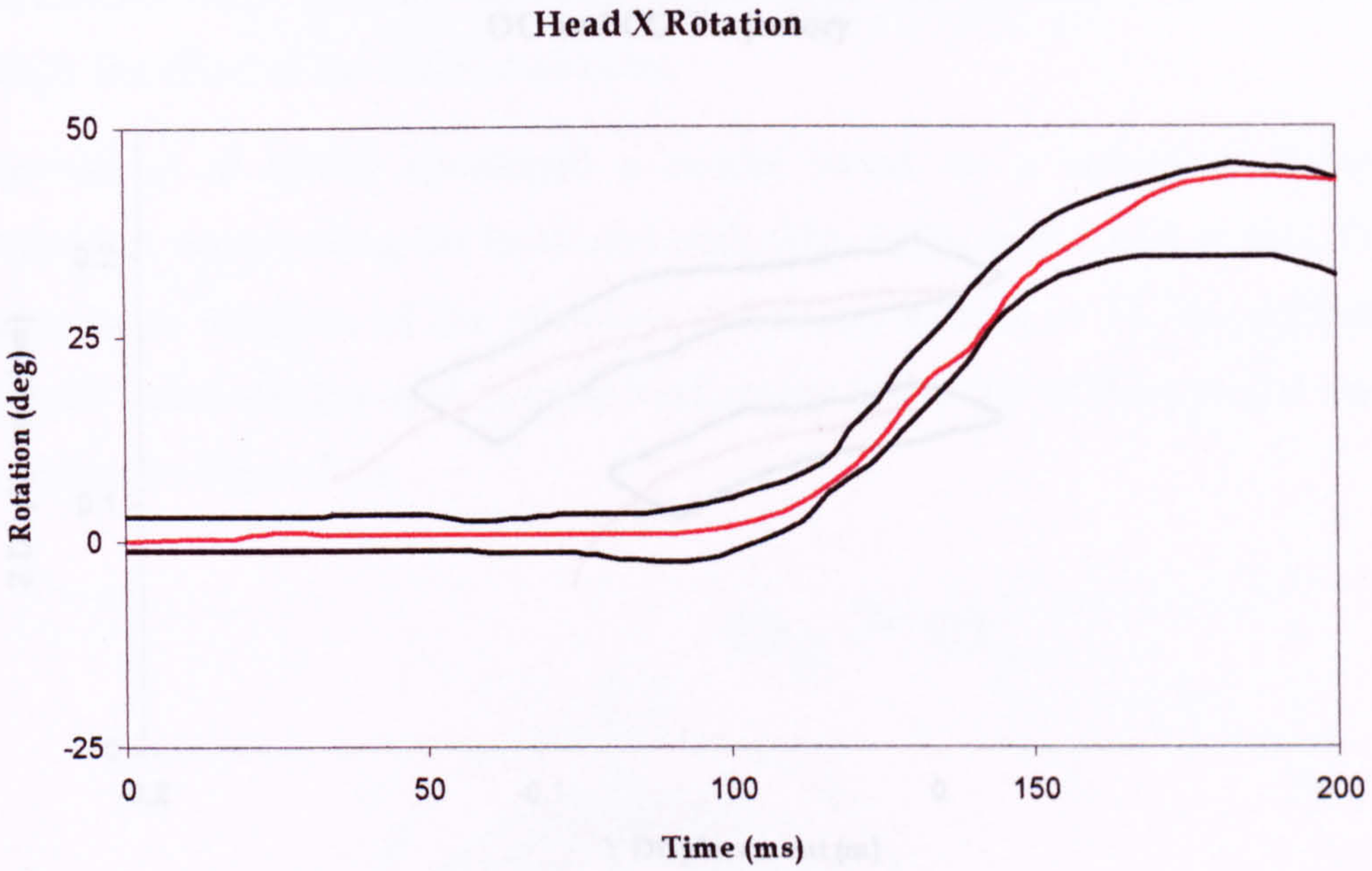

Figure 5.23 Head rotation about x axis

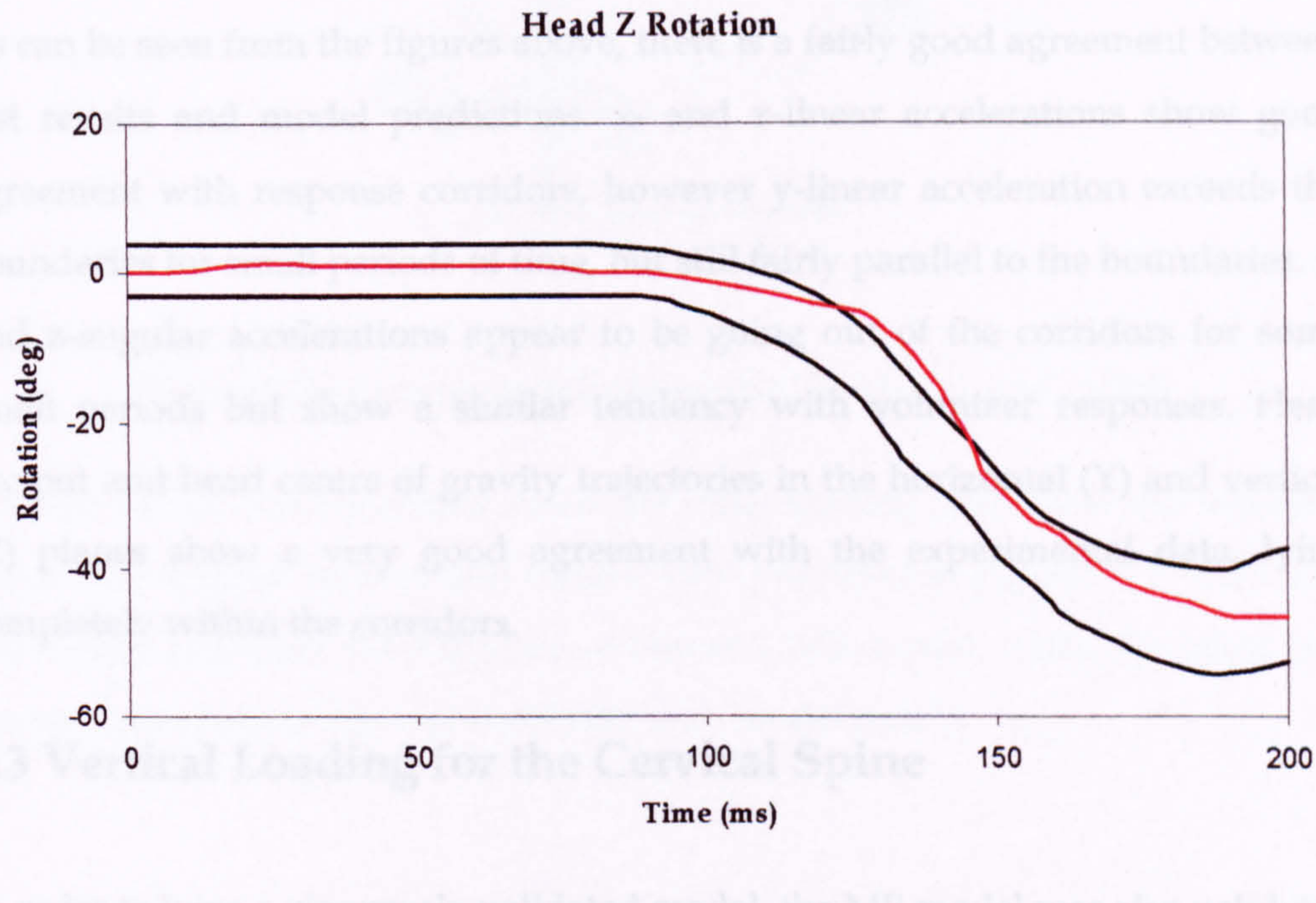

Figure 5.24 Head rotation about z axis

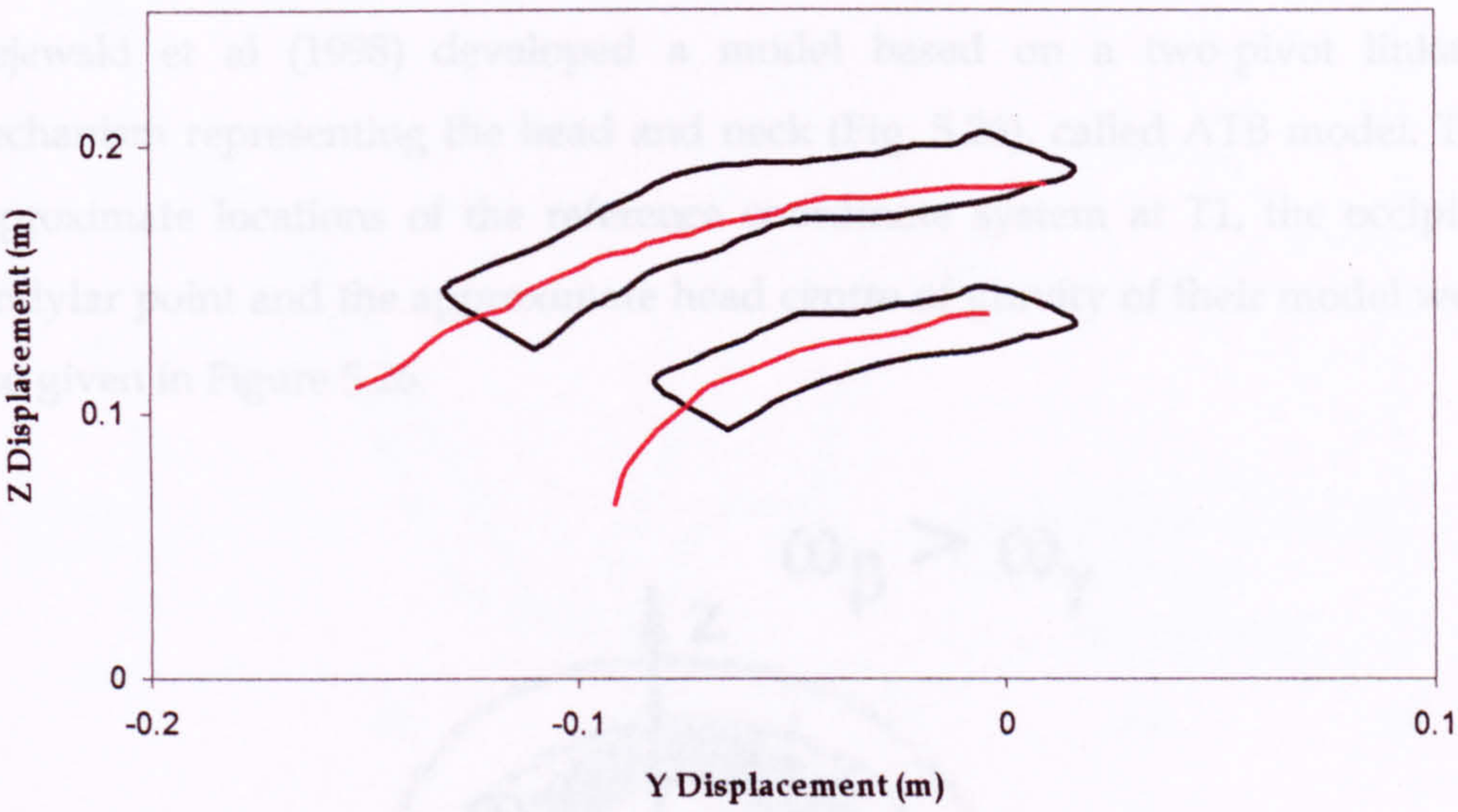

Figure 5.25 Head occiput and head centre of gravity trajectories in the horizontal (Y) and vertical (Z) planes (OC lower, CG upper graph)

As can be seen from the figures above, there is a fairly good agreement between test results and model predictions. x- and z-linear accelerations show good agreement with response corridors, however y-linear acceleration exceeds the boundaries for small periods of time, but still fairly parallel to the boundaries. x- and z-angular accelerations appear to be going out of the corridors for some small periods but show a similar tendency with volunteer responses. Head occiput and head centre of gravity trajectories in the horizontal (Y) and vertical (Z) planes show a very good agreement with the experimental data, lying completely within the corridors.

5.3 Vertical Loading for the Cervical Spine

In order to have a vigorously validated model, the MB model was also validated against vertical loading. Measured acceleration data from human volunteer tests on the Vertical Deceleration Tower (VDT) at Armstrong Laboratory, Wright-Patterson Air Force Base, Ohio, USA (Ziejewski et al., 1998) were used for comparison with MB model results. A peak acceleration of 10g was applied to the model for a duration of 250 ms in vertical direction. As the volunteers in the

experiments wore helmets, the mass of the head was increased by 1.5 kg to include the effect of the additional mass.

Ziejewski et al (1998) developed a model based on a two-pivot linkage mechanism representing the head and neck (Fig. 5.26), called ATB model. The approximate locations of the reference coordinate system at T1, the occipital condylar point and the approximate head centre of gravity of their model were also given in Figure 5.26.

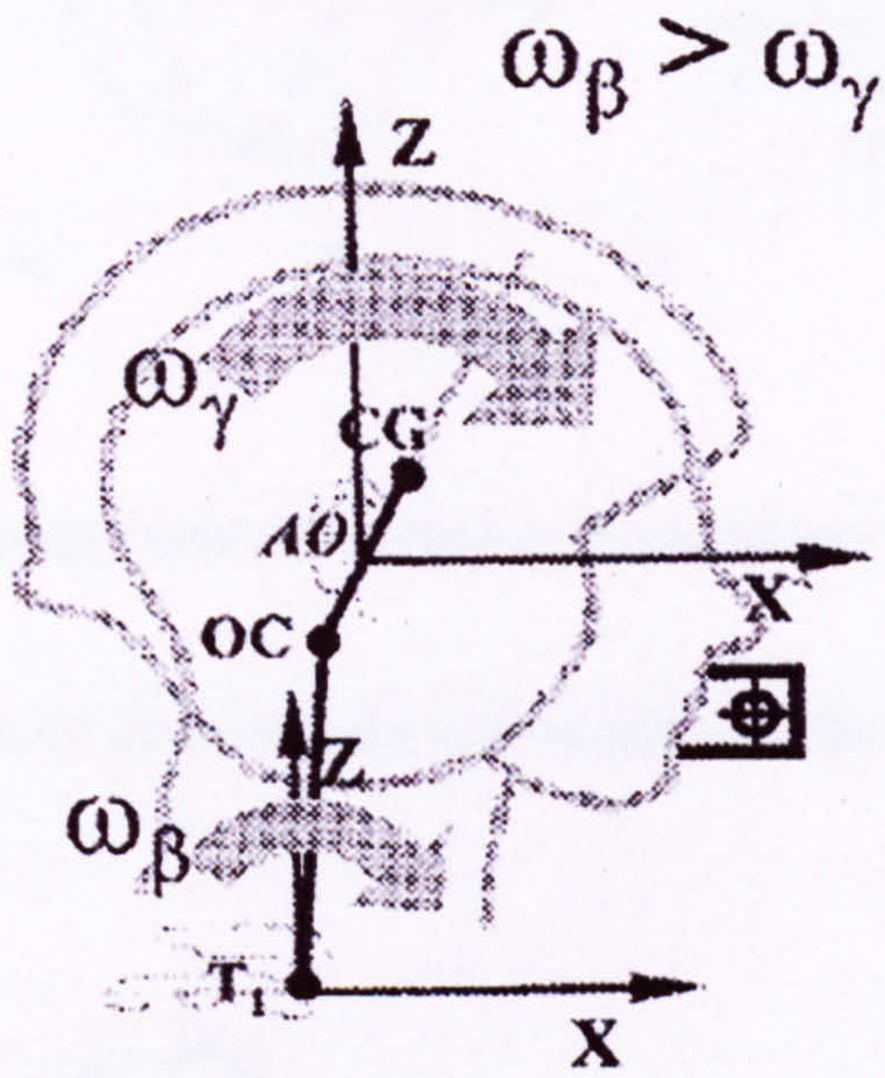

Figure 5.26 Two-pivot linkage model (Ziejewski et al., 1998)

The MB model was simulated under the same loading conditions and resulting linear and angular acceleration results were provided in Figures 5.27-5.29. The red curves represent the response of author's MB model, while the other two curves are experimental and Ziejewski et al. model results.

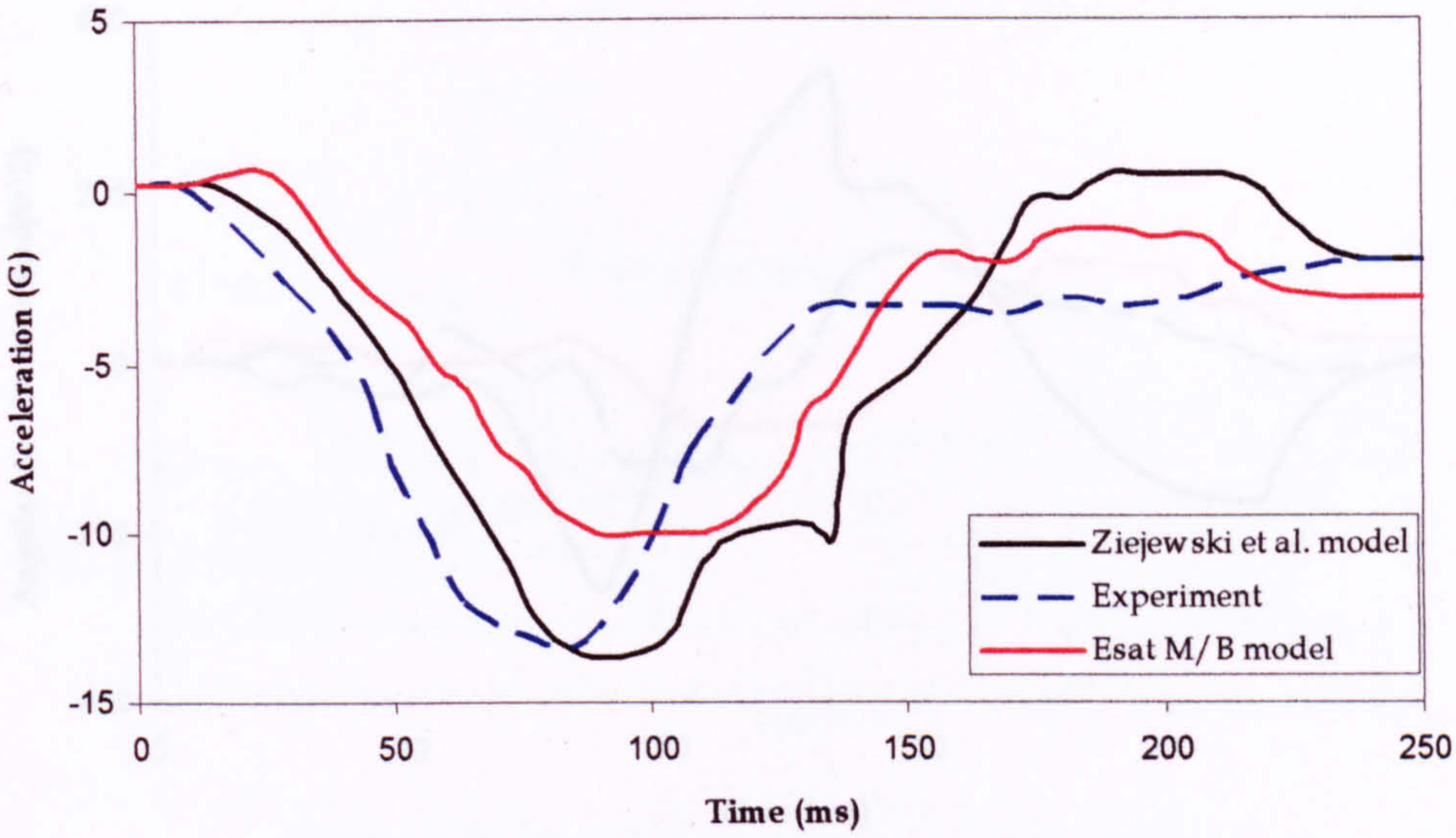

Figure 5.27 Linear head acceleration at mouthpiece in z direction

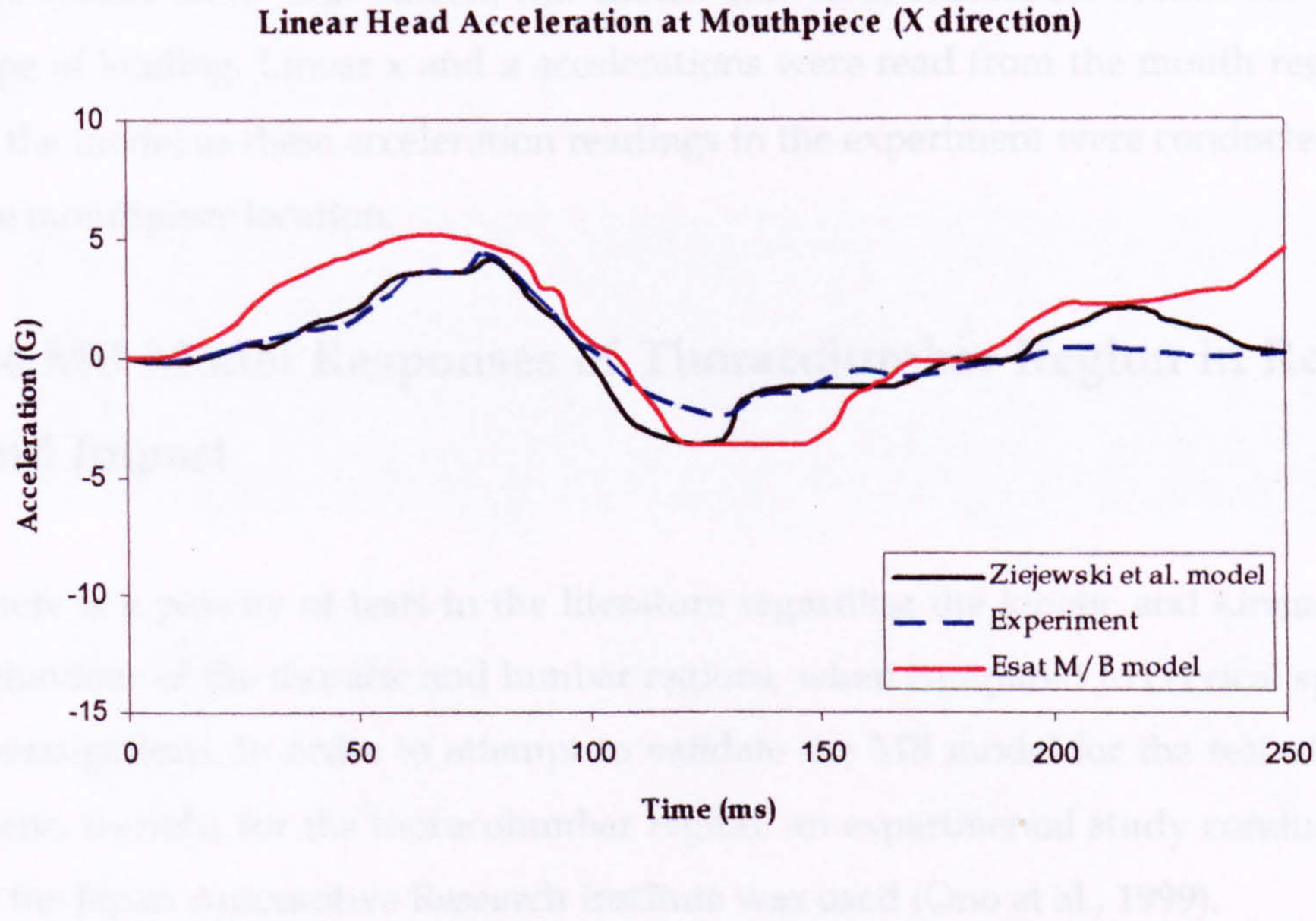

Figure 5.28 Linear head acceleration at mouthpiece in x direction

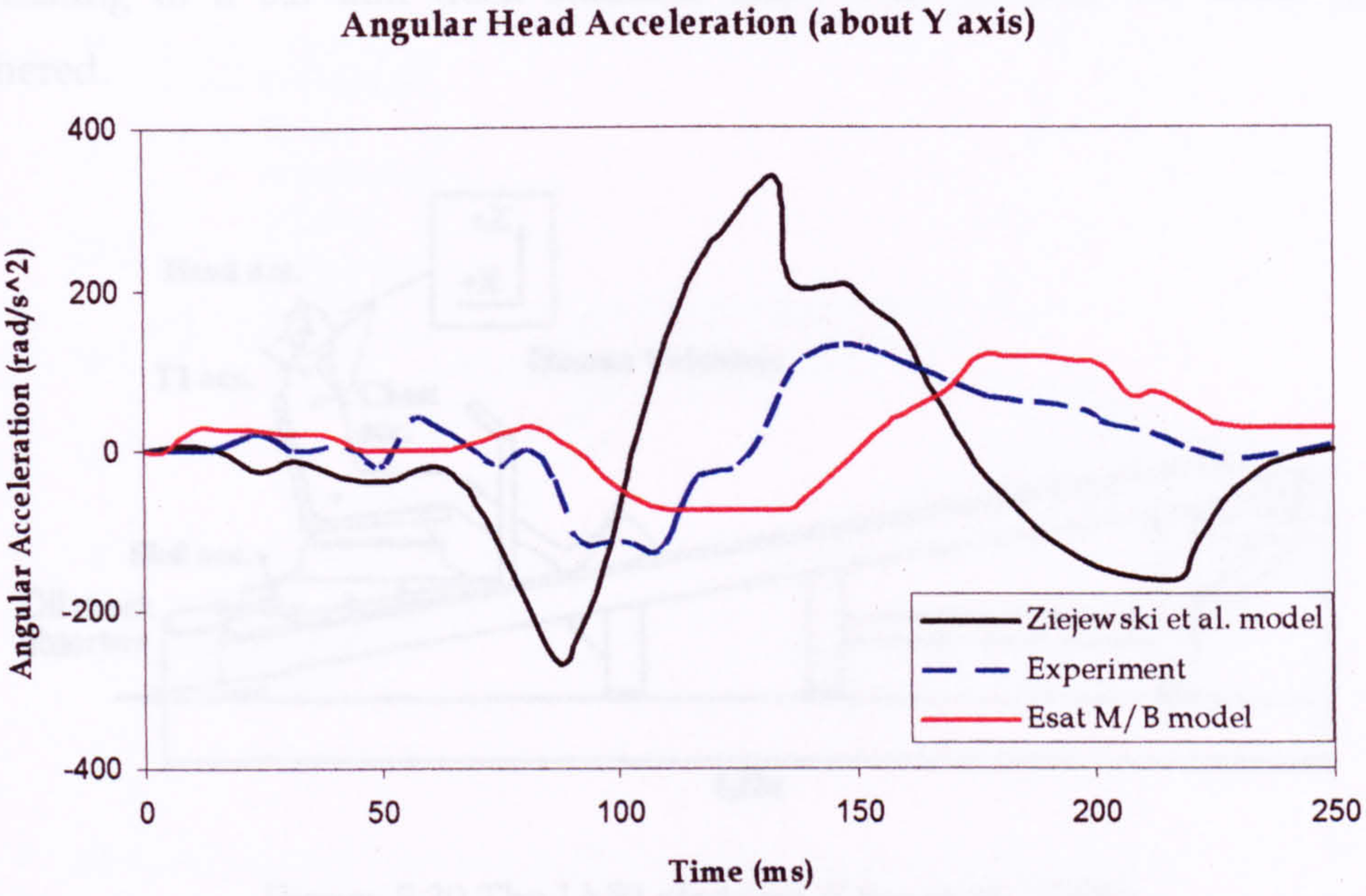

Figure 5.29 Angular head acceleration about y axis

The results show that current MB model can yield reasonable results for this type of loading. Linear x and z accelerations were read from the mouth region of the model as these acceleration readings in the experiment were conducted at the mouthpiece location.

5.4 MB Model Responses of Thoracolumbar Region in Rear-End Impact

There is a paucity of tests in the literature regarding the kinetic and kinematic behaviour of the thoracic and lumbar regions, when compared to cervical spine investigations. In order to attempt to validate the MB model for the rest of the spine, namely, for the thoracolumbar region, an experimental study conducted at the Japan Automotive Research Institute was used (Ono et al., 1999).

The sled apparatus used is provided in Figure 5.30. A cineradiographic system was applied for the analysis of the cervical spine, while the deformations in the thoracic, lumbar and sacral spines were measured via a so-called spinal deformation measurement system. This system works with a tape sensor

consisting of a 0.3 mm thick stainless sheet with 33 pairs of strain gages adhered.

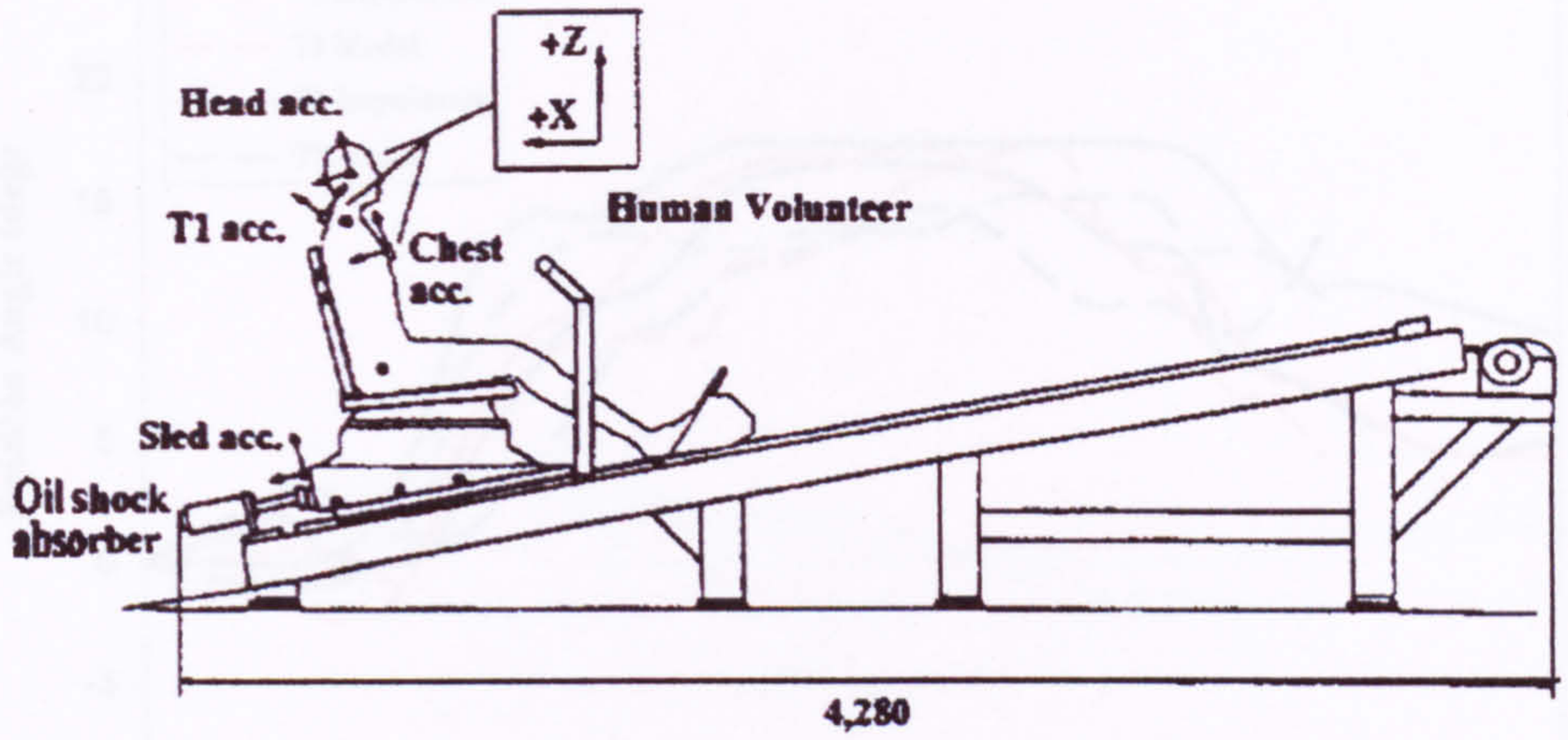

Figure 5.30 The JARI sled test (Ono et al., 1999)

The test was conducted at an impact velocity of 8 km/hr. The comparison of test and model instants together with spinal deformations was given in Figure 5.31. The comparison of the rotational angles of the MB model prediction with the experimental values is provided in Figures 5.32-5.37.

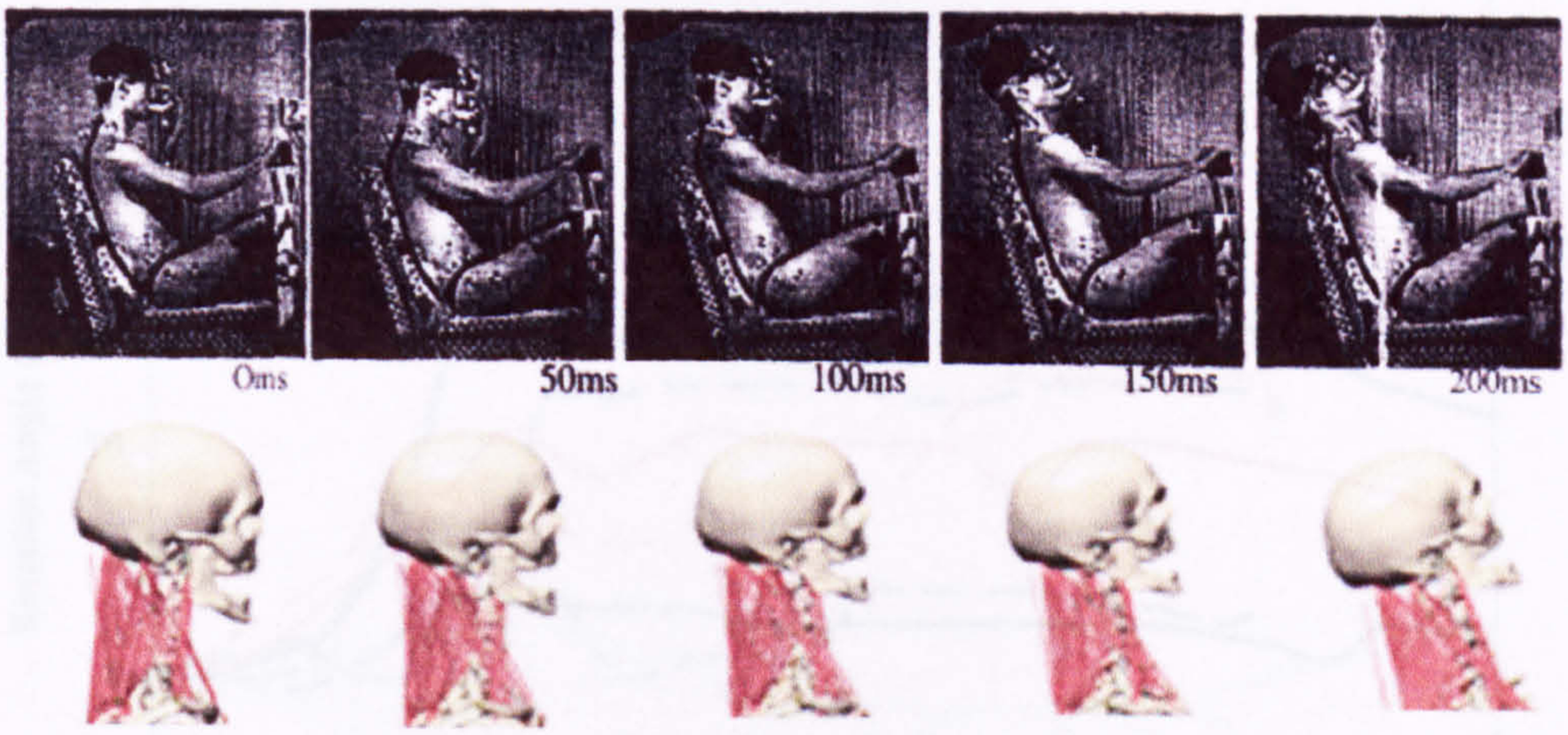

Figure 5.31 Test and model instants for JARI sled test

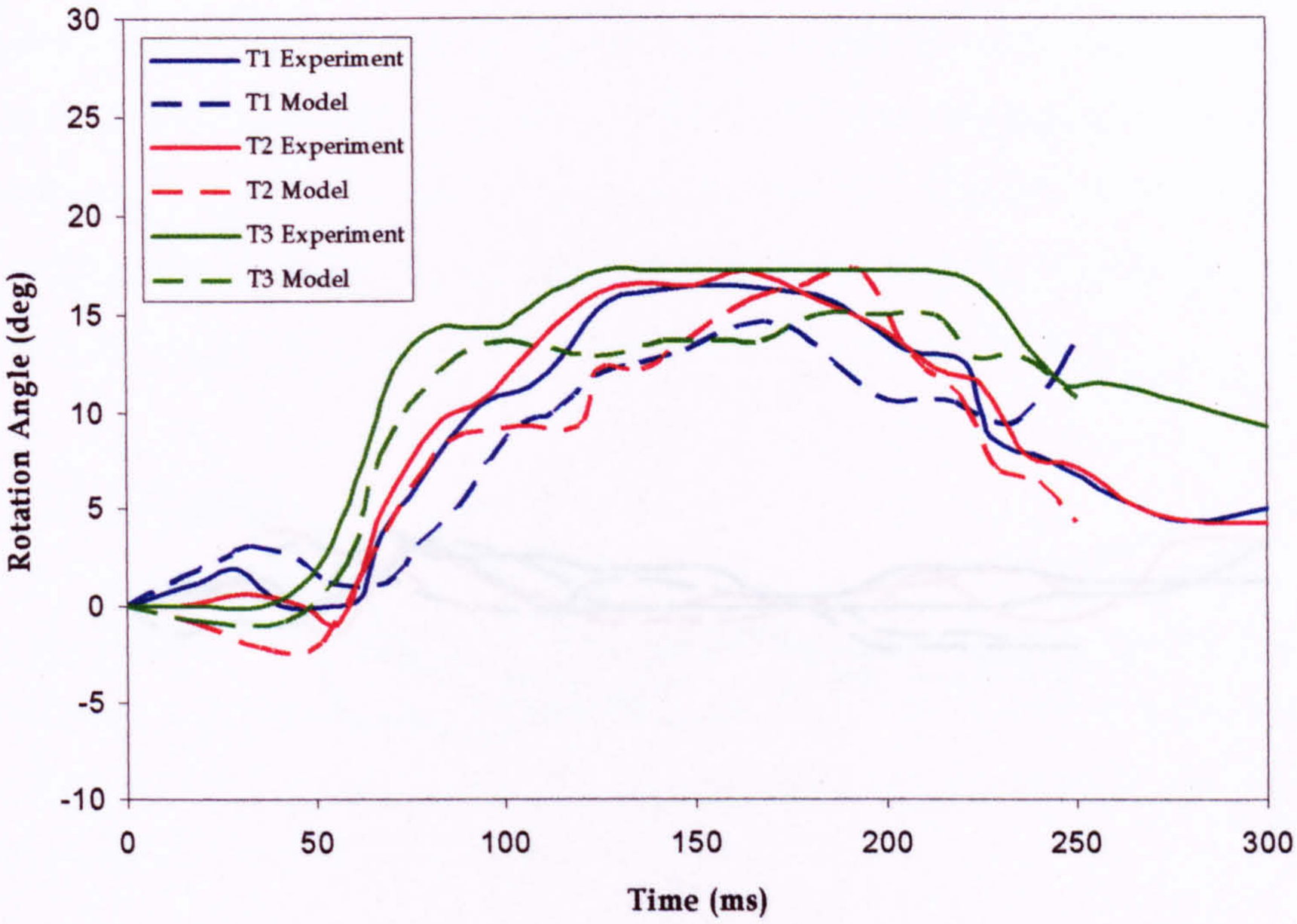

Figure 5.32 Rotational angles of the MB model prediction (in red) compared with the experimental values for T1-T3.

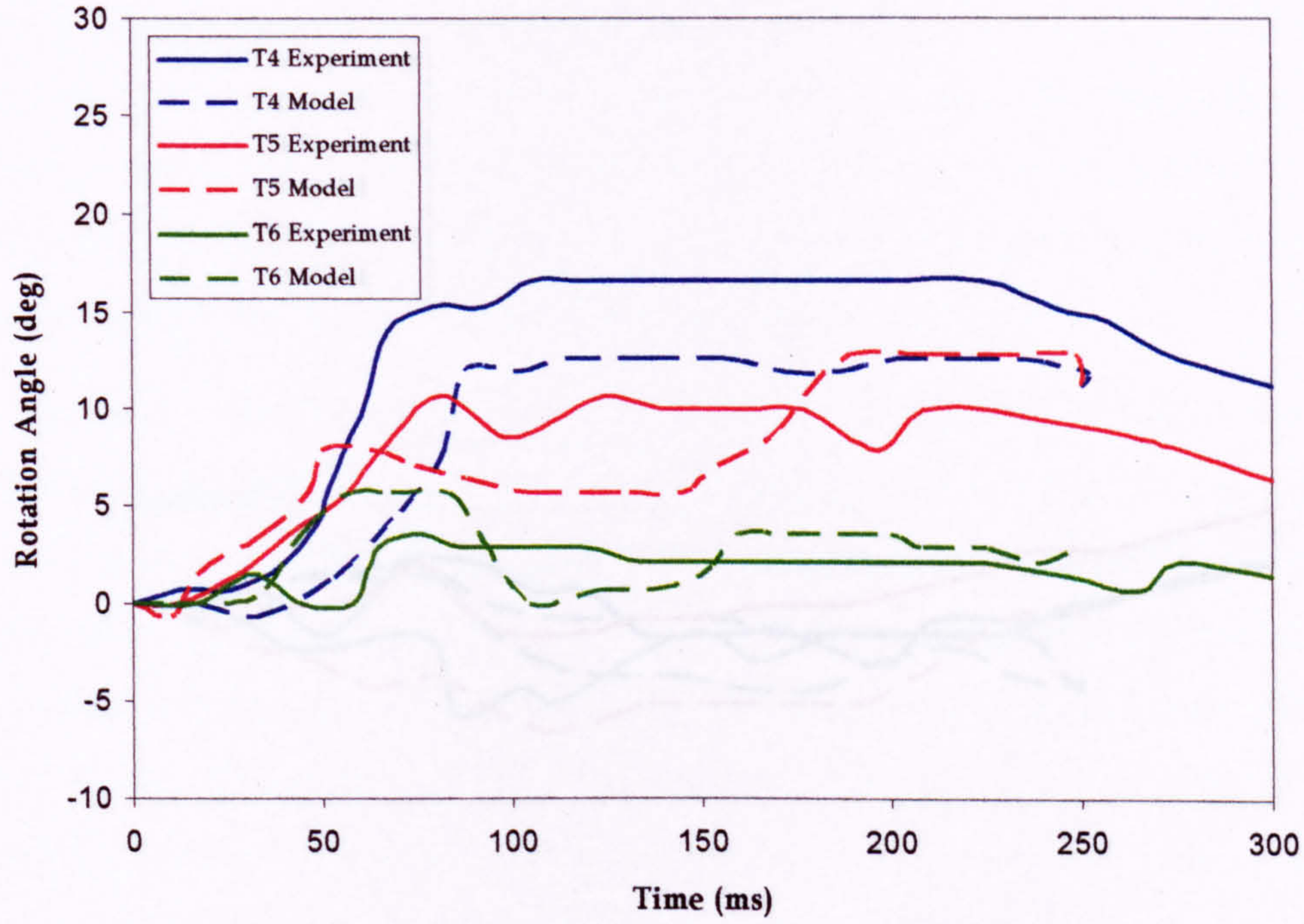

Figure 5.33 Rotational angles of the MB model prediction (in red) compared with the experimental values for T4-T6.

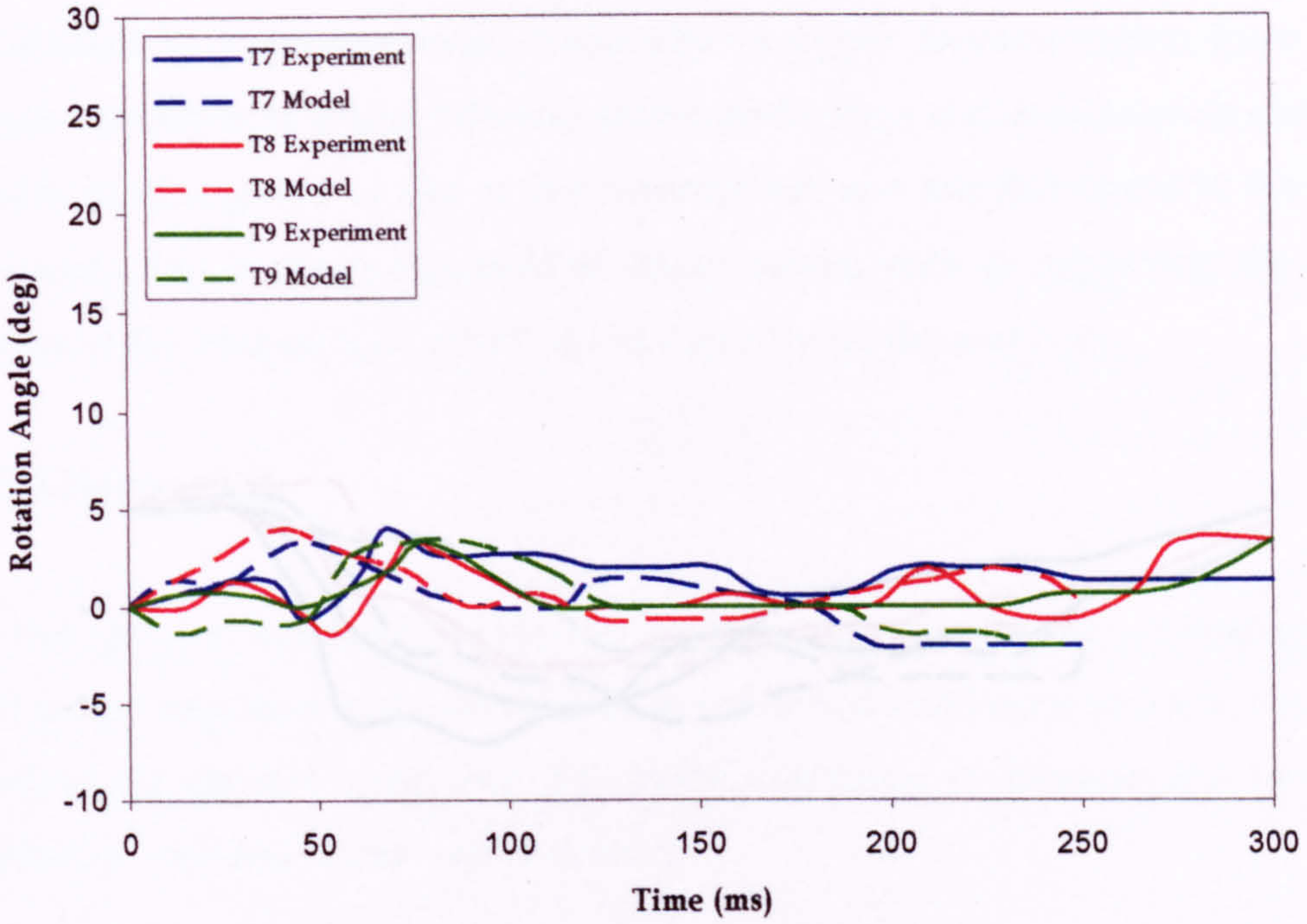

Figure 5.34 Rotational angles of the MB model prediction (in red) compared with the experimental values for T7-T9.

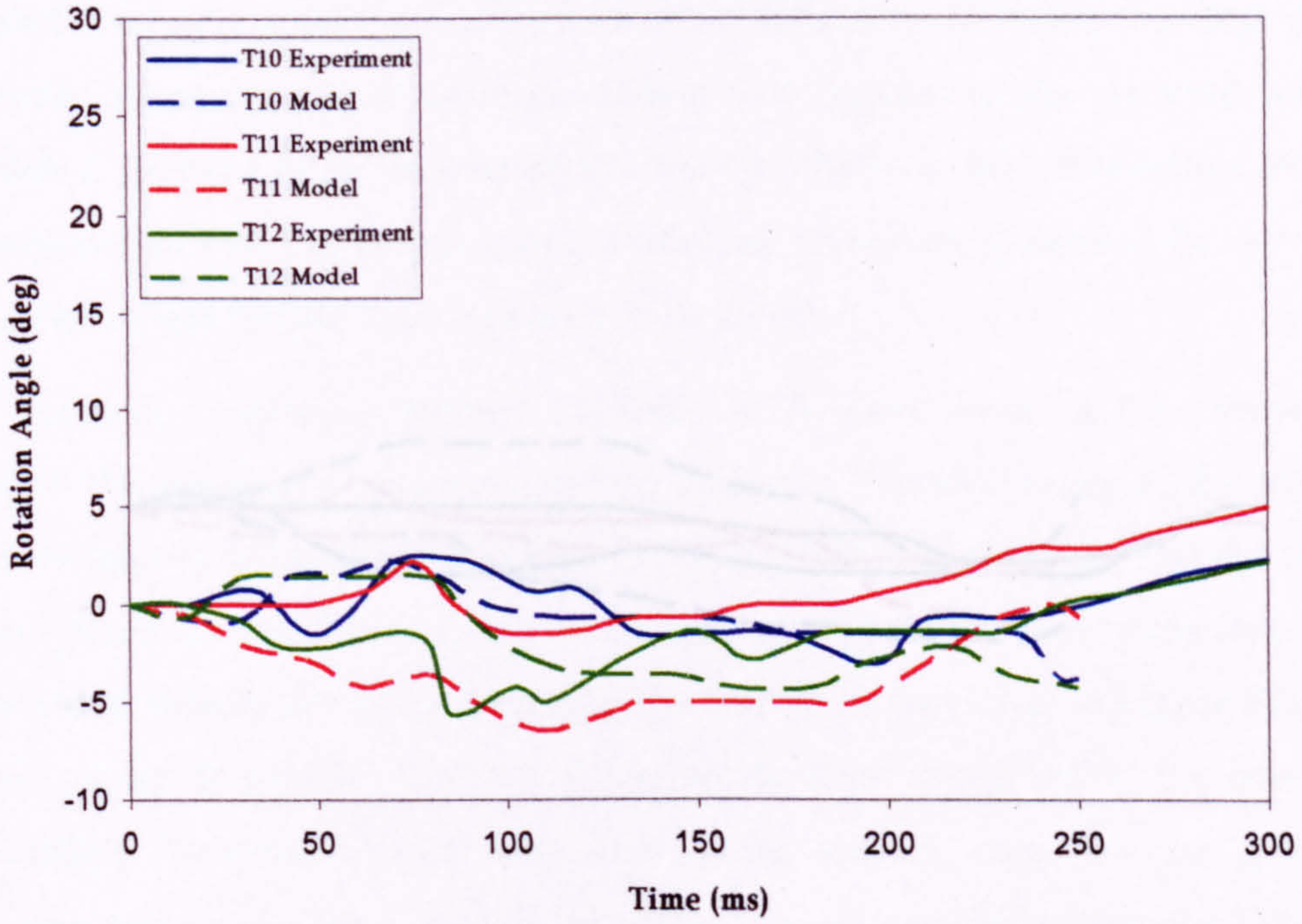

Figure 5.35 Rotational angles of the MB model prediction (in red) compared with the experimental values for T10-T12.

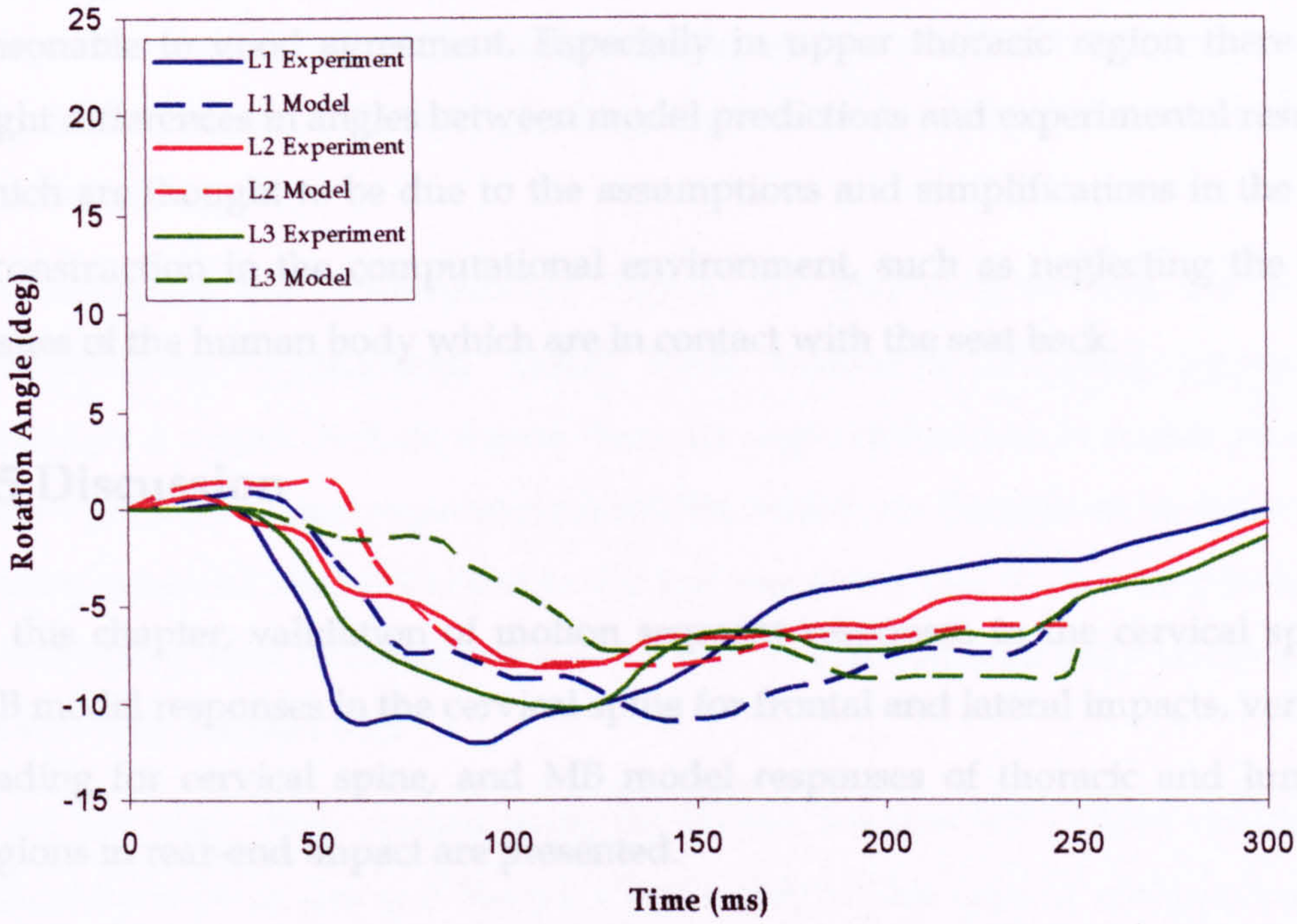

Figure 5.36 Rotational angles of the MB model prediction (in red) compared with the experimental values for L1-L3.

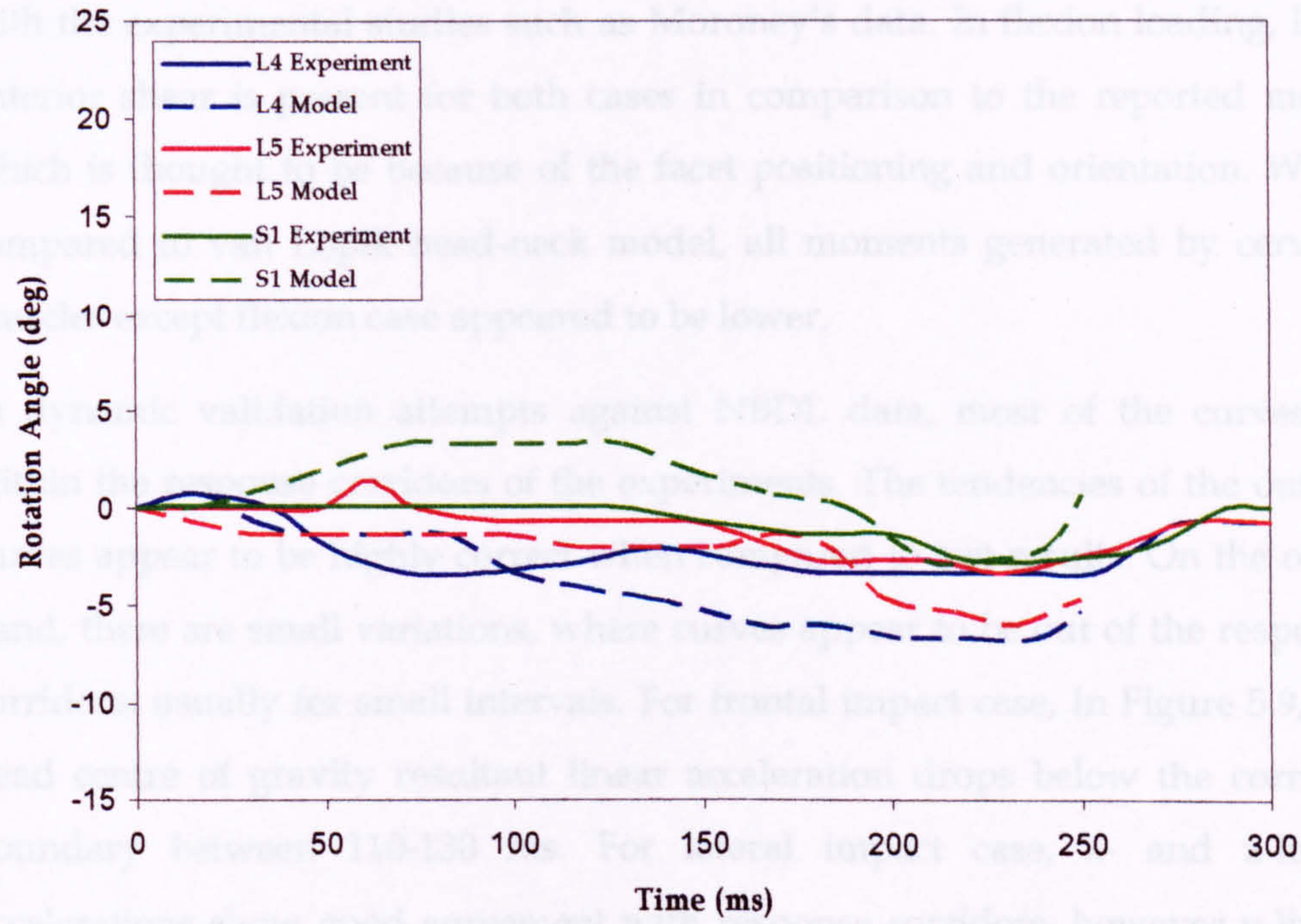

Figure 5.37 Rotational angles of the MB model prediction (in red) compared with the experimental values for L4-S1.

The graphs show that the model predicted the experimental values from reasonable to good agreement. Especially in upper thoracic region there are slight differences in angles between model predictions and experimental results, which are thought to be due to the assumptions and simplifications in the test reconstruction in the computational environment, such as neglecting the soft tissues of the human body which are in contact with the seat back.

5.5 Discussion

In this chapter, validation of motion segment responses in the cervical spine, MB model responses in the cervical spine for frontal and lateral impacts, vertical loading for cervical spine, and MB model responses of thoracic and lumbar regions in rear-end impact are presented.

As there are several experimental studies regarding the impact behaviour of the cervical spine, most of the validation attempts were conducted on the responses of the cervical spine.

The static loading results of the cervical spine seemed to be in good agreement with the experimental studies such as Moroney's data. In flexion loading, little anterior shear is present for both cases in comparison to the reported mean, which is thought to be because of the facet positioning and orientation. When compared to van Lopik head-neck model, all moments generated by cervical muscles except flexion case appeared to be lower.

In dynamic validation attempts against NBDL data, most of the curves lie within the response corridors of the experiments. The tendencies of the output curves appear to be highly correct when compared to test results. On the other hand, there are small variations, where curves appear to be out of the response corridors, usually for small intervals. For frontal impact case, In Figure 5.9, the head centre of gravity resultant linear acceleration drops below the corridor boundary between 110-130 ms. For lateral impact case, x- and z-linear accelerations show good agreement with response corridors, however y-linear acceleration exceeds the boundaries for small periods of time, but still fairly parallel to the boundaries.

The model was also validated against vertical loading. The model and simulation parameters were fairly simple as few data was present in the literature. However, relatively good agreements were achieved in terms of head accelerations.

For validating the thoracolumbar region, the graphs show that the model predicted the experimental values from reasonable to good agreement. Especially in upper thoracic region there are slight differences in angles between model predictions and experimental results, which are thought to be due to the assumptions and simplifications in the test reconstruction in the computational environment, such as neglecting the soft tissues of the human body which are in contact with the seat back.

There are some other studies using the thorax reaction force based results for validation such as Jost and Nurick's study (2001). This type of analysis has the potential to yield good results especially for FE models, where soft tissues and their material properties were incorporated. As multi-body dynamics technique is based on rigid bodies, this type of validation wasn't carried out for the current multi-body model, which is incapable of visualising structural deformations.

CHAPTER 6

A MB Model Application: Simulating Whiplash

Whiplash or Whiplash Associated Disorders (WAD) is a very common injury of the cervical spine, occurring usually as a result of low speed, rear-end car crashes, in which the sudden differential movement between the head and torso results in abnormal motions in the neck causing damage to its soft tissue components. In the resulting head-neck motion a characteristic S-shaped curvature of the neck with lower level hyperextension and upper level flexion is normally observed, which is followed by subsequent C-shaped curvature with extension at all levels of the entire cervical spine (Fig. 6.1).

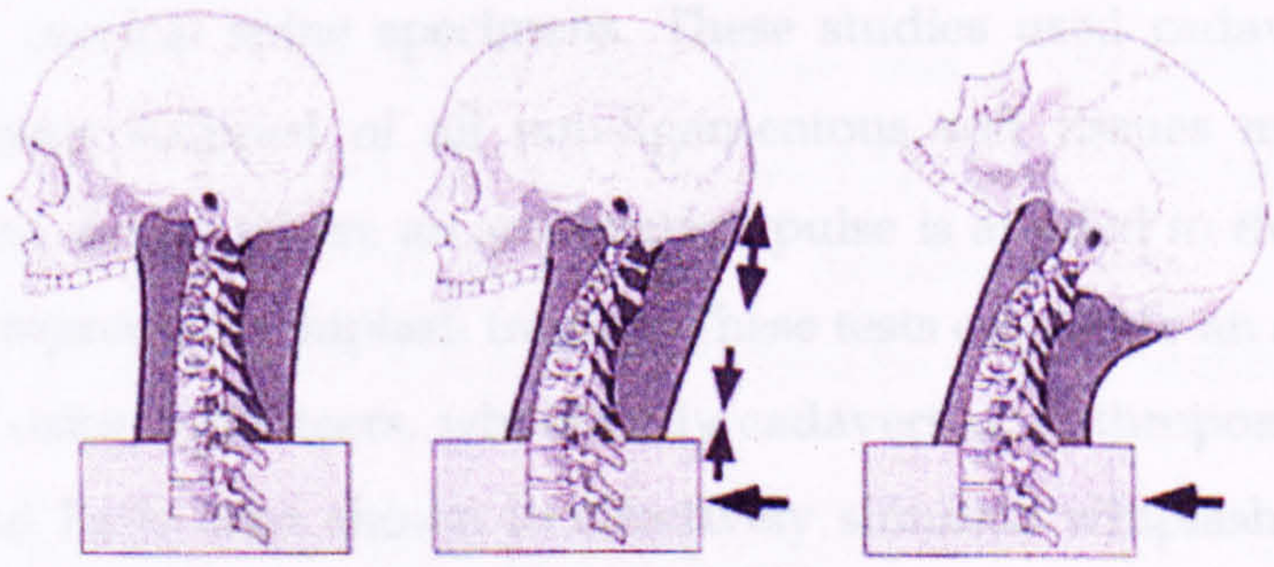

Figure 6.1 Schematic views of S-shaped whiplash injury mechanism in a rear-end impact (S-shaped cervical spine in the middle figure) (Yoganandan et al., 2000)

Whiplash manifests itself in symptoms such as surgical, neurological, audiological, otorhinolaryngological (ear-nose-throat related), sense of balance and teeth occlusion (Hasegawa and Shiomi, 2003). In most cases the injuries are relatively minor and the causes of the disabilities are usually not known

(Galasko, 1998). The injury mechanism of whiplash is insufficiently understood. Recent research has focused on the possibility of internal nerve damage to the spinal canal due to the rapid acceleration of the body with respect to the head, while intersegmental hyperextension, tearing of ligaments and muscles, lesions to discs, and facet joint injuries are also considered to be possible reasons for whiplash.

Whiplash not only leaves some patients with severe residual disability that may interfere with their ability to do their job and quality of life, but also burdens the economy with a huge cost. It has been estimated that 80% of personal injury claims made against British Insurers are related to whiplash, costing well over £1 billion every year and steadily rising (THATCHAM, 2001). In US, neck injuries cost at least $7 billion in U.S. insurance claims per year (IIHS, 2004). Similarly in Japan, neck injury accounted for an annual loss of 192.8 MYen in 2001 (Hasegawa and Shiomi, 2003). The costs in the early nineties have been estimated to be 700 MEuro in Germany, 210 MEuro in Sweden and 300 MEuro in Netherlands (van der Horst, 2002). These data do not include the lost working days due to injuries and their socioeconomic costs.

In this chapter, it is aimed to validate the ligamentous cervical spine model with Panjabi and colleagues' experiments conducted using a bench-top trauma sled and isolated cervical spine specimens. These studies used cadaveric cervical spine specimens stripped of all non-ligamentous soft tissues mounted to a bench top sled device where an acceleration pulse is applied to the base of the specimen to reproduce whiplash trauma. These tests constitute an alternative to experiments using volunteers, whole body cadavers or anthropometrical crash dummies and have been shown to effectively simulate whiplash trauma and have provided valuable insights into the complex events and interactions that cause injuries to the cervical spine (van Lopik, 2004). In the resulting head-neck motion a characteristic S-shaped curvature of the neck with lower level hyperextension and upper level flexion was observed followed by subsequent C-shaped curvature with extension at all levels of the entire cervical spine.

This chapter presents simulations of these rear-end impact sled tests using the ligamentous cervical spine model. The model is firstly used devoid of

musculature with an acceleration pulse applied to T1. Varying levels of impact severity were investigated. Finally, the muscles were activated in the model to study their effect on the head-neck motion.

6.1 Experimental and Simulation Set-ups

Panjabi and co-workers (1997, 1998a, 1998b) utilised a bench-top trauma sled to simulate whiplash trauma on ligamentous human cadaveric cervical spine specimens (Figure 6.2) The spine specimens tested were without all muscle tissue and mounted to the sled at T1. The trauma sled moved on horizontal linear bearings and was accelerated by a pneumatic piston, power springs and an electromagnet release. A steel head surrogate representing a 50th percentile human head was connected to the occiput of the cervical spine with the centre of gravity positioned analogous to that of a real head. The weight of the surrogate head was fully balanced by a pneumatic suspension system effectively negating gravitational pull, however, the inertial components of the head were still effective. Trauma acceleration was exerted onto the specimen by an impactor mounted on the linear bearings. Head motion was monitored with two translational and one rotational potentiometers. The whiplash trauma input was input as the profile of the sled acceleration-time curve to the base of the specimen represented. The acceleration input was a triangular pulse with duration of 105ms and peak accelerations of 2.5g, 4.5g. 6.5g and 8.5g (1g = 9.8m/s^2) (Grauer et al., 1997). The resulting rotation, vertical and horizontal translation of the head with time for the 8.5g trauma were presented.

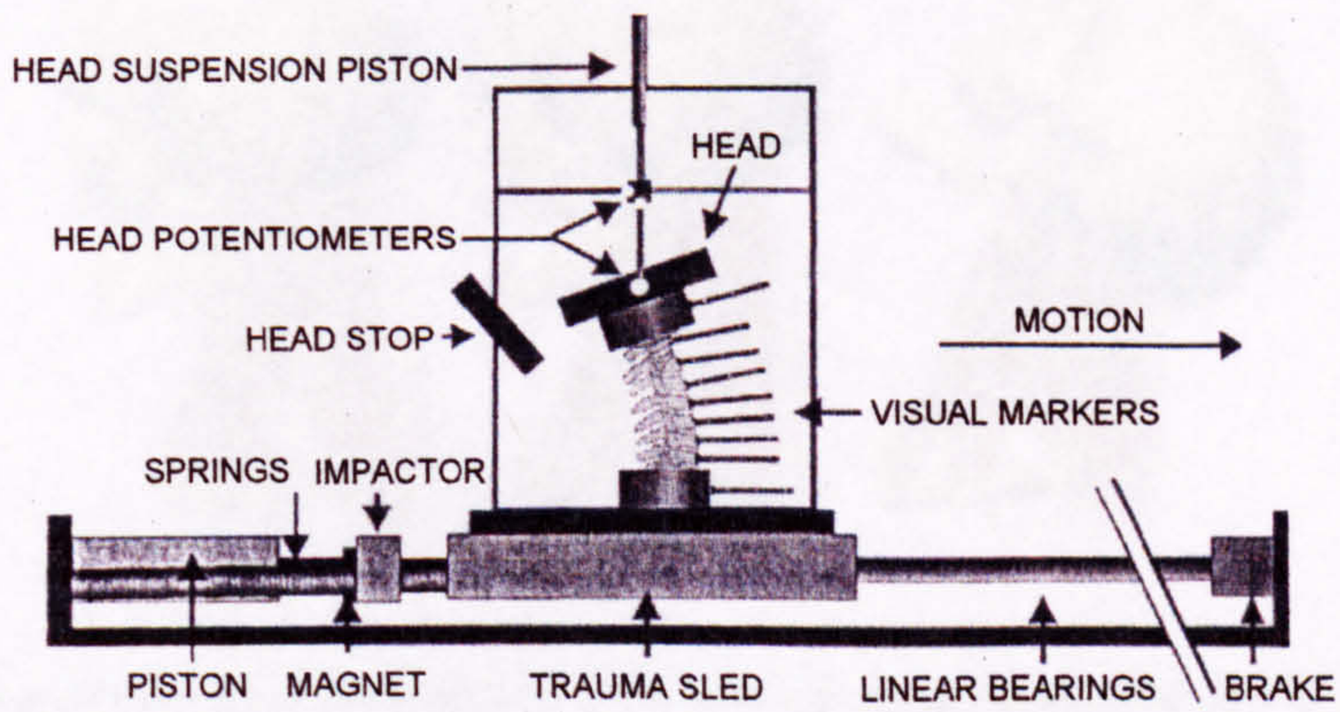

Figure 6.2 Experimental set-up (Grauer et al., 1997)

As simulation set-ups, all muscles were deactivated in the head-neck model. Physically, the muscles were kept on the model but their active and passive properties were deactivated. The motion of T1 was constrained so only translation along the x-axis was allowed. No gravitational effects were taken into consideration at this stage. The acceleration profiles are triangular with the same 105ms duration and corresponding peak accelerations (Figure 6.3). The resulting head rotations and translations are compared against the results for the 8.5g trauma class.

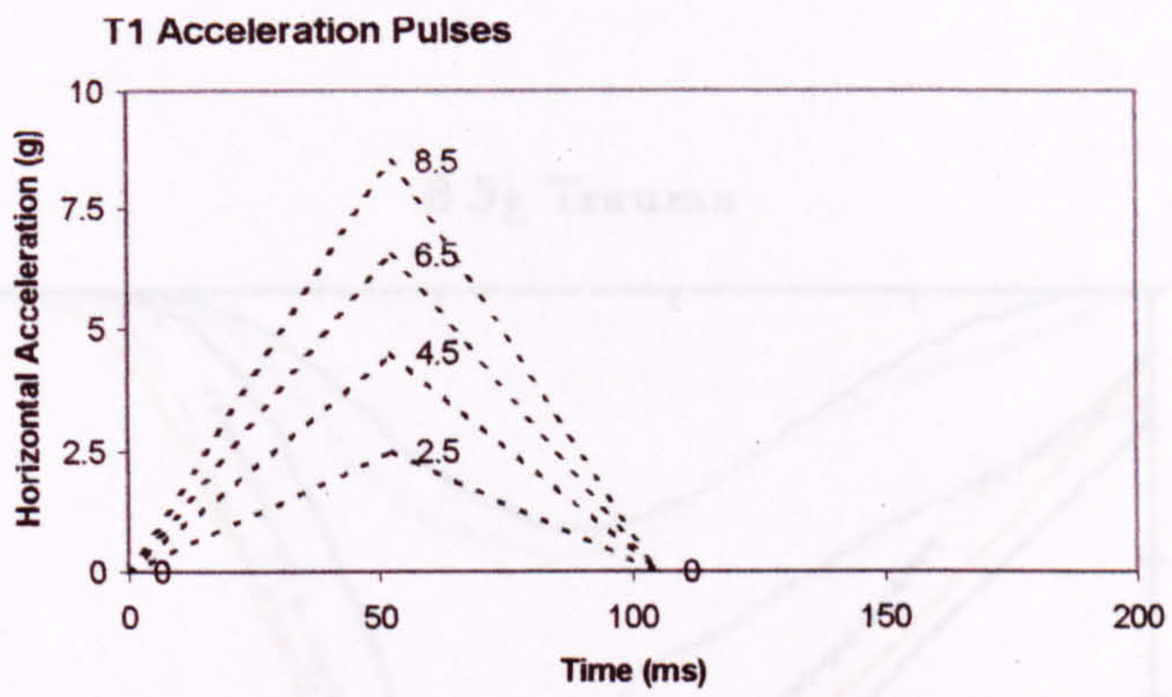

Figure 6.3 T1 acceleration profiles used as input to the cervical spine model

6.2 MB Model Simulation Results

The response of the ligamentous spine model to the 8.5g trauma acceleration is provided schematically in Figure 6.4.

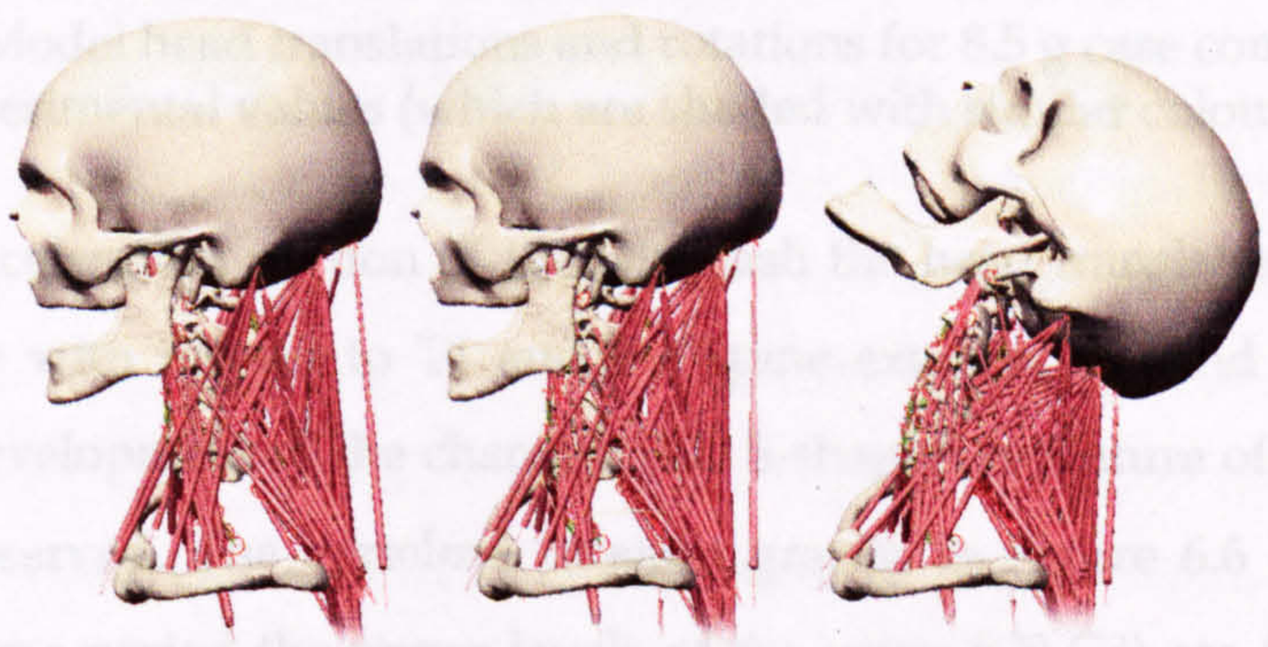

Figure 6.4 Response of the model to 8.5g whiplash acceleration for 0, 60, 120 ms (respectively, from left to right). Muscles were deactivated completely.

The head rotation and head vertical and horizontal translation for the 8.5g case compared to the experimental results of Grauer et al. (1997) is provided in Figure 6.5. The model showed a similar response to the cadaveric spine specimen, where head rotation follows a similar pattern but with a higher peak value. Following the maximum rotation and maximum posterior translation of the head, the model rebounds slightly slower than is seen with the spine specimen. The vertical displacement of the head with respect to the torso is in good agreement with the experimental results reaching a peak of around 6cm below the initial height.

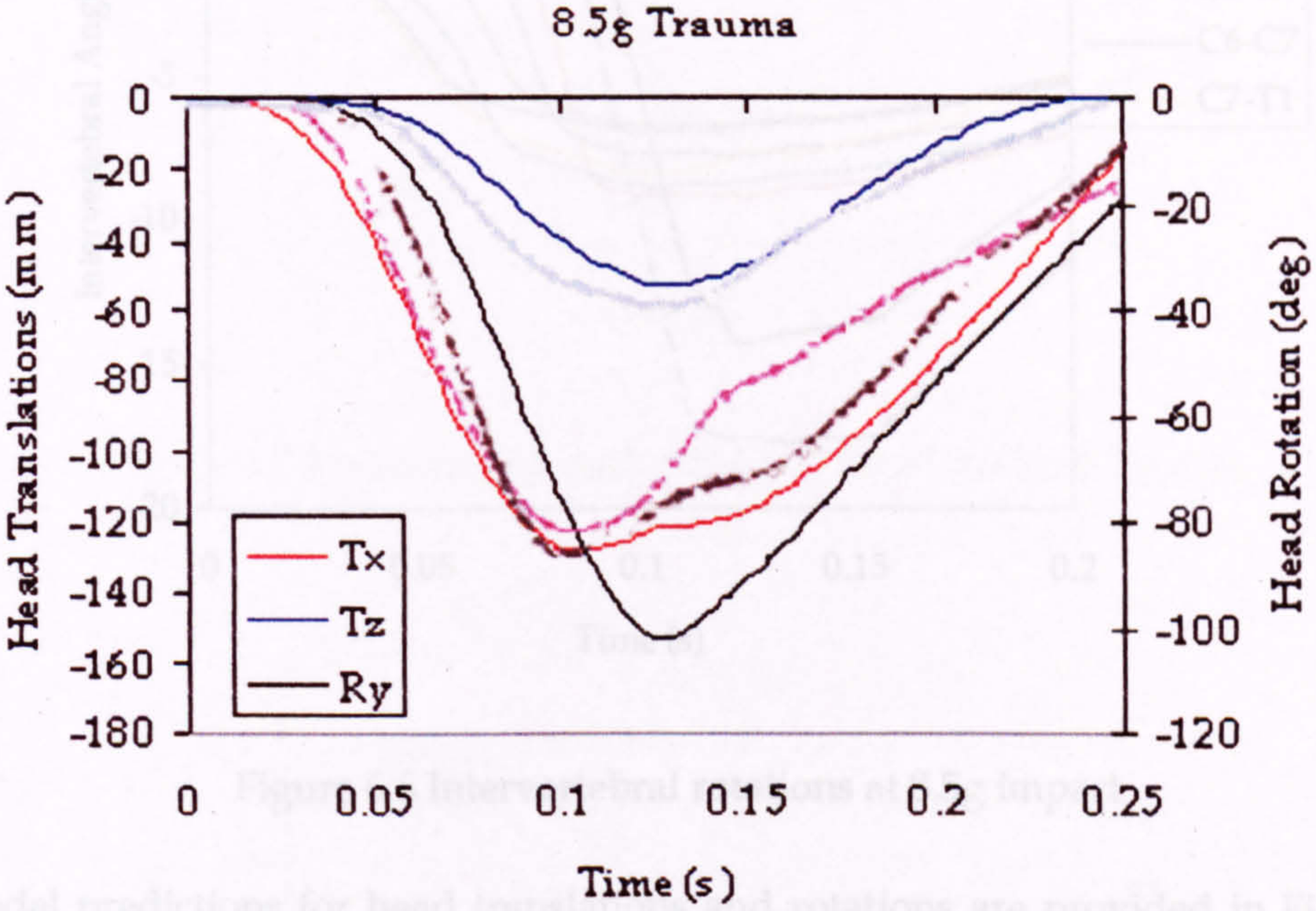

Figure 6.5 Model head translations and rotations for 8.5 g case compared to experimental values (which are shaded with similar colour)

During the acceleration portion of the whiplash the head translates posteriorly and inferiorly with respect to T1 and the spine extends. Around 60 ms time period, the development of the characteristic S-shaped curvature of the cervical spine was observed. The vertebral rotation graphs in Figure 6.6 depicts that during this time period the upper levels of the spine (C0-C3) are flexed while the lower levels (C5-T1) are extended as observed from the experimental results. In the 75-100ms time period, the upper vertebrae of the model change from

flexion to extension as the whole model becomes more and more extended into a C-shaped curvature as also observed in the experiments. Maximum extension of the head and neck was reached at approximately 130ms, slightly later than the experimental results. In the later stages of trauma the head returns towards its initial starting configuration.

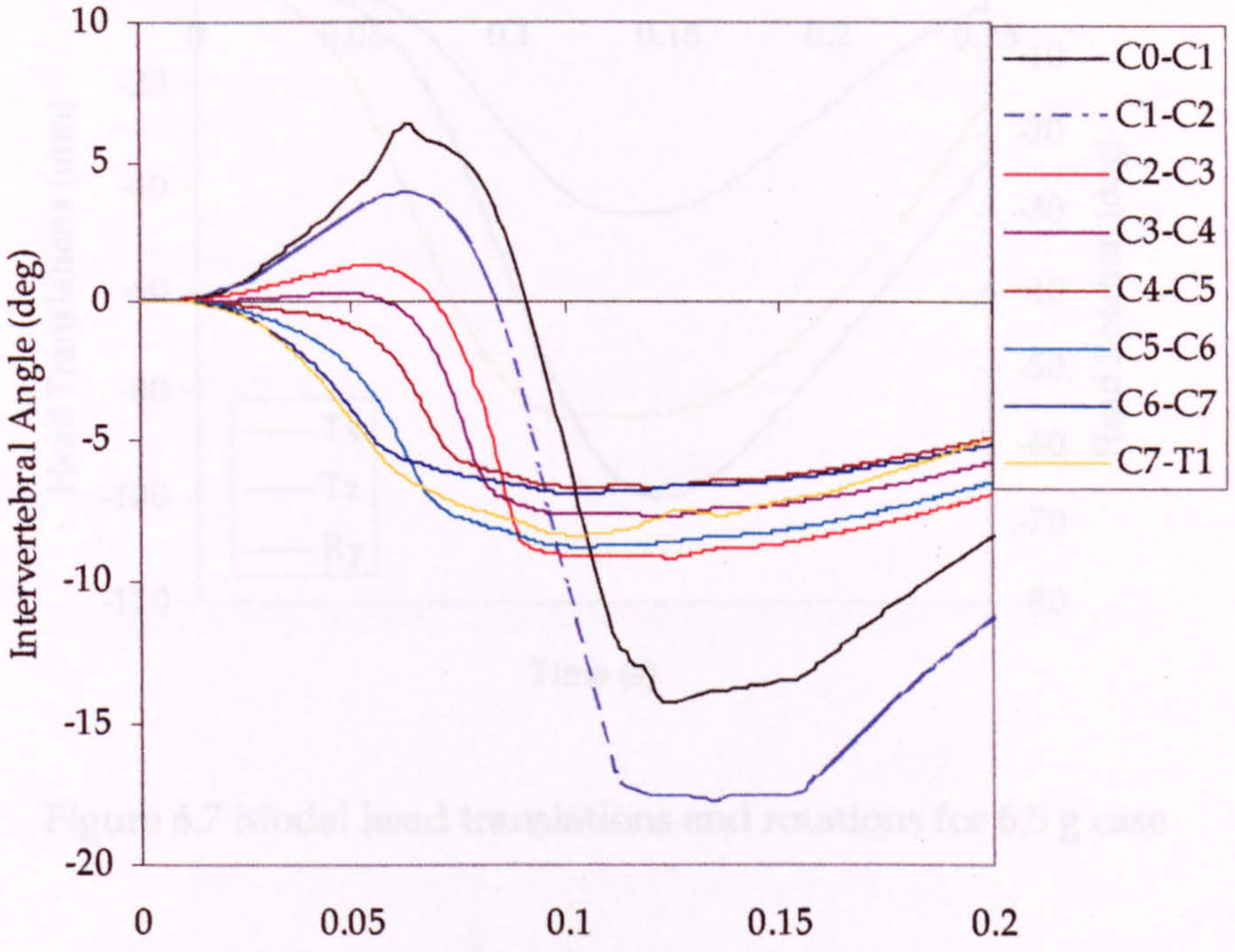

Figure 6.6 Intervertebral rotations at 8.5g impact

Model predictions for head translations and rotations are provided in Figures 6.7-6.9. From the graphs it was observed that the more severe the impact, the more the rotations and translations were. Figures 6.10-6.17 compare the maximum intervertebral rotations of the model for the four cases simulated with those reported for the spine specimens. For the upper three levels of the cervical spine, the graphs (Fig. 6.10-6.12) show that although the upper levels are initially forced into flexion in the model, the levels of flexion experienced are slightly smaller than the experimental values, which may be an indication of the model to be slightly stiff in flexion in these areas. The levels of extension experienced in the later stages of impact show better agreement with the experimental data. Figures 6.13-6.17 show the maximum intervertebral

extension rotations experienced by the lower five levels of the spine model. From the results, it appears that generally level C6-C7 appears to be too stiff when compared to the experimental results.

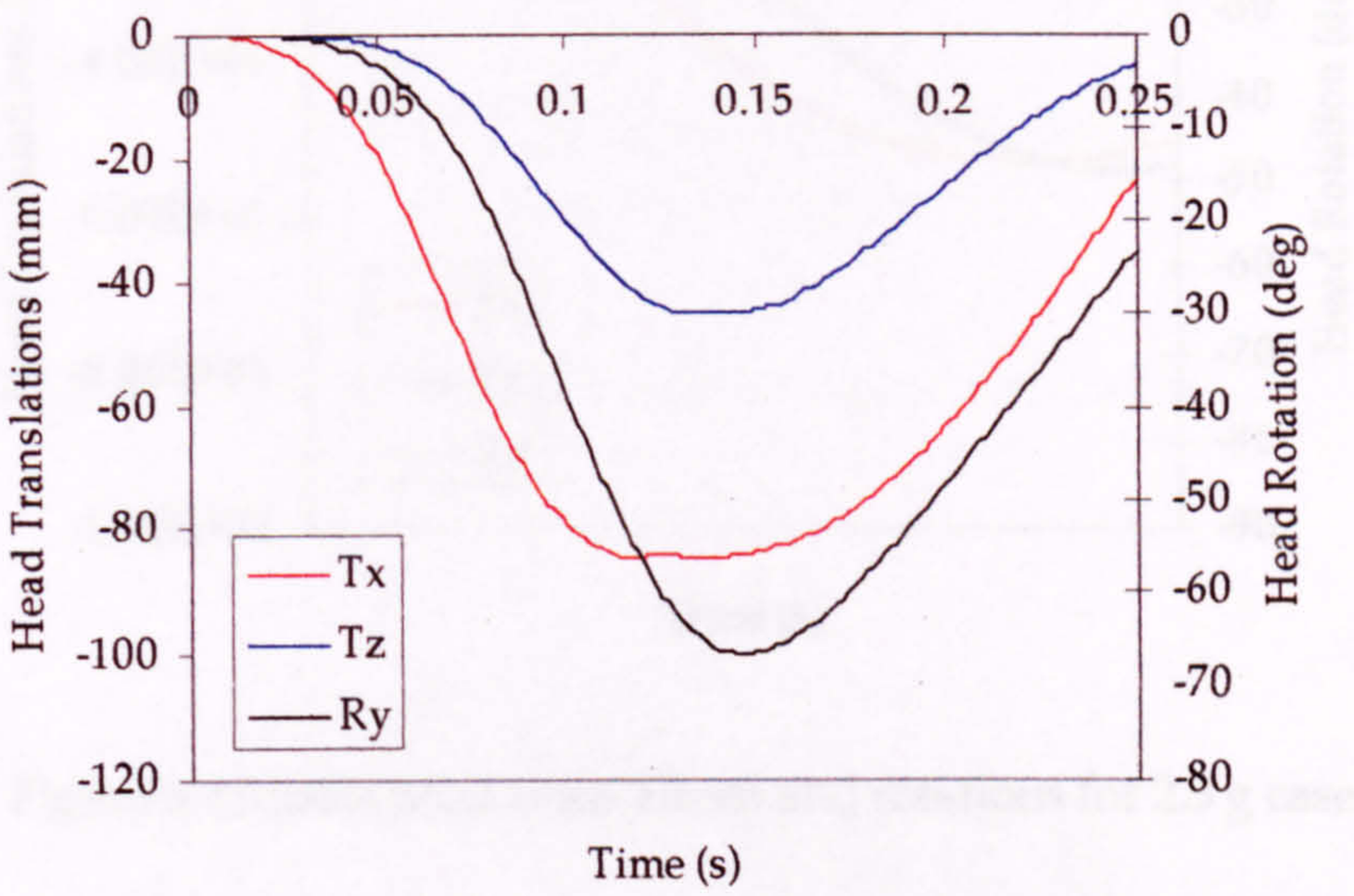

Figure 6.7 Model head translations and rotations for 6.5 g case

Figure 6.8 Model head translations and rotations for 4.5 g case

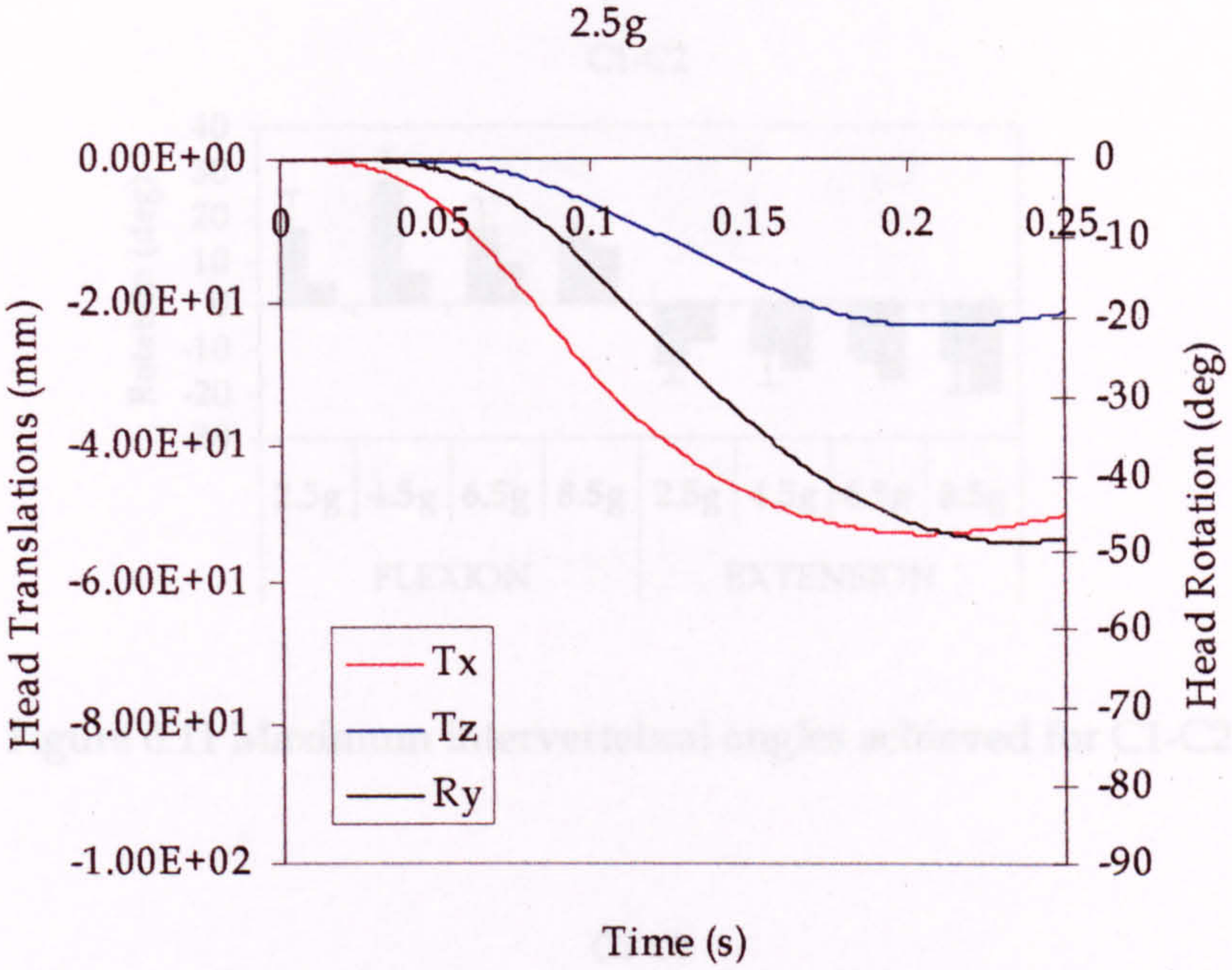

Figure 6.9 Model head translations and rotations for 2.5 g case

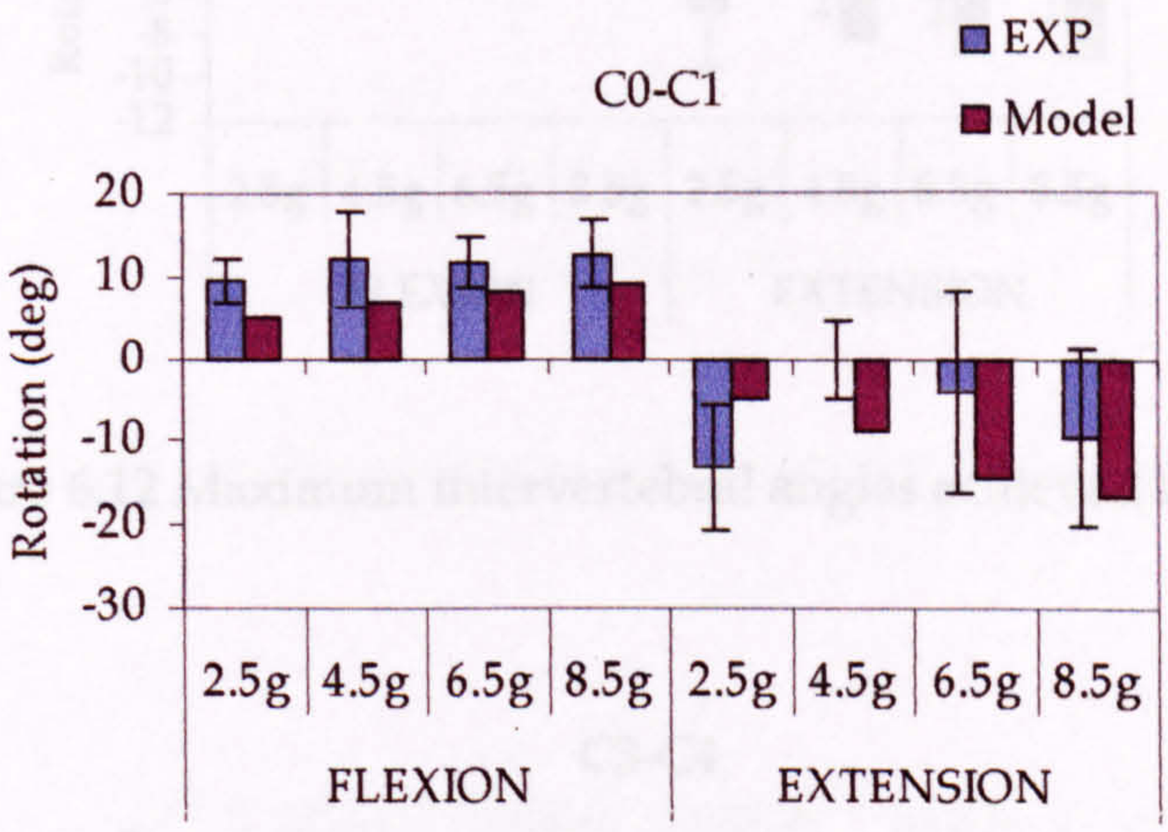

Figure 6.10 Maximum intervertebral angles achieved for C0-C1

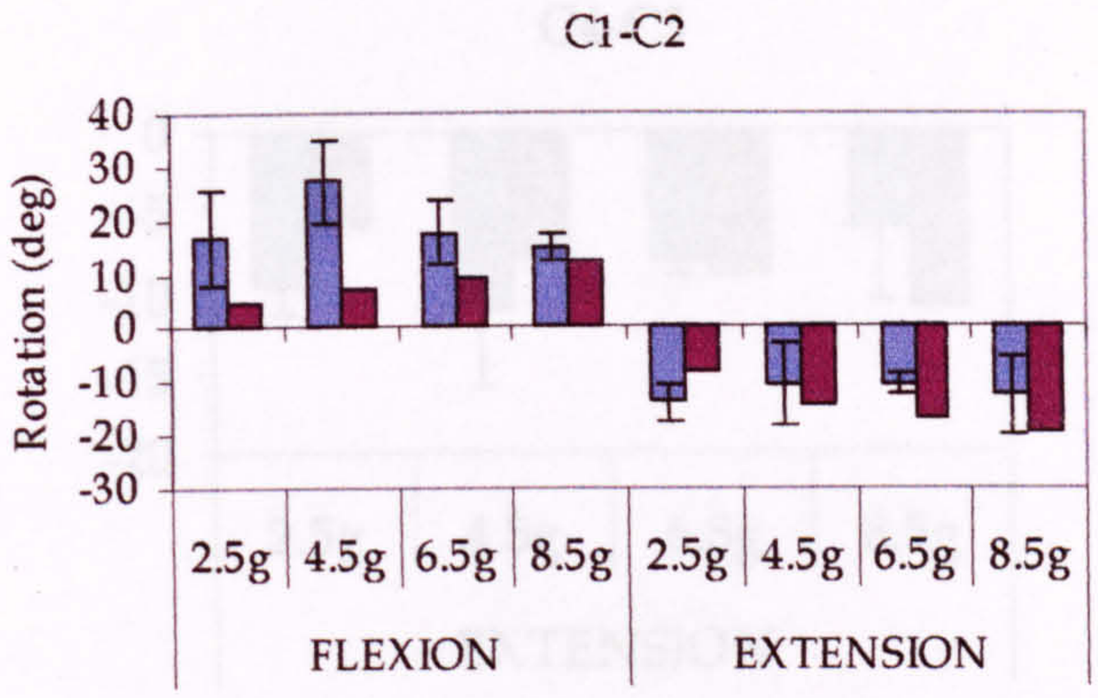

Figure 6.11 Maximum intervertebral angles achieved for C1-C2

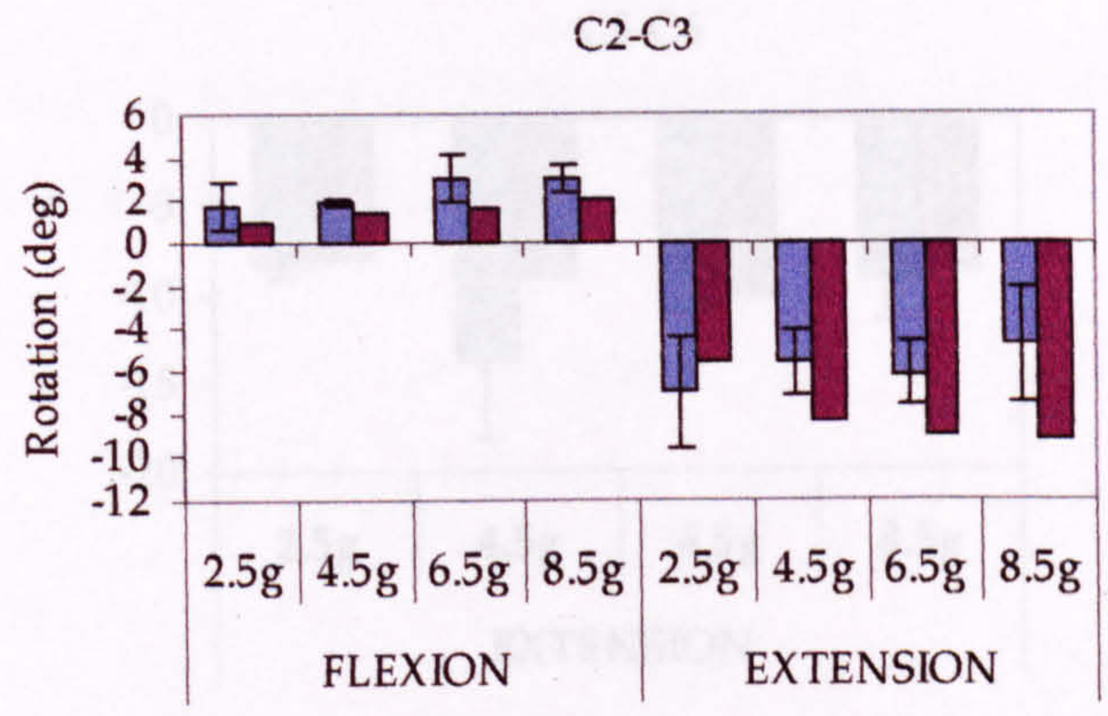

Figure 6.12 Maximum intervertebral angles achieved for C2-C3

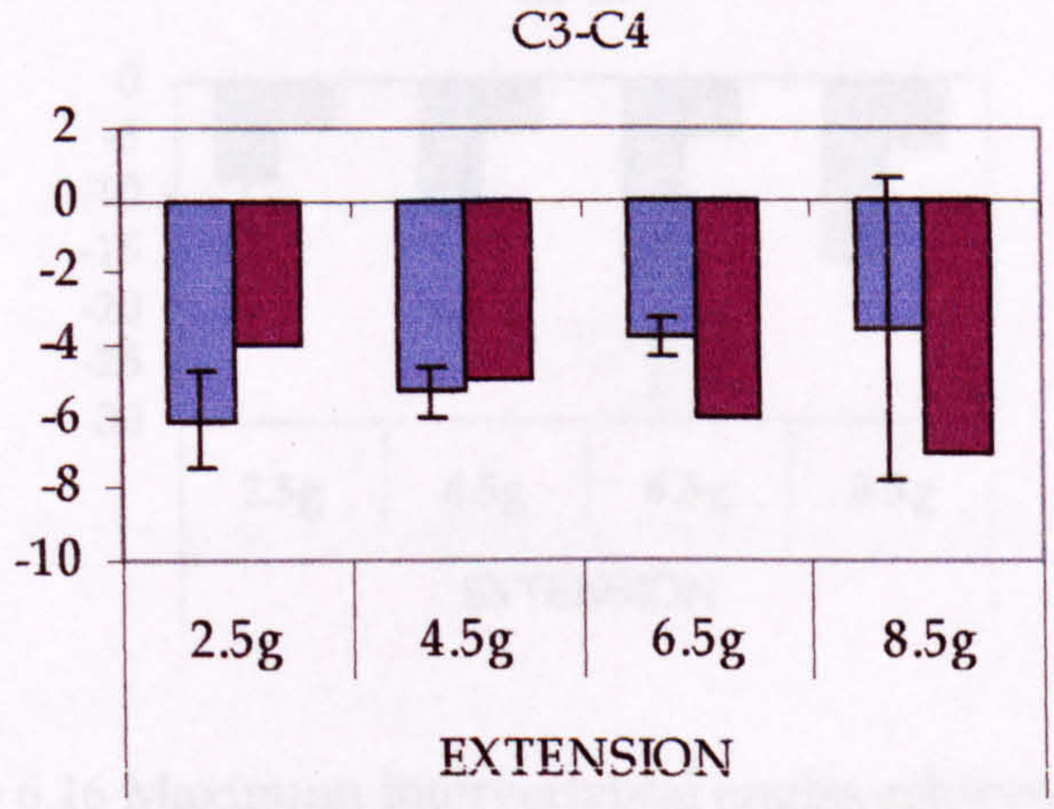

Figure 6.13 Maximum intervertebral angles achieved for C3-C4

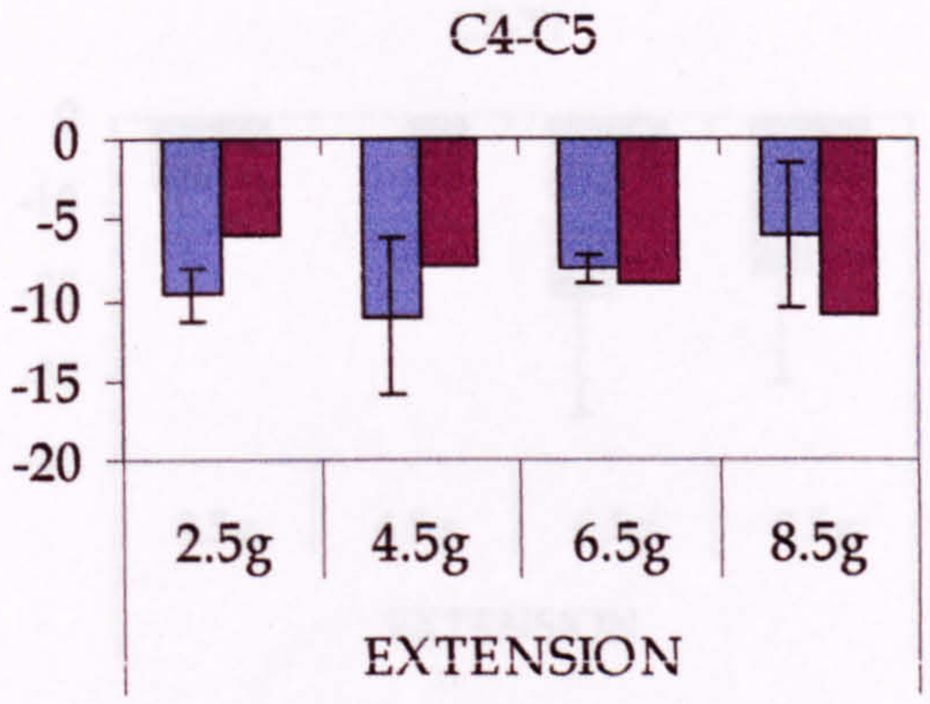

Figure 6.14 Maximum intervertebral angles achieved for C4-C5

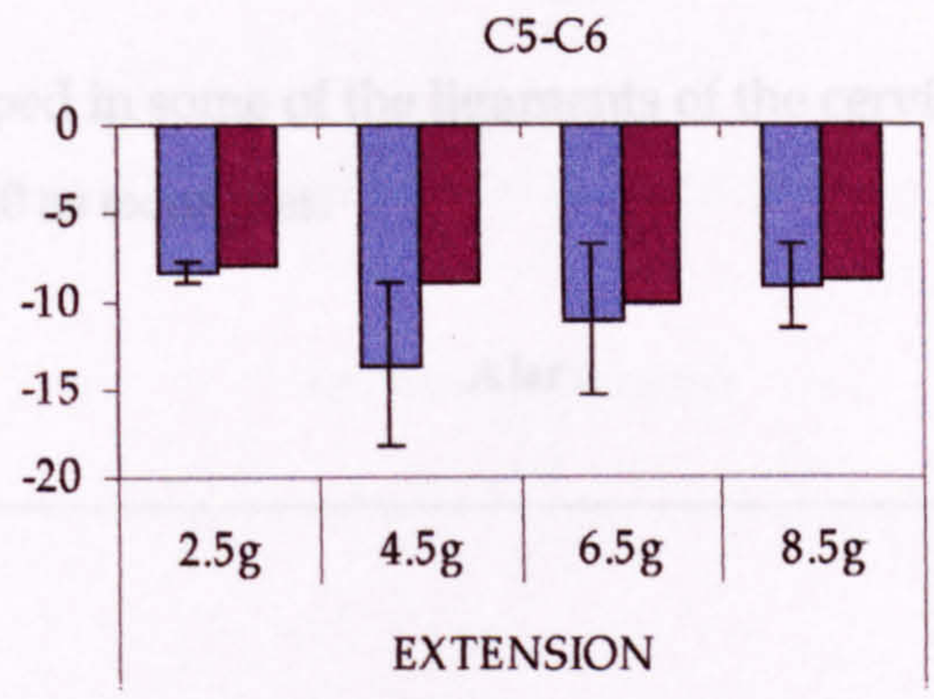

Figure 6.15 Maximum intervertebral angles achieved for C5-C6

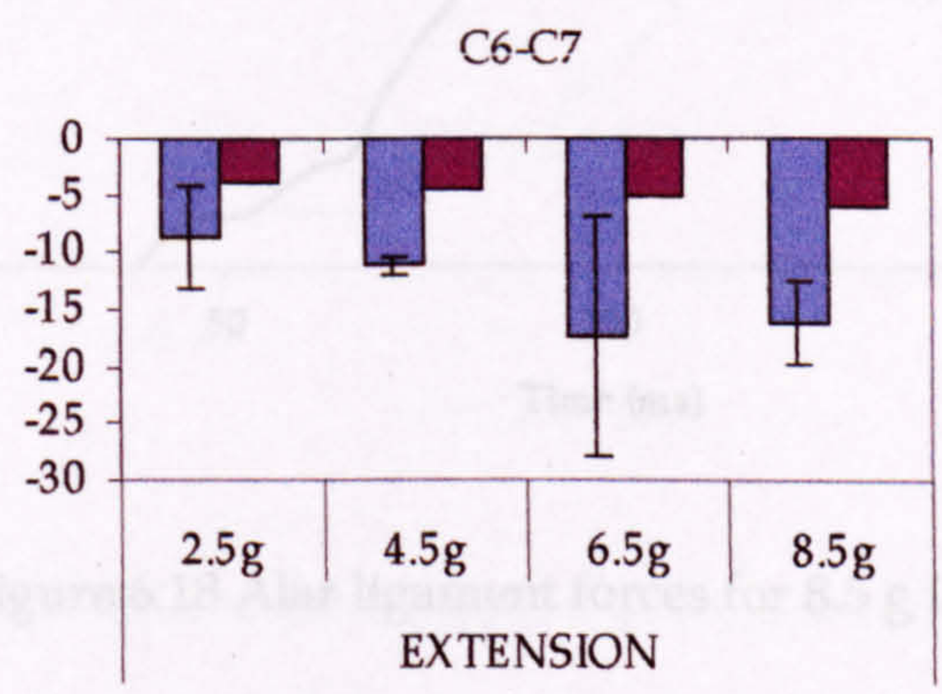

Figure 6.16 Maximum intervertebral angles achieved for C6-C7

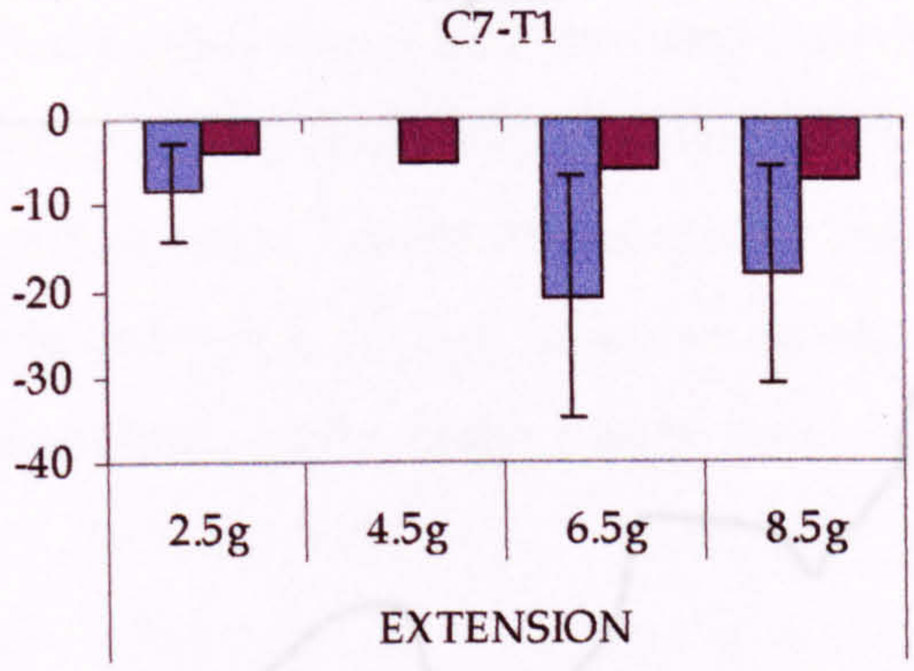

Figure 6.17 Maximum intervertebral angles achieved for C7-T1

6.3 Ligament Forces

The forces developed in some of the ligaments of the cervical spine are provided in Figures 6.18-6.20 as examples.

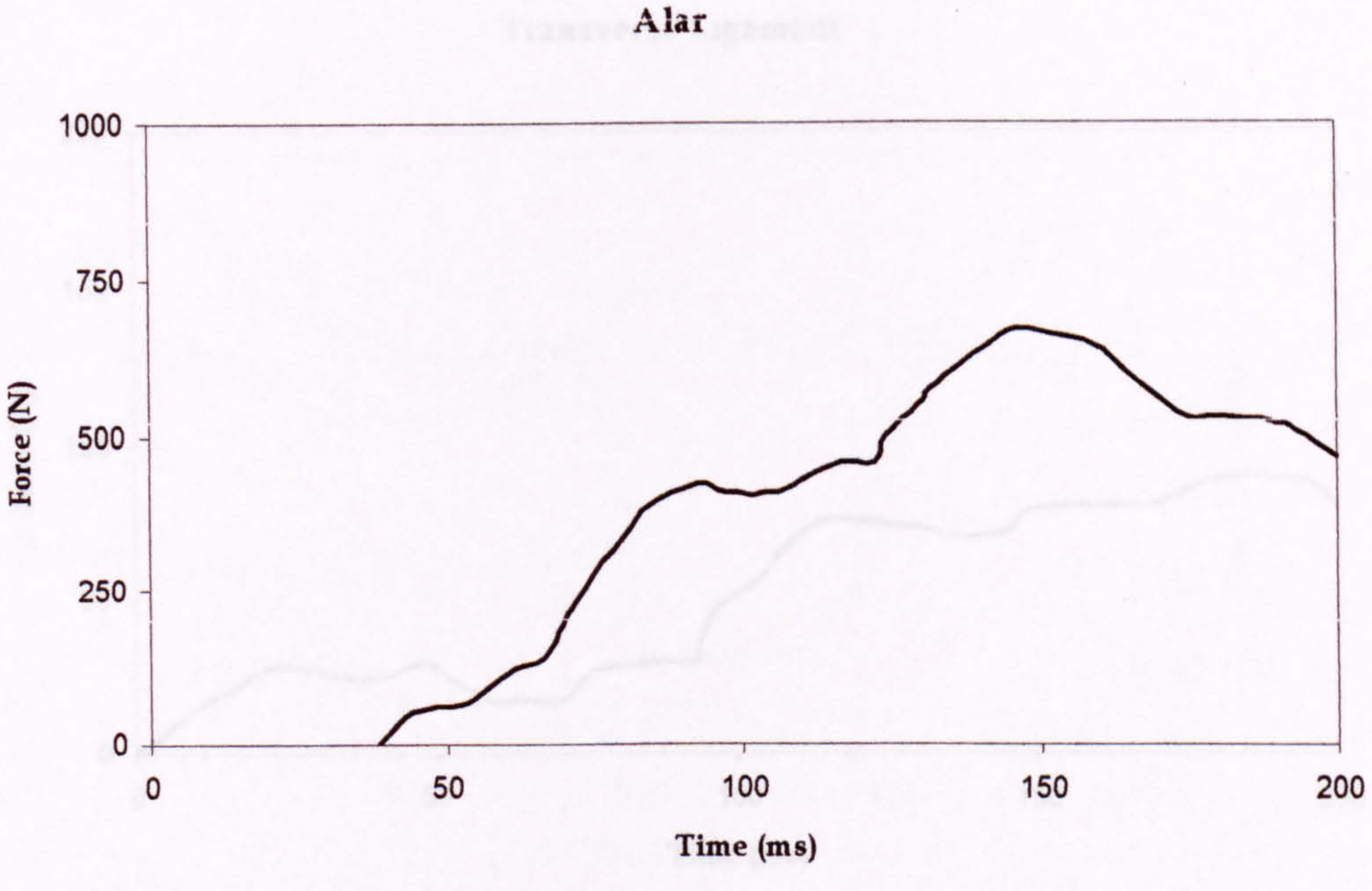

Figure 6.18 Alar ligament forces for 8.5 g impact

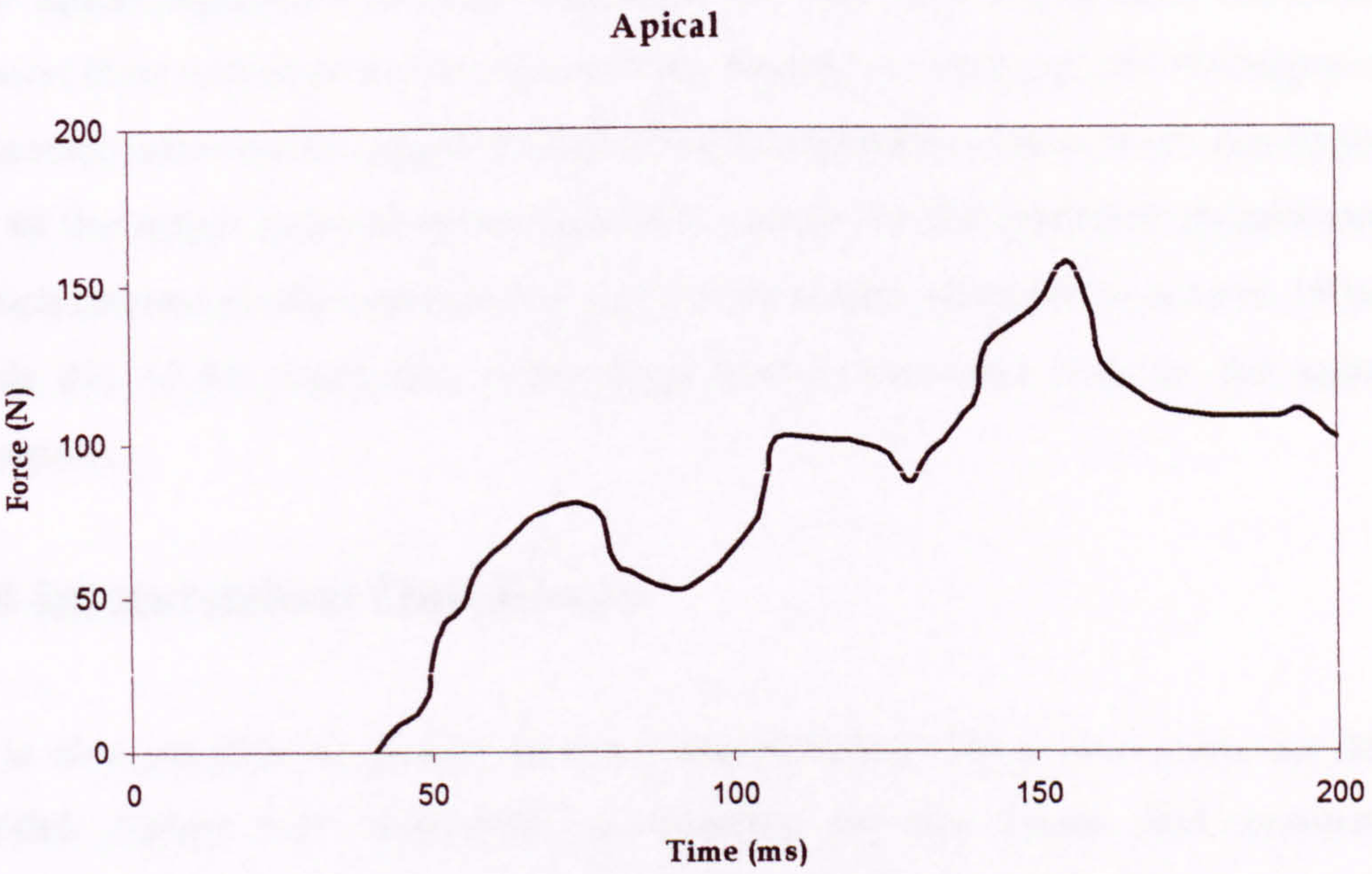

Figure 6.19 Apical ligament forces for 8.5 g impact

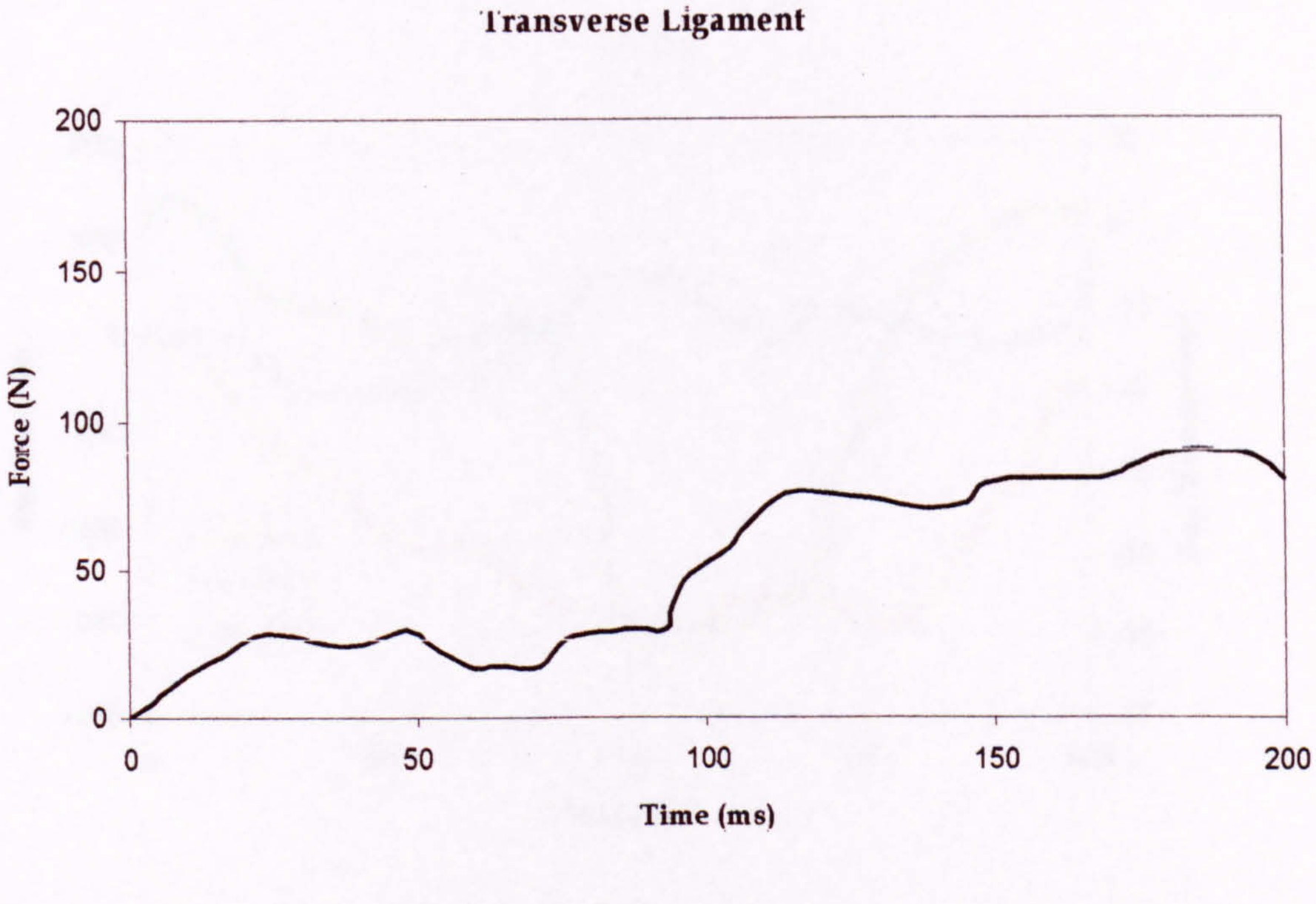

Figure 6.20 Transverse ligament forces for 8.5 g impact

The anterior longitudinal ligaments at all levels experience rapid loading as the lower vertebrae are in extension. The posterior ligaments (PLL, FL and ISL) at all levels below C4 remained unloaded for the duration of the 200ms simulation.

The apical ligaments became loaded as the two joints approach maximum flexion then unloaded as they move from flexion to extension. As the degree of extension between the upper joints increased significant forces were developed in all the upper cervical spine ligaments except for the posterior membranes, which became totally unloaded. A peak in force was observed at around 150ms with the ALAR ligaments while large forces were also seen in the apical ligament.

6.4 Intervertebral Disc Forces

It is also possible to gather dynamic intevertebral disc forces from the MB model. Figure 6.21 illustrates an example for the forces and moments experienced by the intervertebral discs during 200ms impact. As was the case with the frontal impact, no forces were developed in lateral shear and moments were seen about the y-axis only.

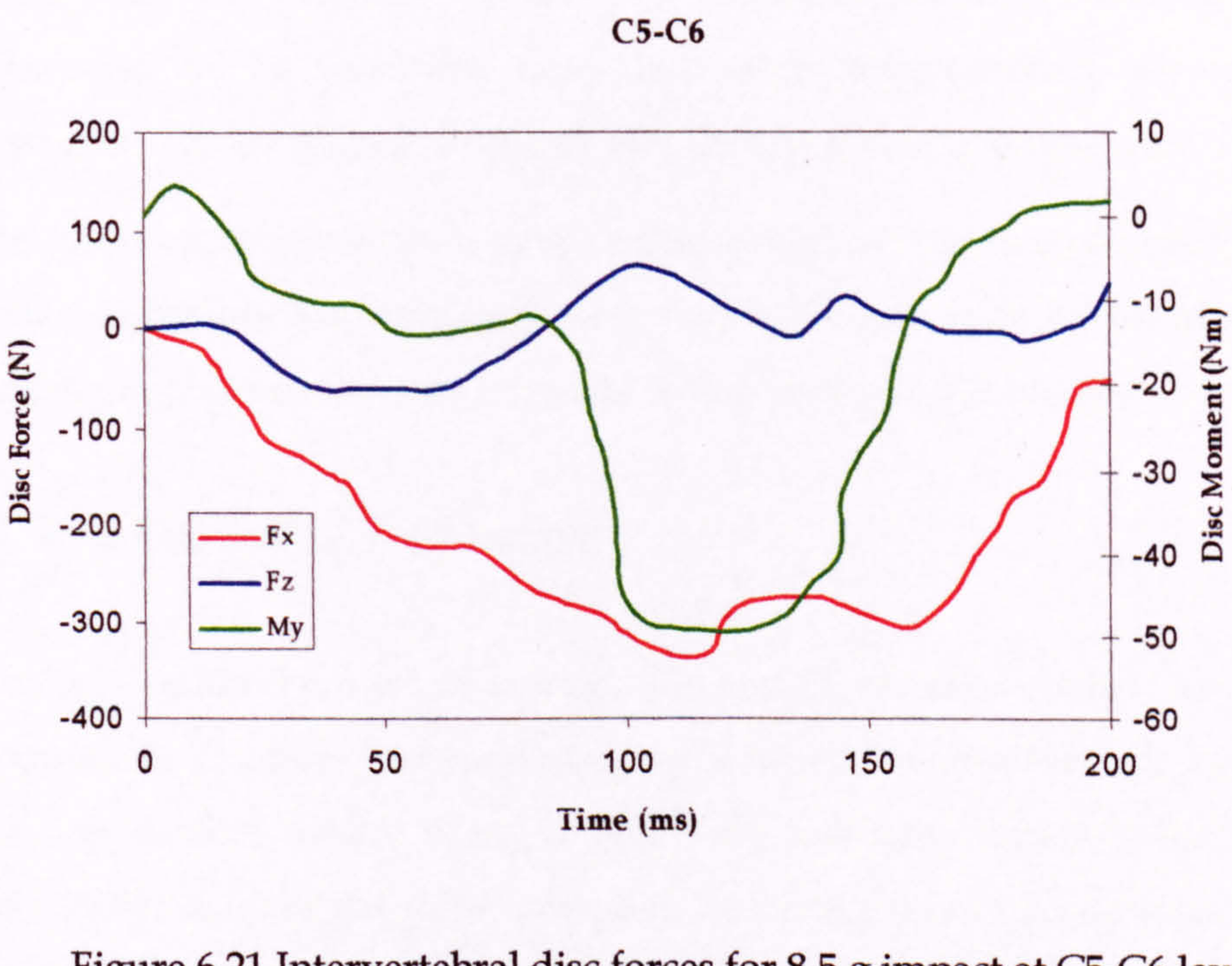

Figure 6.21 Intervertebral disc forces for 8.5 g impact at C5-C6 level

6.5 Discussion

This chapter shows that the MB model can also be used to simulate a ligamentous cervical spine undergoing whiplash trauma. The MB model devoid of muscles was reasonably validated against test results, while most of the simulation results and model predictions showed good agreement with experiments. The model successfully reproduced the characteristic motion of the head and neck when subjected to rear-end impact. The differential movement between the head and T1 caused initial flexion in the upper joints as the head translated backward, without rotation, relative to T1. The formation of this 'S' shaped curvature of the neck with flexion of the upper and extension of the lower joints is typical of 'whiplash' motion, which does not occur under normal physiological movements of the head. Following the development of the 'S' curve, the neck then goes into extension at all levels as the head rotates rearward to a point of maximum extension.

CHAPTER 7

Finite Element Models of the Intervertebral Discs

This chapter covers the use of finite element method in order to investigate intervertebral discs under various loading conditions. Several FE models were gradually developed from simpler ones to more advanced models, incorporating different modelling parameters and techniques each time. Each model has the potential to serve a different purpose, yielding several advantages in its particular case, but often compromising several other parameters for the sake of simplicity and computational requirements.

Also, this chapter presents a proposed approach utilizing multi-body and FE models in conjunction with each other and is thought to be highly novel as an application of it was not seen in spinal biomechanics in the literature.

7.1 The Proposed Approach

In order to make the most of separate MB and FE models, a hybrid approach is proposed to combine two modelling techniques. The approach is basically a one-way method, where firstly a rigorously validated highly detailed multi-body (MB) model of the spine is used to simulate a particular dynamic loading condition. The predictions of the MB model as a result of these simulations such as intervertebral disc loadings will be used as loading boundary conditions for the FE models of the individual elements of the human cervical spine, such as the intervertebral discs. As it is practically almost impossible to determine what these loadings on the discs in a dynamic impact situation are, the validated MB

model will act as a realistic and biofidelic source for determining these loadings on each and every one of the spinal elements, such as intervertebral discs, ligaments, or muscles.

This approach not only helps to visualise the global and local kinematics and kinetics of the human spine via the MB model, but also avoids the modelling, validation and computational power complications of a possible complicated FE model of the whole human spine.

7.2 First Model: A Disc Segment Investigation

In order to investigate a disc segment, and the effects of various loading conditions over the intervertebral disc and the elements of the vertebra, a finite element model is developed by using the commercially available software, Marc/Mentat 2000. The model is one quarter of a functional spine unit, namely two vertebrae and an intervertebral disc, having lateral and sagittal symmetry planes.

The nonlinear model is a three-dimensional finite element model of the L3-L4 spinal segment. All parts of the FSU model were modelled as 8 node brick elements. Only the cortical shell was modelled as 4 node shell elements. The intervertebral disc mainly has two parts; nucleus and annulus fibrosus. In the model all annulus fibrosus are modelled as composite materials with a fibre orientation of 30° with respect to the horizontal axis.

Material properties were taken from a similar study carried out by Lee et al. (2000) (Table 7.1). The loading is assumed to be an impulsive point load of 3000 N. (Figure 7.1).

Table 7.1 Material properties of the disc (Lee et al., 2000)

Material	Young's Modulus (MPa)	Density (kg/mm³)	Poisson's Ratio	Void ratio	Permeability
Cortical Bone	10000	1.83E-06	0.25	-	-
Cancellous Bone	100	1.00E-06	0.25	4	1.0E-10
Endplate	10000	1.83E-06	0.25	4	1.0E-14
Annulus Matrix	0.8	1.20E-06	0.35	3	1.0E-15
Annulus Fibres	175	2.00E-06	-	-	-
Nucleus	0.5	1.36E-06	0.35	6	1.0E-13
Fluid in spinal segment	-	1.00E-06	-	-	-

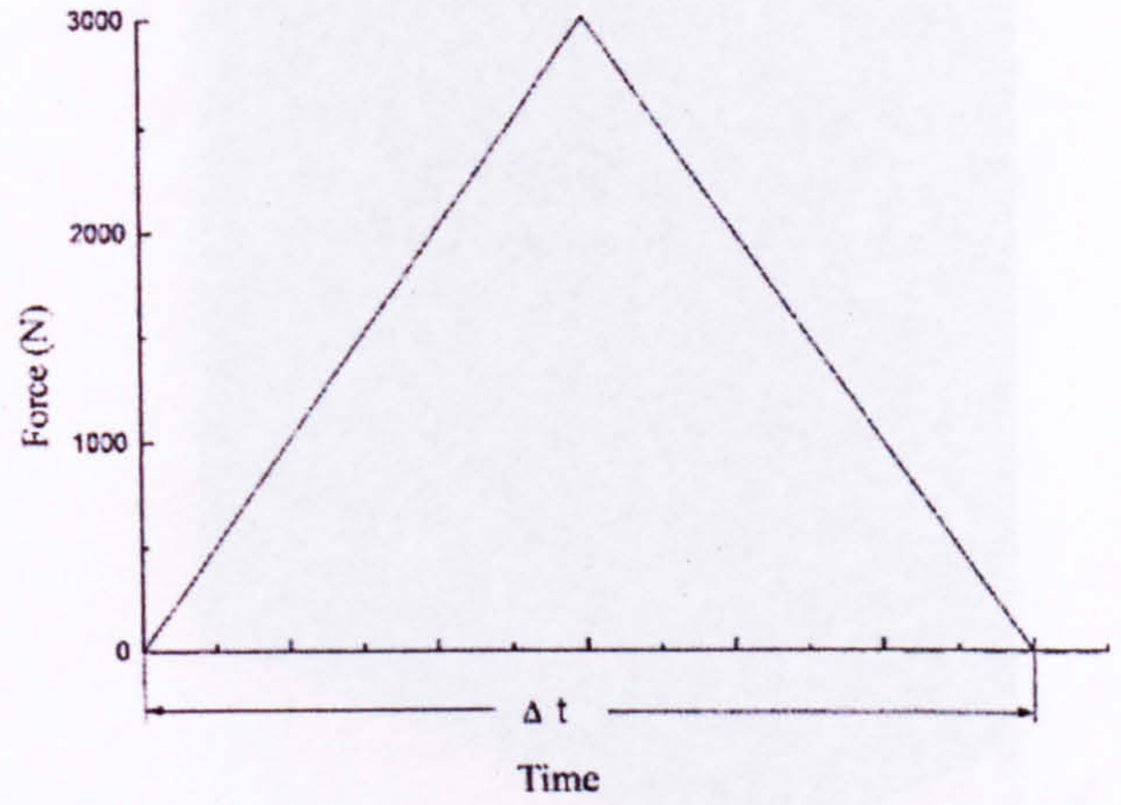

Figure 7.1 The shape of the impulsive force (Lee et al., 2000)

The FE model and the boundary conditions applied are presented in Figures 7.2 – 7.3.

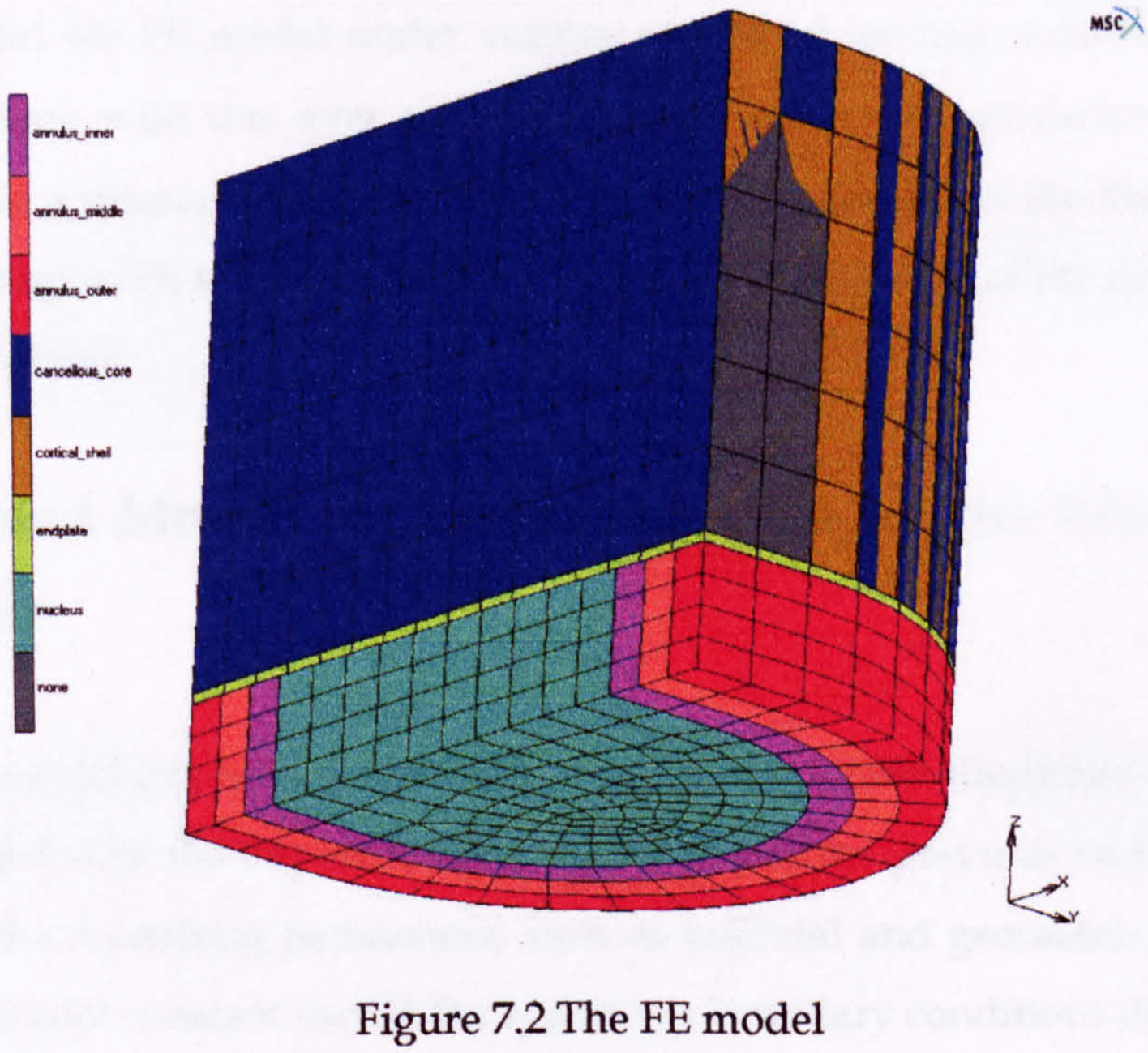

Figure 7.2 The FE model

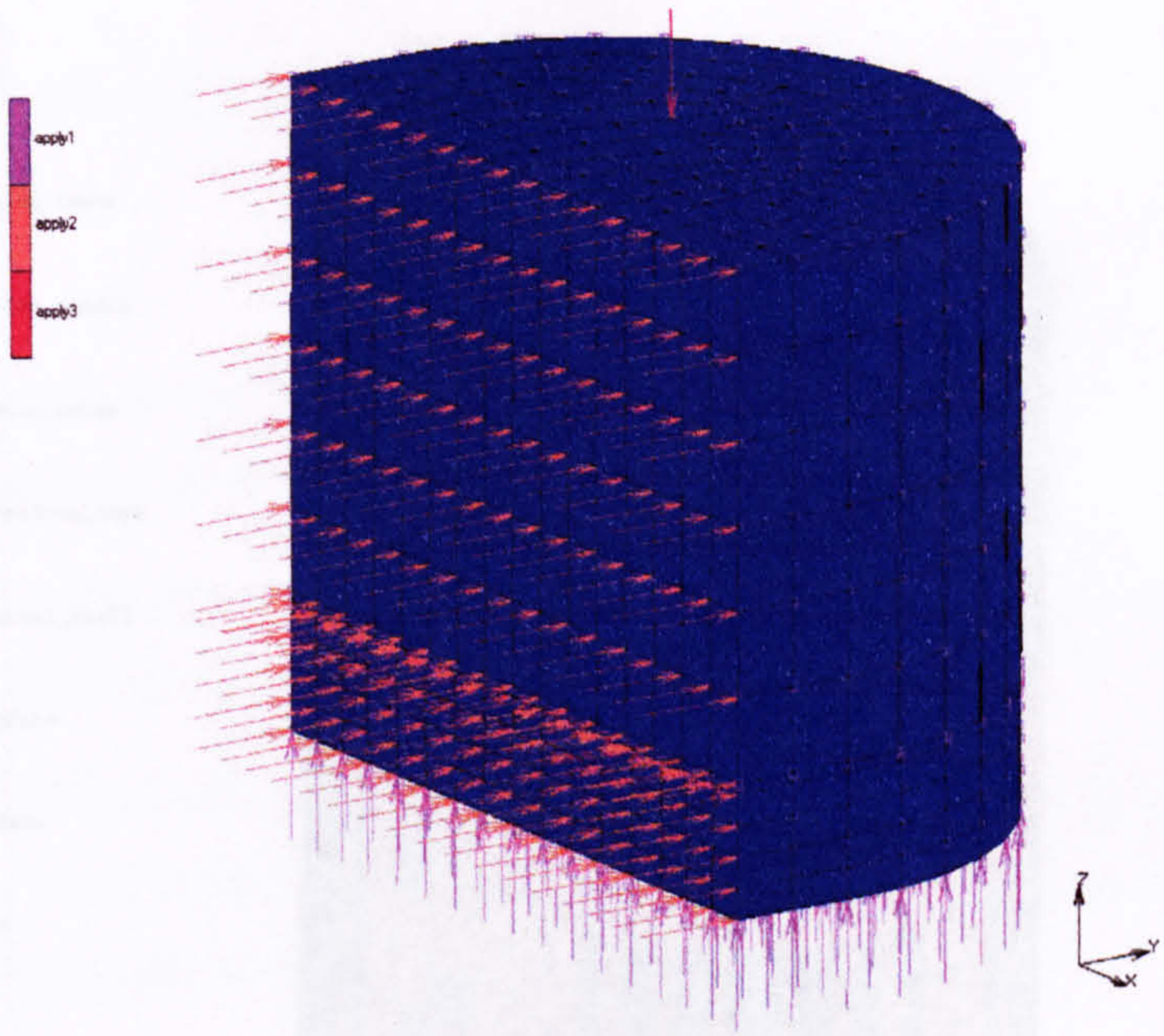

Figure 7.3 The boundary conditions

In order to have a global insight over the results of the FE analyses and to be able to load the FE model under various combined loading conditions, rather than working with this over simplified model, although satisfactory in some cases, there appeared a need for the whole simplistic model of the disc segment. The next step in FE modelling is the whole simplified model of the disc segment motion segment.

7.3 Second Model: An FE Investigation on the Whole Disc Segment

The first model has been extended to develop the whole simplified model and then loaded with the impact loading mentioned in the previous section (Figure 7.4). All the modelling parameters, such as material and geometric properties, have been kept constant except the symmetry boundary conditions illustrated in Figure 7.3, as the new model is a whole disc segment. The equivalent von Mises stress distributions of the disc under a compressive impact load of 3000 N for a duration of t=5 ms have been given in Figure 7.5.

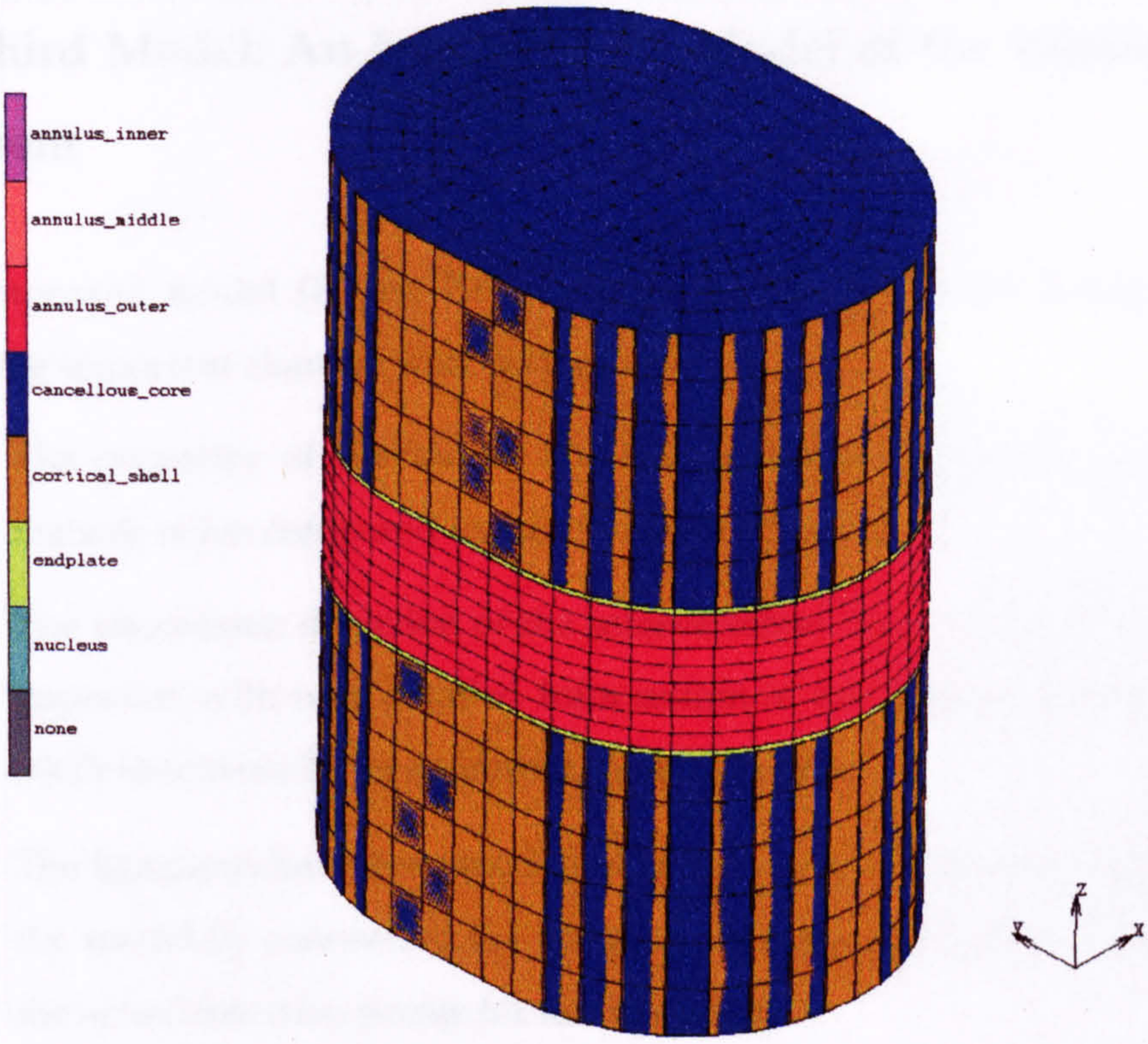

Figure 7.4 The whole FE model of the FSU

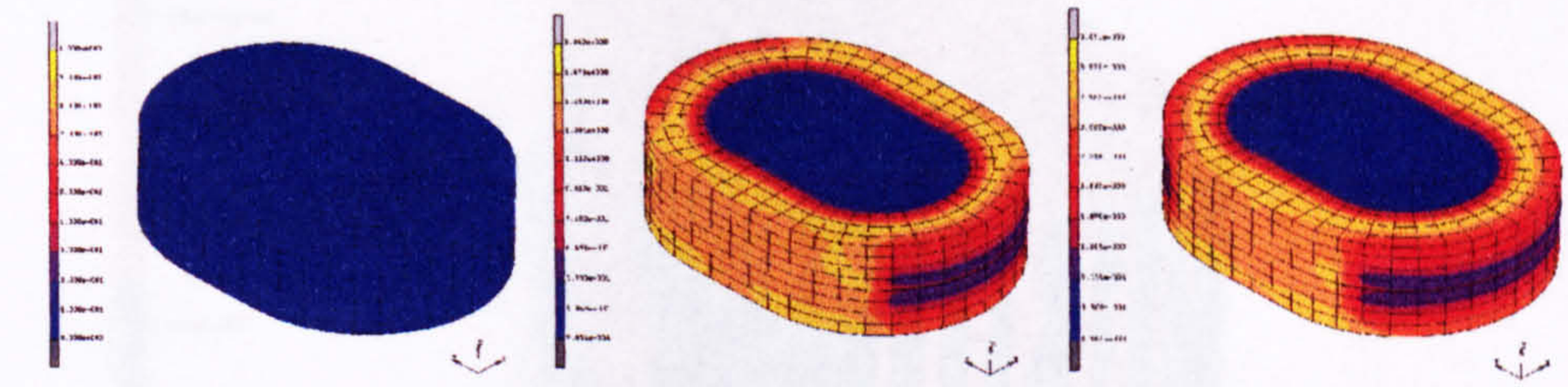

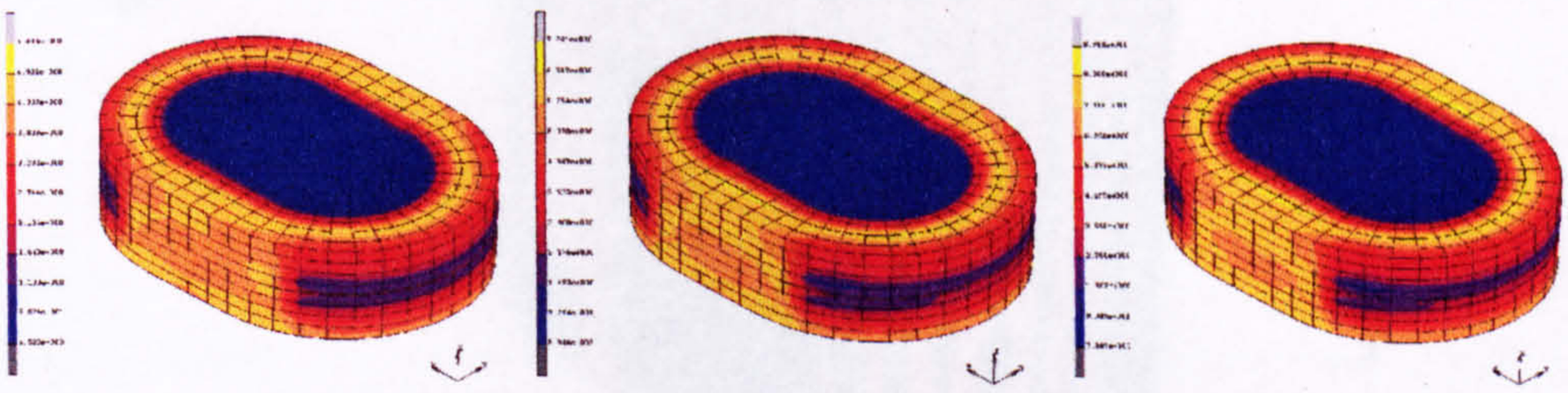

Figure 7.5 The equivalent von Mises stress distributions of the disc under a compressive impact load of 3000 N for a duration of t=5 ms

7.4 Third Model: An Improved FE Model of the Whole Disc Segment

This improved model (Figure 7.6) is based on the 2nd model; however, the following important changes were carried out.

- The geometry of the model and the necessary dimensions are more realistic when compared to the 2nd whole FE model.
- The viscoelastic depiction of the intervertebral disc (Figure 7.7) has been improved with new detailed information in the literature (Wang et al., 2000) to achieve better representation of the disc.
- The ligaments have been modelled as links (Figure 7.8) and integrated to the model by connecting the links between specific nodes, representing the actual insertion points for the ligaments.

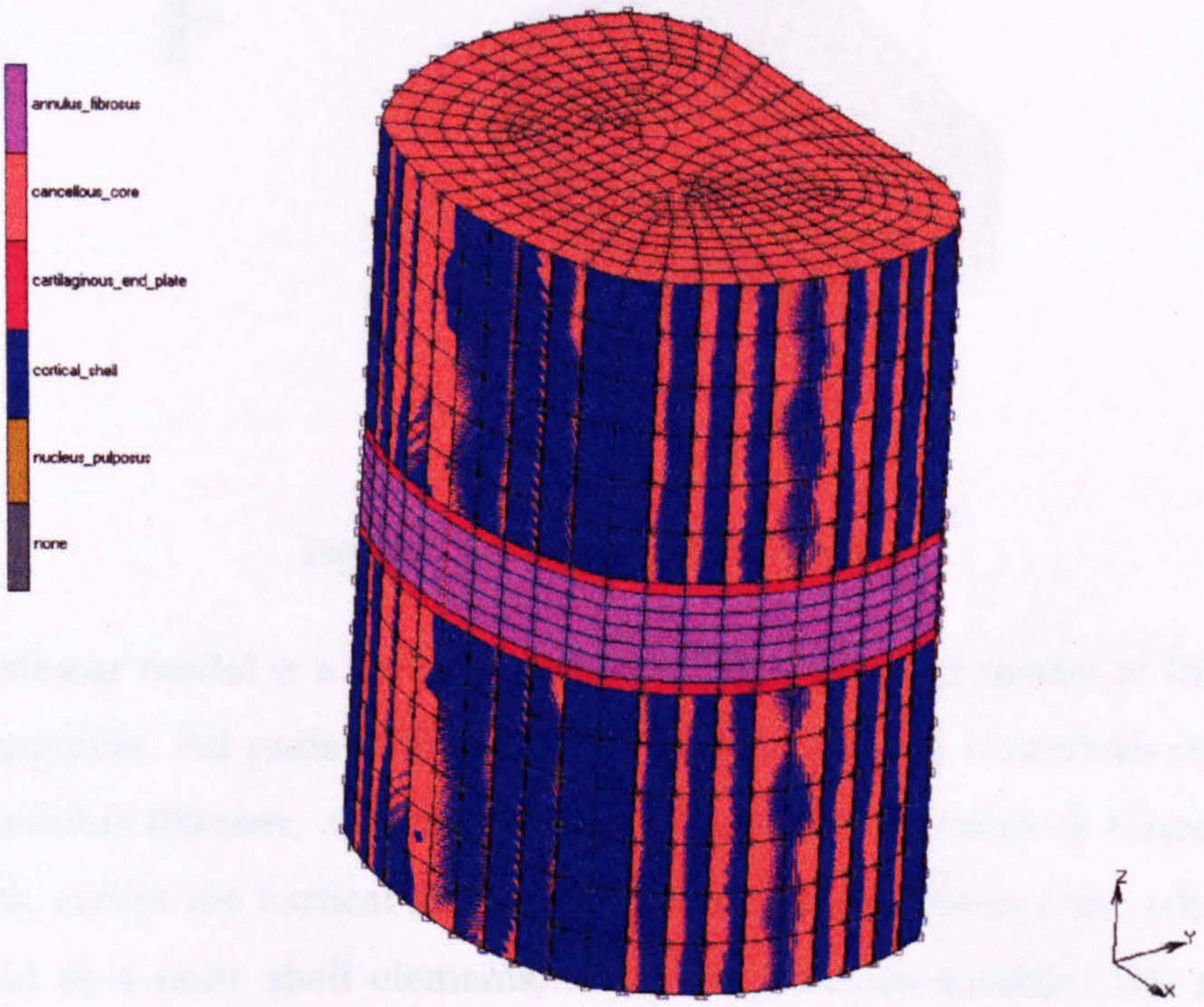

Figure 7.6 The improved model of L2-L3 disc segment

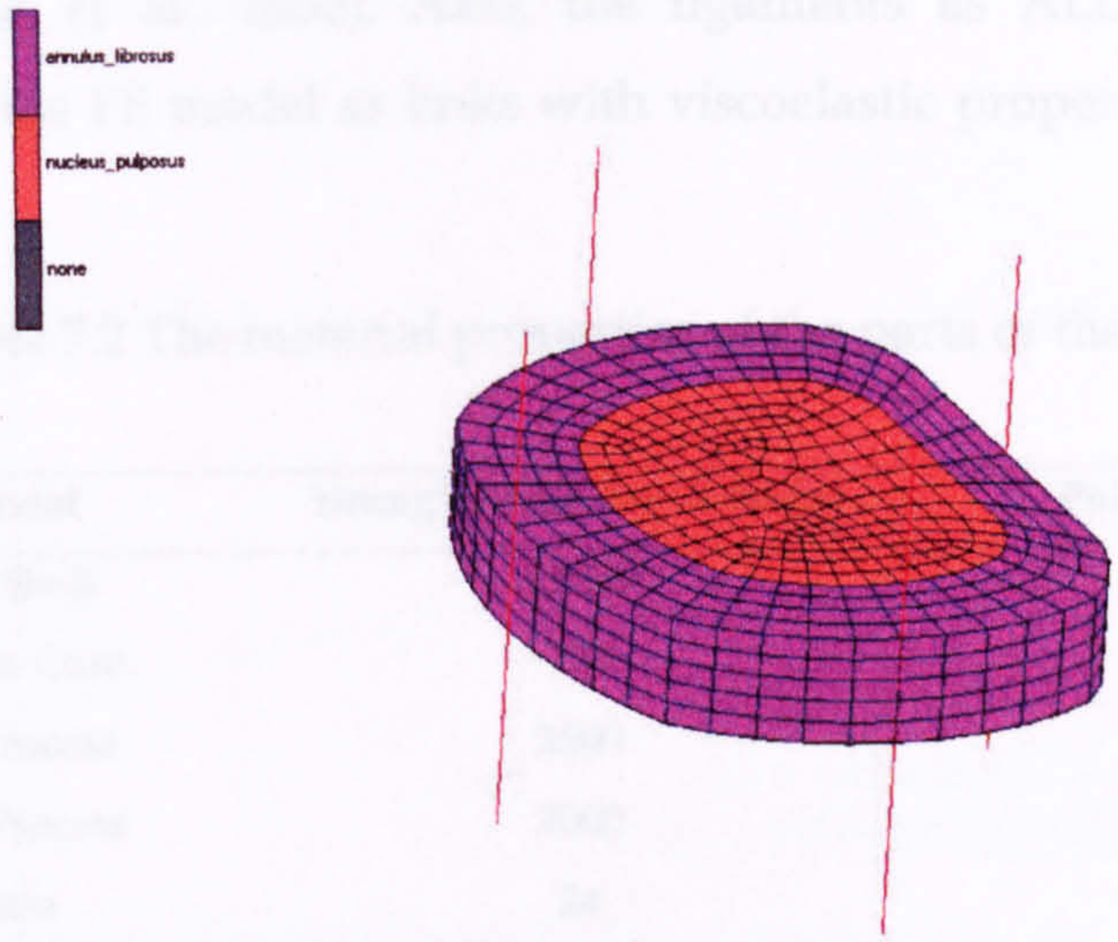

Figure 7.7 The disc, composed of nucleus and annulus

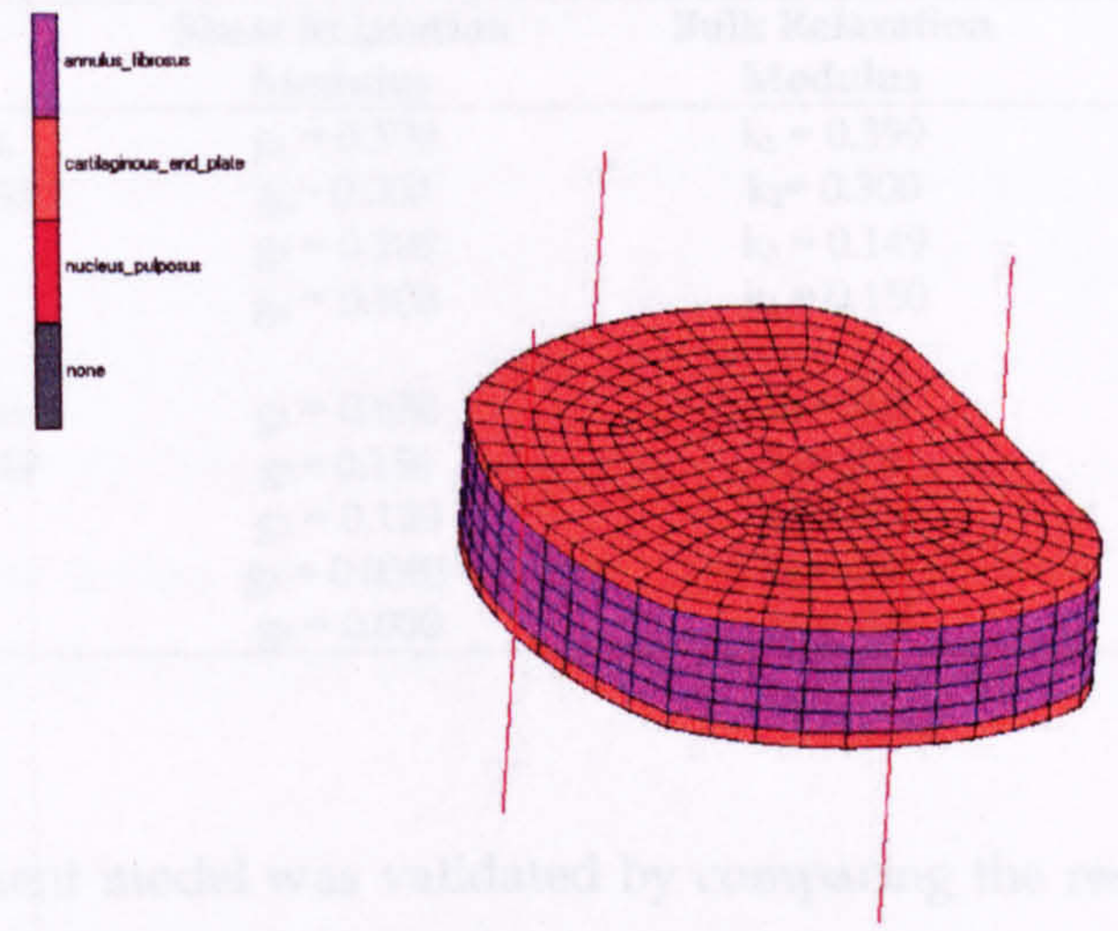

Figure 7.8 The ligaments as links

The nonlinear model is a three-dimensional finite element model of the L2-L3 spinal segment. All parts of the disc segment, which are cancellous core, end plate, annulus fibrosus, and nucleus pulposus were modelled as 8 node brick elements, except the cortical shell surrounding the cancellous core, which was modelled as 4 node shell elements, as in the previous models. The material properties of the parts of the disc segment except the disc were taken from the literature (Wang et al., 2000) (Table 7.2). In the FE model, all annulus fibrosus were modelled with a fibre orientation of 30° with respect to the horizontal axis.

The viscoelastic material properties of the disc (Table 7.3) were taken from the literature (Wang et al., 2000). Also, the ligaments as ALL and PLL were integrated into the FE model as links with viscoelastic properties (Pintar et al., 1992).

Table 7.2 The material properties of the parts of the FSU

Component	**Young's Modulus, E (MPa)**	**Poisson's Ratio, v**
Cortical Shell	12000	0.30
Cancellous Core	100	0.20
Inferior Process	3500	0.25
Superior Process	7000	0.25
Endplate	24	0.40

Table 7.3 Material Constants of Annulus and Nucleus (Wang et al., 2000)

Relaxation of	**Shear Relaxation Modulus**	**Bulk Relaxation Modulus**	**Relaxation Time Constant (sec)**
Annulus Matrix, E=8.0 MPa, υ=0.45	$g_1 = 0.399$	$k_1 = 0.399$	$\tau_1 = 3.45$
	$g_2 = 0.000$	$k_2 = 0.300$	$\tau_2 = 100$
	$g_3 = 0.108$	$k_3 = 0.149$	$\tau_3 = 1000$
	$g_4 = 0.108$	$k_4 = 0.150$	$\tau_4 = 5000$
Nucleus Pulposus, E=2.0 MPa, υ=0.49	$g_1 = 0.638$	$k_1 = 0.0$	$\tau_1 = 0.141$
	$g_2 = 0.156$	$k_2 = 0.0$	$\tau_2 = 2.21$
	$g_3 = 0.120$	$k_3 = 0.0$	$\tau_3 = 39.9$
	$g_4 = 0.0383$	$k_4 = 0.0$	$\tau_4 = 266$
	$g_5 = 0.000$	$k_5 = 0.0$	$\tau_5 = 500$

The finite element model was validated by comparing the results of the model with the results of a L2-L3 segment study in the literature (Shirazi-Adl, A., and Drouin, G., 1988). The intradiscal pressure results of the model in this study appeared to be 0.82 and 1.10 MPa for 5 and 10 Nm flexion moments under a 1000 N compression preload, respectively, while the model in the literature yielded approximately 0.88 and 1.05 MPa, respectively. The results indicate a good agreement for flexion and compression loadings.

The novel approach was utilised for two different loading cases: 10 Nm flexion moment and 2000 N compressive force, both applied at L1 level for a duration of 0.010 s. The vertical forces of the multi-body model at L2-L3 level were

computed from the initial MB model of the lumbar spine (Fig. 7.9) and used as boundary conditions for the FE model of the FSU.

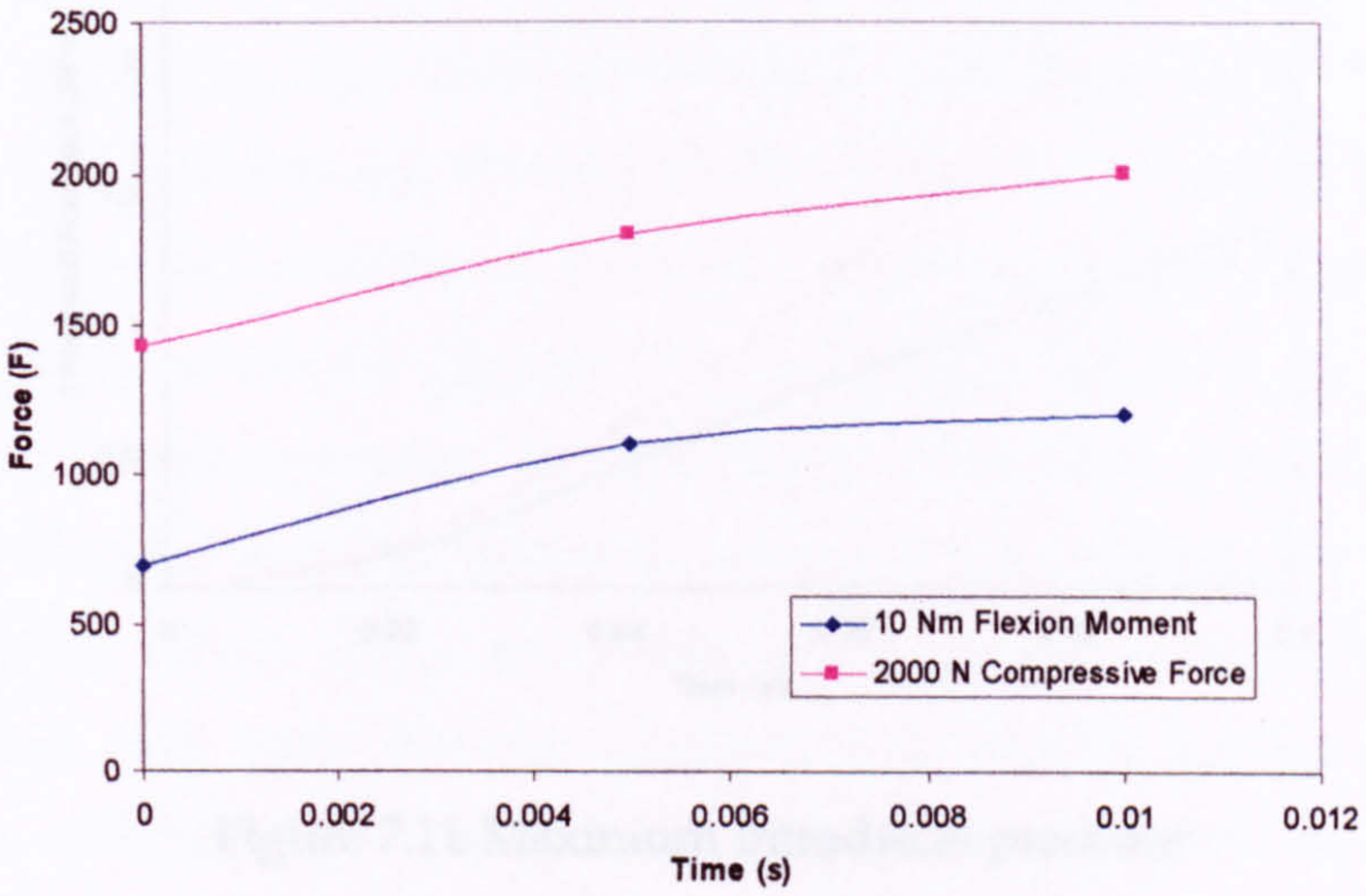

Figure 7.9 The force boundary conditions for the FE model

The maximum equivalent von Mises stress and intradiscal pressure results of the FE model are presented in Figures 7.10 and 7.11, respectively. Also, the maximum equivalent von Mises stress distributions at t = 0.010 s have been given in Figure 7.12. The results show that the stresses created in the annulus and the nucleus under the compressive load of 2000 N are higher than the stresses created by the axial force component resulting from 10 Nm flexion moment.

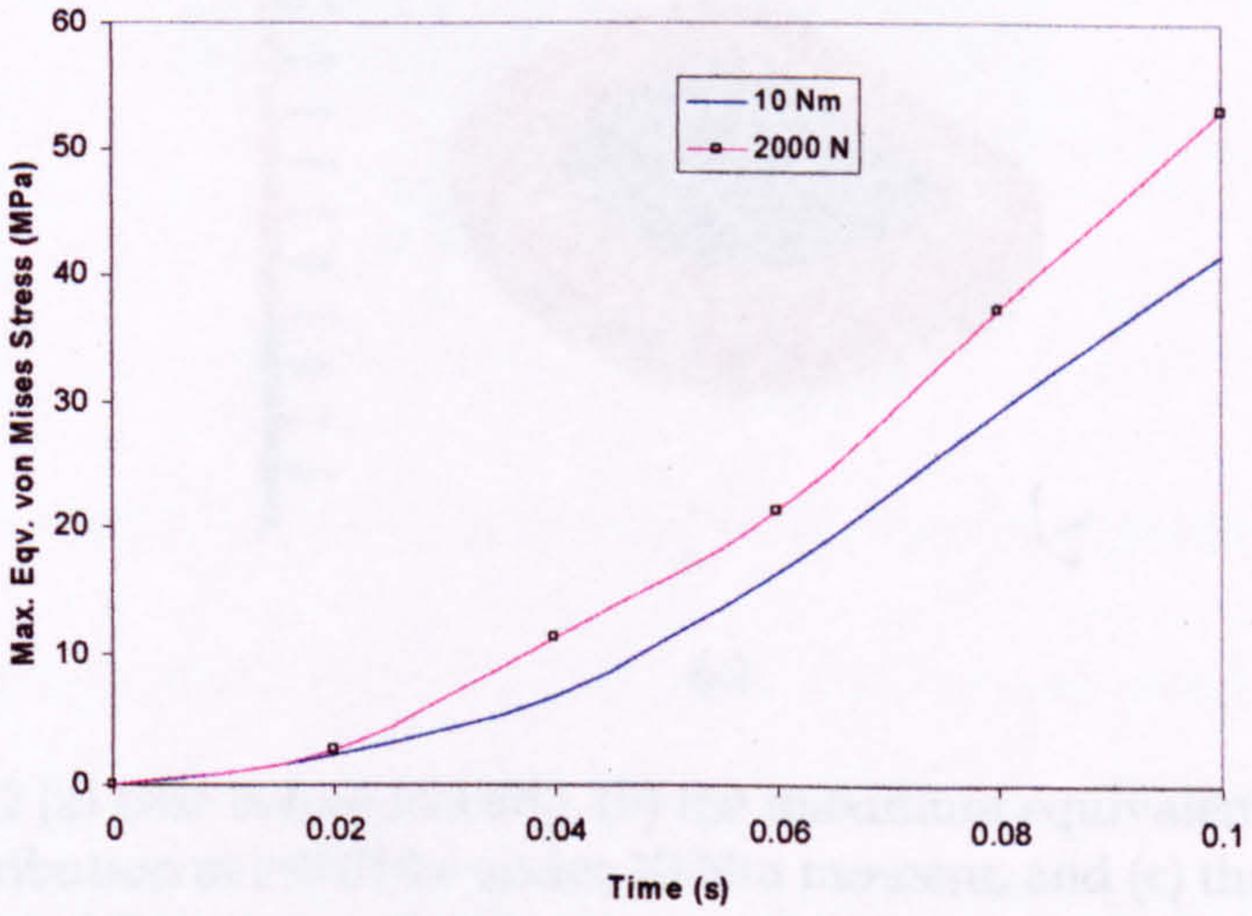

Figure 7.10 Maximum equivalent von Mises stresses

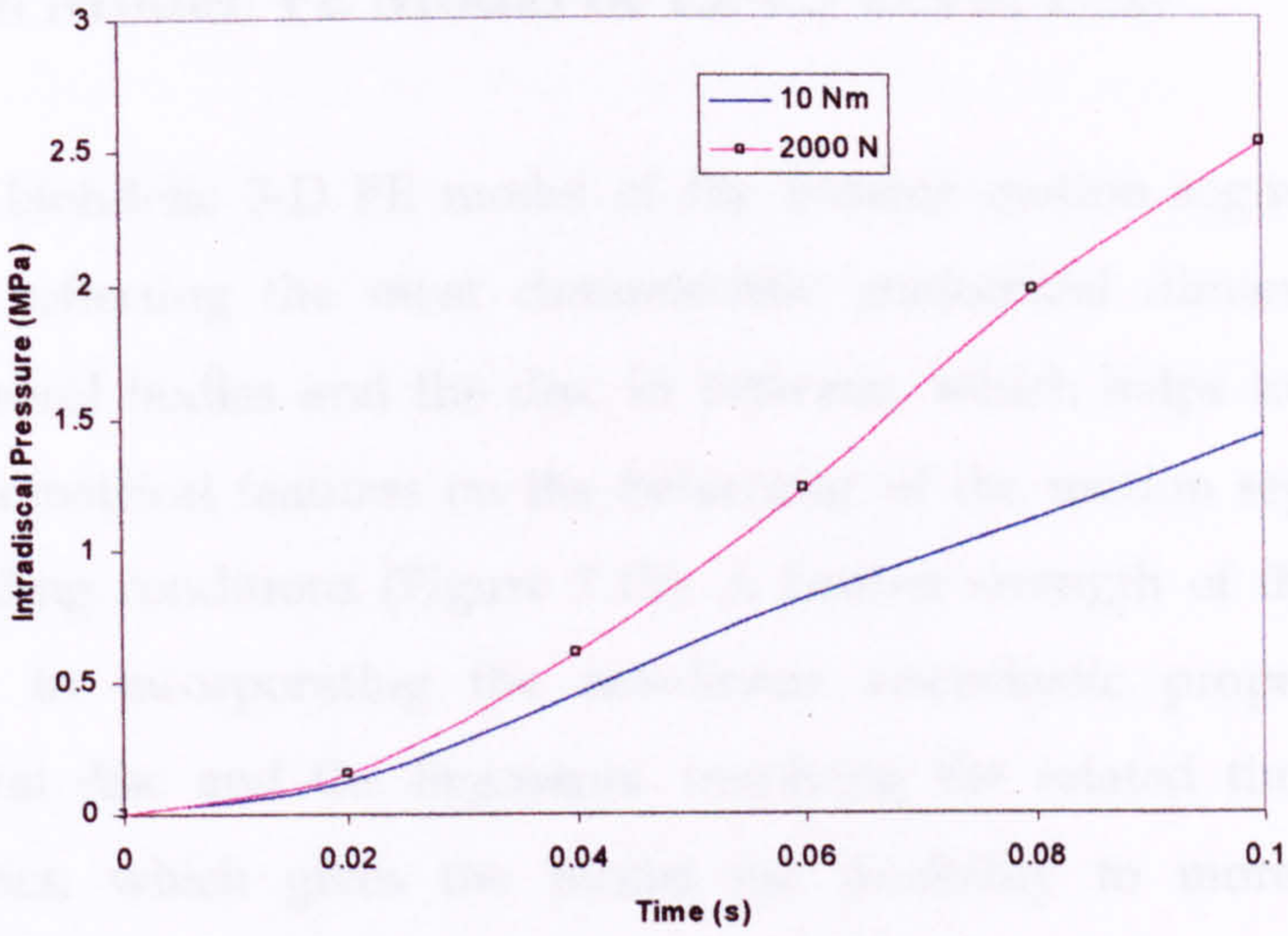

Figure 7.11 Maximum intradiscal pressure

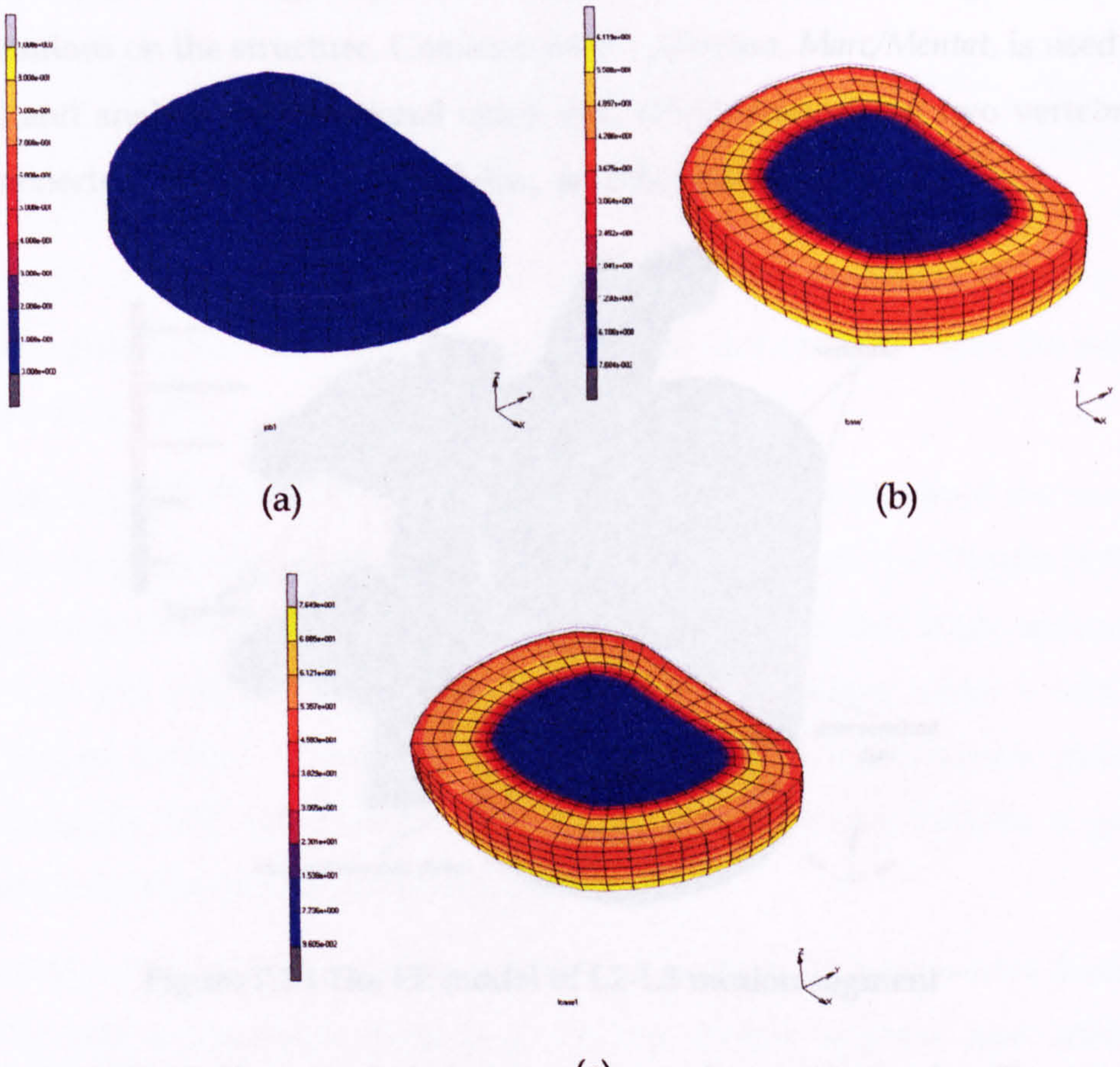

(a) (b)

(c)

Figure 7.12 (a) Disc before loading, (b) the maximum equivalent von Mises stress distribution at t=0.010 s under 10 Nm moment, and (c) the maximum equivalent von Mises stress distribution at t=0.010 s under 2000 N compressive force.

7.5 Fourth Model: FE Model of L2-L3 Level FSU

A detailed biofidelic 3-D FE model of the lumbar motion segment L2-L3 is developed, reflecting the most characteristic anatomical dimensions of the whole vertebral bodies and the disc in between, which helps to analyse the effect of geometrical features on the behaviour of the motion segment under several loading conditions (Figure 7.13). A further strength of the developed model lies in incorporating the non-linear viscoelastic properties of the intervertebral disc and the ligaments, involving the related time-dependant characteristics, which gives the model the flexibility to more realistically simulate not only static but also dynamic and complex loading conditions. Moreover, vertebral bodies and the endplates are modelled as deformable entities, rather than being simplified as rigid bodies, thus, possessing the related deformations on the structure. Commercial FE software, *Marc/Mentat*, is used to model and analyse the functional spine unit (FSU), comprising two vertebrae interconnected, by an intervertebral disc, and the related ligaments.

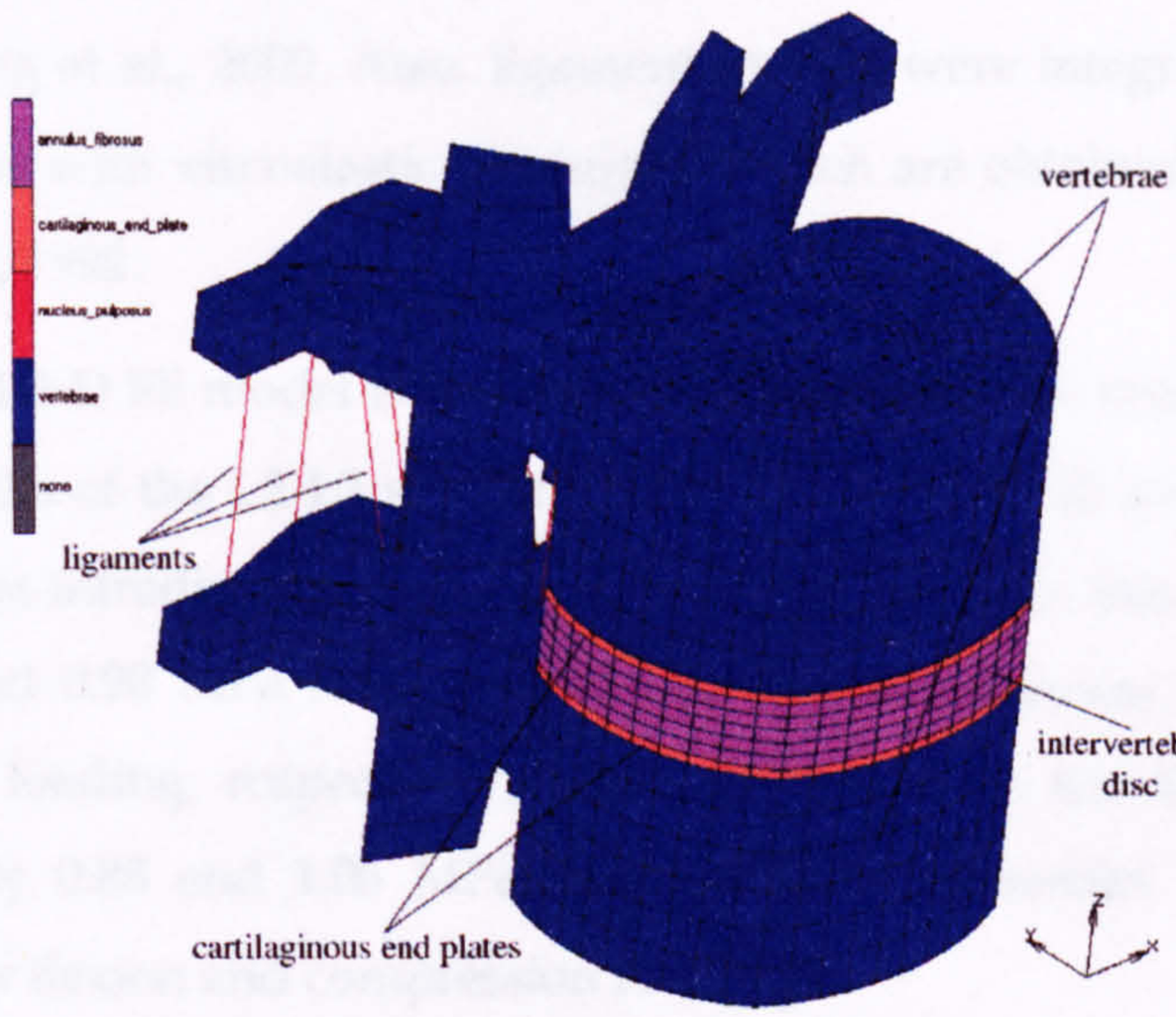

Figure 7.13 The FE model of L2-L3 motion segment

The intervertebral disc mainly has two parts: nucleus and annulus fibrosus. In the model, all annulus fibrosus are modelled as composite materials representing the amorphous matrix and the collagenous fibres, having 30° fibre angle. The fibres are directed in the same direction (30°) in a given band of

annulus but in opposite directions in two adjacent bands. The viscoelastic properties of the disc employed in the modelling are presented in Table 7.4.

Table 7.4 Material constants of annulus and nucleus using Prony series (source: Lee et al.,2000, and Wang et al., 2000)

Relaxation of	Shear Relaxation Modulus	Bulk Relaxation Modulus	Relaxation Time Constant (s)
Annulus Matrix	$g_1 = 0.399$	$k_1 = 0.399$	$\tau_1 = 3.45$
E = 8.0 MPa	$g_2 = 0.000$	$k_2 = 0.300$	$\tau_2 = 100$
$\nu = 0.35$	$g_3 = 0.361$	$k_3 = 0.149$	$\tau_3 = 1000$
	$g_4 = 0.108$	$k_4 = 0.150$	$\tau_4 = 5000$
Nucleus Pulposus	$g_1 = 0.638$	$k_1 = 0.0$	$\tau_1 = 0.141$
E = 0.5 MPa	$g_2 = 0.156$	$k_2 = 0.0$	$\tau_2 = 2.21$
$\nu = 0.49$	$g_3 = 0.120$	$k_3 = 0.0$	$\tau_3 = 39.9$
	$g_4 = 0.0383$	$k_4 = 0.0$	$\tau_4 = 266$
	$g_5 = 0$	$k_5 = 0.0$	$\tau_5 = 500$

All parts of the FSU model are modelled as 8 node brick elements. Only the cortical shell is modelled as 4 node shell elements. The material properties of the remaining parts such as the endplates and cortical shell are adapted from the study of Wang et al., 2000. Also, ligament groups were integrated into the FE model as links with viscoelastic properties, which are obtained from the study of Pintar et al, 1992.

The proposed 3-D FE model is validated by comparing the results of the model with the results of the L2-L3 segment study by Shirazi-Adl and Drouin (1988). The maximum intradiscal pressure results of the model in this study appeared to be 0.79 and 0.98 MPa for 5 and 10 Nm flexion moments under a 1000 N compression loading, respectively, while the model in the literature yielded approximately 0.88 and 1.05 MPa, respectively. The results indicate a good agreement for flexion and compression loadings.

The model is then loaded with two different loadings; a compressive load of 2000 N, and a combined loading of 15 Nm flexion moment and 1000 N compressive force. The average equivalent von Mises stress values in the annulus appear to be around 25 MPa under the compressive load of 2000 N, while the stress values are around 35 MPa under the combined loading of 15 Nm flexion moment and 1000 N compressive force. As a result, the average

equivalent von Mises stress values in the range of 20-35 MPa for both loading conditions, which show good agreement with the stress values ranging between 0-35 MPa in the study of Wang et al. (2000). The equivalent von Mises stress distributions within the intervertebral disc in both loading scenarios are presented in Figure 7.14.

This particular model provides more detailed and realistic results about the exact distribution of stresses and strains within the segments of the lumbar spine, when compared to the simplified models in the literature. Therefore, the proposed model more realistically simulates the behaviour of a FSU, incorporating nonlinearity due to viscoelasticity.

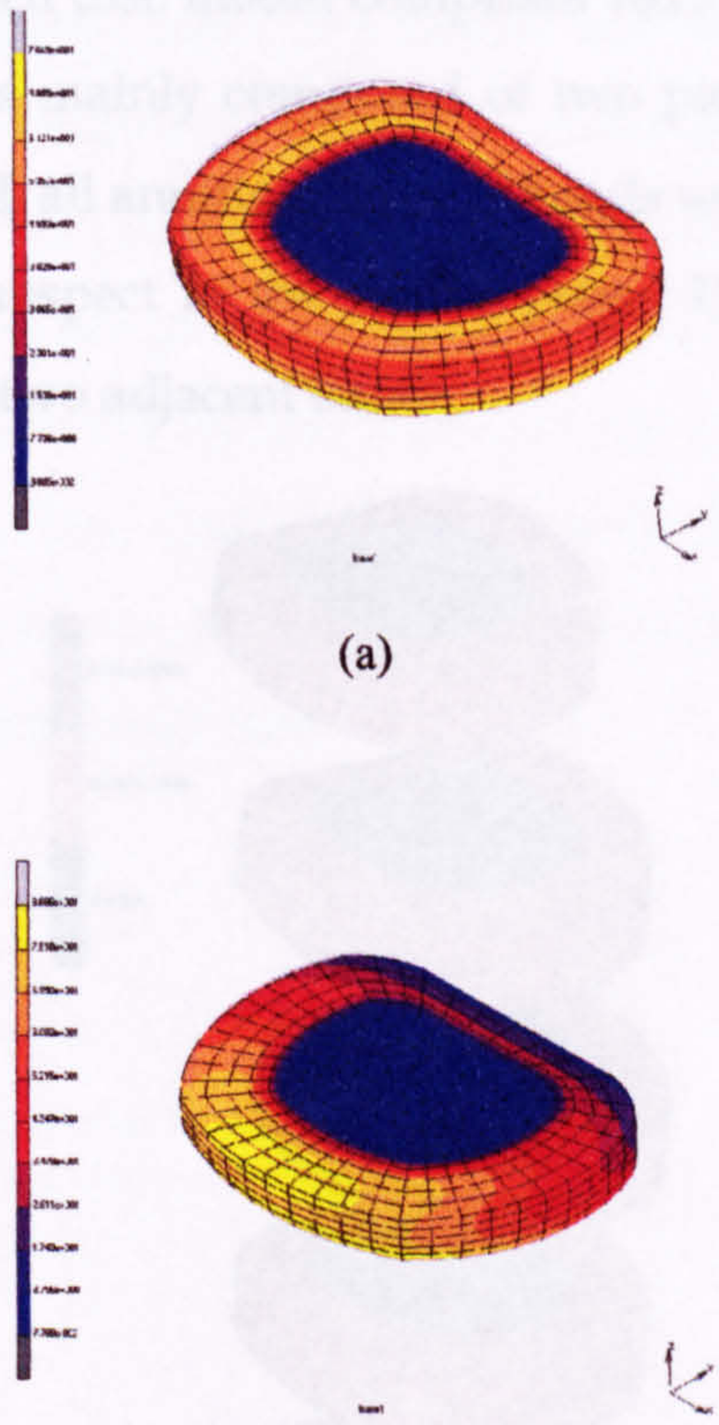

(a)

(b)

Figure 7.14 The equivalent von Mises stress distributions within the disc under (a) the compressive load of 2000 N, and (b) the the combined loading of 15 Nm flexion moment and 1000 N compressive force.

7.6 Fifth Model: Viscoelastic FE Model of Whole Cervical Spine Discs

In order to investigate the effects of the dynamic impact loading on the discs, a 3-D biofidelic FE model of the 6 discs (C23, C34, C45, C56, C67, and C7T1) in the cervical spine has been developed by using commercial software, MSC.Marc/Mentat (Figure 7.15). The dimensions, positions and the orientations of the discs were taken from the quantitative anatomy of the cervical spine in the literature (Panjabi et al., 1992, Nissan and Gilad, 1984) Intervertebral discs were modelled as 8 node brick elements, the material properties of which were adapted from literature (Yang et al., 1998, Yoganandan et al., 2001, and Teo and Ng, 2001) (Table 7.5). Each disc model comprises 1815 elements and 938 nodes. The intervertebral disc is mainly composed of two parts; nucleus and annulus fibrosus. In the FE model, all annulus fibrosus bands were modelled with a fibre orientation of 30° with respect to the lateral plane. The fibres are in opposite alternating directions in two adjacent bands.

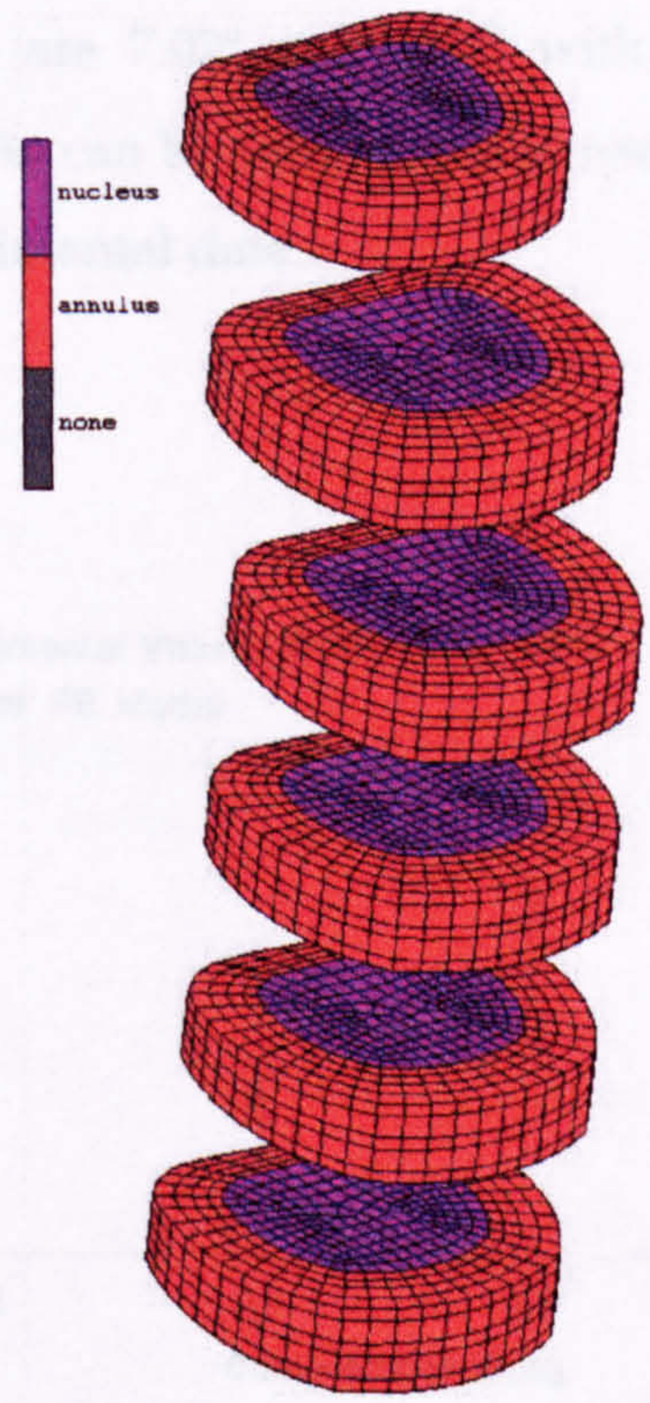

Figure 7.15 The FE model of the discs

Table 7.5 Material properties of the discs

Component	Young's Modulus, E (MPa)	Poisson's Ratio, ν
Cortical Shell	12000	0.30
Cancellous Core	100	0.20
Nucleus Pulposus	3.4	0.49
Annulus Matrix	4.2	0.45
Annulus Fibres	450	0.30
Endplate	600	0.30

The FE model was validated against published experimental measurements. Firstly, C4-C6 model was built in order to comply with the experimental setup. Therefore, for this purpose only, vertebral bodies were built with the endplates, which surround the discs C45 and C56. Table 7.5 illustrates the material properties of these elements. Then, the model was subjected to two different loadings; (a) 1 mm axial compression and (b) 1600 Nmm flexion and extension together with a 73.6 N axial compressive preload. The results from the 1 mm axial compression loading are given in Figure 7.16. For the second loading case, the FE model yielded 6.23° for flexion and 6.60° for extension moments, while the experimental results are 7.02° and 4.80° with 2.23° and 1.41° standard deviations, respectively. As can be seen from the results, a good agreement has been achieved with experimental data.

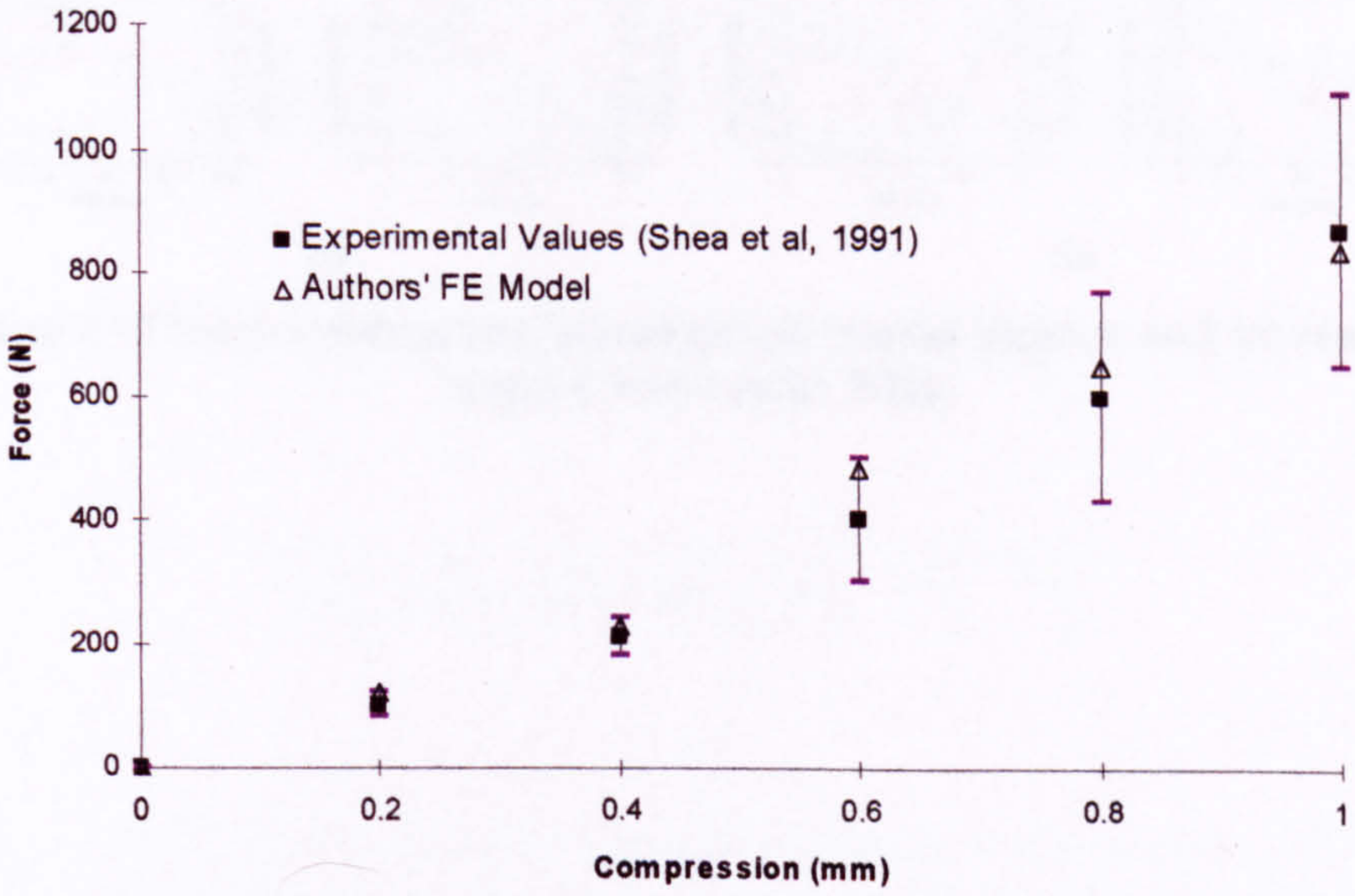

Figure 7.16 Validation of the FE disc

The complete multi-body head and neck model was used to simulate 15g frontal and 8.5g rear-end impacts with the resulting motion compared against response corridors derived from sled acceleration tests using human volunteers (van Lopik, 2004). The intervertebral disc loads from the 15g frontal and 8.5g rear-end impact simulations for the first 200 ms period (Figure 7.17) are used as force boundary conditions for the FE model of the discs. The disc forces F_x and F_z are shown on the left axis and moment M_y on the right axis. The predicted results of maximum von Mises stresses in the annulus and the intradiscal pressure in the nucleus of each disc of the FE model are depicted in Figure 7.18. The intradiscal pressures occurring in the nuclei of the discs have almost the same pattern with the von Mises stress distributions with respect to time increments as in Figure 5, but possessing less magnitudes; a max of 0.5 MPa for the frontal and a max of 0.1 MPa for the rear-end case.

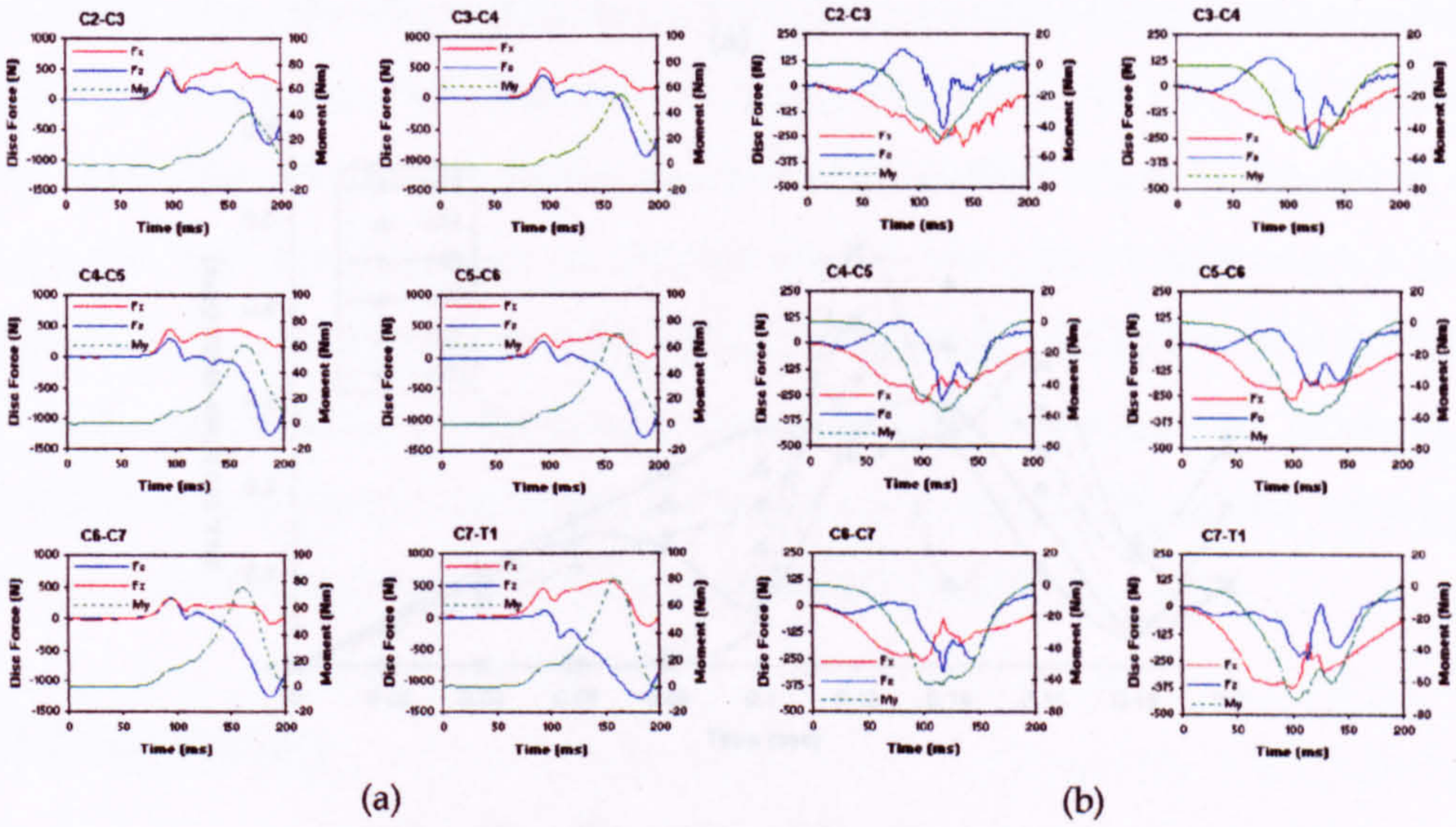

Figure 7.17 Intervertebral disc loadings: (a) frontal impact, and (b) rear-end impact (van Lopik, 2004)

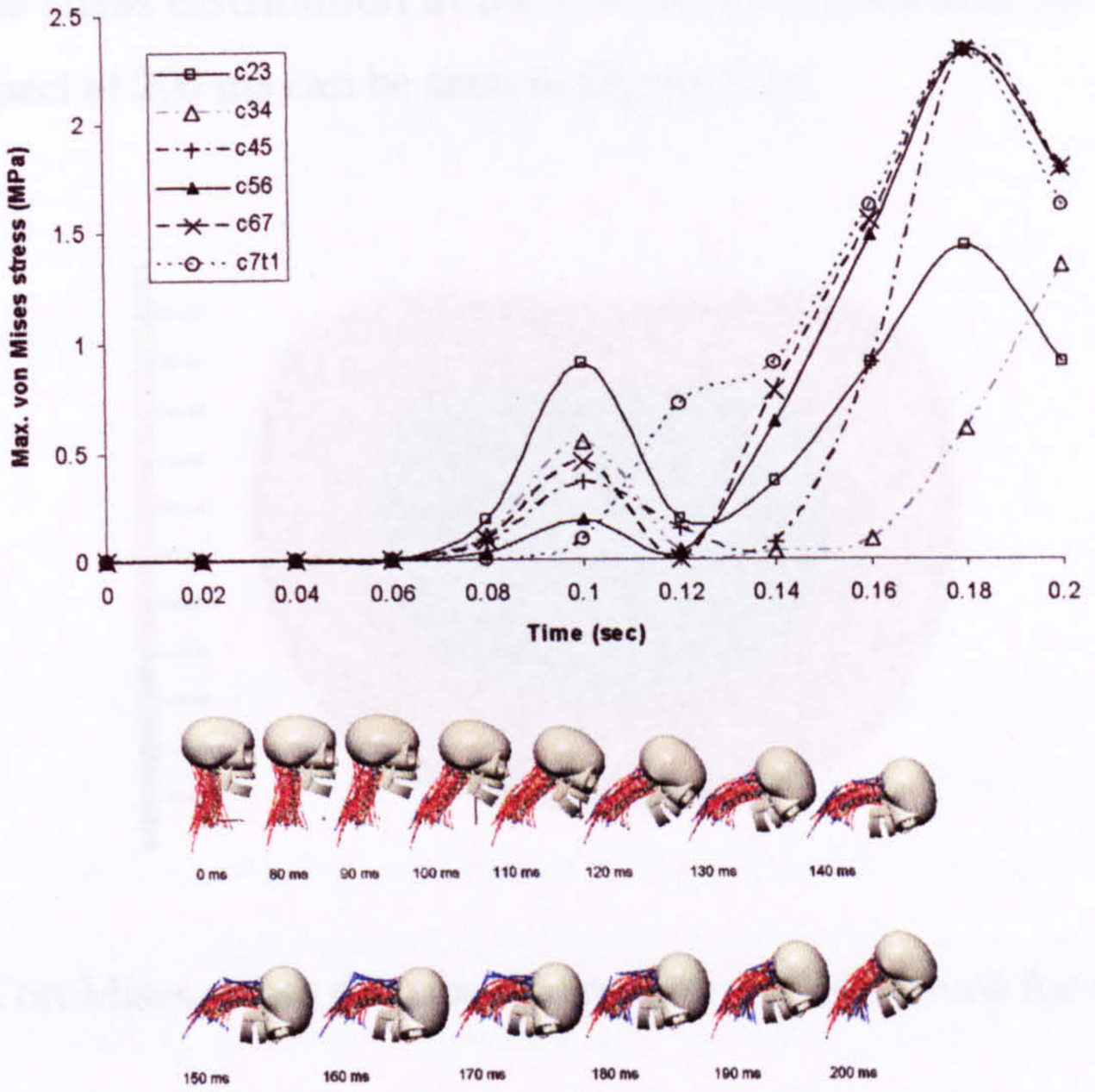

(a)

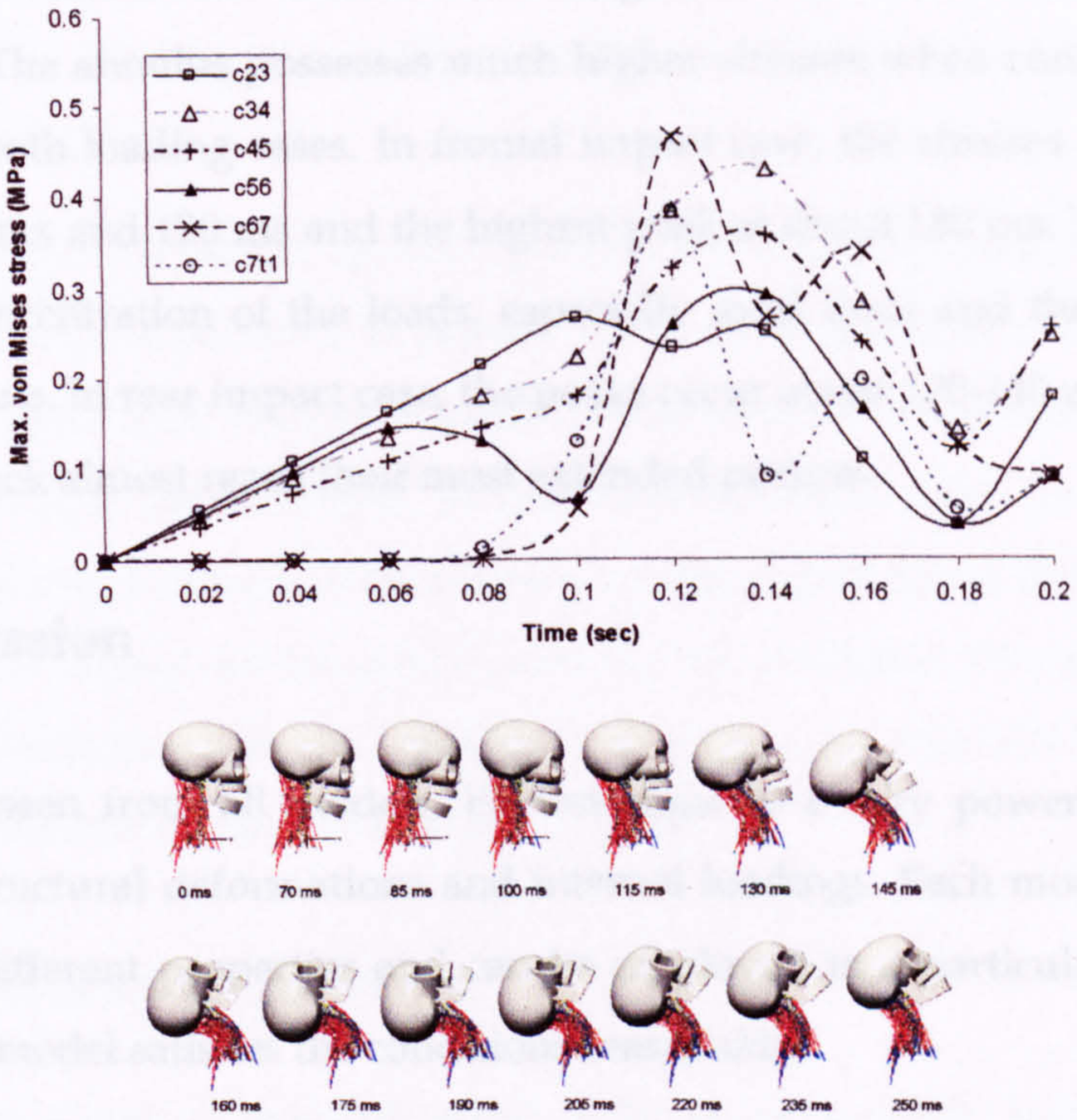

(b)

Figure 7.18 FE results: (a) Max. von Mises stresses in the annulus for frontal impact with multi-body head and neck response illustration, and (b) max. von Mises stresses in the annulus for rear-end impact with multi-body head and neck response illustration

The von Mises stress distribution in the C56 intervertebral disc for the last stage of frontal impact at 200 ms can be seen in Figure 7.19.

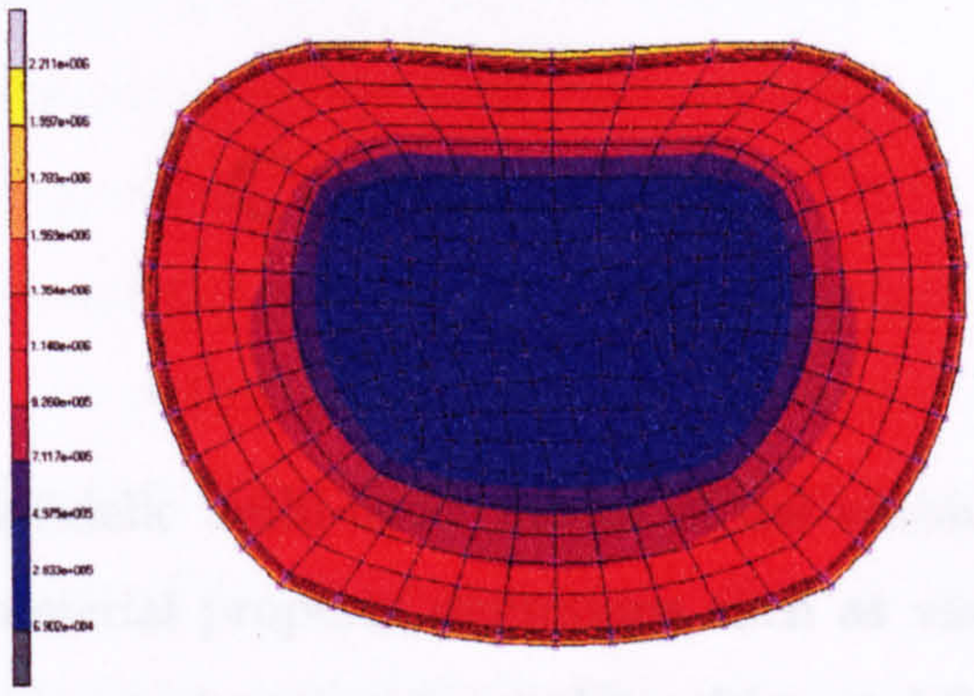

Figure 7.19 Von Mises stress distribution of C56 disc at 200 ms for frontal impact

The results from the FE models show that the responses of the annulus and the nucleus are similar but different in magnitude due to different material properties. The annulus possesses much higher stresses when compared to the nucleus in both loading cases. In frontal impact case, the stresses reach a peak between 80 ms and 120 ms and the highest peak at about 180 ms. This is due to the high concentration of the loads, especially axial force and the moment, at these intervals. In rear impact case, the peaks occur about 120-140 ms, where the head and neck almost reach their most extended posture.

7.7 Discussion

As can be seen from all models, FE technique is a very powerful option to visualise structural deformations and internal loadings. Each model explained possesses different properties and can be employed in a particular analysis as long as the model satisfies the conditions reasonably.

This chapter also shows that the proposed novel approach that combines the multi-body and FE models have the potential to provide a powerful, cost-effective and versatile platform to investigate the kinetics and the kinematics of the whole cervical spine and its components and the response of the intervertebral discs under complex dynamic loading histories.

CHAPTER 8

Conclusions

In this thesis, a biofidelic multi-body model of the whole human spine with highly advanced material property definitions such as viscoelastic behaviour, active-passive muscles, and geometric nonlinearities, and finite element models of the intervertebral discs were developed and validated in order to have a better understanding of injury mechanisms under impact loading conditions. Both models were combined via a novel approach, where the predictions of the MB model as a result of these simulations such as intervertebral disc loadings were used as loading boundary conditions for the FE models of the intervertebral discs.

The proposed novel hybrid approach, which combined the multi-body and FE models, showed the potential to provide a powerful, cost-effective and versatile platform to investigate the kinetics and the kinematics of the whole spine and its components and the response of the intervertebral discs under complex dynamic loading histories. This method not only provided a detailed loading history of the impact on the spinal parts via the validated MB model but also supplied information via the validated FE models on how the intervertebral discs were affected during the loading.

8.1 Assessment of the Work

One of the novelties and advanced features of the MB models was the implementation of the active-passive muscles. The capability of combining multi-body software visualNastran with advanced mathematical package of Matlab/Simulink provided a sophisticated medium to create more biofidelic biomechanical models with advanced muscle properties.

The multi-body model of the lumbar spine included advanced features such as material property and geometric nonlinearities and viscoelastic material properties. One of its strengths was the implementation of Virtual Muscle as an external software to control muscles actively and passively. However, the main shortcoming of the model was the solid body definitions. The vertebrae were modelled by using quantitative anatomy data and therefore reflected average values of some essential dimensions. This led to a relatively poor definition of contact surfaces as well as facet joints. Also, an assumed approximate definition of intervertebral disc damping coefficient appeared to be another shortcoming, which had a significant effect on the kinematic outputs. As another weakness, the muscle fascicles were modelled as one actuator each for the sake of simplicity, which prevented the model from a more realistic description of muscle curving. Due to the paucity of experimental results in the literature regarding lumbar spine dynamics, validation was carried out with small amount of data and good agreements were achieved. The model was validated by comparing the flexion moment results, as rotations, and the intradiscal pressure occurred within the disc after the loadings with a previously validated model in the literature. This model constituted the basis for developing the more advanced, detailed, and biofidelic MB model of the whole human spine.

In the *MB model of the whole human spine*, as a very important improvement to the previous model, the solid bodies comprising the spinal and other skeletal bony elements were no more modelled by using quantitative anatomy data but imported from a CT scanned cadaver human spine study. Due to the technique used, it was highly realistic, and helped define more realistic contact surfaces within the MB model. The intervertebral discs and ligaments were modelled with highly realistic material properties, incorporating nonlinearities and viscoelasticity. All spinal intervertebral discs and all ligaments associated with the spinal column were introduced. The other skeletal parts such as the ribs, clavicles, and scapulae played a very important role especially in attaching the ligaments and muscles into their realistic locations.

Another strength of the model lay in the modelling and defining the muscles. The external software Virtual Muscle was employed again to develop very detailed and realistic muscle behaviour, both active and passive. The

morphological and mechanical properties of all muscle groups were incorporated by using the data available in the literature.

Validation attempts as motion segment responses in the cervical spine, MB model responses in the cervical spine for frontal and lateral impacts, vertical loading for cervical spine, and MB model responses of thoracic and lumbar regions in rear-end impact were carried out in order to validate the *whole human spine MB model* omni-directionally. As there are several experimental studies regarding the impact behaviour of the cervical spine, most of the validation attempts were conducted on the responses of the cervical spine. The static loading results of the cervical spine seemed to be in good agreement with the experimental studies such as Moroney's data. In dynamic validation attempts against NBDL data, most of the curves lie within the response corridors of the experiments. The tendencies of the output curves appear to be highly correct when compared to test results. The model was also validated against vertical loading. The model and simulation parameters were fairly simple as few data was present in the literature. However, relatively good agreements were achieved in terms of head accelerations. Also, for validating the thoracolumbar region, the graphs show that the model predicted the experimental values from reasonable to good agreement.

Similar to the previous lumbar spine MB model, one shortcoming rose from the paucity of data regarding intervertebral disc damping coefficients. Information regarding the other material properties of the intervertebral discs was found to be lacking in the literature; therefore linear stiffness characteristics derived from static testing of isolated disc segments were used to define the response of the discs in most directions while non-linear load curves derived from experiments on intact motion segments were employed to define the response for flexion and extension.

The developed MB model of the whole human spine offered more advanced and realistic features such as active-passive muscle modelling and non-linear viscoelastic material properties when compared to other existing whole spine models. The two similar whole human spine MB models of De Zee et al. (2003) and Ishikawa et al. (2005) were built in a manner close to the techniques

employed in this study. However, De Zee model was an incomplete spine model in terms of only including all lumbar muscle groups and it was solely constructed around lumbar region. Ishikawa et al. musculoskeletal dynamic multi-body spine model was developed in order to perform Functional Electrical Stimulation (FES) but only few details were disclosed about how the components of the spine were modelled, and in particular, how muscles were developed and governed to possess active behaviour.

As the second part of the proposed approach, several FE models were developed from simpler ones to more advanced models, incorporating different modeling parameters and techniques each time. Each model demonstrated a potential to serve for a different purpose, yielding several advantages in its particular case, but often compromising several other parameters for the sake of simplicity and computational requirements. Being the main responsible element for supporting the forces and moments acting on the spine, intervertebral discs were chosen as elements for individual FE models.

Different material properties were introduced into the FE models to obtain accurate results. One of the strengths of the 4th FE model was in incorporating the non-linear viscoelastic properties of the intervertebral disc and the ligaments, involving the related time-dependant characteristics, which gave the model the flexibility to more realistically simulate not only static but also dynamic and complex loading conditions. Moreover, vertebral bodies and the endplates were modelled as deformable entities, rather than being simplified as rigid bodies, thus, possessing the related deformations on the structure. This particular model provided more detailed and realistic results about the exact distribution of stresses and strains within the segments of the lumbar spine, when compared to the simplified models in the literature.

The 5th FE model of the cervical spine discs demonstrated the very first application of the proposed novel approach, where dynamic loading history predictions from the MB model were used to create realistic loading boundary conditions for the FE model. The results from the FE models showed that the responses of the annulus and the nucleus are similar but different in magnitude due to different material properties. The annulus possessed much higher

stresses when compared to the nucleus in both loading cases. In frontal impact case, the stresses reached a peak between 80 ms and 120 ms and the highest peak at about 180 ms. This was probably due to the high concentration of the loads, especially axial force and the moment, at these intervals. In rear impact case, the peaks occured about 120-140 ms, where the head and neck almost reached their most extended posture.

The FE models were validated by using different set of data. The 3rd and the 4th finite element models were validated by comparing the results of the model with the results of a L2-L3 segment study in the literature (Shirazi-Adl, A., and Drouin, G., 1988). The results indicated a good agreement for flexion and compression loadings. The 5th FE model was also validated against published experimental measurements. Firstly, C4-C6 model was built in order to comply with the experimental setup. Therefore, for this purpose only, vertebral bodies were built with the endplates, which surround the discs C45 and C56. Then, the model was subjected to two different loadings; (a) 1 mm axial compression and (b) 1600 Nmm flexion and extension together with a 73.6 N axial compressive preload. Similarly, good agreements were achieved with experimental data.

8.2 Final Conclusions

The main novelty of the thesis and its contribution to knowledge was the multi-body model of the whole human spine itself. This model was built to be one of the most sophisticated MB models in the literature, especially with its highly advanced material property definitions such as viscoelastic behaviour, active-passive muscles, and geometric nonlinearities. On the other hand, considering the size and the detail of the model, there had to be several assumptions and simplifications as in most of the engineering and computational models, especially due to the lack of material property data such as damping characteristics of the intervertebral discs.

The analysis of frontal and lateral impacts revealed that the inclusion of active muscle behaviour is essential in predicting the head-neck response to impact. In both impacts the developed muscle forces limit the movement between the joints of the upper cervical spine by significantly reducing the degree of rotation

of the head in the plane of impact. In lateral impact, the muscle tensioning also showed a strong influence on the rotation of the lower two joints of the cervical spine. With passive properties the response of the head-neck model is similar to the response of cadaveric specimens where the influence of active musculature is missing. The results from the rear-end simulations demonstrated the role of active musculature to have little affect on the resulting head and neck kinematics on contrary to the findings for frontal and lateral impacts.

In whiplash simulation chapter, the MB model was used to simulate a ligamentous cervical spine undergoing whiplash trauma. The MB model devoid of muscles was reasonably validated against test results, while most of the simulation results and model predictions showed good agreement with experiments. The model successfully reproduced the characteristic motion of the head and neck when subjected to rear-end impact.

The proposed novel approach, which combined the multi-body and FE models, exhibited the potential to provide a powerful, cost-effective and versatile platform to investigate the kinetics and the kinematics of the whole spine and its components and the response of the intervertebral discs under complex dynamic loading histories.

CHAPTER 9

Suggestions for Further Work

The current multi-body model of the whole human spine incorporates many advanced features, however there is a huge amount of possibilities in order to develop it further.

In terms of muscle modelling, the muscles in the visual Nastran medium, namely the linear actuator elements can be divided into series of elements in order to visualise muscle bending/curving better. An improved muscle definition will add additional strength to the model towards biofidelity, as the muscle forces can be transferred to the solid bodies in more correct and realistic directions.

Muscle wrapping is another important phenomenon, where all the muscle groups are wrapping around each other as physical entities. In the MB model, due to the software limitations and preferences, the linear actuators are not physical entities. Therefore, muscle wrapping may be considered to probably have a more biofidelic model.

Further measurements of cervical spine muscle morphometry should be conducted to be able to accurately define the properties of all neck muscles. Also the level of activation and onset times of all muscle groups in response to impacts need to be investigated for more realistic simulation purposes.

The mass of the soft tissues such as organs were incorporated into the model in a simple way by increasing the density of the current solid bodies. Although it is thought that the additional effects for a better mass distribution may be minimal, this may be considered for a more realistic multi-body model.

Further experimental work is needed to determine the intervertebral disc properties in response to static and dynamic conditions in all directions of loading for each level of the cervical spine. The dynamic behaviour of all cervical spine ligaments should also be investigated.

Another important issue is validation. More experimental data will not only help improve the model parameters, but also provide confidence through an omni-directional model to be employed in a wide variety of tasks.

The model's ability to predict the forces developed in the soft-tissue components makes it suitable for investigating injury mechanisms and together with experimental research suitable for establishing injury thresholds. Once further experimental work is established to determine the tolerance limits of all the soft-tissues, these can be employed to investigate the possibility of injury occurring in simulated crash scenarios.

Finally, this MB model may well be a step towards a human body modelling, the spine of which may be constituted with this model.

REFERENCES

Acar, B. S., and Grilli, S. L. (2002) Distributed Body Weight over the Whole Spine for Improved Inference in Spine Modelling, *Computer Methods in Biomechanics and Biomedical Engineering*, **5**, No.1, pp. 81-89.

Adler, R. L., Dedieu, J. P., Margulies, J. Y., Martens, M., and Shub, M. (2002) Newton's Method on Riemannian Manifolds and A Geometric Model for the Human Spine, *IMA Journal of Numerical Analysis*, **22**, No. 3, 359-390.

Aspden, R. M. (1988) A New Mathematical Model of the Spine and Its Relationship to Spinal Loading in the Workplace, *Applied Ergonomics*, **19**, No. 4, 319-323.

Aspden, R. M. (1992) Review of the Functional Anatomy of the Spinal Ligaments and the Lumbar Erector Spinae Muscles, *Clinical Anatomy*, **5**, 372-387.

Baer, A. E., Laursen, T. A., and Setton, L. A. (2001) A Finite-Deformation, Anisotropic, Biphasic Finite Element Model of Cell-Matrix Interactions in The Intervertebral Disc, *American Society of Mechanical Engineers, Bioengineering Division (Publication) BED, Advances in Bioengineering*, **50**, 799-800.

Beason, D. P., Dakin, G. J., Alonso, J. E., Lopez, R. R., and Eberhardt, A. W. (2001) Bone Mineral Density Correlates with Fracture Loads in Pelvic Lateral Impacts, *American Society of Mechanical Engineers, Bioengineering Division (Publication) BED, Advances in Bioengineering*, **50**, 883-884.

Bereznick, D. E., Kim Ross, J., and McGill, S. M. (2002) The Frictional Properties at the Thoracic Skin-Fascia Interface: Implications in Spine Manipulation, *Clinical Biomechanics*, **17**, No. 4, 297-303.

Bogduk, N., Macintosh, J. E., and Pearcy, M. J. (1992) A Universal Model of the Lumbar Back Muscles in the Upright Position, *Spine*, **17**, No. 8, 897-913.

Borelli, G. A. (1989) Translation: On the Movement of Animals, Springer-Verlag, Berlin.

Boyd-Clarke, L. C., Briggs, C. A., and Galea, M. P. (2001) Comparative histochemical composition of muscle fibres in a pre- and a postvertebral muscle of the cervical spine, *Journal of Anatomy*, **199**, 709-716.

Bozic, K. J., Keyak, J. H., Skinner, H. B., Bueff, H. U., and Bradford, D. S. (1994) Three Dimensional Finite Element Modelling of a Cervical Vertebra: An Investigation of Burst Fracture Mechanism, *Journal of Spinal Disorders*, **7**, 102-110.

Brault, J. R., Siegmund, G. P., and Wheeler, J. B., (2000) Cervical muscle response during whiplash: evidence of a lengthening muscle contraction, *Clinical Biomechanics*, **15**, 426-443.

Braune, W., and Fischer, O. (1985) Translation: On the Centre of Gravity of the Human Body, Springer-Verlag, Berlin.

Braune, W., and Fischer, O. (1988) Translation: Determination of the Moments of Inertia of the Human Body and Its Limbs, Springer-Verlag, Berlin.

Broman, H., Pope, M., and Hansson, T. (1996) A Mathematical Model Of The Impact Response Of The Seated Subject, *Medical Engineering & Physics*, **18**, No. 5, 410-419.

Brown, I. E., and Loeb, G. E. (2000) Measured and modelled properties of mammalian skeletal muscle: IV. Dynamics of activation and deactivation, *J Muscle Res Cell Motil*, **21**, 33-47.

Camacho, D. L. A., Nightingale, R. W., and Myers, B. S. (2001) The Influence of Surface Padding Properties on Head and Neck Injury Risk, *Journal of Biomechanical Engineering, Transactions of the ASME*, **123**, No. 5, 432-439.

Camacho, D. L., Nightingale, R. W., Robinette, J. J., Vanguri S. K., Coates D. J., and Myers B. S. (1997) Experimental Flexibility Measurements for the Development of a Computational Head-Neck Model Validated for Near-Vertex Head Impact, *Proceedings of the 41st Stapp Car Crash Conference*, Society of Automotive Engineers, SAE Paper No. 973345, 473-486.

Cao, K. D., Grimm, M. J., and Yang, K.-H. (1999) Load Sharing Within The Human Lumbar Vertebral Body Using Finite Element Method, *American Society of Mechanical Engineers, Bioengineering Division (Publication) BED, Advances in Bioengineering*, **42**, 275-276.

Carola, R., Harley, J. P., and Noback, C. R. (1992) *Human Anatomy*, McGraw-Hill, Inc., New York, Ch. 7.

Case, K., Xiao, D. C., Acar, B. S., and Porter, J. M. (1999) Computer Aided Modelling of the Human Spine, *Proceedings of the Institution of Mechanical Engineers Part B - Journal of Engineering Manufacture*, **213**, No. 1, 83-86.

Chang, J. H., Chang, G. L., and Hsu, A. T. (1999) Kinematic Study of Cervical Vertebrae Adjacent to Fixation Procedures, *American Society of Mechanical Engineers, Bioengineering Division (Publication) BED, Advances in Bioengineering*, **42**, 61-62.

Chen, S.-I., Chang, C.-H., and Lin, R. M. (1999) Three Dimensional Finite Element Analysis of the Osteoporotic Lumbar Spine, *American Society of Mechanical Engineers, Bioengineering Division (Publication) BED, Advances in Bioengineering*, **42**, 369-370.

Cheng, E., Brown I., and Loeb J. (2001) Virtual Muscle 3.1.5: Muscle Model For Matlab. Users Manual.

Cholewicki, J., and VanVliet IV, J. J. (2002) Relative Contribution of Trunk Muscles to the Stability of the Lumbar Spine During Isometric Exertions, *Clinical Biomechanics*, **17**, No. 2, 99-105.

Cholewicki, J., Juluru, K., and McGill, S. M. (1999) Intra-abdominal Pressure Mechanism for Stabilizing the Lumbar Spine, *Journal of Biomechanics*, **32**, pp. 13-17.

Cholewicki, J., Simons, A. P. D., and Radebold, A. (2000) Effects of External Trunk Loads on Lumbar Spine Stability, *Journal of Biomechanics*, **33**, pp. 1377-1385.

Chuang, J.-H., and Hwang, W.-C. (1997) Variable-Radius Blending by Constrained Spine Generation, *Visual Computer*, **13**, No. 7, 316-329.

Chung, S. M., Teoh, S. H., Tsai, K. T., and Sin, K. K. (1999) Smart Multi-Axial System for Spinal Research and Testing, *American Society of Mechanical Engineers, Bioengineering Division (Publication) BED, Advances in Bioengineering*, **42**, 177-178.

Chung, S. M., Teoh, S. H., Tsai, K. T., and Sin, K. K. (2002) Multi-Axial Spine Biomechanical Testing System With Speckle Displacement Instrumentation, *Journal of Biomechanical Engineering, Transactions of the ASME*, **124**, No. 4, 471-477.

Clausen, J. D., Goel, V. K., Traynelis, V. C., and Wilder, D. G. (1996) Cervical Spine Biomechanical Investigation Using an Experimentally Validated FE Model of the C5-C6 Motion Segment, *Proceedings Orthopaedic Research Society*, Atlanta GA.

Cooper, R, Cardan, C., and Allen, R. (2001) Computer Visualisation of the Moving Human Lumbar Spine, *Computers in Biology and Medicine*, **31**, 451-469.

Costi, J. J., Hearn, T. C., and Fazzalari, N. L. (2002) The Effect of Hydration on the Stiffness of Intervertebral Discs in an Ovine Model, *Clinical Biomechanics*, **17**, No. 6, 446-455.

Crisco, J.J. III, and Panjabi, M.M. (1992) Euler Stability of the Human Ligamentous Lumbar Spine. Part I: Theory, *Clinical Biomechanics*, **7**, No. 1, 19-26.

Crisco, J.J., Panjabi, M.M., Yamamoto, I., and Oxland, T.R. (1992) Euler Stability of the Human Ligamentous Lumbar Spine. Part II: Experiment, *Clinical Biomechanics*, **7**, No. 1, 27-32.

Cusick, J. F., and Yoganandan, N. (2002) Biomechanics of the Cervical Spine 4: Major Injuries, *Clinical Biomechanics*, **17**, No. 1, 1-20.

Dauvilliers, F., Bendjellal, F., Weiss, M., Lavaste, F., and Tarriere, C. (1994) Development of a Finite Element Model of the Neck, *Proceedings of the 38th Stapp*

Car Crash Conference, Society of Automotive Engineers, SAE Paper No. 942210, 77-91.

De Jager, M. K. J. (1996) Mathematical head-neck models for acceleration impacts, PhD Thesis, Technical University of Eindhoven.

De Oliveira, C. G., Simpson, D. M., and Nadal, J. (2001) Lumbar Back Muscle Activity of Helicopter Pilots and Whole-Body Vibration, *Journal of Biomechanics*, **34**, No. 10, 1309-1315.

De Zee, M., Hansen, L., Andersen, T. B., Wong, C., Rasmussen, J., and Simonsen, E. B. (2003) On the Development of a Detailed Rigid-Body Spine Model, *Proceedings of International Congress on Computational Bioengineering*, Spain, 5pp.

Dean, J. C., Wilcox, C. H., Daniels, A. U., Goodwin, R. R., Vanwagoner, E., and Dunn, H. K. (1991) A New Method for Assessing Relative Dynamic Motion of Vertebral Bodies During Cyclic Loading In Vitro, *Journal of Biomechanics*, **24**, No. 12, 1189-1197.

DeFrate, L. E., Sakai, J. L., Gilbertson, L. G., Moon, S.-H., Nishida, K., Donaldson III, W. F., Kang, J. D., and Woo, S. L.-Y. (1999) Magnetic Tracking/Virtual Reality Based System For Comprehensive Kinematic Assessment of The Cervical Spine, *American Society of Mechanical Engineers, Bioengineering Division (Publication) BED, Advances in Bioengineering*, **42**, 63-64.

Deng, Y. C., and Goldsmith, W. (1987) Response of a Human Head / Neck / Upper-torso Replica to Dynamic Loading-II. Analytical/Numerical Model, *Journal of Biomechanics*, **20, No.** 5, 471-486.

Dietrich, M., Kedzior, K., and Zagrajek, T. (1991) A Biomechanical Model Of The Human Spinal System, *Proceedings of the Institution of Mechanical Engineers, Part H: Journal of Engineering in Medicine*, **205**, No. 1, 19-26.

Doehring, T. C., Gilbertson, L. G., Moon, S.-H., Kang, J. D., and Woo, S. L.-Y. (1999) Delineation of In-Vitro Lumbar Spine Kinetics Using a Robotics/UFS Testing System with Hybrid Control, *American Society of Mechanical Engineers, Bioengineering Division (Publication) BED, Advances in Bioengineering*, **42**, 171-172.

Doherty, B. J., and Heggeness, M. H. (1994) The Quantitative Anatomy of the Atlas, *Spine*, **19**, No. 22, 2497-2500.

Doherty, B. J., and Heggeness, M. H. (1995) Quantitative Anatomy of the Second Cervical Vertebra, *Spine*, **20**, No. 5, 513-517.

Dolan, P., and Adams, M. A. (2001) Recent Advances in Lumbar Spinal Mechanics and Their Significance for Modelling, *Clinical Biomechanics*, **16**, Supp. 1, S8-S16.

Dooris, A. P., Goel, V. K., Todd, D. T., Grosland, N. M., and Wilder, D. G. (1999) Load Sharing in a Lumbar Motion Segment Implanted with an Artificial Disc

Under Combined Sagittal Plane Loading, *American Society of Mechanical Engineers, Bioengineering Division (Publication) BED, Advances in Bioengineering,* **42,** 277-278.

Dozzini, S., Redaelli, A., and Vena, P. (1999) A 3-D Poroelastic Anisotropic Model of a Lumbar Intervertebral Disc, *American Society of Mechanical Engineers, Bioengineering Division (Publication) BED, Advances in Bioengineering,* **42,** 367-368.

Duke, K. K., Hill, D. L., Moreau, M. J., Mahood, J. K., Raso, V. J., and Budney, D. R. (1999) Load Measurement During Scoliosis Surgery, *American Society of Mechanical Engineers, Bioengineering Division (Publication) BED, Advances in Bioengineering,* **42,** 179-180.

Dvorak, J., Schneider, E., Saldinger, P., and Rahn, B. (1988) Biomechanics of the Craniocervical Region: The Alar and Transverse Ligaments, *Journal of Orthopaedic Research,* **6,** No. 3, 452-461.

Essendrop, M., Maul, I., Laubli, T., Riihimaki, H., and Schibye, B. (2002) Measures of Low Back Function: A Review of Reproducibility Studies, *Clinical Biomechanics,* **17,** No. 4, 235-249.

Friedman, K., Gaston, F., and Bish, J. (1999) Experimental Comparison of Inverted Dummy and Living Human Drop Tests, *American Society of Mechanical Engineers, Bioengineering Division (Publication) BED, Advances in Bioengineering,* **42,** 149-150.

Frobin, W., Leivseth, G., Biggemann, M., and Brinckmann, P. (2002a) Sagittal Plane Segmental Motion of the Cervical Spine. A New Precision Measurement Protocol and Normal Motion Data of Healthy Adults, *Clinical Biomechanics,* **17,** No. 1, 21-31.

Frobin, W., Leivseth, G., Biggemann, M., and Brinckmann, P. (2002b) Vertebral Height, Disc Height, Posteroanterior Displacement and Dens-Atlas Gap In The Cervical Spine: Precision Measurement Protocol And Normal Data, *Clinical Biomechanics,* **17,** No. 6, 423-431.

Galasko, C.S.B., The Cost of Whiplash-Associated Disorders (1998) *Whiplash Injuries: Current Concepts in Prevention, Diagnosis, and Treatment of the Cervical Whiplash Syndrome,* Lippincott-Raven Publishers, Philadelphia.

Gardner, W. D., and Osburn, W. A. (1967) *Structure of the Human Body,* W. B. Saunders Company, Philadelphia and London, Ch. 3.

Gardner-Morse, M. G. and Stokes, I. A. F. (2004) Structural Behaviour of Human Lumbar Spinal Motion Segments, *Journal of Biomechanics,* **37,** pp. 205-212.

Gavin, T., Patwardhan, A., and Meade, K. (1999) Preventing Coronal Plane Decompensation in Idiopathic Scoliosis: A Geometric Analysis of Orthotic Correction of Right Thoracic, Left Lumbar Curves, *American Society of Mechanical Engineers, Bioengineering Division (Publication) BED, Advances in Bioengineering,* **42,** 279-280.

Gilad, I., and Tichauer, E. R. (1999) Spinal Geometry During Lifting Tasks, *International Journal of Industrial Ergonomics*, **23**, No. 4, 307-318.

Goel, V. K. (1987) 3-Dimensional Motion Behavior Of The Human Spine - A Question Of Terminology, *Journal of Biomechanical Engineering, Transactions of the ASME*, **109**, No. 4, 353-355.

Goel, V. K., Clark, C. R., Harris, K. G., and Schulte, K. R. (1988) Kinematics of the Cervical Spine: Effects of Multiple Total Laminectomy and Facet Wiring, *Journal of Orthopaedic Research*, **6**, No. 4, 611-619.

Goel, V. K., Clark, C. R., McGowan, D., and Goyal, S. (1984) An In-Vitro Study of the Kinematics of the Normal, Injured and Stabilized Cervical Spine, *Journal of Biomechanics*, **17**, No. 5, 363-376.

Goh, J. C. H., Thambyah, A., Wong, H.-K., and Yu, C.-S. (1999) Biomechanical study of Facetectomised Lumbar Spine, *American Society of Mechanical Engineers, Bioengineering Division (Publication) BED, Advances in Bioengineering*, **42**, 273-274.

Goris, B. C. E., Kuipers, M., De Vries, J., Wever, D. J., Verkerke, G. J., and Veldhuizen, A. G. (2002) On the Determination of the Angular Orientation of a Vertebra, *Journal of Biomechanical Engineering, Transactions of the ASME*, **124**, No. 1, 134-136.

Granata, K. P., and Orishimo, K. F. (2001) Response of Trunk Muscle Coactivation to Changes in Spinal Stability, *Journal of Biomechanics*, **34**, No. 9, 1117-1123.

Granata, K. P., and Wilson, S. E. (2001) Trunk Posture and Spinal Stability, *Clinical Biomechanics*, **16**, No. 8, 650-659.

Grauer, J. N., Panjabi, M. M., Cholewicki, J., Nibu, K., and Dvorak, J. (1997) Whiplash produces an S-shaped curvature of the neck with hyperextension at lower levels, *Spine*, **22**, No. 21, 2489-2494.

Gray, H. (1980) *Grays anatomy*, 36th ed., Edited by Peter L. Williams & Roger Warwick, Churchill Livingstone.

Grilli, S. L. (1997) *Spinal Modelling to Investigate Postural Loading and Stability*, Doctoral (PhD) Thesis, Loughborough University, Loughborough, UK, Ch. 3, 129-240.

Gurumoorthy, D., and Twomey, L. T. (2000) Morhphology of cervical muscles and relevance to whiplash, In *Frontiers in Whiplash Trauma. Clinical and Biomechanical*, Editors: Yoganandan, N., and Pintar, F. A., IOS Press, Amsterdam, ISSN 0929-674360-71.

Hakim, N. S., and King, A. I. (1979) A Three Dimensional Finite Element Dynamic Response Analysis of a Vertebra with Experimental Verification, *Journal of Biomechanics*, **12**, 277-292.

Halidin, P. H., Brolin, K., Kleiven S., Von Hoist, H., Jakobsson, L., and Palmertz, C. (2000) Investigation of Conditions That Affect Neck Compression-Flexion Injuries Using Numerical Techniques, *Stapp Car Crash Journal*, **44**, 127-138.

Hasegawa, J., and Shiomi, A. (2003) A Study of Whiplash Injury Occurrence Mechanisms Using Human Finite Element Model, *Proceedings of ESV 18th International Technical Conference*, paper no: 195.

Herzog, W., Kamal, S., and Clarke, H. D. (1992) Myofilament lengths of cat skeletal muscle: theoretical considerations and functional implications, *Journal of Biomechanics*, **25**, 945-948.

Hill, A.V. (1970) First and Last Experiments in Muscle Mechanics, C.U.P.

Hirschfeld, F. (1982) Human Spine Biomechanics - The Search For Engineering Answers To Medical Problems, *Mechanical Engineering*, **104**, No. 6, 24-29.

Huang, Y., King, A., and Cavanaugh, J. M. (1994) FE Modelling of Gross Motion of Human Cadavers in Side Impact, *Proceedings of the 38th Stapp Car Crash Conference*.

Ishikawa, Y., Shimada, Y., Iwami, T., Kamada, K., Matsunaga, T., Misawa, A., Aizawa, T., and Itoi, E. (2005) Model Simulation for Restoration of Trunk in Complete Paraplegia by Functional Electrical Simulation, *Proceedings of IFESS05 Conference*, Montreal, Canada.

Jaeger, M., and Luttmann, A. (1989) Biomechanical Analysis and Assessment of Lumbar Stress During Load Lifting Using a Dynamic 19-Segment Human Model, *Ergonomics*, **32**, No. 1, 93-112.

Johnson, G., Bogduk, N., Nowitzke, A., and House, D. (1994) Anatomy and actions of the trapezius muscle, *Clinical Biomechanics*, **9**, 44-50.

Jost, R., and Nurick, G. N. (2001) Finite Element Simulation of Biomechanical Response of the Human Body Subjected to Lateral Impact, *International Journal of Crashworthiness*, **6**, No. 1, 123-133.

Kaleps, I. (1998) Model Validation, *Proceedings of Models for Aircrew Safety Assessment: Uses, Limitations, and Requirements, RTO MP-20*, RTO HFM Specialists' Meeting, Ohio, USA, 3pp.

Kamibayashi, L. K., and Richmond F. J. R. (1998) Morphometry of human neck muscles, *Spine*, **23**, No. 12, 1314-1323.

Kasra, M., Shirazi-Adl, A., and Drouin, G. (1992) Dynamics of Human Lumbar Intervertebral Joints: Experimental and Finite Element Investigations, *Spine*, **17**, No. 1, 93-102.

Keller, T. S., Colloca, C. J., and Beliveau, J. G. (2002) Force-Deformation Response of the Lumbar Spine: A Sagittal Plane Model of Posteroanterior Manipulation and Mobilization, *Clinical Biomechanics*, **17**, No. 3, 185-196.

Kettler, A., Hartwig, E., Schulthei, M., Claes, L., and Wilke, H. J. (2002) Mechanically Simulated Muscle Forces Strongly Stabilize Intact and Injured Upper Cervical Spine Specimens, *Journal of Biomechanics*, **35**, No. 3, 339-346.

Kleinberger, M. (1993) Application of Finite Element Techniques to the Study of Cervical Spine Mechanics, *Proceedings of the 37th Stapp Car Crash Conference*, San Antonio, TX, 261-272.

Klisch, S. M., and Lotz, J. C. (2000) A Special Theory of Biphasic Mixtures and Experimental Results for Human Annulus Fibrosus Tested in Confined Compression, *Journal of Biomechanical Engineering, Transactions of the ASME*, **122**, No. 2, 180-188.

Kopperdahl, D. L., and Keaveny, T. M. (1999) Biomechanical Consequences of an Isolated Overload in the Vertebral Body, *American Society of Mechanical Engineers, Bioengineering Division (Publication) BED, Advances in Bioengineering*, **42**, 365-366.

Kumaresan, S., Yoganandan, N., and Pintar, F. A. (1998) Finite Element Modeling Approaches of Human Cervical Spine Facet Joint Capsule, *Journal of Biomechanics*, **31**, No. 4, 371-376.

Kumaresan, S., Yoganandan, N., and Pintar, F. A. (1999a) Biomechanical Responses of Pediatric Cervical Spine Using Nonlinear Finite Element Approach, *American Society of Mechanical Engineers, Bioengineering Division (Publication) BED, Advances in Bioengineering*, **42**, 143-144.

Kumaresan, S., Yoganandan, N., and Pintar, F. A. (1999b) Finite Element Modeling of Spinal Ligaments, *American Society of Mechanical Engineers, Bioengineering Division (Publication) BED, Advances in Bioengineering*, **42**, 281-282.

Kumaresan, S., Yoganandan, N., Pintar, F. A., Maiman, D. J., and Kuppa, S. (2000) Biomechanical Study of Pediatric Human Cervical Spine: A Finite Element Approach, *Journal of Biomechanical Engineering, Transactions of the ASME*, **122**, No. 1, 60-71.

Kumaresan, S., Yoganandan, N., Pintar, F. A., Maiman, D. J., and Goel, V. K. (2001) Contribution of Disc Degeneration to Osteophyte Formation in the Cervical Spine: A Biomechanical Investigation, *Journal of Orthopaedic Research*, **19**, 977-984.

Kumaresan, S., Yoganandan, N., Pintar, F. A., Voo, L., Cusick, J., and Larson, S. (1997) Finite Element Modeling of Cervical Laminectomy with Graded Facetectomy, *Journal of Spinal Disorders*, **10**, No. 1, 40-47.

Laible, J. P., Pflaster, D. S., Krag, M. H., Simon, B. R., and Haugh, L. D. (1993) A Poroelastic-Swelling Finite Element Model with Application to the Intervertebral Disc, *Spine*, **18**, No. 5, 659-670.

Lariviere, C., Gagnon, D., and Loisel, P. (2002) A Biomechanical Comparison Of Lifting Techniques Between Subjects With And Without Chronic Low Back Pain

During Freestyle Lifting And Lowering Tasks, *Clinical Biomechanics*, **17**, No. 2, 89-98.

Lavaste, F., Skalli, W., Robin, S., Roy-Camille, R., and Mazel, C. (1992) Three-Dimensional Geometrical and Mechanical Modelling of the Lumbar Spine, *Journal of Biomechanics*, **25**, No. 10, 1153-1164.

Lee, C.-K., Kim, Y. E., Lee, C.-S., Hong, Y.-M., Jung, J.-M., and Goel, V. K. (2000) Impact Response of the Intervertebral Disc in a Finite-Element Model, *Spine*, **25**, No. 19, 2431-2439.

Lee, M., Kelly, D.W., and Steven, G.P. (1995) A Model Of Spine, Ribcage And Pelvic Responses To A Specific Lumbar Manipulative Force In Relaxed Subjects, *Journal of Biomechanics*, **28**, No. 11, 1403-1408.

Lemosse, D., Le Rue, O., Diop, A., Skalli, W., Marec, P., and Lavaste, F. (1998) Characterization of the Mechanical Behaviour Parameters of the Costo-Vertebral Joint, *European Spine Journal*, **7**, No. 1, 16-23.

Li, S., Patwardhan, A. G., Amirouche, F. M. L., Havey, R., and Meade, K. P. (1995) Limitations of the Standard Linear Solid Model of intervertebral Discs Subject to Prolonged Loading and Low-Frequency Vibration in Axial Compression, *Journal of Biomechanics*, **28**, No. 7, 779-790.

Li, Y., Bishop, P. J., Wells, R. P., and McGill, S. M. (1991) Quasi-Static Analytical Sagittal Plane Model of the Cervical Spine in Extension and Compression, *SAE (Society of Automotive Engineers) Transactions*, **100**, No. 6, 2066-2080.

Lim, T.-H., Goel, V. K., Weinstein, J. N., and Kong, W. (1994) Stress Analysis of a Canine Spinal Motion Segment Using the Finite Element Technique, *Journal of Biomechanics*, **27**, No. 10, 1259-1269.

Lindbeck, L. (1987) Analysis of the Asymmetrically Loaded Spine by Means of a Continuum Beam Model, *Journal of Biomechanics*, **20**, No. 8, 753-765.

Liu, Y. K. (1986) Finite Element Modeling of the Head and Spine, *Mechanical Engineering*, **108**, No. 1, 60-64.

Lizee, E., Robin, S., Song, E., Bertholon, N., LeCoz, J.-Y., Besnault, B., and Lavaste, F. (1998) Development of a 3D Finite Element Model of the Human Body, *Proceedings of the 38th Stapp Car Crash Conference*, 115-138.

Lucas, D. B., and Bressler, B. (1961) Stability of the Ligamentous Spine, Biomechanics Laboratory, University of California, San Francisco, Berkley, 40.

Ma, D., and Lankarani, H.M. (1997) A Multibody/finite element analysis approach for modelling of crash dynamic responses, *Journal of Mechanical Design, Transactions of the ASME*, **119**, No. 3, 382-387.

Maquet, P. (1992) Iatrophysics to Biomechanics: From Borelli (1608-1679) to Pauwels (1885-1980), *J Bone Joint Surg Br*, **74**, No. 3, 335-339.

Merrill, T., Goldsmith, W., and Deng, Y-C. (1984) Three Dimensional Response of a Lumped Parameter Head – Neck Model Due to Impact and Impulsive Loading, *Journal of Biomechancis*, **17**, No. 2, 81-95.

Monheit, G., And Badler N. I. (1991) A Kinematic Model Of The Human Spine And Torso, *IEEE Computer Graphics And Applications*, **11**, No. 2, 29-38.

Montgomery, R. E., Mindrup, S. R., Grobler, L. J., and Goel, V. K. (1999) In Vitro Biomechanics of the Harms Interbody Cage System, *American Society of Mechanical Engineers, Bioengineering Division (Publication) BED, Advances in Bioengineering*, **42**, 283-284.

Moroney, S. P., Schultz, A. B., Miller, J. A. A., and Andersson, G. B. J. (1988) Load-Displacement Properties of Lower Cervical Spine Motion Segments, *Journal of Biomechanics*, **21**, No. 9, 769-779.

Mosekilde, L. (2000) Age-Related Changes in Bone Mass, Structure, and Strength - Effects Of Loading, *Zeitschrift Fur Rheumatologie*, **59**, SUPP/1, 1-9.

MSC visualNastran 2001 Theory Manual (2001) MSC.Software Corporation.

Myklebust, J. B., Pintar, F., Yoganandan, N., Cusick, J. F., Maiman, D., Myers, T. J., and Sances, A. (1988) Tensile Strength of Spinal Ligaments, *Spine*, **13**, No. 5, 526-531.

Nabhani, F., and Wake, M. (2002) Computer Modelling and Stress Analysis of the Lumbar Spine, *Journal of Materials Processing Technology*, **127**, pp. 40-47.

Natarajan, R. N., Chen, B. H., An, H. S., and Andersson, G. B. J. (1999) Biomechanical Study on the Stability of Cervical Graft Fusion, *American Society of Mechanical Engineers, Bioengineering Division (Publication) BED, Advances in Bioengineering*, **42**, 57-58.

Natarajan, R. N., Williams, J. R., and Andersson, G. B. J. (2001) Biomechanical Response in a Lumbar Motion Segment to Dynamic Lifting Activity, *American Society of Mechanical Engineers, Bioengineering Division (Publication) BED, Advances in Bioengineering*, **50**, 823-824.

Ng, H. W., Teo, E. C., and Lee, V. S. (2004) Statistical Factorial Analysis on the Material Property Sensitivity of the Mechanical Responses of the C4-C6 under compression, Anterior, and Posterior Shear, *Journal of Biomechanics*, **37**, 771-777.

Nicholson, L., Maher, C., Adams, R., and Phan-Thien, N. (2001) Stiffness Properties of the Human Lumbar Spine: A Lumped Parameter Model, *Clinical Biomechanics*, **16**, pp. 285-292.

Nightingale, R. W., Winkelstein, B. A., Knaub, K. E., Richardson, W. J., Luck, J. F., and Myers, B. S. (2002) Comparative Strengths and Structural Properties of the Upper and Lower Cervical Spine in Flexion and Extension, *Journal of Biomechanics*, **35**, No. 6, 725-732.

Nissan, M., and Gilad, I. (1984) The Cervical and Lumbar Vertebrae - An Anthropometric Model, *Engineering in Medicine*, **13**, No. 3, 111-114.

Nitsche, S., Krabbel, G., Appel, H., and Haug, E. (1996) Validation of a Finite Element Model of the Human Neck, *International IRCOBI Conference on the Biomechanics of Impact*, Dublin, Ireland, 107-108.

Noone, G., Mazumdar, J., abd Ghista, D. (1991) Continuous Model of the Human Scoliotic Spine, *Journal of Biomedical Engineering*, **13**, No. 6, 473-480.

Nowitzke, A., Westaway, M., and Bogduk, N. (1994) Cervical zygapophysial joints: geometrical parameters and relationship to cervical kinematics, *Clinical Biomechanics*, **9**, 342-347.

Nussbaum, M. A., and Chaffin, D. B. (1996) Development and Evaluation of a Scalable and Deformable Geometric Model of the Human Torso, *Clinical Biomechanics*, **11**, No. 1, 25-34.

Ono, K., Inami, S., Kaneoka, K., Gotou, T., Kisanuki, Y., Sakuma, S., and Miki, K. (1999) Relationship Between Localised Spine Deformation and Cervical Vertebral Motions for Low Speed Rear Impacts Using Human Volunteers, *Proceedings of IRCOBI conference*, Sitges, Spain, 149-163.

Ono, K., Kaneoka, K., Wittek, A., and Kajzer, J. (1997) Cervical injury mechanism based on the analysis of human cervical vertebral motion and head-neck-torso kinematics during low speed rear impacts, In *Proceedings of the 41st Stapp Car Crash Conference*, Society of Automotive Engineers, SAE Paper No. 973340, 339-356.

Overaker, D. W., Langrana, N. A., and Cuitino, A. M. (1999) A Nonlinear Micromechanical Model For Vertebral Trabecular Bone and Application in Whole Bone Finite Element Analysis, *American Society of Mechanical Engineers, Bioengineering Division (Publication) BED, Advances in Bioengineering*, **42**, 361-362.

Panjabi, M. M., Crisco, J. J., Lydon, C., and Dvorak, J. (1998) The Mechanical Properties of Human Alar and Transverse Ligaments at Slow and Fast Extension Rates, *Clinical Biomechanics*, **13**, No. 2, 112-120.

Panjabi, M. M., Duranceau, J., Goel, V., Oxland, T., and Takata, K. (1991a) Cervical Human Vertebrae: Quantitative Three-Dimensional Anatomy of the Middle and Lower Regions, *Spine*, **16**, No. 8, 861-869.

Panjabi, M. M., Dvorak, J., Duranceau, J., Yamamoto, I., Geber, M., Rausching, W., and Bueff, H. U. (1988) Three-dimensional movements of the upper cervical spine, *Spine*, **13**, 726-730.

Panjabi, M. M., Goel, V., Oxland, T., Takata, K., Duranceau, J., Krag, M., and Price, M. (1992) Human Lumbar Vertebrae - Quantitative 3-Dimensional Anatomy, *Spine*, **17**, No. 3, 299-306.

Panjabi, M. M., Krag, M. H., and Goel, V. K. (1981) A Technique for Measurement and Description of 3-Dimensional 6-Degree-of-Freedom Motion of a Body Joint With an Application to the Human Spine, *Journal of Biomechanics*, **14**, No. 7, 447-460.

Panjabi, M. M., Oxland, T. R., and Parks, E. H. (1991b) Quantitative Anatomy of Cervical Spine Ligaments. Part I. Upper Cervical Spine, *Journal of Spinal Disorders*, **4**, No. 3, 270-276.

Panjabi, M. M., Oxland, T. R., and Parks, E. H. (1991c) Quantitative Anatomy of Cervical Spine Ligaments. Part II. Middle and Lower Cervical Spine, *Journal of Spinal Disorders*, **4**, No. 3, 277-285.

Panjabi, M. M., Oxland, T., Takata, K., Goel, V., Duranceau, J., and Krag, M. (1993) Articular Facets of the Human Spine - Quantitative 3-Dimensional Anatomy, *Spine*, **18**, No. 10, 1298-1310.

Patwardhan, A. G., Carandang, G., Ghanayem, A., Voronov, L., Havey, R. M., Phillips, F., Cunningham, B., Simonds, J., Meade, K. P., Lim, T.-H., Gavin, T. M., and Zindrick, M. R. (2001) Effect of Compressive Preload on the Response of the Anterior Lumbar Interbody Fusion Cage Construct and Adjacent Segments, *American Society of Mechanical Engineers, Bioengineering Division (Publication) BED, Advances in Bioengineering*, **50**, 829-830.

Patwardhan, A. G., Havey, R. M., Diener, H., Ghanayem, K. P., Meade, K. P., and Lim, T.-H. (1999) A Follower Load Stabilizes the Whole Lumbar Spine Without Compromising Mobility in The Sagittal Plane, *American Society of Mechanical Engineers, Bioengineering Division (Publication) BED, Advances in Bioengineering*, **42**, 173-174.

Patwardhan, A. G., Meade, K. P., and Lee, B. (2001) A Frontal Plane Model of the Lumbar Spine Subjected to a Follower Load: Implications for the Role of Muscles, *Journal of Biomechanical Engineering, Transactions of the ASME*, **123**, No. 3, 212-217.

Pintar, F. A., Yoganandan, N., Myers, T., Elhagediab, A., and Sances, A. Jr. (1992) Biomechanical Properties of Human Lumbar Spine Ligaments, *Journal of Biomechanics*, **25**, No. 11, 1351-1356.

Puttlitz, C. M., Goel, V. K., Grosland, N. M., Scifert, J. L., Clark, C. R., and Traynelis, V. C. (1999) Biomechanical Aspects of Early Rheumatoid Arthritis Involvement of the Upper Cervical Spine: A Finite Element Investigation, *American Society of Mechanical Engineers, Bioengineering Division (Publication) BED, Advances in Bioengineering*, **42**, 53-54.

Rack, P. M. H., and Westbury, D. R. (1969) The effects of length and stimulus rate on tension in the isometric cat soleus muscle, *J Physiol*, **204**, 443-460.

Reber, J. G., and Goldsmith, W. (1979) Analysis of large head-neck motions, *Journal of Biomechanics*, **12**, 211-222.

Reeves, N. P., and Cholewicki, J. (2003) Modelling the Human Lumbar Spine for Assessing Spinal Loads, Stability, and Risk of Injury, *Critical Reviews in Biomedical Engineering*, **31**, No. 1, 73-139.

Reid, J. E., Meakin, J. R., Robins, S. P., Skakle, J. M. S., and Hukins, D. W. L. (2002) Sheep Lumbar Intervertebral Discs As Models for Human Discs, *Clinical Biomechanics*, **17**, No. 4, 312-314.

Reid, S. E., and Raviv, G. (1981) Neck muscle resistance to head impact, *Aviat Space Environ Med*, 78-84.

Renfroe, D. A., and Partain, J. F. (1999) Dynamics of Vehicle Occupants in Forward and Lateral Impacts, *American Society of Mechanical Engineers, Bioengineering Division (Publication) BED, Advances in Bioengineering*, **42**, 151-152.

Riches, P. E., Dhillon, N., Lotz, J., Woods, A. W., and McNally, D. S. (2002) The Internal Mechanics of the Intervertebral Disc Under Cyclic Loading, *Journal of Biomechanics*, **35**, No. 9, 1263-1271.

Richmond, F. J. R., Singh, K., and Corneil, B. D. (2001) Neck muscles in the rhesus monkey. I. Muscle morphometry and histochemistry, *J Neurosci*, **86**, 1717-1728.

Rothman, R. H., and Simeone, F. A. (1982) *The Spine – Volume I*, 2nd Ed., W.B. Saunders Company, Philadelphia, Ch. 2.

Saito, T., Yamamuro, T., Shikata, J., Oka, M., and Tsutsumi, S. (1991) Analysis and Prevention of Spinal Column Deformity Following Cervical Laminectomy, Pathogenetic Analysis of Post Laminectomy Deformities, *Spine*, **16**, 494-502.

Sakamoto, J., Oda, J., Akamaru, T., Kawahara, N., and Tomita, K. (2001) Mechanical Evaluation of Reconstructed Structure After Total En Bloc Spondylectomy, *American Society of Mechanical Engineers, Bioengineering Division (Publication) BED, Advances in Bioengineering*, **50**, 825-826.

Sakamoto, J., Oda, J., Murakami, H., Kawahara, N., and Tomita, K. (1999) Reconstructed Structure Designs of Total Sacrectomy and Their Mechanical Evaluations, *American Society of Mechanical Engineers, Bioengineering Division (Publication) BED, Advances in Bioengineering*, **42**, 175-176.

Sances, A. Jr. (1999) Biomechanics of Airbag Injuries, *American Society of Mechanical Engineers, Bioengineering Division (Publication) BED, Advances in Bioengineering*, **42**, 147-148.

Sances, A., Friedman, K., Gaston, F., Bish, J., and Rogers, C. (1999) Experimental Investigation and Finite Element Analysis of Vehicle Restraint Systems, *American Society of Mechanical Engineers, Bioengineering Division (Publication) BED, Advances in Bioengineering*, **42**, 153-154.

Schibye, B., Sogaard, K., Martinsen, D., and Klausen, K. (2001) Mechanical Load on the Low Back and Shoulders During Pushing and Pulling of Two-Wheeled

Waste Containers Compared with Lifting and Carrying of Bags and Bins, *Clinical Biomechanics*, **16**, No. 7, 549-559.

Schultz, A. B., and Galante, J. O. (1970) A Mathematical Model for the Study of the Mechanics of the Human Vertebral Column, *Journal of Biomechanics*, **3**, 405-416.

Scifert, J. L., Goel, V. K., Grosland, N. M., Puttlitz, C. M., Totoribe, K., and Traynelis, V. C. (1999) Finite Element Investigation of Anterior Plate and Bone Graft Load Sharing in the Cervical Spine, *American Society of Mechanical Engineers, Bioengineering Division (Publication) BED, Advances in Bioengineering*, **42**, 51-52.

Scott, S. H., Brown, I. E., and Loeb, G. E. (1996) Mechanics of feline soleus: I. Effect of fascicle length and velocity on force output, *J Muscle Res Cell Motil*, **17**, 207-219.

Seng, K.-Y. (2001) An Advanced Method to Measure Isometric Strength of the Cervical Musculature, *American Society of Mechanical Engineers, Bioengineering Division (Publication) BED, Advances in Bioengineering*, **50**, 261-262.

Shirazi-Adl, A. (1994) Biomechanics of the Lumbar Spine in Sagittal/Lateral Moments, *Spine*, **19**, No. 21, 2407-2414.

Shirazi-Adl, A., and Drouin, G. (1988) Nonlinear Gross Response Analysis Of A Lumbar Motion Segment In Combined Sagittal Loadings, *Journal of Biomechanical Engineering, Transactions of the ASME*, **110**, No. 3, 216-222.

Shirazi-Adl, A., and Parnianpour, M. (1996) Stabilizing Role of Moments and Pelvic Rotation on the Human Spine in Compression, *Journal of Biomechanical Engineering, Transactions of the ASME*, **118**, No. 1, 26-31.

Shirazi-Adl, A., and Parnianpour, M. (2000) Load-Bearing and Stress Analysis of the Human Spine Under a Novel Wrapping Compression Loading, *Clinical Biomechanics*, **15**, No. 10, 718-725.

Siegmund, G. P., and Brault, J. R. (2000) Role of cervical muscles during whiplash, In N. Yoganandan and F.A. Pintar, editors, *Frontiers in Whiplash Trauma, Clinical and Biomechanical*, IOS Press, Amsterdam, 295–320.

Silva, M. P. T., and Ambrosio, J. A. C. (2004) Sensitivity of the Results Produced by the Inverse Dynamic Analysis of a Human Stride to Perturbed Input Data, *Gait and Posture*, **19**, 35-49.

Snyder, R. G., Chaffin, D. B., and Foust, D. R. (1975) Bioengineering study of basic physical measurements related to susceptibility to cervical hyperextension-hyperflexion injury, *Report UM-HSRI-BI-75-6*, Highway Safety Research Institute, University of Michigan, Ann Arbor, Michigan.

Spilker, R. l., Daugirda, D. M., and Schultz, A. B. (1984) Mechanical Response of a Simple Finite-Element Model of the Intervertebral Disc Under Complex Loading, *Journal of Biomechanics*, **17**, No. 2, 103-112.

Stokes, I. A., Gardner-Morse, M., Churchill, D., and Laible, J. P. (2002) Measurement of a Spinal Motion Segment Stiffness Matrix, *Journal of Biomechanics*, **35**, No. 4, 517-521.

Swartz, D. E., Wittenberg, R. H., Shea, M., White, A. A., and Hayes, W. C. (1991) Physical and Mechanical Properties of Calf Lumbosacral Trabecular Bone, *Journal of Biomechanics*, **24**, No. 11, 1059-1068.

Tan, S. H., Teo, E. C., and Chua, H. C. (2002) Quantitative Three-Dimensional Anatomy of Lumbar Vertebrae in Singaporean Asians, *European Spine Journal*, **11**, No. 2, 152-158.

Teo, E. C., and Ng, H. W. (2001) Evaluation of the Role of Ligaments, Facets, and Disc Nucleus in Lower Cervical Spine Under Compression and Sagittal Moments Using Finite Element Method, *Medical Engineering and Physics*, **23**, 155-164.

Teo, E. C., Paul, J. P., and Evans, J. H. (1994) Finite Element Stress Analysis of a Cadaver Second Cervical Vertebra, *Med Biol Eng Comput*, **32**, 236-238.

Thacker, B. H., Nicolella, D. P., and Jones, G. M. (1999) Development of a Parametric Cervical Spine Model for Risk of Injury Assessment Using Probabilistic Finite Element Methods, *American Society of Mechanical Engineers, Bioengineering Division (Publication) BED, Advances in Bioengineering*, **42**, 59-60.

Thacker, B. H., Nicolella, D. P., Kumaresan, S., Yoganandan, N., and Pintar, F. A. (2001) Probabilistic Injury Analysis of the Human Cervical Spine, *American Society of Mechanical Engineers, Bioengineering Division (Publication) BED, Advances in Bioengineering*, **50**, 879-880.

Thunnissen, J., Wismans, J., Ewing, C. L., and Thomas, D. J. (1995) Human volunteer head-neck response in frontal flexion: A new Analysis. In *Proceedings of the 39th STAPP Car Crash Confernece*, Society of Automotive Engineers, SAE Paper No. 952721, 439-460.

Tominaga, T., Dickman, C. A., Sonntag, V. K. H., and Coons, S. (1995) Comparative Anatomy of the Baboon and the Human Cervical Spine, *Spine*, **20**, No. 2, 131-137.

Tözeren, A. (2000) *Human Body Dynamics – Classical Mechanics and Human Movement*, Springer-Verlag Inc., New York, Ch. 1.

Van Der Horst, M. J. (2002) Human Head Neck Response in Frontal, Lateral and Rear End Impact Loading - modelling and validation, PhD Thesis, Technical University of Eindhoven.

Van Der Horst, M. J., Thunnsissen, J. G. M., Happee, R., Van Haaster, R. M. H. P., and Wismans, J. S. H. M., (1997) The influence of muscle activity on the head-neck response during impact, *SAE conference proceedings*, **315**, 487-508.

Van Dieen, J. H., Hoozemans, M. J., van der Beek, A. J., and Mullender, M. (2002) Precision of Estimates of Mean and Peak Spinal Loads in Lifting, *Journal of Biomechanics*, **35**, No. 7, 976-982.

Van Ee, C. A., Nightingale, R. W., Camacho, D. L. A., Chancey, V. C., Knaub, K. E., Sun, E. A., and Myers, B. A. (2000) Tensile Properties of the Human Muscular and Ligamentous Cervical Spine, *Proceedings of 44th Stapp Car Crash Conference*, Society of Automotive Engineers, 85-102.

Van Lopik, D. W. (2004) A Computational Model of the Human Head and Cervical Spine for Dynamic Impact Simulation, PhD Thesis, Loughborough University, UK.

Van Lopik, D. W., and Acar, M. (2002) The Development of a Multibody Head-Neck System for Impact Dynamics Using visualNastran 4D, *Proceedings of ESDA2002*.

Van Lopik, D. W., and Acar, M. (2004) A Computational Model of the Human Head and Neck System for the Analysis of Whiplash Motion, *International Journal of Crashworthiness*, **9**, No. 5, 465-473.

Van Sint Jan, S. (2005) Introducing Anatomical and Physiological Accuracy in Computerized Anthropometry for Increasing the Clinical Usefulness of Modeling Systems, *Critical Reviews in Physical and Rehabilitation Medicine*, **17**, No. 4, 249-274.

Van Sint Jan, S., Lufimpadio, J., Manero, C., Hilal, I., Sholukha, V., Salvia, P., Feipel, V., Sobczak, S., Dugailly, P-M., and Rooze, M. (2004) Methods for musculo-skeletal modeling: data collection and data processing, *Proceedings of the 14th conference of the European Society of Biomechanics*, 's-Hertogenbosch (Netherlands).

Vanderby, R. Jr., Daniele, M., Patwardhan, A., and Bunch, W. (1986) A Method For The Identification Of In-Vivo Segmental Stiffness Properties Of The Spine, *Journal of Biomechanical Engineering, Transactions of the ASME*, **108**, No. 4, 312-316.

Vasavada, A. N., Li, S., and Delp, S. L. (1998) Influence of muscle morphometry and moment arms on the moment-generating capacity of human neck muscles, *Spine*, **23**, No. 4, 412-422.

Vogt, L., Pfeifer, K., and Banzer, W. (2002) Comparison of Angular Lumbar Spine and Pelvis Kinematics During Treadmill and Overground Locomotion, *Clinical Biomechanics*, **17**, No. 2, 162-165.

Wagner, D. R., Klisch, S. M., and Lotz, J. C. (1999) A Constitutive Formulation Which Simultaneously Predicts The Response of The Annulus Fibrosus To

Seven Distinct Deformations, *American Society of Mechanical Engineers, Bioengineering Division (Publication) BED, Advances in Bioengineering*, **42**, 363-364.

Walker, L. B., Harris, E. H., and Pontius, U. R. (1973) Mass, volume, centre of mass, and mass moment of inertia of head and head and neck of the human body, *17th Stapp Car Crash Conference*, Society of Automotive Engineers. SAE Paper No. 730985, 525-537.

Wang, J.-L., Parnianpour, M., Shirazi-Adl, A., and Engin, A. E. (2000) Viscoelastic Finite-Element Analysis of a Lumbar Motion Segment in Combined Compression and Sagittal Flexion: Effect of Loading Rate, *Spine*, **25**, No. 3, 310-318.

Ward, C.C., and Hoffman, M. (1999) Interaction of Head and Neck with Head Restraints During Low Speed Rear End Impacts, *American Society of Mechanical Engineers, Bioengineering Division (Publication) BED, Advances in Bioengineering*, **42**, 145-146.

Warfel, J. H. (1985) *The Head, Neck, and Trunk*, 5th Ed., Lea & Febiger, Philadelphia.

Weber, W., and Weber, E. (1992) Translation: Mechanics of the Human Walking Apparatus, Springer-Verlag, Berlin.

Whealan, K. M., Kwak, S. D., Tedrow, J. R., Inoue, K., and Snyder, B. D. (1999) Composite Beam Theory Predicts The Fracture Load of Spines with Simulated Osteolytic Defects Using QCT, *American Society of Mechanical Engineers, Bioengineering Division (Publication) BED, Advances in Bioengineering*, **42**, 359-360.

White, A. A., and Panjabi, M. M. (1990) *Clinical Biomechanics of the Spine*, 2nd Ed., Lippincott - Raven Publishers, Philadelphia, Ch. 1, 2, 3, and 5.

Williams, J. L.., and Belytschko, T. B. (1983) A Three-Dimensional Model of the Human Cervical Spine for Impact Simulation, *Journal of Biomechanical Engineering, Transactions of the ASME*, **105**, No. 4, 321-331.

Winkelstein, B. A., and Myers, B. S. (2002) Importance of Nonlinear and Multivariable Flexibility Coefficients in the Prediction of Human Cervical Spine Motion, *Journal of Biomechanical Engineering, Transactions of the ASME*, **124**, No. 5, 504-511.

Winkelstein, B. A., Richardson, W. J., and Myers, B. S. (1999) A Mechanical Investigation of The Role of The Cervical Facet Capsule in Whiplash Injury, *American Society of Mechanical Engineers, Bioengineering Division (Publication) BED, Advances in Bioengineering*, **42**, 169-170.

Winters, J. M., and Stark, L. (1988) Estimated mechanical properties of synergistic muscles involved in movements of a variety of human joints, *Journal of Biomechanics*, **21**, 1027-1041.

Winters, J. M., and Woo, S. L-Y. (1990) Multiple Muscle Systems: Biomechanics and Movement Organization. Springer-Verlag.

Wismans, J., Happee, R., and van Dommelen, J. A. W. (2005) Computational Human Body Models, *Proceedings of IUTAM Symposium on Impact Biomechanics: From Fundamental Insights to Applications*, Dublin, Springer, 417-429.

Wismans, J., Van Oorshot, E., and Woltring, H. J. (1986) Omni-directional human head-neck response, *30th Stapp Car Crash Proceedings*, Society of Automotive Engineers, SAE Paper No. 861893, 313-331.

Wittek, A, Ono, K., and Kajzer, J. (2000) Finite Element Model for Simulation of Muscle Effects on Kinematic Response of Cervical Spine in Low-Speed Rear-End Impacts, *JARI Research Journal*, **22**, No. 5, 224-227.

Wu, G., Siegler, S., Allard, P., Kirtley, C., Leardini, A., Rosenbaum, D., Whittle, M., D`Lima, D. D., Cristofolini, L., and Witte, H. (2002) ISB Recommendation on Definitions of Joint Coordinate System of Various Joints for the Reporting of Human Joint Motion - Part I: Ankle, Hip, and Spine, *Journal of Biomechanics*, **35**, No. 4, 543-548.

Wynarsky, G. T., and Schultz, A. B. (1991) Optimization of Skeletal Configuration - Studies Of Scoliosis Correction Biomechanics, *Journal of Biomechanics*, **24**, No. 8, 721-732.

Xinghua, Z., He, G., Dong, Z., and Bingzhao, G. (2002) A Study Of The Effect Of Non-Linearities In The Equation Of Bone Remodeling, *Journal of Biomechanics*, **35**, No. 7, 951-960.

Xu, R., Nadaud, M. C., Ebraheim, N. A., and Yeasting, R. A. (1995) Morphology of the Second Cervical Vertebra and the Posterior Projection of the C2 Pedicle Axis, *Spine*, **20**, No. 3, 259-263.

Yamada, H. (1970) Strength of Biological Materials, The Williams & Wilkins Company, Baltimore.

Yamaguchi, G. T., Sawa, A. G. U., Moran, D. W., Fessler, M. J., and Winters, J. M. (1990) A Survey of Human Musculotendon Actuator Parameters, *Multiple Muscle Systems: Biomechanics and Movement Organization*, Springer-Verlag, New York.

Yamamoto, S., Tanaka, E., and Watanebe, Y. (2001) Effects of Spondylolytic Defect on the Stress Distributions in Intervertebral Discs in Lower Lumbar Spine, *American Society of Mechanical Engineers, Bioengineering Division (Publication) BED, Advances in Bioengineering*, **50**, 827-828.

Yang, K. H., Zhu, F., Luan, F., Zhao, L., and Begeman, P. C. (1998) Development of a Finite Element Model of the Human Neck, *Proceedings of the 42nd Stapp Car Crash Conference*, Society of Automotive Engineers, SAE Paper No. 983157, 195-205.

Yeni, Y. N., Vashishth, D., and Fyhrie, D. P. (2001) Variations in Apparent Strength and Stiffness of Human Vertebral Cancellous Bone Are Consistent With Trabecular Shear Stress Distribution Statistics Along the Spine, *American Society of Mechanical Engineers, Bioengineering Division (Publication) BED, Advances in Bioengineering*, **50**, 19-20.

Yoganandan, N., and Pintar, F. A. (1999) Tension-Extension Biomechanics of the Cervical Spine, *American Society of Mechanical Engineers, Bioengineering Division (Publication) BED, Advances in Bioengineering*, **42**, 55-56.

Yoganandan, N., Kumaresan, S., and Pintar, F. A. (2000) Geometric and Mechanical Properties of Human Cervical Spine Ligaments, *Journal of Biomedical Engineering*, **122**, No. 6, 623-629.

Yoganandan, N., Pintar, F. A., Kumaresan, S., and Elhagediab, A. (1999) Biomechanical Assessment of Human Cervical Spine Ligaments, *SAE (Society of Automotive Engineers) Transactions*, **107**, No. 6, 2852-2861.

Yoganandan, N., Pintar, F. A., Maiman, D. J., Cusick, J. F., Sances, A. Jr., and Walsh, P. R. (1996) Human Head-Neck Biomechanics Under Axial Tension, *Medical Engineering & Physics*, **18**, No. 4, 289-294.

Yoganandan, N., Pintar, F., Butler, J., Reinartz, J., Sances, A., and Larson, S. J. (1989) Dynamic Response of Human Cervical Spine Ligaments, *Spine*, **14**, No. 10, 1102-1110.

Zajac, F. E. (1989) Muscle and tendon: Properties, models, scaling, and application to biomechanics and motor control, *Critical Reviews in Biomedical Engineering*, **17**, 359-411.

Zander, T., Rohlmann, A., Klockner, C., and Bergmann, G. (2002) Comparison of the Mechanical Behavior of the Lumbar Spine Following Mono- and Bisegmental Stabilization, *Clinical Biomechanics*, **17**, No. 6, 439-445.

Zander, T., Rohlmann, A., Klockner, C., and Bergmann, G. (2002) Effect of Bone Graft Characteristics on the Mechanical Behavior of the Lumbar Spine, *Journal of Biomechanics*, **35**, No. 4, 491-497.

Ziejewski, M., Obergefell, L., Perry, C., and Anderson, B. (1998) Modes of Human Head/Neck Response to Vertical Impact, *Proceedings of Models for Aircrew Safety Assessment: Uses, Limitations, and Requirements, RTO MP-20*, RTO HFM Specialists' Meeting, Ohio, USA, 3-1 – 3-10.

APPENDICES

Appendix A Modelling/Material Property Data for Spinal Elements

Appendix B Mean and Standard Deviation Values for Force and Deflection at Failure for Human Spinal Ligaments

Appendix C Equations and Coefficients for 'Virtual Muscle' Muscle Model

Appendix D A Survey of Human Musculotendon Actuator Parameters (Yamaguchi et al., 1990)

Appendix A: Modelling/Material Property Data for Spinal Elements

Table A.1 The failure strength of spinal ligaments (White and Panjabi, 1990)

	Load (N)		Deformation (mm)		Stress (MPa)		Strain (%)	
	Average	Range	Average	Range	Average	Range	Average	Range
Upper Cervical								
C0–C1								
Ant. atlantooccip. memb.	233		18.9					
Post. atlantooccip. memb.	83		18.1					
C1–C2								
ALL	281		12.3					
Atlanto-axial membrane	113		8.7					
CL	157		11.4					
Transverse ligament	354	170–700						
C0–C2								
Apical	214		11.5					
Alar	286	215–357	14.1					
Vert. cruciate	436		25.2					
Tectorial membrane	76		11.9					
Lower Cervical								
ALL	111.5	47–176	8.95	4.2–13.7				
PLL	74.5	47–102	6.4	3.4–9.4				
LF	138.5	56–221	8.3	3.7–12.9				
CL	204	144–264	8.4	6.8–10				
ISL	35.5	26–45	7.35	5.5–9.2				
SSL								
Thoracic								
ALL	295.5	123–468	10.25	6.3–14.2				
PLL	106	74–138	5.25	3.2–7.3				
LF	200	135–265	8.65	6.3–11				
CL	168	63–273	6.75	3.9–9.6				
ISL	75.5	31–120	5.25	3.8–6.7				
SSL	319.5	101–538	14.1	7.2–21				
Lumbar								
ALL	450	390–510	15.2	7–20	11.6	2.4–21	36.5	16–57.
PLL	324	264–384	5.1	4.2–7.0	11.5	2.9–20	26.0	8–44
LF	285	230–340	12.7	12.0–14.5	8.7	2.4–15	26.0	10–46
CL	222	160–284	11.3	9.8–12.8	7.6	7.6	12.0	12.0
ISL	125	120–130	13.0	7.4–17.8	3.2	1.8–4.6	13.0	13.0
SSL	150	100–200	25.9	22.1–28.1	5.4	2.0–8.7	32.5	26–39

ALL = anterior longitudinal ligament
PLL = posterior longitudinal ligament
LF = ligamentum falvum
CL = capsular ligament
ISL = interspinous ligament
SSL = supraspinous ligament

(Data from Chazal, et. al.,[48] Dvorak, et al.,[52] Goel, et al.,[54] Myklebust, et al.,[100] Nachemson and Evans,[104] Panjabi, et al.,[106] and Tkaczuk.[110])

Table A.2 Quantitative anatomy of vertebrae from T1 to T12 (White and Panjabi, 1990)

	T1	T2	T3	T4	T5	T6	T7	T8	T9	T10	T11	T12
UEW (mm)	24.5	24.9	24.6	24.5	24.9	26.2	27.8	29.5	30.6	31.9	34.9	39.0
UED (mm)	18.5	19.6	22.7	23.3	24.3	26.0	27.4	27.9	29.3	30.5	31.9	32.8
LEW (mm)	27.8	27.4	25.9	26.0	27.0	28.2	29.1	30.5	33.0	35.4	39.1	42.1
LED (mm)	19.7	21.6	23.3	24.5	25.8	26.9	28.5	29.4	31.0	31.6	31.8	33.4
VBHp (mm)	14.1	15.6	15.7	16.2	16.2	17.4	18.2	18.7	19.3	20.2	21.3	22.7
UEA (mm^2)	300.	333.	373.	381.	426.	483.	547.	603.	678.	727.	842.	954.
LEA (mm^2)	376.	398.	412.	444.	495.	552.	603.	664.	755.	834.	945.	1024.
UEIt (degrees)	0.8	1.7	2.4	1.5	2.1	2.1	1.6	1.3	0.9	0.5	2.7	2.2
LEIt (degrees)	3.9	1.8	2.1	2.0	1.8	2.0	2.3	1.2	1.2	2.2	1.8	2.0
SCW (mm)	21.8	19.5	18.3	17.0	17.1	17.3	17.3	17.7	17.9	18.2	19.4	22.2
SCD (mm)	16.4	15.3	15.9	16.2	16.3	16.5	16.1	15.9	15.7	15.5	16.0	18.1
SCA (mm)	213.	200.	189.	192.	201.	206.	199.	194.	200.	202.	220.	280.
PDW (mm)	8.2	8.4	7.0	5.5	6.2	6.0	6.5	6.7	7.6	8.3	8.6	8.8
PDH (mm)	9.3	11.1	11.8	11.9	11.2	12.0	11.8	12.5	13.9	14.7	16.9	16.5
PDA (mm^2)	52.2	46.3	38.1	32.5	31.6	3.5	36.8	43.8	52.3	64.8	88.4	90.9
PDIs (degrees)	28.1	28.9	22.5	21.8	20.2	19.4	23.4	22.5	19.3	14.4	12.0	8.0
PDIt (degrees)	4.6	16.5	8.1	6.4	8.6	7.0	10.9	12.1	8.3	8.8	8.9	4.8
SPL (mm)	50.1	52.1	51.7	51.1	52.1	53.8	50.5	52.8	51.3	49.3	45.6	47.4
TPW (mm)	73.3	69.4	60.8	56.9	61.1	61.3	60.4	59.9	59.3	58.4	52.2	46.9

Key: The first two letters indicate anatomic part; the third letter indicates dimension. Figure 1-18 depicts the anatomy of a vertebra in detail

UE = upper end-plate
LE = lower end-plate
PD = pedicle
SP = spinous process
SC = spinal canal
TP = transverse process
PI = pars interarticularis
VB = vertebral body
W = width
A = area
D = depth
H = height
I = inclination
t = transverse plane
p = posterior

(Based upon data from Berry, et al.,[11] Cotterill, et al.,[47] and Panjabi, et al.[182])

Table A.3 Rotation ranges for the middle and lower cervical spine (White and Panjabi, 1990)

	Combined Flexion/Extension (±x-axis rotation)		One Side Lateral Bending (z-axis rotation)		One Side Axial Rotation (y-axis rotation)	
Interspace	Limits of Ranges (degrees)	Representative Angle (degrees)	Limits of Ranges (degrees)	Representative Angle (degrees)	Limits of Ranges (degrees)	Representative Angle (degrees)
Middle						
C2–3	5–16	10	11–20	10	0–10	3
C3–4	7–26	15	9–13	11	3–10	7
C4–5	13–29	20	0–16	11	1–12	7
Lower						
C5–6	13–29	20	0–16	8	2–12	7
C6–7	6–26	17	0–17	7	2–10	6
C7–T1	4–7	9	0–17	4	0–7	2

Table A.4 Nomenclature for a typical lumbar vertebra (Panjabi et al., 1992)

Mnemonics	*Dimension*	*Reference*
EPWu	End-Plate Width, Upper	Panjabi et al. (1992)
EPWl	End-Plate Width, Lower	
TPW	Transverse Process Width	
SCW	Spinal Canal Width	
SCD	Spinal Canal Depth	
PA	Pedicle Angle	
PW	Pedicle Width	
PH	Pedicle Height	
IFWu	Interfacet Width, Upper	Panjabi et al. (1993)
IFWl	Interfacet Width, Lower	
FW	Facet Width	
FH	Facet Height	

Table A.5 Lumbar vertebral body dimensions (Panjabi et al., 1992)

	Lumbar Vertebral Level				
	L1	*L2*	*L3*	*L4*	*L5*
Linear dimensions (mm)					
EPDu	34.1 ± 1.34	34.6 ± 1.10	35.2 ± 1.10	35.5 ± 0.80	34.7 ± 1.17
EPWu	41.2 ± 1.03	42.8 ± 0.74	44.1 ± 0.63	46.6† (L1) ± 1.20	47.3† (L1) ± 1.20
EPDl	35.3 ± 1.27	34.9 ± 0.74	34.8 ± 1.24	33.9 ± 0.85	33.2 ± 0.92
EPWl	43.3 ± 0.78	45.5 ± 1.10	48.0 ± 1.24	49.5† (L1) ± 1.38	49.4† (L1) ± 1.41
VBHp	23.8 ± 1.03	24.3 ± 0.95	23.6 ± 1.10	24.1 ± 1.10	22.9 ± 0.95
EPWu/EPDu	1.21	1.23	1.25	1.31	1.36
EPWl/EPDl	1.23	1.30	1.38	1.46	1.49
Surface Areas (mm²)					
EPAu	1057 ± 60.78	1136 ± 61.84	1194 ± 55.19	1239 ± 58.41	1237 ± 58.48
EPAl	1117 ± 43.00	1197 ± 51.41	1290 ± 64.35	1273 ± 51.72	1218 ± 59.43
Angular measures (deg)					
EPIu	2.7 ± 0.77	3.5 ± 1.5	1.7 ± 0.43	4.7 ± 1.1	2.2 ± 0.54
EPIl	4.0 ± 0.54	2.1 ± 0.4	2.7 ± 1.1	2.7 ± 0.69	1.8 ± 0.42

Table A.6 Lumbar spinal canal dimensions (Panjabi et al., 1992)

	Lumbar Vertebral Level				
	L1	*L2*	*L3*	*L4*	*L5*
Linear dimensions (mm)					
SCW	23.7 ± 0.92*	23.8 ± 0.71	24.3 ± 0.84	25.4 ± 0.49	27.1 ± 0.88
SCD	19.0 ± 0.67	18.2 ± 0.53	17.5 ± 0.53	18.6 ± 0.71	19.7 ± 0.49
SCW/SCD	1.25	1.31	1.39	1.37	1.38
Cross-sectional areas (mm²)					
SCA	320 ± 18.10	281 ± 15.38	280 ± 14.64	290 ± 15.17	330 ± 21.2*

Table A.7 Lumbar pedicle dimesions (Panjabi et al., 1992)

	Lumbar Vertebral Level				
	L1	L2	L3	L4	L5
Linear dimensions (mm)					
PDWr	8.0 ± 0.95*	7.8 ± 0.57	10.2 ± 0.67	13.4† (L1-L2) ± 0.19	12.3* (L1-L4) ± 1.0*
PDHr	15.9 ± 0.81	15.0 ± 0.53	14.2 ± 0.64	15.7 ± 0.57	15.6* (L1-L4) ± 0.74
PDWl	9.2 ± 0.68	8.7 ± 0.78	10.1 ± 0.53	11.7* (L1-L3) ± 0.45	13.2† (L1-L4) ± 1.1*
PDHl	15.8 ± 0.72	14.9 ± 0.51	14.6 ± 0.60	15.2 ± 0.46	15.5† (L1-L4) ± 0.91
PDHr/PDWr	2.00	1.91	1.39	1.17	1.09
PDHl/PDWl	1.72	1.71	1.44	1.03	1.02
Cross-sectional areas (mm^2)					
PDAr	88.4 ± 11.42	83.0 ± 8.94	92.9 ± 7.71	102.8 ± 6.65	143.9† (L1-L3) ± 9.5*
PDAl	88.5 ± 11.74	93.6 ± 8.87	95.3 ± 9.17	112.3 ± 7.53	158.7* (L1-L4) ± 10.5*
Angular dimensions (°)					
PDtr	16.5 ± 5.02	17.1 ± 3.75	19.8 ± 2.33	18.4 ± 1.66	25.9 ± 1.73
PDsl	2.2 ± 0.67	3.3 ± 0.67	2.9 ± 1.06	4.8 ± 1.06	5.7 ± 1.85
PDtl	12.4 ± 1.87	11.2 ± 2.02	11.7 ± 1.56	14.7 ± 2.15	23.2* (L1-L2 ± 2.51
PDtl	2.9 ± 0.74	3.1 ± 0.64	2.4 ± 0.67	3.0 ± 1.17	5.7 ± 1.48

Table A.8 Geometric and morphologic features of the lumbar muscles (Bogduk et al., 1992)

Fascicle	Angle POA (degrees)	BC (mm)	PO (mm)	PCSA (mm^2)	SD	F_{avg} (N)	F_v (N)	F_h (N)
m1s	−7	17.5	111	40	14	39.5K	39.2K	−4.8K
m1L1	−8	20.6	146	42	17	41.6K	41.2K	−5.9K
m1T.2	−2	22.2	177	36	9	35.7K	35.6K	−1.1K
m1L3	14	27.7	190	60	41	59.4K	57.6K	14.4K
m2s	0	20.6	98	39	13	38.2K	38.2K	0.0K
m2L1	−1	22.2	124	39	06	38.4K	38.2K	−0.8K
m2L2-3	22	30.4	154	99	30	97.1K	90.1K	36.6K
m3s	1	22.2	80	54	16	52.0K	51.6K	1.1K
m3L1-3	23	31.3	119	157	51	151.6K	139.7K	59.7K
m4s-m4L3	8	20.3	73	185	38	179.2K	176.7K	24.2K
m5s-m5L3	−11	7.6	41	90	34	88.5K	87.2K	17.1K
l1	22	9.2	224	108	20	107.4K	100.4K	40.0K
l2	21	7.5	152	154	37	153.8K	143.2K	55.4K
l3	20	4.4	102	182	62	181.8K	171.1K	61.9K
l4	18	3.2	54	199	80	188.6K	162.5K	94.5K
l1	21	17.3	244	79	32	78.8K	73.5K	28.4K
l2	27	15.1	191	91	22	90.7K	81.0K	41.0K
l3	28	11.3	140	103	44	102.7K	90.6K	48.4K
l4	28	14.6	89	110	39	108.8K	95.7K	50.6K
l5	41	3.3	44	116	51	115.7K	87.0K	75.4K

Table A.9 Moment arms of lumbar muscles (Bogduk et al., 1992)

Fascicle	Moment Arms (mm) by Segment				
	L1–2	L2–3	L3–4	L4–5	L5–S1
m1s	44.1	41.7	34.6	—	—
m1t.1	54.6	51.3	43.3	28.3	—
m1t.2	54.8	55.5	51.5	40.1	24.6
m1t.3	52.5	63.6	69.8	68.2	60.2
m2s	—	45.5	41.6	30.3	—
m2t.1	—	56.0	51.7	40.0	24.5
m2t.2–3	—	53.4	63.3	65.4	60.1
m3s	—	—	45.1	39.1	27.7
m3t.1–3	—	—	52.3	59.5	58.6
m4s–m4t.3	—	—	—	46.7	47.2
m5s–m5t.3	—	—	—	—	42.0
i1	34.8	49.6	62.0	56.9	56.9
i2	—	35.4	46.0	47.8	42.4
i3	—	—	35.2	40.6	39.3
i4	—	—	—	21.9	35.0
l1	32.6	47.9	58.3	61.0	56.3
l2	—	35.5	49.0	54.5	52.2
l3	—	—	35.3	45.9	47.9
l4	—	—	—	33.3	41.8
l5	—	—	—	—	28.2
IT5	53	57	62	57	68
IT6	53	57	62	57	57
IT7	53	57	62	57	45
IT8	53	57	62	46	36
IT9	53	57	52	46	26
IT10	53	43	52	46	26
IT11	31	40	52	46	25
IT12	31	30	43	35	25
LT1	53	—	—	—	—
LT2	53	—	—	—	—
LT3	53	47	—	—	—
LT4	53	57	62	—	—
LT5	53	57	62	—	—
LT6	53	57	62	57	—
LT7	53	57	62	57	45
LT8	53	57	62	57	45
LT9	53	57	62	57	45
LT10	46	57	62	57	45
LT11	38	49	62	57	45
LT12	31	40	52	57	45

Table A.10 Maximum moments generated by lumbar muscles (Bogduk et al., 1992)

	Maximum Force (N) and Moments (Nm) by Segment					
Fascicle	Force	L1-2	L2-3	L3-4	L4-5	L5-S1
m1s	39.5K	1.7K	1.7K	1.4K	—	—
m1t.1	41.6K	2.3K	2.1K	1.8K	1.2K	—
m1t.2	35.7K	2.0K	2.0K	1.8K	1.4K	0.9K
m1t.3	53.4K	3.1K	3.8K	4.2K	4.1K	3.5K
m2s	38.2K	—	1.7K	1.6K	1.2K	—
m2t.1	33.4K	—	2.2K	2.0K	1.5K	0.3K
m2t-2-3	97.1K	—	5.2K	6.2K	6.4K	5.2K
m3s	52.0K	—	—	2.4K	2.4K	1.4K
m3t.1-3	151.8K	—	—	7.9K	9.0K	8.9K
m4s-m4t.3	179.2K	—	—	—	8.7K	8.5K
m5s-m5t.3	68.5K	—	—	—	—	3.7K
i1	107.4K	3.3K	5.6K	6.7K	6.7K	5.1K
i2	153.8K	—	5.6K	7.1K	7.3K	6.5K
i3	181.9K	—	—	6.4K	7.3K	7.0K
i4	188.7K	—	—	—	6.0K	6.6K
l1	78.3K	2.6K	3.8K	4.6K	4.8K	4.4K
l2	90.7K	—	3.2K	4.4K	4.9K	4.7K
l3	102.7K	—	—	3.6K	4.7K	4.9K
l4	108.6K	—	—	—	3.6K	4.5K
l5	115.7K	—	—	—	—	3.3K
Total						
One side		16K	37K	62K	81K	82K
Bilateral		31K	73K	124K	162K	163K

Table A.11 Biomechanical parameters of human lumbar ligaments (Pintar et al., 1992)

Parameter	Ligament	T12-L1	L1-L2	L2-L3	L3-L4	L4-L5	L5-S1
Stiffness ($N\ mm^{-1}$)	ALL	32.9 ± 20.9	32.4 ± 13.0	20.8 ± 14.0	39.5 ± 20.3	40.5 ± 14.3	13.2 ± 10.2
	PLL	10.0 ± 5.5	17.1 ± 9.6	36.6 ± 15.2	10.6 ± 8.5	25.8 ± 15.8	21.8 ± 16.0
	JC	31.7 ± 7.9	42.5 ± 0.8	33.9 ± 19.2	32.3 ± 3.3	30.6 ± 1.5	29.9 ± 22.0
	LF	24.2 ± 3.6	23.0 ± 7.8	25.1 ± 10.9	34.5 ± 6.2	27.2 ± 12.2	20.2 ± 8.4
	ISL	12.1 ± 2.6	10.0 ± 5.0	9.6 ± 4.8	18.1 ± 15.9	8.7 ± 6.5	16.3 ± 15.0
	SSL	15.1 ± 6.9	23.0 ± 17.3	24.8 ± 14.5	34.8 ± 11.7	18.0 ± 6.9	17.8 ± 3.8
Energy to failure (J)	ALL	3.30 ± 2.01	3.58 ± 2.34	5.31 ± 1.98	5.35 ± 4.54	8.68 ± 7.99	0.82 ± 0.54
	PLL	0.22 ± 0.15	0.22 ± 0.21	0.33 ± 0.11	0.11 ± 0.04	0.07 ± 0.05	0.29 ± 0.27
	JC	1.55 ± 0.55	4.18 ± 2.15	3.50 ± 1.61	2.35 ± 1.88	2.05 ± 0.99	2.54 ± 1.31
	LF	2.18 ± 1.89	1.58 ± 0.93	0.56 ± 0.46	2.63 ± 2.09	3.31 ± 1.20	2.47 ± 0.60
	ISL	0.72 ± 0.47	2.65 ± 0.25	1.06 ± 0.73	0.59 ± 0.29	1.13 ± 0.91	0.78 ± 0.56
	SSL	3.75 ± 2.78	4.09 ± 2.00	4.72 ± 5.77	11.64 ± 5.39	3.40 ± 2.59	3.18 ± 1.94
Stress at failure (MPa)	ALL	9.1 ± 0.6	13.4 ± 3.9	16.1 ± 6.2	12.8 ± 7.0	15.8 ± 1.9	8.2 ± 2.5
	PLL	7.2 ± 4.1	11.5 ± 10.0	28.4 ± 11.3	12.2 ± 1.9	20.6 ± 7.3	19.7 ± 7.1
	JC	13.2 ± 1.1	10.3 ± 2.9	14.4 ± 1.4	7.7 ± 1.6	3.5 ± 1.2	5.6 ± 2.5
	LF	4.0 ± 1.2	2.5 ± 0.8	1.3 ± 0.4	2.9 ± 1.7	2.9 ± 1.4	4.1 ± 0.5
	ISL	4.2 ± 0.2	5.9 ± 1.8	1.8 ± 0.1	1.8 ± 0.3	2.9 ± 1.9	5.5 ± 0.1
	SSL	8.9 ± 3.2	15.5 ± 5.1	9.9 ± 5.8	12.6 ± 2.7	12.7 ± 7.1	14.0 ± 1.7
Strain at failure (%)	ALL	31.9 ± 24.5	44.0 ± 23.7	49.0 ± 31.7	32.8 ± 23.5	44.7 ± 27.4	28.1 ± 18.3
	PLL	16.2 ± 9.3	15.7 ± 7.4	11.3 ± 0.2	15.8 ± 3.7	12.7 ± 6.3	15.0 ± 8.4
	JC	78.2 ± 24.3	90.4 ± 17.7	70.0 ± 27.5	52.7 ± 7.2	47.9 ± 5.4	53.8 ± 28.8
	LF	61.5 ± 11.9	78.6 ± 6.7	28.8 ± 8.2	70.6 ± 13.6	102.0 ± 12.9	83.1 ± 19.3
	ISL	59.4 ± 36.1	119.7 ± 14.7	51.5 ± 2.9	96.5 ± 35.8	87.4 ± 6.7	52.9 ± 23.2
	SSL	75.0 ± 7.1	83.4 ± 21.4	70.6 ± 45.0	109.4 ± 2.5	106.3 ± 9.7	115.1 ± 49.1

Appendix B: Mean and Standard Deviation Values for Force and Deflection at Failure for Human Spinal Ligaments

Table 1. Mean and Standard Deviation values for Force and Deflection at Failure for Human Spinal Ligaments

	Anterior longitudinal		Posterior longitudinal		Ligamentum flavum		Joint capsules		Interspinous		Supraspinous	
Spinal level	Force (N)	Defl. (mm)	Force (N)	Defl. (mm)	Force (N)	Defl. (mm)	Force (N)	Defl. (mm)	Force (N)	Defl. (mm)	Force (N)	Defl. (mm)
C2-C3	207 (98)	8.7 (3.8)	84 (81)	9.6 (9.3)	86 (61)	5.8 (0.8)	211 (130)	8.9 (4.6)	37 (2)	7.0 (1.6)	*	*
C3-C4	47 (14)	4.2 (1.8)	82 (66)	7.4 (7.1)	75 (8)	3.7 (1.5)	224 (60)	8.7 (2.2)	33 (2)	6.8 (8.1)	*	*
C4-C5	47 (13)	4.8 (2.9)	47 (11)	3.4 (1.4)	56 (17)	12.8 (7.3)	170 (20)	9.1 (6.0)	26 (24)	6.9 (2.9)	*	*
C5-C6	89 (67)	5.0 (1.7)	85 (50)	4.8 (2.0)	89 (48)	8.0 (4.4)	144 (36)	8.7 (7.9)	33 (15)	5.5 (3.1)	*	*
C6-C7	176 (25)	13.7 (5.7)	102 (29)	5.0 (1.6)	160 (38)	7.7 (0.4)	277 (147)	10.0 (3.9)	31 (12)	9.2 (6.6)	*	*
C7-T1	97 (28)	7.6 (3.8)	95 (23)	6.4 (1.6)	221 (67)	9.9 (6.0)	264 (88)	6.8 (2.8)	45 (32)	8.7 (5.9)	†	†
T1-T2	182 (101)	8.3 (5.9)	86 (53)	3.6 (1.6)	135 (84)	6.4 (5.5)	182 (69)	7.4 (3.5)	31 (25)	6.6 (2.9)	†	†
T2-T3	123 (48)	7.3 (1.4)	116 (85)	3.2 (1.8)	144 (21)	10.4 (1.1)	63 (9)	4.1 (1.4)	44 (6)	6.7 (2.0)	186 (24)	13.9 (1.4)
T3-T4	154 (43)	7.5 (4.8)	67 (20)	3.9 (1.2)	161 (67)	6.3 (3.1)	180 (73)	8.3 (3.8)	84 (36)	5.8 (4.0)	133 (†)	19.3 (†)
T4-T5	169 (46)	6.9 (2.9)	99 (9)	3.7 (0.5)	182 (23)	9.1 (3.5)	250 (150)	8.0 (2.7)	51 (40)	8.8 (6.1)	345 (173)	14.9 (0.9)
T5-T6	284 (25)	10.6 (3.0)	82 (7)	7.3 (6.9)	128 (46)	6.3 (2.2)	272 (111)	6.4 (0.9)	64 (54)	8.7 (6.4)	92 (†)	7.2 (†)
T6-T7	332 (214)	7.6 (2.2)	138 (123)	5.7 (1.7)	281 (115)	10.2 (0.2)	153 (103)	5.1 (0.8)	64 (69)	5.2 (3.1)	184 (133)	17.0 (1.3)
T7-T8	213 (58)	17.7 (6.8)	74 (59)	3.6 (2.0)	221 (79)	10.4 (5.1)	237 (103)	8.2 (4.4)	41 (29)	3.8 (0.9)	101 (17)	8.4 (3.6)
T8-T9	332 (53)	13.2 (1.7)	76 (45)	3.0 (2.3)	200 (55)	6.7 (3.1)	174 (61)	5.9 (1.7)	30 (24)	5.4 (1.1)	167 (84)	15.5 (8.3)
T9-T10	408 (192)	14.2 (4.9)	75 (18)	4.7 (3.1)	221 (119)	10.3 (4.4)	216 (186)	3.9 (1.2)	24 (4)	4.2 (3.4)	212 (28)	12.9 (0.3)
T10-T11	408 (253)	11.6 (4.0)	116 (116)	5.9 (3.0)	265 (25)	11.0 (6.3)	258 (151)	9.6 (5.0)	173 (69)	7.0 (3.8)	538 (130)	17.5 (7.9)
T11-T12	281 (88)	13.7 (3.6)	116 (38)	3.3 (1.6)	282 (57)	10.1 (2.3)	244 (46)	11.6 (2.1)	92 (37)	10.2 (5.0)	273 (54)	11.4 (1.7)
T12-L1	276 (81)	12.7 (9.1)	66 (32)	4.8 (4.0)	278 (134)	9.2 (1.8)	252 (22)	10.2 (2.6)	108 (24)	7.6 (4.0)	226 (†)	21.1 (†)
L1-L2	341 (72)	11.5 (12.1)	91 (46)	5.2 (3.1)	215 (72)	12.1 (1.0)	429 (122)	12.8 (2.5)	185 (41)	17.8 (0.6)	378 (160)	28.1 (8.8)
L2-L3	504 (218)	15.7 (7.0)	160 (82)	4.2 (0.1)	133 (41)	4.5 (1.3)	299 (28)	11.9 (5.9)	98 (13)	8.8 (0.5)	742 (†)	29.2 (†)
L3-L4	676 (359)	20.4 (3.5)	38 (15)	7.0 (3.2)	251 (176)	12.2 (3.6)	290 (101)	9.8 (1.6)	95 (22)	14.8 (4.7)	750 (159)	22.5 (5.9)
L4-L5	606 (191)	14.9 (7.2)	53 (7)	4.3 (2.1)	334 (158)	14.5 (3.4)	353 (35)	11.0 (0.4)	115 (76)	16.6 (1.3)	329 (161)	22.1 (1.8)
L5-S1	209 (196)	13.4 (9.3)	108 (53)	4.7 (3.1)	287 (47)	11.9 (3.4)	326 (116)	11.1 (8.2)	118 (10)	7.4 (3.3)	293 (†)	27.5 (†)

Mean and standard deviations are based on 2 to 5 samples
*Supraspinous Ligament does not exist at these spinal levels.
†Only one sample or insufficient data to calculate mean and STD.

Appendix C: Equations and Coefficients for 'Virtual Muscle' Muscle Model

Extrapolated parameters for human skeletal muscle fiber types and associated model equations (Cheng et al., 2000)

CURVE	Typical slow-twitch fibers				Fast-twitch fibers			
Tendon Elasticity								
$F_{SE}(L^T) = c^T k^T \ln\left\{\exp\left[\frac{(L^T - L_r^T)}{k^T}\right] + 1\right\}$	c^T 27.8	k^T 0.0047	L_r^T 0.964		c^T (same as slow twitch)	k^T	L_r^T	
Parallel Elastic Element								
$F_{PE1}(L) = c_1 k_1 \ln\left\{\exp\left[\frac{(L/L_{max} - L_{r1})}{k_1}\right] + 1\right\} + \eta V$	c_1 23.0	k_1 0.046	L_{r1} 1.17	η 0.001	c_1 (same as slow twitch)	k_2	L_{r2}	
Thick Filament Compression								
$F_{PE2}(L) = c_2\{\exp[k_2(L - L_{r2})] - 1\}, \quad F_{PE2} \le 0$	c_2 −0.020	k_2 −21.0	L_{r2} 0.70		c_2 (same as slow twitch)	k_2	L_{r2}	
Force-Length								
$FL(L) = \exp\left(-\text{abs}\left\|\frac{L^\beta - 1}{\omega}\right\|^\rho\right)$	ω 1.12	β 2.30	ρ 1.62		ω 0.75	β 1.55	ρ 2.12	
Force-Velocity								
$FV(V, L) = \begin{cases} (V_{max} - V)/(V_{max} \pm (c_{v0} + c_{v1} L)V), & V \le 0 \\ (b_v - (a_{v0} + a_{v1} L + a_{v2} L^2)V)/(b_v + V), & V > 0 \end{cases}$	V_{max} −7.88	c_{v0} 5.88	c_{v1} 0		V_{max} −9.15	c_{v0} −5.70	c_{v1} 9.18	
Effective Activation								
$Af(f_{eff}, L_{eff}, Y, S) = 1 - \exp\left[-\left(\frac{YSf_{eff}}{a_f n_f}\right)^{n_f}\right], \quad n_f = n_{f0} + n_{f1}\left(\frac{1}{L_{eff}} - 1\right)$	a_{v0} −4.70 a_f 0.56	a_{v1} 8.41 n_{f0} 2.1	a_{v2} −5.34 n_{f1} 5	b_v 0.35	a_{v0} −1.53 a_f 0.56	a_{v1} 0 n_{f0} 2.1	a_{v2} 0 n_{f1} 3.3	
Activation Delay								
$\dot{L}_{eff}(t) = \frac{[L(t) - L_{eff}(t)]^3}{T_L(1 - Af)}$	T_L(ms) 0.088				T_L(ms) (same as slow twitch)			
Sag								
$\dot{S}(t, f_{eff}) = \frac{a_s - S(t)}{T_s}, \quad a_s = \begin{cases} a_{s1}, f_{eff}(t) < 0.1 \\ a_{s2}, f_{eff}(t) \ge 0.1 \end{cases}$	a_{s1} 1.0	a_{s2} 1.0	T_s(ms) –		a_{s1} 1.76	a_{s2} 0.96	T_s(ms) 43	
Yield								
$\dot{Y}(t) = \frac{1 - c_Y[1 - \exp(-\text{abs}\lvert V\rvert/V_Y)] - Y(t)}{T_Y}$	c_Y 0.35	V_Y 0.1	T_Y(ms) 200		c_Y 0	V_Y –	T_Y(ms) –	
Rise and Fall Time								
$\dot{f}_{int}(t, f_{env}, L) = \frac{f_{env}(t) - f_{int}(t)}{T_f}$, $\dot{f}_{eff}(t, f_{int}, L) = \frac{f_{int}(t) - f_{eff}(t)}{T_f}$, $\quad T_f = \begin{cases} T_{f1} L^2 + T_{f2} f_{env}(t), & \dot{f}_{eff}(t) \ge 0 \\ (T_{f3} + T_{f4} Af)/(L), & \dot{f}_{eff}(t) < 0 \end{cases}$	T_{f1}(ms) 24.2	T_{f2}(ms) 16	T_{f3}(ms) 33.2	T_{f4}(ms) 17.8	T_{f1}(ms) 20.6	T_{f2}(ms) 13.6	T_{f3}(ms) 28.2	

Appendix D: A Survey of Human Musculotendon Actuator Parameters (Yamaguchi et al., 1990)

TRUNK MUSCULATURE

MUSCLE		SOURCE	MUSCLE LENGTH ML (m)	FIBER LENGTH LM (m)	VOLUME V (m³)	MUSCLE PCSA =V/L (cm²)	PENNATION ANGLE (deg)	MUSCLE FIBER TYPE %SO	%FO	%FG
1st dorsal interosseous		[14]	–	–	–	–	–	57.4	–	42.6
erector spinae	(1)	[7]	–	–	–	–	–	–	–	–
	(2)	[7]	–	–	–	–	–	–	–	–
	(3)	[7]	–	–	–	–	–	–	–	–
	(4)	[7]	–	–	–	–	–	–	–	–
	(5)	[7]	–	–	–	–	–	–	–	–
	(6)	[7]	–	–	–	–	–	–	–	–
	(7)	[7]	–	–	–	–	–	–	–	–
	(8)	[7]	–	–	–	–	–	–	–	–
	(9)	[7]	–	–	–	–	–	–	–	–
	(10)	[7]	–	–	–	–	–	–	–	–
	(11)	[7]	–	–	–	–	–	–	–	–
	(12)	[7]	–	–	–	–	–	–	–	–
	(13)	[7]	–	–	–	–	–	–	–	–
	(14)	[7]	–	–	–	–	–	–	–	–
	(15)	[7]	–	–	–	–	–	–	–	–
	(16)	[7]	–	–	–	–	–	–	–	–
	(L)	[13]	–	–	426.89	16.02	–	–	–	–
	(R)	[13]	–	–	417.87	16.73	–	–	–	–
	(surface)	[14]	–	–	–	–	–	58.4	–	41.6
	(deep)	[14]	–	–	–	–	–	54.9	–	45.1
external obliquus abdominis		[12]	–	–	–	5.86	–	–	–	–
	(1)	[7]	–	–	–	–	–	–	–	–
	(2)	[7]	–	–	–	–	–	–	–	–
iliocostalis dorsi		[12]	–	–	–	0.80	–	–	–	–
iliocostalis lumborum		[12]	–	–	–	1.00	–	–	–	–
iliopsoas	(1)	[7]	–	–	–	–	–	–	–	–
	(2)	[7]	–	–	–	–	–	–	–	–
	(3)	[7]	–	–	–	–	–	–	–	–
	(4)	[7]	–	–	–	–	–	–	–	–
	(5)	[7]	–	–	–	–	–	–	–	–
	(6)	[7]	–	–	–	–	–	–	–	–
	(7)	[7]	–	–	–	–	–	–	–	–
	(8)	[7]	–	–	–	–	–	–	–	–
	(9)	[7]	–	–	–	–	–	–	–	–
internal obliquus abdominis		[7]	–	–	–	–	–	–	–	–
		[12]	–	–	–	5.60	–	–	–	–
interspinalis	(1)	[12]	–	–	–	0.30	–	–	–	–
	(2)	[12]	–	–	–	–	–	–	–	–
intertransversarii	(1)	[12]	–	–	–	0.25	–	–	–	–
	(2)	[12]	–	–	–	–	–	–	–	–
latissimus dorsi	(1)	[7]	–	–	–	–	–	–	–	–
	(2)	[7]	–	–	–	–	–	–	–	–
	(3)	[7]	–	–	–	–	–	–	–	–
	(4)	[7]	–	–	–	–	–	–	–	–
	(5)	[7]	–	–	–	–	–	–	–	–
		[14]	–	–	–	–	–	59.5	–	40.5
longissimus dorsi		[12]	–	–	–	1.0	–	–	–	–
multifidus	(1)	[13]	–	–	–	1.26	–	–	–	–
	(2)	[13]	–	–	–	–	–	–	–	–
multifidus lumborum	(1)	[7]	–	–	–	–	–	–	–	–
	(2)	[7]	–	–	–	–	–	–	–	–
	(3)	[7]	–	–	–	–	–	–	–	–
	(4)	[7]	–	–	–	–	–	–	–	–
	(5)	[7]	–	–	–	–	–	–	–	–
	(6)	[7]	–	–	–	–	–	–	–	–
	(7)	[7]	–	–	–	–	–	–	–	–
	(8)	[7]	–	–	–	–	–	–	–	–
	(9)	[7]	–	–	–	–	–	–	–	–
	(10)	[7]	–	–	–	–	–	–	–	–
	(11)	[7]	–	–	–	–	–	–	–	–
quadratus lumborum	(1)	[7]	–	–	–	–	–	–	–	–
	(2)	[7]	–	–	–	–	–	–	–	–
	(3)	[7]	–	–	–	–	–	–	–	–
	(4)	[7]	–	–	–	–	–	–	–	–
	(5)	[7]	–	–	–	–	–	–	–	–
		[12]	–	–	–	2.80	–	–	–	–
rectus abdominis		[7]	–	–	–	–	–	–	–	–
		[13]	–	–	–	2.06	–	–	–	–
		[13]	–	–	366.16	10.80	–	–	–	–
		[14]	–	–	–	–	–	46.1	–	53.9
rotatores lumborum	(1)	[7]	–	–	–	–	–	–	–	–
	(2)	[7]	–	–	–	–	–	–	–	–
	(3)	[7]	–	–	–	–	–	–	–	–
	(4)	[7]	–	–	–	–	–	–	–	–
	(5)	[7]	–	–	–	–	–	–	–	–

TENDON LENGTH LT (m)	TENDON PCSA (mm²)	ORIGIN COORD. SYSTEM	ORIGIN X (m)	ORIGIN Y (m)	ORIGIN Z (m)	INSERTION COORD. SYSTEM	INSERTION X (m)	INSERTION Y (m)	INSERTION Z (m)
–	–	–	–	–	–	–	–	–	–
–	–	Thorax	-0.0800	-0.0700	0.1000	Pelvis	-0.0850	-0.0800	0.1400
–	–	Thorax	-0.0800	-0.0700	0.1000	Pelvis	-0.0850	-0.0800	0.0800
–	–	L1	-0.0850	0.0000	0.0100	Thorax	-0.0400	-0.0800	0.1350
–	–	Thorax	0.0000	-0.0800	0.2300	Thorax	-0.0400	-0.0800	0.1350
–	–	L2	-0.0850	0.0000	0.0100	Thorax	-0.0400	-0.0800	0.1350
–	–	Thorax	0.0200	-0.0800	0.2300	Thorax	-0.0400	-0.0800	0.1350
–	–	L3	-0.0850	0.0000	0.0100	Thorax	-0.0400	-0.0800	0.1350
–	–	Thorax	0.0200	-0.0800	0.2300	Thorax	-0.0400	-0.0800	0.1350
–	–	L4	-0.0850	0.0000	0.0100	Thorax	-0.0400	-0.0870	0.1350
–	–	Thorax	0.0200	-0.0800	0.2300	Thorax	-0.0400	-0.0870	0.1350
–	–	L5	-0.0850	0.0000	0.0100	Thorax	-0.0400	-0.0800	0.1350
–	–	Thorax	0.0200	-0.0800	0.2300	Thorax	-0.0400	-0.0800	0.1350
–	–	Pelvis	-0.0950	-0.0800	0.0800	Thorax	-0.0400	-0.0800	0.1350
–	–	Thorax	0.0800	-0.0800	0.2300	Thorax	-0.0400	-0.0800	0.1350
–	–	Pelvis	-0.0950	-0.0800	0.1400	Thorax	-0.0400	-0.0420	0.1350
–	–	Thorax	0.0200	-0.0800	0.2300	Thorax	-0.0400	-0.0420	0.1350
–	–	–	–	–	–	–	–	–	–
–	–	–	–	–	–	–	–	–	–
–	–	–	–	–	–	–	–	–	–
–	–	–	–	–	–	–	–	–	–
–	–	Pelvis	0.0782	0.0884	-0.0782	ConTorso	0.0800	0.0884	0.0079
–	–	Thorax	-0.0400	-0.1300	-0.0850	Pelvis	0.0400	-0.1150	0.1150
–	–	Thorax	0.0700	-0.1300	0.0800	Pelvis	0.0800	0.0000	-0.0100
–	–	ConTorso	-0.0884	0.0782	0.0079	UpTorso	-0.0884	0.0782	0.0000
–	–	Pelvis	-0.0884	0.0881	0.0879	ConTorso	-0.0884	0.0782	0.0079
–	–	L1	-0.0050	-0.0800	0.0200	Pelvis	0.0850	-0.0750	0.0000
–	–	Femur	-0.0100	-0.0850	0.3450	Pelvis	0.0850	-0.0750	0.0000
–	–	L2	-0.0050	-0.0850	0.0200	Pelvis	0.0850	-0.0750	0.0000
–	–	L3	-0.0050	-0.0850	0.0200	Pelvis	0.0850	-0.0750	0.0000
–	–	Femur	-0.0100	-0.0850	0.3450	Pelvis	0.0850	-0.0750	0.0000
–	–	L4	-0.0050	-0.0870	0.0200	Pelvis	0.0850	-0.0750	0.0000
–	–	Femur	-0.0100	-0.0850	0.3450	Pelvis	0.0850	-0.0750	0.0000
–	–	L5	-0.0050	-0.0850	0.0200	Pelvis	0.0850	-0.0750	0.0000
–	–	Femur	-0.0100	-0.0850	0.3450	Pelvis	0.0850	-0.0750	0.0000
–	–	Thorax	0.1450	-0.0850	0.0200	Pelvis	0.0850	-0.1250	0.1250
–	–	Pelvis	0.0000	0.0884	-0.0782	ConTorso	0.0782	0.0884	0.0079
–	–	ConTorso	0.0254	0.0000	-0.0734	UpTorso	-0.0150	0.0000	0.1074
–	–	UpTorso	-0.0150	0.0000	-0.0518	Neck	-0.0150	0.0000	0.0716
–	–	ConTorso	-0.0254	0.0881	-0.0734	UpTorso	-0.0150	0.0254	0.1074
–	–	UpTorso	-0.0150	0.0254	-0.0518	Neck	-0.0150	0.0254	0.0716
–	–	L1	-0.0450	0.0000	0.0100	Thorax	-0.0400	-0.1150	0.0400
–	–	L2	-0.0450	0.0000	0.0100	Thorax	-0.0400	-0.1150	0.0400
–	–	L3	-0.0450	0.0000	0.0100	Thorax	-0.0400	-0.1150	0.0400
–	–	L4	-0.0450	0.0000	0.0100	Thorax	-0.0400	-0.1150	0.0400
–	–	L5	-0.0450	0.0000	0.0100	Thorax	-0.0400	-0.1150	0.0100
–	–	–	–	–	–	–	–	–	–
–	–	ConTorso	-0.0254	0.0881	-0.0048	UpTorso	-0.0150	0.0254	0.0150
–	–	ConTorso	-0.0884	0.0881	-0.0734	UpTorso	-0.0150	0.0000	0.1074
–	–	UpTorso	-0.0150	0.0884	-0.0518	Neck	-0.0150	0.0000	0.0716
–	–	Thorax	-0.0800	0.0000	0.0200	L1	-0.0450	-0.0800	0.0000
–	–	Thorax	-0.0850	0.0000	0.0200	L1	-0.0450	-0.0800	0.0000
–	–	Thorax	-0.0800	0.0000	0.0200	L2	-0.0450	-0.0800	0.0000
–	–	Thorax	-0.0800	0.0000	0.0200	L2	-0.0450	-0.0800	0.0000
–	–	Thorax	-0.0800	0.0000	0.0200	L3	-0.0450	-0.0800	0.0000
–	–	Thorax	-0.0800	0.0000	0.0200	L3	-0.0450	-0.0800	0.0000
–	–	Thorax	-0.0800	0.0000	0.0200	L4	-0.0450	-0.0800	0.0000
–	–	L1	-0.0800	0.0000	0.0100	L4	-0.0450	-0.0800	0.0000
–	–	L1	-0.0800	0.0000	0.0100	L5	-0.0450	-0.0800	0.0000
–	–	L2	-0.0800	0.0000	0.0100	L5	-0.0450	-0.0800	0.0000
–	–	L5	-0.0800	0.0000	0.0100	Pelvis	-0.0800	-0.0800	0.0000
–	–	Thorax	-0.0800	-0.0850	0.0100	Pelvis	-0.0400	-0.0780	0.1000
–	–	L1	-0.0800	-0.0850	0.0200	Pelvis	-0.0400	-0.0780	0.1000
–	–	L1	-0.0800	-0.0870	0.0200	Pelvis	-0.0400	-0.0780	0.1000
–	–	L3	-0.0800	-0.0450	0.0200	Pelvis	-0.0400	-0.0780	0.1000
–	–	L4	-0.0800	-0.0450	0.0200	Pelvis	-0.0400	-0.0780	0.1000
–	–	Pelvis	0.0800	0.0884	-0.0782	ConTorso	-0.0780	0.0884	-0.0048
–	–	Thorax	0.1800	-0.0400	0.0800	Pelvis	0.0850	-0.0800	-0.0100
–	–	Pelvis	0.0884	0.0127	0.0467	ConTorso	0.0782	0.0127	-0.1074
–	–	–	–	–	–	–	–	–	–
–	–	Thorax	-0.0850	0.0000	0.0800	L2	-0.0450	-0.0200	0.0850
–	–	Thorax	-0.0850	0.0000	0.0800	L2	-0.0450	-0.0200	0.0850
–	–	L1	-0.0850	0.0000	0.0100	L3	-0.0450	-0.0800	0.0850
–	–	L2	-0.0850	0.0000	0.0100	L4	-0.0450	-0.0800	0.0850
–	–	L3	-0.0850	0.0000	0.0100	L5	-0.0450	-0.0800	0.0850

UPPER EXTREMITY MUSCULATURE

MUSCLE		SOURCE	MUSCLE LENGTH ML (m)	FIBER LENGTH LM (m)	VOLUME V (ml)	MUSCLE PCSA =V/L (cm^2)	PENNATION ANGLE (deg)	MUSCLE FIBER TYPE %SO	%FO	%FG
[illegible]		[7]	–	–	–	–	–	–	–	–
		[12]	–	–	–	0.84	–	–	–	–
		[15]	–	–	–	3.18	–	–	–	–
		[22]	–	0.027	*67	2.5	–	–	–	–
biceps brachii	(LH)	[15]	–	–	–	3.33	–	–	–	–
	(LH)	[19]	0.3124	–	70.46	1.84	–	–	–	–
	(LH)	[21]	–	–	–	–	–	–	–	–
	(LH)	[22]	–	0.136	33.4	2.5	–	–	–	–
	(SH)	[19]	–	–	–	3.22	–	–	–	–
	(SH)	[19]	0.2327	–	57.09	1.39	–	–	–	–
	(SH)	[21]	–	–	–	–	–	–	–	–
	(SH)	[22]	–	0.150	30.9	2.1	–	–	–	–
	(1)	[17]	–	–	–	–	–	–	–	–
	(surface)	[22]	–	–	–	–	–	42.3	–	57.7
	(deep)	[22]	–	–	–	–	–	50.5	–	49.5
brachialis		[15]	–	–	–	3.55	–	–	–	–
		[19]	–	–	–	–	–	–	–	–
		[21]	–	–	–	–	–	–	–	–
		[22]	–	–	–	4.05	–	–	–	–
		[22]	–	–	–	5.40	–	–	–	–
	(low head)	[19]	0.0782	–	34.41	4.82	–	–	–	–
	(top head)	[19]	0.1409	–	66.46	4.82	–	–	–	–
		[15]	0.12	0.080	–	8	–	–	–	–
brachioradialis		[22]	–	0.080	28.3	7.0	–	–	–	–
		[15]	–	–	–	–	–	–	–	–
		[22]	–	–	–	1.37	–	–	–	–
		[19]	–	–	–	1.86	–	–	–	–
		[22]	–	–	–	–	–	39.8	–	60.2
		[19]	0.2870	–	40.97	1.39	–	–	–	–
		[15]	0.24	0.16	–	9	–	–	–	–
		[22]	–	0.104	21.9	1.5	–	–	–	–
coracobrachialis		[15]	–	–	–	–	–	–	–	–
		[22]	–	–	–	1.52	–	–	–	–
		[19]	0.1054	–	21.50	1.39	–	–	–	–
		[22]	–	–	–	5.8	–	–	–	–
deltoideus		[22]	–	–	–	–	–	–	–	–
		[22]	–	–	–	–	–	–	–	–
		[22]	–	–	–	–	–	–	–	–
		[22]	–	–	–	11.01	–	–	–	–
	(3)	[22]	–	–	–	–	–	–	–	–
		[22]	–	–	–	–	–	–	–	–
		[22]	–	–	–	–	–	–	–	–
		[22]	–	–	–	–	–	–	–	–
	(superior)	[22]	–	–	–	–	–	52.3	–	46.7
	(deep)	[22]	–	–	–	–	–	61.0	–	39.0
	(acromial)	[19]	0.1051	–	222.84	13.55	–	–	–	–
	(clavicular)	[19]	0.1035	–	88.49	4.82	–	–	–	–
	(scapular)	[19]	0.1035	–	76.36	3.57	–	–	–	–
extensor carpi radialis brevis		[22]	–	–	–	–	–	–	–	–
		[15]	–	–	–	2.22	–	–	–	–
		[22]	–	0.053	15.9	2.8	–	–	–	–
extensor carpi radialis longus		[22]	–	–	–	–	–	–	–	–
		[15]	–	–	–	3.14	–	–	–	–
		[22]	0.22	0.080	–	7	–	–	–	–
		[22]	–	0.078	16.3	2.4	–	–	–	–
extensor carpi ulnaris		[22]	–	–	–	–	–	–	–	–
		[15]	–	–	–	5.20	–	–	–	–
		[22]	–	0.045	14.9	3.4	–	–	–	–
extensor digitorum communis		[22]	–	–	–	–	–	–	–	–
		[22]	–	–	–	–	–	47.3	–	52.7
		[15]	–	–	–	4.20	–	–	–	–

TENDON LENGTH LT (m)	TENDON PCSA (mm²)	ORIGIN COORD. SYSTEM	X (m)	Y (m)	Z (m)	INSERTION COORD. SYSTEM	X (m)	Y (m)	Z (m)
–	–	Humerus	-0.016	-0.025	-0.300	Ulna	-0.018	-0.005	-0.040
–	–	Humerus	0.000	0.000	0.132	Forearm	0.010	0.000	-0.176
–	–	–	–	–	–	–	–	–	–
–	–	–	–	–	–	–	–	–	–
–	–	–	–	–	–	–			
–	–	Scapula	0.1629	0.1921	0.0985	Radius	0.0081	-0.1473	0.0045
–	–	Shoulder	0.025	0.000	-0.005	Shoulder	0.006	-0.018	-0.003
–	–	–	–	–	–	–	–	–	–
–	–	–	–	–	–	–	–	–	–
–	–	Scapula	0.1854	0.1270	0.7239	Radius	0.0405	-0.1448	0.0045
–	–	Shoulder	0.029	0.006	-0.015	Shoulder	0.006	-0.016	-0.005
–	–	–	–	–	–	–	–	–	–
–	–	–	–	–	–	Scapula	0.0160	0.0028	0.0028
–	–	–	–	–	–	Scapula	0.0050	0.0012	0.0402
–	–	–	–	–	–	–	–	–	–
–	–	–	–	–	–	–	–	–	–
–	–	Scapula	-0.005	0.020	-0.020	Humerus	0.005	0.005	0.495
–	–	Humerus	0.025	0.000	0.910	Radius	0.001	0.000	-0.005
–	–	UpTorso	0.0000	0.1395	-0.0724	Forearm	0.0000	0.0000	-0.1957
–	–	Scapula	0.010	0.000	-0.025	Radius	0.000	0.000	-0.005
–	–	UpTorso	0.0000	0.1395	-0.0525	Forearm	0.0000	0.0000	-0.1957
–	–	Humerus	0.010	-0.005	-0.300	Ulna	0.000	0.000	-0.000
–	–	Humerus	0.0000	0.0000	-0.0991	Forearm	0.0000	0.0000	-0.1916
–	–	–	–	–	–	–	–	–	–
–	–	Humerus	0.1016	-0.0782	0.5918	Ulna	0.0003	-0.1426	0.0020
–	–	Humerus	0.1270	-0.0178	0.4223	Ulna	0.0000	-0.1600	0.0020
–	–	Shoulder	0.001	-0.162	-0.005	Shoulder	-0.003	-0.304	-0.013
–	–	–	–	–	–	–	–	–	–
–	–	Humerus	0.000	-0.015	-0.270	Radius	0.000	-0.020	-0.240
–	–	Humerus	0.0000	0.0000	0.0917	Forearm	0.0000	0.0291	0.0084
–	–	–	–	–	–	–	–	–	–
–	–	–	–	–	–	–	–	–	–
–	–	Humerus	0.1041	-0.0737	0.5967	Radius	-0.0018	-0.1448	0.7995
–	–	Shoulder	-0.005	-0.195	0.005	Shoulder	0.010	-0.005	0.027
–	–	–	–	–	–	–	–	–	–
–	–	Scapula	0.010	0.000	-0.025	Humerus	0.010	0.000	-0.182
–	–	UpTorso	0.0000	0.1849	-0.0920	Humerus	0.0000	-0.0000	-0.0183
–	–	Scapula	0.1905	0.1218	0.7214	Humerus	0.1287	-0.0178	0.6274
–	–	–	–	–	–	–	–	–	–
–	–	–	–	–	–	Scapula	0.0209	-0.0025	0.0042
–	–	–	–	–	–	Humerus	0.1185	0.0042	-0.0054
–	–	Scapula	-0.005	0.000	-0.025	Humerus	-0.010	0.000	-0.120
–	–	Scapula	0.000	-0.025	-0.015	Humerus	0.010	-0.010	-0.120
–	–	Clavicle	0.000	-0.130	-0.005	Humerus	0.010	-0.005	-0.130
–	–	UpTorso	-0.0207	0.1648	-0.0908	Humerus	0.0000	0.0000	0.0010
–	–	UpTorso	0.0207	0.1648	-0.0908	Humerus	0.0000	0.0000	0.0010
–	–	–	–	–	–	Scapula	-0.0016	-0.0030	-0.0109
–	–	–	–	–	–	Scapula	0.0427	0.0052	-0.0008
–	–	–	–	–	–	Clavicle	0.1110	-0.0009	0.0021
–	–	–	–	–	–	Humerus	0.1185	-0.0012	0.0120
–	–	–	–	–	–	–	–	–	–
–	–	–	–	–	–	–	–	–	–
–	–	Scapula	0.1885	0.1422	0.6604	Humerus	0.1184	-0.0051	0.5228
–	–	Clavicle	0.1885	0.1473	0.7169	Humerus	0.1270	0.0203	0.6380
–	–	Scapula	0.2957	0.1270	0.8756	Humerus	0.1321	0.0127	0.5248
–	–	Humerus	-0.010	-0.030	-0.200	Hand	-0.008	-0.009	-0.006
–	–	–	–	–	–	–	–	–	–
–	–	–	–	–	–	–	–	–	–
–	–	Humerus	-0.010	-0.028	-0.200	Hand	-0.008	-0.013	-0.004
–	–	–	–	–	–	–	–	–	–
–	–	Shoulder	-0.008	-0.200	0.000	Shoulder	0.011	-0.000	0.004
–	–	–	–	–	–	–	–	–	–
–	–	Humerus	-0.014	-0.027	-0.200	Hand	-0.008	0.005	-0.000
–	–	–	–	–	–	–	–	–	–
–	–	–	–	–	–	–	–	–	–
–	–	Humerus	-0.012	-0.030	-0.206	Hand	-0.070	0.000	-0.016
–	–	–	–	–	–	–	–	–	–
–	–	–	–	–	–	–	–	–	–

MUSCLE	SOURCE	MUSCLE LENGTH ML (m)	FIBER LENGTH LM (m)	VOLUME V (m^3)	MUSCLE PCSA $\cdot$VL (mm^2)	PENNATION ANGLE (deg)	MUSCLE FIBER TYPE %SO	%FO	%FG
flexor carpi radialis	[7]	–	–	–	–	–	–	–	–
	[15]	–	–	–	2.16	–	–	–	–
	[23]	–	0.058	12.4	2.0	–	–	–	–
flexor carpi ulnaris	[7]	–	–	–	–	–	–	–	–
	[14]	–	–	–	–	–	44.5	–	55.5
	[15]	–	–	–	5.0	–	–	–	–
	[23]	–	0.068	16.2	3.2	–	–	–	–
flexor digitorum profundus	[14]	–	–	–	–	–	47.3	–	52.7
	[15]	–	–	–	10.8	–	–	–	–
flexor digitorum sublimis	[7]	–	–	–	–	–	–	–	–
	[15]	–	–	–	10.7	–	–	–	–
flexor pollicis longus	[7]	–	–	–	–	–	–	–	–
	[15]	–	–	–	2.9	–	–	–	–
gemelli	[15]	–	–	–	–	–	–	–	–
	[15]	–	–	–	–	–	–	–	–
	[15]	–	–	–	–	–	–	–	–
gluteus maximus	[15]	–	–	–	–	–	–	–	–
	[15]	–	–	–	–	–	–	–	–
	[15]	–	–	–	–	–	–	–	–
	[15]	–	–	–	–	–	–	–	–
	[15]	–	–	–	–	–	–	–	–
	[15]	–	–	–	16.5	–	–	–	–
gracilis	[15]	–	–	–	–	–	–	–	–
	[15]	–	–	–	–	–	–	–	–
	[15]	–	–	–	–	–	–	–	–
	[15]	–	–	–	5.27	–	–	–	–
	[15]	–	–	–	–	–	–	–	–
	[15]	–	–	–	–	–	–	–	–
	[15]	0.2002	–	338.21	12.69	–	–	–	–
hamstrings	[15]	–	–	–	–	–	–	–	–
	[15]	–	–	–	–	–	–	–	–
	[15]	–	–	–	–	–	–	–	–
	[15]	–	–	–	17.76	–	–	–	–
	[15]	–	–	–	–	–	–	–	–
iliacus	[15]	–	–	–	–	–	–	–	–
psoas major	[15]	–	–	–	5.93	–	–	–	–
	[15]	–	0.057	6.1	0.9	–	–	–	–
pectineus	[15]	–	–	–	–	–	–	–	–
	[15]	–	–	–	–	–	–	–	–
	[15]	–	–	–	–	–	–	–	–
	[15]	–	–	–	8.6	–	–	–	–
piriformis	[15]	–	–	–	–	–	–	–	–
(clavicular)	[14]	–	–	–	–	–	42.3	–	57.7
(sternal)	[14]	–	–	–	–	–	49.1	–	50.9
(abdom.)	[14]	0.2134	–	78.66	3.67	–	–	–	–
(clav.)	[14]	0.1954	–	93.40	5.16	–	–	–	–
(ster.)	[14]	0.2189	–	96.66	4.92	–	–	–	–
plantaris	[17]	–	–	–	–	–	–	–	–
	[17]	–	–	–	–	–	–	–	–
	[17]	–	–	–	–	–	–	–	–
popliteus	[14]	0.1348	–	58.44	3.67	–	–	–	–
pronator teres	[7]	–	–	–	–	–	–	–	–
	[15]	–	–	–	1.61	–	–	–	–
	[15]	–	–	–	3.56	–	–	–	–
	[23]	0.14	0.070	–	4	–	–	–	–
	[23]	–	0.036	18.7	3.4	–	–	–	–
pronator quadratus	[15]	–	–	–	2.22	–	–	–	–
	[15]	–	–	–	–	–	–	–	–
rectus femoris	[7]	–	–	–	–	–	–	–	–
	[15]	–	–	–	–	–	–	–	–
	[15]	–	–	–	–	–	–	–	–
	[15]	–	–	–	–	–	–	–	–
	[15]	–	–	–	–	–	–	–	–
	[15]	–	–	–	–	–	–	–	–
	[14]	–	–	–	–	–	44.6	–	55.4
rhomboid (major)	[15]	0.1143	–	49.97	3.67	–	–	–	–
(minor)	[15]	0.0707	–	27.56	3.23	–	–	–	–
sartorius (proximal)	[17]	–	–	–	–	–	–	–	–
(middle)	[17]	–	–	–	–	–	–	–	–

TENDON LENGTH LT (m)	TENDON PCSA (mm²)	ORIGIN COORD. SYSTEM	X (m)	Y (m)	Z (m)	INSERTION COORD. SYSTEM	X (m)	Y (m)	Z (m)
—	—	Humerus	-0.000	0.006	-0.295	Hand	0.000	-0.016	-0.025
—	—	—	—	—	—	—	—	—	—
—	—	—	—	—	—	—	—	—	—
—	—	Humerus	-0.012	0.000	-0.295	Hand	0.007	0.016	-0.012
—	—	—	—	—	—	—	—	—	—
—	—	—	—	—	—	—	—	—	—
—	—	—	—	—	—	—	—	—	—
—	—	—	—	—	—	—	—	—	—
—	—	—	—	—	—	—	—	—	—
—	—	Humerus	-0.006	0.005	-0.295	Hand	0.007	0.000	-0.025
—	—	—	—	—	—	—	—	—	—
—	—	Humerus	-0.006	0.006	-0.295	Hand	0.007	-0.000	-0.000
—	—	—	—	—	—	—	—	—	—
—	—	—	—	—	—	Scapula	0.1464	-0.0108	-0.0011
—	—	—	—	—	—	Humerus	0.0468	0.0111	-0.0068
—	—	—	—	—	—	—	—	—	—
—	—	Scapula	0.2972	0.0767	0.0000	Humerus	0.1669	0.1346	0.0004
—	—	Scapula	-0.006	0.000	-0.000	Humerus	-0.008	-0.000	0.004
—	—	UpTorso	-0.0000	0.1148	-0.0071	Humerus	0.0000	0.0160	-0.1362
—	—	—	—	—	—	Humerus	-0.0084	-0.0075	0.0001
—	—	—	—	—	—	Scapula	0.1062	0.0426	-0.0158
—	—	—	—	—	—	Scapula	0.1346	0.0004	-0.0122
—	—	—	—	—	—	—	—	—	—
—	—	Thorax	-0.106	-0.000	-0.220	Humerus	0.010	0.000	-0.004
—	—	Thorax	-0.006	-0.116	-0.200	Humerus	0.016	0.006	-0.040
—	—	Pelvis	-0.116	-0.006	-0.200	Humerus	0.016	0.006	-0.040
—	—	ConTorso	-0.0000	0.0000	0.0070	Humerus	0.0000	0.0000	-0.0001
—	—	ConTorso	-0.0000	0.0000	0.0160	Humerus	0.0000	0.0000	-0.0001
—	—	—	—	—	—	Humerus	0.0000	0.0100	0.0001
—	—	Thorax	0.2848	-0.1219	0.0020	Humerus	0.1702	0.0000	0.0731
—	—	C1	0.0000	-0.0000	0.0070	Scapula	-0.0570	0.0000	-0.0040
—	—	C2	-0.0040	-0.0000	0.0060	Scapula	-0.0000	0.0000	-0.0120
—	—	C3	-0.0040	-0.0000	0.0060	Scapula	-0.0000	0.0070	-0.0260
—	—	UpTorso	-0.0000	0.1067	-0.0470	ConTorso	-0.0070	0.0114	-0.0470
—	—	—	—	—	—	Scapula	0.0002	0.0731	-0.0021
—	—	—	—	—	—	Scapula	0.0428	0.0056	0.0005
—	—	—	—	—	—	—	—	—	—
—	—	—	—	—	—	—	—	—	—
—	—	Thorax	0.040	0.010	0.070	Humerus	0.000	-0.000	-0.040
—	—	Thorax	0.040	-0.020	-0.100	Humerus	0.000	-0.000	-0.040
—	—	Clavicle	0.018	-0.050	0.007	Humerus	0.000	-0.000	-0.040
—	—	UpTorso	0.0000	0.0000	-0.0071	Humerus	0.0000	0.0000	-0.0401
—	—	UpTorso	0.0000	0.0040	-0.0070	Humerus	0.0000	0.0000	-0.0401
—	—	—	—	—	—	—	—	—	—
—	—	—	—	—	—	—	—	—	—
—	—	Thorax	0.1401	-0.0254	0.0703	Humerus	0.1473	0.0711	0.0020
—	—	Clavicle	0.2002	0.1104	0.0170	Humerus	0.1372	0.0432	0.0025
—	—	Thorax	0.2007	0.0403	0.0015	Humerus	0.1401	0.0000	0.0004
—	—	—	—	—	—	Humerus	0.0020	0.0110	0.0120
—	—	—	—	—	—	Clavicle	0.0022	0.0130	0.0000
—	—	—	—	—	—	Scapula	0.0000	0.0004	0.0047
—	—	Thorax	0.1540	0.0000	0.0001	Scapula	0.0007	0.1340	0.7200
—	—	Humerus	-0.006	0.006	-0.200	Radius	0.006	-0.010	-0.100
—	—	Humerus	0.0000	0.0000	0.1105	Forearm	0.0000	0.0100	-0.0000
—	—	—	—	—	—	—	—	—	—
—	—	Shoulder	-0.004	-0.047	-0.027	Shoulder	0.006	-0.000	0.005
—	—	—	—	—	—	—	—	—	—
—	—	—	—	—	—	—	—	—	—
—	—	Shoulder	0.010	-0.006	-0.010	Shoulder	0.014	-0.003	0.000
—	—	C3	-0.0000	-0.0040	-0.0070	Scapula	-0.1100	0.0000	-0.0400
—	—	C7	-0.0000	-0.0040	-0.0100	Scapula	-0.1100	0.0000	-0.0000
—	—	Thorax	0.0000	0.0000	0.2700	Scapula	-0.1100	0.0000	-0.0000
—	—	Thorax	0.0000	0.0000	0.2000	Scapula	-0.1300	0.0000	-0.1100
—	—	Thorax	0.0000	0.0000	0.2000	Scapula	-0.1300	0.0700	-0.1000
—	—	—	—	—	—	—	—	—	—
—	—	Thorax	0.2005	0.1016	0.7722	Scapula	0.2100	0.0530	0.0000
—	—	Thorax	0.2404	0.1321	0.7023	Scapula	0.2100	0.1100	0.7001
—	—	—	—	—	—	Scapula	0.1006	0.0430	-0.0240
—	—	—	—	—	—	Scapula	0.0040	0.0004	-0.0041

MUSCLE		SOURCE	MUSCLE LENGTH ML (m)	FIBER LENGTH LM (m)	VOLUME V (ml)	MUSCLE PCSA =V/L (cm²)	PENNATION ANGLE (deg)	MUSCLE FIBER TYPE %SO	%FO	%FG
serratus anterior	(1)	[7]	–	–	–	–	–	–	–	–
	(2)	[7]	–	–	–	–	–	–	–	–
	(3)	[7]	–	–	–	–	–	–	–	–
	(4)	[7]	–	–	–	–	–	–	–	–
	(1)	[17]	–	–	–	–	–	–	–	–
	(2)	[17]	–	–	–	–	–	–	–	–
	(3)	[17]	–	–	–	–	–	–	–	–
	(lower)	[16]	0.1727	–	102.23	9.09	–	–	–	–
	(upper)	[16]	0.1041	–	31.14	3.29	–	–	–	–
smaller round	(1)	[17]	–	–	–	–	–	–	–	–
	(2)	[17]	–	–	–	–	–	–	–	–
sternocleido-mastoid		[17]	–	–	–	–	–	–	–	–
sternohyoid		[17]	–	–	–	–	–	–	–	–
subclavius		[7]	–	–	–	–	–	–	–	–
		[17]	–	–	–	–	–	–	–	–
		[16]	0.0762	–	–	–	–	–	–	–
subscapularis		[7]	–	–	–	–	–	–	–	–
		[12]	–	–	–	8.9	–	–	–	–
		[16]	0.1219	–	121.38	9.88	–	–	–	–
		[16]	–	–	–	25.24	–	–	–	–
		[17]	–	–	–	–	–	–	–	–
	(1)	[17]	–	–	–	–	–	–	–	–
	(2)	[17]	–	–	–	–	–	–	–	–
	(3)	[17]	–	–	–	–	–	–	–	–
supinator		[7]	–	–	–	–	–	–	–	–
		[7]	–	–	–	–	–	–	–	–
		[12]	–	–	–	1.77	–	–	–	–
		[16]	–	–	–	2.30	–	–	–	–
		[21]	–	0.083	–	4.8	–	–	–	–
		[22]	–	0.083	10.9	3.4	–	–	–	–
supraspinatus		[7]	–	–	–	–	–	–	–	–
		[14]	–	–	–	–	–	59.3	–	40.7
		[12]	–	–	–	8.3	–	–	–	–
		[16]	0.0884	–	30.33	4.32	–	–	–	–
		[15]	–	–	–	7.7	–	–	–	–
	(1)	[17]	–	–	–	–	–	–	–	–
	(2)	[17]	–	–	–	–	–	–	–	–
teres major		[7]	–	–	–	–	–	–	–	–
		[12]	–	–	–	4.07	–	–	–	–
		[16]	0.1216	–	70.46	5.81	–	–	–	–
		[15]	–	–	–	9.8	–	–	–	–
teres minor		[7]	–	–	–	–	–	–	–	–
		[12]	–	–	–	1.57	–	–	–	–
		[16]	0.1041	–	34.38	2.88	–	–	–	–
trapezius	(1)	[7]	–	–	–	–	–	–	–	–
	(2)	[7]	–	–	–	–	–	–	–	–
	(3)	[7]	–	–	–	–	–	–	–	–
	(4)	[7]	–	–	–	–	–	–	–	–
	(5)	[7]	–	–	–	–	–	–	–	–
	(6)	[7]	–	–	–	–	–	–	–	–
	(7)	[7]	–	–	–	–	–	–	–	–
	(8)	[7]	–	–	–	–	–	–	–	–
	(9)	[7]	–	–	–	–	–	–	–	–
	(10)	[7]	–	–	–	–	–	–	–	–
	(11)	[7]	–	–	–	–	–	–	–	–
	(12)	[7]	–	–	–	–	–	–	–	–
	(13)	[7]	–	–	–	–	–	–	–	–
	(14)	[7]	–	–	–	–	–	–	–	–
	(15)	[7]	–	–	–	–	–	–	–	–
	(16)	[7]	–	–	–	–	–	–	–	–
	(17)	[7]	–	–	–	–	–	–	–	–
	(18)	[7]	–	–	–	–	–	–	–	–
	(19)	[7]	–	–	–	–	–	–	–	–
	(20)	[7]	–	–	–	–	–	–	–	–
		[12]	–	–	–	16.60	–	–	–	–
	(lower)	[16]	0.2085	–	190.82	9.88	–	–	–	–
	(medial)	[16]	0.1345	–	90.13	7.10	–	–	–	–
	(upper)	[16]	0.1194	–	80.30	6.46	–	–	–	–

TENDON LENGTH LT (m)	TENDON PCSA (mm²)	ORIGIN COORD. SYSTEM	ORIGIN X (m)	ORIGIN Y (m)	ORIGIN Z (m)	INSERTION COORD. SYSTEM	INSERTION X (m)	INSERTION Y (m)	INSERTION Z (m)
–	–	Thorax	0.0650	-0.0650	0.2200	Scapula	-0.0550	0.0500	0.0200
–	–	Thorax	0.0650	-0.1000	0.1900	Thorax	0.0800	-0.1100	0.1900
–	–	Scapula	-0.1250	0.0500	-0.0650	Thorax	0.0800	-0.1100	0.1900
–	–	Thorax	0.0800	-0.1400	0.0700	Scapula	-0.1300	0.0500	-0.1400
–	–	–	–	–	–	Scapula	0.0552	0.0504	-0.0101
–	–	–	–	–	–	Scapula	0.1342	0.0546	-0.0204
–	–	–	–	–	–	Scapula	0.1453	0.0147	0.0087
–	–	Thorax	0.1727	-0.0264	0.7264	Scapula	0.3134	0.0000	0.0500
–	–	Thorax	0.2261	0.1016	0.7518	Scapula	0.3079	0.0838	0.7188
–	–	–	–	–	–	Scapula	0.1052	-0.0057	-0.0042
–	–	–	–	–	–	Humerus	0.0117	-0.0136	-0.0111
–	–	–	–	–	–	Clavicle	0.0252	0.0047	0.0008
–	–	–	–	–	–	Clavicle	0.0052	-0.0084	0.0008
–	–	Thorax	0.1150	-0.0500	0.2120	Clavicle	0.0000	0.0000	0.0000
–	–	–	–	–	–	Clavicle	0.0708	-0.0039	-0.0038
–	–	Thorax	0.2511	0.1016	0.8230	Clavicle	0.2159	0.1372	0.7566
–	–	Scapula	-0.030	0.065	-0.035	Humerus	0.016	0.012	0.020
–	–	UpTorso	0.0000	0.1350	0.0150	Humerus	0.0150	0.0150	-0.1350
–	–	Scapula	0.3048	0.0711	0.6909	Humerus	0.3048	0.1067	0.6350
–	–	–	–	–	–	–	–	–	–
–	–	–	–	–	–	Humerus	0.0035	0.0254	0.0000
–	–	–	–	–	–	Scapula	0.0035	0.0546	-0.0342
–	–	–	–	–	–	Scapula	0.1152	0.0250	-0.0150
–	–	–	–	–	–	Scapula	0.1348	0.0152	-0.0115
–	–	Humerus	-0.013	-0.028	-0.300	Radius	0.006	-0.006	-0.005
–	–	Arm	-0.0150	-0.0280	0.1600	Radius	0.0050	-0.0050	0.0050
–	–	Humerus	0.0000	0.0000	0.1516	Forearm	0.0000	0.0150	-0.1500
–	–	–	–	–	–	–	–	–	–
–	–	Shoulder	0.015	-0.285	0.010	Shoulder	0.007	-0.340	-0.014
–	–	–	–	–	–	–	–	–	–
–	–	Scapula	-0.050	0.075	-0.005	Humerus	0.010	-0.000	0.005
–	–	–	–	–	–	–	–	–	–
–	–	UpTorso	0.0000	0.0000	-0.0470	Humerus	0.0000	0.0000	-0.1401
–	–	Scapula	0.2870	0.1397	0.7239	Humerus	0.1061	0.1397	0.6833
–	–	–	–	–	–	–	–	–	–
–	–	–	–	–	–	Scapula	0.0540	0.0516	-0.0100
–	–	–	–	–	–	Humerus	-0.0126	0.0003	0.0236
–	–	Scapula	-0.110	0.080	-0.140	Humerus	0.014	0.008	-0.084
–	–	UpTorso	0.0000	0.1250	0.0531	Humerus	0.0000	-0.0050	-0.0782
–	–	Scapula	0.2794	0.0305	0.6543	Humerus	0.1702	0.0510	0.0005
–	–	–	–	–	–	–	–	–	–
–	–	Scapula	-0.070	0.025	-0.005	Humerus	-0.004	-0.003	-0.006
–	–	UpTorso	0.0000	0.1460	0.0130	Humerus	0.0000	0.0000	-0.1302
–	–	Scapula	0.2967	0.0460	0.6904	Humerus	0.1005	0.1116	0.6804
–	–	Skull	-0.0960	-0.0100	0.0270	Clavicle	-0.0100	0.1300	0.0300
–	–	C1	-0.0270	0.0000	0.0060	Clavicle	-0.0100	0.1300	0.0060
–	–	C2	-0.0270	-0.0040	-0.0060	Clavicle	-0.0100	0.1300	0.0060
–	–	C3	-0.0350	-0.0040	-0.0070	Clavicle	-0.0100	0.1300	0.0060
–	–	C4	-0.0350	-0.0040	-0.0070	Clavicle	-0.0100	0.1300	0.0060
–	–	C5	-0.0350	-0.0040	-0.0070	Clavicle	-0.0100	0.1300	0.0060
–	–	C6	-0.0350	-0.0040	-0.0070	Clavicle	-0.0100	0.1300	0.0060
–	–	Skull	-0.0960	-0.0100	0.0270	Scapula	-0.0500	-0.0100	-0.0100
–	–	C1	-0.0270	0.0000	0.0060	Scapula	-0.0500	-0.0100	-0.0100
–	–	C2	-0.0270	-0.0040	-0.0060	Scapula	-0.0500	-0.0100	-0.0100
–	–	C3	-0.0350	-0.0040	-0.0070	Scapula	-0.0500	-0.0100	-0.0100
–	–	C4	-0.0350	-0.0040	-0.0070	Scapula	-0.0500	-0.0100	-0.0100
–	–	C5	-0.0350	-0.0040	-0.0070	Scapula	-0.0500	-0.0100	-0.0100
–	–	C6	-0.0350	-0.0040	-0.0070	Scapula	-0.0500	-0.0100	-0.0100
–	–	C7	-0.0400	-0.0040	-0.0100	Scapula	-0.0500	0.0000	-0.0500
–	–	Thorax	0.0000	0.0000	0.2000	Scapula	-0.0500	0.0000	-0.0500
–	–	Thorax	-0.0070	0.0000	0.1500	Scapula	-0.1150	0.0000	-0.0500
–	–	Scapula	-0.0800	0.0000	-0.0270	Scapula	-0.1150	0.0000	-0.0500
–	–	Thorax	-0.0450	0.0000	0.0800	Scapula	-0.1350	0.0000	-0.0500
–	–	Scapula	-0.0000	0.0000	-0.0270	Scapula	-0.1350	0.0000	-0.0500
–	–	UpTorso	0.0000	0.1048	-0.0507	Head	-0.0500	0.0000	0.0548
–	–	Thorax	0.2610	-0.0483	0.7544	Scapula	0.2073	0.1116	0.6858
–	–	Thorax	0.2048	0.1651	0.7772	Clavicle	0.2088	0.1575	0.7112

MUSCLE		SOURCE	MUSCLE LENGTH ML (m)	FIBER LENGTH LM (m)	VOLUME V (ml)	MUSCLE PCSA =V/L (cm²)	PENNATION ANGLE (deg)	MUSCLE FIBER TYPE %SO	%FO	%FG
	(1)	[16]	0.1900	–	–	8.11	10	16	–	–
	(2)	[16]	0.1675	–	–	1.14	10	16	–	–
		[14]	–	–	–	–	–	50.7	–	49.2
	(1)	[17]	–	–	–	–	–	–	–	–
	(2)	[17]	–	–	–	–	–	–	–	–
	(3)	[17]	–	–	–	–	–	–	–	–
	(4)	[17]	–	–	–	–	–	–	–	–
biceps brachii		[17]	–	–	–	–	–	–	–	–
	(1)	[18]	–	–	–	6.78	–	–	–	–
	(2)	[18]	–	–	–	5.66	–	–	–	–
	(3)	[18]	–	–	–	4.76	–	–	–	–
	(surface)	[14]	–	–	–	–	–	32.5	–	67.5
	(deep)	[14]	–	–	–	–	–	89.7	–	10.6
	(lateral)	[16]	0.2404	–	108.16	4.82	–	–	–	–
	(lateral)	[22]	–	0.084	47.3	6.0	–	–	–	–
	(medial)	[16]	0.2134	–	62.27	3.28	–	–	–	–
	(medial)	[22]	–	0.083	50.7	6.1	–	–	–	–
	(long)	[16]	0.3124	–	127.82	3.87	–	–	–	–
	(long)	[22]	–	0.102	66.6	6.7	–	–	–	–
	(1)	[7]	–	–	–	–	–	–	–	–
	(2)	[7]	–	–	–	–	–	–	–	–
	(3)	[7]	–	–	–	–	–	–	–	–
	(1)	[12]	–	–	–	16.30	–	–	–	–
	(2)	[12]	–	–	–	–	–	–	–	–
	(3)	[12]	–	–	–	–	–	–	–	–

TENDON LENGTH LT (m)	TENDON PCSA (mm²)	ORIGIN COORD. SYSTEM	X (m)	Y (m)	Z (m)	INSERTION COORD. SYSTEM	X (m)	Y (m)	Z (m)
0.0935	–	–	–	–	–	–	–	–	–
0.01875	–	–	–	–	–	–	–	–	–
–	–	–	–	–	–	–	–	–	–
–	–	–	–	–	–	Scapula	0.0875	0.0534	-0.0899
–	–	–	–	–	–	Scapula	0.0535	0.0535	-0.0822
–	–	–	–	–	–	Scapula	0.0147	0.0158	-0.0178
–	–	–	–	–	–	Clavicle	0.1186	-0.0216	0.0046
–	–	–	–	–	–	Scapula	0.0546	-0.0166	0.0079
–	–	–	–	–	–	–	–	–	–
–	–	–	–	–	–	–	–	–	–
–	–	–	–	–	–	–	–	–	–
–	–	–	–	–	–	–	–	–	–
–	–	–	–	–	–	–	–	–	–
–	–	Humerus	0.1448	0.0051	0.0121	Ulna	0.0006	-0.1051	0.0007
–	–	–	–	–	–	–	–	–	–
–	–	Humerus	0.1345	-0.0050	0.0071	Ulna	0.0707	-0.1782	0.0008
–	–	–	–	–	–	–	–	–	–
–	–	Scapula	0.2219	0.0014	0.0706	Ulna	0.0008	-0.1051	0.0009
–	–	–	–	–	–	–	–	–	–
–	–	Scapula	-0.016	0.005	-0.050	Ulna	-0.016	0.009	0.005
–	–	Humerus	-0.010	0.012	-0.200	Ulna	-0.016	0.000	0.005
–	–	Humerus	-0.008	-0.016	-0.100	Ulna	-0.016	0.009	0.005
–	–	Humerus	-0.0008	0.0000	-0.0165	Forearm	-0.0160	0.000	-0.2167
–	–	Humerus	-0.0008	0.0000	-0.0051	Forearm	-0.0160	0.000	-0.2167
–	–	UpTorso	0.0000	0.1746	-0.0470	Forearm	-0.0160	0.000	-0.2167

HEAD AND NECK MUSCULATURE

MUSCLE		SOURCE	MUSCLE LENGTH ML (m)	FIBER LENGTH LM (m)	VOLUME V (ml)	MUSCLE PCSA =V/L (cm²)	PENNATION ANGLE (deg)	MUSCLE FIBER TYPE %SO	%FO	%FG
[illegible]		[14]	–	–	–	–	–	64.1	–	35.9
iliocostalis cervicis	(1)	[7]	–	–	–	–	–	–	–	–
	(2)	[7]	–	–	–	–	–	–	–	–
	(3)	[7]	–	–	–	–	–	–	–	–
longissimus	(1)	[16]	0.0700	–	–	1.88	10	30	–	–
	(2)	[16]	0.0860	–	–	1.88	10	40	–	–
	(3)	[16]	0.0860	–	–	1.88	10	[illegible]	–	–
longissimus capitis		[12]	–	–	–	0.80	–	–	–	–
	(1)	[7]	–	–	–	–	–	–	–	–
	(2)	[7]	–	–	–	–	–	–	–	–
	(3)	[7]	–	–	–	–	–	–	–	–
	(4)	[7]	–	–	–	–	–	–	–	–
	(5)	[7]	–	–	–	–	–	–	–	–
	(6)	[7]	–	–	–	–	–	–	–	–
		[16]	0.1200	–	–	1.22	10	30	–	–
longissimus cervicis		[12]	–	–	–	0.80	–	–	–	–
	(1)	[7]	–	–	–	–	–	–	–	–
	(2)	[7]	–	–	–	–	–	–	–	–
	(3)	[7]	–	–	–	–	–	–	–	–
	(4)	[7]	–	–	–	–	–	–	–	–
	(5)	[7]	–	–	–	–	–	–	–	–
	(6)	[7]	–	–	–	–	–	–	–	–
	(7)	[7]	–	–	–	–	–	–	–	–
	(8)	[7]	–	–	–	–	–	–	–	–
	(9)	[7]	–	–	–	–	–	–	–	–
	(10)	[7]	–	–	–	–	–	–	–	–
longus capitis		[12]	–	–	–	0.75	–	–	–	–
	(1)	[7]	–	–	–	–	–	–	–	–
	(2)	[7]	–	–	–	–	–	–	–	–
	(3)	[7]	–	–	–	–	–	–	–	–
	(4)	[7]	–	–	–	–	–	–	–	–
longus colli		[12]	–	–	–	0.75	–	–	–	–
		[16]	0.0880	–	–	0.82	10	80	–	–
longus colli vertical	(1)	[7]	–	–	–	–	–	–	–	–
	(2)	[7]	–	–	–	–	–	–	–	–
	(3)	[7]	–	–	–	–	–	–	–	–
	(4)	[7]	–	–	–	–	–	–	–	–
	(5)	[7]	–	–	–	–	–	–	–	–
	(6)	[7]	–	–	–	–	–	–	–	–
	(7)	[7]	–	–	–	–	–	–	–	–
	(8)	[7]	–	–	–	–	–	–	–	–
	(9)	[7]	–	–	–	–	–	–	–	–
	(10)	[7]	–	–	–	–	–	–	–	–
	(11)	[7]	–	–	–	–	–	–	–	–
	(12)	[7]	–	–	–	–	–	–	–	–
	(13)	[7]	–	–	–	–	–	–	–	–
	(14)	[7]	–	–	–	–	–	–	–	–
	(15)	[7]	–	–	–	–	–	–	–	–
	(16)	[7]	–	–	–	–	–	–	–	–
longus colli inferior oblique		[7]	–	–	–	–	–	–	–	–
	(2)	[7]	–	–	–	–	–	–	–	–
longus colli superior oblique		[7]	–	–	–	–	–	–	–	–
	(2)	[7]	–	–	–	–	–	–	–	–
	(3)	[7]	–	–	–	–	–	–	–	–
	(4)	[7]	–	–	–	–	–	–	–	–
	(5)	[7]	–	–	–	–	–	–	–	–
	(6)	[7]	–	–	–	–	–	–	–	–
multifidus cervicis	(1)	[7]	–	–	–	–	–	–	–	–
	(2)	[7]	–	–	–	–	–	–	–	–
	(3)	[7]	–	–	–	–	–	–	–	–
	(4)	[7]	–	–	–	–	–	–	–	–
	(5)	[7]	–	–	–	–	–	–	–	–
	(6)	[7]	–	–	–	–	–	–	–	–
	(7)	[7]	–	–	–	–	–	–	–	–
	(8)	[7]	–	–	–	–	–	–	–	–
	(9)	[7]	–	–	–	–	–	–	–	–
	(10)	[7]	–	–	–	–	–	–	–	–
	(11)	[7]	–	–	–	–	–	–	–	–
	(12)	[7]	–	–	–	–	–	–	–	–
oblique capitis superior		[7]	–	–	–	–	–	–	–	–
		[12]	–	–	–	1.00	–	–	–	–
		[16]	0.0800	–	–	1.78	10	80	–	–
oblique capitis inferior		[7]	–	–	–	–	–	–	–	–
		[16]	0.0880	–	–	0.88	10	30	–	–

TENDON LENGTH LT (m)	TENDON PCSA (mm²)	ORIGIN COORD. SYSTEM	ORIGIN X (m)	ORIGIN Y (m)	ORIGIN Z (m)	INSERTION COORD. SYSTEM	INSERTION X (m)	INSERTION Y (m)	INSERTION Z (m)
–	–	–	–	–	–	–	–	–	–
–	–	C4	-0.0040	-0.0280	0.0060	Thorax	0.0150	-0.0460	0.2160
–	–	C6	-0.0040	-0.0280	0.0060	Thorax	0.0150	-0.0460	0.2160
–	–	C6	-0.0040	-0.0280	0.0060	Thorax	0.0150	-0.0460	0.2160
0.0175	–	–	–	–	–	–	–	–	–
0.0300	–	–	–	–	–	–	–	–	–
0.0212	–	–	–	–	–	–	–	–	–
–	–	Neck	-0.0150	0.0254	0.0540	Head	0.0000	0.0340	0.0578
–	–	Shoulder	-0.0150	-0.0420	0.0060	C3	0.0000	-0.0660	0.0160
–	–	Shoulder	-0.0150	-0.0460	0.0060	C4	0.0000	-0.0660	0.0160
–	–	Shoulder	-0.0150	-0.0460	0.0060	C5	0.0000	-0.0660	0.0160
–	–	Shoulder	-0.0150	-0.0460	0.0060	C6	0.0000	-0.0660	0.0160
–	–	Shoulder	-0.0150	-0.0460	0.0060	C7	0.0000	-0.0660	0.0160
–	–	Shoulder	-0.0150	-0.0460	0.0060	Thorax	0.0000	-0.0660	0.2200
0.0300	–	–	–	–	–	–	–	–	–
–	–	UpTorso	-0.0150	0.0254	-0.0020	Neck	-0.0150	0.0254	0.0157
–	–	C2	-0.0040	-0.0280	0.0060	Thorax	0.0150	-0.0460	0.2160
–	–	C3	-0.0040	-0.0280	0.0060	Thorax	0.0150	-0.0460	0.2160
–	–	C4	-0.0040	-0.0280	0.0060	Thorax	0.0150	-0.0460	0.2160
–	–	C5	-0.0040	-0.0280	0.0060	Thorax	0.0150	-0.0460	0.2160
–	–	C6	-0.0040	-0.0280	0.0060	Thorax	0.0150	-0.0460	0.2160
–	–	C2	-0.0040	-0.0280	0.0060	C7	-0.0060	-0.0660	0.0670
–	–	C3	-0.0040	-0.0280	0.0060	C7	-0.0060	-0.0660	0.0670
–	–	C4	-0.0040	-0.0280	0.0060	C7	-0.0060	-0.0660	0.0670
–	–	C5	-0.0040	-0.0280	0.0060	C7	-0.0060	-0.0660	0.0670
–	–	C6	-0.0040	-0.0280	0.0060	C7	-0.0060	-0.0660	0.0670
–	–	Neck	-0.0150	0.0254	-0.0157	Head	0.0001	0.0000	0.0000
–	–	Shoulder	0.0170	-0.0040	0.0060	C3	0.0000	-0.0060	0.0160
–	–	Shoulder	0.0170	-0.0040	0.0060	C4	0.0000	-0.0060	0.0160
–	–	Shoulder	0.0170	-0.0040	0.0060	C5	0.0000	-0.0060	0.0160
–	–	Shoulder	0.0170	-0.0040	0.0060	C6	0.0000	-0.0060	0.0160
–	–	UpTorso	0.0150	0.0000	-0.0020	Neck	0.0150	0.0000	-0.0157
0.0256	–	–	–	–	–	–	–	–	–
–	–	C1	0.0150	0.0000	0.0100	C6	0.0150	0.0000	0.0000
–	–	C2	0.0150	0.0000	0.0060	C6	0.0150	0.0000	0.0000
–	–	C3	0.0150	0.0000	0.0060	C6	0.0150	0.0000	0.0000
–	–	C4	0.0150	0.0000	0.0060	C6	0.0150	0.0000	0.0000
–	–	C1	0.0150	0.0000	0.0100	C6	0.0150	0.0000	0.0000
–	–	C2	0.0150	0.0000	0.0060	C6	0.0150	0.0000	0.0000
–	–	C3	0.0150	0.0000	0.0060	C6	0.0150	0.0000	0.0000
–	–	C4	0.0150	0.0000	0.0060	C6	0.0150	0.0000	0.0000
–	–	C1	0.0150	0.0000	0.0100	C7	0.0150	0.0000	0.0000
–	–	C2	0.0150	0.0000	0.0060	C7	0.0150	0.0000	0.0000
–	–	C3	0.0150	0.0000	0.0060	C7	0.0150	0.0000	0.0000
–	–	C4	0.0150	0.0000	0.0060	C7	0.0150	0.0000	0.0000
–	–	C1	0.0150	0.0000	0.0100	Thorax	0.1050	0.0000	0.2760
–	–	C2	0.0150	0.0000	0.0060	Thorax	0.1050	0.0000	0.2760
–	–	C3	0.0150	0.0000	0.0060	Thorax	0.1050	0.0000	0.2760
–	–	C4	0.0150	0.0000	0.0060	Thorax	0.1050	0.0000	0.2760
–	–	C5	0.0150	-0.0060	0.0100	Thorax	0.1050	0.0000	0.2760
–	–	C6	0.0150	-0.0060	0.0100	Thorax	0.1050	0.0000	0.2760
–	–	C1	0.0150	0.0000	0.0100	C6	0.0150	-0.0060	0.0160
–	–	C2	0.0150	0.0000	0.0060	C4	0.0150	-0.0060	0.0160
–	–	C1	0.0150	0.0000	0.0100	C6	0.0150	-0.0060	0.0160
–	–	C2	0.0150	0.0000	0.0060	C5	0.0150	-0.0060	0.0160
–	–	C1	0.0150	0.0000	0.0100	C4	0.0150	-0.0060	0.0160
–	–	C2	0.0150	0.0000	0.0060	C5	0.0150	-0.0060	0.0160
–	–	C5	-0.0270	-0.0040	-0.0020	C6	-0.0130	-0.0620	0.0000
–	–	C6	-0.0270	-0.0040	-0.0020	C6	-0.0130	-0.0620	0.0000
–	–	C5	-0.0250	-0.0040	-0.0070	C6	-0.0130	-0.0620	0.0000
–	–	C5	-0.0250	-0.0040	-0.0070	C7	-0.0130	-0.0620	0.0000
–	–	C4	-0.0250	-0.0040	-0.0070	C7	-0.0130	-0.0620	0.0000
–	–	C4	-0.0250	-0.0040	-0.0070	Thorax	0.0700	-0.0660	0.2600
–	–	C5	-0.0250	-0.0040	-0.0070	Thorax	0.0700	-0.0660	0.2600
–	–	C5	-0.0250	-0.0040	-0.0070	Thorax	0.0650	-0.0660	0.2600
–	–	C6	-0.0250	-0.0040	-0.0070	Thorax	0.0650	-0.0660	0.2600
–	–	C6	-0.0250	-0.0040	-0.0070	Thorax	0.0650	-0.0660	0.2600
–	–	C7	-0.0400	-0.0040	-0.0100	Thorax	0.0650	-0.0660	0.2600
–	–	C7	-0.0400	-0.0040	-0.0100	Thorax	0.0400	-0.0660	0.2600
–	–	Shoulder	-0.0170	-0.0420	0.0170	C1	0.0000	-0.0640	0.0070
–	–	Neck	-0.0150	0.0254	-0.0540	Head	-0.0140	0.0000	0.0578
0.0120	–	–	–	–	–	–	–	–	–
–	–	C1	0.0000	-0.0060	0.0070	C2	-0.0070	-0.0040	-0.0060
0.0138	–	–	–	–	–	–	–	–	–

MUSCLE		SOURCE	MUSCLE LENGTH ML (m)	FIBER LENGTH LM (m)	VOLUME V (ml)	MUSCLE PCSA =V/L (cm²)	PENNATION ANGLE (deg)	MUSCLE FIBER TYPE %SO	%FO	%FG
orbicularis oculi		[14]	–	–	–	–	–	16.4	–	83.6
rectus capitis posterior major		[7]	–	–	–	–	–	–	–	–
		[12]	–	–	–	0.80	–	–	–	–
		[16]	0.0800	–	–	1.10	10	60	–	–
rectus capitis posterior minor		[7]	–	–	–	–	–	–	–	–
		[12]	–	–	–	0.386	–	–	–	–
		[16]	0.0600	–	–	1.06	10	60	–	–
rectus capitis anterior		[7]	–	–	–	–	–	–	–	–
		[12]	–	–	–	0.85	–	–	–	–
		[16]	0.0800	–	–	0.15	10	50	–	–
rectus capitis lateral		[7]	–	–	–	–	–	–	–	–
		[12]	–	–	–	0.25	–	–	–	–
		[16]	0.0350	–	–	0.21	10	50	–	–
rotatores cervicis	(1)	[7]	–	–	–	–	–	–	–	–
	(2)	[7]	–	–	–	–	–	–	–	–
	(3)	[7]	–	–	–	–	–	–	–	–
	(4)	[7]	–	–	–	–	–	–	–	–
	(5)	[7]	–	–	–	–	–	–	–	–
	(6)	[7]	–	–	–	–	–	–	–	–
	(7)	[7]	–	–	–	–	–	–	–	–
	(8)	[7]	–	–	–	–	–	–	–	–
	(9)	[7]	–	–	–	–	–	–	–	–
	(10)	[7]	–	–	–	–	–	–	–	–
	(11)	[7]	–	–	–	–	–	–	–	–
scalenus		[12]	–	–	–	1.75	–	–	–	–
		[16]	0.0922	–	–	2.80	10	50	–	–
scalenus anterior	(1)	[7]	–	–	–	–	–	–	–	–
	(2)	[7]	–	–	–	–	–	–	–	–
	(3)	[7]	–	–	–	–	–	–	–	–
	(4)	[7]	–	–	–	–	–	–	–	–
scalenus medial	(1)	[7]	–	–	–	–	–	–	–	–
	(2)	[7]	–	–	–	–	–	–	–	–
	(3)	[7]	–	–	–	–	–	–	–	–
	(4)	[7]	–	–	–	–	–	–	–	–
	(5)	[7]	–	–	–	–	–	–	–	–
	(6)	[7]	–	–	–	–	–	–	–	–
	(7)	[7]	–	–	–	–	–	–	–	–
scalenus posterior	(1)	[7]	–	–	–	–	–	–	–	–
	(2)	[7]	–	–	–	–	–	–	–	–
	(3)	[7]	–	–	–	–	–	–	–	–
semispinalis	(1)	[16]	0.1012	–	–	1.60	10	40	–	–
	(2)	[16]	0.1200	–	–	3.75	10	50	–	–
semispinalis capitis		[12]	–	–	–	2.35	–	–	–	–
	(1)	[7]	–	–	–	–	–	–	–	–
	(2)	[7]	–	–	–	–	–	–	–	–
	(3)	[7]	–	–	–	–	–	–	–	–
	(4)	[7]	–	–	–	–	–	–	–	–
	(5)	[7]	–	–	–	–	–	–	–	–
semispinalis cervicis		[12]	–	–	–	2.00	–	–	–	–
	(1)	[7]	–	–	–	–	–	–	–	–
	(2)	[7]	–	–	–	–	–	–	–	–
	(3)	[7]	–	–	–	–	–	–	–	–
	(4)	[7]	–	–	–	–	–	–	–	–
	(5)	[7]	–	–	–	–	–	–	–	–
	(6)	[7]	–	–	–	–	–	–	–	–
semispinalis dorsi		[12]	–	–	–	1.00	–	–	–	–
spinalis capitis		[12]	–	–	–	0.80	–	–	–	–
spinalis dorsi		[12]	–	–	–	1.00	–	–	–	–
splenius capitis		[12]	–	–	–	1.22	–	–	–	–
		[16]	0.1382	–	–	3.73	10	35	–	–
	(1)	[7]	–	–	–	–	–	–	–	–
	(2)	[7]	–	–	–	–	–	–	–	–
splenius cervicis		[16]	0.1650	–	–	2.73	10	60	–	–
	(1)	[12]	–	–	–	1.25	–	–	–	–
	(2)	[12]	–	–	–	0.70	–	–	–	–
	(1)	[7]	–	–	–	–	–	–	–	–
	(2)	[7]	–	–	–	–	–	–	–	–
	(3)	[7]	–	–	–	–	–	–	–	–
sternocleidomastoid		[12]	–	–	–	1.80	–	–	–	–
		[16]	0.2008	–	–	2.08	10	35	–	–
	(1)	[7]	–	–	–	–	–	–	–	–
	(2)	[7]	–	–	–	–	–	–	–	–
		[14]	–	–	–	–	–	38.2	–	61.8
temporalis		[14]	–	–	–	–	–	46.5	–	53.5

TENDON LENGTH LT (m)	TENDON PCSA (m²)	ORIGIN COORD. SYSTEM	X (m)	Y (m)	Z (m)	INSERTION COORD. SYSTEM	X (m)	Y (m)	Z (m)
–	–	–	–	–	–	–	–	–	–
–	–	Skull	-0.0460	-0.0350	0.0120	C2	-0.0070	-0.0040	-0.0080
–	–	Neck	-0.0190	0.0000	-0.0472	Head	-0.0140	0.0280	0.0710
0.0960	–	–	–	–	–	–	–	–	–
–	–	Skull	-0.0070	-0.0100	0.0080	C1	-0.0070	0.0000	0.0080
–	–	Neck	-0.0190	0.0000	-0.0640	Head	-0.0140	0.0070	0.0757
0.0045	–	–	–	–	–	–	–	–	–
–	–	Skull	0.0100	-0.0080	0.0080	C1	0.0000	-0.0270	0.0080
–	–	Neck	-0.0190	0.0054	-0.0640	Head	0.0020	0.0000	0.0808
0.0045	–	–	–	–	–	–	–	–	–
–	–	Skull	-0.0000	-0.0000	0.0000	C1	0.0000	-0.0050	0.0070
–	–	Neck	-0.0190	0.0054	-0.0640	Head	0.0021	0.0000	0.0808
0.0088	–	–	–	–	–	–	–	–	–
–	–	C2	-0.0270	-0.0040	-0.0080	C4	0.0080	-0.0080	0.0160
–	–	C3	-0.0280	-0.0040	-0.0070	C4	0.0080	-0.0080	0.0160
–	–	C3	-0.0280	-0.0040	-0.0070	C5	0.0080	-0.0080	0.0160
–	–	C4	-0.0280	-0.0040	-0.0070	C5	0.0080	-0.0080	0.0160
–	–	C4	-0.0280	-0.0040	-0.0070	C6	0.0080	-0.0080	0.0160
–	–	C5	-0.0280	-0.0040	-0.0070	C6	0.0080	-0.0080	0.0160
–	–	C5	-0.0280	-0.0040	-0.0070	C7	0.0080	-0.0080	0.0160
–	–	C6	-0.0280	-0.0040	-0.0070	C7	0.0080	-0.0080	0.0160
–	–	C6	-0.0280	-0.0040	-0.0070	Thorax	0.0700	-0.0080	0.2360
–	–	C7	-0.0400	-0.0040	-0.0160	Thorax	0.0700	-0.0080	0.2360
–	–	C7	-0.0400	-0.0040	-0.0160	Thorax	0.0080	-0.0080	0.2760
–	–	UpTorso	0.0762	0.0020	-0.0470	Neck	-0.0190	0.0054	0.0061
0.0194	–	–	–	–	–	–	–	–	–
–	–	C3	0.0080	-0.0220	0.0100	Thorax	0.1000	-0.0080	0.2460
–	–	C4	0.0080	-0.0220	0.0100	Thorax	0.1000	-0.0080	0.2460
–	–	C5	0.0080	-0.0220	0.0100	Thorax	0.1000	-0.0080	0.2460
–	–	C6	0.0080	-0.0220	0.0100	Thorax	0.1000	-0.0080	0.2460
–	–	C1	0.0000	-0.0080	0.0070	Thorax	0.0700	-0.0080	0.2700
–	–	C2	-0.0040	-0.0080	0.0080	Thorax	0.0700	-0.0080	0.2700
–	–	C3	-0.0040	-0.0080	0.0080	Thorax	0.0700	-0.0080	0.2700
–	–	C4	-0.0040	-0.0080	0.0080	Thorax	0.0700	-0.0080	0.2700
–	–	C5	-0.0040	-0.0080	0.0080	Thorax	0.0700	-0.0080	0.2700
–	–	C6	-0.0040	-0.0080	0.0080	Thorax	0.0700	-0.0080	0.2700
–	–	C7	-0.0040	-0.0080	0.0080	Thorax	0.0700	-0.0080	0.2700
–	–	C8	-0.0040	-0.0080	0.0080	Thorax	0.0400	-0.0080	0.2660
–	–	C8	-0.0040	-0.0080	0.0080	Thorax	0.0400	-0.0080	0.2660
–	–	C7	-0.0040	-0.0080	0.0080	Thorax	0.0400	-0.0080	0.2660
0.0202	–	–	–	–	–	–	–	–	–
0.0040	–	–	–	–	–	–	–	–	–
–	–	Neck	-0.0190	0.0054	0.0548	Head	-0.0061	0.0201	0.0678
–	–	Skull	-0.0530	-0.0190	0.0260	C4	-0.0120	-0.0020	0.0800
–	–	Skull	-0.0530	-0.0190	0.0260	C5	-0.0120	-0.0020	0.0800
–	–	Skull	-0.0530	-0.0190	0.0260	C6	-0.0120	-0.0020	0.0800
–	–	Skull	-0.0530	-0.0190	0.0260	C7	0.0000	-0.0280	0.0100
–	–	Skull	-0.0530	-0.0190	0.0260	Thorax	-0.0400	-0.0800	0.2400
–	–	UpTorso	-0.0190	0.0054	-0.0660	Neck	-0.0190	0.0000	-0.0806
–	–	C2	-0.0270	-0.0040	-0.0080	Thorax	0.0180	-0.0800	0.2360
–	–	C3	-0.0280	-0.0040	-0.0070	Thorax	0.0180	-0.0800	0.2360
–	–	C4	-0.0280	-0.0040	-0.0070	Thorax	0.0180	-0.0800	0.2360
–	–	C5	-0.0280	-0.0040	-0.0070	Thorax	0.0180	-0.0800	0.2360
–	–	C6	-0.0280	-0.0040	-0.0070	Thorax	-0.0100	-0.0800	0.1900
–	–	C7	-0.0400	-0.0040	-0.0100	Thorax	-0.0100	-0.0800	0.1900
–	–	UpTorso	-0.0190	0.0054	0.0480	Neck	-0.0190	0.0054	0.0061
–	–	Neck	-0.0190	0.0054	0.0548	Head	-0.0021	0.0061	0.0710
–	–	CenTorso	-0.0054	0.0000	-0.1074	UpTorso	-0.0190	0.0054	0.0190
–	–	Neck	-0.0190	0.0000	0.0548	Head	-0.0069	0.0069	0.0678
0.021	–	–	–	–	–	–	–	–	–
–	–	Skull	-0.0300	-0.0140	0.0180	C7	-0.0400	-0.0040	-0.0100
–	–	Skull	-0.0300	-0.0140	0.0180	Thorax	0.0300	0.0000	0.2800
0.033	–	–	–	–	–	–	–	–	–
–	–	UpTorso	-0.0190	0.0000	-0.0660	Neck	-0.0190	0.0000	-0.0472
–	–	UpTorso	-0.0190	0.0000	-0.0660	Neck	-0.0190	0.0054	-0.0472
–	–	C1	0.0000	-0.0260	0.0070	Thorax	0.0180	0.0000	0.2260
–	–	C2	-0.0040	-0.0260	0.0080	Thorax	0.0180	0.0000	0.2260
–	–	C3	-0.0040	-0.0260	0.0080	Thorax	0.0180	0.0000	0.2260
–	–	UpTorso	0.0762	0.0000	-0.0558	Head	-0.0069	0.0069	0.0678
0.040	–	–	–	–	–	–	–	–	–
–	–	Skull	-0.0000	-0.0260	0.0000	Thorax	0.1300	-0.0100	0.2800
–	–	Skull	-0.0000	-0.0260	0.0260	Clavicle	0.0020	0.0000	0.0120
–	–	–	–	–	–	–	–	–	–
–	–	–	–	–	–	–	–	–	–

VITA

PERSONAL INFORMATION

Surname, Name: Esat, Volkan
Nationality: Turkish (TC)
Date and Place of Birth: 26 May 1976, Ankara, Turkey
Marital Status: Married
Phone: +90 312 2791682 (home/Turkey)
+44 1509 554737 (home/UK)
+44 7951560801 (mobile/UK)
email: volkanesat@yahoo.com, volkanesat@hotmail.com, volkanesat@gmail.com

EDUCATION

Degree	Institution	Year of Graduation
MSc	Mechanical Engineering, METU, Ankara, Turkey	2002
BSc	Mechanical Engineering, Gazi University, Ankara, Turkey	1999
High School	Ankara Atatürk Anatolian High School	1994

WORK EXPERIENCE

Year	Place	Enrollment
2003- Present	Wolfson School of Mechanical and Manufacturing Engineering, Loughborough University, UK	University Teacher (temporary part-time)
1999-2002	Department of Mechanical Engineering, METU, Ankara, Turkey	Teaching Assistant

FOREIGN LANGUAGES

Skilful and fluent in **English**, intermediate knowledge of **German**, basic knowledge of **French**

PUBLICATIONS

1. Esat, V., and Acar, M., "A Multi-Body Model of the Whole Human Spine for Dynamic Analysis of Impact Situations", Proceedings of CMBBE06 International Symposium on Computer Methods in Biomechanics and Biomedical Engineering, Cote d'Azur, France, 2006, 6pp.
2. Esat, V., van Lopik, D. W., and Acar, M., "Combined Multi-Body Dynamic and FE Models of Human Head and Neck", Proceedings of IUTAM Symposium on Impact Biomechanics, Dublin, Ireland, 2005, pp. 91-100.
3. Esat, V., and Acar, M., "A Multi-Body Human Spine Model for Dynamic Analysis in Conjunction with the FE Analysis of Spinal Parts", Proceedings of 1st Annual Injury Biomechanics Symposium, The Ohio State University, Columbus, USA, 2005, 12 pp.
4. Esat, V., and Acar, M., "Biomechanical Response of a Functional Spine Unit under Various Loading Conditions: A Viscoelastic Finite Element Approach", Proceedings of IMECE04 - 2004 ASME International Mechanical Engineering Congress And RD&D Expo, Anaheim, California, USA, 2004, 2pp.
5. Esat, V., and Acar, M., "A Finite Element Investigation of a Functional Spine Unit in Conjunction with a Multi-Body Model of the Lumbar Spine for Impact Dynamics", Proceedings of ESDA04 - 7TH Biennial ASME Conference on Engineering Systems Design and Analysis, Manchester, UK, 2004, 7 pp.
6. Esat, V., Darendeliler, H., and Gokler, M. I., "Finite Element Analysis of Springback in Bending of Aluminium Sheets", Materials & Design, Vol. 23, No. 2, 2002, pp. 223-229.
7. Esat, V., Darendeliler, H., and Gokler, M. I., "Springback Analysis in Various Bending Dies by Using Finite Element Method", 2nd International Conference and Exhibition on Design and Production of Dies and Molds, Kuşadası, Turkey, 2001.
8. Esat, V., Darendeliler, H., and Gokler, M. I., "Finite Element Analysis of Springback in Bending of Aluminium Sheets", Proceedings of APPA 2001, pp. 12-1-1 – 12-1-9.